

Enclosure 3 to E-53168

**Updated Final Safety Analysis Report for the
NUHOMS® EOS System, Revision 2
(Public Version)**

PUBLIC VERSION



TN Americas LLC
(formerly AREVA TN Americas,
an operating division of AREVA Inc.)

NUHOMS[®] EOS System
Updated Final Safety Analysis Report

Docket Number 72-1042

Revision 2

January 2020

The proprietary notice is withheld from this public UFSAR version.

REVISION LOG

UFSAR Revision	Date	Record of Changes/FCNs
0	8/15/17	Initial Issue
1	1/31/18	721042-001 R1,002 R1,003 R1,004 R1,005 R1,006 R1,007 R1,008 R1,009 R1,010 R1,011 R1,012 R1,013 R1,014 R1,015 R1,016 R1,017 R1,018 R1,021,022,023 R1,024, 026 R1,027 R1,028 R2,029, 038
2	1/29/20	721042-020, 030, 031, 032, 034, 035, 037, 039, 040, 041, 045, 046 R1, 047 R1, 048, 054, 055, 056, 057, 064, 065, 067 R1, 070, 075, 079, 080, 083, 084, 086, 088, 091 R1, 099, 100, 103, 105, 112, 115, 121, 126, 127, 129, 136, 137, 140, 144, 146, 156, 158, 169

Table of Contents

1.	GENERAL INFORMATION.....	1-1
1.1	Introduction.....	1-2
1.2	General Description and Operational Features of the NUHOMS® EOS System.....	1-5
1.2.1	NUHOMS® EOS System Characteristics.....	1-6
1.2.2	Transfer Equipment	1-11
1.2.3	Operational Features.....	1-11
1.3	Drawings.....	1-16
1.3.1	NUHOMS® EOS-37PTH DSC	1-16
1.3.2	NUHOMS® EOS-89BTH DSC	1-17
1.3.3	NUHOMS® EOS-HSM/EOS-HSMS.....	1-18
1.3.4	NUHOMS® EOS-TCs (EOS-TC108 and EOS-TC125/135).....	1-19
1.4	NUHOMS® EOS System Contents.....	1-20
1.4.1	EOS-37PTH DSC Contents.....	1-20
1.4.2	EOS-89BTH DSC Contents.....	1-20
1.5	Qualification of TN Americas LLC (Applicant).....	1-22
1.6	Quality Assurance.....	1-23
1.7	References	1-24
1.8	Supplemental Data.....	1-25
1.8.1	Generic Cask Arrays.....	1-25
2.	PRINCIPAL DESIGN CRITERIA.....	2-1
2.1	SSCs Important to Safety	2-2
2.1.1	Dry Shielded Canisters	2-2
2.1.2	Horizontal Storage Module (EOS-HSM/EOS-HSMS).....	2-2
2.1.3	ISFSI Basemat and Approach Slabs	2-3
2.1.4	Transfer Equipment	2-3
2.1.5	Auxiliary Equipment.....	2-4
2.2	Spent Fuel to Be Stored	2-5
2.2.1	EOS-37PTH DSC	2-6
2.2.2	EOS-89BTH DSC	2-7

2.3	Design Criteria for Environmental Conditions and Natural Phenomena.....	2-8
2.3.1	Tornado Wind and Tornado Missiles for EOS-HSM	2-8
2.3.2	Tornado Wind and Tornado Missiles for EOS-TC.....	2-10
2.3.3	Water Level (Flood) Design	2-11
2.3.4	Seismic Design.....	2-11
2.3.5	Snow and Ice Loading	2-12
2.3.6	Tsunami.....	2-12
2.3.7	Lightning.....	2-12
2.4	Safety Protection Systems	2-13
2.4.1	General	2-13
2.4.2	Structural.....	2-15
2.4.3	Thermal	2-16
2.4.4	Shielding/Confinement/Radiation Protection	2-16
2.4.5	Criticality	2-17
2.4.6	Material Selection	2-18
2.4.7	Operating Procedures.....	2-19
2.4.8	Acceptance Tests and Maintenance	2-19
2.4.9	Decommissioning	2-19
2.5	References	2-20
3.	STRUCTURAL EVALUATION.....	3-1
3.1	Structural Design	3-2
3.1.1	Design Criteria	3-2
3.2	Weight and Centers of Gravity.....	3-5
3.3	Mechanical Properties of Materials	3-6
3.3.1	EOS-37PTH DSC/EOS-89BTH DSC	3-6
3.3.2	EOS-HSM.....	3-6
3.3.3	EOS-TC.....	3-6
3.4	General Standards for EOS System.....	3-7
3.4.1	Chemical and Galvanic Reaction.....	3-7
3.4.2	Positive Closure	3-7
3.4.3	Lifting Devices.....	3-7

3.4.4	Heat	3-7
3.4.5	Cold.....	3-15
3.5	Fuel Rods General Standards for NUHOMS® EOS System.....	3-16
3.5.1	Fuel Rod Temperature Limits.....	3-16
3.5.2	Fuel Assembly Thermal and Irradiation Growth.....	3-16
3.5.3	Fuel Rod Integrity during Drop Scenarios.....	3-16
3.6	Normal Conditions of Storage and Transfer.....	3-17
3.6.1	EOS-37PTH DSC/89BTH DSC	3-17
3.6.2	EOS-HSM.....	3-18
3.6.3	EOS-TC.....	3-19
3.7	Off-Normal and Hypothetical Accident Conditions of Storage and Transfer.....	3-20
3.7.1	EOS-37PTH DSC/89BTH DSC	3-20
3.7.2	EOS-HSM.....	3-22
3.7.3	EOS-TC.....	3-22
3.8	References	3-23
3.9.1	<i>DSC SHELL STRUCTURAL ANALYSIS</i>	<i>3.9.1-1</i>
3.9.1.1	<i>General Description</i>	<i>3.9.1-1</i>
3.9.1.2	<i>DSC Shell Assembly Stress Analysis.....</i>	<i>3.9.1-1</i>
3.9.1.3	<i>DSC Shell Buckling Evaluation.....</i>	<i>3.9.1-25</i>
3.9.1.4	<i>DSC Fatigue Analysis.....</i>	<i>3.9.1-25</i>
3.9.1.5	<i>DSC Weld Flaw Size Evaluation.....</i>	<i>3.9.1-28</i>
3.9.1.6	<i>Conclusions</i>	<i>3.9.1-30</i>
3.9.1.7	<i>References</i>	<i>3.9.1-31</i>
3.9.2	<i>EOS-37PTH AND EOS-89BTH BASKET STRUCTURAL ANALYSIS</i>	<i>3.9.2-1</i>
3.9.2.1	<i>EOS-37PTH Basket Structural Evaluation for Normal/Off-Normal Loads.....</i>	<i>3.9.2-1</i>
3.9.2.2	<i>EOS-89BTH Basket Structural Evaluation for Normal/Off-Normal Loads.....</i>	<i>3.9.2-9</i>
3.9.2.3	<i>EOS-37PTH Basket Structural Evaluation for On-Site Accident Drop Loads.....</i>	<i>3.9.2-14</i>

3.9.2.4	<i>EOS-89BTH Basket Structural Evaluation for On-Site Accident Drop Loads</i>	3.9.2-23
3.9.2.5	<i>References</i>	3.9.2-30
3.9.3	NUHOMS® EOS SYSTEM ACCIDENT DROP EVALUATION	3.9.3-1
3.9.3.1	Application Independent Parameters and Background	3.9.3-1
3.9.3.2	Benchmarking and Sensitivity	3.9.3-1
3.9.3.3	NUHOMS® EOS System with EOS-TC108 and EOS-37PTH Side and Corner Drop Evaluation using LS-DYNA	3.9.3-2
3.9.3.4	NUHOMS® EOS System with EOS-TC108 and EOS-89BTH Side and Corner Drop Evaluation using LS-DYNA	3.9.3-5
3.9.3.5	References	3.9.3-5
3.9.4	EOS-HSM STRUCTURAL ANALYSIS	3.9.4-1
3.9.4.1	<i>General Description</i>	3.9.4-1
3.9.4.2	<i>Material Properties</i>	3.9.4-3
3.9.4.3	<i>Design Criteria</i>	3.9.4-3
3.9.4.4	<i>Load Cases</i>	3.9.4-5
3.9.4.5	<i>Load Combination</i>	3.9.4-5
3.9.4.6	<i>Finite Element Models</i>	3.9.4-5
3.9.4.7	<i>Normal Operation Structural Analysis</i>	3.9.4-9
3.9.4.8	<i>Off-Normal Operation Structural Analysis</i>	3.9.4-10
3.9.4.9	<i>Accident Condition Structural Analysis</i>	3.9.4-11
3.9.4.10	<i>Structural Evaluation</i>	3.9.4-17
3.9.4.11	<i>Conclusions</i>	3.9.4-28
3.9.4.12	<i>References</i>	3.9.4-28
3.9.5	NUHOMS® EOS-TC BODY STRUCTURAL ANALYSIS	3.9.5-1
3.9.5.1	General Information	3.9.5-1
3.9.5.2	EOS Transfer Cask Accident (Side and End) Drop Evaluation for 65g Static Load	3.9.5-1
3.9.5.3	Lead Gamma Shielding Slump Evaluation	3.9.5-2
3.9.5.4	EOS Transfer Cask Trunnions and Local Shell Stress Evaluation	3.9.5-3
3.9.5.5	EOS Transfer Cask Neutron Shield Shell Structural Evaluation	3.9.5-9

3.9.5.6	EOS Transfer Cask, Trunnion, and Neutron Shield Shell Fatigue Requirements.....	3.9.5-14
3.9.5.7	References	3.9.5-15
3.9.6	NUHOMS® EOS FUEL CLADDING EVALUATION	3.9.6-1
3.9.6.1	General Description	3.9.6-1
3.9.6.2	Material Properties	3.9.6-1
3.9.6.3	Evaluation of Effect of Side Drop on PWR Fuel Assemblies.....	3.9.6-1
3.9.6.4	Evaluation of Effect of Corner Drop on PWR Fuel Assemblies.....	3.9.6-3
3.9.6.5	Evaluation of Effect of Side Drop on BWR Fuel Assemblies.....	3.9.6-10
3.9.6.6	Evaluation of Effect of Corner Drop on BWR Fuel Assemblies	3.9.6-13
3.9.6.7	References	3.9.6-16
3.9.7	NUHOMS® EOS SYSTEM STABILITY ANALYSIS	3.9.7-1
3.9.7.1	EOS-HSM Stability Evaluation	3.9.7-1
3.9.7.2	EOS Transfer Cask Missile Stability and Stress Evaluation	3.9.7-14
3.9.7.3	References	3.9.7-31
4.	<i>THERMAL EVALUATION.....</i>	<i>4-1</i>
4.1	<i>Discussion of Decay Heat Removal System</i>	<i>4-2</i>
4.2	<i>Material and Design Limits</i>	<i>4-4</i>
4.2.1	<i>Summary of Thermal Properties of Materials</i>	<i>4-5</i>
4.2.2	<i>Neutron Absorber Plate Conductivity Requirements.....</i>	<i>4-27</i>
4.3	<i>Thermal Loads and Environmental Conditions</i>	<i>4-28</i>
4.4	<i>Thermal Evaluation for Storage</i>	<i>4-29</i>
4.4.1	<i>EOS-37PTH DSC - Description of Loading Cases for Storage</i>	<i>4-29</i>
4.4.2	<i>EOS-37PTH DSC - Thermal Model for Storage in EOS-HSM.....</i>	<i>4-31</i>
4.4.3	<i>EOS-37PTH DSC - Normal Conditions of Storage</i>	<i>4-53</i>
4.4.4	<i>EOS-37PTH DSC - Off-Normal Conditions of Storage.....</i>	<i>4-54</i>
4.4.5	<i>EOS-37PTH DSC - Hypothetical Accident Conditions of Storage</i>	<i>4-55</i>
4.4.6	<i>EOS-89BTH DSC - Description of Loading Cases for Storage</i>	<i>4-55</i>
4.4.7	<i>EOS-89BTH DSC - Thermal Model for Storage in EOS-HSM.....</i>	<i>4-57</i>
4.4.8	<i>EOS-89BTH DSC - Justification for Use of Temperatures Determined for EOS-37PTH DSC in EOS-HSM</i>	<i>4-65</i>

4.4.9	<i>EOS-89BTH DSC - Normal Conditions of Storage</i>	4-68
4.4.10	<i>EOS-89BTH DSC - Off-Normal Conditions of Storage</i>	4-69
4.4.11	<i>EOS-89BTH DSC - Hypothetical Accident Conditions of Storage</i>	4-69
4.5	<i>Thermal Evaluation for Transfer in EOS-TC125 or EOS-TC135</i>	4-70
4.5.1	<i>EOS-37PTH DSC - Description of Load Cases for Transfer</i>	4-71
4.5.2	<i>EOS-37PTH DSC - Thermal Model for Transfer in EOS-TC125</i>	4-74
4.5.3	<i>EOS-37PTH DSC - Normal and Off-Normal Conditions of Transfer</i>	4-82
4.5.4	<i>EOS-37PTH DSC - Time Limits for Normal/Off-Normal Transfer Operations</i>	4-86
4.5.5	<i>EOS-37PTH DSC - Hypothetical Accident Conditions of Transfer</i>	4-88
4.5.6	<i>EOS-89BTH DSC - Description of Load Cases for Transfer</i>	4-88
4.5.7	<i>EOS-89TBH DSC - Thermal Model for Transfer in EOS-TC125</i>	4-91
4.5.8	<i>EOS-89BTH DSC - Normal and Off-Normal Conditions of Transfer</i>	4-91
4.5.9	<i>EOS-89BTH DSC - Time Limits for Normal/Off-Normal Transfer Operations</i>	4-93
4.5.10	<i>EOS-89BTH DSC - Hypothetical Accident Conditions of Transfer</i>	4-93
4.5.11	<i>Thermal Evaluation for Loading/Unloading Conditions</i>	4-94
4.5.12	<i>Acceptance Criteria of EOS-TC125/135 Transfer Cask Coating Damage</i>	4-96
4.6	<i>Thermal Evaluation for Transfer in EOS-TC108</i>	4-98
4.6.1	<i>Description of Load Cases for Transfer</i>	4-98
4.6.2	<i>Normal and Off-Normal Conditions of Transfer</i>	4-100
4.6.3	<i>Time Limits for Normal/Off-Normal Transfer Operations in EOS-TC108</i>	4-102
4.6.4	<i>Hypothetical Accident Conditions of Transfer</i>	4-103
4.7	<i>Maximum Internal Pressure</i>	4-104
4.7.1	<i>Maximum Internal Pressure in EOS-37PTH DSC</i>	4-106
4.7.2	<i>Maximum Internal Pressure in EOS-89BTH DSC</i>	4-108
4.8	<i>References</i>	4-109

4.9.1 CALCULATION OF EFFECTIVE PROPERTIES FOR HOMOGENIZED FUEL ASSEMBLIES.....	4.9.1-1
4.9.1.1 Effective Thermal Properties for PWR Spent Fuel Assemblies in EOS-37PTH DSC.....	4.9.1-2
4.9.1.2 Effective Thermal Properties for BWR Spent Fuel Assemblies in EOS-89BTH DSC	4.9.1-3
4.9.1.3 Scaling Factors for Short and Long Fuel Assemblies.....	4.9.1-5
4.9.1.3A Acceptance Criteria of Basket Plate Coating Damage.....	4.9.1-7
4.9.1.4 References	4.9.1-8
 4.9.2 BENCHMARKING OF THE CFD MODEL AGAINST THERMAL TEST OF HSM-H MOCKUP	4.9.2-1
4.9.2.1 Assumptions.....	4.9.2-1
4.9.2.2 Methodology	4.9.2-2
4.9.2.3 Computations	4.9.2-2
4.9.2.4 Results, Conclusions, and Recommendations	4.9.2-10
4.9.2.5 References	4.9.2-14
 4.9.3 MESH SENSITIVITY	4.9.3-1
4.9.3.1 Mesh Sensitivity for Storage Analysis.....	4.9.3-1
4.9.3.2 Mesh Sensitivity for Transfer Analysis.....	4.9.3-10
4.9.3.3 References	4.9.3-19
 4.9.4 WIND IMPACT ON THE THERMAL PERFORMANCE OF THE EOS-HSM.....	4.9.4-1
4.9.4.1 Introduction to Wind Impact on the EOS-HSM.....	4.9.4-1
4.9.4.2 Thermal Model for Wind Impact Analysis	4.9.4-3
4.9.4.3 Baseline Model (Load Case #1).....	4.9.4-7
4.9.4.4 Frontal Wind Effect (Load Case #F-1 through #F-3).....	4.9.4-7
4.9.4.5 Back Wind Effect (Load Case #B-1 through #B-3).....	4.9.4-8
4.9.4.6 Side Wind Effect (Load Case #S-1 through #S-3).....	4.9.4-8
4.9.4.7 Summary of Wind Impact on Thermal Performance of EOS-HSM	4.9.4-10
4.9.4.8 Evaluation of Grid Convergence Index for Wind Impact	4.9.4-12
4.9.4.9 References	4.9.4-17

4.9.5 THERMAL PERFORMANCE OF THE FLAT PLATE SUPPORT STRUCTURE (FPS) OPTION OF EOS-HSM	4.9.5-1
4.9.5.1 Design of FPS Option of EOS-HSM.....	4.9.5-1
4.9.5.2 Thermal Model.....	4.9.5-4
4.9.5.3 Normal Hot, Steady State with HLZC #1 (LC #1).....	4.9.5-8
4.9.5.4 Off-Normal Hot, Steady State (LC #3)	4.9.5-8
4.9.5.5 Accident, Blocked Inlet and Outlet for 40 Hours (LC #4)	4.9.5-9
4.9.5.6 Normal Hot, Steady State with HLZC #2.....	4.9.5-9
4.9.5.7 Grid Convergence Index Study of CFD Model of FPS Option of EOS-HSM Loaded with EOS-37PTH DSC Basket	4.9.5-10
4.9.5.8 Summary of Thermal Performance of FPS Option of EOS- HSM	4.9.5-10
4.9.5.9 References	4.9.5-11
5. CONFINEMENT	5-1
5.1 Confinement Boundary	5-2
5.1.1 Boundary Definition/Design Features	5-2
5.1.2 Confinement Penetrations.....	5-3
5.1.3 Seals and Welds	5-3
5.1.4 Closure	5-3
5.2 Design Criteria	5-4
5.2.1 Requirements for Normal Conditions of Storage	5-4
5.2.2 Confinement Requirements for Hypothetical Accident Conditions	5-4
5.3 References	5-6
6. SHIELDING EVALUATION.....	6-1
6.1 Discussions and Results	6-2
6.2 Source Specification.....	6-6
6.2.1 Computer Programs	6-7
6.2.2 PWR and BWR Source Terms.....	6-7
6.2.3 Axial Source Distributions and Subcritical Neutron Multiplication.....	6-11
6.2.4 Control Components	6-13
6.2.5 Blended Low Enriched Uranium Fuel	6-16

6.2.6	Reconstituted Fuel	6-16
6.2.7	Irradiation Gases	6-18
6.3	Model Specification.....	6-20
6.3.1	Material Properties.....	6-20
6.3.2	MCNP Model Geometry for the EOS-TC	6-21
6.3.3	MCNP Model Geometry for the EOS-HSM.....	6-24
6.4	Shielding Analysis	6-28
6.4.1	Computer Codes.....	6-28
6.4.2	Flux-to-Dose Rate Conversion	6-28
6.4.3	EOS-TC Dose Rates	6-28
6.4.4	EOS-HSM Dose Rates.....	6-29
6.5	Supplemental Information	6-33
6.5.1	References.....	6-33
7.	CRITICALITY EVALUATION	7-1
7.1	Discussion and Results.....	7-3
7.2	Package Fuel Loading.....	7-5
7.3	Model Specification.....	7-6
7.3.1	Description of Criticality Analysis Model	7-6
7.3.2	Package Regional Densities	7-11
7.4	Criticality Calculation	7-12
7.4.1	Calculational Method.....	7-13
7.4.2	EOS 37PTH Fuel Loading Optimization.....	7-15
7.4.3	EOS 89BTH Fuel Loading Optimization	7-22
7.4.4	Criticality Results.....	7-26
7.5	Critical Benchmark Experiments.....	7-28
7.5.1	Benchmark Experiments and Applicability	7-29
7.5.2	Statistical Analysis and Determination of USL	7-31
7.5.3	Results of the Benchmark Calculations	7-32
7.6	References	7-33

8.	MATERIALS EVALUATION	8-1
8.1	General Information	8-1
8.1.1	NUHOMS® EOS System Materials	8-1
8.1.2	Environmental Conditions	8-1
8.1.3	Engineering Drawings	8-2
8.2	Materials Selection	8-3
8.2.1	Applicable Codes and Standards and Alternatives	8-3
8.2.2	Material Properties	8-6
8.2.3	Materials for ISFSI Sites with Experience of Atmospheric Chloride Corrosion	8-8
8.2.4	Weld Design and Inspection	8-8
8.2.5	Galvanic and Corrosive Reactions	8-8
8.2.6	Creep Behavior of Aluminum	8-12
8.2.7	Bolt Applications	8-13
8.2.8	Protective Coatings and Surface Treatments	8-14
8.2.9	Neutron Shielding Materials	8-14
8.2.10	Materials for Criticality Control	8-15
8.2.11	Concrete and Reinforcing Steel	8-15
8.2.12	Seals	8-15
8.2.13	Low Temperature Ductility of Ferritic Steels	8-16
8.3	Fuel Cladding	8-17
8.3.1	Fuel Burnup	8-17
8.3.2	Cladding Temperature Limits	8-17
8.4	Prevention of Oxidation Damage During Loading of Fuel	8-18
8.5	Flammable Gas Generation	8-19
8.6	DSC Closure Weld Testing	8-20
8.6.1	Periodic Inspections	8-20
8.7	References	8-21
9.	OPERATING PROCEDURES	9-1
9.1	<i>Procedures for Loading the DSC and Transfer to the HSM</i>	<i>9-3</i>
9.1.1	<i>TC and DSC Preparation</i>	<i>9-3</i>
9.1.2	<i>DSC Fuel Loading</i>	<i>9-5</i>

9.1.3	<i>DSC Drying and Backfilling</i>	9-7
9.1.4	<i>DSC Sealing Operations</i>	9-11
9.1.5	<i>TC Downending and Transfer to ISFSI</i>	9-12
9.1.6	<i>DSC Transfer to the EOS-HSM</i>	9-13
9.1.7	<i>Monitoring Operations</i>	9-15
9.2	<i>Procedures for Unloading the DSC</i>	9-16
9.2.1	<i>DSC Retrieval from the HSM</i>	9-16
9.2.2	<i>Removal of Fuel from the DSC</i>	9-17
9.3	<i>References</i>	9-21
10.	ACCEPTANCE TESTS AND MAINTENANCE PROGRAM	10-1
10.1	Acceptance Tests	10-2
10.1.1	Structural and Pressure Tests	10-2
10.1.2	Leak Tests	10-3
10.1.3	Visual Inspection and Non-Destructive Examinations	10-4
10.1.4	Shielding Tests	10-4
10.1.5	Neutron Absorber Tests	10-5
10.1.6	Thermal Acceptance	10-10
10.1.7	Low Alloy High Strength Steel for Basket Structure	10-10
10.1.8	Cask Identification	10-11
10.2	Maintenance Program	10-12
10.2.1	Inspection	10-12
10.2.2	Tests	10-12
10.3	Repair, Replacement, and Maintenance	10-13
10.3.1	Transfer Cask Repair, Replacement, and Maintenance	10-13
10.3.2	HSM Repair, Replacement, and Maintenance	10-13
10.3.3	Maintenance of Thermal Monitoring System	10-14
10.4	References	10-15
11.	RADIATION PROTECTION	11-1
11.1	Radiation Protection Design Features	11-2
11.2	Occupational Dose Assessment	11-3
11.2.1	EOS-DSC Loading, Transfer, and Storage Operations	11-3

11.2.2	EOS-DSC Retrieval Operations.....	11-4
11.2.3	Fuel Unloading Operations	11-5
11.2.4	Maintenance Operations	11-5
11.2.5	Doses during ISFSI Array Expansion.....	11-5
11.3	Offsite Dose Calculations	11-6
11.3.1	Normal Conditions (10 CFR 72.104)	11-6
11.3.2	Accident Conditions (10 CFR 72.106)	11-9
11.4	Ensuring that Occupational Radiation Exposures Are ALARA.....	11-10
11.4.1	Policy Considerations	11-10
11.4.2	Design Considerations	11-10
11.4.3	Operational Considerations.....	11-12
11.5	References	11-13
12.	ACCIDENT ANALYSIS	12-1
12.1	Introduction.....	12-1
12.2	Off-Normal Events.....	12-2
12.2.1	Off-Normal Transfer Load.....	12-2
12.2.2	Extreme Temperature.....	12-4
12.3	Postulated Accident	12-5
12.3.1	EOS-TC Drop	12-5
12.3.2	Earthquake	12-8
12.3.3	Tornado Wind and Tornado Missiles Effect on EOS-HSM	12-9
12.3.4	Tornado Wind and Tornado Missiles Effect on EOS-TC.....	12-10
12.3.5	Flood	12-11
12.3.6	Blockage of EOS-HSM Air Inlet and Outlet Openings or Loss/Damage of Wind Deflectors.....	12-12
12.3.7	Lightning.....	12-13
12.3.8	Fire/Explosion.....	12-13
12.4	References	12-15
13.	OPERATING CONTROLS AND LIMITS.....	13-1
13.1	Operating Controls and Limits.....	13-2
13.1.1	NUREG-1536 [13-1] (Standard Review Plan) Acceptance Criteria	13-2

13.2	Development of Operating Controls and Limits.....	13-3
13.2.1	Training Program	13-3
13.2.2	Retraining Program	13-4
13.2.3	Administration and Records	13-4
13.2.4	Dry Run Training.....	13-4
13.2.5	Functional and Operating Limits, Monitoring Instruments, and Limiting Control Settings	13-4
13.2.6	Limiting Conditions for Operation (LCO).....	13-5
13.2.7	Surveillance Requirements	13-5
13.2.8	Design Features.....	13-5
13.2.9	Administrative Controls.....	13-5
13.3	Technical Specifications	13-6
13.4	References	13-7

TECHNICAL SPECIFICATION BASES

B 2.0	SAFETY LIMITS (SLS).....	13.A-3
B 3.0	LIMITING CONDITION FOR OPERATION (LCO) APPLICABILITY	13.A-4
B 3.0	SURVEILLANCE REQUIREMENT (SR) APPLICABILITY.....	13.A-8
B.3.1	DSC FUEL INTEGRITY	13.A-13
B.3.2	CASK CRITICALITY CONTROL	13.A-20
B.3.3	RADIATION PROTECTION	13.A-22
14.	<i>QUALITY ASSURANCE</i>	<i>14-1</i>
14.1	<i>Introduction.....</i>	<i>14-2</i>
14.2	<i>“Important-to-Safety and “Safety-Related” NUHOMS® EOS System Components</i>	<i>14-3</i>
14.3	<i>Description of TN Americas LLC 10 CFR 72, Subpart G QA Program.....</i>	<i>14-5</i>
14.3.1	<i>Project Organization</i>	<i>14-5</i>
14.3.2	<i>QA Program.....</i>	<i>14-5</i>
14.3.3	<i>Design Control.....</i>	<i>14-6</i>
14.3.4	<i>Procurement Document Control.....</i>	<i>14-6</i>

14.3.5	<i>Procedures, Instructions, and Drawings</i>	<i>14-6</i>
14.3.6	<i>Document Control.....</i>	<i>14-7</i>
14.3.7	<i>Control of Purchased Items and Services</i>	<i>14-7</i>
14.3.8	<i>Identification and Control of Materials, Parts, and Components.....</i>	<i>14-7</i>
14.3.9	<i>Control of Special Processes</i>	<i>14-7</i>
14.3.10	<i>Inspection.....</i>	<i>14-8</i>
14.3.11	<i>Test Control</i>	<i>14-8</i>
14.3.12	<i>Control of Measuring and Test Equipment.....</i>	<i>14-8</i>
14.3.13	<i>Handling, Storage and Shipping.....</i>	<i>14-8</i>
14.3.14	<i>Inspection and Test Status</i>	<i>14-8</i>
14.3.15	<i>Control of Nonconforming Items</i>	<i>14-8</i>
14.3.16	<i>Corrective Action</i>	<i>14-9</i>
14.3.17	<i>Records</i>	<i>14-9</i>
14.3.18	<i>Audits and Surveillances.....</i>	<i>14-9</i>
14.4	<i>Conditions of Approval Records.....</i>	<i>14-10</i>
14.5	<i>Supplemental Information.....</i>	<i>14-11</i>
14.5.1	<i>References</i>	<i>14-11</i>

Acronym List

(3 pages)

Acronym	Definition
3D	Three-Dimensional
AEG	Average Energy Group Causing Fission
ALARA	As Low As Reasonably Achievable
APSRA	Axial Power Shaping Rod Assembly
ASME	American Society of Mechanical Engineers
ASTM	American Society for Testing and Materials
AWS	Automated Welding System
B&W	Babcock and Wilcox
BLEU	Blended Low-Enriched Uranium
BPRA	Burnable Poison Rod Assembly
BRC	Below Regulatory Concern
BWR	Boiling Water Reactor
CC	Control Component
CE	Combustion Engineering
CEA	Control Element Assembly
CFD	Computational Fluid Dynamics
CISCC	Chloride-Induced Stress Corrosion Cracking
CoC	Certificate of Compliance
COR	Coefficient of Restitution
CRA	Control Rod Assembly
CTE	Coefficient of Thermal Expansion
DBT	Design Basis Tornado
DO	Discrete Ordinates
DOE	Department of Energy
DOF	Degrees of Freedom
DRL	Dose Rate Location
DSC	Dry Shielded Canister
DW	Dead Weight
EALF	Energy of Average Lethargy of Fission
FA	Fuel Assembly
FE	Finite Element
FEM	Finite Element Model
GCI	Grid Convergence Index
GTAW	Gas Tungsten Arc Welding

Acronym List

(3 pages)

Acronym	Definition
HLZC	Heat Load Zone Configuration
HSM	Horizontal Storage Module
IBCP	Inner Bottom Cover Plates
IBS	Inner Bottom Shield
IFBA	Integral Fuel Burnable Absorber
IMD	Internal Moderator Density
ISFSI	Independent Spent Fuel Storage Installation
ITCP	Inner Top Cover Plate
LWR	Light Water Reactor
MCNP	Monte Carlo N-Particle
MMC	Metal Matrix Composite
MRF	Most Reactive Fuel
MRC	Most Reactive Configuration
MRS	Monitored Retrievable Storage
NDE	Non-Destructive Examination
NDRC	National Defense Research Committee
NFAH	Non-Fuel Assembly Hardware
NRC	U.S. Nuclear Regulatory Commission
NSA	Neutron Source Assembly
OBCP	Outer Bottom Cover Plate
ORA	Orifice Rod Assembly
ORNL	Oak Ridge National Laboratory
OTCP	Outer Top Cover Plate
PPSS	Peripheral Power Suppression Assemblies
ppm	Parts Per Million
PT	Liquid Penetrant Testing
PWR	Pressurized Water Reactor
QA	Quality Assurance
RCCA	Rod Cluster Control Assembly
SAR	Safety Analysis Report
SFA	Spent Fuel Assembly
TC	Transfer Cask
TD	Theoretical Density
TPA	Thimble Plug Assembly

Acronym List
(3 pages)

Acronym	Definition
TSP	Top Shield Plug
UDF	User Defined Function
UFSAR	Updated Final Safety Analysis Report
USL	Upper Subcritical Limit
VDS	Vacuum Drying System
VSI	Vibration Suppression Insert
WABA	Wet Annular Burnable Absorber
WE	Westinghouse
ZPA	Zero Period Acceleration

CHAPTER 1 GENERAL INFORMATION

Table of Contents

1. GENERAL INFORMATION.....	1-1
1.1 Introduction.....	1-2
1.2 General Description and Operational Features of the NUHOMS® EOS System	1-5
1.2.1 NUHOMS® EOS System Characteristics.....	1-6
1.2.2 Transfer Equipment	1-11
1.2.3 Operational Features.....	1-11
1.3 Drawings.....	1-16
1.3.1 NUHOMS® EOS-37PTH DSC	1-16
1.3.2 NUHOMS® EOS-89BTH DSC	1-17
1.3.3 NUHOMS® EOS-HSM/EOS-HSMS.....	1-18
1.3.4 NUHOMS® EOS-TCs (EOS-TC108 and EOS-TC125/135).....	1-19
1.4 NUHOMS® EOS System Contents.....	1-20
1.4.1 EOS-37PTH DSC Contents.....	1-20
1.4.2 EOS-89BTH DSC Contents.....	1-20
1.5 Qualification of TN Americas LLC (Applicant)	1-22
1.6 Quality Assurance.....	1-23
1.7 References	1-24
1.8 Supplemental Data.....	1-25
1.8.1 Generic Cask Arrays.....	1-25

List of Tables

Table 1-1	Key Design Parameters of the NUHOMS® EOS System Components.....	1-26
-----------	---	------

List of Figures

Figure 1-1	EOS-37PTH DSC	1-28
Figure 1-2	EOS-37PTH Basket	1-29
Figure 1-3	EOS-89BTH DSC	1-30
Figure 1-4	EOS-89BTH Basket.....	1-31
Figure 1-5	EOS-HSM	1-32
Figure 1-6	TC125/135 Transfer Cask.....	1-33
Figure 1-7	TC108 Transfer Cask.....	1-34
Figure 1-8	NUHOMS® EOS System Components, Structures, and Transfer Equipment	1-35
Figure 1-9	Typical Transfer Trailer	1-36
Figure 1-10	Typical Cask Support Skid	1-37
Figure 1-11	Typical Double Module Row ISFSI Layout with EOS-Medium Modules	1-38
Figure 1-12	Typical Single Module Row ISFSI Layout with EOS-Medium Modules.....	1-39
Figure 1-13	Typical Combined Single and Double Module Row ISFSI Layout with EOS-Medium Modules	1-40

1. GENERAL INFORMATION

This Updated Final Safety Analysis Report (UFSAR) describes the design and forms the licensing basis for 10 CFR 72 [1-1], Subpart L certification of the NUHOMS® EOS dry spent fuel storage system. The NUHOMS® EOS System provides for the horizontal storage of high burnup spent pressurized water reactor (PWR) and boiling water reactor (BWR) fuel assemblies (FAs) in dry shielded canisters (DSCs) that are placed in an EOS horizontal storage module (EOS-HSM) utilizing an EOS transfer cask (EOS-TC). The NUHOMS® EOS System is designed to be installed in an independent spent fuel storage installation (ISFSI) at power reactor sites under the provision of a general license in accordance with 10 CFR 72, Subpart K. This system has been specifically optimized for high thermal loads, limited space, and needs for superior radiation shielding performance.

The quality assurance (QA) program applicable to this design satisfies the requirements of 10 CFR 72, Subpart G and is described in Chapter 14. To facilitate U.S. Nuclear Regulatory Commission (NRC) review of this application, this UFSAR has been prepared in compliance with the information and methods defined in Revision 1 to NRC NUREG-1536 [1-2].

The NUHOMS® EOS System is an improved version of the NUHOMS® HD System described in Certificate of Compliance (CoC) No. 1030 [1-3]. The EOS-DSCs included in this application are similar to the DSCs licensed in the NUHOMS® HD Horizontal Modular Storage System For Irradiated Nuclear Fuel Updated Final Safety Analysis Report (UFSAR), Revision 4 [1-4]. The EOS-HSMs are similar to the previously licensed HSM-H. The EOS-TCs are similar to the previously licensed TCs, but with a larger diameter.

The NUHOMS® EOS System is designed for enhanced heat rejection capabilities, and to permit storage of intact PWR spent fuel assemblies (SFAs) with or without control components (CCs), and BWR SFAs with or without channels. Protection afforded to the public is similar to the HSM-H designs described in the NUHOMS® HD System UFSAR. Details of the system design, analyses, operation, and margins are provided in the remainder of this UFSAR.

1.1 Introduction

The type of fuel to be stored in the NUHOMS® EOS System is light water reactor (LWR) fuel of the PWR and BWR type. The EOS-37PTH DSC is designed to accommodate up to 37 intact PWR FAs with uranium dioxide (UO₂) fuel, zirconium alloy cladding, and with or without control components (CCs). The EOS-89BTH DSC is designed to accommodate up to 89 intact BWR FAs with uranium dioxide (UO₂) fuel, zirconium alloy cladding, and with or without fuel channels. The physical and radiological characteristics of these payloads are provided in Chapter 2.

The NUHOMS® EOS System consists of the following components as shown in Figure 1-1 through Figure 1-7:

- Two new dual-purpose (storage and transportation) DSCs that provide confinement in an inert environment, structural support and criticality control for the FAs; the EOS-37PTH DSC and the EOS-89BTH DSC. The DSC shells are welded stainless or duplex steel pressure vessels that includes thick shield plugs at either end to maintain occupational exposures as-low-as reasonably-achievable (ALARA).
- Two new DSC basket designs. In addition, depending on the boron content and neutron poison material in the basket poison plates, and the heat load zone configuration (HLZC), each basket type is designated as follows:

EOS 37PTH Basket Types

Neutron Poison Loading Option	HLZC		
	HLZC 1 (max. 50 kW)	HLZC 2 (max. 41.8 kW)	HLZC 3 (max. 36.35 kW)
A (Low B10)	A1	A2	A3
B (High B10)	B1	B2	B3

EOS 89BTH Basket Types

Neutron Poison Loading Option	HLZC		
	HLZC 1 (max. 43.6 kW)	HLZC 2 (max. 41.6 kW)	HLZC 3 (max. 34.44 kW)
M1-A (Low B-10)	A1	A2	A3
M1-B (Moderate B-10)	B1	B2	B3
M2-A (High B-10)	C1	C2	C3

The criticality evaluations in Chapter 7 refer to the basket types based on the boron content in the poison plates. In Chapter 7, the references to the basket types differ from the above table. The correlations between the basket types used in Chapter 7 and basket types identified in the above table are clarified below:

- EOS-37PTH basket types A1, A2, and/or A3 are identified as EOS-37PTH basket type A in Chapter 7
- EOS-37PTH basket types B1, B2, and/or B3 are identified as EOS-37PTH basket type B in Chapter 7
- EOS-89BTH basket types A1, A2, and/or A3 are identified as EOS-89BTH basket type M1-A in Chapter 7
- EOS-89BTH basket types B1, B2, and/or B3 are identified as EOS-89BTH basket type M1-B in Chapter 7
- EOS-89BTH basket types C1, C2, and/or C3 are identified as EOS-89BTH basket type M2-A in Chapter 7

The thermal evaluation in Chapter 4 refers directly to the HLZC instead of using the basket types.

- A new HSM design, designated as either the EOS-HSM or the EOS-HSMS, is equipped with special design features for enhanced shielding and heat rejection capabilities. The HSM base has two alternatives, a single piece or a split base. The HSM with the split base is designated as the EOS-HSMS. Finally, the EOS-HSM and EOS-HSMS can be fabricated with three lengths to accommodate the range of DSC lengths, provided in the table below.

NUHOMS® Module	DSC Length without Grapple Ring (in.)		Total EOS- HSM Length (in.)
	Minimum (in.)	Maximum (in.)	
EOS-Short	165.5	179.5	228
EOS-Medium	185.5	199.5	248
EOS-Long	205.5	219.5	268

- EOS-HSM and EOS-HSMS modules are arranged in arrays to minimize space and maximize self-shielding. The DSCs are longitudinally restrained to prevent movement during seismic events. Arrays are fully expandable to permit modular expansion in support of operating power plants.
- The EOS-HSM and EOS-HSMS provides the bulk of the radiation shielding for the DSCs. The EOS-HSM/EOS-HSMS can be arranged in either a single-row or a back-to-back arrangement. Thick concrete supplemental shield walls are used at either end of an EOS-HSM and EOS-HSMS array and along the back wall of single-row arrays to minimize radiation dose rates both onsite and offsite. Two or more empty modules can be substituted for the end walls until the array is fully built.

- A new EOS-TC system is provided with a top cover plate that allows air circulation through the TC/DSC annulus during transfer operations at certain heat loads when time limits for transfer operations cannot be satisfied. The EOS-TC system consists of a 135-ton cask (EOS-TC135), a 125-ton cask (EOS-TC125), and a 108-ton cask (EOS-TC108).

The EOS-37PTH DSC is designed for a maximum heat load of 50 kW when transferred in the EOS-TC125/135, and a maximum heat load of 41.8 kW when transferred in the EOS-TC108. The EOS-89BTH DSC is designed for a maximum heat load of 43.6 kW when transferred in the EOS-TC125/135, and a maximum heat load of 41.6 kW when transferred in the EOS-TC108. The EOS-37PTH DSC can be transferred in any EOS-TC with a maximum heat load of 36.35 kW without air circulation available and, similarly, the EOS-89BTH with a maximum heat load of 34.4 kW.

The NUHOMS® EOS System is designed to be compatible with removal of the stored DSC for transportation and ultimate disposal by the Department of Energy, in accordance with 10 CFR 236(m). However, this application only addresses the storage of the spent fuel in the NUHOMS® EOS System.

The cavity length of the DSCs is adjustable to match the length of the fuel to be stored. This eliminates or reduces the need for fuel spacers to address secondary impact of the fuel on the lids during transportation accident scenarios.

The NUHOMS® EOS System provides structural integrity, confinement, shielding, criticality control, and passive heat removal independent of any other facility structures or components.

Approval of the NUHOMS® EOS System components described above is sought under the provisions of 10 CFR 72, Subpart L for use under the general license provisions of 10 CFR 72, Subpart K. The EOS-HSMs and DSCs are intended for outdoor or sheltered storage on a reinforced concrete pad at a nuclear power plant. In addition to these components, the system requires use of an onsite TC, transfer trailer, and other auxiliary equipment that are described in this UFSAR. Similar equipment was previously licensed under NUHOMS® HD System UFSAR, Revision 4. Sufficient information for the transfer system and auxiliary equipment is included in this SAR to demonstrate that means for safe operation of the system are provided.

1.2 General Description and Operational Features of the NUHOMS® EOS System

The NUHOMS® EOS System provides for the horizontal, dry storage of canisterized SFAs in a concrete EOS-HSM. The storage system components consist of a reinforced concrete EOS-HSM and a stainless or duplex steel DSC confinement vessel that houses the SFAs. The general arrangement of the NUHOMS® EOS System components is shown in Figure 1-8. The confinement boundary is defined in Section 5.1 and shown in Figure 5-1. This UFSAR addresses the design and analysis of the storage system components, including the EOS-37PTH DSC, the EOS-89BTH DSC, the TC135, the TC125, the TC108, the EOS-HSM, and the EOS-HSMS, which are important to safety in accordance with 10 CFR 72.

In addition to these storage system components, the NUHOMS® EOS System also utilizes transfer equipment to move the DSCs from the plant's fuel or reactor building, where they are loaded with SFAs and prepared for storage in the EOS-HSM where they are stored. This transfer system consists of a TC, a lifting yoke, a ram system, a prime mover, a transfer trailer, a cask support skid, and a skid positioning system. This transfer system interfaces with the existing plant fuel pool, the cask handling crane, the site infrastructure (i.e., roadways and topography) and other site-specific conditions and procedural requirements. Auxiliary equipment, such as a TC/DSC annulus seal, a vacuum drying system, and a welding system, are also used to facilitate DSC loading, draining, drying, inerting, and sealing operations. Similar transfer system and auxiliary equipment has been previously licensed under the NUHOMS® HD System.

During dry storage of the spent fuel, no active systems are required for the removal and dissipation of the decay heat from the fuel. The NUHOMS® EOS System is designed to transfer the decay heat from the fuel to the DSC and from the DSC to the surrounding air by conduction, radiation and natural convection. The NUHOMS® EOS System ISFSI can also be housed in enclosed buildings provided the ISFSI with the building design is bounded by the design criteria described in Chapter 2 and the Technical Specification. No credit is taken for the building in the Safety Analysis of the NUHOMS® EOS System.

Each PWR DSC is identified by a Model Number, XXX-EOS-37PTH-YYY-Z, where XXX typically identifies the site for which the EOS-37PTH DSC was fabricated, Z designates the basket type, and YYY is a sequential number corresponding to a specific DSC. The basket types are defined by both the HLZC and neutron poison loading and are described in UFSAR drawing no. EOS01-1010-SAR. Similarly, each BWR DSC is identified by a Model Number, XXX-EOS-89BTH-YYY-Z. The basket types are described in UFSAR drawing no. EOS01-1020-SAR.

The NUHOMS® EOS System components do not include receptacles, valves, sampling ports, impact limiters, protrusions, or pressure relief systems, except for the neutron shield tanks on the EOS-TCs, which include pressure relief valves.

1.2.1 NUHOMS® EOS System Characteristics

1.2.1.1 EOS-37PTH DSC

The key design parameters of the EOS-37PTH DSC are listed in Table 1-1. The primary confinement boundary for the EOS-37PTH DSC consists of the cylindrical shell, the top and bottom inner cover plates, the *siphon*/drain port cover plate, vent plug, and the associated welds. *Note that the terms 'drain port' and 'siphon' are used interchangeably throughout the UFSAR and TS.* The outer top cover plate and the test port plug provide the redundant sealing required by 10 CFR 72.236(e). The top and bottom shield plugs provide shielding for the EOS-37PTH DSC so that occupational doses at the ends are minimized during drying, sealing, handling, and transfer operations.

The cylindrical shell and inner bottom cover plate confinement boundary welds are fully compliant with Subsection NB of the ASME Code and are made during fabrication. The confinement boundary weld between the shell and the inner top cover (including drain port cover plate and vent plug welds), and the structural attachment weld between the shell and the outer top cover plate (including the test port weld) are in accordance with Alternatives to the ASME code as described in Section 4.4.4 of the Technical Specifications [1-7].

Both drain port cover plate and vent plug welds are made after drying operations are completed. There are no credible accidents that could breach the confinement boundary of the EOS-37PTH DSC, as documented in Chapters 3 and 12.

The EOS-37PTH DSC basket structure, shown schematically in Figure 1-2, consists of interlocking slotted plates to form an egg-crate type structure. The egg-crate structure forms a grid of 37 fuel compartments that house the PWR SFAs. The egg-crate grid structure is composed of one or more of the following: a steel plate, an aluminum plate and a neutron absorber plate. The steel plates are fabricated from high-strength low-alloy (HSLA) steels such as ASTM A829 Gr 4130 (AISI 4130) steel, hot rolled, heat-treated and tempered to provide structural support for the FAs. The poison plates are made of borated metal matrix composites (MMCs) and provide the necessary criticality control. The aluminum plates, together with the poison plates, provide a heat conduction path from the FAs to the DSC rails and shell.

Basket “transition rails” provide the transition between the rectangular basket structure and the cylindrical DSC shell. The transition rails are made of extruded aluminum open or solid sections, which are reinforced with internal steel, as necessary. These transition rails provide the transition to a cylindrical exterior surface to match the inside surface of the DSC shell. The transition rails support the fuel basket egg-crate structure and transfer mechanical loads to the DSC shell. They also provide the thermal conduction path from the basket assembly to the DSC shell wall, making the basket assembly efficient in rejecting heat from its payload. The nominal dimension of each fuel compartment opening is sized to accommodate the limiting assembly with sufficient clearance around the FA.

The EOS-37PTH DSC is designed for a maximum heat load of 50.0 kW. The internal basket assembly contains a storage position for each FA. The criticality analysis credits the fixed borated neutron absorbing material placed between the FAs. The analysis also takes credit for soluble boron during loading operations. Sub-criticality during wet loading/unloading, drying, sealing, transfer, and storage operations is maintained through the geometric separation of the FAs by the basket assembly, the boron loading of the pool water, and the neutron absorbing capability of the EOS-37PTH DSC materials, as applicable. Based on poison material and boron loading, and the HLZC, six basket types are provided, as shown on drawing EOS01-1010-SAR and described in Chapter 10.

In general, the dimensions of the EOS-37PTH DSC components described in the text and provided in figures and tables of this UFSAR are nominal dimensions for general system description purposes. Actual design dimensions are contained in the drawings in Section 1.3.1 of this UFSAR. See Sections 1.4.1 and 2.2.1 for a discussion of the contents authorized to be stored in this DSC.

1.2.1.2 EOS-89BTH DSC

The key design parameters of the EOS-89BTH DSC are listed in Table 1-1. The primary confinement boundary for the EOS-89BTH DSC consists of the cylindrical shell, the top and bottom inner cover plates, the drain port cover plate, vent plug, and the associated welds. The outer top and bottom cover plates, test port plug and associated welds form the redundant confinement boundary. The top and bottom shield plugs provide shielding for the EOS-89BTH DSC to minimize occupational doses at the ends during drying, sealing, handling, and transfer operations.

The cylindrical shell and inner bottom cover plate confinement boundary welds are fully compliant with Subsection NB of the ASME Code and are made during fabrication. The confinement boundary weld between the shell and the inner top cover (including drain port cover plate and vent plug welds), and structural attachment weld between the shell and the outer top cover plate (including the test plug weld) are in accordance with Alternatives to the ASME code as described in Section 4.4.4 of the Technical Specifications [1-7].

Both drain port cover plate and vent plug welds are made after drying operations are complete. There are no credible accidents that could breach the confinement boundary of the EOS-89BTH DSC as documented in Chapters 3 and 12.

The EOS-89BTH DSC basket structure, shown schematically in Figure 1-4, consists of interlocking slotted plates to form an egg-crate-type structure. The egg-crate structure forms a grid of 89 fuel compartments that house the BWR SFAs. The egg-crate grid structure is composed of one or more of the following: a steel plate, an aluminum plate, and a neutron absorber plate. The steel plates are fabricated from HSLA steels such as ASTM A829 Gr 4130 (AISI 4130) steel, hot rolled, heat-treated and tempered to provide structural support for the FAs. The poison plates are made of borated MMCs or BORAL® and provide the necessary criticality control. The aluminum plates, together with the poison plates, provide a heat conduction path from the FAs to the DSC rails and shell.

Basket “transition rails” provide the transition between the rectangular basket structure and the cylindrical DSC shell. The transition rails are made of extruded aluminum open or solid sections, which are reinforced with internal steel as necessary. These transition rails provide the transition to a cylindrical exterior surface to match the inside surface of the DSC shell. The transition rails support the fuel basket egg-crate structure and transfer mechanical loads to the DSC shell. They also provide the thermal conduction path from the basket assembly to the DSC shell wall, making the basket assembly efficient in rejecting heat from its payload. The nominal dimension of each fuel compartment opening is sized to accommodate the limiting assembly with sufficient clearance around the FA.

The EOS-89BTH DSC is designed for a maximum heat load of 43.6 kW. The internal basket assembly contains a storage position for each FA. The criticality analysis credits the fixed borated neutron absorbing material placed between the FAs. Sub-criticality during wet loading/unloading, drying, sealing, transfer, and storage operations is maintained through the geometric separation of the FAs by the basket assembly, and the neutron absorbing capability of the EOS-89BTH DSC materials, as applicable. Based on poison material and boron loading, and the HLZC, nine basket types are provided, as shown on drawing EOS01-1020-SAR and described in Chapter 10.

In general, the dimensions of the EOS-89BTH DSC components described in the text and provided in figures and tables of this UFSAR are nominal dimensions for general system description purposes. Actual design dimensions are contained in the drawings in Section 1.3.2 of this UFSAR. See Sections 1.4.2 and 2.2.2 for a discussion of the contents authorized to be stored in this DSC.

1.2.1.3 Horizontal Storage Module

Each EOS-HSM or EOS-HSMS provides a self-contained modular structure for storage of spent fuel canisterized in an EOS-37PTH or EOS-89BTH DSC. The EOS-HSMS is essentially identical to the EOS-HSM except that the base is split into two sections (upper and lower), which are tied together via shear keys and six grouted tie rods. Henceforth in this UFSAR, EOS-HSM is used interchangeably for both the EOS-HSM and EOS-HSMS. The EOS-HSM is constructed from reinforced concrete and structural steel. The thick concrete roof and walls provide substantial neutron and gamma shielding. Contact doses for the EOS-HSM are designed to be ALARA. The key design parameters of the EOS-HSM are listed in Table 1-1.

The nominal thickness of the EOS-HSM roof is four feet for biological shielding. Separate shield walls at the end of a module row in conjunction with the module base wall, provide a minimum total thickness of four feet for shielding. Similarly, an additional shield wall is used at the rear of the module if the ISFSI is configured as single module arrays to provide a minimum total thickness of four feet of shielding with the module base rear wall. Sufficient shielding is provided by thick concrete side walls between EOS-HSMs in an array to minimize doses in adjacent EOS-HSMs during loading and retrieval operations.

The EOS-HSMs provide an independent, passive system with substantial structural capacity to ensure the safe dry storage of SFAs. To this end, the EOS-HSMs are designed to ensure that normal transfer operations and postulated accidents or natural phenomena do not impair the DSC or pose a hazard to the public or plant personnel.

The EOS-HSM provides a means of removing spent fuel decay heat by a combination of radiation, conduction and convection. Ambient air enters the EOS-HSM through ventilation inlet openings located on both sides of the lower front wall of the EOS-HSM and circulates around the DSC and the heat shields. Air exits through air outlet openings located on each side of the top of the EOS-HSM. The EOS-HSM is designed to remove up to 50.0 kW of decay heat from the bounding EOS-37PTH DSC.

Decay heat is rejected from the DSC to the EOS-HSM air space by convection and then removed from the EOS-HSM by natural circulation air flow. Heat is also radiated from the DSC surface to the heat shields and EOS-HSM walls and roof, where the natural convection air flow and conduction through the walls and roof aid in the removal of the decay heat. The passive cooling system for the EOS-HSM is designed to preserve fuel cladding integrity by maintaining SFA peak cladding temperatures below acceptable limits during long-term storage. Wind deflectors are installed on the EOS-HSM to mitigate the effect of sustained winds for high heat load DSCs.

The EOS-HSMs are installed on a load bearing foundation, which consists of a reinforced concrete basemat on a subgrade suitable to support the loads. The EOS-HSMs are not tied to the basemat.

Dimensions of the EOS-HSM components described in the text and provided in figures and tables of this UFSAR are, in general, nominal dimensions for general system description purposes. Actual design dimensions are contained in the drawings in Section 1.3.3.

1.2.1.4 Transfer Casks

The EOS-TCs are designed to provide shielding and protection from potential hazards during DSC loading and closure operations and transfer to the EOS-HSM. The key design parameters of the TC are listed in Table 1-1. The EOS-TCs included in this UFSAR are limited to onsite use under 10 CFR 72. The EOS-TCs are non-pressure-retaining, except the neutron shield tanks, atmospheric cylindrical vessels with welded bottom assemblies, and bolted top cover plates, and they are designed to ASME Division III Subsection NF Class 1 criteria. The neutron shield tanks retain pressure and are designed to ASME III Subsection ND criteria. The primary function of the EOS-TC is to provide onsite transport of loaded DSCs between the plant's spent fuel pool and the plant's onsite ISFSI. The TC provides the principal biological shielding and heat rejection mechanism for the EOS-DSC and SFAs during handling in the fuel or reactor building, EOS-DSC closure operations, transfer to the ISFSI, and placement in the EOS-HSM.

The TC is designed to provide sufficient shielding to provide reasonable assurance that dose rates are ALARA. Two top-lifting trunnions are provided for handling the TC using a lifting yoke and overhead crane. Lower pocket trunnions are provided for rotating the cask from/to the vertical and horizontal positions on the support skid/transport trailer.

The EOS-TC108 is designed with a removable neutron shield for use at nuclear plant sites with space limitations and/or crane capacity limits and, therefore, cannot use one of the other EOS-TCs. A schematic sketch of the EOS-TC125/135 is shown in Figure 1-6, and of the EOS-TC108 with removable neutron shield is shown in Figure 1-7.

A cask spacer is required in the bottom of the EOS-TC to provide the correct interface at the top of the EOS-TC during loading, drying, and sealing operations for DSCs that are shorter than the cavity length. All EOS-TCs utilize a bottom cover incorporating wedges and top cover assembly that allows for air circulation. This mechanism enables cooling air to travel through the annular space between the EOS-DSC and the TC inner diameter through the entire cask length and to exit through the vent passages in the modified top cover assembly of the cask.

Dimensions of the EOS-TC components described in the text and provided in figures and tables of this UFSAR are in general nominal dimensions for general system description purposes. Actual design dimensions are contained in the drawings in Section 1.3.4.

1.2.2 Transfer Equipment

Transfer Trailer:

The typical transfer trailer for the NUHOMS® EOS System consists of a heavy industrial trailer used to transfer the empty cask, support skid and the loaded transfer cask between the plant's fuel or reactor building and the ISFSI. The trailer is designed to ride as low to the ground as possible to minimize the overall EOS-HSM height and the transfer cask height during DSC transfer operations. The trailer is equipped with leveling jacks to provide vertical alignment of the cask with the EOS-HSM. The trailer is self-powered or towed by a conventional heavy-haul truck tractor or other suitable prime mover. A typical transfer trailer is depicted in Figure 1-9.

Cask Support Skid:

A typical cask support skid for the NUHOMS® EOS System is shown in Figure 1-10, and is similar to the cask support skids described in the NUHOMS® HD System UFSAR. Key design features are:

- The skid is mounted on a surface with sliding support bearings and hydraulic positioners to provide alignment of the cask with the EOS-HSM. A mechanism is provided to prevent movement during trailer towing.
- A hydraulic or mechanical ram is mounted on the skid to insert or retrieve the DSC from the EOS-HSM.
- The cask support skid is mounted on a low profile heavy-haul or self-powered industrial trailer.

The plant's fuel or reactor building crane or other suitable lifting device is used to lower the cask onto the support skid, which is secured to the transfer trailer. Specific details of this operation and the plant-specific building arrangement are covered by the provisions of the 10 CFR 50 operating license for the plant.

Ram:

A hydraulic or mechanical ram system consists of a hydraulic cylinder or mechanical frame with a capacity and a reach sufficient for DSC insertion into and retrieval from the EOS-HSM. The design of the ram support system provides a direct load path for the ram reaction forces during DSC insertion and retrieval. The system uses a rear ram support for alignment of the ram to the DSC. The design provides positive alignment of the major components during DSC insertion and retrieval.

1.2.3 Operational Features

This section provides a discussion of the sequence of operations involving the NUHOMS® EOS System components.

1.2.3.1 Spent Fuel Assembly Loading Operations

The primary operations (in sequence of occurrence) for the NUHOMS® EOS System with the EOS-TC125 or EOS-TC135 are:

1. Prepare TC
2. Prepare DSC
3. Place DSC in TC
4. Fill TC/DSC Annulus with clean water and seal
5. Fill DSC cavity with water (may be accomplished in step 6)
6. Lift TC and place in fuel pool
7. Load spent fuel
8. Place top shield plug
9. Lift TC from pool (DSC water may be drained and replaced with helium during draindown)
10. Seal inner top cover
11. Vacuum Dry and Backfill
12. Pressure test
13. Leak test
14. Seal outer top cover plate
15. Drain TC/DSC annulus and place TC top cover plate
16. Place loaded TC on transfer skid/trailer
17. Move loaded TC to EOS-HSM
18. Prepare and align TC/EOS-HSM
19. Insert DSC into EOS-HSM
20. Close EOS-HSM

For operations (in sequence of occurrence) for the NUHOMS® EOS System with the EOS-TC108 the following additional steps may be used to meet crane limits.

- Concurrent with Step 1 the TC108 neutron shield tank may be removed from the cask and positioned for installation onto the cask once it is loaded and removed from the fuel pool.
- Between Step 9 and Step 10, the neutron shield tank is reinstalled and filled with water.

These operations are described in the following paragraphs. The descriptions are intended to be generic and are described in greater detail in Chapter 9. Plant specific requirements may affect these operations and are to be addressed by the licensee.

Prepare TC:

Transfer cask preparation includes exterior washdown and interior decontamination. These operations are performed on the decontamination pad/pit outside the fuel pool area. The operations are similar to those for a shipping cask, which are performed by plant personnel using existing procedures. For the TC108, this includes removing the neutron shield tank if required to meet crane capacity limits or cask loading space considerations.

Prepare DSC:

The internals and externals of the DSC are inspected and cleaned if necessary. This ensures that the DSC will meet plant cleanliness requirements for placement in the spent fuel pool. If the neutron shield tank is removed from the TC108, position the tank such that it can be installed onto the cask once the cask is loaded and removed from the fuel pool.

Place DSC in TC:

The empty DSC is inserted into the TC.

Fill TC/DSC annulus with clean water and seal:

The TC/DSC annulus is filled with uncontaminated water and is then sealed prior to placement in the pool. This prevents contamination of the DSC outer surface and the transfer cask inner surface by the pool water.

Fill DSC cavity with water:

The DSC cavity is filled with pool water to prevent an in-rush of water as the transfer cask is lowered into the pool.

Lift TC and place in fuel pool:

The TC, with the water-filled DSC inside, is then lowered into the fuel pool. The TC125 and TC135 liquid neutron shield may be left unfilled to meet hook weight limitations.

Load spent fuel:

Spent fuel assemblies are placed into the DSC. This operation is identical to that presently used at plants for shipping cask loading.

Place top shield plug:

This operation consists of placing the top shield plug into the DSC using the plant's crane or other suitable lifting device.

Lift TC from pool:

The loaded TC is lifted out of the pool and placed (in the vertical position) on the drying pad in the decontamination pit. This operation is similar to that used for shipping cask handling operations. If the neutron shield for the EOS-TC125 and EOS-TC135 is not filled, fill tank at this time. If using the EOS-TC108 without the neutron shield tank installed, install the neutron shield tank and fill with water.

Seal inner top cover:

The water contained in the space above the shield plug is drained. The inner top cover plate is installed and welded to the shell. This weld provides the top (confinement) seal for the DSC.

Vacuum dry and backfill:

The initial draining of the DSC is accomplished by pumping from the DSC cavity through the drain port while backfilling the cavity with helium through the vent port. The water in the cavity is pumped out through the siphon tube and routed back to the fuel pool or to the plant's liquid radwaste processing system via appropriate size flexible hose or pipe, as appropriate. The DSC is then evacuated to remove the residual liquid water and water vapor, and helium in the cavity. When the system pressure has stabilized, the DSC is backfilled with helium.

Pressure test:

A pressure test of inner top cover weld is performed by backfilling the DSC cavity with helium. After the pressure test, remove the helium lines. Then, the drain port cover plate and vent plug are installed and welded to the inner top cover.

Leak test:

A leak test of the inner top cover to the DSC shell weld, drain port cover plate and vent plug welds is performed using a temporary test head or after the root pass on the outer top cover plate through the test port or any other alternative means.

Seal outer top cover plate:

After helium backfilling, the DSC outer top cover plate is installed by using a partial penetration weld between the outer top cover plate and the DSC shell.

The outer cover plate to shell weld and inner top cover plate weld provide redundant seals at the upper end of the DSC.

Drain TC/DSC annulus and place TC top cover plate:

The TC/DSC annulus is drained. A swipe is then taken over the DSC exterior at the top cover plate and the upper portion of the shell. Demineralized water is flushed through the TC/DSC annulus, as required, to remove any contamination left on the DSC exterior. The TC top cover plate is installed, using the plant's crane or other suitable lifting device, and bolted closed.

Place Loaded Transfer Cask on Transfer Skid/Trailer:

The TC is lifted onto the TC support skid and downended onto the transfer trailer from the vertical to horizontal position.

Move Loaded Transfer Cask to EOS-HSM:

The transfer trailer is moved to the ISFSI along a predetermined route on a prepared road surface. Upon entering the ISFSI, the cask is positioned and aligned with the designated EOS-HSM into which the DSC is to be transferred.

Prepare and align TC/EOS-HSM:

At the ISFSI with the TC positioned in front of the EOS-HSM, the TC top cover plate is removed. The EOS-HSM door is removed and the transfer trailer is then backed into close proximity with the EOS-HSM. The skid positioning system is then used for the final alignment and docking of the TC with the EOS-HSM and the cask restraint installed.

Insert DSC into EOS-HSM:

After final alignment of the TC, EOS-HSM, and ram, the DSC is pushed into the EOS-HSM by the ram.

Close EOS-HSM:

Install DSC axial retainer and install EOS-HSM door.

1.3 Drawings

1.3.1 NUHOMS® EOS-37PTH DSC

EOS01-1000-SAR	NUHOMS® EOS System Transportable Canister 37PTH DSC Main Assembly	
EOS01-1001-SAR	NUHOMS® EOS System Transportable Canister 37PTH DSC Shell Assembly	
EOS01-1010-SAR	NUHOMS® EOS System Transportable Canister 37PTH Basket Assembly	
EOS01-1011-SAR	NUHOMS® EOS System Transportable Canister 37PTH Basket Transition Rails	

**Proprietary and Security Related Information
for Drawing EOS01-1000-SAR, Rev. 2
Withheld Pursuant to 10 CFR 2.390**

**Proprietary and Security Related Information
for Drawing EOS01-1001-SAR, Rev. 2
Withheld Pursuant to 10 CFR 2.390**

**Proprietary and Security Related Information
for Drawing EOS01-1010-SAR, Rev. 2
Withheld Pursuant to 10 CFR 2.390**

**Proprietary and Security Related Information
for Drawing EOS01-1011-SAR, Rev. 2
Withheld Pursuant to 10 CFR 2.390**

1.3.2 NUHOMS® EOS-89BTH DSC

EOS01-1005-SAR	NUHOMS® EOS System Transportable Canister 89BTH DSC Main Assembly	
EOS01-1006-SAR	NUHOMS® EOS System Transportable Canister 89BTH DSC Shell Assembly	
EOS01-1020-SAR	NUHOMS® EOS System Transportable Canister 89BTH Basket Assembly	
EOS01-1021-SAR	NUHOMS® EOS System Transportable Canister 89BTH Basket Transition Rails	

**Proprietary and Security Related Information
for Drawing EOS01-1005-SAR, Rev. 2
Withheld Pursuant to 10 CFR 2.390**

**Proprietary and Security Related Information
for Drawing EOS01-1006-SAR, Rev. 1
Withheld Pursuant to 10 CFR 2.390**

**Proprietary and Security Related Information
for Drawing EOS01-1020-SAR, Rev. 0
Withheld Pursuant to 10 CFR 2.390**

**Proprietary and Security Related Information
for Drawing EOS01-1021-SAR, Rev. 0
Withheld Pursuant to 10 CFR 2.390**

1.3.3 NUHOMS® EOS-HSM/EOS-HSMS

EOS01-3000-SAR	NUHOMS® EOS System Horizontal Storage Module (EOS-HSM) Main Assembly
EOS01-3016-SAR	NUHOMS® EOS System Wind Deflector Assembly

**Proprietary and Security Related Information
for Drawing EOS01-3000-SAR, Rev. 2
Withheld Pursuant to 10 CFR 2.390**

**Proprietary and Security Related Information
for Drawing EOS01-3016-SAR, Rev. 1
Withheld Pursuant to 10 CFR 2.390**

1.3.4 NUHOMS® EOS-TCs (EOS-TC108 and EOS-TC125/135)

EOS01-2000-SAR	NUHOMS® EOS System Onsite Transfer Cask EOS-TC108 Main Assembly	
EOS01-2001-SAR	NUHOMS® EOS System Onsite Transfer Cask EOS-TC108 Inner and Outer Shells	
EOS01-2002-SAR	NUHOMS® EOS System Onsite Transfer Cask EOS-TC108 Shielding and Rails Details	
EOS01-2003-SAR	NUHOMS® EOS System Onsite Transfer Cask EOS-TC108 Removable Neutron Shield	
EOS01-2010-SAR	NUHOMS® EOS System Onsite Transfer Cask EOS-TC125/TC135 Main Assembly	
EOS01-2011-SAR	NUHOMS® EOS System Onsite Transfer Cask EOS-TC125/TC135 Inner and Outer Shells	
EOS01-2012-SAR	NUHOMS® EOS System Onsite Transfer Cask E EOS-TC125/TC135 Shielding and Rails Details	

**Proprietary and Security Related Information
for Drawing EOS01-2000-SAR, Rev. 1
Withheld Pursuant to 10 CFR 2.390**

**Proprietary and Security Related Information
for Drawing EOS01-2001-SAR, Rev. 1
Withheld Pursuant to 10 CFR 2.390**

**Proprietary and Security Related Information
for Drawing EOS01-2002-SAR, Rev. 1
Withheld Pursuant to 10 CFR 2.390**

**Proprietary and Security Related Information
for Drawing EOS01-2003-SAR, Rev. 0
Withheld Pursuant to 10 CFR 2.390**

**Proprietary and Security Related Information
for Drawing EOS01-2010-SAR, Rev. 2
Withheld Pursuant to 10 CFR 2.390**

**Proprietary and Security Related Information
for Drawing EOS01-2011-SAR, Rev. 2
Withheld Pursuant to 10 CFR 2.390**

**Proprietary and Security Related Information
for Drawing EOS01-2012-SAR, Rev. 2
Withheld Pursuant to 10 CFR 2.390**

1.4 NUHOMS® EOS System Contents

1.4.1 EOS-37PTH DSC Contents

The EOS-37PTH DSC is designed to store up to 37 intact PWR FAs with or without CCs.

The EOS-37PTH DSC is qualified for storage of Babcock and Wilcox (B&W) 15 x 15 class, Combustion Engineering (CE) 14 x 14 class, CE 15 x 15 class, CE 16 x 16 class, Westinghouse (WE) 14 x 14 class, WE 15 x 15 class, and WE 17x17 class PWR FA designs, as described in Chapter 2.

The EOS-37PTH DSC payload may include CCs that are contained within the FA, such as described in Chapter 2.

Reconstituted assemblies containing up to five replacement irradiated stainless steel rods per assembly or an unlimited number of low enriched or natural uranium fuel rods or non-fuel rods are acceptable for storage in an EOS-37PTH DSC as intact FAs.

The EOS-37PTH DSC is also authorized to store FAs containing blended low enriched uranium (BLEU) fuel material. Limitations for storing BLEU fuel are provided in Chapter 2.

The contents of the DSC are stored in an inert atmosphere of helium.

The maximum allowable planar average initial enrichment of the fuel to be stored is 5.00 wt. % U-235, and the maximum assembly average burnup is 62,000 MWd/MTU. The FAs (with or without CCs) must be cooled to meet the decay heat limits specified in Figure 1 of the Technical Specifications [1-7] prior to storage.

The criticality control features of the EOS-37PTH DSC are designed to maintain the neutron multiplication factor k-effective (including uncertainties and calculational bias) at less than 0.95 under normal, off-normal, and accident conditions.

The quantity and type of radionuclides in the SFAs are described and tabulated in Chapter 6. Chapter 7 covers the criticality safety of the EOS-37PTH DSC and its parameters. These parameters include rod pitch, rod outside diameter, material densities, moderator ratios, soluble boron content and geometric configurations. The maximum pressure buildup in the EOS-37PTH DSC cavity is addressed in Chapter 4.

1.4.2 EOS-89BTH DSC Contents

The EOS-89BTH DSC is designed to store up to 89 intact BWR FAs with or without channels.

The EOS-89BTH DSC is qualified for storage of 7x7, 8x8, 9x9, and 10x10 class BWR FAs of initial design or equivalent reload FAs as described in Chapter 2.

Reconstituted assemblies containing up to five replacement irradiated stainless steel rods per assembly or an unlimited number of low enriched or natural uranium fuel rods or non-fuel rods are acceptable for storage in an EOS-89BTH DSC as intact FAs.

The EOS-89BTH DSC is also authorized to store FAs containing BLEU fuel material. Limitations for storing BLEU fuel are provided in Chapter 2.

The contents of the DSC are stored in an inert atmosphere of helium.

The maximum allowable lattice average initial enrichment of the fuel to be stored is 4.80 wt. % U-235 and the maximum assembly average burnup is 62,000 MWd/MTU. The FAs (with or without channels) must be cooled to meet the decay heat limits specified in Figure 2 of the Technical Specifications [1-7] prior to storage.

The criticality control features of the EOS-89BTH DSC are designed to maintain the neutron multiplication factor k -effective (including uncertainties and calculational bias) at less than 0.95 under normal, off-normal, and accident conditions.

The quantity and type of radionuclides in the SFAs are described and tabulated in Chapter 6. Chapter 7 covers the criticality safety of the EOS-89BTH DSC and its parameters. These parameters include rod pitch, rod outside diameter, material densities, moderator ratios, and geometric configurations. The maximum pressure buildup in the EOS-89BTH DSC cavity is addressed in Chapter 4.

1.5 Qualification of *TN Americas LLC* (Applicant)

The prime contractor for design and procurement of the NUHOMS® EOS System components is TN Americas *LLC* (*TN*). TN Americas will subcontract the fabrication, testing, onsite construction, and QA services, as necessary, to qualified firms on a project-specific basis, in accordance with TN's QA program requirements.

The design activities for the NUHOMS® EOS Updated Final Safety Analysis Report were performed by TN and subcontractors, in accordance with TN's QA program requirements. TN is responsible for the design and analysis of the EOS-37PTH DSC, the EOS-89BTH DSC, the EOS-HSMs, the onsite EOS-TCs, and the associated transfer equipment.

Closure activities associated with welding the top cover plates on the DSCs following fuel loading are typically performed by the licensee under the licensee's NRC approved QA program.

1.6 Quality Assurance

The TN QA program has been established in accordance with the requirements of 10 CFR 72, Subpart G [1-1]. The QA program applies to the design, purchase, fabrication, handling, shipping, storing, cleaning, assembly, inspection, testing, operation, maintenance, repair, and modification of the NUHOMS® EOS System and components identified as “important to safety” and “safety-related.” These components and systems are defined in Chapter 2.

The complete description and specific commitments of the *TN* QA program are contained in the *TN* QA Program Description Manual [1-6]. This manual has been approved by the NRC for performing 10 CFR Part 72-related activities.

1.7 References

- 1-1 Title 10, Code of Federal Regulations, Part 72, “Licensing Requirements for the Independent Storage of Spent Nuclear Fuel, High-Level Radioactive Waste, and Reactor-Related Greater Than Class C Waste.”
- 1-2 NUREG-1536, “Standard Review Plan for Spent Fuel Dry Storage Systems at a General License Facility,” Revision 1, U.S. Nuclear Regulatory Commission, Office of Nuclear Material Safety and Safeguards, July 2010.
- 1-3 U.S. Nuclear Regulatory Commission, “Certificate of Compliance 72-1030, NUHOMS® HD Horizontal Modular Storage System for Irradiated Nuclear Fuel,” Amendment No. 2, October 14, 2014.
- 1-4 AREVA Transnuclear, Updated Final Safety Analysis Report, “NUHOMS® HD Horizontal Modular Storage System for Irradiated Nuclear Fuel,” Revision 4, U.S. Nuclear Regulatory Commission Docket No. 72-1030, September 2013.
- 1-5 Title 10, Code of Federal Regulations, Part 50, “Domestic Licensing of Production and Utilization Facilities.”
- 1-6 *TN Americas LLC*, “*TN Americas LLC* Quality Assurance Program Description Manual for 10 CFR Part 71, Subpart H and 10 CFR Part 72, Subpart G,” current revision.
- 1-7 CoC 1042 Appendix A, NUHOMS® EOS System Generic Technical Specifications, Amendment 0.

1.8 Supplemental Data

1.8.1 Generic Cask Arrays

The DSC containing the SFAs is transferred to, and stored in, an EOS-HSM in the horizontal position. Multiple EOS-HSMs are grouped together to form arrays whose size is determined to meet plant-specific needs. Arrays of EOS-HSMs are arranged within the ISFSI site on a concrete basemat(s) with the entire area enclosed by a security fence. Individual EOS-HSMs are arranged adjacent to each other. The decay heat for each EOS-HSM is primarily removed by internal natural circulation flow and conduction through the EOS-HSM walls. Figure 1-11, Figure 1-12 and Figure 1-13 show typical layouts for NUHOMS® EOS System ISFSIs, which are capable of modular expansion to any capacity. These are typical layouts only and do not represent limitations in number of modules, number of rows, and orientation of modules in rows. *A minimum of one empty module with an end wall is required at the end of an array to allow for future expansion until the array is complete. The end wall may be removed for expansion, provided compensatory shielding and limitations on personnel access to the area are employed. Alternatively, two empty modules with the side inlet vent of the outer module blocked may be used. In any expansion configuration, compensatory measures shall be considered for radiation shielding.* Back-to-back module configurations require expansion in sets of pairs. Expansion can be accomplished, as necessary, by the licensee provided the criteria of 10 CFR 72.104, 10 CFR 72.106 and Chapter 14 are met. The parameters of interest in planning the installation layout are the configuration of the EOS-HSM array and an area in front of each EOS-HSM to provide adequate space for backing and aligning the transfer trailer.

Table 1-1
Key Design Parameters of the NUHOMS® EOS System
Components
(2 Pages)

EOS-37PTH DSC	
Overall Length (in.)	219.12 (max for TC135)
	197.65 (max for TC125 and TC108)
Outside Diameter (in.)	75.50
Cavity Length (in.)	To fit fuel to be stored accounting for irradiation growth and differential thermal growth.
Shell Thickness (in.)	0.5
Design Weight of Loaded EOS-37PTH DSC (lbs.)	135,000 (max for TC135)
	124,000 (max for TC125 and TC108)
Materials of Construction	Stainless steel or duplex shell assembly and carbon steel internals, carbon steel shield plugs, aluminum
Neutron Absorbing Material	MMC as specified in Chapter 10
Internal Atmosphere	Helium
EOS-89BTH DSC	
Overall Length (in.)	197.65 (max. for TC125 and TC108)
Outside Diameter (in.)	75.50
Cavity Length (in.)	To fit fuel to be stored accounting for irradiation growth and differential thermal growth.
Shell Thickness (in.)	0.5
Design Weight of Loaded EOS-89BTH DSC (lbs.)	124,000 (max for TC125 and TC108)
Materials of Construction	Stainless steel or duplex shell assembly and carbon steel internals, carbon steel shield plugs, aluminum
Neutron Absorbing Material	BORAL™, MMC, as specified in Chapter 10
Internal Atmosphere	Helium

Table 1-1
Key Design Parameters of the NUHOMS® EOS System
Components
(2 Pages)

Horizontal Storage Module (EOS-HSM/EOS-HSMS):	
Overall length (without back shield wall)	19' EOS-Short
	20' 8" EOS-Medium
	22' 4" EOS-Long
Overall width (without end shield walls)	9'-8"
Overall height (without vent covers)	18' 6"
Total Weight not including DSC (lbs.)	311,000 EOS-Short
	334,000 EOS-Medium
	351,000 EOS-Long
Materials of Construction	Reinforced concrete and structural steel
Heat Removal	Conduction, convection, and radiation
OnSite Transfer Cask (EOS-TC)	
Overall Length (in)	206.76 EOS-TC108
	208.21 EOS-TC125
	228.71 EOS-TC135
Outside Diameter (in)	90.61 EOS-TC108 w/ NS tank
	88.50 EOS-TC108 w/o NS tank
	95.38 EOS-TC125
	95.38 EOS-TC125
Cavity Length (in)	199.17 EOS-TC108
	199.25 EOS-TC125
	219.75 EOS-TC135
Lead Thickness (in)	2.50 EOS-TC108
	3.56 EOS-TC125
	3.56 EOS-TC135
Gross Weight (with neutron shield and steel lid and no payload) (tons)	46.5 EOS-TC108
	62.1 EOS-TC125
	67.9 EOS-TC135
Materials of Construction	Carbon steel shell assemblies and closures with lead shielding, aluminum and carbon steel lids and aluminum neutron shield tank for the TC108
Internal Atmosphere	Air

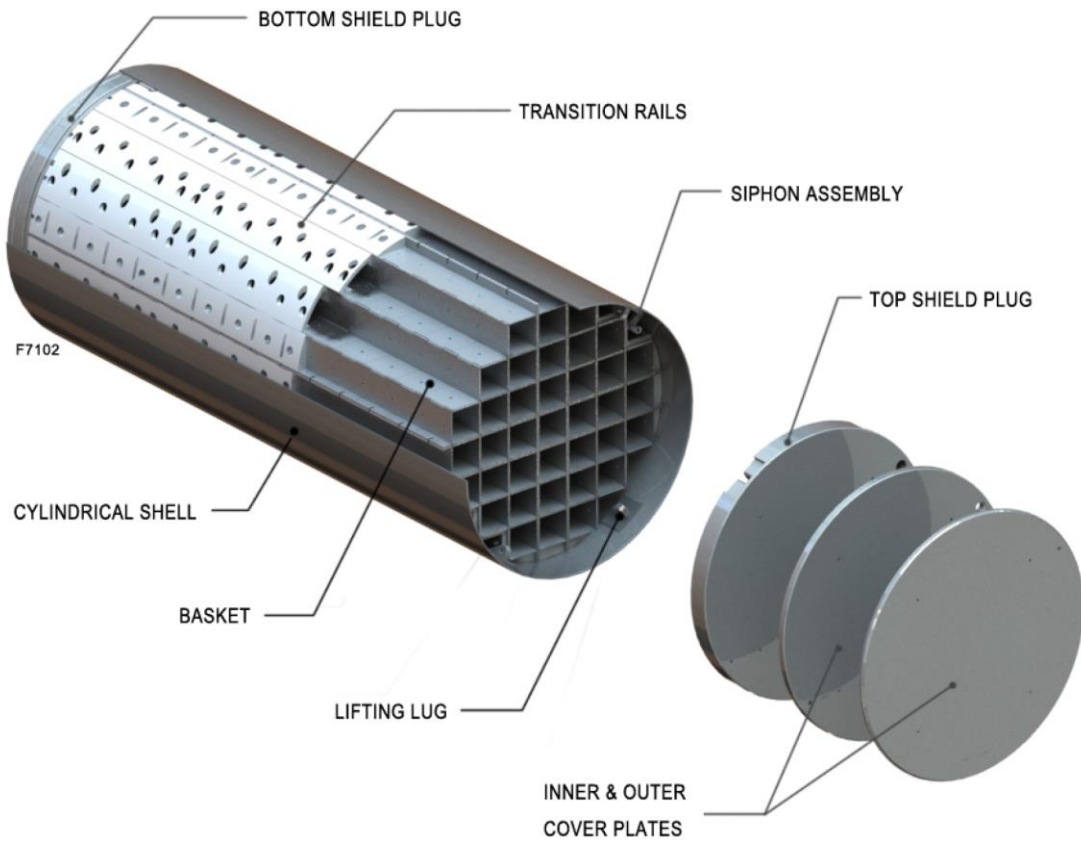


Figure 1-1
EOS-37PTH DSC

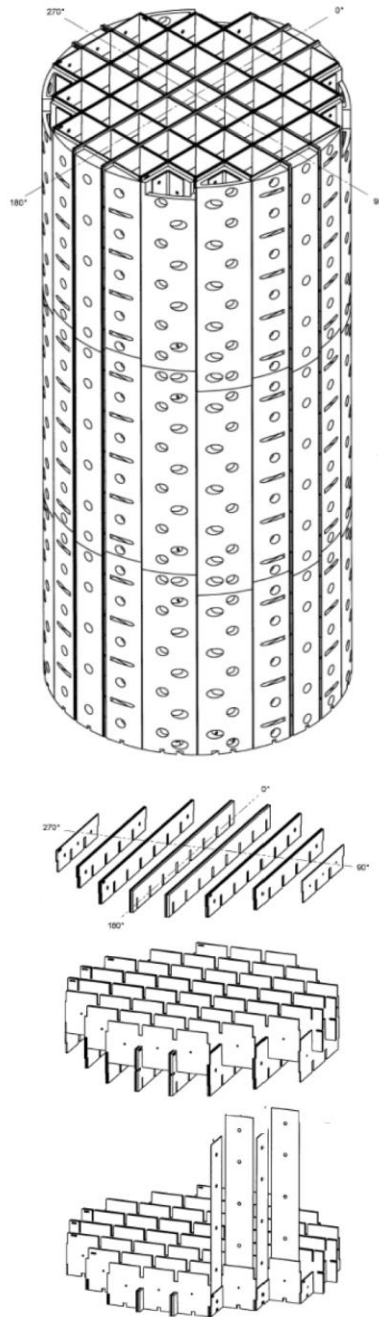


Figure 1-2
EOS-37PTH Basket

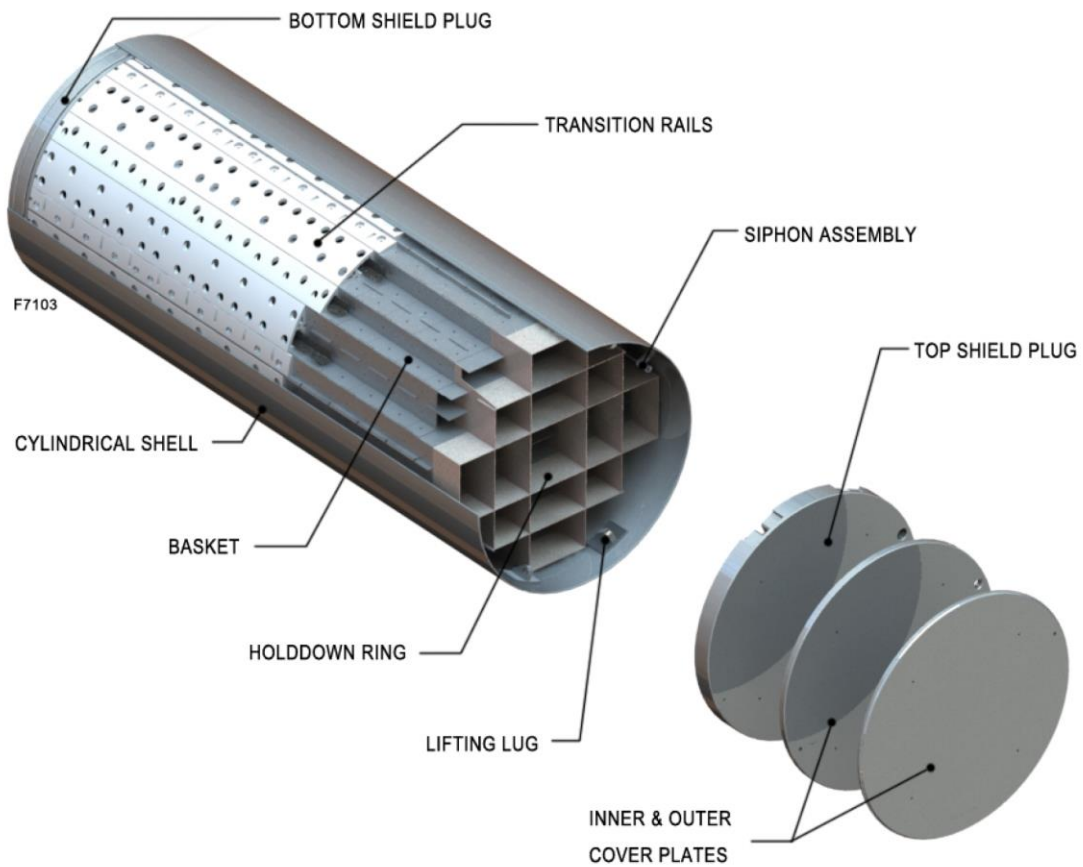


Figure 1-3
EOS-89BTH DSC

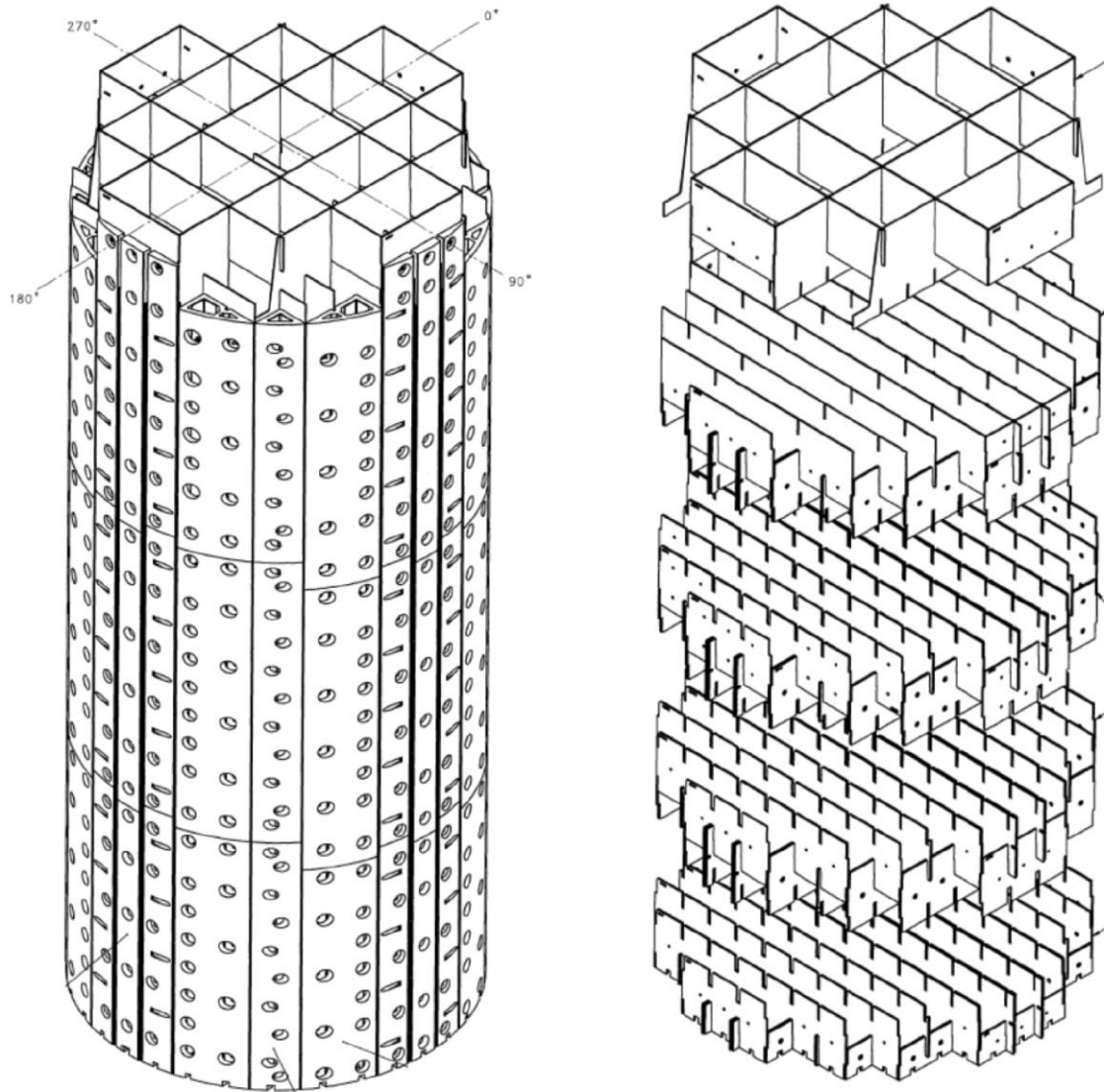
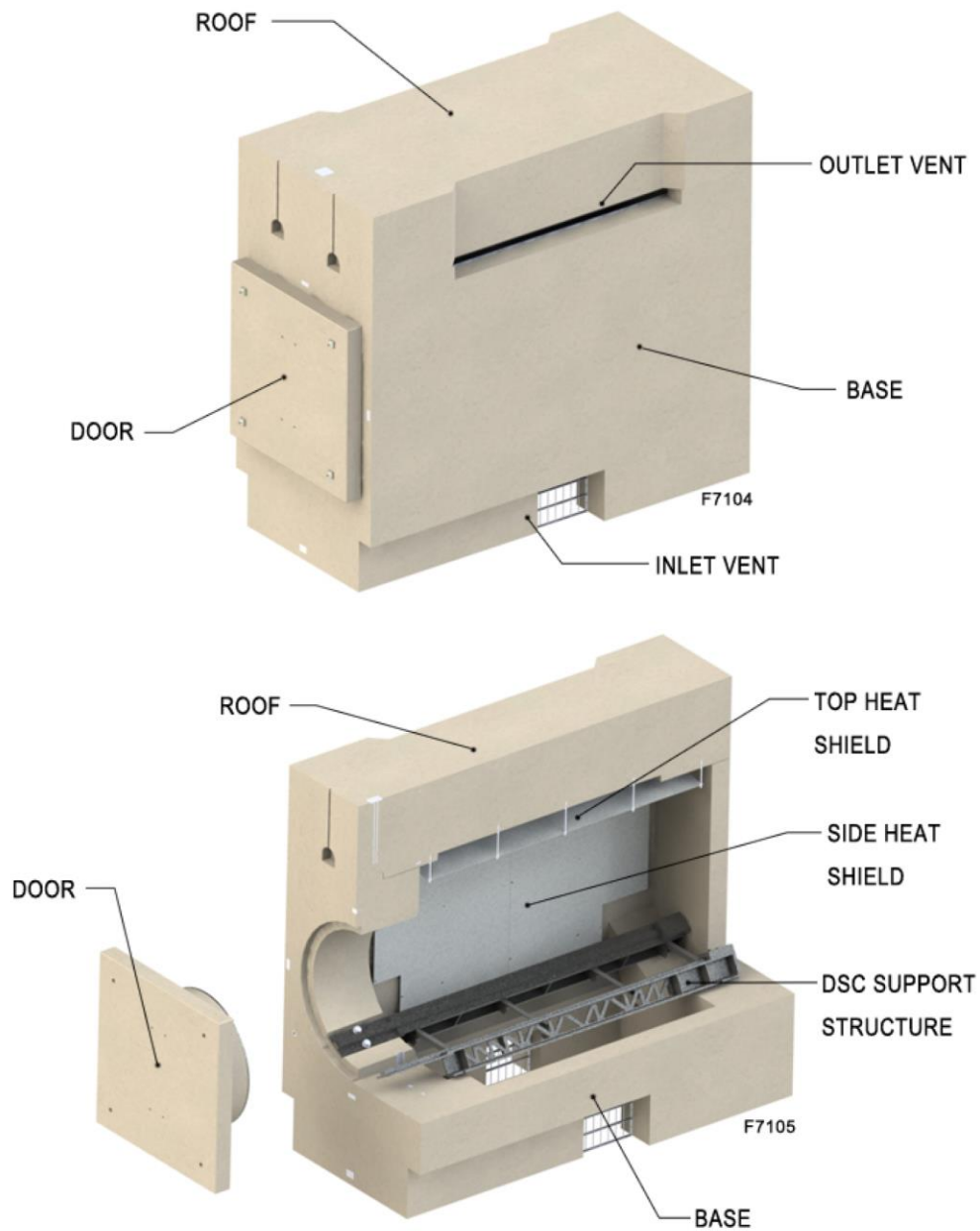


Figure 1-4
EOS-89BTH Basket



**Figure 1-5
EOS-HSM**

Note: Alternative HSM (EOS-HSM-FPS) and support structure (FPS DSC support structure) are not shown in this figure

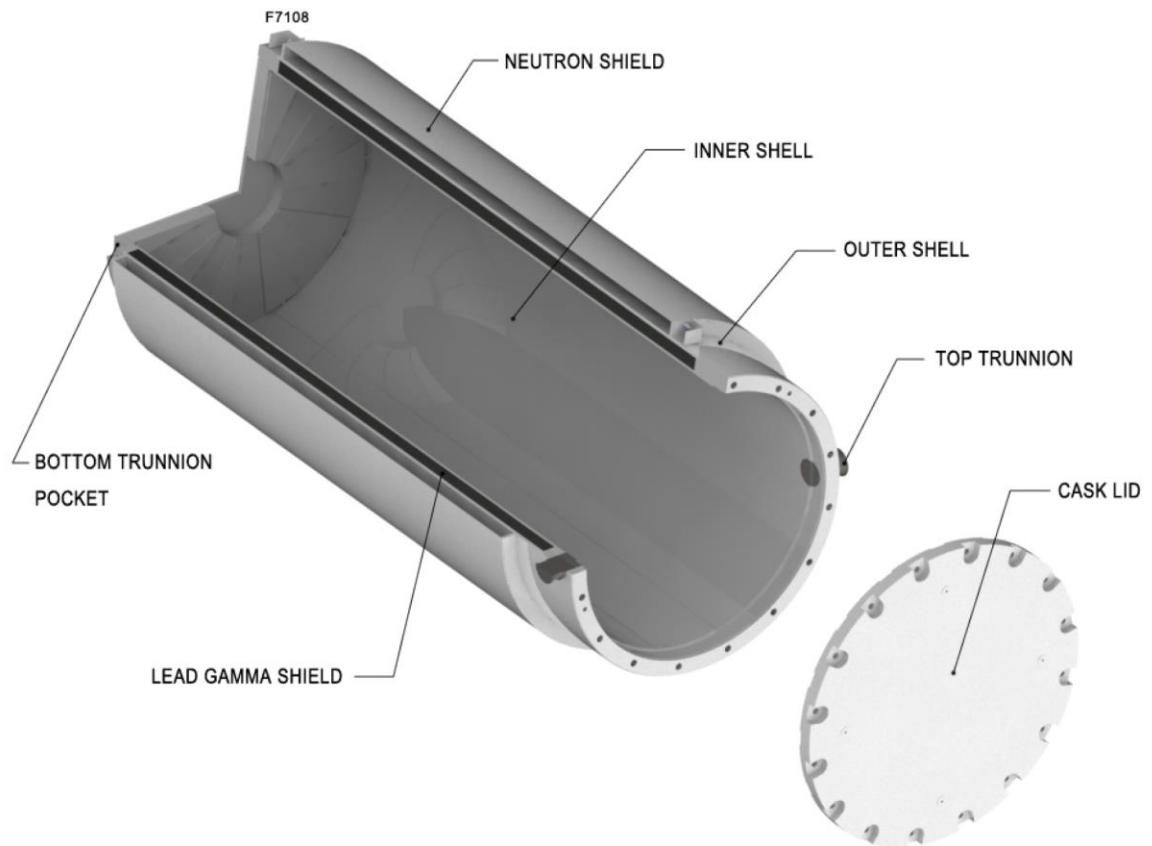


Figure 1-6
TC125/135 Transfer Cask

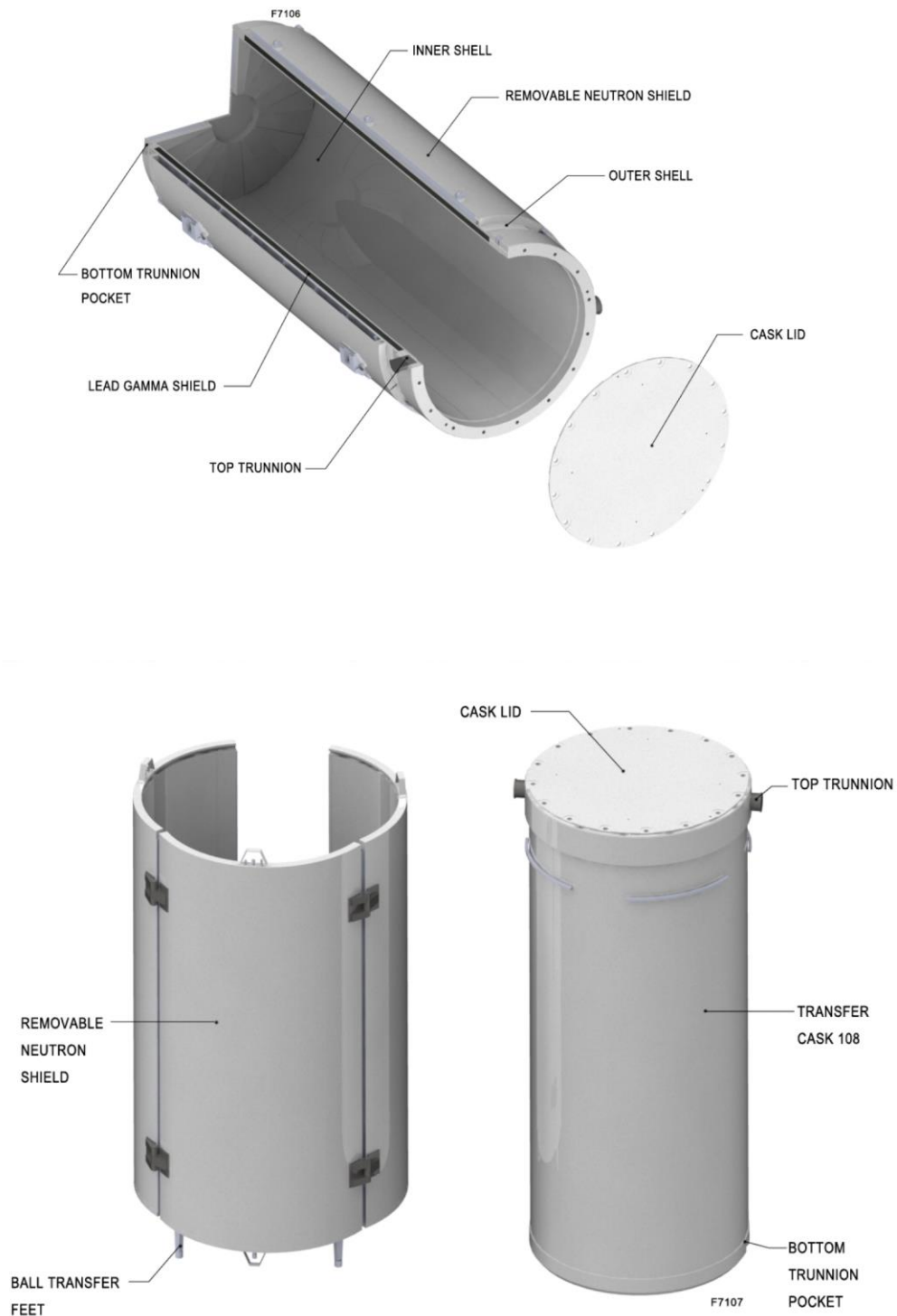


Figure 1-7
TC108 Transfer Cask

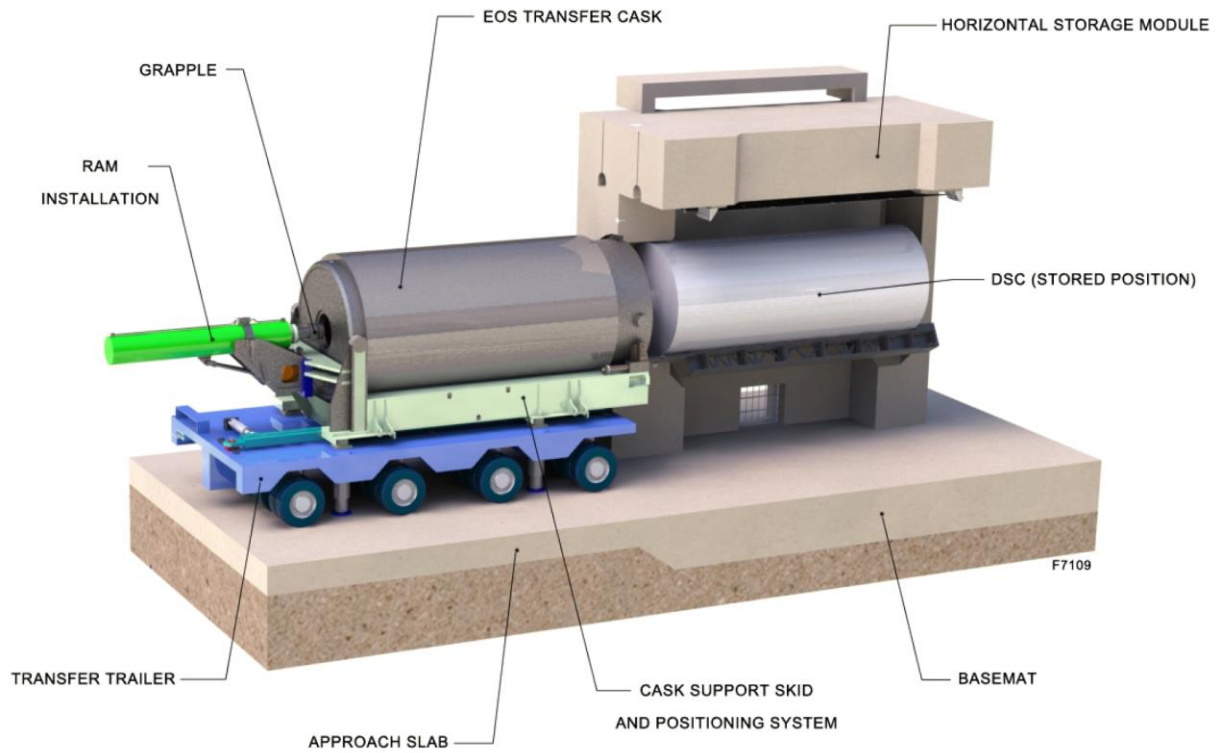


Figure 1-8
NUHOMS® EOS System Components, Structures, and
Transfer Equipment

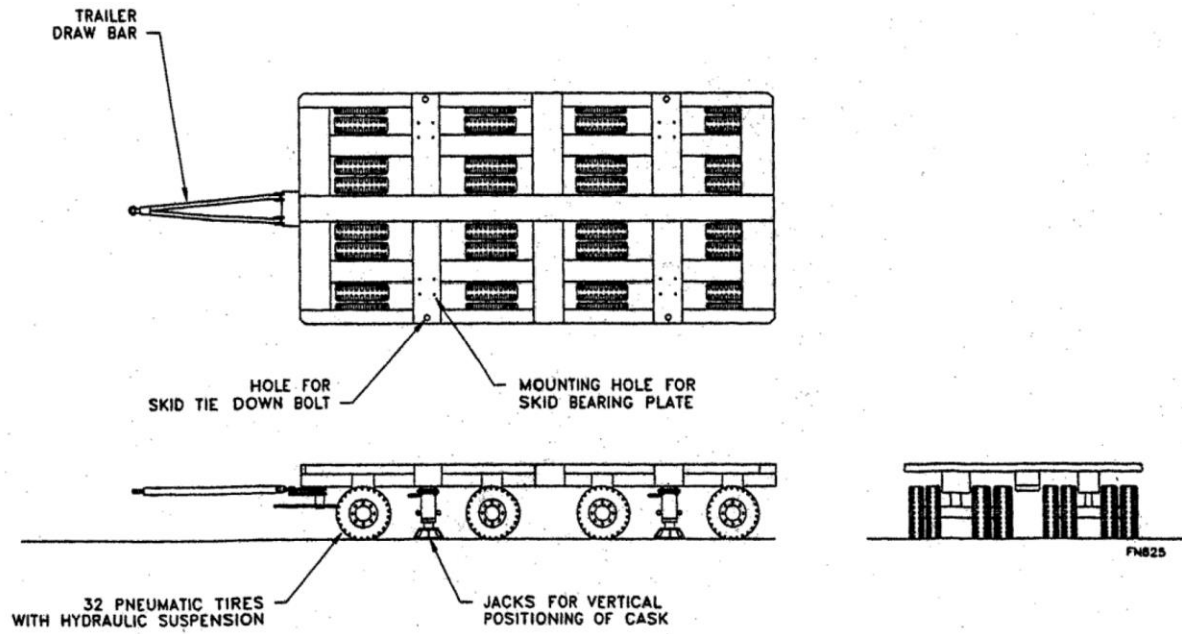


Figure 1-9
Typical Transfer Trailer

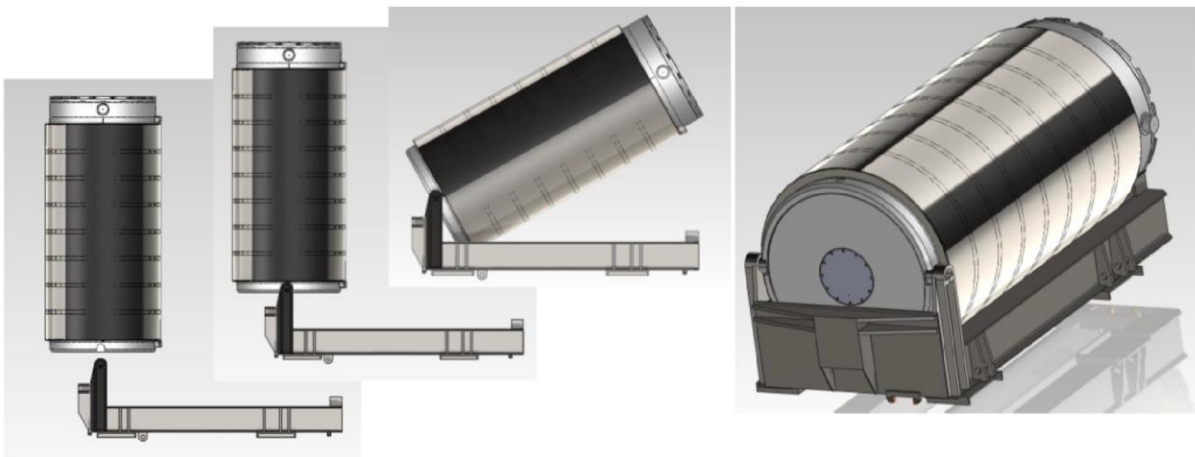
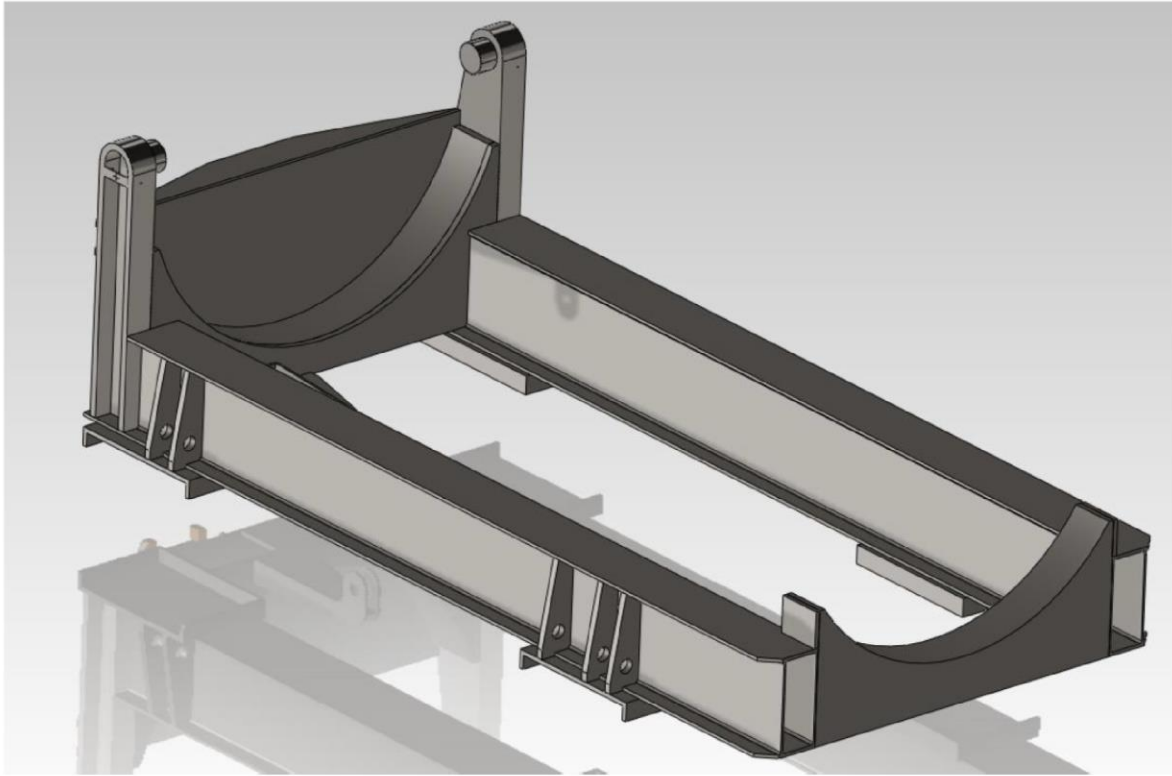
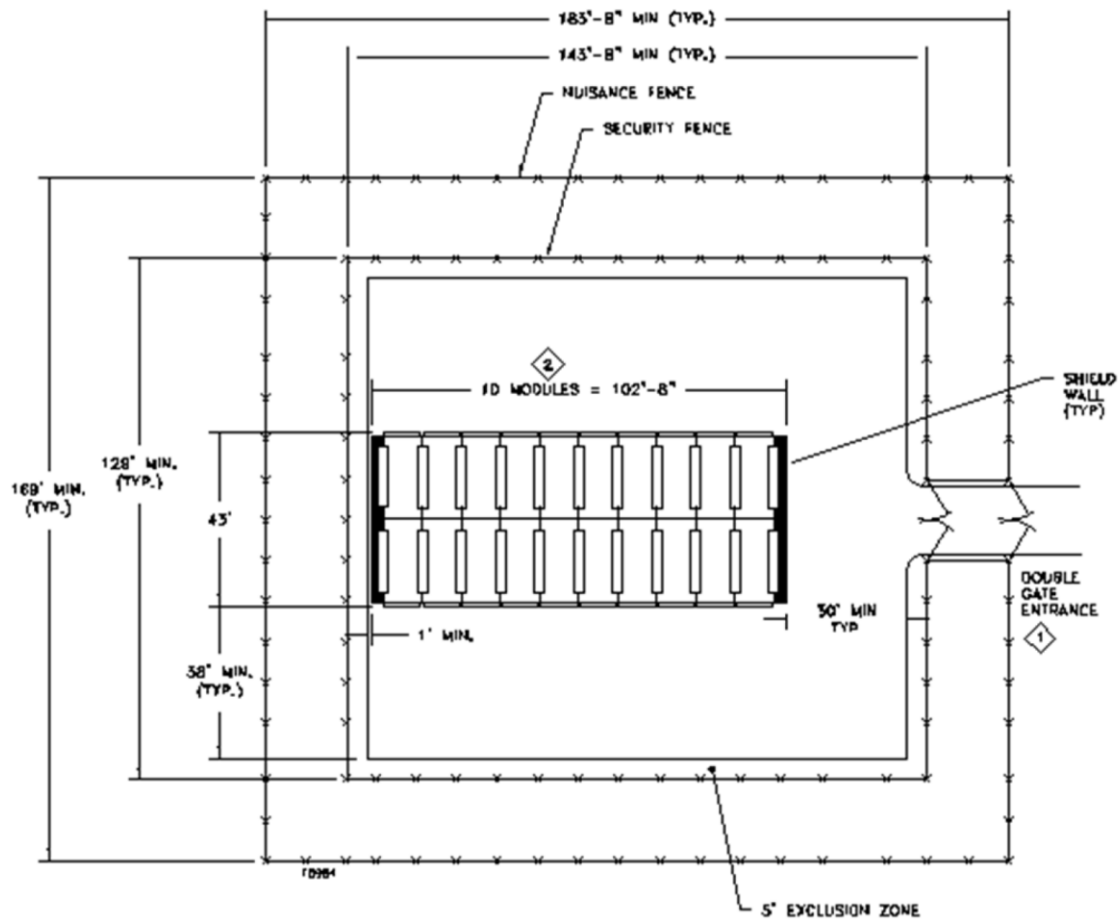
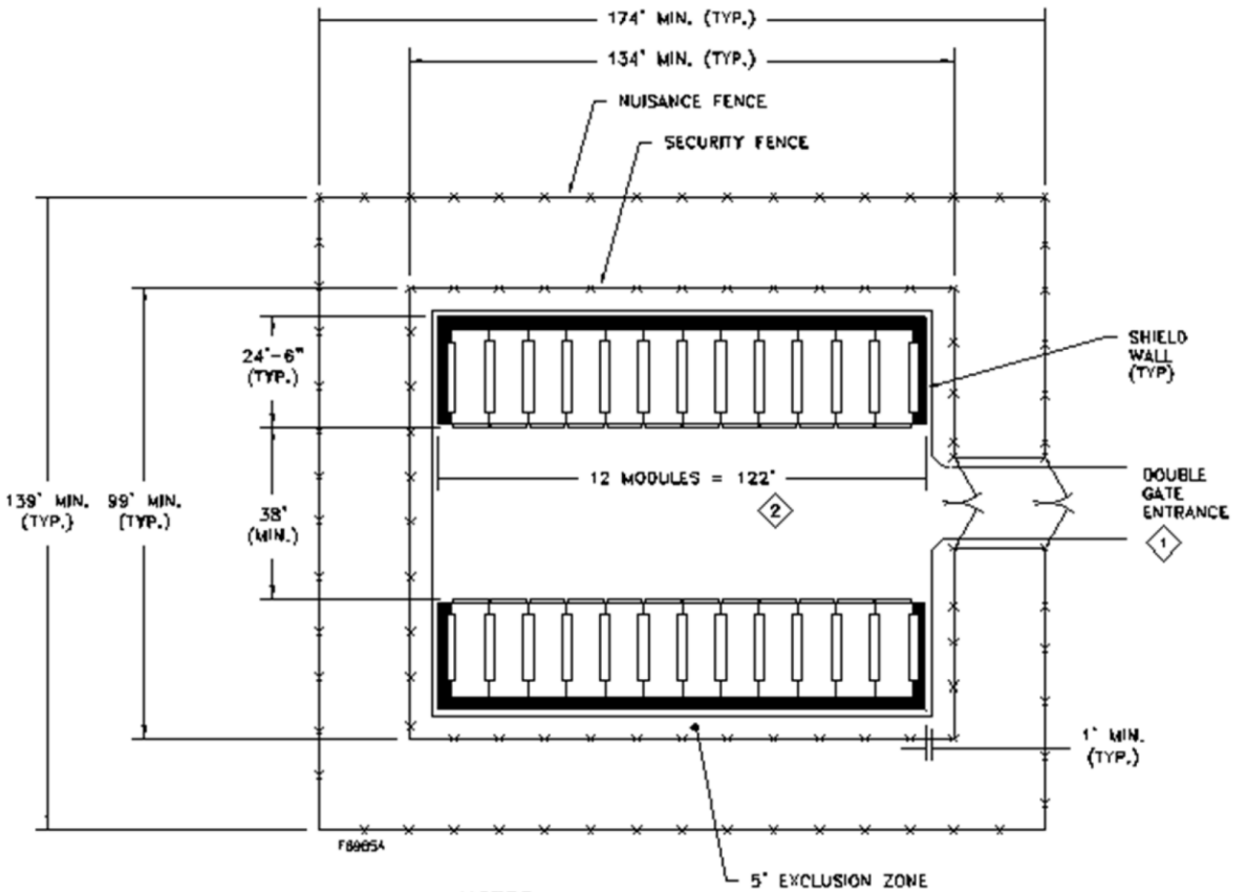


Figure 1-10
Typical Cask Support Skid

**NOTES:**

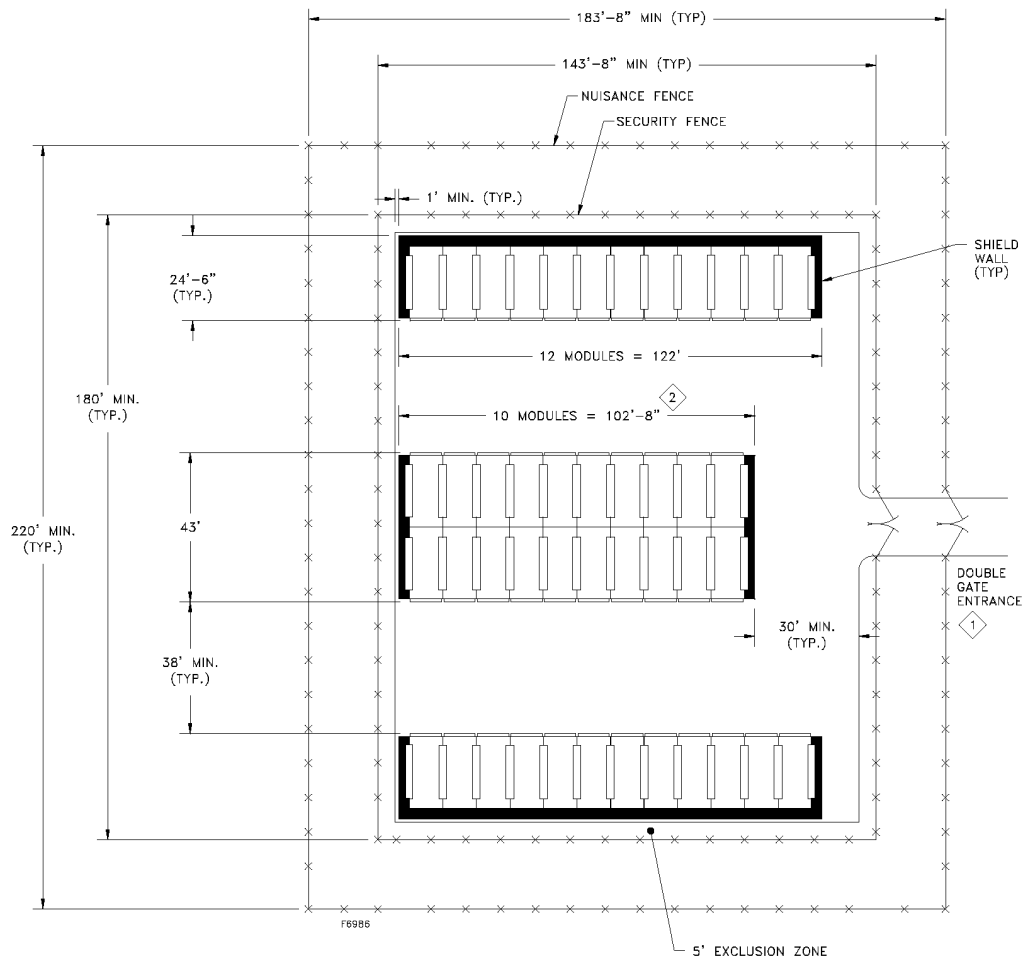
- 1 LOCATION OF ENTRANCE TO ISFSI TO BE COMPATIBLE WITH PLANT SITE ROADS.
- 2 NUMBER OF MODULES DETERMINED BY USER BASED ON PLANT DISCHARGE RATES AND DRY STORAGE NEEDS.
3. HSM ARRAYS CAN BE EXPANDED BY ADDING ADDITIONAL HSM UNITS. THIS CAN BE DONE WITH OR WITHOUT RELOCATING END SHIELD WALLS.

Figure 1-11
Typical Double Module Row ISFSI Layout with EOS-Medium Modules

**NOTES:**

- ① LOCATION OF ENTRANCE TO ISFSI TO BE COMPATIBLE WITH PLANT SITE ROADS.
- ② NUMBER OF MODULES DETERMINED BY USER BASED ON PLANT DISCHARGE RATES AND DRY STORAGE NEEDS.
3. HSM ARRAYS CAN BE EXPANDED BY ADDING ADDITIONAL HSM UNITS. THIS CAN BE DONE WITH OR WITHOUT RELOCATING END SHIELD WALLS.

Figure 1-12
Typical Single Module Row ISFSI Layout with EOS-Medium Modules



NOTES:

- ① LOCATION OF ENTRANCE TO ISFSI TO BE COMPATIBLE WITH PLANT SITE ROADS.
- ② NUMBER OF MODULES DETERMINED BY USER BASED ON PLANT DISCHARGE RATES AND DRY STORAGE NEEDS.
3. HSM ARRAYS CAN BE EXPANDED BY ADDING ADDITIONAL HSM UNITS. THIS CAN BE DONE WITH OR WITHOUT RELOCATING END SHIELD WALLS.

Figure 1-13
Typical Combined Single and Double Module Row ISFSI Layout with
EOS-Medium Modules

CHAPTER 2 PRINCIPAL DESIGN CRITERIA

Table of Contents

2.	PRINCIPAL DESIGN CRITERIA	2-1
2.1	SSCs Important to Safety	2-2
2.1.1	Dry Shielded Canisters	2-2
2.1.2	Horizontal Storage Module (EOS-HSM/EOS-HSMS).....	2-2
2.1.3	ISFSI Basemat and Approach Slabs	2-3
2.1.4	Transfer Equipment	2-3
2.1.5	Auxiliary Equipment.....	2-4
2.2	Spent Fuel to Be Stored	2-5
2.2.1	EOS-37PTH DSC	2-6
2.2.2	EOS-89BTH DSC	2-7
2.3	Design Criteria for Environmental Conditions and Natural Phenomena.....	2-8
2.3.1	Tornado Wind and Tornado Missiles for EOS-HSM	2-8
2.3.2	Tornado Wind and Tornado Missiles for EOS-TC.....	2-10
2.3.3	Water Level (Flood) Design	2-11
2.3.4	Seismic Design.....	2-11
2.3.5	Snow and Ice Loading	2-12
2.3.6	Tsunami.....	2-12
2.3.7	Lightning.....	2-12
2.4	Safety Protection Systems	2-13
2.4.1	General	2-13
2.4.2	Structural.....	2-15
2.4.3	Thermal	2-16
2.4.4	Shielding/Confinement/Radiation Protection	2-16
2.4.5	Criticality	2-17
2.4.6	Material Selection	2-18
2.4.7	Operating Procedures.....	2-19
2.4.8	Acceptance Tests and Maintenance	2-19
2.4.9	Decommissioning	2-19

2.5	References	2-20
------------	-------------------------	-------------

List of Tables

Table 2-1	NUHOMS® EOS System Major Components and Safety Classification.....	2-22
Table 2-2	PWR Fuel Assembly Design Characteristics.....	2-23
Table 2-3	BWR Fuel Assembly Design Characteristics	2-26
Table 2-4	Additional PWR and BWR Fuel Assembly Design Characteristics.....	2-30
Table 2-5	EOS-37PTH/EOS-89BTH DSC Shell Assembly Loads and Load Combinations	2-32
Table 2-6	EOS-37PTH/EOS-89BTH DSC Basket Assembly Load Combinations.....	2-34
Table 2-7	EOS-HSM Design Criteria	2-35
Table 2-8	EOS-TC Load Combinations and Service Levels	2-36
Table 2-9	Thermal Conditions for NUHOMS® EOS System Analyses	2-37

List of Figures

Figure 2-1	RG 1.60 Response Spectra with Enhancement in Frequencies above 9.0 Hz.....	2-38
------------	---	------

2. PRINCIPAL DESIGN CRITERIA

This section provides the principal design criteria for the NUHOMS® EOS System described in Chapter 1. Section 2.1 identifies the structures, systems, and components (SSCs) important-to-safety (ITS) for the NUHOMS® EOS System design. Section 2.2 presents a general description of the spent fuel to be stored. Section 2.3 provides the design criteria for environmental conditions and natural phenomena. Section 2.4 discusses safety protection systems.

2.1 SSCs Important to Safety

Table 2-1 provides a list of major NUHOMS® EOS System independent spent fuel storage installation (ISFSI) components and their classification. Table 2-1 identifies all SSCs that are ITS. Components are classified in accordance with the criteria of 10 CFR Part 72. Structures, systems, and components classified as ITS are defined in 10 CFR 72.3 as the features of the ISFSI whose function is:

- To maintain the conditions required to store spent fuel safely.
- To prevent damage to the spent fuel container during handling and storage.
- To provide reasonable assurance that spent fuel can be received, handled, packaged, stored, and retrieved without undue risk to the health and safety of the public.

These criteria are applied to the NUHOMS® EOS System components in determining their classification in the paragraphs that follow.

2.1.1 Dry Shielded Canisters

The EOS-37PTH dry shielded canister (DSC) and EOS-89BTH DSC provide the fuel assembly (FA) support required to maintain the fuel geometry for criticality control. Accidental criticality inside a DSC could lead to offsite doses comparable with the limits in 10 CFR Part 100 [2-1], which must be prevented. The DSCs also provide the confinement boundary for radioactive materials. Therefore, the DSCs are designed to maintain structural integrity under all accident conditions identified in Chapters 12 without losing its function to provide confinement of the spent fuel assemblies (SFAs). The DSCs are designed, constructed, and tested in accordance with a quality assurance (QA) program incorporating a graded quality approach for ITS requirements as defined by 10 CFR Part 72, Subpart G, paragraph 72.140(b) and described in Chapter 14.

2.1.2 Horizontal Storage Module (EOS-HSM/EOS-HSMS)

The EOS horizontal storage module (HSM) and EOS-HSMS are essentially identical except the EOS-HSMS base is split into two parts. EOS-HSM is used herein for both the EOS-HSM and EOS-HSMS. The EOS-HSMs are considered ITS since these provide physical protection and shielding for the DSC during storage. The reinforced concrete HSM is designed in accordance with American Concrete Institute (ACI) 349-06 [2-3] and constructed to ACI-318-08 [2-4]. The level of testing, inspection, and documentation provided during construction and maintenance is in accordance with the quality assurance requirements as defined in 10 CFR Part 72, Subpart G and as described in Chapter 14. Thermal instrumentation for monitoring EOS-HSM concrete temperatures is considered “not important-to-safety” (NITS).

2.1.3 ISFSI Basemat and Approach Slabs

The ISFSI basemat and approach slabs and buildings for indoor storage are considered NITS and are designed, constructed, maintained, and tested as commercial-grade items.

Licensees are required to perform an assessment to confirm that the license seismic criteria described in Section 2.3.4 are met.

2.1.4 Transfer Equipment

2.1.4.1 Transfer Cask and Yoke

The transfer casks (EOS-TCs) are ITS since they protect the DSC during handling and are part of the primary load path used while handling the DSCs in the fuel/reactor building. An accidental drop of a loaded transfer cask (TC) (weighing up to 135 tons) has the potential for creating conditions in the plant that must be evaluated. These possible drop conditions are evaluated with respect to the impact on the DSC in Chapters 3 and 12. Therefore, the EOS-TCs are designed, constructed, and tested in accordance with a QA program incorporating a graded quality approach for ITS requirements as defined by 10 CFR Part 72, Subpart G, paragraph 72.140(b) and described in Chapter 14.

A lifting yoke is used for handling the TC within the fuel/reactor building and it is used by the licensee (utility) under their 10 CFR Part 50 [2-5] program requirements.

Due to site-unique requirements, rigid or sling lifting members can be used to augment the lifting yoke. These members shall be designed, fabricated and tested in accordance with the same requirements as the cask lifting yoke.

2.1.4.2 Other Transfer Equipment

The NUHOMS® EOS System transfer equipment (i.e., ram, skid, transfer trailer) are necessary for the successful loading of the DSCs into the EOS-HSM. However, these items are not required to provide reasonable assurance that spent fuel can be received, handled, packaged, stored, and retrieved without undue risk to the health and safety of the public. Therefore, these components are considered NITS and need not comply with the requirements of 10 CFR Part 72. These components are designed, constructed, and tested in accordance with good industry practices.

2.1.5 Auxiliary Equipment

The vacuum drying system and the automated welding system are NITS. Performance of these items is not required to provide reasonable assurance that spent fuel can be received, handled, packaged, stored, and retrieved without undue risk to the health and safety of the public. Failure of any part of these systems may result in a delay of operations, but will not result in a hazard to the public or operating personnel. These components are designed, constructed, and tested in accordance with good industry practices.

2.2 Spent Fuel to Be Stored

The NUHOMS® EOS System is designed to accommodate pressurized water reactor (PWR) (14x14, 15x15, 16x16 and 17x17 array designs) and boiling water reactor (BWR) (7x7, 8x8, 9x9 and 10x10 array designs) fuel types and reload assemblies that are available for storage. As described in Chapter 1, there are two DSC designs for the NUHOMS® EOS System: the EOS-37PTH DSC for PWR fuel and EOS-89BTH DSC for BWR fuel. The EOS-37PTH DSC is designed to accommodate up to 37 intact PWR FAs with uranium dioxide (UO₂) fuel, zirconium-alloy cladding, and with or without control components. The EOS-89BTH DSC is designed to accommodate up to 89 intact BWR FAs with UO₂ fuel, zirconium-alloy cladding, and with or without fuel channels.

The cavity length of the DSC is determined for a specific site to match the FA length used at that site, including control components (CCs), as applicable. Both DSCs store intact, including reconstituted and blended low enriched uranium (BLEU), FAs as specified in Table 2-2, Table 2-3 and Table 2-4. Any FA that has fuel characteristics within the range of Table 2-2, Table 2-3 and Table 2-4 and meets the other limits specified for initial enrichment, burnup and heat loads is acceptable for storage in the NUHOMS® EOS System.

The maximum allowable assembly average burnup is limited to 62 GWd/MTU and the minimum cooling time is three years. Dummy FAs, reconstituted FAs are also included in the EOS-37PTH DSC and EOS-89BTH DSC payloads. Reconstituted assemblies containing up to five replacement irradiated stainless steel rods per assembly or an unlimited number of low enriched or natural uranium fuel rods or non-fuel rods are acceptable for storage in an EOS-37PTH DSC and EOS-89BTH DSC as intact FAs.

Fuel assemblies that contain fixed integral non-fuel rods are also considered as intact FAs. These FAs are different than reconstituted assemblies because fuel rods are not “replaced” by non-fuel rods, rather the non-fuel rods are part of the initial fuel design. The non-fuel rods displace the same amount of moderator, with zirconium-alloy (or aluminum) cladding and typically contain burnable absorber (or other non-fuel) material. The radiation and thermal source terms for the non-fuel rods are significantly lower than those of the fuel rods since there is no significant radioactive decay source. The internal pressure of the non-fuel rods after irradiation is lower than those of the fuel rods since there is no fission gas generation. The reactivity of the fuel rods (from a criticality standpoint) is significantly higher than that of non-fuel rods. In summary, the mechanical, thermal, shielding, and criticality evaluations for these rods are bounded by those of the regular fuel rods. Therefore, no further evaluations are required for the qualification of these FAs.

For FAs with up to five irradiated stainless steel rods the minimum cooling time is 15 years or the cooling time to meet the decay heat limit for the location it is to be stored in the DSC basket, whichever is longer. The stainless steel rods are assumed to have two-thirds the irradiation time as the remaining fuel rods of the assembly. The reconstituted UO_2 rods are assumed to have the same irradiation history as the entire FA. The reconstituted rods can be at any location in the FAs.

There is no limit on the number of reconstituted FAs per DSC. For BLEU fuel the Co-60 activity in the BLEU fuel must be limited to the values shown in Tables 2 and 7 of the Technical Specifications [2-18]. The EOS-37PTH DSC may contain less than 37 FAs and the EOS-89BTH DSC may contain less than 89 FAs. In both DSCs, the basket slots not loaded with FAs shall be loaded with dummy FAs. The dummy FAs approximate the weight and center of gravity of an FA.

Following loading, each DSC is evacuated and then backfilled with an inert gas, helium, to preclude detrimental chemical reaction between the fuel and the DSC interior atmosphere during storage. Multilayer, double seal welds at each end of the DSC and multi-layer circumferential and longitudinal DSC shell welds ensure retention of the helium atmosphere for the full storage period.

2.2.1 EOS-37PTH DSC

The EOS-37PTH DSC stores up to 37 intact PWR FAs with characteristics as described in Table 2-2 and the PWR FAs listed in Table 2-4. One or more PWR fuel designs are grouped under a “PWR class”. EOS-37PTH DSC payloads may also contain Control Components (CCs), such as identified below, with thermal and radiological characteristics as listed in Table 3 and Figure 1 of the Technical Specifications [2-18]:

- Control spiders,
- Burnable poison rod assemblies (BPRAs),
- Neutron source assemblies (NSAs),
- Thimble plug assemblies (TPAs),
- Control rod assemblies (CRAs),
- Axial power shaping rod assemblies (APSRAs),
- Orifice rod assemblies (ORAs),
- Integral fuel burnable absorber assemblies (IFBAs),
- Peripheral power suppression assemblies (PPSAs),
- Rod cluster control assemblies (RCCAs),
- Wet annular burnable absorbers (WABAs),
- Vibration suppression inserts (VSIs),
- Neutron sources and,

- Control element assemblies (CEAs)

Furthermore, non-fuel hardware that is positioned within the fuel assembly after the fuel assembly is discharged from the core such as guide tube or instrument tube tie rods or anchors, guide tube inserts, BPRA spacer plates or devices that are positioned and operated within the FA during reactor operation such as those listed above are also considered as CCs.

Figure 1 of the Technical Specifications [2-18] defines the maximum decay heat and other parameters for PWR fuel assemblies, with or without CCs, authorized for storage. These tables are used to ensure that the decay heat load of the FA to be stored is less than that as specified in each table, and that the corresponding radiation source term is consistent with the shielding analysis presented in Chapter 6. The maximum weight of a FA plus CC, if applicable, is 1,900 lbs.

Calculations were performed to determine the FA type that was most limiting for each of the analyses including shielding, criticality, thermal and confinement. These evaluations are performed in Chapter 6, 7, 4 and 5, respectively.

2.2.2 EOS-89BTH DSC

The EOS-89BTH DSC design accommodates up to 89 intact BWR FAs with characteristics as described in Table 2-3, and the BWR FAs listed in Table 2-4. One or more BWR FA designs are grouped under a “BWR Fuel ID”. The EOS-89BTH accommodates:

- Fuel assemblies with and without channels,
- Fuel assemblies with and without channel fasteners.

Figure 2 of the Technical Specifications [2-18] define the maximum decay heat and other parameters for BWR fuel assemblies authorized for storage. These tables are used to ensure that the decay heat load of the fuel assembly to be stored is less than that as specified in each table, and that the corresponding radiation source term is consistent with the shielding analysis presented in Chapter 6. The maximum weight of an FA plus channel, if applicable, is 705 lbs.

Calculations were performed to determine the FA type that was most limiting for each of the analyses including shielding, criticality, thermal and confinement. These evaluations are performed in Chapter 6, 7, 4 and 5, respectively.

2.3 Design Criteria for Environmental Conditions and Natural Phenomena

The NUHOMS® EOS System ITS SSCs described in Section 2.1 are designed consistent with the 10 CFR Part 72 [2-6] §122(b) requirement for protection against environmental conditions and natural phenomena. The criterion used in the design of the NUHOMS® EOS System ensures that exposure to credible site hazards does not impair their safety functions.

2.3.1 Tornado Wind and Tornado Missiles for EOS-HSM

The EOS-HSM is designed to safely withstand 10 CFR 72.122 (b)(2) tornado missiles. The tornado characteristics as specified in NRC Regulatory Guide 1.76, Revision 1 [2-8] are the design bases for the EOS-HSM. The missiles spectrum of NUREG-0800, Revision 3, Section 3.5.1.4 [2-10] with missile velocity for Region I is the design basis for the EOS-HSM.

Extreme wind effects are much less severe than the specified design basis tornado (DBT) wind forces. The design basis extreme wind for the EOS-HSM is calculated per [2-12].

2.3.1.1 Tornado Wind Design Parameters

The design basis tornado wind intensities for the EOS-HSM design are obtained from NRC Regulatory Guide 1.76, Revision 1 [2-8]. Region I intensities are utilized since they result in the most severe loading parameters. For this region, the maximum wind speed is 230 mph, the rotational speed is 184 mph and the maximum translational speed is 46 mph. The radius of the maximum rotational speed is 150 feet, the pressure drop across the tornado is 1.2 psi and the rate of pressure drop is 0.5 psi per second. The structural evaluations may be performed using more bounding tornado wind parameters.

2.3.1.2 Determination of Forces on Structures

Tornado loads result from three separate loading phenomena and these loading effects are combined in accordance with Section 3.3.2 of NUREG-0800, Revision 3 [2-10]:

- Pressure or suction forces created by drag as air impinges on and flows past the EOS-HSM. These pressure or suction forces are due to tornado-generated wind with maximum wind speed of 230 mph.
- Pressure or suction forces created by tornado generated pressure drop or differential pressure load of 1.2 psi.
- Impact forces created by tornado-generated missiles striking the EOS-HSM.

The determination of the DBT velocity pressure is in accordance with the requirements of American Society of Civil Engineers (ASCE) 7-10 [2-12]. The resistance to overturning and sliding of the EOS-HSM under these design pressures is determined considering the bounding condition of a single EOS-HSM with end shield walls.

2.3.1.3 Tornado Missiles

The design basis tornado missiles specified in NRC Regulatory Guide 1.76, Revision 1 [2-8] are used to evaluate the EOS-HSM. As specified in NUREG-0800, Revision 3, Section 3.5.1.4 [2-10], the postulated missiles include at least:

- A massive high-kinetic-energy missile that deforms on impact.
- A rigid missile to test penetration resistance.
- A small rigid missile of a size sufficient to just pass through any openings in protective barriers.

The DBT missiles for the EOS-HSM are listed below:

Missile Type	Schedule 40 Pipe	Automobile	Solid Steel Sphere
Dimensions	6.625 in. dia x 15 ft long	16.4 ft x 6.6 ft x 4.3 ft	1 in. dia
Mass	287 lb	4000 lb	0.147 lb
$C_D A/m$	0.0212 ft ² /lb	0.0343 ft ² /lb	0.0166 ft ² /lb
V_{Mh}^{max}	135 ft/s	135 ft/s	26 ft/s

Evaluation for the effects of small diameter solid spherical missiles is not required because there are no openings in the EOS-HSM leading directly to the DSC through which such missiles could pass. Barrier design should be evaluated assuming a normal impact to the surface for the Schedule 40 pipe and automobile missiles. The automobile missile is considered to impact at all altitudes less than 30 feet above grade level. While the design basis missiles are described above, the structural evaluations may be performed using more bounding missiles and additional missiles.

In determining the overall effects of a DBT missile impact, overturning, and sliding of the EOS-HSM, the force due to the missile impact is applied to the structure at the most adverse location. For hand calculations, conservation of momentum is used to demonstrate that sliding and/or tipping of a single module does not result in an unstable condition for the module. The coefficient of restitution is conservatively assumed as zero so that 100% of the missile energy is transferred to the EOS-HSM. The missile energy transferred to the EOS-HSM dissipates by sliding friction and/or an increase in potential energy by raising the EOS-HSM center of gravity. The calculations assume the missile impact force as evenly distributed over the impact area, and use a 0.6 coefficient of friction for concrete on concrete surfaces.

For localized damage of the EOS-HSM resulting from DBT missile impact, the four postulated missiles are used in the evaluation of concrete penetration, scabbing, and perforation thickness. The modified National Defense Research Committee (NDRC) empirical formula is used for this evaluation as recommended in NUREG-0800, Section 3.5.3, Revision 3 [2-11].

2.3.2 Tornado Wind and Tornado Missiles for EOS-TC

The EOS-TC is evaluated for the tornado characteristics as specified in NRC Regulatory Guide 1.76, Revision 1 [2-8] and the missiles spectrum of NUREG-0800, Revision 3, Section 3.5.1.4 [2-10] with missile velocity for Region I. The evaluation is performed for an EOS-TC secured horizontally to the cask support skid/transport trailer. Both overall stability and maximum cask stresses are evaluated.

2.3.2.1 Tornado Wind Design Parameters

The DBT wind intensities used for the EOS-TC designs are obtained from NRC Regulatory Guide 1.76, Revision 1 [2-8]. Region I intensities are utilized since they result in the most severe loading parameters. For this region, the maximum wind speed is 230 mph, the rotational speed is 184 mph and the maximum translational speed is 46 mph. The radius of the maximum rotational speed is 150 feet, the pressure drop across the tornado is 1.2 psi and the rate of pressure drop is 0.5 psi per second.

2.3.2.2 Tornado Missiles

The tornado missiles specified in NRC Regulatory Guide 1.76, Revision 1 [2-8] are used to evaluate the EOS-TC. As specified in NUREG-0800, Revision 3, Section 3.5.1.4 [2-10], the postulated missiles include at least (1) a massive high-kinetic-energy missile that deforms on impact, (2) a rigid missile to test penetration resistance, and (3) a small rigid missile of a size sufficient to just pass through any openings in protective barriers. The DBT missiles used in the evaluation of EOS-TC are listed below:

Missile Type	Schedule 40 Pipe	Automobile	Solid Steel Sphere
Dimensions	6.625 in. dia x 15 ft long	16.4 ft x 6.6 ft x 4.3 ft	1 in. dia
Mass	287 lb	4000 lb	0.147 lb
$C_D A/m$	0.0212 ft ² /lb	0.0343 ft ² /lb	0.0166 ft ² /lb
V_{Mh}^{max}	135 ft/s	135 ft/s	26 ft/s

Barrier design should be evaluated assuming a normal impact to the surface for the Schedule 40 pipe and automobile missiles. The automobile missile is considered to impact at all altitudes less than 30 feet above grade level.

2.3.3 Water Level (Flood) Design

EOS-HSM inlet vents are blocked when the depth of flooding is greater than 0.76 m (2 ft-6 in.) above the level of the ISFSI basemat. The DSC is wetted when flooding exceeds a depth of 1.7 m (5 ft-8 in.) above ISFSI basemat. Greater flood heights result in submersion of the DSC and blockage of the EOS-HSM outlet vents.

The DSC and EOS-HSM are conservatively designed for an enveloping design basis flood. The flood is postulated to result from natural phenomena such as tsunamis and seiches as specified by 10 CFR 72.122(b) [2-6]. A bounding assumption of a 15-meter (50-foot) flood height and water velocity of 4.6 m/sec (15 fps) is used for the flood evaluation. The EOS-HSM is evaluated for the effects of the 4.6 m/sec (15 fps) water current impinging upon the side of the submerged EOS-HSM. The DSC is subjected to an external pressure equivalent to a 15-meter (50-foot) head of water. These evaluations are presented in Chapter 3 and Section 12.3.5. The effects of water reflection on DSC criticality safety are addressed in Chapter 7. Due to its short term infrequent use, the onsite EOS-TC is not explicitly evaluated for flood effects. ISFSI procedures should ensure that the EOS-TC is not used for DSC transfer during flood conditions.

The plant-specific design basis flood (if the possibility for flooding exists at a particular ISFSI site) should be evaluated by the licensee and shown to be enveloped by the flooding conditions used for this generic evaluation of the NUHOMS® EOS System.

2.3.4 Seismic Design

The seismic design criteria for the EOS-HSM are based on the NRC Regulatory Guide 1.60 [2-13] response spectra anchored at a zero period acceleration (ZPA) of 0.45g in the horizontal direction and 0.30g in the vertical direction and enhanced frequency content above 9 Hz. The horizontal and vertical components of the design response spectra correspond to a maximum horizontal ground acceleration of 1.0g are shown in Figure 2-1. The seismic structural evaluations consider both stability evaluation and stress qualification of the EOS-HSM. The structural stress qualifications of the HSM concrete and steel components are conservatively based on the spectra shown in Figure 2-1 anchored at 0.50g in the horizontal direction and 0.33g in the vertical direction. The stability criteria for seismic loading are based on the stability response of a single, freestanding EOS-HSM with and without an end shield wall.

The EOS-HSMs in the array have no anchorage to the concrete basemat and there are no positive structural connections between HSMs. The stability analyses consider the effects of sliding and rocking motions, and determine the maximum possible sliding of a single module with and without an end shield wall. The EOS-HSM will neither slide nor overturn at design ZPA of 0.45g in the horizontal direction and 0.30g in the vertical direction.

The licensee shall determine if, based on ISFSI-specific site investigations, a soil structure interaction (SSI) analyses ought to be performed to assess potential site-specific amplifications. The SSI evaluations are based on ISFSI site-specific parameters (free-field accelerations, strain-dependent soil properties, HSM array configurations, etc.). The SSI response spectra at the base of the HSMs are to be bounded by the HSM design basis seismic criteria response spectra, i.e., the Regulatory Guide 1.60 response spectra shape, with enhanced spectral accelerations above 9 Hz, and anchored at 0.45g horizontal and 0.30g vertical directions. The licensee shall reconcile spectral accelerations from the SSI analysis response spectra that exceed the seismic criteria spectra (if any); 5% damped response spectra may be used in making these determinations.

For dynamic analysis, the stability evaluation shall be performed using the methodology in CoC 2029 [2-19].

Since the DSC can be considered to act as a large diameter pipe for the purpose of evaluating seismic effects, the "Equipment and Large Diameter Piping System" category in NRC Regulatory Guide 1.61, Table 1 [2-16] is applicable. Therefore, a damping value of 3% of critical damping for the design bases safe shutdown earthquake is used. Similarly, from the same Regulatory Guide table, a damping value of 7% of critical damping is used for the reinforced concrete structural components of the EOS-HSM.

2.3.5 Snow and Ice Loading

Snow and ice loads for the EOS-HSM are derived from ASCE 7-10 [2-12]. The maximum 100-year roof snow load, specified for most areas of the continental United States for an unheated structure, of 110 psf is assumed.

Snow and ice loads for the onsite TC with a loaded DSC are not evaluated because these are negligible due to the smooth curved surface of the cask, the heat rejection of the SFAs, and the infrequent short term use of the cask.

2.3.6 Tsunami

Specific analyses including analysis for tip-over are not done for tsunamis as they are typically bounded by the tornado wind and flooding load conditions. The licensee should evaluate site-specific impacts of a tsunami.

2.3.7 Lightning

A lightning strike will not cause a significant thermal effect on the EOS-HSM or stored DSC. The effects on the EOS-HSM resulting from a lightning strike are discussed in Section 12.3.7.

2.4 Safety Protection Systems

2.4.1 General

The NUHOMS® EOS System is designed to provide long-term storage of spent fuel. The DSC materials are selected for degradation to not be expected during the storage period. The DSC shell and bottom end assembly confinement boundary weld is made during fabrication of the DSC in accordance with the subsection NB of the ASME code. The top and bottom shield plugs and covers provide shielding for the DSC so that occupational doses are minimized during drying, sealing, and handling operations. The confinement boundary weld between the DSC shell and inner top cover (including drain port cover and vent plug welds) and structural attachment weld between the DSC shell and outer top cover plate are in accordance with alternatives to the ASME code as described in Section 4.4.4 of the Technical Specifications [2-18].

The radioactive material stored in the NUHOMS® EOS System is the SFAs and the associated contaminated or activated materials.

During fuel loading operations, the radioactive material in the plant's fuel pool is prevented from contacting the DSC exterior by filling the TC/DSC annulus with uncontaminated, demineralized water prior to placing the cask and DSC in the fuel pool. In addition, the TC/DSC annulus opening at the top of the EOS-TC is sealed using an inflatable seal to prevent pool water from entering the annulus. This procedure minimizes the likelihood of contaminating the DSC exterior surface. The combination of the above operations ensures that the DSC surface loose contamination levels are within those required for shipping cask externals. Compliance with these contamination limits is ensured by taking surface swipes of the upper end of the DSC before transferring the cask from the fuel building.

Once inside the DSC, the contents are confined by the DSC confinement boundary. The fuel cladding integrity is ensured by maintaining the storage cladding temperatures below levels that are known to cause degradation of the cladding. In addition, the SFAs are stored in an inert atmosphere to prevent degradation of the cladding, specifically cladding rupture due to oxidation and its resulting volumetric expansion of the fuel. Thus, a helium atmosphere for the DSC is incorporated into the design to protect the fuel cladding integrity by inhibiting the ingress of oxygen into the cavity.

Helium is known to leak through valves, mechanical seals, and escape through very small passages because it has a small atomic diameter, is an inert element, and exists in a monatomic species. Helium will not, to any practical extent, diffuse through stainless or duplex steel. For this reason, the DSC has been designed as a welded confinement pressure vessel with no mechanical or electrical penetrations and meets the leak-tight criteria as described in Chapter 10. See Chapter 5 for a detailed discussion of the confinement boundary design.

The DSC itself has a series of barriers to ensure the confinement of radioactive materials. The cylindrical shell is fabricated from rolled ASME stainless steel plate or duplex steel, which is joined with full penetration welds that are 100% inspected by non-destructive examination. All top and bottom end closure welds are multiple-layer welds. This effectively eliminates any pinhole leaks that might occur in a single pass weld, since the chance of pinholes being in alignment on successive weld passes is not credible. Furthermore, the cover plates are sealed by separate, redundant closure welds. Pressure boundary welds and welders are qualified in accordance with Section IX of the ASME Boiler and Pressure Vessel Code and inspected according to the appropriate articles of Section III, Division 1, Subsection NB including alternatives to ASME Code as specified in Section 4.4.4 of the Technical Specifications [2-18]. These criteria ensure that the as-deposited weld filler metal is as sound as the parent metal of the pressure vessel.

Pressure monitoring instrumentation is not used since penetration of the pressure boundary would be required. The penetration itself would then become a potential leakage path and by its presence compromise the integrity of the DSC design. The shell and welded cover plates provide total confinement of radioactive materials. Once the DSC is sealed, there are no credible events, as discussed in Chapter 12, which could fail the cylindrical shell or the closure plates that form the confinement boundary.

The NUHOMS® EOS System provides safe and long-term dry storage of SFAs. The key elements of the NUHOMS® EOS System, and its operation requiring special design consideration, are:

- A. Minimizing contamination of the DSC exterior by fuel pool water.
- B. Double-closure seal welds on the DSC shell to form a pressure retaining containment boundary, and to maintain the DSC interior helium atmosphere.
- C. Minimizing personnel radiation exposure during DSC loading, closure, and transfer operations.
- D. Maintaining EOS-TC and DSC ITS features under postulated accident conditions.
- E. Passive ventilation of the EOS-HSM providing effective decay heat removal thereby maintaining fuel cladding temperature below the maximum limit.
- F. DSC basket assembly to ensure that the SFAs are maintained in a subcritical configuration.

Components of the NUHOMS® EOS System that are ITS and NITS are listed in Table 2-1.

2.4.2 Structural

2.4.2.1 EOS-DSC Design Criteria

The principal design criteria for the DSCs are presented in Table 2-5 and Table 2-6. The EOS-37PTH DSC is designed to store intact PWR FAs with or without CCs. The EOS-89BTH DSC is designed to store intact BWR FAs with or without fuel channels. The maximum total heat generation rate of the stored fuel is limited to 50 kW per DSC for the EOS-37PTH DSC and 43.6 kW per DSC for the EOS-89BTH DSC, in order to keep the maximum fuel cladding temperature below the limit necessary to ensure cladding integrity. The maximum heat load for any single assembly is 2 kW for the EOS-37PTH DSC and 0.6 kW for the EOS-89BTH DSC. The fuel cladding integrity is assured by limiting fuel cladding temperature and maintaining a nonoxidizing environment in the DSC cavity as described in Chapter 4.

2.4.2.2 EOS-HSM Design Criteria

The principal design criteria for the EOS-HSM/EOS-HSMS, both the module and DSC support structure, are presented in Table 2-7.

The EOS reinforced concrete EOS-HSM is designed to meet the requirements of ACI 349-06 [2-3]. The ultimate strength method of analysis is utilized with the appropriate strength reduction factors as described in Appendix 3.9.4. The load combinations specified in Section 6.17.3.1 of ANSI 57.9-1984 are used for combining normal operating, off-normal, and accident loads for the EOS-HSM. All seven load combinations specified are considered and the governing combinations are selected for detailed design and analysis. The resulting EOS-HSM load combinations and the appropriate load factors are presented in Appendix 3.9.4. The effects of duty cycle on the EOS-HSM are considered and found to have negligible effect on the design.

2.4.2.3 EOS-TC Design Criteria

The EOS-TCs are designed in accordance with the applicable portions of the ASME Code, Section III, Division 1, Subsection NF for Class 1 vessels, except for the neutron shield tank, which is designed to ASME Code, Section III, Division 1, Subsection ND, since it will see pressure greater than 15 psig. The load combinations considered for the TC normal, off-normal, and postulated accident loadings are shown in Table 2-8. Service Levels A and B allowables are used for all normal operating and off-normal loadings. Service Levels C and D allowables are used for load combinations that include postulated accident loadings. The maximum shear stress theory is used to calculate principal stresses in the cask structural shell. Allowable stress limits for the lifting trunnions conservatively meet the requirements of ANSI N14.6- 1993 [2-14] for critical loads.

2.4.3 Thermal

The NUHOMS® EOS System relies on natural convection through the air space in the EOS-HSM to cool the DSC. This passive convective ventilation system is driven by the pressure difference due to the stack effect (ΔP_s) provided by the height difference between the bottom of the DSC and the EOS-HSM air outlet. This pressure difference is greater than the flow pressure drop (ΔP_f) at the design air inlet and outlet temperatures. The details of the ventilation system design are provided in Chapter 4.

Thermal analysis is based on FAs with decay heat up to 50.0 kW per DSC for the EOS-37PTH and up to 43.6 kW per DSC for the EOS-89BTH. Zoning is used to accommodate high per assembly heat loads. The heat load zoning configurations (HLZCs) for the DSCs are shown in Figures 1 and 2 of the Technical Specifications [2-18].

The thermal analyses is performed for the environmental conditions listed in Table 2-9.

Peak clad temperature of the fuel at the beginning of the long-term storage does not exceed 400 °C for normal conditions of storage, and for short-term operations, including DSC drying and backfilling. Fuel cladding temperature shall be maintained below 570 °C (1058 °F) for accident conditions involving fire or off-normal storage conditions.

For onsite transfer in the EOS-TC, air circulation may be used, as a recovery action, to facilitate transfer operations when the heat loads in the EOS-37PTH DSC are above 36.35 kW and 34.3 kW in the EOS-89BTH DSC as described in the Technical Specifications [2-18].

Wind deflectors are installed on the EOS-HSM to eliminate the effect of sustained winds for DSCs with Type 1 or Type 2 baskets as described in Section 5.5 of the Technical Specifications [2-18].

2.4.4 Shielding/Confinement/Radiation Protection

As described earlier, the DSC shells are a welded stainless or duplex steel pressure vessel that includes thick shield plugs at both ends to maintain occupational exposures as-low-as-reasonably-achievable (ALARA). The top end of the DSC has nominally 10 inches of steel shielding and the bottom eight inches of steel shielding. The confinement boundary is designed, fabricated, and tested to ensure that it is leaktight in accordance with [2-15]. Section 2.4.2.1 provides a summary of the features of the DSCs that ensure confinement of the contents.

The EOS-HSM/EOS-HSMS provides the bulk of the radiation shielding for the DSCs. The EOS-HSM designs can be arranged in either a single-row or a back-to-back arrangement. Thick concrete supplemental shield walls are used at either end of an EOS-HSM array and along the back wall of single-row arrays to minimize radiation dose rates both onsite and offsite. The nominal thickness of the EOS-HSM roof is 44 inches for biological shielding. Separate shield walls at the end of a module row, in conjunction with the module wall, provide a minimum thickness of four feet for shielding. Similarly, an additional shield wall is used at the rear of the module if the ISFSI is configured as single module arrays. Sufficient shielding is provided by thick concrete side walls between EOS-HSMs in an array to minimize doses in adjacent EOS-HSMs during loading and retrieval operations. Section 11.3 provides a summary of the offsite dose calculations for representative arrays of design basis EOS-HSMs providing assurance that the limits in 10 CFR 72.104 and 10 CFR 72.106(b) are not exceeded.

The EOS-TCs are designed to provide sufficient shielding to ensure dose rates are ALARA. The EOS-TCs are constructed of steel and lead gamma shielding with high-density polyethylene neutron shielding at the bottom and water neutron shielding jackets/tanks. The dose rates on and around the EOS-TCs are provided in Chapter 6 and the occupational exposures associated with a loading campaign are provided in Section 11.2. Off-normal and accident doses and dose rates are provided in Chapters 6 and 12.

There are no radioactive releases of effluents during normal and off-normal storage operations. Also, there are no credible accidents that cause significant releases of radioactive effluents from the DSC. Therefore, there are no off-gas or monitoring systems required for the EOS-HSM. An off-gas system is required only during DSC drying operations. During this operation, the spent fuel pool or plant's radwaste system is used to process the air and helium exchanges required to establish a DSC interior inert atmosphere.

2.4.5 Criticality

The criticality analyses are performed with the CSAS5 module of the SCALE system [2-17]. For the EOS-37PTH DSC a combination of soluble boron in the fuel pool, the fixed poison in the basket and geometry are relied on to maintain criticality control. The structural analysis shows that there is no deformation of the basket under accident conditions that would increase reactivity. The EOS-37PTH basket is fabricated with one of two neutron poison loading options as shown in Table 5 of the Technical Specifications [2-18].

These two neutron poison loading options allow flexibility to accommodate the payload fuel types and initial enrichments, with and without CCs, and credit for soluble boron (2000 – 2500 ppm) in the fuel pool during loading and unloading operations. Table 4 of the Technical Specifications [2-18] and Chapter 7 documents the minimum soluble boron required as a function of basket type and FA design/initial enrichment to be stored. Pressurized water reactor FAs with maximum planar average enrichments up to 5.0 wt. % U-235 can be stored.

For the EOS-89BTH DSC, a combination of fixed poison in the basket and geometry are relied on to maintain criticality control. The structural analysis shows that there is no deformation of the basket under accident conditions that would increase reactivity. The EOS-89BTH basket is fabricated with one of three neutron poison loading options as shown in Table 8 of the Technical Specifications [2-18].

These three neutron poison loading options allow flexibility to accommodate the payload fuel types and initial enrichments, with and without channels during loading and unloading operations. Table 8 of the Technical Specifications [2-18] and Chapter 7 documents the allowed fuel assembly design/initial enrichment as a function of neutron poison loading allowed to be stored. Fuel assemblies with maximum lattice average enrichments up to 4.8 wt. % U-235 can be stored in the EOS-89BTH with neutron poison loading option C.

The criticality analysis in Chapter 7 takes 90% credit for the B-10 content of the metal matrix composite (MMC) material and 75% credit for the B-10 content of the BORAL® material. Chapter 10 provides the testing requirements to justify the B-10 credit used in the criticality analysis.

2.4.6 Material Selection

Materials are selected based on their corrosion resistance, susceptibility to stress corrosion cracking, embrittlement properties, and the environment in which they operate during normal off-normal and accident conditions. The confinement boundary for the DSC materials meet the requirements of ASME Boiler and Pressure Vessel Code, Section III, Article NB-2000 and the specification requirements of Section II, Part D, with code alternatives provided in Section 4.4.4 of the Technical Specifications [2-18]. The DSC and TC materials are resistant to corrosion and are not susceptible to other galvanic reactions. Studies under severe marine environments have demonstrated that the shell materials used in the DSC shells are expected to demonstrate minimal corrosion during a 80-year exposure. The DSC internals are enveloped in a dry, helium-inerted environment and are designed for all postulated environmental conditions. The EOS-HSM is a reinforced concrete component with an internal DSC support structure that is fabricated to ACI and AISC Code requirements with code alternatives provided in Section 4.4.4 of the Technical Specifications [2-18], respectively; both have durability well beyond their design life of 80 years. Chapter 8 provides an additional discussion related to the materials used for the NUHOMS® EOS System.

2.4.7 Operating Procedures

The sequence of operations are outlined for the NUHOMS® EOS System in Chapter 9 for loading of fuel, closure of the DSC, transfer to the ISFSI using the TC, insertion into the HSM, monitoring operations, and retrieval and unloading. Throughout Chapter 9, CAUTION statements are provided at the step where special notice is needed to maintain ALARA, protect the contents of the DSC, protect the public and/or ITS components of the NUHOMS® EOS System.

2.4.8 Acceptance Tests and Maintenance

Chapter 10 specifies the acceptance testing and maintenance program for important to safety components of the NUHOMS® EOS System (DSC, EOS-HSM and EOS-TCs).

2.4.9 Decommissioning

The DSC is designed to interface with a transportation system for the eventual offsite transport of stored canisters by the Department of Energy (DOE) to either a monitored retrievable storage (MRS) facility or a permanent geologic repository.

Decommissioning of the ISFSI will be performed in a manner consistent with the decommissioning of the plant itself since all NUHOMS® EOS System components are constructed of materials similar to those found in existing plants.

If the fuel is to be removed from the DSC at the plant prior to shipment, the DSC will likely be contaminated internally by crud from the spent fuel, and may be slightly activated by neutron emissions from the spent fuel. The DSC internals can be cleaned to remove surface contamination and the DSC disposed of as low-level waste.

Alternatively, if the contamination and activation levels of the DSC are small enough (to be determined on a case-by-case basis), it may be possible to decontaminate the DSC and dispose of it as commercial scrap pending NRC rulings on below regulatory concern (BRC) waste disposal issues.

While the intent for the NUHOMS® EOS System includes the eventual disposal of each DSC following fuel removal, current closure weld designs do not preclude future development of a non-destructive closure removal technique that allows for reuse of the DSC shell/basket assembly. Economic and technical conditions existing at the time of fuel removal would be assessed prior to making a decision to reuse the DSC.

The exact decommissioning plan for the ISFSI will be dependent on the DOE's fuel transportation system capability and requirements for a specific plant. Because of the minimal contamination of the outer surface of the DSC, no contamination is expected on the internal passages of the EOS-HSM. It is anticipated that the prefabricated EOS-HSMs can be dismantled and disposed of using commercial demolition and disposal techniques. Alternatively, the EOS-HSMs may be refurbished and reused at another site, or at the MRS for storage of intact DSCs transported from the plant.

2.5 References

- 2-1 Title 10, Code of Federal Regulations, Part 100, "Reactor Site Criteria."
- 2-2 American Society of Mechanical Engineers, "ASME Boiler and Pressure Vessel Code," Section III, Division 1, Subsections NB, NF, ND and NCA, 2010 Edition with 2011 Addenda.
- 2-3 ACI 349-06, "Code Requirements for Nuclear Safety Related Concrete Structures," American Concrete Institute.
- 2-4 ACI 318-08, "Building Code Requirements for Structural Concrete and Commentary," American Concrete Institute.
- 2-5 Title 10, Code of Federal Regulations, Part 50, "Domestic Licensing of Production and Utilization Facilities."
- 2-6 Title 10, Code of Federal Regulations, Part 72, "Licensing Requirements for the Independent Storage of Spent Nuclear Fuel, High-Level Radioactive Waste, and Reactor-Related Greater Than Class C Waste."
- 2-7 Not Used.
- 2-8 U.S. Nuclear Regulatory Commission, Regulatory Guide 1.76, "Design Basis Tornado and Tornado Missiles for Nuclear Power Plants," Rev. 1, March 2007.
- 2-9 Not Used.
- 2-10 NUREG-0800, Standard Review Plan, Section 3.3.1 "Wind Loading", Section 3.3.2 "Tornado Loads", and Section 3.5.1.4 "Missiles Generated by Tornado and Extreme Winds," Rev. 3, March 2007.
- 2-11 NUREG-0800, Standard Review Plan, Section 3.5.3 "Barrier Design Procedures," Rev. 3, March 2007.
- 2-12 American Society of Civil Engineers, ASCE 7-10, "Minimum Design Loads for Buildings and Other Structures," (formerly ANSI A58.1).
- 2-13 NRC Regulatory Guide 1.60, "Design Response Spectra for Seismic Design of Nuclear Power Plants" Rev. 1, December 1973.
- 2-14 ANSI N14.6, "American National Standard for Special Lifting Device for Shipping Containers Weighing 10,000 lbs. or More for Nuclear Materials," American National Standards Institute, Inc., 1993.
- 2-15 ANSI N14.5, "Leakage Tests on Packages for Shipment of Radioactive Materials," American National Standards Institute, Inc., 1997.
- 2-16 U.S. Nuclear Regulatory Commission, Regulatory Guide 1.61, "Damping Values for Seismic Design of Nuclear Power Plants," Rev 1, March 2007.
- 2-17 SCALE 6: Modular Code System for Performing Standardized Computer Analyses for Licensing Evaluation for Workstations and Personal Computers, Oak Ridge National Laboratory, Radiation Shielding Information Center Code Package CCC-750, February 2009.

- 2-18 CoC 1042 Appendix A, NUHOMS® EOS System Generic Technical Specifications, Amendment 0.
- 2-19 Updated Final Safety Analysis Report For The Standardized Advanced NUHOMS® Horizontal Modular Storage System For Irradiated Nuclear Fuel, 72-1029, Revision 6

Table 2-1
NUHOMS® EOS System Major Components and Safety Classification

Component	10 CFR 72 Classification⁽¹⁾
Dry Shielded Canister (EOS-37PTH DSC and EOS-89BTH DSC)	
Basket Steel Plate	ITS
Poison Plate	ITS
Basket Aluminum Plate	ITS
Transition Rails	ITS
Transition Rail Tie Rod and Nuts	ITS
Transition Rail Angle Plates	ITS
Transition Rail Screw, Washer and Nut	ITS
Shell	ITS
Outer Top Cover Plate	ITS
Top Shield Plug	ITS
Inner Top Cover Plate	ITS
Inner Bottom Cover Plate	ITS
Bottom Shield Plug	ITS
Outer Bottom Cover Plate	ITS
<i>Lifting Lug Plate</i>	<i>ITS</i>
DSC Lifting Lug	NITS
Siphon Assembly	NITS
Drain Port Cover and Vent Plug	ITS
Test Port Plug	ITS
Grapple Ring and Grapple Support	ITS
Basket Key	ITS
Weld Filler Metal	ITS
Horizontal Storage Module (EOS-HSM/EOS-HSMS)	
Reinforced Concrete	ITS
DSC Support Structure	ITS
Thermal Instrumentation (if used)	NITS
ISFSI Basemat and Approach Slabs	NITS
Transfer Equipment	
Eos-TC (TC135/TC125/TC108)	ITS
Cask Lifting Yoke	See Note 2
Transfer Trailer/Skid	NITS
Ram Assembly	NITS
Dry Film Lubricant	NITS
Auxiliary Equipment	
Vacuum Drying System	NITS
Automatic Welding System	NITS
TC/DSC Annulus Seal	NITS

Notes:

- SSCs ITS are defined in 10 CFR 72.3 as those features of the ISFSI whose function is (1) to maintain the conditions required to store spent fuel safely, (2) to prevent damage to the spent fuel container during handling and storage, or (3) to provide reasonable assurance that spent fuel can be received, handled, packaged, stored, and retrieved without undue risk to the health and safety of the public.
- Safety classification shall be per existing plant-specific requirements under the user's 10 CFR 50 heavy loads program.

Table 2-2
PWR Fuel Assembly Design Characteristics
 3 Pages

Fuel Class	B&W 15x15				WE 17x17
Assembly Type	Mark B2 - B8	Mark B9	Mark B10	Mark B11	BW 17x17 Mark C
Fuel Parameters					
Number of Rods	208	208	208	208	264
Active Fuel Length (in.)	≤150	≤150	≤150	≤150	≤150
Pellet Diameter (in.)	0.3686	0.37	0.3735	0.3615	0.3232
Fuel Rod Pitch (in.)	0.568	0.568	0.568	0.568	0.502
Clad Outer Diameter (OD) (in.)	0.43	0.43	0.43	0.416	0.379
Clad Thickness (in.)	0.0265	0.0265	0.025	0.024	0.024
Guide and Instrument Tubes					
Number of Guide/Instrument Tubes	17	17	17	17	17
Guide/Instrument Tube Thickness (in.)	≥0.016	≥0.016	≥0.016	≥0.016	≥0.026

Fuel Class	WE 14 x 14			
Assembly Type	Std/LOPAR/ ZCA/ZCB	OFA	Exxon/ANF (ANP) WE	Exxon/ANF (ANP) Top rod
Fuel Parameters				
Number of Rods	179	179	179	179
Active Fuel Length (in.)	≤150	≤150	≤150	≤150
Pellet Diameter (in.)	0.364-0.3674	0.364-0.3674	0.3505	0.3505
Fuel Rod Pitch (in.)	0.556	0.556	0.556	0.556
Clad OD (in.)	0.422	0.400	0.424	0.417
Clad Thickness (in.)	0.0225-0.030	0.0243-0.034	0.024-0.030	0.024-0.0295
Guide and Instrument Tubes				
Number of Guide/Instrument Tubes	17	17	17	17
Guide/Instrument Tube Thickness (in.)	≥0.015	≥0.015	≥0.016	≥0.019

Fuel Class	WE 17x17			
Assembly Type	LOPAR	OFA/ Van 5	Framatome 17x17 STD/Van 5H/RFA	Framatome 17x17 MK BW
Fuel Parameters				
Number of Rods	264	264	264	264
Active Fuel Length (in.)	≤150	≤150	≤150	≤150
Pellet Diameter (in.)	0.3225	0.3088	0.3225	0.3195
Fuel Rod Pitch (in.)	0.496	0.496	0.496	0.496
Clad OD (in.)	0.374	0.360	0.374	0.374
Clad Thickness (in.)	0.0225	0.0225	0.0225	0.0240
Guide and Instrument Tubes				
Number of Guide/Instrument Tubes	25	25	25	25
Guide/Instrument Tube Thickness (in.)	≥0.015	≥0.015	≥0.015	≥0.016

Table 2-2
PWR Fuel Assembly Design Characteristics
 3 Pages

Fuel Class	CE 14 x 14		
Assembly Type	Std/Gen/St. Lucie	Fort Calhoun	Framatome CE
Fuel Parameters			
Number of Rods	176	168	176
Active Fuel Length (in.)	≤150	≤150	≤150
Pellet Diameter (in.)	0.370 – 0.3805	0.3765	0.3805
Fuel Rod Pitch (in.)	0.58	0.580	0.580
Clad OD (in.)	0.44	0.440	0.440
Clad Thickness (in.)	0.026 – 0.031	0.0280	0.0280
Guide and Instrument Tubes			
Number of Guide/Instrument Tubes	5	5	5
Guide/Instrument Tube Thickness (in.)	≥0.040	≥0.040	≥0.040

Fuel Class	WE 15 x 15			CE 15x15	
Assembly Type	LOPAR/ OFA DRFA/ Van5	Std/ZC	Exxon ANF (ANP) WE	CE 15x15 Palisades	CE 15x15 Exxon/ ANF (ANP)
Fuel Parameters					
Number of Rods	204	204	204	216	216
Active Fuel Length (in.)	≤150	≤150	≤150	≤150	≤150
Pellet Diameter (in.)	0.3659	0.3559	0.3565	0.3150 - 0.3600	0.3565
Fuel Rod Pitch (in.)	0.563	0.563	0.563	0.550	0.550
Clad OD (in.)	0.422	0.422	0.424	0.4138 - 0.4180	0.417
Clad Thickness (in.)	0.0280	0.0242	0.0300	0.024 – 0.0295	0.0300
Guide and Instrument Tubes					
Number of Guide/Instrument Tubes	21	21	21	8	Note 3
Guide/Instrument Tube Thickness (in.)	≥0.015	≥0.015	≥0.017	≥0.024	≥0.027

Table 2-2
PWR Fuel Assembly Design Characteristics
 3 Pages

Fuel Class	CE 16x16			
Assembly Type	Standard	System 80	CE 16 x 16 SCE U2/3 Westinghouse Designs	CE 16 x 16 SCE U2/3 AREVA Designs
Fuel Parameters				
Number of Rods	236	236	236	236
Active Fuel Length (in.)	≤150	≤150	≤150	≤150
Pellet Diameter (in.)	0.3250	0.3250	0.3255	0.3255
Fuel Rod Pitch (in.)	0.506	0.506	0.506	0.506
Clad OD (in.)	0.382	0.382	0.382	0.382
Clad Thickness (in.)	0.025	0.023	0.025	0.025
Guide and Instrument Tubes				
Number of Guide/Instrument Tubes	5	5	5	5
Guide/Instrument Tube Thickness (in.)	≥0.041	≥0.041	≥0.040	≥0.040

Notes:

1. All dimensions shown are nominal.
2. Reload FAs from other manufacturers with these parameters are also acceptable.
3. One instrument tube and eight guide bars (solid Zr).

Table 2-3
BWR Fuel Assembly Design Characteristics
 4 Pages

BWR Fuel ID/(Fuel Class)	GE-7-A (7 x 7)	GE-8-A (8 x 8)	GE-8-B (8 x 8)	GE-8-C (8 x 8)	GE-8-D (8 x 8)	GE-9-A (9 x 9)	GE-10-A (10 x 10)	GE-10-B (10 x 10)	ENC-7-B (7 x 7)
FA Design	7 x 7- 49/0	8 x 8- 63/1	8 x 8- 62/2	8 x 8- 60/4	8 x 8- 60/1	9 x 9- 74/2	10x10- 92/2	10x10	7 x 7- 48/0
Reload Fuel Designation ⁽¹⁾⁽²⁾	GE1 GE2 GE3	GE4	GE-5 GE-Pres GE-Barrier GE8 Type I	GE8 Type II	GE9 GE10	GE11 GE13	GE12 GE14	GNF2	ENC-III ⁽¹¹⁾
Rod Pitch (in.)	0.738	0.640	0.640	0.640	0.640	0.566	0.510	0.510	0.738
No of Fueled Rods	49	63	62	60	60	66 full 8 partial	78 full 14 partial	78 full 14 partial	48
Maximum Active Fuel Length (in.)	≤150	≤150	≤150	≤150	≤150	146" full 90" partial 108" partial GE13	150" full 93" partial 84" partial GE14	150.3" full 110.81" partial 59.4" partial	≤150
Fuel Rod OD (in.)	0.563	0.493	0.483	0.483	0.483	0.440	0.404	0.404	0.570
Clad Thickness (in.)	0.032 0.037	0.034	0.032	0.032	0.032	0.028	0.026	0.0236	≥0.0355
Fuel Pellet OD (in.)	0.491 0.477	0.416	0.410 0.411	0.410 0.411	0.411	0.376	0.345	0.350	0.468 - 0.491
No of Water Rods	0	1	2	4	1	2	2	2	1 (Note 3)
Water Rod OD (in.)	---	0.493	0.591	2 @ 0.591 2 @ 0.483	1.340	0.980	0.980	0.98	0.572 ⁽³⁾
Water Rod Inner Diameter ID (in.)	---	0.425	0.531	2 @ 0.531 2 @ 0.419	1.260	0.920	0.920	0.92	Note 3

Table 2-3
BWR Fuel Assembly Design Characteristics
 4 Pages

BWR Fuel ID/(Fuel Class)	ENC-7-A (7 x 7)	ENC-8-A (8 x 8)	FANP-8-A (8 x 8)	FANP-9-A (9 x 9)	FANP-9-B (9 x 9)	FANP-10-A (10 x 10)	GE-8-A (8 x 8)	GE-8-A (8 x 8)	FANP-9-A (9 x 9)
FA Design	7 x 7- 49/0	8 x 8- 60/4	8 x 8- 62/2	9 x 9- 79/2	9 x 9	10x10- 91/1	8 x 8- 59/5	8 x 8- 63/1	9 x 9- 81
Reload Fuel Designation ⁽¹⁾⁽²⁾	ENC-III A	ENC Va and Vb	FANP 8X8-2	FANP 9X9-2	Siemens QFA 9X9 ATRIUM 9	ATRIUM- 10 ATRIUM- 10XM	XXX-RCN	STD GE-4 w/ higher exposure	FANP 9X9
Rod Pitch (in.)	0.738	0.642	0.641	0.572	0.569	0.510	0.640	0.640	0.572
No of Fueled Rods	49	60	62	79	72	83 full 8 partial	59 to 64	63	72, 80, 81
Maximum Active Fuel Length (in.)	≤150	≤150	≤150	≤150	≤150	149.54" full 149.45"full 90" partial	150	146	150
Fuel Rod OD (in.)	0.570	0.5015	0.484	0.424	0.433	0.3957	0.493	0.493	0.424
Clad Thickness (in.)	≥0.0355	0.036	0.035	0.030	0.0262	0.0239	0.034	0.034	0.030
Fuel Pellet OD (in.)	0.468- 0.488	0.4195	0.4045 - 0.4055	0.3565	0.3737	0.3413	0.416	0.416	0.3565
No of Water Rods	0	4 ⁽³⁾	2	2	1 (9 pins)	1	5	1	2 max.
Water Rod OD (in.)	---	0.5015 ⁽³⁾	0.484	0.425 - 0.424	1.516 square	1.378 square	0.493	0.493	0.425 -0.424
Water Rod ID (in.)	---	Note 3	0.414	0.364	1.458 square	1.321 square	0.425	0.425	0.364

Table 2-3
BWR Fuel Assembly Design Characteristics
 4 Pages

BWR Fuel ID /(Fuel Class)	ABB-8-A (8 x 8)	ABB-8-B (8 x 8)	ABB-10-A (10 x 10)	ABB-10-B (10 x 10)	ABB-10-B (10 x 10)	ABB-10-B (10 x 10)	ABB-10-A (10 x 10)	ABB-10-B (10 x 10)
FA Design	4x(4 x 4)	4x(4 x 4)	4x(5x5-2)	4x(5x5-2)	4x(5x5-1)	4x(5x5-1)	4x(5x5)	4x(5x5)
Reload Fuel Designation ⁽¹⁾⁽²⁾	SVEA-64	SVEA-64	SVEA-92	SVEA-92	SVEA-96 ⁽⁵⁾	SVEA-96 ⁽⁵⁾	SVEA-100	SVEA-100
Rod Pitch (in.)	0.610	0.622	0.500	0.500	0.496	0.488	0.500	0.496
No. of Fueled Rods	64	64	96	96	96	96	100	100
Maximum Active Fuel Length (in.)	150.59	150.59	150.59	150.59	150.59	150.59	151	151
Fuel Rod OD (in.)	0.461	0.483	0.387	0.378	0.387	0.378	0.443	0.387
Clad Thickness (in.)	0.027	0.031	0.0243	0.0243	0.0243	0.0243	0.028	0.0243
Fuel Pellet OD (in.)	0.3940	0.4110	0.3350	0.3224	0.3350	0.3224	0.3745	0.3350
No. of Water Rods	0	0	0	0	0	0	0	0
Water Rod OD (in.)	---	---	---	---	---	---	---	---
Water Rod ID (in.)	---	---	---	---	---	---	---	---

Table 2-3
BWR Fuel Assembly Design Characteristics
 4 Pages

BWR Fuel ID /(Fuel Class)	ABB-10-A (10 x 10)	ABB-10-C (10 x 10)
FA Design	4x(5x5-3) 4x(5x5-1) Optima	4x(5x5-4) 4x(5x5-2) 4x(5x5-1) Optima2
Reload Fuel Designation ⁽¹⁾⁽²⁾	SVEA-96Opt ⁽⁴⁾⁽⁵⁾	SVEA-96Op2 ⁽⁴⁾⁽⁵⁾
Rod Pitch (in.)	0.496 - 0.500	0.484 - 0.512
No of Fueled Rods	96	96
Maximum Active Fuel Length (in.)	150.42	150.42
Fuel Rod OD (in.)	0.379-0.406	0.387
Clad Thickness (in.)	0.0248 -0.0268	0.0238
Fuel Pellet OD (in.)	0.323-0.346	0.334
No of Water Rods	0	0
Water Rod OD (in.)	---	---
Water Rod ID (in.)	---	---

Notes:

1. All dimensions shown are nominal.
2. Reload FAs from other manufacturers with these parameters are also acceptable.
3. Solid Zircaloy rod(s).
4. Fuel bundles designated as ABB or SVEA are typically assembled from four sub-assemblies. There is a cruciform internal water channel between the sub-assemblies. The thickness of the water channel is 0.8 mm, the inner width of the channel is 4 mm for most ABB or SVEA bundles, except 2.4 mm for SVEA-Optima 1 and SVEA-Optima 2.
5. There is one rod that occupies the four central fuel rod locations and four water bars/channels that divide the FA into four quadrants.

Table 2-4
Additional PWR and BWR Fuel Assembly Design Characteristics
 2 Pages

Fuel Class	WE 14x14	WE17x17	WE17x17	WE15x15	WE17x17	WE17x17
FA Design	Doel 1&2 14x14	Doel 3 17x17	Doel 4 17x17	Tihange 1 15x15	Tihange 2 17x17	Tihange 3 17x17
Fuel Parameters						
No. of Rods	179	264	264	204	264	264
Active Fuel Length (in.)	96	145	169	145	145	169
Pellet Diameter (in.)	0.368	0.322	0.323	0.368	0.323	0.323
Fuel Rod Pitch (in.)	0.556	0.496	0.496	0.563	0.496	0.496
Clad OD (in.)	0.424	0.376	0.376	0.426	0.376	0.376
Clad Thickness (in.)	0.0225-0.030	0.0225	0.0225	0.0242	0.0225	0.0225
Guide and Instrument Tubes						
No. of Guide/Instrument Tubes	17	25	25	21	25	25
Guide/Instrument Tube Thickness (in.)	≥0.015	≥0.015	≥0.015	≥0.015	≥0.015	≥0.015
Fuel Class / BWR Fuel ID	WE 14x14	WE 15x15	WE 17x17	GE-8-C (8 x 8)	WE 17x17	WE 17x17
FA Design ^{(1) (2)}	Kansai 14x14 Step I Type A	Kansai 15x15 Step I Type A	Kansai 17x17 Step II	8x8 Step II	17x17	17x17
Fuel Parameters						
No. of Rods	179	204	264	60	264	264
Active Fuel Length (in.)	143	143	144	146	144	165
Pellet Diameter (in.)	0.366	0.366	0.317	0.409	0.322	0.322
Fuel Rod Pitch (in.)	0.555	0.563	0.496	0.642	0.496	0.496
Clad OD (in.)	0.422	0.422	0.374	0.484	0.36	0.372
Clad Thickness (in.)	0.0225-0.030	0.0242	0.0225	0.036	0.0225	0.0225
Guide and Instrument Tubes						
No. of Guide/Instrument Tubes	17	21	25	4 (Note 3)	25	25
Guide/Instrument Tube Thickness (in.)	≥0.015	≥0.015	≥0.015	0.5015 ⁽³⁾	≥0.015	≥0.015

Table 2-4
Additional PWR and BWR Fuel Assembly Design Characteristics
 2 Pages

BWR Fuel ID/Fuel Class	GE-8-C what (8 x 8)	GE-9-A (9 x 9)	GE-10-A (10 x 10)	ABB-8-A (8 x 8)	ABB-10-B (10 x 10)	ABB-10-A (10 x 10)	ABB-10-C (10 x 10)
	BWR 1/4	BWR 2/5/8	BWR 3/9/12/13	BWR 6	BWR 7/14	BWR 10/15	BWR 11/16
FA Design	KKL 8x8	KKL 9x9	KKL 10x10	KKL 4x4x4	KKL 4x(5x5-1)	KKL 4x(5x5-3)/ 4x(5x5-1)	KKL 4x(5x5-4)/ 4x(5x5-2)/ 4x(5x5-1)
Fuel Parameters							
Number of Rods	62	74	92	64	96	88-96	84-96
Active Fuel Length (in.)	150	146	148	151	151	151	151
Pellet Diameter (in.)	0.413	0.378	0.35	0.394	0.323	0.323 - 0.346	0.334 - 0.335
Fuel Rod Pitch (in.)	0.64	0.566	0.51	0.61	0.488	0.496 - 0.502	0.512
Clad OD (in.)	0.483	0.441	0.431	0.461	0.369 - 0.378	0.379 - 0.406	0.369 - 0.387
Clad Thickness (in.)	0.036	0.028	0.026	0.027	0.0228	0.023	0.024
Number of Water Rods	4 (Note 3)	2	2	0	0	0	0
Water Rod OD	0.5015 ⁽³⁾	0.98	0.98	---	---	---	---
Water Rod ID	Note 3	0.92	0.92	---	---	---	---

Notes:

1. All dimensions shown are nominal.
2. Reload fuel assemblies from other manufacturers with these parameters are also acceptable.
3. Solid Zirc rod(s).

Table 2-5
EOS-37PTH/EOS-89BTH DSC Shell Assembly Loads and Load
Combinations

Loading Type	DSC Orientation	Load for Analysis	Load Combination	Service Level	Load Combination No.
Dead weight (DW)	Vertical ⁽¹⁾	1g down (axial)	DW + Normal Pressure + Normal Thermal ⁽²⁾	A	1
Blowdown/Pressure Test		20 psig internal pressure			
Thermal		Normal vertical orientation thermal			
Dead weight	Horizontal ⁽³⁾	1g down	DW + H + Pressure + Thermal (117 °F)	A	2
Thermal – Off-Normal Hot		Off-Normal –Hot (117 °F)			
Thermal – Off-Normal Cold		Off-Normal Cold (-40 °F)			
Internal Pressure – Off-Normal		20 psig	DW + H + Pressure + Thermal (-40 °F)		3
Handling (H) in TC ⁽¹⁶⁾		H = ± ½ g axial ± ½ g trans. ± ½ g vertical and 1g vertical, 1g trans., 1g axial applied individually			
Dead weight	Horizontal ⁽³⁾	1g down	DW + Hydraulic Ram (135 kips insertion) + Pressure + Thermal	A/B ⁽⁷⁾	4
Hydraulic Ram Loads (push/pull)		135 kips (push) ⁽⁵⁾			
Internal pressure-Off-Normal		80 kips (pull) ⁽⁶⁾	DW + Hydraulic Ram (80 kips, retrieval) + Pressure + Thermal		5
Thermal — Off-Normal		20 psig ⁽⁹⁾			
		Thermal –Off Normal ⁽⁸⁾			
Dead weight	Horizontal ⁽³⁾	1g down	DW + Hydraulic Ram (135 kips retrieval) + Pressure	D	6
Hydraulic Ram Loads (pull)		135 kips ⁽⁶⁾			
Internal pressure – Off-Normal		20 psig ⁽⁹⁾			
Dead Weight	Horizontal	1g down	DW + Pressure + 65 inch Accident Drop	D	7
Internal pressure – Off-Normal		20 psig ⁽⁹⁾			
Accident Side/corner drop ⁽¹⁷⁾		65 inch drop			
Dead Weight	Horizontal	1g down	DW + Accident Pressure	D	8
Internal pressure – Accident		130 psig ⁽³⁾⁽⁹⁾⁽¹⁰⁾			
Dead Weight	Horizontal ⁽¹¹⁾	1g down	DW + Pressure + Thermal	A	9
Internal Pressure – Off-Normal		20 psig			
Thermal – Off-Normal		Thermal-Off Normal			
Dead Weight	Horizontal ⁽¹¹⁾	1 g down	DW + Pressure + Seismic (S)	D	10
Internal Pressure – Off-Normal		20 psig			
Seismic (S)		S = ± 1.25g (axial) ± 2g (transverse) ± 1g (vertical)			
Test Pressure at fabricator – 18 psig ⁽¹²⁾	Vertical	18 psig internal pressure	18 psig internal pressure	Test	11
External pressure	Horizontal	See Note 14		D	12

Notes

1. DSC in EOS-TC in vertical orientation. Only inner top cover is installed.
2. Bounding thermal case for normal operations of TC in vertical orientation.
3. DSC in EOS-TC; EOS-TC is in horizontal orientation and supported at the trunnion and saddle locations.
4. Not used.
5. The hydraulic push loads are applied at the canister bottom surface within the grapple ring support.
6. The hydraulic pull loads are applied at the inner surface of the grapple ring.
7. Level B evaluations may take credit for 10% increase in allowable per NB-3223(a).
8. Controlling thermal off-normal case.
9. Load combination results to bound cases with and without internal pressure. Level B is used for the case with internal pressure. Level A is used for the case without internal pressure.
10. Bounding pressure of EOS-HSM blocked vent accident or TC accident fire conditions.
11. DSC in EOS-HSM supported on the steel rails.
12. Conservatively used 18 psig as the test pressure; test configuration is circular shell and inner bottom welded to shell; a top end lid with a 155 kips clamping force used to seal the test assembly.
13. (General) Material properties at temperature.
14. The maximum accident condition external pressure before DSC collapse/buckling is determined.
15. (General) In addition to the Part 72 loads, postulated end, corner, and side drops associated with 10 CFR Part 71 are evaluated to ensure that the DSC can be licensed as a transportable system.
16. These handling loads in conjunction with Level A limits bounds case of EOS-TC in fuel building under seismic loads (Level D accident condition).
17. The top end drop and bottom end drop are not credible events under 10 CFR Part 72; therefore these drop analyses are not required. However, consideration of end drops (for 10 CFR Part 71 conditions) and the 65-inch side drop conservatively envelope the effects of a corner drop.

Table 2-6
EOS-37PTH/EOS-89BTH DSC Basket Assembly Load Combinations

Loading	Canister w/Transfer Cask Orientation	Load for Analysis	Load Combinations	Service Level	Notes
Dead Weight Thermal	Vertical	1 g down (axial) Thermal	DW + Thermal	A	Note 1
Dead Weight Handling Thermal	Horizontal	1g down H = + ½ g axial + ½ g trans.+ ½ g vertical and 1g vertical, 1g trans., 1g axial applied individually Thermal Off Normal hot and cold	DW + H + Thermal (117 °F) DW + H + Thermal (-40 °F)	A	Notes 2
Dead Weight Side Drop	Horizontal	65-inch side drop	65" side drop	D	Notes 3
Dead Weight Corner Drop	30 Degrees from Horizontal	65-inch corner drop	1g down+65" side drop	D	Notes 5

Notes:

1. Basket and FAs are supported at the bottom of the DSC. No mechanical loads other than basket self-weight. Due to its egg-crate, segmental, and non-welded construction, basket deformations due to thermal expansion/gradients are not expected to be significant. Not a bounding case.
2. Basket cells deformations due to FA inertia. Bounding case for Normal/Off-Normal conditions.
3. Seismic loads bounded by Dead Weight Side Drop load.
4. Not used
5. The top end drop and bottom end drop are not credible events under 10 CFR Part 72; therefore these drop analyses are not required. However, consideration of end drops (for 10 CFR Part 71 conditions) and the 65-inch side drop to conservatively envelope the effects of a corner drop.

Table 2-7
EOS-HSM Design Criteria

Number	Load Combination	Event
Concrete Structures		
1	$U > 1.4 D + 1.7 (L + R_o)$	Normal
2	$U > 1.05 D + 1.275 (L + T_o + W)$	Off-Normal – Wind
3	$U > 1.05 D + 1.275 (L + T_o + R_a)$	Off-Normal – Handling
4	$U > D + L + T_o + E$	Accident – Earthquake
5	$U > D + L + T_o + W_t$	Accident – Tornado
6	$U > D + L + T_o + FL$	Accident – Flood
7	$U > D + L + T_a$	Accident – Thermal
Steel Structures Allowable Stress Design		
1	$S > D + L + R_o$	Normal
2	$1.3 S > D + L + W$	Off-Normal – Wind
3	$1.3 S > D + L + T_o + R_a$	Off-Normal – Handling
4	$(1.5 S \text{ or } 1.4 S_v) > D + L + T_o + W$	Off-Normal – Wind with Thermal
5	$(1.6 S \text{ or } 1.4 S_v) > D + L + T_o + E$	Accident – Earthquake
6	$(1.6 S \text{ or } 1.4 S_v) > D + L + T_o + W_t$	Accident – Tornado
7	$(1.6 S \text{ or } 1.4 S_v) > D + L + T_o + FL$	Accident – Flood
8	$(1.7 S \text{ or } 1.4 S_v) > D + L + T_a$	Accident – Thermal
Steel Structures Plastic Strength Design		
1	$U_s > 1.7 (D + L)$	Normal
2	$U_s > 1.3 (D + L + W)$	Off-Normal – Wind
3	$U_s > 1.3 (D + L + R_a)$	Off-Normal – Handling
4	$U_s > 1.3 (D + L + T_o + W)$	Off-Normal – Wind with Thermal
5	$U_s > 1.1 (D + L + T_o + E)$	Accident – Earthquake
6	$U_s > 1.1 (D + L + T_o + W_t)$	Accident – Tornado
7	$U_s > 1.1 (D + L + T_o + FL)$	Accident – Flood
8	$U_s > 1.1 (D + L + T_a)$	Accident – Thermal

Table 2-8
EOS-TC Load Combinations and Service Levels

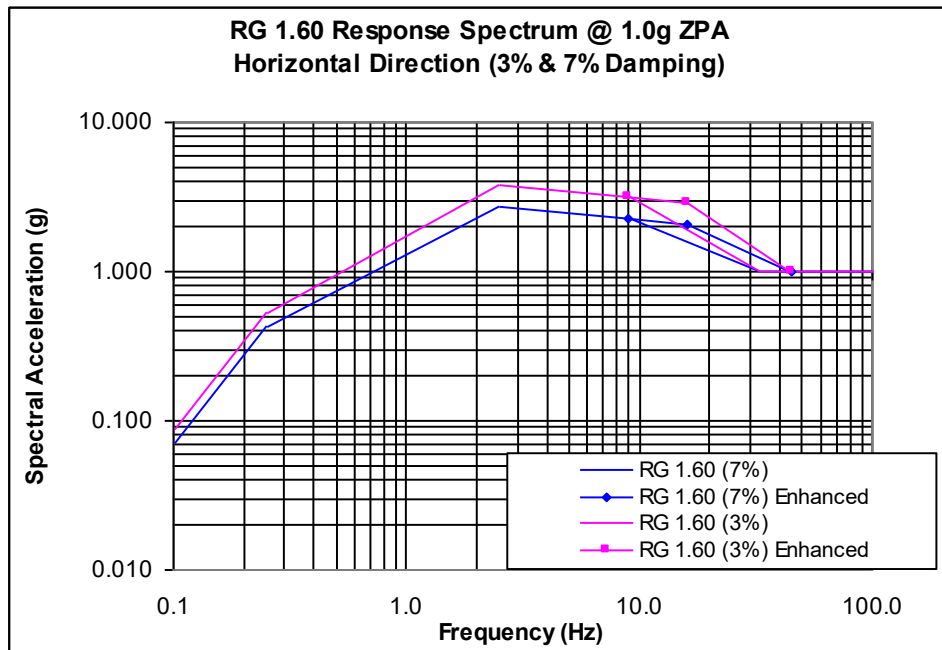
Load Case		Normal Conditions			Off-Normal			Accident Conditions			
		1	2	3	1	2	3	1	2	1	2
Dead Load / Live Load		X		X		X		X			
Thermal w/EOS-DSC	Normal	X	X	X							
	Off-normal				X	X					
Handling Loads (Critical Lifts)	Vertical	X									
	Downending	X									
	Horizontal	X									
Load Test	300% of Design Load						X				
Transfer Handling Loads	±1g Ax. + DW		X		X						
	±1g Tran. + DW		X		X						
	±1g Vert + DW		X		X						
	± ½g Ax. ± ½g Tran. ± ½g Vert + DW		X		X						
HSM Loading/ EOS-DSC Transfer	Normal (135k) Insertion			X		X					
	Normal (80k) Retrieval			X		X					
	"Accident" (135k) Insertion							X			
	"Accident" (135k) Retrieval							X			
Seismic	± 0.5g Ax. ± 0.5g Tran. ± 0.33g Vert +DW								X		
Drop Loads	65" Side Drop									X	
	65"End Drop										X
ASME Code Service Level		A	A	A	B	B	B	C	C	D	D
Load Combination Number		A1	A2	A3	B1	B2	B3	C1	C2	D1	D2

Table 2-9
Thermal Conditions for NUHOMS® EOS System Analyses

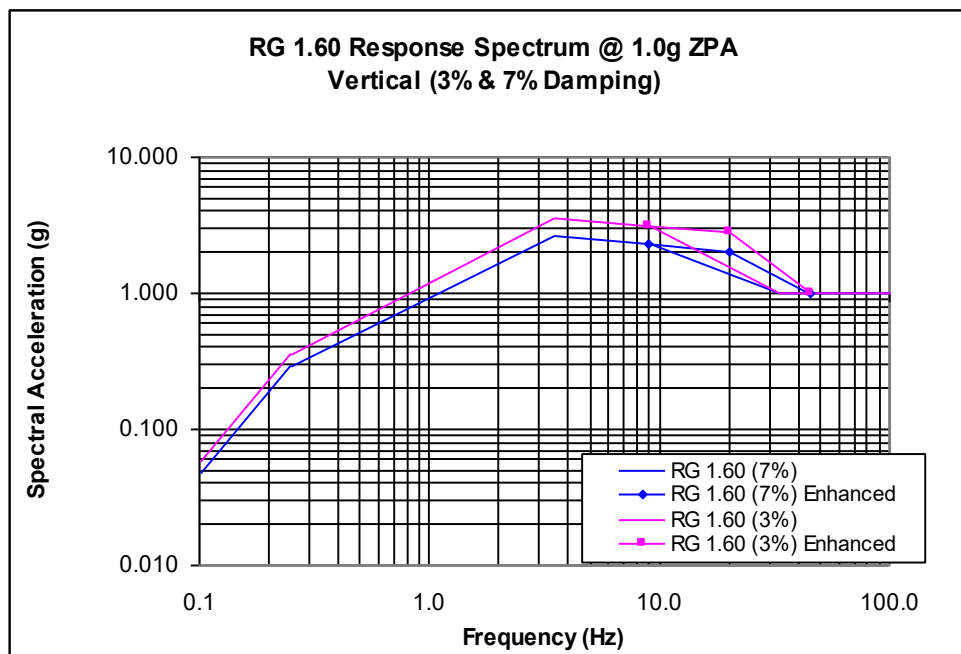
Operating Conditions	EOS-37PTH/EOS-89BTH DSC Location	Minimum Ambient Temperature	Maximum Ambient Temperature
Normal	Transfer Cask (Refuel Floor)	0 °F	120 °F
	Transfer Cask	0 °F	100 °F
	EOS-HSM/EOS-HSMS	-20 °F	Note 5
	Transportation Cask ⁽¹⁾	-20 °F	100 °F
Off-Normal	Transfer Cask	0 °F	117 °F
	EOS-HSM/EOS-HSMS	-40 °F	117 °F
	Transportation Cask	n/a	n/a
Accident	Transfer Cask ⁽²⁾	n/a	117 °F
	EOS-HSM/EOS-HSMS (Blocked inlet and outlet vents) ⁽³⁾	n/a	117 °F
	Transportation Cask ⁽¹⁾	-40 °F	100 °F

Notes:

1. For information only.
2. Loss of forced air, loss of neutron shield, ambient at 117 °F.
3. 10% rod rupture is considered for this blocked vent accident condition for DSC internal pressure calculation.
4. Assume pool water temperature = 125 °F.
5. For EOS-37PTH DSCs with a heat load less than or equal to 41.8kW, and EOS-89BTH DSCs with a heat load less or equal to 41.6 kW, the maximum ambient temperature is 100 °F. For EOS-37PTH DSCs with a heat load greater than 41.8 kW and EOS-89BTH DSCs with a heat load greater than 41.6 kW, maximum ambient temperatures are as discussed in Section 4.3.



RG 1.60 (3%, Horiz. Enhanced)	
Freq (Hz)	Acc. (g)
0.10	0.085
0.25	0.529
2.5	3.755
9.0	3.130
16.0	2.885
45.0	1.000
100.0	1.000
RG 1.60 (7%, Horiz. Enhanced)	
Freq (Hz)	Acc. (g)
0.10	0.069
0.25	0.432
2.5	2.720
9.0	2.270
16.0	2.093
45.0	1.000
100.0	1.000

HORIZONTAL

RG 1.60 (3%, Vert. Enhanced)	
Freq (Hz)	Acc. (g)
0.10	0.056
0.25	0.353
3.5	3.577
9.0	3.130
20.0	2.797
45.0	1.000
100.0	1.000
RG 1.60 (7%, Vert. Enhanced)	
Freq (Hz)	Acc. (g)
0.10	0.046
0.25	0.287
3.5	2.590
9.0	2.270
20.0	2.030
45.0	1.000
100.0	1.000

VERTICAL

Figure 2-1
RG 1.60 Response Spectra with Enhancement in Frequencies above 9.0 Hz

CHAPTER 3 STRUCTURAL EVALUATION

Table of Contents

3.	STRUCTURAL EVALUATION.....	3-1
3.1	Structural Design	3-2
3.1.1	Design Criteria	3-2
3.2	Weight and Centers of Gravity.....	3-5
3.3	Mechanical Properties of Materials	3-6
3.3.1	EOS-37PTH DSC/EOS-89BTH DSC	3-6
3.3.2	EOS-HSM	3-6
3.3.3	EOS-TC.....	3-6
3.4	General Standards for EOS System.....	3-7
3.4.1	Chemical and Galvanic Reaction.....	3-7
3.4.2	Positive Closure	3-7
3.4.3	Lifting Devices.....	3-7
3.4.4	Heat	3-7
3.4.5	Cold.....	3-15
3.5	Fuel Rods General Standards for NUHOMS® EOS System.....	3-16
3.5.1	Fuel Rod Temperature Limits.....	3-16
3.5.2	Fuel Assembly Thermal and Irradiation Growth	3-16
3.5.3	Fuel Rod Integrity during Drop Scenarios.....	3-16
3.6	Normal Conditions of Storage and Transfer.....	3-17
3.6.1	EOS-37PTH DSC/89BTH DSC	3-17
3.6.2	EOS-HSM	3-18
3.6.3	EOS-TC.....	3-19
3.7	Off-Normal and Hypothetical Accident Conditions of Storage and Transfer	3-20
3.7.1	EOS-37PTH DSC/89BTH DSC	3-20
3.7.2	EOS-HSM	3-22
3.7.3	EOS-TC.....	3-22
3.8	References	3-23

List of Tables

Table 3-1	Summary of Stress Criteria for Subsection NB Pressure Boundary Components Shells and Cover Plates	3-24
Table 3-2	EOS-37PTH/EOS-89BTH Basket Assembly Stress Criteria for Subsection NG Components.....	3-26
Table 3-3	Plate and Shell Type Support for Transfer Cask Structural Shell	3-28
Table 3-4	Structural Shell Structural Stress Criteria for Transfer Cask Bolts	3-31
Table 3-5	Structural Stress Criteria for Neutron Shield	3-32
Table 3-6	Summary of EOS-37PTH DSC Component Weights	3-33
Table 3-7	Summary of EOS-89BTH DSC Component Weights	3-34
Table 3-8	Summary of EOS-HSM Weight and Center of Gravity	3-34
Table 3-9	Summary of EOS-TC Component Weight	3-35

3. STRUCTURAL EVALUATION

This chapter and its appendices describe the structural evaluation of the NUHOMS® EOS System, described in Chapter 1, under normal and off-normal conditions, accident conditions, and natural phenomena events. Structural evaluations are performed for the important-to-safety components, which are the EOS-37PTH dry shielded canister (DSC), the EOS-89BTH DSC, the EOS horizontal storage module (EOS-HSM), and the EOS transfer casks (EOS-TCs). The DSC functions as the confinement boundary, and restrains and positions the fuel assemblies (FAs) in the DSC.

3.1 Structural Design

The NUHOMS® EOS System provides for the horizontal, dry storage of canisterized spent fuel assemblies (SFAs) in a concrete EOS horizontal storage module (HSM). The storage system components consist of a reinforced concrete EOS-HSM and a stainless or duplex steel DSC confinement vessel that houses the SFAs. A general description and operational features of the NUHOMS® EOS System is provided in Chapter 1, and the confinement boundary is defined in Chapter 5. This chapter addresses the structural design and analysis of the storage system components, including the EOS-37PTH DSC, the EOS-89BTH DSC, the TC135, the TC125, TC108, the EOS-HSM, and the EOS-HSMS, which are important-to-safety in accordance with 10 CFR Part 72 [3-13].

3.1.1 Design Criteria

3.1.1.1 EOS-37PTH DSC/EOS-89BTH DSC Design Criteria

The EOS-37PTH DSC/EOS-89BTH DSC are designed using the American Society of Mechanical Engineers (ASME) Boiler and Pressure Vessel (B&PV) Code, Section III, Division 1, Subsections NB, NG, NF, ND and NCA [3-2] criteria with the code Alternatives as described in Section 8.2.1.

3.1.1.1.1 Stress Criteria

EOS-37PTH DSC/EOS-89BTH DSC Shell Assembly Stress Limits

The stress limits for the DSC shell are taken from the ASME B&PV Code, Section III, Subsection NB, Article NB-3200 for Level A and B Service Limits [3-2]. In accordance with NB-3225, Appendix F is used for accident condition loads (Level D). Service Level A and B stress limits apply to normal and off-normal conditions, respectively, and Service Level D stress limits apply to accident conditions. Elastic system analysis is used for calculation of stresses for normal, off-normal, and accident conditions, except that plastic analysis is used for side drop accident conditions.

Stress limits for Level A, B and D service loading conditions are summarized in Table 3-1. The stress due to each load type is identified as to the type of stress induced, such as membrane or membrane plus bending, and classified accordingly as primary, secondary, peak, etc. Local yielding is permitted at the point of contact where Level D load is applied. In accordance with NB-3222, the plastic analysis provisions of NB-3228 may be used if the Level A Service Limits for local membrane stress intensity and/or primary membrane plus primary bending stress intensity are not satisfied.

Finite element, non-linear analysis models, or hand calculations using actual material properties, are used to calculate the critical buckling load of the DSC shell.

The allowable stress intensity value, S_m , as defined by the Code, is based on the calculated (or a bounding) temperature for each service load condition.

The DSC closure welds are designed in accordance with the guidance of NUREG-1536 [3-1], using a stress reduction factor of 0.8 on weld strength. Weld inspection interval requirements are based on calculation of critical flaw depth using ASME Section XI. See Section 8.4.7.4 of NUREG-1536.

EOS-37PTH/EOS-89BTH Basket Stress/Strain Limits

The basis for the steel basket stress allowables is the ASME Code, Section III, Subsection NG [3-2]. Stress limits for Level A through D service loading conditions are summarized in Table 3-2. The design stress intensity, S_m , is defined as the lower of $2/3S_y$ or $1/3 S_u$ (Appendix 2 of ASME B&PV, Section II [3-3]).

The hypothetical impact accidents are evaluated as short duration Level D conditions. Secondary and peak stresses are not required to be evaluated for Level D events, but should be evaluated to ensure that they are not a source of uncontrolled crack initiation. Appendix 3.9.2 classifies the rails as "non-code," and does not perform any stress analysis of the rail aluminum or steel plates. The membrane equivalent plastic strain in the steel grid plate is limited to 1%. Membrane + bending equivalent plastic strain is limited to 3% and peak equivalent plastic strain is limited to 10%. This ensures that displacement and permanent deformation of the steel grid is small and within failure limits for high-strength low-alloy steel such as American Iron and Steel Institute (AISI) 4130 material.

3.1.1.1.2 Stability Criteria

Stability of the EOS-37PTH DSC/EOS-89BTH DSC shell assembly is addressed for load conditions in which the DSC is under external hydrostatic pressure (such as vacuum drying and external flood load cases) and/or axial compression, (e.g., loading the shell due to the shield plug's dead weight). Stability criteria are from ASME Section III, NB-3133.3 and NB-3133.6 [3-2].

3.1.1.2 EOS-HSM Design Criteria

The EOS-HSM concrete and steel components are designed to the requirements of American Concrete Institute (ACI) 349-06 [3-4] and the American Institute of Steel Construction (AISC) Manual of Steel Construction [3-5], respectively, meeting the load combinations in accordance with the requirements of ANSI 57.9 [3-6]. The load combination and design criteria for concrete and support structure components are described in Appendix 3.9.4.

3.1.1.3 EOS-TC Design Criteria

The onsite TC is a non-pressure retaining component, which is conservatively designed by analysis to meet the stress allowables of the ASME Code [3-2] Subsection NF Class 1 criteria. Service Levels A and B allowables are used for all normal operating and off-normal loadings. Service Levels C and D allowables are used for load combinations that include postulated accident loadings. Stress limits for Level A, B, C and D service loading conditions are summarized in Table 3-3. The stress due to each load type is identified as to the type of stress induced and classified accordingly. Allowable stress limits for the upper lifting trunnions and lower trunnion sleeves are conservatively developed to meet the requirements of ANSI N14.6- 1993 [3-7] for a non-redundant lifting device for all cask movements within the fuel/reactor building.

The TC structural design criteria are summarized in Table 3-3, Table 3-4 and Table 3-5.

3.2 Weight and Centers of Gravity

Table 3-6 through Table 3-9 summarize the bounding weights of the various components in the NUHOMS® EOS system. The dead weights of the components are determined based on nominal dimensions.

3.3 Mechanical Properties of Materials

3.3.1 EOS-37PTH DSC/EOS-89BTH DSC

Material properties for EOS-37PTH DSC and EOS-89BTH DSC are summarized in Chapter 8.

The analyses are performed based on the least favorable set of properties to ensure that the analysis results are conservative. For example, for stress analysis it is conservative to use the minimum stress intensity allowables.

3.3.2 EOS-HSM

The material properties for the EOS-HSMs are summarized in Chapter 8.

3.3.3 EOS-TC

The material properties for EOS-TCs are summarized in Chapter 8, and are taken from the ASME B&PV Code, Section II, Part D [3-3].

3.4 General Standards for EOS System

3.4.1 Chemical and Galvanic Reaction

Chemical and galvanic reactions for the NUHOMS® EOS System are presented in Chapter 8.

3.4.2 Positive Closure

Positive closure is provided by the the presence of redundant closure welds in the DSC, which precludes unintentional opening.

3.4.3 Lifting Devices

There are no permanent lifting devices used for lifting a loaded DSC. The loaded DSC is inside a TC during handling.

The evaluation of upper trunnions is performed in the EOS -TC body analysis (see Appendix 3.9.5).

3.4.4 Heat

3.4.4.1 Summary of Pressures and Temperatures

Temperatures and pressures for the NUHOMS® EOS System are described in Chapter 4. The thermal evaluations for storage and transfer conditions are performed in Chapter 4 for normal, off-normal, and accident conditions. The internal pressure evaluation is performed in Chapter 4, Section 4.7.

Maximum temperatures for the various components of the EOS-HSM, loaded with EOS-37PTH DSC and EOS-89BTH DSC under normal, off-normal and accident conditions are summarized in Table 4-5, Table 4-6, Table 4-17 and Table 4-18.

These temperatures are used for the structural evaluations documented in Appendices 3.9.1 through 3.9.6. Stress allowables for the components are a function of component temperature. The temperatures used to perform the structural analyses are based on actual calculated temperatures or conservatively selected higher temperatures.

3.4.4.2 Differential Thermal Expansion

Clearances are provided between the various components of the DSC to accommodate differential thermal expansion and to minimize thermal stress. The radial direction clearance is provided between the basket outer diameter and DSC shell inside diameter, and between the poison/aluminum plates and the interfacing basket components. In the axial direction, clearances are provided between the DSC cavity and all the basket parts. Additionally, the connections between the transition rails and the fuel support structure are designed to permit relative axial growth.

The thermal analyses of the basket for handling/transfer conditions are described in Chapter 4. The thermal analyses are performed to determine the basket/DSC temperatures and thermal expansion for -40 °F ambient, 0 °F ambient, 117 °F ambient, and vacuum drying conditions. The temperatures are used to evaluate the effects of axial and radial thermal expansion in the basket/DSC components

To verify that adequate clearance exists, the thermal expansion of different components are calculated in the following sections.

3.4.4.2.1 Minimum Gaps within the Interlocking Slots

EOS-37PTH DSC

The EOS-37PTH DSC basket assembly is made up of interlocking slotted plates to form an egg-crate type structure. To avoid interference between the perpendicular plates, the width of the slots is varied between the various basket assembly plates. This section presents the thermal expansion evaluation to demonstrate that the aluminum/metal matrix composite (MMC) plates do not extend past the steel plates at the interlocking slot location.

To avoid any interference between the perpendicular basket assembly plates, the location of slots within the aluminum/MMC plates should not extend past the location of the slots within the steel plates. The thermal expansion of the basket assembly plates is calculated as:

$$L_{Hot,i} = L_{Cold,i} + [L_{Cold,i} \times \alpha_i (T_{avg,B} - T_{ref})]$$

Where,

$L_{Hot,i}$ = Hot length of the steel plates ($L_{Hot,St}$) and the aluminum plates ($L_{Hot,Al}$)

$L_{Cold,i}$ = Cold length of the steel plates ($L_{Cold,St}$) and the aluminum plates ($L_{Cold,Al}$)

α_i = Thermal expansion coefficient of the steel (α_{St}) and aluminum plates (α_{Al}) at $T_{avg,B}$

$T_{avg,B}$ = Average temperature of the basket assembly plates based at hottest cross section

T_{ref} = Reference ambient temperature

The minimum gap between each location of the slots within the steel plates and the location of the slots within the aluminum/MMC plates is calculated as:

$$\Delta_{St-Al} = L_{Hot,St} - L_{Hot,Al}$$

The minimum gap between the slots of the steel plates with aluminum/MMC plates is 0.01 inch. Therefore, the slots within the aluminum/MMC plates provide sufficient space to accommodate any differential thermal growth.

EOS-89BTH DSC

Similar to the EOS-37PTH DSC design, the minimum gaps between the slots of the steel plates with aluminum/MMC plates is calculated to be 0.02 inch. Therefore, the slots within the aluminum/MMC plates provide sufficient space to accommodate any differential thermal growth.

3.4.4.2.2 Axial Gaps between the Basket Assembly Plates

EOS-37PTH DSC

To accommodate the axial thermal growth between the various basket assembly plates, the aluminum/MMC plates are designed to be smaller than the paired steel plates. Each aluminum/MMC plate and the steel plates have a nominal cold gap of 0.06 inch.

Similar to Section 3.4.4.2.1, the hot gap between the steel and aluminum/MMC plates due to the axial thermal expansion of the basket assembly plates is 0.015 inch. There is sufficient clearance for the thermal growth of aluminum/MMC plates.

EOS-89BTH DSC

Similar to the EOS-37PTH DSC design, the minimum gaps between the steel and aluminum/MMC plates due to the axial thermal expansion of the basket assembly plates is 0.015 inch. Therefore, the slots within the aluminum/MMC plates provide sufficient space to accommodate any differential thermal growth.

3.4.4.2.3 Radial Gap between the Basket Assembly and the DSC Shell

EOS-37PTH DSC

The nominal diametrical cold gap between the basket rails and the EOS-37PTH DSC shell is 0.40 inches. The hot diametrical gap is calculated as:

$$ID_1 = ID_{SHELL} \cdot [1 + \alpha_{SHELL} (T_{avg, SHELL} - 70)] - \sum_{n=1}^N L_n [1 + \alpha_n \cdot (T_{avg, n} - 70)]$$

Where,

ID_{SHELL}	is the DSC shell inner diameter
$T_{avg, SHELL}$	is the DSC shell volumetric average temperature
n	represents a basket component rail

N is total number of components considered

L_n is the nominal length of basket component n in the radial direction

$T_{avg, n}$ is the volumetric average temperature of basket component n

α_n is the expansion coefficient of basket component n at T_n

$$\text{Hot Radial Gap} = ID_1 / 2$$

Using the above-formula and bounding conditions, the minimum hot radial gap (clearance) is calculated as 0.065 inch. Therefore, there is no interference between the basket and the DSC shell.

EOS-89BTH DSC

Similar to EOS-37PTH DSC, the minimum hot radial gap (clearance) for the EOS-89BTH DSC is calculated as 0.067 inch. Therefore, there is no interference between the basket and the DSC shell.

3.4.4.2.4 Axial Gaps between Fuel Assemblies and the DSC Cavity

EOS-37PTH DSC

To accommodate this variation in the axial length, and also due to the effect of various parameters such as burnup or irradiation growth on the FA, this evaluation considers one approach to determine the minimum gap and is repeated for each type of FA and the DSC size.

The DSC cavity length is chosen to ensure a minimum of 1-inch cold gap exists as a starting point and is verified to ensure that no interference exists as described below. Furthermore, if available, the methodology presented below to determine the irradiation growth can be replaced with an appropriate methodology from the license.

A bounding average temperature is used in determining the thermal expansion for the fuel assemblies. The hot length of the fuel assemblies within the EOS-37PTH DSC is calculated as:

$$L_{Fuel, Total, Hot} = L_{Fuel, Hot} + L_{Fuel, Irrad}$$

Where,

$L_{Fuel, Hot}$ = Total hot length of un-irradiated FA

$L_{Fuel, Irrad}$ = Net irradiation growth of the FA

The total hot length of the FA without irradiation growth is:

$$L_{Fuel,Hot} = L_{Fuel,Cold} + \alpha_{Zr} \cdot L_{Fuel,Cold}$$

Where,

α_{Zr} = Zircaloy axial thermal expansion

T_{Zr} = Average temperature of Zircaloy (FA)

$L_{Fuel,Cold}$ = Maximum cold length of the un-irradiated FA

The irradiation growth model presented in equation 3.7-2 of [3-9] for a PWR fuel rod is:

$$\Delta x = 2.18 \times 10^{-21} \times \Phi^{0.845}$$

Where,

Δx = irradiation growth (m/m) or (in/in)

Φ = fast neutron fluence (n/cm²) (E > 1.0 MeV).

However, FA designs include gaps to accommodate a portion of the irradiation growth without increasing the overall length.

$$L_{Fuel,Irrad} = L_{Fuel,Irrad,Total} - L_{Fuel,Gap}$$

The total hot length of the fuel, including the net irradiation growth is:

$$L_{Fuel,Total,Hot} = L_{Fuel,Hot} + L_{Fuel,Irrad}$$

The length of the DSC cavity is calculated as:

$$L_{DSC,Cav,Hot} = L_{DSC,Cav} \cdot [1 + \alpha_{DSC} \cdot (T_{DSC} - 70)]$$

Where,

α_{DSC} = Coefficient of thermal expansion for DSC shell

T_{DSC} = Average temperature of DSC shell

$L_{DSC,Cav}$ = Cold length of the DSC Cavity

The bounding gap between the irradiated fuel assemblies and the DSC cavity is calculated as:

$$\Delta_{FA-DSC\ Cav} = L_{DSC,Cav,Hot} - L_{Fuel,Total,Hot}$$

Using the approach presented above, it would be ensured that a positive gap exists to avoid any interference between the FAs and the DSC cavity.

EOS-89BTH DSC

Similar to EOS-37PTH DSC, the minimum axial gap (clearance) between the FAs and the DSC cavity is calculated.

3.4.4.2.5 Axial Gap between the Basket Assembly and the DSC Cavity

EOS-37PTH DSC

The following steps present the methodology to determine a bounding cold gap between the basket assembly and the DSC cavity that will encompass any variations due to the different FAs.

1. The maximum hot lengths of the basket assembly are calculated for a nominal cold length and a maximum cold length

$$L_{BSK,Nom,Hot} = L_{BSK,Nom} \cdot [1 + \alpha_{Bsk} \cdot (T_{Bsk} - 70)]$$

$$L_{BSK,Long,Hot} = L_{BSK,Long} \cdot [1 + \alpha_{Bsk} \cdot (T_{Bsk} - 70)]$$

Where,

α_{Bsk} = Coefficient of thermal expansion of basket assembly

T_{Bsk} = Average temperature of basket assembly

$L_{Bsk,Nom}$ = Nominal cold length of the basket assembly

$L_{Bsk,Long}$ = Maximum cold length of the basket assembly

2. Assuming a zero gap under hot conditions, the maximum hot length of the DSC cavity is assumed to be equal to the hot length of the basket assembly.

$$L_{BSK,Nom,Hot} = L_{DSC,Nom,Hot}$$

$$L_{BSK,Long,Hot} = L_{DSC,Long,Hot}$$

Where,

$L_{DSC,Nom,Hot}$ = Nominal hot length of the DSC cavity

$L_{DSC,Long,Hot}$ = Maximum hot length of the DSC cavity

3. Using the hot length of the DSC cavity, the cold lengths of the DSC cavity are determined as:

$$L_{DSC,Nom} = \frac{L_{DSC,Nom,Hot}}{1 + \alpha_{DSC} \cdot (T_{DSC} - 70)}$$

$$L_{DSC,Long} = \frac{L_{DSC,Long,Hot}}{1 + \alpha_{DSC} \cdot (T_{DSC} - 70)}$$

Where,

$L_{DSC,Nom}$ = Nominal Cold length of the DSC cavity

$L_{DSC,Long}$ = Maximum Cold length of the DSC cavity

4. The net gap at cold conditions between the DSC cavity and the basket assembly is determined.

$$\Delta_{DSC-Bsk,Nom} = L_{DSC,Nom} - L_{Bsk,Nom}$$

$$\Delta_{DSC-Bsk,Long} = L_{DSC,Long} - L_{Bsk,Long}$$

5. As long as the cold gap calculated in Step 4 is maintained, there will be no interference under hot conditions.

To bound any uncertainties a minimum axial cold gap of 0.6 inch is recommended between the DSC cavity and the basket assembly.

EOS-89BTH DSC

Similar to EOS-37PTH DSC, the minimum axial cold gap of 0.6 inch is recommended between the DSC cavity and the basket assembly.

3.4.4.2.6 Axial Gap between the Transition Rails and the DSC Cavity

EOS-37PTH DSC

To determine the bounding cold gap to avoid interference between the transition rails and the EOS-37PTH DSC cavity, the steps outlined in Section 3.4.4.2.5 are repeated for the transition rails.

To bound any uncertainties a minimum axial cold gap of 1.2 inches is recommended between the DSC cavity and the transition rails.

EOS-89BTH DSC

Similar to EOS-37PTH DSC, the minimum axial cold gap of 1.2 inches is recommended between the DSC cavity and the transition rails.

3.4.4.2.7 Axial Gap between the TC125/TC135 Cavity and the DSC Shell

EOS-37PTH DSC

To determine the bounding cold gap to avoid interference between the EOS-TC and the EOS-37PTH DSC cavity, the steps outlined in Section 3.4.4.2.5 are repeated for the EOS-TC cold gap.

To bound any uncertainties, a minimum axial cold gap of 0.6 inch in is recommended between the TC cavity and the DSC shell, including the cask spacer.

EOS-89BTH DSC

Similar to EOS-37PTH DSC, the minimum axial cold gap of 0.6 inch is recommended between the TC cavity and the DSC shell including the cask spacer.

3.4.4.2.8 Axial Gap between the EOS-HSM Support Structure and the EOS-HSM Cavity

EOS-37PTH DSC/EOS-89BTH DSC

A 1-inch gap is provided between the EOS-HSM support structure and the EOS-HSM cavity to accommodate any thermal growth. This section verifies that there is no interference between the EOS-HSM cavity and the support structure.

The maximum support structure temperature ($T_{EOS-HSM,SS}$) and is selected to determine the maximum length of support structure within EOS-HSM long cavity. The maximum support structure temperature is conservatively applied as the average temperature as it maximizes the thermal expansion.

The thermal growth of the support structure is determined as:

$$\Delta L_{EOS-HSM,SS,Hot} = L_{EOS-HSM,SS,Cold} \times \alpha_{EOS-HSM,SS} \times (T_{EOS-HSM,SS} - 70)$$

Where,

$L_{EOS-HSM,SS,Cold}$ = Cold length of the EOS-HSM long support structure ,

$\alpha_{EOS-HSM,SS}$ = Thermal expansion coefficient for EOS-HSM support structure

$T_{EOS-HSM,SS}$ = Maximum EOS-HSM support structure temperature.

The maximum thermal growth of the EOS-HSM support structure is 0.46 inch and is less than the 1-inch gap. Therefore, sufficient clearance exists within the EOS-HSM cavity for free thermal expansion of the support structure.

3.4.5 Cold

Impact on material properties of cold ambient temperatures is discussed in Chapter 8. Structural analyses performed for all components account for both hot and cold ambient conditions.

3.5 Fuel Rods General Standards for NUHOMS® EOS System

This section provides the temperature criteria used in the EOS-37PTH DSC and EOS-89BTH DSC thermal evaluation for the safe storage and handling of SFAs in accordance with the requirements of 10 CFR Part 72 [3-13]. This section also contains the analysis of the thermal and irradiation growth of the FAs to ensure adequate space exists within the EOS-37PTH DSC and EOS-89BTH DSC cavity for the FAs to grow thermally under all conditions. In addition, this section provides an evaluation of the fuel rod stresses due to accident drop loads.

3.5.1 Fuel Rod Temperature Limits

The fuel rod temperature limits during transfer operation and storage are defined by Interim Staff Guidance, ISG-11, Revision 3 [3-11]. The temperature limits are summarized in the following table.

Transfer		Storage	
Normal/Off-Normal	Accident	Normal	Off-Normal / Accident
752 °F	1058 °F	752 °F	1058 °F

3.5.2 Fuel Assembly Thermal and Irradiation Growth

The thermal and irradiation growth of the FAs were calculated to ensure that there is adequate space for the FAs to grow within the cavity of the EOS-37PTH DSC and EOS-89BTH DSC. Detailed thermal expansion evaluations of the DSC cavity versus lengths of the basket and the FA, the DSC internal diameter (ID) versus the basket outer diameter (OD), the DSC OD versus the TC ID, and the overall length of the DSC versus the TC cavity length are included in Section 3.4.4.2.

3.5.3 Fuel Rod Integrity during Drop Scenarios

The fuel rod integrity is demonstrated in Appendix 3.9.6.

3.6 Normal Conditions of Storage and Transfer

This section presents the structural analyses of the EOS-37PTH DSC/ EOS-89BTH DSC, the EOS-HSM and the EOS-TC subjected to normal conditions of storage and transfer. The analyses performed evaluate these three major NUHOMS® EOS System components for the design criteria described in Section 3.1.1.

The EOS-37PTH DSC/EOS-89BTH DSC are subjected to both storage and transfer loading conditions, while the EOS-HSM is only subjected to storage loading conditions and the EOS-TC is only subjected to transfer loading conditions.

Numerical analyses have been performed for the normal and accident conditions, as well as for the lifting loads. In general, numerical analyses have been performed for the regulatory events. These analyses are summarized in this section, and described in detail in Appendix 3.9.1 through 3.9.7.

The detailed structural analysis of the NUHOMS® EOS System is included in the following appendices:

- Appendix 3.9.1 DSC Shell Structural Analysis
- Appendix 3.9.2 EOS-37PTH and EOS-89BTH Basket Structural Analysis
- Appendix 3.9.3 NUHOMS® EOS System Accident Drop Evaluation
- Appendix 3.9.4 EOS-HSM Structural Analysis
- Appendix 3.9.5 NUHOMS® EOS-TC Body Structural Analysis
- Appendix 3.9.6 NUHOMS® EOS Fuel Cladding Evaluation
- Appendix 3.9.7 NUHOMS® EOS System Stability Analysis

3.6.1 EOS-37PTH DSC/89BTH DSC

The basket and DSC shell are analyzed independently. Details of the structural analyses of the EOS-37PTH DSC and EOS-89BTH DSC shell assemblies are provided in Appendix 3.9.1, while the structural analyses for the basket assemblies are provided in Appendix 3.9.2.

3.6.1.1 EOS-37PTH DSC/89BTH DSC Shell Normal Condition Structural Evaluation

This section summarizes the evaluation of the structural adequacy of the EOS-37PTH DSC and EOS-89BTH DSC under all applied normal condition loads. Detailed evaluation of the stresses generated in the DSC is presented in Appendix 3.9.1. The DSC shell buckling evaluation is presented in Appendix 3.9.1.

An enveloping technique of combining various individual loads in a single analysis is used in this evaluation for several load combinations. This approach greatly reduces the number of computer runs while remains conservative. For some load combinations, the stress intensities under individual loads are added to obtain resultant stress intensities for the specified combined loads. This stress addition at the stress intensity level for the combined loads, instead of at the component stress level, is also a conservative way to reduce the number of analysis runs.

Elastic and elastic-plastic analyses are performed to calculate the stresses in the EOS-37PTH DSC under the transfer and storage loads. These detailed load cases are summarized in Appendix 3.9.1.

Based on the results of these analyses, the design of the EOS-37PTH DSC/EOS-89BTH DSC canister is structurally adequate with respect to both transfer and storage loads under normal conditions.

3.6.1.2 EOS-37PTH DSC/89BTH DSC Basket Normal Condition Structural Evaluation

The fuel basket stress analysis is performed for normal conditions loads during fuel transfer and storage. The detailed stress analysis is presented in Appendix 3.9.2. A summary of the fuel basket load cases is provided in Appendix 3.9.2. The basket stress analysis is performed using a finite element method for the transfer handling, storage dead weight, and both transfer and storage thermal load cases. The finite element model (FEM) is described in detail in Appendix 3.9.2.

Basket component stress results for normal condition dead weight + handling loads are listed in Appendix 3.9.2. Thermal stress analysis results are listed in Appendix 3.9.2. Combined results with controlling stress ratios are listed in Appendix 3.9.2.

Based on the results of these analyses, the design of the EOS-37PTH DSC/ EOS-89BTH DSC basket is structurally adequate with respect to both transfer and storage loads under normal conditions.

3.6.2 EOS-HSM

The EOS-HSM design has variable lengths to accommodate DSC lengths. For the structural evaluation, EOS-HSM Long bounds the three sizes. The following table shows how the bounding loads are used for structural evaluation of the EOS-HSM.

Component	Weight (kips)	Thermal Heat Load
EOS-37PTH DSC (Loaded Weight)	134	50 kW
EOS-89BTH DSC (Loaded Weight)	120	43.6 kW
Bounding EOS-HSM	135 ⁽²⁾	50 kW ⁽¹⁾

Notes:

1. The thermal loading condition of the EOS-HSM is based on the most conservative thermal loading configuration.
2. For stability evaluation, several different combinations of DSC and HSM bounding weights are considered.

Detailed geometry descriptions, material properties, loadings, and structural evaluation for the EOS-HSM is presented in Appendix 3.9.4.

3.6.3 EOS-TC

Details of the structural analysis of the EOS-TC are provided in Appendices 3.9.3 and 3.9.5.

The details of the structural analyses of the EOS-TC body, including the cylindrical shell assembly and bottom assembly, the top cover, and the local stresses at the trunnion/cask body interface are presented in Appendix 3.9.5. The specific methods, models and assumptions used to analyze the cask body for the various individual loading conditions specified in 10 CFR Part 72 [3-13] are described in that appendix.

The EOS-TC body structural analyses use static or quasistatic linear elastic methods. The stresses and deformations due to the applied loads are determined using the ANSYS [3-12] computer program.

Appendix 3.9.5 presents the evaluation of the trunnion stresses in the EOS-TC due to all applied loads during fuel loading and transfer operations.

Based on the loading and transfer scenario, the top trunnions are analyzed per ANSI N14.6 [3-7] for vertical lifting loads.

The evaluations summarized in Appendix 3.9.5 show that all calculated trunnion stresses are less than their corresponding allowable stresses. Therefore, the EOS-TC top and bottom trunnions are structurally adequate to withstand loads during lifting and transfer operations.

Appendix 3.9.5 presents the evaluation of the stresses in the EOS-TC neutron shield shell due to all applied loads during fuel loading and transfer operations. An FEM was built for the structural analysis of the neutron shield shell, end closure, central plates and structural shell. These structural components were modeled with ANSYS shell elements.

Appendix 3.9.5 summarizes the calculated stresses for the EOS-TC neutron shield shell. Based on the results of the analysis, it is concluded that the outer neutron shield shell structure is structurally adequate for the specified transfer loads.

3.7 Off-Normal and Hypothetical Accident Conditions of Storage and Transfer

This section presents the structural analyses of the EOS-37PTH DSC and EOS-89BTH DSC, the EOS-HSM and the EOS-TC subjected to off-normal and hypothetical accident conditions of storage and transfer. These analyses are summarized in this section, and described in detail in Appendices 3.9.1 through 3.9.7.

3.7.1 EOS-37PTH DSC/89BTH DSC

The basket and DSC shell are analyzed independently. Details of the structural analyses of the EOS-37PTH DSC and EOS-89BTH DSC shell assemblies are provided in Appendix 3.9.1, while the structural analyses for the basket assemblies are provided in Appendix 3.9.2. Accident drop loads are analyzed using ANSYS quasi-static analysis methods with deceleration values that bound those obtained from the LS-DYNA analyses of Appendix 3.9.3.

LS-DYNA evaluations are also performed for drop conditions. The analysis includes DSC (DSC shell and basket) and TC. The details of the analysis are presented in Appendix 3.9.3. Two scenarios are analyzed for the drop conditions: a side drop and a corner drop. The drop height is based on the 65-inch height of the transfer trailer on which the EOS-TC is transferred.

3.7.1.1 EOS-37PTH DSC/89BTH DSC Shell Off-Normal/Accident Condition Structural Evaluation

This section summarizes the evaluation of the structural adequacy of the EOS-37PTH DSC shell and EOS-89BTH DSC shell under all applied off-normal and accident condition loads.

3.7.1.1.1 Stress Analysis

An enveloping technique of combining various individual loads in a single analysis is used in this evaluation for several load combinations. This approach greatly reduces the number of computer runs, while remaining conservative. However, for some load combinations, the stress intensities under individual loads are added to obtain resultant stress intensities for the specified combined loads. This stress addition at the stress intensity level for the combined loads, instead of at component stress level, is also a conservative way to reduce numbers of analysis runs.

Elastic and elastic-plastic analyses are performed to calculate the stresses in the EOS-37PTH DSC/EOS-89BTH DSC under the off-normal and accident loads. These load cases are summarized in Appendix 3.9.1. All side drop loads are analyzed by elastic-plastic analyses and the rest by elastic analyses.

The calculated stresses in the DSC shell due to off-normal and accident transfer loading conditions are summarized in Appendix 3.9.1. The stresses due to accident storage loading conditions are summarized in Appendix 3.9.1.

Based on the results of these analyses, the design of the EOS-37PTH DSC/EOS-89BTH DSC is structurally adequate with respect to off-normal and accident condition transfer and storage loads.

3.7.1.1.2 Buckling Analysis

This section summarizes the evaluation of EOS-37PTH DSC and EOS-89BTH DSC against buckling under a vertical end drop during transfer operations. The detail of the DSC shell buckling analysis is provided in Appendix 3.9.1. A finite element plastic analysis with large displacement option is performed to monitor the occurrence of DSC shell buckling under the specified loads.

The thermal evaluation presented in Chapter 4 shows that the metal temperatures of the entire DSC are below 500 °F during the transfer operations. The material properties of the DSC at 500 °F are, therefore, conservatively used for the DSC buckling analysis.

The FEM of the DSC described in Appendix 3.9.1 for the DSC stress analysis is used for this analysis. Since the top end of the DSC is heavier than the bottom end, it is a more severe case when the DSC drops on its bottom end. A bottom end drop is therefore chosen for analysis in this calculation. The DSC shell does not buckle up to a load of 130g. For further details about the results refer Appendix 3.9.1.

3.7.1.2 EOS-37PTH DSC/89BTH DSC Basket Off-Normal/Accident Condition Structural Evaluation

This section summarizes the evaluation of the structural adequacy of the EOS-37PTH DSC and EOS-89BTH DSC baskets under all applied off-normal and accident condition loads.

The basket analyses are performed for off-normal/accident condition loads during fuel transfer and storage. The detailed analyses are presented in Appendix 3.9.2. A summary of the fuel basket load cases is provided in Appendix 3.9.2. The basket analyses are performed using a finite element method for the off-normal transfer and storage thermal load cases and for the accident side drop load cases. The finite element models (FEM) are described in detail in Appendix 3.9.2. Basket component stress and strain results for off-normal thermal and accident drop condition loads, respectively, are listed in Appendix 3.9.2. Combined results with controlling stress and strain ratios are listed in Appendix 3.9.2. Based on the results of these analyses, the EOS-37PTH DSC/ EOS-89BTH DSC basket designs are structurally adequate with respect to both off-normal and accident loads. The DSC basket buckling evaluation is also presented in Appendix 3.9.2.

3.7.2 EOS-HSM

This section summarizes the evaluation of the structural adequacy of the EOS-HSM under all applied off-normal and accident condition loads. Detailed evaluation of the geometry descriptions, material properties, loadings, and structural evaluation for the EOS-HSM is presented in Appendix 3.9.4.

3.7.3 EOS-TC

The main accident condition for the EOS-TC is the drop load combination, which is analyzed via a LS-DYNA analysis. The details of the analysis is presented in Appendix 3.9.3. All other off-normal and accident load cases that are not bounded by the normal condition analyses are presented in Appendix 3.9.5.

3.8 References

- 3-1 NUREG-1536, Revision 1, “Standard Review Plan for Spent Fuel Dry Cask Storage Systems at a General License Facility,” July 2010.
- 3-2 American Society of Mechanical Engineers, “ASME Boiler and Pressure Vessel Code,” Section III, Division 1, Subsections NB, NG, NF, ND and NCA, 2010 Edition through 2011 Addenda.
- 3-3 American Society of Mechanical Engineers, “ASME Boiler and Pressure Vessel Code,” Section II, Materials Specifications, Parts A, B, C and D, 2010 Edition through 2011 Addenda.
- 3-4 ACI 349-06, “Code Requirements for Nuclear Safety Related Concrete Structures,” American Concrete Institute, November 2006.
- 3-5 American Institute of Steel Construction, “AISC Manual of Steel Construction,” 13th Edition or later.
- 3-6 ANSI/ANS 57.9-1984, “Design Criteria for an Independent Spent Fuel Storage Installation (Dry Storage Type),” American National Standards Institute.
- 3-7 ANSI N14.6-1993, “American National Standard for Special Lifting Device for Shipping Containers Weighing 10,000 lbs. or More for Nuclear Materials,” American National Standards Institute.
- 3-8 U.S. Nuclear Regulatory Commission, Regulatory Guide 1.124, “Service Limits and Loading Combination for Class 1 Linear-Type Supports,” February 2007.
- 3-9 NUREG/CR-7024, “Material Property Correlations: Comparisons between FRAPCON-3.4, FRAPTRAN 1.4, and MATPRO,” U.S. Nuclear Regulatory Commission, August 2010.
- 3-10 Nuclear Assurance Corporation, “Domestic Light Water Reactor Fuel Design Evolution,” Volume III, 1981.
- 3-11 U.S. Nuclear Regulatory Commission Interim Staff Guidance No. 11, Revision 3, “Cladding Considerations for the Transportation and Storage of Spent Fuel,” November 17, 2003.
- 3-12 “ANSYS Computer Code and User’s Manual”, Release 14.0.3.
- 3-13 Title 10, Code of Federal Regulations, Part 72, “Licensing Requirements for the Storage of Spent Fuel in the Independent Spent Fuel Storage Installation,” U.S. Nuclear Regulatory Commission, August 3, 1988.
- 3-14 NUREG/CR-6007, “Stress Analysis of Closure Bolts for Shipping Casks,” U.S. Nuclear Regulatory Commission, 1993.

Table 3-1
Summary of Stress Criteria for Subsection NB Pressure Boundary
Components
Shells and Cover Plates
 2 Pages

Service Level	Stress Category	References	Notes
Design (NB-3221)	$P_m \leq 1.0S_m$ $P_L \leq 1.5S_m$ $P_m (or P_L) + P_b \leq 1.5S_m$ $F_p \leq 1.0S_y or 1.5S_y$ $\sigma_1 + \sigma_2 + \sigma_3 \leq 4S_m$ External Pressure: NB-3133	NB-3221.1, NB-3221.2, NB 3221.3, NB 3227.1 and NB-3227.4	2 and 8
Level A (NB-3222)	$P_m \leq 1.0S_m$ $P_L \leq 1.5S_m$ $P_m (or P_L) + P_b \leq 1.5S_m$ $P_m (or P_L) + P_b + Q \leq 3.0S_m$ $F_p \leq 1.0S_y or 1.5S_y$ $\sigma_1 + \sigma_2 + \sigma_3 \leq 4S_m$ External Pressure: NB-3133	NB-3222, NB-3227.1, and NB-3227.4	1, 2 and 8
Level B (NB-3223)	$P_m \leq 1.0S_m$ $P_L \leq 1.5S_m$ $P_m (or P_L) + P_b \leq 1.5S_m$ $P_m (or P_L) + P_b + Q \leq 3.0S_m$ $F_p \leq 1.0S_y or 1.5S_y$ $\sigma_1 + \sigma_2 + \sigma_3 \leq 4S_m$ External Pressure: NB-3133	NB-3223, NB-3227.1, and NB-3227.4	8
Carbon Steel Components (e.g., shield plugs)			
Level D Elastic Analysis (NB-3225, App. F)	$P_m \leq 0.7S_u$ $P_m (or P_L) + P_b \leq 1.0S_u$ $P_m + P_b + Q \leq note 4$ $F_p \leq note 5$ External Pressure = 1.5 * NB-3133	NB-3225, F-1331.1, and F-1331.5(b)	Note 6

Table 3-1
Summary of Stress Criteria for Subsection NB Pressure Boundary
Components
Shells and Cover Plates
 2 Pages

Service Level	Stress Category	References	Notes
Level D Plastic Analysis (NB-3225, App. F)	$P_m \leq 0.7S_u$ $P_m \text{ (or } P_L) + P_b \leq 0.9S_u$ $P_m + P_b + Q \leq \text{note 4}$ $F_p \leq \text{note 5}$ External Pressure = 1.5 * NB-3133	NB-3225, F-1341.2, and F-1331.5(b)	Note 6
Austenitic Steel Components (e.g., Shell)			
Level D Elastic Analysis (NB-3225, App. F)	$P_m \leq \min(2.4S_m, 0.7S_u)$ $P_m \text{ (or } P_L) + P_b \leq \min(3.6S_m, 1.0S_u)$ $P_m + P_b + Q \leq \text{note 4}$ $F_p \leq \text{note 5}$ External Pressure = 1.5 * NB-3133	NB-3225, F-1331.1, and F-1331.5(b)	Note 7
Level D Plastic Analysis (NB-3225, App. F)	$P_m \leq \max(0.7S_u, S_y + (S_u - S_y)/3)$ $P_m \text{ (or } P_L) + P_b \leq 0.9S_u$ $P_m + P_b + Q \leq \text{note 4}$ $F_p \leq \text{note 5}$ External Pressure = 1.5 * NB-3133	NB-3225, F-1341.2, and F-1331.5(b)	Note 7

Notes:

1. The Level A limit of NB-3222.2 may be exceeded provided the criteria of NB-3228.5 are satisfied.
2. There are no specific limits on primary stresses for Level A events. However, the stresses due to primary loads during normal service must be computed and combined with the effects of other loadings in satisfying other limits. See NB-3222.1. The Code Design limits on primary stresses used for Service Level A.
3. Not used.
4. Evaluation of secondary stresses not required for Level D events.
5. Evaluation of bearing stresses, F_p , not required for Level D events.
6. Criteria listed are for carbon steel components (e.g., shield plugs).
7. Criteria listed are for austenitic parts including shells, cover plates, and the grapple assembly.
8. The bearing stress category is referred to as F_p .

Table 3-2
EOS-37PTH/EOS-89BTH Basket Assembly Stress Criteria for Subsection NG Components

Service Level	Stress Category ⁽⁵⁾	References	Notes
Design (NG-3221)	$P_m \leq 1.0S_m$ $P_m + P_b \leq 1.5S_m$	NG-3221.1 NG-3222.2	
Level A (NG-3222)	$P_m \leq 1.0S_m$ $P_m + P_b \leq 1.5S_m$ $P_m + P_b + Q \leq 3.0S_m$ (Note 4)	NG-3222.1, NG-3221.1 NG-3222.1, NG-3221.2 NG-3222.2	Note 6
Level B (NG-3223) Note 1	$P_m \leq 1.0S_m$ $P_m + P_b \leq 1.5S_m$ $P_m + P_b + Q \leq 3.0S_m$ (Note 4)	NG-3223(a), NG-3222.1, NG-3221.1 NG-3223(a), NG-3222.1, NG-3221.2 NG-3223(a), NG-3222.2	Note 1
Level C Elastic Analysis (NG-3224)	$P_m \leq 1.5S_m$ $P_m + P_b \leq 2.25S_m$ $P_m + P_b + Q \leq \text{Note 2}$	NG-3224.1(a)(1) NG-3224.1(a)(2) Figure NG-3224 - 1	Notes 2 and 3
Level D Elastic Analysis (NG-3225, App. F)	$P_m \leq (\max(1.2S_y, 1.5S_m), 0.7S_u)$ $P_m + P_b \leq (\max(1.8S_y, 2.2S_m), S_u)$ $P_m + P_b + Q \leq \text{Note 2}$	NG-3225, F- 1440, F- 1332 NG-3225, F- 1440, F- 1332	
Level D Plastic Analysis (Austenitic) (NG-3225, App. F)	$P_m \leq \max(0.7S_u, S_y + 1/3(S_u - S_y))$ $P_m + P_b \leq 0.9S_u$ $P_m + P_b + Q \leq (\text{Note 2})$	NG-3225, F - 1440, F - 1341.2(a) NG-3225, F - 1440, F - 1341.2(b)	Note 7
Level D Plastic Analysis (Ferritic) (NG-3225, App. F)	$P_m \leq 0.7S_u$ $P_m + P_b \leq 0.9S_u$ $P_m + P_b + Q \leq (\text{Note 2})$	NG-3225, F-1440, F-1341.2(a) NG-3225, F-1440, F-1341.2(b)	Note 8

Notes:

1. There are no pressure loads on the basket, therefore the 10% increase permitted by NG-3223(a) for pressures exceeding the design pressure are not included.

2. Evaluation of secondary stresses not required for Level C and D events.
3. Criteria listed are for elastic analyses, other analysis methods permitted by NG-3224.1 are acceptable if performed in accordance with the appropriate paragraph of NG-3224.1.
4. This limit may be exceeded provided the requirements of NG-3228.3 are satisfied, see NG-3222.2 and NG-3228.3.
5. As appropriate, the special stress limits of NG-3227 should be applied.
6. In accordance with NG-3222 and Note 9 of Figure NG-3221-1, the Limit Analysis provisions of NG-3228 may be used.
7. Level D criteria for austenitic materials are also applicable to high-nickel alloy and copper nickel alloy materials.
8. Alternatively, the criteria in the table may be exceeded for the steel basket plates if equivalent plastic strains are within 1% for membrane, 3% for membrane plus bending and 10% for peak equivalent plastic strains.

Table 3-3
Plate and Shell Type Support for Transfer Cask Structural Shell
 2 Pages

Service Level	Stress/Stress Intensity Limits	Reference	Notes
Support Component			
Design, Level A	<i>Membrane and Bending:</i> $P_m \leq 1.0S_m$ $P_m + P_b \leq 1.5S_m$ $P_m + P_b + Q \leq 3.0S_m$ <i>Triaxial:</i> $(\sigma_t + \sigma_l + \sigma_r) \leq 4 S_m$	NF-3142, NF-3220 NF-3522, Table NF-3221.2-1, NF-3223.3	(1), (2)
Level B	<i>Membrane and Bending:</i> $P_m \leq 1.0S_m \times 1.33$ $P_m + P_b \leq 1.5S_m \times 1.33$ $P_m + P_b + Q \leq 3.0S_m \times 1.33$ <i>Triaxial:</i> $(\sigma_t + \sigma_l + \sigma_r) \leq 4 S_m \times 1.33$		
Level C	<i>Membrane and Bending:</i> $P_m \leq \min(1.0 S_m \times 1.5, 0.7S_u)$ $P_m + P_b \leq \min(1.5 S_m \times 1.5, 0.7S_u)$ <i>Triaxial:</i> $(\sigma_t + \sigma_l + \sigma_r) \leq 4 S_m \times 1.5$		
Design, Levels A, B, C	<i>Bearing:</i> Average bearing stress S_y	NF-3223.1	(1)(12)
Level A	<i>Shear:</i> Average pure shear $0.6S_m$ Maximum pure shear $0.8S_m$ <i>Primary + Secondary Shear</i> Average pure shear $1.2S_m$ Maximum pure shear $1.6S_m$	NF-3223.2 Table NF-3221.2-1	
Level B	<i>Shear:</i> Average pure shear $0.6S_m \times 1.33$ Maximum pure shear $0.8S_m \times 1.33$		
Level C	<i>Shear:</i> Average pure shear $\min(0.6S_m \times 1.5, 0.7S_u)$ Maximum pure shear $\min(0.8S_m \times 1.5, 0.7S_u)$		

Table 3-3
Plate and Shell Type Support for Transfer Cask Structural Shell
 2 Pages

Service Level	Stress/Stress Intensity Limits	Reference	Notes
Level D (Elastic Analysis)	<i>Membrane and Bending:</i> $P_m \leq \min (\max(1.2S_y, 1.5S_m), 0.7S_u)$ $P_m + P_b \leq 1.5 \times \min (\max(1.2S_y, 1.5S_m), 0.7S_u)$ <i>Pure Shear:</i> $V_u \leq 0.42S_u$ <i>Bearing:</i> NA <i>Compression:</i> $(2/3)F_a$	F-1332.1 F-1332.4 F-1332.3 F-1331.5(a)	(3)
Level D (Plastic Analysis)	<i>Membrane and Bending:</i> $P_m \leq \max(S_y + (S_u - S_y)/3, 0.7S_u)$ $P_m \text{ (or } P_L) + P_b \leq 0.9S_u$ <i>Primary Shear:</i> $0.42S_u$ <i>Compression:</i> $(2/3)F_a$	F-1342 F-1341 F-1341.8 F-1331.5a	(3),(4),(5)
Support Weld			
Design, Levels A, B	<i>Full Penetration Groove Weld:</i> Same as base metal <i>Partial Penetration Groove/Fillet Weld:</i> (i) Normal compression – same as base metal (ii) Shear stress on fillet weld, normal tension on partial pen. Groove weld, shear stress on plug/slot weld <i>Level A</i> $0.3x F_{u, \text{ weld metal}}$ $0.4x F_{y, \text{ base metal}}$ <i>Level B</i> $K_v .0.3x F_{u, \text{ weld metal}}$ $K_v .0.4x F_{y, \text{ base metal}}$	NF-3226.2 NF-3256 Table NF-3324.5(a)-1 Table NF-3523(b)-1	(8)
Level D	<i>Partial Penetration Groove/Fillet Weld:</i> Level A allowable stresses can be increased by $\min(2, 1.167S_u/S_y)$ if $S_u > 1.2S_y$ 1.4 if $S_u \leq 1.2S_y$	F-1334	

Notes:

1. Limit Analysis may be used if stress intensity is not satisfied at a specific location per the criteria of NF-3221.4.
2. S_u is on net effective area.
3. F_a : Buckling load or stress.
4. Plastic analysis for Level D implies plastic system and component analysis.
5. P_m : General primary membrane stress intensity
 - a. P_L : Local primary membrane stress intensity
 - b. P_b : Primary bending stress intensity
6. For P_b , other conditions specified in NF-3322.1 must be specified.
7. Incorporates provisions of Reg. Guide 1.124 Rev2, 2007 Paragraphs C.2, C.3 and C.4 [3-8).
8. Base metal stress should be checked on appropriate shear plane.
9. Rigorous analysis of member stability may be used to determine critical bending stress for non-compact sections. A factor of safety of 1.5 is used in determining allowable bending stress.
10. Thermal load is considered even though ASME Section III Subsection NF does not require thermal stress evaluations. For Service Levels A and B, primary plus secondary stresses is limited to a range of $2S_y$ or S_u at temperature, whichever is less.
11. Primary plus secondary stresses are evaluated for critical buckling loads for all loading categories.
12. For bearing loads applied near free edges, consider shear failure. Average sheer stress is limited to $0.6 S_m$ in the case of primary stress and $0.5 S_y$ for primary stress plus secondary stress.

Table 3-4
Structural Shell Structural Stress Criteria for Transfer Cask Bolts

Stress Category	Fastener Allowable Stress		
	Normal Conditions ⁽¹⁾		Accident Conditions ⁽²⁾
	Ferritic Steels	Austenitic Steels	
Average Tensile Stress	$\frac{S_u}{2} K_{bo}$	$\frac{S_u}{3.33} K_{bo}$	Lesser of: 0.7 S _u or S _y
Average Shear Stress	$\frac{0.625S_u}{3} K_{bo}$	$\frac{0.625S_u}{5} K_{bo}$	Lesser of: 0.42 S _u or 0.6 S _y
Combined Shear and Tension	$\frac{f_t^2}{f_{tb}^2} + \frac{f_v^2}{f_{vb}^2} \leq 1$		$\frac{f_t^2}{f_{tb}^2} + \frac{f_v^2}{f_{vb}^2} \leq 1$

Notes:

1. Stress limits are as defined in ASME Code, Section III, Subsection NF 3324.6 (a) with stress limit factors (K_{bo}) as defined in Table NF 3225.2-1. Service level A K_{bo}= 1.0, Service level B K_{bo}= 1.15, Service level C K_{bo}= 1.25.
2. Stress limits for Service Level D conditions are as defined in Appendix F.

Table 3-5
Structural Stress Criteria for Neutron Shield

Item Shell Component	Stress Type		
Stress Type	Service Levels A	Service Level B	Service Level C
$\sigma_m^{(1)}$	1.0S	1.10 S	1.5 S
$(\sigma_m \text{ or } \sigma_L) + \sigma_b^{(1)}$	1.5S	1.65 S	1.8S
$(\sigma_m \text{ or } \sigma_L) + \sigma_b + Q^{(1, 5)}$	2.4S	2.4S	Note 6
Fillet Welds			
Allowable Load (P) ^(3, 4)	.55SA	.61 SA	.825 SA

Notes:

- Per ASME Subsection ND Table 3321-1,
 - σ_m : General membrane stress
 - σ_L : Membrane stress
 - σ_b : Bending stress
 - Q: Stresses due to thermal gradient
- Joint efficiency to be 1.00 for determining shell thickness/allowable pressure; analysis to provide justification for assumption.
- ASME Subsection ND 3356.1(c)- The allowable load on fillet welds are the product of the weld area based on minimum leg dimensions , the allowable stress value in tension of the material being welded, and a joint efficiency of 0.55.
- Per ASME Subsection ND 3356. Stress limits for components based on Table ND-3321-1. P = Allowable load, S = maximum allowable stress, A = weld area based on minimum leg dimensions.
- Primary membrane + bending + thermal stress acceptance limits are based on Subsection NB allowables, but not to exceed the Level D limits as listed in Table ND-3321-1.
- Evaluation of secondary membrane plus bending stresses (Q) are required for Service Level A and B loadings only per Figure NB-3222-1.

Table 3-6
Summary of EOS-37PTH DSC Component Weights

Component Description	Weight (lb)
DSC Shell ⁽¹⁾	17,700
Basket Assembly	33,500
Dry/Unloaded/Open DSC ⁽⁵⁾	51,200
37 Fuel Assemblies	70,300
DSC Top Shield Plug	7,340
Flooding Water in Loaded DSC	15,300
Flooded/Loaded Open DSC ⁽⁶⁾	145,000
DSC Top Cover Plates	5060
Sealed/Loaded DSC Weight ⁽⁷⁾	134,000

Table 3-7
Summary of EOS-89BTH DSC Component Weights

Component Description	Weight (lb)
DSC Shell	17,000
Basket Assembly	27,400
Dry/Unloaded/Open DSC	44,400
89 Fuel Assemblies	62,800
DSC Top Shield Plug	7,340
Flooding Water in Loaded DSC	15,900
Flooded/Loaded Open DSC	131,000
DSC Top Cover Plates	5060
Sealed/Loaded DSC Weight	120,000

Table 3-8
Summary of EOS-HSM Weight and Center of Gravity

Component	Description	Value
Empty EOS-HSM Long	Total Weight (lb)	350,000
	Center of Gravity from Bottom in Vertical Direction	126.5 inches
EOS-HSM Long Loaded with EOS-37PTH DSC	Maximum Weight (lb)	484,000
	Center of Gravity from Bottom in Vertical Direction	120.8 inches

Notes:

1. The weight and center of gravity values listed in the table are corresponding to the maximum concrete density of 160 pcf.

Table 3-9
Summary of EOS-TC Component Weight

Transfer Cask Component	Calculated Weight (lb)		
	TC108	TC125	TC135
Outer Shell	13,451	13,800	15,400
Inner Shell including Rails	9,653	9,652	10,680
Lead Gamma Shielding	47,221	71,500	79,300
Top Ring	4,391	5,340	5,340
Bottom Ring	2,512	3,170	3,170
3¼" Nominal Top Cover Plate (LID)	4,692	4,790	4,790
Bottom Assembly	4,113	4,137	4,137
Neutron Shield Panel including Water	6,652	11,550	12,720
Upper Trunnion	256	256	256
Total	92,941	124,195	135,793

APPENDIX 3.9.1 DSC SHELL STRUCTURAL ANALYSIS

Table of Contents

<i>3.9.1 DSC SHELL STRUCTURAL ANALYSIS</i>	<i>3.9.1-1</i>
<i>3.9.1.1 General Description</i>	<i>3.9.1-1</i>
<i>3.9.1.2 DSC Shell Assembly Stress Analysis</i>	<i>3.9.1-1</i>
<i>3.9.1.3 DSC Shell Buckling Evaluation</i>	<i>3.9.1-25</i>
<i>3.9.1.4 DSC Fatigue Analysis</i>	<i>3.9.1-25</i>
<i>3.9.1.5 DSC Weld Flaw Size Evaluation</i>	<i>3.9.1-28</i>
<i>3.9.1.6 Conclusions</i>	<i>3.9.1-30</i>
<i>3.9.1.7 References</i>	<i>3.9.1-31</i>

List of Tables

<i>Table 3.9.1-1</i>	<i>EOS37PTH DSC Major Dimensions</i>	<i>3.9.1-33</i>
<i>Table 3.9.1-2</i>	<i>Material of EOS DSC Components (Analysis)</i>	<i>3.9.1-33</i>
<i>Table 3.9.1-3</i>	<i>Elastic-Plastic Material Properties</i>	<i>3.9.1-34</i>
<i>Table 3.9.1-4</i>	<i>Allowable Weld Stresses for Pressure Boundary Partial Penetration Welds, Material Type 304</i>	<i>3.9.1-35</i>
<i>Table 3.9.1-5</i>	<i>SA-240/SA-479 304 & SA-182 F304 -Stress Allowables.....</i>	<i>3.9.1-35</i>
<i>Table 3.9.1-6</i>	<i>Allowable Base Metal Stresses for Non Pressure Boundary Partial Penetration and Fillet Welds Type 304 Base Metal</i>	<i>3.9.1-36</i>
<i>Table 3.9.1-7</i>	<i>DSC Shell Stress Results, Confinement Boundary – Load Combinations</i>	<i>3.9.1-37</i>
<i>Table 3.9.1-7a</i>	<i>DSC Shell Stress Results, Non-Confinement Boundary – Load Combinations</i>	<i>3.9.1-40</i>
<i>Table 3.9.1-7b</i>	<i>DSC Shell Stress Results, Confinement Boundary - Load Combinations (Supported by FPS DSC Support Structure)</i>	<i>3.9.1-43</i>
<i>Table 3.9.1-7c</i>	<i>DSC Shell Stress Results, Non-Confinement Boundary - Load Combinations (Supported by FPS DSC Support Structure)</i>	<i>3.9.1-46</i>
<i>Table 3.9.1-8</i>	<i>OTCP Stress Results – Load Combinations.....</i>	<i>3.9.1-49</i>
<i>Table 3.9.1-8a</i>	<i>OTCP Stress Results- Load Combination (Supported by FPS DSC Support Structure).....</i>	<i>3.9.1-52</i>
<i>Table 3.9.1-9</i>	<i>ITCP Stress Results – Load Combinations</i>	<i>3.9.1-55</i>
<i>Table 3.9.1-9a</i>	<i>ITCP Stress Results- Load Combinations (Supported by FPS DSC Support Structure).....</i>	<i>3.9.1-58</i>
<i>Table 3.9.1-10</i>	<i>IBCP Stress Results – Load Combinations.....</i>	<i>3.9.1-61</i>
<i>Table 3.9.1-10a</i>	<i>IBCP Stress Results - Load Combinations (Supported by FPS DSC Support Structure).....</i>	<i>3.9.1-64</i>
<i>Table 3.9.1-11</i>	<i>ITCP-DSC Shell Weld Stress Results – Load Combinations.....</i>	<i>3.9.1-67</i>
<i>Table 3.9.1-11a</i>	<i>ITCP-DSC Shell Weld Stress Results - Load Combinations (Supported by FPS DSC Support Structure).....</i>	<i>3.9.1-69</i>
<i>Table 3.9.1-12</i>	<i>OTCP-DSC Shell Weld Stress Results – Load Combinations</i>	<i>3.9.1-71</i>
<i>Table 3.9.1-12a</i>	<i>OTCP-DSC Shell Weld Stress Results - Load Combinations (Supported by FPS DSC Support Structure).....</i>	<i>3.9.1-73</i>
<i>Table 3.9.1-13</i>	<i>Weld Flaw Size for Controlling Load Combination</i>	<i>3.9.1-75</i>
<i>Table 3.9.1-14</i>	<i>Lifting Lug Plate-DSC Shell Weld Stress Results – Load Combinations</i>	<i>3.9.1-76</i>
<i>Table 3.9.1-15</i>	<i>Summary of Maximum Strain for Side Drop (Strain Criteria)</i>	<i>3.9.1-77</i>

List of Figures

Figure 3.9.1-1	DSC FEM.....	3.9.1-78
Figure 3.9.1-2	DSC FEM-Top End.....	3.9.1-79
Figure 3.9.1-3	DSC FEM-Bottom End	3.9.1-80
Figure 3.9.1-4	Mesh detail – Grapple Assembly	3.9.1-81
Figure 3.9.1-5	Not Used.....	3.9.1-82
Figure 3.9.1-6	Internal Pressure – Load Application.....	3.9.1-83
Figure 3.9.1-7	Dead Weight Simulation in EOS-HSM – Boundary Conditions	3.9.1-84
Figure 3.9.1-7a	Dead Weight Simulation in EOS-HSM Detail	3.9.1-85
Figure 3.9.1-8	Dead Weight Simulation in EOS-TC.....	3.9.1-86
Figure 3.9.1-8a	Dead Weight Simulation in Cask Detail	3.9.1-87
Figure 3.9.1-9	Pull Load with Internal Pressure.....	3.9.1-88
Figure 3.9.1-9a	Pull Load with Internal Pressure Detail.....	3.9.1-89
Figure 3.9.1-10	Push Load with Internal Pressure	3.9.1-90
Figure 3.9.1-10a	Push Load with Internal Pressure Detail	3.9.1-91
Figure 3.9.1-11	Side Drop away from Cask Rail.....	3.9.1-92
Figure 3.9.1-11a	Side Drop away from Cask Rail– Boundary Condition Details	3.9.1-93
Figure 3.9.1-12	Bottom End Drop Simulation.....	3.9.1-94
Figure 3.9.1-12a	Bottom End Drop Simulation Detail.....	3.9.1-95
Figure 3.9.1-13	Seismic in EOS-HSM Simulation	3.9.1-96
Figure 3.9.1-13a	High Seismic in EOS-HSM-FPS Simulation.....	3.9.1-97
Figure 3.9.1-14	Stresses for Internal Pressure (Normal) Load Case.....	3.9.1-98
Figure 3.9.1-15	Stresses for Internal Pressure (Accident) Load Case	3.9.1-99
Figure 3.9.1-16	Stresses for Side Drop (away from Rails) Load Case.....	3.9.1-100
Figure 3.9.1-17	Not Used.....	3.9.1-101
Figure 3.9.1-18	Stresses for Seismic (Top) Load Case.....	3.9.1-102
Figure 3.9.1-19	Stress Linearization Paths for the DSC Components and Welds	3.9.1-103
Figure 3.9.1-20	Maximum Linearized Component Stresses for Internal Pressure (Normal) Load Case	3.9.1-104
Figure 3.9.1-21	Mesh Sensitivity Study 01 – Models and ITCP Weld Stresses	3.9.1-105
Figure 3.9.1-22	Mesh Sensitivity Study 02 – Models and ITCP Weld Stresses	3.9.1-106
Figure 3.9.1-23	Mesh Sensitivity Study 03 – Models and ITCP Weld Stresses	3.9.1-107

<i>Figure 3.9.1-23a</i>	<i>Membrane Stresses around the Circumference within the ITCP Weld</i>	<i>3.9.1-108</i>
<i>Figure 3.9.1-24</i>	<i>Limit Load – Load vs. Deflection – Internal Pressure.....</i>	<i>3.9.1-109</i>
<i>Figure 3.9.1-25</i>	<i>Limit Load – Load vs. Deflection – Side Drop Acceleration.....</i>	<i>3.9.1-110</i>
<i>Figure 3.9.1-26</i>	<i>Equivalent Plastic Strain at 75g Side Drop Load for Strain Criteria Analysis</i>	<i>3.9.1-111</i>
<i>Figure 3.9.1-27</i>	<i>OTCP and ITCP Confinement Weld Equivalent Plastic Strain Distribution for Strain Criteria Analysis</i>	<i>3.9.1-112</i>

3.9.1 DSC SHELL STRUCTURAL ANALYSIS

The purpose of this appendix is to present the structural evaluation of the shell assembly of the EOS-37PTH dry shielded canister (DSC) and the EOS-89BTH DSC under all applicable normal, off-normal and accident loading conditions during storage in the EOS horizontal storage module (HSM) and during transfer in the EOS transfer cask (TC). The EOS system consists of the EOS-HSM, the EOS-TC, the dual-purpose (transportable/storage) EOS-37PTH and EOS-89BTH DSC, and associated ancillary equipment.

The design of the DSC includes five design options: EOS-37PTH (short, medium and long) and EOS-89BTH (short and medium). The longest and heaviest EOS-37PTH DSC, which uses TC135 for transfer operations, is analyzed to bound all DSC design options in the NUHOMS® EOS System.

3.9.1.1 General Description

The DSC consists of a fuel basket and a shell assembly. The DSC pressure boundary consists of DSC shell with two cover plates at each end. Non-pressure boundary shield plugs are included at each end of the assembly. The inner bottom shield (IBS) is confined between the inner bottom cover plate (IBCP) and outer bottom cover plate (OBCP). The top shield plug (TSP) is confined by the inner top cover plate (ITCP) and four lifting lugs, which are welded to the inside of the DSC shell. The grapple ring support is welded to the OBCP using full penetration weld. The ITCP is welded along the top perimeter with partial penetration weld. The IBCP is welded using a full penetration weld. Grapple ring assembly connections are all made using full penetration welds.

The DSC shell thickness is 0.50 inch, and the top and bottom closure assemblies are 10.0 inches and 8.0 inches, respectively. The DSC shell is constructed entirely from stainless steel or duplex steel. There are no penetrations through the pressure boundary. The draining and venting systems are covered by the port plugs. The outer top cover plate (OTCP) and the ITCP are welded to the cylindrical shell with multilayer welds. The DSC cavity is pressurized above atmospheric pressure with helium. The DSC shell assembly geometry and the materials used for its analysis and fabrication are shown on drawings EOS01-1000-SAR, EOS01-1001-SAR, EOS01-1005-SAR and EOS01-1006-SAR included in Chapter 1.

3.9.1.2 DSC Shell Assembly Stress Analysis

An enveloping technique of combining various individual loads in a single analysis is used in this evaluation for several load combinations. This approach reduces the number of computer runs, while remaining conservative. For some load combinations, stress intensities under individual loads are added to obtain resultant stress intensities for the specified combined loads. This addition at the

stress intensity level for the combined loads, instead of at component stress level, is also a conservative method for reducing the number of analysis runs.

The stresses of all components are assessed by means of elastic analysis methodology for all load combinations, except for accident loading conditions. Elastic-plastic analysis methodology is used to assess the stresses for Service Level D load combinations.

A detailed description of each load combination is provided in Section 3.9.1.2.8.

3.9.1.2.1 Material Properties

For elastic analysis, temperature dependent material properties used for each component of DSC shell assembly are obtained from the American Society of Mechanical Engineers (ASME) code [3.9.1-2], and are summarized in Chapter 8. Material properties used for stress evaluations are conservatively taken at 500 °F. For the partial penetration welds and grapple assembly, 350 °F allowable stresses are used for comparison to load induced stresses as these components remain below this lower temperature.

For plastic analysis, a bilinear stress-strain curve with a 5% tangent modulus is used for steel components. The non-linear material properties at 500 °F for side drop analysis are shown in Table 3.9.1-3. Steel material (except shield plugs) is modeled by bilinear kinematic hardening method (TB, BKIN – [3.9.1-9]).

3.9.1.2.2 DSC Shell Stress Criteria

The calculated stresses in the DSC shell assembly structural components are compared with the allowable stresses set forth by ASME Boiler and Pressure Vessel (B&PV) Code, Section III, Subsection NB [3.9.1-3] under normal (Level A), and off-normal (Level B) loading conditions. Appendix F of the ASME B&PV Code is used to evaluate the calculated stresses in the DSC shell assembly under accident (Level D) loading conditions. Allowable stress limits for Levels A, B and D service loading conditions, as appropriate, are summarized in Table 3-1, and the corresponding allowable stress values at different temperatures are summarized in Table 3.9.1-5.

The OTCP-to-DSC shell weld and the ITCP-to-DSC shell weld, which are both partial penetration welds, are to be evaluated using a joint efficiency factor of 0.8. Per NUREG-1536 [3.9.1-7], the minimum inspection requirement for end closure welds is multi-pass dye penetrant testing (PT) using a stress (allowable) reduction factor of 0.8. The allowable weld stresses are summarized in Table 3.9.1-4.

3.9.1.2.3 Finite Element Model Description

The EOS DSC shell assembly is analyzed for the postulated load conditions using a three-dimensional (3D) 180° half- symmetric finite element model (FEM). The FEM is developed using the nominal dimensions of the long cavity DSC.

Each of the DSC shell assembly components is modeled using (ANSYS SOLID185) 3D solid elements. The elements have translational degrees of freedom (DOF) at each of the eight nodes (no rotational DOF). The top end of the DSC is assembled such that no axial gaps initially exist between the OTCP, ITCP, and TSP. Similarly, the bottom end of the DSC is assembled so that no axial gaps initially exist between the OBCP, IBS, and IBCP. The interfaces between the mating surfaces are modeled using (ANSYS CONTA178) 3D node-to-node contact elements that allow the transfer of compressive (bearing) loads.

Contact is not modeled between the cover plates and the shell. This modeling approach is conservative as it forces all loads to be transferred through the welds.

Figure 3.9.1-1 through Figure 3.9.1-4 depict the components and meshed model of the DSC. Table 3.9.1-1 lists the major dimensions of the bounding model and Table 3.9.1-2 lists the material designations of each modeled component.

A description of the FEM for the DSC components is shown below.

DSC Shell

The DSC shell is modeled using 3D solid elements (ANSYS element SOLID185) and has five elements through the thickness of the component. The shell is connected to the OTCP, ITCP, and OBCP with partial penetration welds and is connected to the IBCP using a full penetration weld.

Outer Top Cover Plate

The OTCP is modeled using 3D solid elements (ANSYS element SOLID185) and has 15 elements through the thickness of the component. The plate is connected to the DSC shell with partial penetration welds.

Inner Top Cover Plate

The ITCP is modeled using 3D solid elements (ANSYS element SOLID185) and has 15 elements through the thickness of the component. The plate is connected to the DSC shell with partial penetration welds.

Top Shield Plug

The TSP is modeled using 3D solid elements (ANSYS element SOLID185) and has 11 elements through the thickness of the component. The TSP is confined by the ITCP and four lifting lugs, which are welded to the inside of the DSC shell.

Outer Bottom Cover Plate

The OBCP is modeled using 3D solid elements (ANSYS element SOLID185) and has 15 elements through the thickness of the component. The plate is connected to the DSC shell with partial penetration welds and to the grapple ring assembly (grapple ring and grapple ring support) with full penetration welds.

Inner Bottom Shield

The IBS is modeled using 3D solid elements (ANSYS element SOLID185) and has eight elements through the thickness of the component. The IBS is confined between the IBCP and OBCP.

Inner Bottom Cover Plate

The IBCP is modeled using 3D solid elements (ANSYS element SOLID185) and has six elements through the thickness of the component. The plate is connected to the DSC shell with a full penetration weld.

Grapple Ring

The grapple ring is modeled using 3D solid elements (ANSYS element SOLID185) and has four elements through the thickness of the component. The grapple ring is connected to the grapple ring support with full penetration welds.

Grapple Ring Support

The grapple ring support is modeled using 3D solid elements (ANSYS element SOLID185) and has two elements through the thickness of the component. The grapple ring support is connected to the OBCP with full penetration welds.

Weld Components

Partial penetration welds are used between the DSC shell and the OBCP, OTCP and ITCP and are modeled by merging the nodes of the appropriate components. The OBCP-to-DSC shell weld and OTCP-to-DSC shell weld are 0.5 inch with five elements through the thickness of the weld. The ITCP-to-DSC shell weld is 3/16 inch with five elements through the thickness of the weld.

Full penetration welds are used between the DSC shell and the IBCP; therefore, all nodes through the thickness of the plate along the perimeter are merged with the DSC shell nodes.

Full penetration welds are also used between the grapple ring support and the OBCP. The grapple ring and grapple support plate welds are also full penetration welds. Therefore, for these components, nodes at the interfaces are merged.

The top shield plug (TSP) is confined by the inner top cover plate (ITCP) and four lifting lug plates, which are welded to the inside of the DSC shell. All four sides of the lifting lug plate to shell weld are modeled as coupled set nodes as a line weld. Lifting lug plate stresses are not evaluated since the welds at the lug plate-to-DSC shell interface support the TSP loads.

3.9.1.2.4 Mesh Sensitivity

Mesh sensitivity studies are a validation that a model produces accurate results by refining a mesh and studying the change in results. A model is shown to be valid when the solution from increasingly refined meshes under a particular set of loadings and boundary conditions results in only negligible differences in relevant output. As one study cannot encompass all general load paths and configurations, multiple studies must be performed with each modeling a particular “archetype” of the overall simulation in order to keep the influence of unintended variables as small as possible. Aspects of the mesh relevant for each archetype are then combined to constitute the base model for the analysis. Figure 3.9.1-21 through Figure 3.9.1-23a show that the chosen model (using the relevant aspects of model 4 in both cases) produces an accurate solution for the foreseeable loads.

Three sensitivity studies were performed. The first studied the impact of mathematical versus geometric/visual gap modeling to represent the interface between the top cover plates and the DSC shell under a side drop loading. The second studied the effect of mesh density in the radial and axial dimensions near the welds between the top cover plates and the DSC shell in an axisymmetric internal pressure loading. The third studied the effect of mesh density (principally) in the circumferential direction under a side drop loading.

Effect of Gap Modeling Methodology upon Results (Study No. 1)

Two models were compared, where all details were identical except for the radial locations of the outer-most five layers of nodes in the top cover plates. These models, shown in Figure 3.9.1-21, used the side drop load case as the basis for comparison.

In the first model, these outer-most nodes were coincident with the adjacent inner-surface nodes of the DSC shell, with the nominal radial gap incorporated as a parameter in the contact elements between the bodies that allows for a specific amount of penetration before contact effects were introduced. In the second model, the above-referenced outer-most nodes of the cover plates were moved inward by the magnitude of the nominal gap.

The modeling methodology of visual versus strictly mathematical representation of the nominal radial gaps has no effect on the results, as shown in Figure 3.9.1-21.

Effect on Results of Mesh Refinement in Axisymmetric Loading (Study No. 2)

Six models were compared, where all details were identical except for the radial lengths of the outer-most elements in the top cover plates, as well as the elements throughout the thickness of the DSC shell. In models four, five, and six, the circumferential length of the elements is halved in order to keep elemental aspect ratios within reasonable limits, although this circumferential sensitivity is explored in Study No. 3. Model five is identical to model four, except that solid185 elements have been replaced with solid186 elements with midside nodes. These models, shown in Figure 3.9.1-22, used the normal internal pressure load case as the basis for comparison.

The model's accuracy is sensitive to radial element length, but only at the largest value tested – 0.69 inches. A radial length of 0.17 inch for the weld between the OTCP and the DSC shell, and a radial length of 0.125 inch for the weld between the ITCP and the DSC shell, produces accurate results as shown in Figure 3.9.1-22. The more refined model (model 6) shows a slight increase in the membrane plus bending stresses, as well a decrease in the membrane stress. The membrane stresses are more critical for this evaluation; therefore, it is concluded that model 4 has adequate mesh characteristics for this study.

Effect of Higher Order Elements with Midside Nodes

The internal pressure load case is evaluated with higher order elements with midside nodes. The results with low order nodes show conservative results as shown in Figure 3.9.1-22.

Effect on Results of Mesh Refinement in Side Drop Loading (Study No. 3)

Five models were compared, where all facets were identical except for the circumferential lengths of the outer-most elements in the top cover plates, as well as the elements throughout the thickness of the DSC shell. These models, shown in Figure 3.9.1-23, used the side drop load case as the basis for comparison.

The model is more sensitive to radial element lengths than circumferential lengths in low gradient areas away from the areas impacted by the presence of boundary conditions, where the 1.4-inch elements from model 2 produce results that are not appreciably different from the highly refined model. In high gradient areas near boundary conditions, a smaller element length of 0.36 inch produces accurate results as shown in Figure 3.9.1-23a.

3.9.1.2.5 Post-Processing

The DSC component stress results were post-processed using the ANSYS LPATH and PRSECT commands, which linearize the stress distribution through the requested section. Stress linearization for the DSC components are performed on all possible paths, both radially and circumferentially, through the thickness of a component or weld as appropriate, using the ANSYS post-processing macro. Stress linearization for weld stresses are performed on stress paths at the throat location of the weld, including the elements adjacent to the weld. Figure 3.9.1-19 shows examples of the stress linearization paths for the components and welds. The methodology employed is location agnostic - reported peak membrane stresses are combined with reported peak membrane + bending stresses even if they occur in disparate locations of a particular component. However, locations are tracked on the basis of proximity to the confinement boundary welds and gross structural discontinuities, or proximity to boundary conditions.

Stress Linearization Method

Stress evaluation on predefined paths and the stress linearization procedure are based on the method employed in the ANSYS code. Stress results are mapped onto a path by first interpolating stress components (σ_x , σ_y , σ_z , σ_{xy} , σ_{yz} , σ_{zx}) at the path location. Then, stress averaging and linearization on the path are done independently for all six stress components.

Principal membrane stresses and membrane stress intensity are then derived from membrane parts of the individual stress components. Similarly, linearized principal stresses and linearized stress intensity at the path section surface are derived from linearized individual stress components of that surface.

The stress path evaluation in ANSYS brings the information about membrane stress intensity across the path, as well as maximum linearized stress membrane plus bending at classification path surface.

ASME NB-3213.2 defines a gross structural discontinuity as a geometric or material discontinuity, which affects the stress or strain distribution through the entire wall thickness of the pressure-retaining member. Examples of gross structural discontinuities are head-to-shell junctions, flange-to-shell junctions, and nozzles. ASME Table NB-3217-1 concludes that at the junction of shell and head, the membrane stresses are P_L and bending stresses are Q , provided that the edge restraint is not required to maintain the bending stress in the middle to acceptable limits. Section NB-3224.4 states that the requirement of primary plus secondary stress intensity does not need to be satisfied for Level C service limits. Appendix F, Section F-1332.3 states that bearing stress does not need to be evaluated for Level D service limits.

Membrane stresses distant from gross structural discontinuities are compared against primary membrane (P_m) allowable stresses. Analogous membrane + bending stresses are compared against primary membrane + bending ($P_m + P_b$) allowable stresses.

Membrane stresses proximate to gross structural discontinuities are compared against primary local membrane (P_L) allowable stresses. Membrane + bending stresses proximate to gross structural discontinuities are compared against secondary allowable stresses.

3.9.1.2.6 Stress Categorization Sensitivity Studies

Limit Load Analysis

Limit load analysis sensitivity studies are performed on the internal pressure and side drop load combination to supplement the stress categorization. The analysis directly relates the gross plastic deformation of primary stresses to failure and removes the stress categorization uncertainties. Limit load analysis is performed per Paragraph NB-3228.1, where the acceptance criterion is that the specified loading does not exceed two-thirds of the lower bound collapse load. The lower bound collapse load is determined using an ideally plastic (non-strain hardening) material model, with a yield stress of $1.5S_m$. This criterion is used for Service Level A and B load cases. For Service Level D load cases, the rules of ASME Section III Appendix F Paragraph F-1341.3 [3.9.1-3] are used, which states that the loads “shall not exceed 90% of the limit analysis collapse load using a yield stress which is the lesser of $2.3S_m$ and $0.7S_u$.”

For both the internal pressure and side drop load cases, all materials are modeled as elastic-perfectly plastic with a yield stress based on $1.5S_m$. Elastic-perfectly plastic is described as an idealized material that behaves in a linear-elastic manner up to its yield point, and thereafter is perfectly plastic (i.e., non-strain hardening). Also note that, even though the side drop is a Level D event, the $1.5S_m$ value is conservatively used, which inherently adds an approximate safety factor equal to:

$$\frac{\frac{0.7 \cdot S_u}{1.1}}{\frac{1.5 \cdot S_m}{1.5}} \geq 2$$

Both analyses use small deflection theory (NLGEOM, OFF). This is necessary since deflections are unrealistically high in limit load analysis due to the lower-bound, non-strain-hardening material properties. If large deflections are used, the beneficial effects of membrane action would result in a higher collapse load.

The FEM described in Section 3.9.1.2.3 is used for the internal pressure load case, except that the material properties are changed to an elastic-perfectly plastic model. A reduction factor of 0.8 is used for elements in the partial penetration ITCP to DSC shell and OTCP to DSC shell welds such that the yield stress is equal to:

$$\sigma_{yield} = 0.8 \cdot 1.5 \cdot S_m$$

The internal pressure is linearly increased until the solution fails to converge.

The FEM described in Section 3.9.1.2.3 is used for the internal pressure plus side drop load case, except that the material properties are changed to an elastic-perfectly plastic model. A reduction factor of 0.8 is used as above for elements in the partial penetration ITCP to DSC shell and OTCP to DSC shell welds. Furthermore, contact between the DSC shell and the inner surface of the cask is neglected. The loads (20 psig internal pressure and 1g acceleration) are applied at a time value of 1. The loads are then increased with the time step until the solution fails to converge. Figure 3.9.1-24 and Figure 3.9.1-25 show the maximum displacement history and indicate the expected plastic instability that occurs as the limit load is approached. The last converged solution was at a pressure of 270 psig for internal pressure load and a deceleration of 217 g for the side drop load case.

Strain Criteria Analysis

Similar to the limit load analysis sensitivity studies, a strain criteria sensitivity study is performed on the side drop load combination to supplement the stress categorization. The strain criterion directly relates equivalent plastic strain to failure and removes the stress categorization uncertainties. Strain criteria analyses are performed per non-mandatory Appendix FF of the ASME Code [3.9.1-10].

Since the critical areas for the DSC Shell are the partial penetration welds between ITCP and DSC Shell and OTCP and DSC Shell, the average and the maximum equivalent plastic strain, ϵ_{eq}^p , multiplied by the triaxiality factor (TF) at 75g are compared against following criteria:

$$\begin{aligned} [TF \cdot (\epsilon_{eq}^p)]_{avg} &\leq (0.85 \cdot \epsilon_{uniform}) \\ [TF \cdot (\epsilon_{eq}^p)]_{max} &\leq [\epsilon_{uniform} + 0.25 \cdot (\epsilon_{fracture} - \epsilon_{uniform})] \end{aligned}$$

Where:

$$TF = \frac{(\sigma_1 + \sigma_2 + \sigma_3)}{\sqrt{\frac{1}{2} \cdot [(\sigma_1 - \sigma_2)^2 + (\sigma_2 - \sigma_3)^2 + (\sigma_3 - \sigma_1)^2]}}$$

Where σ_1 , σ_2 , and σ_3 are the principal stresses at the location, and:

ϵ_{eq}^p is equal to the equivalent plastic strain.

$\epsilon_{uniform}$ is equal to the true strain just prior to the onset of necking in a uniaxial tensile test.

$\epsilon_{fracture}$ is equal to the true strain at fracture in a uniaxial tensile test.

At this time, ASME standard true stress-strain curves, true uniform strain, and true fracture strain are under development. Therefore, the following assumptions are made for the material properties, which may not be sufficient for a full qualification using strain criteria, but are determined to be sufficient for this sensitivity study:

A bilinear curve is used for the analysis where the material behaves in a linear-elastic manner up to its ASME specified yield point and, thereafter, a slope of 2.59×10^4 psi is used (i.e., the tangent modulus after yield strength is 1% of the Young's modulus). This tangent modulus, along with the ASME specified yield strength, is conservatively low, especially considering the low level of strains resulting from the analysis.

ASME Section II, Part C specifies a 30% elongation limit for the E316-XX electrode. This electrode is chosen as a conservative representative design, as the elongation limit is lower than that of a 304 SS matching electrode. Furthermore, Figure EE-1230-1 in Appendix EE [3.9.1-10] shows that the engineering uniform strain is approximately 75% of the elongation limit. Therefore, the value used for the uniform strain is equal to:

$$\epsilon_{uniform} = \ln(1 + 0.75 \cdot 0.3) = 0.2 \cdot \frac{in}{in}$$

The bounding 75g side drop load case on rails with 20 psig internal pressure is evaluated using the above material properties. Furthermore, per Section FF-1145, strain rate effects are considered with two additional analyses; the yield strength value was increased by 20%, successively, while the slope was unchanged.

To decrease the resources required in post processing, the maximum equivalent plastic strain (including consideration of the triaxiality factor) was conservatively compared against the uniform strain limit, ϵ_{limit} , equal to:

$$\epsilon_{limit} = 0.85 \cdot \epsilon_{uniform} = 0.17 \frac{in}{in}$$

The results are shown in Table 3.9.1-15. Figure 3.9.1-27 shows the confinement weld strain distribution along the entire circumference of the DSC.

3.9.1.2.7 Load Cases for DSC Shell Stress Analysis

This section discusses the different load cases considered to evaluate the stresses generated in the EOS-37PTH DSC and EOS-89BTH DSC shell assembly during transfer operations and in storage conditions under normal, off-normal and accident loading. During fuel transfer, the DSC is oriented horizontally inside the EOS-TC, which is mounted to the transfer skid and transferred from the reactor or fuel building to the independent spent fuel storage installation (ISFSI). During storage, the DSC is in the horizontal position within EOS-HSM.

Each load case analysis utilizes the FEM that is described in Section 3.9.1.2.3, along with pertinent loads and boundary conditions. Bounding storage load cases, transfer load cases and load combinations used to evaluate the DSC shell assembly are tabulated in Table 2-5. In general, major loads (ram push/pull loading with internal/external pressure) are combined within the ANSYS analyses, while stress intensities from minor loads (i.e. dead weight and pressure) are added algebraically.

3.9.1.2.7.1 Dead Weight

The dead weight is analyzed for the following three basic configurations:

- When the DSC is vertical in the EOS-TC135,
- When the DSC is horizontal in the EOS-TC135,
- When the DSC is horizontal in the EOS-HSM.

The model for the EOS-TC135 and EOS-HSM differ in boundary conditions representing support rails.

Vertical in EOS-TC

The DSC shell supports the entire weight of the top end components in addition to its self-weight. The weight of the fuel is assumed to be uniformly distributed over the area of the IBCP. The fuel load and the weight of the bottom end components are transferred directly to the ground through bearing between the IBCP, IBS, and OBCP.

The bottom end surface of the EOS-TC135 is constrained in the vertical direction. The contact elements are generated between DSC shell and OBCP outermost nodes (excluding the surface of OBCP, which is bounded by the grapple ring support) and the EOS-TC135 surface. The payload of 105 kips is applied as uniform pressure acting on the IBCP.

Horizontal in EOS-TC

When the DSC is in a horizontal position, the end components and basket assembly bear against the DSC shell.

The inertial loads for DSC internals are accounted for by applying an equivalent pressure on the inside surface of the DSC represented by the projection of first 6.5° support rail only. This pressure is determined based on the payload of 105 kips and the projected area of the DSC shell that is in interface with the EOS-TC135 support rail. Figure 3.9.1-7 and Figure 3.9.1-7a show the pressure load and boundary conditions applied to the FEM.

The interface between the DSC and the EOS-TC135 support rails is modeled through node-to-node contact elements (CONTA178). Nodes that interface with the rails are selected and copied, creating new nodes that are restrained in all DOF and connected to the original nodes belonging to the DSC shell through the CONTA178 contact elements.

Three sets of rails, at 6.5°, 17.5° and 25.5°, are modeled in the FEM. The 6.5° rail is modeled as contacts with closed gaps between the DSC shell and the EOS-TC135 rail. For the second and third rail, at 17.5° and 25.5°, respectively, from the plane of symmetry, contact elements between the rail nodes and the DSC shell nodes are created through the same type of contact element, but the real constant of these elements is modified to the true geometric gap value between the DSC shell and the EOS-TC135 rail.

Horizontal Position in EOS-HSM

When stored in the EOS-HSM, the DSC shell is supported by two, 3-inch wide EOS-HSM slide rails at $\pm 30^\circ$ from the bottom centerline. The inertial loads for DSC internals are accounted for by applying equivalent pressure onto the inner surface of DSC shell representing the EOS-HSM support rail or EOS-HSM-FPS support rail only. The magnitude of the pressure is determined based on the payload of 105 kips and projected area that are in interface with the EOS-HSM support rail.

The interface between the DSC and the EOS-HSM support rail is modeled through node-to-node contact elements (CONTA178). Nodes that interface with the EOS-HSM support rail are selected and copied, creating new nodes. Each row of nodes represents the width of the EOS-HSM support rail (there are three nodes across the width of the rail). Each node of the row is coupled with its neighboring node in all DOF using CERIG command, creating a rigid platform. Figure 3.9.1-7 and Figure 3.9.1-7a show the pressure load and boundary conditions applied to the FEM.

Each middle node of this platform is connected in the axial direction of the DSC through BEAM188 element. Finally, these new nodes representing the EOS-HSM are connected to the original nodes belonging to the DSC shell through the CONTA178 contact elements. Gaps are set to zero, placing the DSC shell and the EOS-HSM support rail in initial contact. Nodes representing the EOS-HSM support rail are constrained in all DOF along a length of 16.5 inches from bottom end and 20.5 inches from the top end. The BEAM188 elements have the properties of the wide-flange steel beam that supports the DSC when inside the EOS-HSM or the plate that supports the DSC when inside the EOS-HSM-FPS.

3.9.1.2.7.2 Fabrication Pressure and Leak Testing

Pressurization and leak testing is performed on the DSC shell and IBCP during fabrication. No other DSC components are in place during this test. A seal plate is placed on the open top of the DSC shell and preloaded through the application of torque on eight bolts that are connected with a flange at the bottom of the DSC shell. The resulting preload to be considered in the evaluation is 155 kips. The DSC is then evacuated to a partial vacuum (simplified to full vacuum) and then re-pressurized with helium. Therefore, two load conditions are evaluated for the DSC shell and IBCP:

1. Leak Test: 155 kip axial compression + 14.7 psi external pressure (full vacuum) on the DSC shell between the top edge and the IBCP + 14.7 psi external pressure on the IBCP. Note that the vacuum will add axial load to the 155 kips preload.
2. Pressure Test: 155 kip axial compression + 23.0 psig internal pressure on the DSC shell between the top edge and the IBCP + 23.0 psig internal pressure on the IBCP. Note that the internal pressure will not affect the reaction on the DSC shell due to the preload.

In order to simulate the leak testing conditions, the OTCP, ITCP and OBCP, TSP and IBS, grapple ring and its support are removed from the FEM, including all contact pair elements.

The bottom surface of the DSC shell surface is constrained in the vertical direction. The 155 kips load is represented by equivalent pressure that is applied at the top surface of the DSC shell.

External pressure is applied at all external nodes of the DSC shell-IBCP assembly with the exception of the top surface of the DSC shell that is loaded with the 155 kips preload. Internal pressure is applied at all nodes on the inside surface of the DSC shell-IBCP assembly. Two load steps are performed, one for the internal pressure and the second one for the external pressure as stated above.

3.9.1.2.7.3 Internal and External Pressure

The DSC pressure boundary is defined by the DSC shell, the IBCP, the ITCP and the associated welds. Since there are no gaps between the top end plate components, the ITCP bears against the OTCP. Since the ITCP meets the leaktight requirements of ANSI N14.5, no leakage is feasible and, therefore, the pressure load is shared by the two plates according to their relative stiffness. Similarly, the absence of gaps between the bottom end components allows the IBCP to bear against the IBS, which, in turn, bears against the OBCP.

Normal (Level A) 15 psig (Elastic)

Off-Normal (Level B) 20 psig (Elastic)

Accident (Level D) 130 psig (Elastic-plastic)

The design pressure of the DSC is 15 psig. A bounding pressure of 20 psig was used in structural evaluations for normal and off-normal conditions. Two load cases were analyzed: one with an internal pressure of 20 psig and the second with an internal pressure of 130 psig.

All of the nodes of the inner surface of DSC shell confined by ITCP and IBCP are selected for application of internal pressure. A node of the grapple is constrained in axial (z-direction) and vertical (x-direction) directions and a node of the OTCP is also constrained in the vertical direction to prevent rigid body motion. Figure 3.9.1-6 shows the internal pressure applied onto the inside of the DSC cavity.

In addition to the internal pressure loads listed above, the DSC will be subjected to hydrostatic, blowdown, vacuum, and test pressures during the fuel loading and draining/drying processes. Prior to loading fuel and without the top end components in place, the TC/DSC annulus is filled with water resulting in a hydrostatic external load on the DSC shell. The hydrostatic load is then balanced by filling the DSC with water.

After the fuel is loaded, the TSP and ITCP are installed and an internal blowdown pressure of 15 psig is applied to evacuate the DSC of water. The DSC internals are then dried under vacuum conditions. The DSC is backfilled with helium at 20 psig. The pressure is then reduced to 3.5 psig and the OTCP is welded in place.

External pressure is applied at all external nodes of the DSC at a level below 12 inches from the top of the DSC. Internal pressure is applied at all surface nodes inside the DSC from the inside of the IBCP up to the ITCP-DSC shell weld. Nodes in contact between the lifting lugs and the DSC shell are not subject to pressure load. Contact elements are modeled on the lateral surface of the shell and the bottom of the OBCP.

Two load steps are performed for the blowdown/pressure test and the vacuum drying with combinations of internal and external pressures without the OTCP installed. Figure 3.9.1-14 and Figure 3.9.1-15 show the stress results for normal and accident internal pressure load cases.

3.9.1.2.7.4 EOS-HSM Loading/Unloading

To load the DSC into the EOS-HSM, the DSC is pushed out of the EOS-TC using a hydraulic ram. The load is applied at the center of the OBCP within the diameter of the grapple ring support. Based on the relative stiffnesses of the cover plates and the IBS, a portion of the insertion load will be transferred through the IBS to the IBCP and associated welds.

Loading is defined as:

Level A/B/C/D: 135 kips (Ram Push)

Unloading (grapple) loads are defined as:

Level A/B: 80 kips (Grapple Pull)

Level C/D: 135 kips (Grapple Pull)

To unload the EOS-HSM, the DSC is pulled using grapple hooks, which engage the grapple ring. The loads applied by the hydraulic ram are balanced by friction between the DSC shell and the EOS-TC135 and/or DSC support structure or FPS DSC support structure.

For the grapple push simulation, the cask is modeled by copying the outer surface nodes of the DSC, creating a new pattern of nodes representing the cask inner surface. These new nodes are restrained in all DOF and connected to the original nodes belonging to the DSC shell through the CONTA178 contact elements. Furthermore, gaps are set to zero at the first rail placing the DSC and the first rail in initial contact. Real constants of contact elements at the second and third rail are set to the gap calculated based on the nodal coordinates of the contact element nodes on both the DSC side and the rail side.

The outer top nodes of the DSC shell are constrained in the axial direction and a node of the ITCP is constrained in the vertical direction to aid in convergence. The insertion force is modeled through a uniform pressure applied within the inner diameter of the grapple support. Two load cases were analyzed: one with a push load of 135 kips, and the second with an internal pressure of 20 psig and a push load of 135 kips. Table 3.9.1-12 and Table 3.9.1-12a lists the load conditions. Figure 3.9.1-10 and Figure 3.9.1-10a show the load and boundary conditions applied to the FEM.

For the grapple pull simulation, the outer top nodes of the DSC shell are constrained in the axial direction and a node of ITCP is constrained in the vertical direction to aid in convergence. The extraction force is modeled through nodal forces applied on selected nodes within the footprint of the grapple hook. Five load cases were analyzed combining pressure loads and are described in the table below. Refer to Table 3.9.1-12 and Table 3.9.1-12a for load combinations. Figure 3.9.1-9 and Figure 3.9.1-9a show the load and boundary conditions applied to the FEM.

Internal Pressure	Pull Force (kips)	Analysis Type
0	80	Elastic
20	80	Elastic
0	135	Elastic-plastic
20	135	Elastic-plastic
20	80	Limit Load Elastic-perfectly plastic

For the normal condition pull load cases, a limit load analysis is performed to show that the stresses at the junction between the grapple ring support and the outer bottom cover plate are secondary stresses. The limit load analysis is described in NB-3228.1 [3.9.1-2]. The grapple ring assembly is acceptable for the normal pull load if the lower bound limit load (LL) is equal to or greater than 1.5 times the normal pull load ($2/3 * LL$) without any excessive deformation and plastic strain. The lower bound limit load is determined using elastic-perfect plastic material properties with a yield strength defined as $1.5S_m$. The last converged load step for the limit load analysis corresponds to a 200 kip axial pull load, which is greater than $1.5 * 80 \text{ kip} = 120 \text{ kip}$.

3.9.1.2.7.5 Transfer/Handling Load

The same model described above for HSM loading and unloading is used and updated to reflect the effect of the vertical 1g load, transverse 1g load, axial 1g load and internal pressure of 20 psig.

Two runs were performed for this load:

1. Deadweight + 1g vertical + 1g transverse + 1g axial with the weight of DSC internals modeled by equivalent pressure application on TSP with addition of internal pressure of 20 psig.
2. Deadweight + 1g vertical + 1g transverse + 1g axial with the weight of DSC internals modeled by equivalent pressure application on IBCP with addition of internal pressure of 20 psig.

3.9.1.2.7.6 Seismic Load during Storage

The same model described in Section 3.9.1.2.7.1 for dead weight in EOS-HSM is used and updated to reflect the effect of the vertical 1g load, transverse 2g load, axial (longitudinal) 1.25g load, and the internal pressure load of 20 psig.

Two elastic-plastic runs are performed for this load:

1. 1g vertical + 2g transverse + 1.25g axial with the weight of DSC internals modeled by equivalent pressure application on TSP with addition of internal pressure of 20 psig.
2. 1g vertical + 2g transverse + 1.25g axial with the weight of DSC internals modeled by equivalent pressure application on IBS with addition of internal pressure of 20 psig.

The dead weight and 1g vertical and 2g transverse effect is modeled by multiplying the pressure projected at the EOS-HSM support rail through the DSC shell by a conservative factor of 5.

DSC support within an EOS-HSM is provided by two, 3.00-inch wide rails at $\pm 30^\circ$ from the bottom centerline. Seismic axial forces toward the EOS-HSM door are resisted by the axial retainer. The retainer is a 4-inch x 2-inch steel bar located on the vertical centerline, at the edge of the DSC shell below the center of the DSC. The retainer bears against the edge of the DSC shell and OBCP. The nodes of DSC shell and OBCP, which bears against the area of the retainer bar, are restrained in the axial direction. Figure 3.9.1-13 shows the pressure load and boundary conditions applied to the DSC while supported by the DSC support rail. Figure 3.9.1-13a shows the pressure load and boundary conditions applied to the DSC while supported by the FPS DSC support *structure*.

The DSC shell and the OBCP experience compressive bearing stress in the vicinity of the axial retainer. The bearing stresses experienced by the DSC shell and OBCP need not be evaluated for Service Level D loads.

Seismic axial forces away from the EOS-HSM door are resisted by the canister stop plates located at the ends of the support rails. The stop plates are 11 inches wide. Because the top cover plate is recessed from the edge of the DSC shell, the stop plates bear against the bottom edge of the DSC shell only. The nodes of the top end of DSC shell, which come into contact with the DSC stop plate, are restrained in the axial direction. Figure 3.9.1-18 shows the stress results for seismic load acting towards the stop plates of the DSC support structure.

3.9.1.2.7.7 Cask Drop

Side and end drop accelerations of 75g are applied. Drops are only postulated for the DSC when positioned inside of the EOS-TC135. The following accident drops are analyzed:

- 65-inch side drop of the TC onto a concrete pad above a generic soil profile.
- A corner drop from a height of 65 inches at an angle of 30° to the horizontal, onto the top or bottom corner of the TC (two cases) using the bounding deceleration based on a 65-inch drop.

The top end drop and bottom end drop are not credible events under 10 CFR Part 72; therefore, these drop analyses are not required. However, consideration of end drops (for 10 CFR Part 71 conditions) and the 65-inch side drop is performed to conservatively envelope the effects of a corner drop.

In summary, three drop conditions are considered in the analyses:

- 75g bottom end drop
- 75g top end drop
- 75g side drop

End Drop

For the bottom end drop, the interface between the bottom surface of DSC shell and OBCP (excluding the OBCP surface, which falls inside the grapple ring support) with the EOS-TC135 is modeled through CONTA178 node-to-node contact elements. The nodes of the EOS-TC135 are constrained in the vertical direction representing TC as a rigid surface. The payload is applied as a load of 105 kips multiplied by 75. The inertial load of the basket assembly and fuel is applied as uniform pressure acting on the IBCP. An elastic-plastic material model is used in the analysis. In addition to pressure representing the payload inertia load, conservative internal pressure of 20 psig is added.

For the bottom end drop, the couplings (CP) representing the welds between the lug plate and the DSC shell are deleted from the model and these welds are modeled by spring elements (COMBIN14). Figure 3.9.1-12 and Figure 3.9.1-12a show the pressure load and boundary conditions applied to the FEM.

Two load cases are performed for bottom end drop:

- Bottom end drop without internal pressure
- Bottom end drop with internal pressure

For the top end drop, the interface between the top surface of the DSC and the EOS-TC135 is modeled through CONTA178 node-to-node contact elements. The nodes of the EOS-TC135 (node position 2 of CONTA178 elements) are constrained in all directions representing TC as a rigid surface. The payload is applied as a total load of 105 kips multiplied by 75g. The inertial load of the basket assembly and fuel is applied as uniform pressure acting on the bottom side of the TSP. An elastic-plastic material model is used in the analysis. In addition to pressure representing the payload inertia load, this load case includes a 20 psig internal pressure in the model, as opposed to adding the internal pressure load case later.

Two load cases are performed for top end drop:

- Top end drop without internal pressure
- Top end drop with internal pressure

Side Drop

The side drop analysis of the DSC shell assembly is simplified by considering the distribution of the basket load to the DSC as uniform. The basket is flexible enough to deform under the action of 75g deceleration of its contents and, therefore, during an accident side drop, the basket will tend to bend under the action of the higher g-loads on its contents. This results in a uniform radial pressure load applied to the inner surface of the DSC to represent the basket load.

An elastic-plastic analysis was performed for side drop analysis. For elastic-plastic analyses, the steel components (except shield plugs) are modeled by a bilinear kinematic hardening method. At the specified yield stress, the curve continues along the second slope defined by the plastic modulus. It is assumed that the plastic modulus is 5% of the elastic modulus, except for shield plugs, which are modeled with elastic material properties.

Side Drop on Cask Rails

A uniform pressure load is applied to the DSC inner surface. The inner nodes of the DSC are selected from 0° to 45° and a uniform pressure is applied. The interface between the DSC and the EOS-TC135 is modeled through node-to-node contact elements CONTA178. Nodes that interface with the DSC are selected and copied, creating new pattern of nodes. These new nodes are restrained in all DOF and connected to the original nodes belonging to the DSC shell through the CONTA178 contact elements. Gaps are set to zero at the 6.5° and 17.5° rail, placing the DSC and the 6.5° and 17.5° rail in initial contact. Real constants of contact elements at the 25.5° rail are set to a gap calculated based on the nodal coordinates of the contact element node at the DSC side and the rail side. The small radial gaps between the shield plugs and the DSC shell are set to zero, since during a side drop event these gaps will close.

In addition to pressure representing the payload inertial load, this load case includes a 20 psig internal pressure in the model, as opposed to adding the internal pressure load case later.

Two load cases are analyzed for the side drop onto the cask rail:

- Side drop onto the cask rail without internal pressure
- Side drop onto the cask rail with internal pressure

Side Drop Away From Cask Rails

The interface between the DSC and the EOS-TC135 is modeled through node-to-node contact elements CONTA178. Nodes that interface with the DSC are selected and copied, creating new pattern of nodes. These new nodes are restrained in all DOF and connected to the original nodes belonging to the DSC shell through the CONTA178 contact elements. Gaps between the DSC shell and the cask inner surface are set to the gap calculated based on nodal coordinates of the contact element node at the DSC side and the cask side. At the point where the DSC contacts the rigid cask, the initial contact gap is zero. Circumferentially away from this initial contact point, the initial contact gap increases. The small radial gap between the shield plugs and the DSC shell is set to zero since during a side drop event, this gap will close.

In addition to pressure representing the payload inertial load, this load case includes a 20 psig internal pressure in the model, as opposed to adding the internal pressure load case later. Figure 3.9.1-11 and Figure 3.9.1-11a show the load and boundary conditions applied to the FEM.

Two load cases are analyzed for side drop away from the cask rail:

- Side drop away from the cask rail without internal pressure
- Side drop away from the cask rail with internal pressure

Figure 3.9.1-16 shows the stress results for side drop away from cask rails without internal pressure.

3.9.1.2.7.8 Thermal Loads

Per Chapter 4, the thermal storage load cases have lower temperature gradients in the DSC shell compared to thermal transfer load cases. Therefore, only bounding off-normal thermal transfer load cases have been selected for thermal stress analysis of the EOS-37PTH DSC.

For thermal stress analysis, temperature profiles and maximum component temperatures are based on the thermal analyses of the EOS-37PTH DSC in TC125 for transfer conditions, which is discussed in Chapter 4. Only the off-normal load cases with higher temperature gradients in the DSC shell are taken for thermal stress analysis.

Since the TC125 is shorter than TC135, there is a higher temperature distribution in TC125. Therefore, the thermal analysis of the EOS-37PTH in TC125 bounds the thermal analysis of EOS-37PTH in TC135. The thermal conditions have been evaluated separately to minimize the number of analyses to be performed. For all DSC components, the thermal stresses have been combined by adding the maximum stress intensities of components from thermal load runs to the primary membrane plus bending stresses of components from mechanical load runs.

Thermal stresses are classified as secondary stresses per the ASME Code, [3.9.1-3]. These secondary stresses are a result of dissimilar material properties, primarily differential thermal growth of a structure due to material thermal expansion coefficient differences between different materials used for construction of the structure, or differential temperature distribution throughout the structure, or a combination of both.

Nodal temperature from thermal analyses is transferred to the structural model described in Section 3.9.1.2.3. The structural model is solved and stresses of thermal load of each load step are post-processed and the largest stresses for all the transfer cases are selected. Only the largest selected stresses are used for further stress evaluation and stress combination.

3.9.1.2.8 Load Combinations

The bounding load combinations, along with the applicable ASME service level, are listed in Chapter 2, Table 2-5 for the shell assembly. Stresses generated by applied loads described in Section 3.9.1.2.7.1 are combined in a manner that bounds all load conditions under consideration. The methodologies for combining the load cases into their corresponding load combinations are described in the following sections.

Load Combination 1

Load Combination 1 (LC1) addresses the DSC when it is in a vertical position. LC1 is developed by adding the linearized stress intensities of a vertical dead weight load case, an internal pressure of 20 psig within the DSC and the maximum stress intensities due to thermal loading.

Load Combinations 2 and 3

Load Combinations 2 and 3 (LC23) addresses the DSC when it is in a horizontal position. LC23 is developed by adding linearized stress intensities from a model comprised of the dead weight, an internal pressure of 20 psig within the DSC and handling loads with thermal loads.

Load Combination 4

Load Combination 4 (LC4) addresses the DSC when it is in a horizontal position. LC4 describes a hydraulic ram push case. The stress intensities from the dead weight load case, the 135-kip insertion load cases and thermal load cases are determined independently and subsequently added together to develop the maximum stress intensity on the DSC components and welds. The 135-kip insertion model evaluates the system with and without a 20-psig internal pressure load.

Load Combination 5

Load Combination 5 (LC5) addresses the DSC when it is in a horizontal position. LC5 describes a hydraulic ram pull case. The stress intensities from the dead weight load case, the 80-kip retrieval load cases and thermal load cases are determined independently and subsequently added to develop the maximum stress intensity on the DSC component and weld. The 80-kip retrieval model evaluates the system with and without a 20-psig internal pressure load.

Load Combination 6

Load Combination 6 (LC6) addresses the DSC when it is in a horizontal position. LC6 describes a hydraulic ram pull case. The stress intensities from the dead weight load case and the 135-kip retrieval load cases are determined independently and subsequently added to develop the maximum stress intensity on the DSC component and weld. The 135-kip retrieval model evaluates the system with and without a 20-psig internal pressure load.

Load Combination 7A

Load Combination 7A (LC7A) addresses the DSC when it is in a horizontal position. LC7A describes the 65-inch accident drop condition. LC7A is developed by post-processing the stresses from a FEM that includes the 20-psig off-normal internal pressure load and the 75g side drop load.

Load Combination 7B

Load Combination 7B (LC7B) addresses the DSC when it is in a vertical position. LC7B describes the 65-inch accident drop condition. LC7B is developed by post-processing the stresses from a FEM that includes the 20-psig off-normal internal pressure load and the 75g end drop load.

Load Combination 8

Load Combination 8 (LC8) addresses the DSC when it is in the horizontal position. LC8 describes the accident internal pressure load case. The stress intensities from the dead weight load case and the 130-psig internal pressure load case are determined independently and subsequently added to develop the maximum stress intensity on the DSC component and weld.

Load Combination 9

Load Combination 9 (LC9) addresses the DSC when it is in the horizontal position. LC9 describes the off-normal internal pressure load case. The stress intensities from the dead weight load case, 20-psig internal pressure load case and thermal load cases are determined independently and subsequently added to develop the maximum stress intensity on the DSC component and weld.

Load Combination 10

Load Combination 10 (LC10) addresses the DSC when it is in the horizontal position. LC10 describes the seismic load case. LC10 is developed by post-processing the stresses from an FEM that includes the internal off-normal pressure loads and the seismic loads.

Load Combination 11

Load Combination 11 (LC11) addresses the DSC when it is in the vertical position. LC11 describes the fabrication pressure and leak testing loads. LC11 is developed by post-processing the stresses from stresses from the fabrication pressure/leak test load case.

3.9.1.3 DSC Shell Buckling Evaluation

An FE plastic analysis with large displacement option is performed to monitor occurrence of canister shell buckling under the specified loads.

The bottom end drop envelopes the top end drop because the top end structure is heavier than the bottom end structure, which will impose a larger load on the DSC shell. A drop on the bottom end is therefore chosen for buckling analysis.

The buckling analysis uses the same model as the end drop simulation.

The inertia load of the basket assembly and fuel is applied as uniform pressure acting on the IBCP. Elastic-plastic bilinear kinematic hardening material model is used at a uniform temperature of 500 °F with a plastic tangent modulus conservatively taken at 1% of the elastic modulus for buckling. Conservatively, no internal pressure that could have a stabilizing effect is applied. Large deformation effect NLGEOM is enabled in the ANSYS model.

The uniform pressure at the IBCP that represents the payload is multiplied by acceleration as a g-factor that is computed at two values, 75g and 130g. The 130g simulation represents the stability load qualification.

The 130g load is conservatively used as the buckling load. Two thirds of the maximum compressive load of 130g is equal to the 87g limit load per F-1331.5 of Appendix F, [3.9.1-3], which is higher than required load of 75g. It is, therefore, concluded that buckling of the DSC will not occur during a hypothetical accident end drop.

3.9.1.4 DSC Fatigue Analysis

Fatigue effects on the EOS-37PTH DSC is addressed using NB-3222.4 criteria of [3.9.1-3]. Fatigue effects need not be specifically evaluated, provided the criteria contained in NB-3222.4(d) are met. A summary of the six criteria and their application to the DSC is presented below:

- A. The first criterion states that the DSC is adequate for fatigue effects, provided that the total number of atmospheric-to-operating pressure cycles during normal operation (including startup and shutdown) does not exceed the number of cycles on the applicable fatigue curve corresponding to a S_a value of three times the S_m value of the material at operating temperatures. This condition is satisfied for the DSC since the pressure is not cycled during its design life. The pressure established at the time that the DSC is sealed following fuel loading and DSC closure operations is maintained during normal storage in the EOS-HSM.
- B. The second criterion states that DSC is adequate for fatigue effects, provided that the specified full range of pressure fluctuations during normal operation does not exceed the quantity $(1/3) \times \text{design pressure} \times (S_a/S_m)$, where S_a is the value obtained from the applicable fatigue curve for the total specified number of significant pressure fluctuations, and S_m is the allowable stress intensity for the material at operating temperatures.

Significant pressure fluctuations are those for which the total excursion exceeds $(1/3) \times \text{design pressure} \times (S/S_m)$, where S equals the value of S_a for 10^6 cycles. Using a design pressure of 20.0 psig, an S_m value of 17,500 psi, and an S value of 28,200 psi, the total range for a significant pressure fluctuation is 10.7 psig. This pressure fluctuation is not expected to occur during normal storage as a result of seasonal ambient temperature changes.

Ambient temperature cycles significant enough to cause a measurable pressure fluctuation are assumed to occur five times per year for 80 years. The number of fluctuations with this pressure range is expected to be 400 for the DSC. The value of S_a associated with this number of cycles is 170 ksi. Therefore, the value of $(1/3) \times \text{design pressure} \times (S_a/S_m)$ is equal to 64.76 psig. Clearly, this value will not be exceeded during the normal condition lifetime of the DSC. Therefore, the second criterion is satisfied for the DSC.

- C. The third criterion states that the DSC is adequate for fatigue effects, provided that the temperature differences between any two adjacent points on the DSC during normal operation do not exceed $S_a/2E\alpha$, where S_a is the value obtained from the applicable fatigue curve for the specified number of startup-shutdown cycles, α is the instantaneous coefficient of thermal expansion at the mean value of the temperatures at the two points, and E is the modulus of elasticity at the mean value of the temperatures at the two points.

For an operational cycle of the DSC, thermal gradients occur during fuel loading, DSC closure, transport to the EOS-HSM, and transfer of the DSC to the EOS-HSM. This half-cycle is approximately reversed for DSC unloading operations. However, this normal operational cycle occurs only once in the design service life of a DSC. Since there is only one startup-shutdown cycle associated with the DSC, the value of S_a is very large (>800 ksi). Therefore, the value of $S_m/2E\alpha$ is very large ($>1500^\circ\text{F}$). This is far greater than the temperature difference between any two adjacent points on the dry shielded canister. Therefore, the third criterion is satisfied for the DSC.

- D. The fourth criterion states that the DSC is adequate for fatigue effects, provided that the temperature difference between any two adjacent points on the DSC does not change during normal operation by more than the quantity $S_a/2E\alpha$, where S_a is the value obtained from the applicable fatigue curve for the total specified number of significant temperature difference fluctuations.

A temperature difference fluctuation is considered to be significant if its total algebraic range exceeds the quantity $S/2E\alpha$ where S is value of S_a (28,200 psi) obtained from the applicable fatigue curve for 10^6 cycles if the number of cycles is 10^6 or less.

Small fluctuations in the DSC thermal gradients during normal storage in the EOS-HSM occur as a result of seasonal ambient temperature changes. Ambient temperature cycles significant enough to cause a measurable thermal gradient fluctuation are assumed to occur five times per year for 80 years. The temperature gradient fluctuation is 250 cycles. Since this is less than 10^6 cycles, the value of $S/2E\alpha$ at 10^6 cycles is 112.7°F .

The most significant fluctuation in normal operating temperature occurs during a change in ambient temperature from -20°F to 100°F . A review of thermal evaluation of EOS-HSM loaded with EOS-37PTH DSC storage load cases in Chapter 4 concluded that the temperature difference between adjacent points in the DSC does not exceed the quantity 112.7°F , therefore the fourth condition is satisfied for the DSC.

- E. The fifth criterion states that for components fabricated from materials of differing moduli of elasticity or coefficients of thermal expansion, the total algebraic range of temperature fluctuation experienced by the component during normal operation must not exceed the magnitude $S_a/2(E_1\alpha_1 - E_2\alpha_2)$, where S_a is the value obtained from the applicable fatigue curve for the total specified number of significant temperature fluctuations, E_1 and E_2 are the moduli of elasticity, and α_1 and α_2 are the values of the instantaneous coefficients of thermal expansion at the mean temperature value involved for the two materials of construction.

A temperature fluctuation is considered to be significant if its total excursion exceeds the quantity $S/2(E_1\alpha_1 - E_2\alpha_2)$, where S is the value of S_a obtained from the applicable fatigue curve for 10^6 cycles. If the two materials have different applicable design fatigue curves, the lower value of S_a has to be used. Since the structural material used to construct the DSC shell is 240 Type 304 and shield plug is A-36, therefore taking the values of $E_1 = 25.9 \times 10^6$ psi, $E_2 = 27.3 \times 10^6$, $\alpha_1 = 10.5 \times 10^{-6}$ and $\alpha_2 = 8.0 \times 10^{-6}$ (Section II, Part D, [3.9.1-2]), the quantity $S/2(E_1\alpha_1 - E_2\alpha_2) = 268.6^\circ\text{F}$.

Since the DSC experiences temperature fluctuation from -20°F to 100°F , the range of temperature fluctuation is 120°F which is less than 268.6°F . Therefore, the fifth criterion is satisfied for the DSC.

- F. The sixth criterion states that the DSC is adequate for fatigue effects, provided that the specified full range of mechanical loads does not result in a stress range that exceeds the S_a value obtained from the applicable fatigue curve for the total specified number of significant load fluctuations. If the total specified number of significant load fluctuations exceeds 10^6 , the S_a value at $N = 10^6$ can be used.

A load fluctuation is considered to be significant if the total excursion of stresses exceed the value of S_a obtained from the applicable fatigue curve for 10^6 cycles. The only mechanical loads that affect the DSC are those associated with handling loads and a seismic event. One handling load cycle and a major seismic event are postulated during the design life of the DSC. The DSC stresses resulting from these mechanical load fluctuations are small since the structural capacity of the DSC is designed for extreme accident loads such as a postulated cask drop.

The number of significant cycles associated with mechanical load fluctuations is conservatively assumed to be 1,000. The value of S_a associated with this number of cycles is 120 ksi. Since the maximum stress range intensity permitted by the code is $3.0 S_m$, or 52.5 ksi for SA-240, Type 304 stainless steel at 500°F , this sixth condition is satisfied for the DSC.

The evaluation presented in the preceding paragraphs demonstrates that the six criteria contained in NB-3222.4(d) are satisfied for all components of the EOS-37PTH DSC.

3.9.1.5 DSC Weld Flaw Size Evaluation

EOS-37PTH DSC is considered as the bounding DSC for weld flaw evaluation because the weight of EOS-37PTH DSC (long) is greater than the weight of EOS-89BTH DSC.

3.9.1.5.1 Methodology

It is stipulated that the critical flaw configuration is a circumferential weld flaw exposed to the tensile component radial stress. The determination of the allowable surface and sub-surface flaw depth is accomplished by means of the methodology outlined below.

- Determine the tensile radial membrane stresses in the weld. Evaluate membrane radial stresses occurring at the weld between the OTCP and the DSC shell for all individual loads.
- Determine limiting membrane radial stresses in the OTCP weld for all load combinations, for Service levels A, B, C, and D.
- Limiting stresses are multiplied by safety factors SF_m for the corresponding service levels.
- Since OTCP weld is gas tungsten arc welding (GTAW) (non-flux weld), according to ASME Code Sec XI, Division 1, Figure C-4210-1 [3.9.1-4], maximum allowable flaw depth is estimated using limit load criteria.

The allowable membrane stress, S_t , in the flawed section for each service level is determined from Article C-5322, Appendix C [3.9.1-4] where the relation between the applied membrane stress and flaw depth at incipient stress is given.

3.9.1.5.2 Flaw Size Calculation

For 3D, half-symmetric model, as described in Section 3.9.1.2.3, the tensile radial membrane stresses in the weld are evaluated by the stress linearization method explained in Section 3.9.1.2.5.

Radial stresses for controlling load combination are calculated by adding individual load cases. Bounding radial tensile stresses in OTCP weld for all load combinations for Service Level A, B, and D are assessed. The allowable flaw depths, calculated by means of the methodology described in previous Section and are shown in Table 3.9.1-13.

Based on the evaluation, requirements for welding and weld inspections should be based on limiting the weld critical depth for surface and subsurface flaws to the following values:

- Surface Crack: 0.38 inch.
- Subsurface Crack: 0.38 inch.

3.9.1.6 Conclusions

The EOS DSC shell assembly has been analyzed for normal, off-normal, and accident load conditions using three dimensional finite element analyses. The load combinations provided in Section 3.9.1.2.8 are used in the analysis of the EOS DSC. Stress intensities in different components of the DSC shell assembly, compared with ASME code stress intensity allowables and the resulting stress ratios are summarized in Table 3.9.1-7, Table 3.9.1-7a, Table 3.9.1-8, Table 3.9.1-9, Table 3.9.1-10, Table 3.9.1-11, Table 3.9.1-12, and Table 3.9.1-14 for DSCs supported by the DSC support structure and Table 3.9.1-7b, Table 3.9.1-7c, Table 3.9.1-8a, Table 3.9.1-9a, Table 3.9.1-10a, Table 3.9.1-11a, and Table 3.9.1-12a for DSCs supported by the FPS DSC support structure. *FPS DSC support structure evaluations provide results for the maximum and the minimum lengths of canisters for the EOS-HSM-FPS and EOS-HSMS-FPS designs. Minimum length DSC is determined to be the controlling configuration in DSC evaluations. Results obtained for minimum canister length are documented in this chapter.* The stress ratio is calculated by dividing the maximum stress intensity by the stress intensity allowable value, with the stress ratio required to be less than 1. Figure 3.9.1-20 shows the linearized component stresses for the DSC shell for the internal pressure (normal) load case. Figure 3.9.1-27 shows the strain criteria state of the DSC.

For DSCs supported by the DSC support structure, the maximum ratio of induced load to allowable load for a confinement boundary area is 0.76, in the weld between the ITCP and the DSC shell during a side drop event. The maximum overall ratio of 0.92 occurs in the grapple ring support, seconded by a ratio of 0.85 in the non-confinement area of the DSC shell during a grapple pull/accident scenario.

For DSCs supported by the FPS DSC support structure, the maximum ratio of induced load to allowable load for a confinement boundary area is 0.74 and occurs in the confinement boundary area of the DSC shell while the DSC is in horizontal position as described in LC9. The maximum overall stress ratio is 0.92 and occurs in the grapple ring support, seconded by a ratio of 0.85 in the non-confinement area of the DSC shell during a grapple pull/accident scenario.

The above evaluations, specifically the closure welds, are supplemented with additional limit load and strain criteria analyses. These analyses are presented in Section 3.9.1.2.6. The results of the limit load analysis show that there is sufficient margin compared to the design loads. The results of the strain criteria analysis show a maximum equivalent plastic strain of 0.065 in/in during a side drop event, compared to the allowable uniform strain limit of 0.17 in/in, demonstrating a minimum factor of safety of 2.6 in the design. The factor of safety is calculated by dividing the maximum allowable strain by the maximum equivalent plastic strain, and must be greater than 1.

The structural integrity of the DSC shell, including closure welds, is maintained since the maximum stress ratio is less than 1 and the limit load and strain criteria analyses results were lower than their respective limits.

Convergence/Sensitivity Studies

The base model and mesh used to evaluate the EOS DSC is validated by three sensitivity studies focused on gap modeling methodology, radial and longitudinal element size in an axisymmetric internal pressure environment, and circumferential element sizes in a lateral load side drop environment. A model with midside nodes was added to the axisymmetric model and showed lower stresses than the other models, and thus these midside nodes were conservatively excluded from the analytical model. No significant difference in results were observed between the employed model and the refined models, therefore the employed model is producing accurate results.

It is on these bases that the EOS DSC assembly is determined to be, as designed, structurally adequate under all anticipated load conditions for service during storage and transfer.

3.9.1.7 References

- 3.9.1-1 Title 10, Code of Federal Regulations, Part 72, "Licensing Requirements for the Independent Storage of Spent Nuclear Fuel, High-Level Radioactive Waste, and Reactor-Related Greater than Class C Waste."
- 3.9.1-2 American Society of Mechanical Engineers, ASME Boiler and Pressure Vessel Code, Section II, Part D, 2010 Edition through 2011 Addenda.
- 3.9.1-3 American Society of Mechanical Engineers, ASME Boiler and Pressure Vessel Code, Section III, 2010 Edition through 2011 Addenda.
- 3.9.1-4 American Society of Mechanical Engineers, ASME Boiler and Pressure Vessel Code, Section XI, Division 1, Appendix C, 2010 Edition Addenda through 2011 Addenda.
- 3.9.1-5 ANSI N14.5, "Leakage Tests on Packages for Shipment of Radioactive Materials," 1997.
- 3.9.1-6 ANSI N14.6 – 1993, "American National Standard for Radioactive Materials – Special Lifting Devices for Shipping Containers Weighing 10000 pounds (4500 kg) or More," American National Standards Institute, Inc., New York.
- 3.9.1-7 NUREG-1536, "Standard Review Plan for Spent Fuel Dry Cask Storage Systems at a General License Facility," Revision 1, U.S. Nuclear Regulatory Commission, July 2010.
- 3.9.1-8 U.S. Nuclear Regulatory Commission, Regulatory Guide 1.60, "Design Response Spectra for Seismic Design of Nuclear Power Plants," Revision 1, 1973.
- 3.9.1-9 ANSYS Computer Code and User's Manual, Release 14.0, 14.0.3, and 17.1.

3.9.1-10 American Society of Mechanical Engineers, ASME Boiler and Pressure Vessel Code, 2013, Section III Appendices.

Table 3.9.1-1
EOS37PTH DSC Major Dimensions

Component	Dimensions
Outer Diameter of DSC Shell	75.50 inches
DSC Shell Thickness	0.5 inch
DSC Length	219 inches ⁽¹⁾
OTCP Thickness	2 inches
ITCP Thickness	2 inches
TSP Thickness	6 inches
OBCP Thickness	2 inches
IBCP Thickness	2 inches
IBS	4 inches

(1) Indicated length is for longest EOS-37PTH DSC

Table 3.9.1-2
Material of EOS DSC Components (Analysis)

DSC Shell	ASME SA-240 Type 304
OTCP	ASME SA-240 Type 304
ITCP	ASME SA-240 Type 304
TSP	ASTM A36
OBCP	ASTM A240 Type 304
IBCP	ASME SA-240 Type 304
IBS	ASTM A36
Grapple Ring Support	ASTM A240 Type 304
Grapple Ring	ASTM A240 Type 304
Lifting Lug Plate	ASME SA-240 Type 304
Lifting Lug	ASTM A240 Type 304

Table 3.9.1-3
Elastic-Plastic Material Properties

Material Property	SA-240 Type 304 at 500 °F	SA-36 at 500 °F
Elastic Modulus (psi)	25.9×10^6	27.3×10^6
Yield Strength (psi)	19,400	29,300
Tangent Modulus, E_t (psi)	5% of E = 1.295×10^6	5% of E = 1.365×10^6

Table 3.9.1-4
Allowable Weld Stresses for Pressure Boundary Partial Penetration Welds,
Material Type 304

Service Level	Stress Region / Category	Stress Criteria	Allowable Stress Value at 350 °F [ksi]
Level A / Level B	Primary Local Membrane Stress, P_L	$P_L = 0.8 [1.5 S_m]$	23.2
	Primary Local Membrane + Bending Stress, $P_L + P_b$	$P_L + P_b = 0.8 [1.5 S_m]$	23.2
	Primary + Secondary Stress, $P+Q$	$P_L + P_b + Q = 0.8 [3.0 S_m]$	46.3
Level D (Elastic)	Primary Local Membrane Stress, P_L	$0.8 [\text{Min}(3.6 S_m, S_u)]$	52.08
	Primary Local Membrane + Bending Stress, $P_L + P_b$	$0.8 [\text{Min}(3.6 S_m, S_u)]$	52.08
Level D (Elastic Plastic)	Primary Local Membrane Stress, P_L	$0.8 [0.9 S_u]$	46.9
	Primary Local Membrane + Bending Stress, $P_L + P_b$	$0.8 [0.9 S_u]$	46.9

Table 3.9.1-5
SA-240/SA-479 304 & SA-182 F304 -Stress Allowables

Temp (°F)	S_m (ksi)	S_y (ksi)	S_u (ksi)	Level A/B			Level D (Elastic)		Level D (Plastic)	
				P_m	$P_m + P_b$	$P_m + P_b + Q$	P_m	$P_m + P_b$	P_m	$P_m + P_b$
70	20	30	75	20.0	30.0	60.0	48.0	72.0	52.5	67.5
200	20	25	71	20.0	30.0	60.0	48.0	71.0	49.7	63.9
300	20	22.4	66.2	20.0	30.0	60.0	46.3	66.2	46.3	59.6
400	18.6	20.7	64	18.6	27.9	55.8	44.6	64.0	44.8	57.6
500	17.5	19.4	63.4	17.5	26.3	52.5	42.0	63.0	44.4	57.1
600	16.6	18.4	63.4	16.6	24.9	49.8	39.8	59.8	44.4	57.1
700	15.8	17.6	63.4	15.8	23.7	47.4	37.9	56.9	44.4	57.1

Table 3.9.1-6
Allowable Base Metal Stresses for Non Pressure Boundary Partial
Penetration and Fillet Welds Type 304 Base Metal

Temp. (°F)	S_y (ksi)	Level A F_w = .40S_y	Level B F_w = .53S_y	Level C F_w = .60S_y	Level D F_w = .80S_y
100	30	12	15.9	18	24
200	25	10	13.3	15	20
300	22.4	8.96	11.9	13.4	17.9
400	20.7	8.28	11	12.4	16.6
500	19.4	7.76	10.3	11.6	15.5
600	18.4	7.36	9.75	11	14.7
650	18	7.2	9.54	10.8	14.4
700	17.6	7.04	9.33	10.6	14.1

Table 3.9.1-7
DSC Shell Stress Results, Confinement Boundary – Load Combinations
 3 Pages

Load Comb No.	Service Level	DSC Orientation	Stress Category	Loads	Stress intensity (ksi)	Allowable Stress (ksi)	Stress Ratio
1	A	Vertical ⁽¹⁾	P_m	DWv + max($PI_{(20)}$, BD, VD)	2.51	17.50	0.14
			$P_m + P_b$	DWv + max($PI_{(20)}$, BD, VD)	7.87	26.25	0.30
			P_L	DWv + max($PI_{(20)}$, BD, VD)	6.80	26.25	0.26
			P_m (or P_L) + P_b + Q	DWv + max($PI_{(20)}$, BD, VD)	12.28	52.50	0.23
			P_m (or P_L) + P_b + Q + P_e	DWv + max($PI_{(20)}$, BD, VD) + TH	29.82	52.50	0.57
2/3	A	Horizontal ⁽²⁾	P_m	DWh + 1g axial + 1g transverse + 1g Vertical + $PI_{(20)}$	2.49	17.50	0.14
			$P_m + P_b$	DWh + 1g axial + 1g transverse + 1g Vertical + $PI_{(20)}$	3.30	26.25	0.13
			P_L	DWh + 1g axial + 1g transverse + 1g Vertical + $PI_{(20)}$	6.21	26.25	0.24
			P_m (or P_L) + P_b + Q	DWh + 1g axial + 1g transverse + 1g Vertical + $PI_{(20)}$	10.98	52.50	0.21
			P_m (or P_L) + P_b + Q + P_e	DWh + 1g axial + 1g transverse + 1g Vertical + $PI_{(20)}$ + TH	28.52	52.50	0.54
4	A/B	Horizontal ⁽²⁾	P_m	DWh + 135kips + $PI_{(20)}$	2.89	17.50	0.17
			$P_m + P_b$	DWh + 135kips + $PI_{(20)}$	4.19	26.25	0.16
			P_L	DWh + 135kips + $PI_{(20)}$	7.17	26.25	0.27
			P_m (or P_L) + P_b + Q	DWh + 135kips + $PI_{(20)}$	16.09	52.50	0.31
			P_m (or P_L) + P_b + Q + P_e	DWh + 135kips + TH	33.63	52.50	0.64
5	A/B	Horizontal ⁽²⁾	P_m	DWh + 80 kips + $PI_{(20)}$	2.20	17.50	0.13
			$P_m + P_b$	DWh + 80 kips + $PI_{(20)}$	3.75	26.25	0.14
			P_L	DWh + 80 kips + $PI_{(20)}$	6.31	26.25	0.24
			P_m (or P_L) + P_b + Q	DWh + 80 kips + $PI_{(20)}$	13.50	52.50	0.26
			P_m (or P_L) + P_b + Q + P_e	DWh + 80 kips + TH	31.04	52.50	0.59

Table 3.9.1-7
DSC Shell Stress Results, Confinement Boundary – Load Combinations
 3 Pages

Load Comb No.	Service Level	DSC Orientation	Stress Category	Loads	Stress intensity (ksi)	Allowable Stress (ksi)	Stress Ratio
6	D	Horizontal ⁽²⁾	P_m	DWh + 135 kips + $PI_{(20)}$	2.81	44.38	0.06
			$P_m + P_b$	DWh + 135 kips + $PI_{(20)}$	4.62	57.06	0.08
			P_L	DWh + 135 kips + $PI_{(20)}$	6.67	57.06	0.12
			P_m (or P_L) + P_b + Q	DWh + 135 kips + $PI_{(20)}$	NA		
7A	D	Horizontal ⁽²⁾	P_m	DWh + max.(SD_AWAY, SD_RAIL_EP, SD_TOP_RAIL_EP) + $PI_{(20)}$	24.36	44.38	0.55
			$P_m + P_b$	DWh + max.(SD_AWAY_EP, SD_RAIL_EP) + $PI_{(20)}$	41.08	57.06	0.72
			P_L	DWh + max.(SD_AWAY, SD_RAIL_EP, SD_TOP_RAIL_EP) + $PI_{(20)}$	34.25	57.06	0.60
			P_m (or P_L) + P_b + Q	DWh + max.(SD_AWAY_EP, SD_RAIL_EP) + $PI_{(20)}$	NA		
7B	D	Vertical	P_m	DWv + max.(ED_TOP, ED_BOT) + $PI_{(20)}$	21.48	44.38	0.48
			$P_m + P_b$	DWv + max.(ED_TOP, ED_BOT) + $PI_{(20)}$	33.49	57.06	0.59
			P_L	DWv + max.(ED_TOP, ED_BOT) + $PI_{(20)}$	15.84	57.06	0.28
			P_m (or P_L) + P_b + Q	DWv + max.(ED_TOP, ED_BOT) + $PI_{(20)}$	NA		
8	D	Horizontal ⁽²⁾	P_m	DWh + $PI_{(130)}$	12.26	44.38	0.28
			$P_m + P_b$	DWh + $PI_{(130)}$	19.19	57.06	0.34
			P_L	DWh + $PI_{(130)}$	16.91	57.06	0.30
			P_m (or P_L) + P_b + Q	DWh + $PI_{(130)}$	NA		
9	A	Horizontal ⁽³⁾	P_m	DWh + $PI_{(20)}$	3.65	17.50	0.21
			$P_m + P_b$	DWh + $PI_{(20)}$	7.78	26.25	0.30
			P_L	DWh + $PI_{(20)}$	9.23	26.25	0.35
			P_m (or P_L) + P_b + Q	DWh + $PI_{(20)}$	16.56	52.50	0.32
			P_m (or P_L) + P_b + Q + P_e	DWh + $PI_{(20)}$ + TH	34.10	52.50	0.65

Table 3.9.1-7
DSC Shell Stress Results, Confinement Boundary – Load Combinations
 3 Pages

Load Comb No.	Service Level	DSC Orientation	Stress Category	Loads	Stress intensity (ksi)	Allowable Stress (ksi)	Stress Ratio
10	D	Horizontal ⁽³⁾	P_m	DWh + max.(HS_TOP, HS_BOT)+PI ₍₂₀₎	9.25	44.38	0.21
			P_m+P_b	DWh + max.(HS_TOP, HS_BOT)+PI ₍₂₀₎	28.98	57.06	0.51
			P_L	DWh + max.(HS_TOP, HS_BOT)+PI ₍₂₀₎	21.50	57.06	0.38
			P_m (or P_L)+ P_b +Q	DWh + max.(HS_TOP, HS_BOT)+PI ₍₂₀₎	NA		
11	Test	Vertical	P_m	max. (PI(23)+155 kips ,PE _(14.7) +155 kips)	3.97	17.50	0.23
			P_m+P_b	max. (PI(23)+155 kips,PE _(14.7) +155 kips)	9.00	26.25	0.34
			P_L	max. (PI(23)+155 kips ,PE _(14.7) +155 kips)	3.21	26.25	0.12
			P_m (or P_L)+ P_b +Q	max. (PI(23)+155 kips,PE _(14.7) +155 kips)	NA		
12	D	Horizontal	External Pressure		21.70	45.10	0.48

Notes:

- (1) DSC in transfer cask in vertical orientation. Only inner top cover is installed
- (2) DSC in TC with TC in a horizontal orientation.
- (3) DSC in EOS-HSM supported on the steel rails

Table 3.9.1-7a
DSC Shell Stress Results, Non-Confinement Boundary – Load Combinations
 3 Pages

Load Comb No.	Service Level	DSC Orientation	Stress Category	Loads	Stress intensity (ksi)	Allowable Stress (ksi)	Stress Ratio
1	A	Vertical ⁽¹⁾	P_m	DWv + max($PI_{(20)}$, BD, VD)	0.82	17.50	0.05
			$P_m + P_b$	DWv + max($PI_{(20)}$, BD, VD)	2.25	26.25	0.09
			P_L	DWv + max($PI_{(20)}$, BD, VD)	1.28	26.25	0.05
			P_m (or P_L) + P_b + Q	DWv + max($PI_{(20)}$, BD, VD)	3.88	52.50	0.07
			P_m (or P_L) + P_b + Q + P_e	DWv + max($PI_{(20)}$, BD, VD) + TH	23.27	52.50	0.44
2/3	A	Horizontal ⁽²⁾	P_m	DWh + 1g axial + 1g transverse + 1g Vertical + $PI_{(20)}$	3.46	17.50	0.20
			$P_m + P_b$	DWh + 1g axial + 1g transverse + 1g Vertical + $PI_{(20)}$	4.49	26.25	0.17
			P_L	DWh + 1g axial + 1g transverse + 1g Vertical + $PI_{(20)}$	4.80	26.25	0.18
			P_m (or P_L) + P_b + Q	DWh + 1g axial + 1g transverse + 1g Vertical + $PI_{(20)}$	5.30	52.50	0.10
			P_m (or P_L) + P_b + Q + P_e	DWh + 1g axial + 1g transverse + 1g Vertical + $PI_{(20)}$ + TH	24.69	52.50	0.47
4	A/B	Horizontal ⁽²⁾	P_m	DWh + 135kips + $PI_{(20)}$	1.69	17.50	0.10
			$P_m + P_b$	DWh + 135kips + $PI_{(20)}$	5.78	26.25	0.22
			P_L	DWh + 135kips + $PI_{(20)}$	7.92	26.25	0.30
			P_m (or P_L) + P_b + Q	DWh + 135kips + $PI_{(20)}$	18.95	52.50	0.36
			P_m (or P_L) + P_b + Q + P_e	DWh + 135kips + TH	38.34	52.50	0.73
5	A/B	Horizontal ⁽²⁾	P_m	DWh + 80 kips + $PI_{(20)}$	2.98	17.50	0.17
			$P_m + P_b$	DWh + 80 kips + $PI_{(20)}$	13.40	26.25	0.51
			P_L	DWh + 80 kips + $PI_{(20)}$	8.36	26.25	0.32
			P_m (or P_L) + P_b + Q	DWh + 80 kips + $PI_{(20)}$	25.22	52.50	0.48
			P_m (or P_L) + P_b + Q + P_e	DWh + 80 kips + TH	44.61	52.50	0.85

Table 3.9.1-7a
DSC Shell Stress Results, Non-Confinement Boundary – Load Combinations
 3 Pages

Load Comb No.	Service Level	DSC Orientation	Stress Category	Loads	Stress intensity (ksi)	Allowable Stress (ksi)	Stress Ratio
6	D	Horizontal ⁽²⁾	P_m	DWh + 135 kips + $PI_{(20)}$	4.47	44.38	0.10
			P_m+P_b	DWh + 135 kips + $PI_{(20)}$	20.49	57.06	0.36
			P_L	DWh + 135 kips + $PI_{(20)}$	11.76	57.06	0.21
			P_m (or P_L) + P_b + Q	DWh + 135 kips + $PI_{(20)}$	NA		
7A	D	Horizontal ⁽²⁾	P_m	DWh + max.(SD_AWAY, SD_RAIL_EP, SD_TOP_RAIL_EP) + $PI_{(20)}$	21.44	44.38	0.48
			P_m+P_b	DWh + max.(SD_AWAY_EP, SD_RAIL_EP) + $PI_{(20)}$	24.63	57.06	0.43
			P_L	DWh + max.(SD_AWAY, SD_RAIL_EP, SD_TOP_RAIL_EP) + $PI_{(20)}$	29.17	57.06	0.51
			P_m (or P_L) + P_b + Q	DWh + max.(SD_AWAY_EP, SD_RAIL_EP) + $PI_{(20)}$	NA		
7B	D	Vertical	P_m	DWv + max.(ED_TOP, ED_BOT) + $PI_{(20)}$	15.14	44.38	0.34
			P_m+P_b	DWv + max.(ED_TOP, ED_BOT) + $PI_{(20)}$	24.68	57.06	0.43
			P_L	DWv + max.(ED_TOP, ED_BOT) + $PI_{(20)}$	16.10	57.06	0.28
			P_m (or P_L) + P_b + Q	DWv + max.(ED_TOP, ED_BOT) + $PI_{(20)}$	NA		
8	D	Horizontal ⁽²⁾	P_m	DWh + $PI_{(130)}$	3.43	44.38	0.08
			P_m+P_b	DWh + $PI_{(130)}$	11.77	57.06	0.21
			P_L	DWh + $PI_{(130)}$	7.95	57.06	0.14
			P_m (or P_L) + P_b + Q	DWh + $PI_{(130)}$	NA		
9	A	Horizontal ⁽³⁾	P_m	DWh + $PI_{(20)}$	2.06	17.50	0.12
			P_m+P_b	DWh + $PI_{(20)}$	3.78	26.25	0.14
			P_L	DWh + $PI_{(20)}$	2.97	26.25	0.11
			P_m (or P_L) + P_b + Q	DWh + $PI_{(20)}$	5.03	52.50	0.10
			P_m (or P_L) + P_b + Q + P_e	DWh + $PI_{(20)}$ + TH	24.42	52.50	0.47

Table 3.9.1-7a
DSC Shell Stress Results, Non-Confinement Boundary – Load Combinations
 3 Pages

Load Comb No.	Service Level	DSC Orientation	Stress Category	Loads	Stress intensity (ksi)	Allowable Stress (ksi)	Stress Ratio
10	D	Horizontal ⁽³⁾	P_m	DWh + max.(HS_TOP, HS_BOT)+PI ₍₂₀₎	15.53	44.38	0.35
			P_m+P_b	DWh + max.(HS_TOP, HS_BOT)+PI ₍₂₀₎	20.26	57.06	0.36
			P_L	DWh + max.(HS_TOP, HS_BOT)+PI ₍₂₀₎	21.19	57.06	0.37
			P_m (or P_L)+ P_b +Q	DWh + max.(HS_TOP, HS_BOT)+PI ₍₂₀₎	NA		
11	Test	Vertical	P_m	max. (PI(23)+155 kips ,PE _(14.7) +155 kips)	4.98	17.50	0.28
			P_m+P_b	max. (PI(23)+155 kips,PE _(14.7) +155 kips)	10.70	26.25	0.41
			P_L	max. (PI(23)+155 kips ,PE _(14.7) +155 kips)	4.72	26.25	0.18
			P_m or P_L)+ P_b +Q	max. (PI(23)+155 kips,PE _(14.7) +155 kips)	NA		
12	D	Horizontal	External Pressure		21.7	45.1	0.481

Notes:

- (1) DSC in transfer cask in vertical orientation. Only inner top cover is installed.
- (2) DSC in TC with TC in a horizontal orientation.
- (3) DSC in EOS-HSM supported on the steel rails.

Table 3.9.1-7b
DSC Shell Stress Results, Confinement Boundary - Load Combinations (Supported by FPS DSC Support Structure)
 3 Pages

Load Comb No.	Service Level	DSC Orientation	Stress Category	Loads	Stress intensity (ksi)	Allowable Stress (ksi)	Stress Ratio
1	A	Vertical	P_m	$DW_v + \max(PI(20), BD, VD)$	2.51	17.50	0.14
			$P_m + P_b$	$DW_v + \max(PI(20), BD, VD)$	7.87	26.25	0.30
			P_L	$DW_v + \max(PI(20), BD, VD)$	6.80	26.25	0.26
			$P_m \text{ (or } P_L) + P_b + Q$	$DW_v + \max(PI(20), BD, VD)$	12.28	52.50	0.23
			$P_m \text{ (or } P_L) + P_b + Q + P_e$	$DW_v + \max(PI(20), BD, VD) + TH$	29.82	52.50	0.57
2/3	A	Horizontal ⁽²⁾	P_m	$DW_h + 1g \text{ axial} + 1g \text{ transverse} + 1g \text{ Vertical} + PI(20)$	2.49	17.50	0.14
			$P_m + P_b$	$DW_h + 1g \text{ axial} + 1g \text{ transverse} + 1g \text{ Vertical} + PI(20)$	3.30	26.25	0.13
			P_L	$DW_h + 1g \text{ axial} + 1g \text{ transverse} + 1g \text{ Vertical} + PI(20)$	6.21	26.25	0.24
			$P_m \text{ (or } P_L) + P_b + Q$	$DW_h + 1g \text{ axial} + 1g \text{ transverse} + 1g \text{ Vertical} + PI(20)$	10.98	52.50	0.21
			$P_m \text{ (or } P_L) + P_b + Q + P_e$	$DW_h + 1g \text{ axial} + 1g \text{ transverse} + 1g \text{ Vertical} + PI(20) + TH$	28.52	52.50	0.54
4	A/B	Horizontal ⁽²⁾	P_m	$DW_h + 135\text{kips} + PI(20)$	2.89	17.50	0.17
			$P_m + P_b$	$DW_h + 135\text{kips} + PI(20)$	4.19	26.25	0.16
			P_L	$DW_h + 135\text{kips} + PI(20)$	7.17	26.25	0.27
			$P_m \text{ (or } P_L) + P_b + Q$	$DW_h + 135\text{kips} + PI(20)$	16.09	52.50	0.31
			$P_m \text{ (or } P_L) + P_b + Q + P_e$	$DW_h + 135\text{kips} + TH$	33.63	52.50	0.64
5	A/B	Horizontal ⁽²⁾	P_m	$DW_h + 80 \text{ kips} + PI(20)$	2.20	17.50	0.13
			$P_m + P_b$	$DW_h + 80 \text{ kips} + PI(20)$	3.75	26.25	0.14
			P_L	$DW_h + 80 \text{ kips} + PI(20)$	6.31	26.25	0.24
			$P_m \text{ (or } P_L) + P_b + Q$	$DW_h + 80 \text{ kips} + PI(20)$	13.50	52.50	0.26
			$P_m \text{ (or } P_L) + P_b + Q + P_e$	$DW_h + 80 \text{ kips} + TH$	31.04	52.50	0.59

Table 3.9.1-7b
DSC Shell Stress Results, Confinement Boundary - Load Combinations (Supported by FPS DSC Support Structure)
 3 Pages

Load Comb No.	Service Level	DSC Orientation	Stress Category	Loads	Stress intensity (ksi)	Allowable Stress (ksi)	Stress Ratio
6	D	Horizontal ⁽²⁾	P_m	DWh + 135 kips + PI(20)	2.81	44.38	0.06
			P_m+P_b	DWh + 135 kips + PI(20)	4.62	57.06	0.08
			P_L	DWh + 135 kips + PI(20)	6.67	57.06	0.12
			P_m (or P_L)+ P_b +Q	DWh + 135 kips + PI(20)	NA		
7A	D	Horizontal ⁽²⁾	P_m	DWh + max.(SD_AWAY, SD_RAIL_EP,SD_TOP_RAIL_EP)+ PI(20)	24.36	44.38	0.55
			P_m+P_b	DWh + max.(SD_AWAY_EP, SD_RAIL_EP)+ PI(20)	41.08	57.06	0.72
			P_L	DWh + max.(SD_AWAY, SD_RAIL_EP,SD_TOP_RAIL_EP)+ PI(20)	34.25	57.06	0.60
			P_m (or P_L)+ P_b +Q	DWh + max.(SD_AWAY_EP, SD_RAIL_EP)+ PI(20)	NA		
7B	D	Vertical	P_m	DWv + max.(ED_TOP, ED_BOT)+ PI(20)	21.48	44.38	0.48
			P_m+P_b	DWv + max.(ED_TOP, ED_BOT)+ PI(20)	33.49	57.06	0.59
			P_L	DWv + max.(ED_TOP, ED_BOT)+ PI(20)	15.84	57.06	0.28
			P_m (or P_L)+ P_b +Q	DWv + max.(ED_TOP, ED_BOT)+ PI(20)	NA		
8	D	Horizontal ⁽²⁾	P_m	DWh + PI(130)	12.26	44.38	0.28
			P_m+P_b	DWh + PI(130)	19.19	57.06	0.34
			P_L	DWh + PI(130)	16.91	57.06	0.30
			P_m (or P_L)+ P_b +Q	DWh + PI(130)	NA		

Table 3.9.1-7b
DSC Shell Stress Results, Confinement Boundary - Load Combinations (Supported by FPS DSC Support Structure)
 3 Pages

Load Comb No.	Service Level	DSC Orientation	Stress Category	Loads	Stress intensity (ksi)	Allowable Stress (ksi)	Stress Ratio
9	A	Horizontal ⁽³⁾	P_m	DWh + PI(20)	4.76	17.50	0.27
			$P_m + P_b$	DWh + PI(20)	10.20	26.25	0.39
			P_L	DWh + PI(20)	14.02	26.25	0.53
			P_m (or P_L) + P_b + Q	DWh + PI(20)	21.11	52.50	0.40
			P_m (or P_L) + P_b + Q + P_e	DWh + PI(20) + TH	38.65	52.50	0.74
10	D	Horizontal ⁽³⁾	P_m	DWh + max.(HS_TOP, HS_BOT) + PI(20)	12.55	44.38	0.28
			$P_m + P_b$	DWh + max.(HS_TOP, HS_BOT) + PI(20)	32.29	57.06	0.57
			P_L	DWh + max.(HS_TOP, HS_BOT) + PI(20)	23.99	57.06	0.42
			P_m (or P_L) + P_b + Q	DWh + max.(HS_TOP, HS_BOT) + PI(20)	NA		
11	Test	Vertical	P_m	max. (PI(23)+155 kips , PE(14.7)+155 kips)	3.97	17.50	0.23
			$P_m + P_b$	max. (PI(23)+155 kips, PE(14.7)+155 kips)	9.00	26.25	0.34
			P_L	max. (PI(23)+155 kips , PE(14.7)+155 kips)	3.21	26.25	0.12
			P_m (or P_L) + P_b + Q	max. (PI(23)+155 kips, PE(14.7)+155 kips)	NA		
12	D	Horizontal	External Pressure		21.70	45.10	0.48

Notes:

- (1) DSC in transfer cask in vertical orientation. Only inner top cover is installed.
- (2) DSC in transfer cask, TC is in horizontal orientation.
- (3) DSC in EOS-HSM-FPS supported by FPS DSC support structure.
- (4) Only load combinations 9 and 10 have results that differ from Table 3.9.1-7.

Table 3.9.1-7c
DSC Shell Stress Results, Non-Confinement Boundary - Load Combinations (Supported by FPS DSC Support Structure)
 3 Pages

Load Comb No.	Service Level	DSC Orientation	Stress Category	Loads	Stress intensity (ksi)	Allowable Stress (ksi)	Stress Ratio
1	A	Vertical ⁽¹⁾	P_m	DWv + max(PI(20),BD,VD)	0.82	17.50	0.05
			P_m+P_b	DWv + max(PI(20),BD,VD)	2.25	26.25	0.09
			P_L	DWv + max(PI(20),BD,VD)	1.28	26.25	0.05
			P_m (or P_L)+ P_b +Q	DWv + max(PI(20),BD,VD)	3.88	52.50	0.07
			P_m (or P_L)+ P_b +Q+ P_e	DWv + max(PI(20),BD,VD)+TH	23.27	52.50	0.44
2/3	A	Horizontal ⁽²⁾	P_m	DWh + 1g axial + 1g transverse + 1g Vertical + PI(20)	3.46	17.50	0.20
			P_m+P_b	DWh + 1g axial + 1g transverse + 1g Vertical + PI(20)	4.49	26.25	0.17
			P_L	DWh + 1g axial + 1g transverse + 1g Vertical + PI(20)	4.80	26.25	0.18
			P_m (or P_L)+ P_b +Q	DWh + 1g axial + 1g transverse + 1g Vertical + PI(20)	5.30	52.50	0.10
			P_m (or P_L)+ P_b +Q+ P_e	DWh + 1g axial + 1g transverse + 1g Vertical + PI(20) +TH	24.69	52.50	0.47
4	A/B	Horizontal ⁽²⁾	P_m	DWh + 135kips + PI(20)	1.69	17.50	0.10
			P_m+P_b	DWh + 135kips + PI(20)	5.78	26.25	0.22
			P_L	DWh + 135kips + PI(20)	7.92	26.25	0.30
			P_m (or P_L)+ P_b +Q	DWh + 135kips + PI(20)	18.95	52.50	0.36
			P_m (or P_L)+ P_b +Q+ P_e	DWh + 135kips + TH	38.34	52.50	0.73
5	A/B	Horizontal ⁽²⁾	P_m	DWh + 80 kips + PI(20)	2.98	17.50	0.17
			P_m+P_b	DWh + 80 kips + PI(20)	13.40	26.25	0.51
			P_L	DWh + 80 kips + PI(20)	8.36	26.25	0.32
			P_m (or P_L)+ P_b +Q	DWh + 80 kips + PI(20)	25.22	52.50	0.48
			P_m (or P_L)+ P_b +Q+ P_e	DWh + 80 kips + TH	44.61	52.50	0.85

Table 3.9.1-7c
DSC Shell Stress Results, Non-Confinement Boundary - Load Combinations (Supported by FPS DSC Support Structure)
 3 Pages

Load Comb No.	Service Level	DSC Orientation	Stress Category	Loads	Stress intensity (ksi)	Allowable Stress (ksi)	Stress Ratio
6	D	Horizontal ⁽²⁾	P_m	DWh + 135 kips + PI(20)	4.47	44.38	0.10
			P_m+P_b	DWh + 135 kips + PI(20)	20.49	57.06	0.36
			P_L	DWh + 135 kips + PI(20)	11.76	57.06	0.21
			P_m (or P_L)+ P_b +Q	DWh + 135 kips + PI(20)	NA		
7A	D	Horizontal ⁽²⁾	P_m	DWh + max.(SD_AWAY, SD_RAIL_EP,SD_TOP_RAIL_EP)+ PI(20)	21.44	44.38	0.48
			P_m+P_b	DWh + max.(SD_AWAY_EP, SD_RAIL_EP)+ PI(20)	24.63	57.06	0.43
			P_L	DWh + max.(SD_AWAY, SD_RAIL_EP,SD_TOP_RAIL_EP)+ PI(20)	29.17	57.06	0.51
			P_m (or P_L)+ P_b +Q	DWh + max.(SD_AWAY_EP, SD_RAIL_EP)+ PI(20)	NA		
7B	D	Vertical	P_m	DW _v + max.(ED_TOP, ED_BOT)+ PI(20)	15.14	44.38	0.34
			P_m+P_b	DW _v + max.(ED_TOP, ED_BOT)+ PI(20)	24.68	57.06	0.43
			P_L	DW _v + max.(ED_TOP, ED_BOT)+ PI(20)	16.10	57.06	0.28
			P_m (or P_L)+ P_b +Q	DW _v + max.(ED_TOP, ED_BOT)+ PI(20)	NA		
8	D	Horizontal ⁽²⁾	P_m	DWh + PI(130)	3.43	44.38	0.08
			P_m+P_b	DWh + PI(130)	11.77	57.06	0.21
			P_L	DWh + PI(130)	7.95	57.06	0.14
			P_m (or P_L)+ P_b +Q	DWh + PI(130)	NA		

Table 3.9.1-7c
DSC Shell Stress Results, Non-Confinement Boundary - Load Combinations (Supported by FPS DSC Support Structure)
 3 Pages

Load Comb No.	Service Level	DSC Orientation	Stress Category	Loads	Stress intensity (ksi)	Allowable Stress (ksi)	Stress Ratio
9	A	Horizontal ⁽³⁾	P_m	DWh + PI(20)	2.59	17.50	0.15
			$P_m + P_b$	DWh + PI(20)	4.59	26.25	0.17
			P_L	DWh + PI(20)	4.16	26.25	0.16
			P_m (or P_L) + P_b + Q	DWh + PI(20)	7.06	52.50	0.13
			P_m (or P_L) + P_b + Q + P_e	DWh + PI(20) + TH	26.45	52.50	0.50
10	D	Horizontal ⁽³⁾	P_m	DWh + max.(HS_TOP, HS_BOT) + PI(20)	16.71	44.38	0.38
			$P_m + P_b$	DWh + max.(HS_TOP, HS_BOT) + PI(20)	21.81	57.06	0.38
			P_L	DWh + max.(HS_TOP, HS_BOT) + PI(20)	22.02	57.06	0.39
			P_m (or P_L) + P_b + Q	DWh + max.(HS_TOP, HS_BOT) + PI(20)	NA		
11	Test	Vertical	P_m	max. (PI(23)+155 kips , PE(14.7)+155 kips)	4.98	17.50	0.28
			$P_m + P_b$	max. (PI(23)+155 kips, PE(14.7)+155 kips)	10.70	26.25	0.41
			P_L	max. (PI(23)+155 kips , PE(14.7)+155 kips)	4.72	26.25	0.18
			P_m (or P_L) + P_b + Q	max. (PI(23)+155 kips, PE(14.7)+155 kips)	NA		
12	D	Horizontal	External Pressure		21.70	45.10	0.48

Notes:

- (1) DSC in transfer cask in vertical orientation. Only inner top cover is installed.
- (2) DSC in transfer cask, TC is in horizontal orientation.
- (3) DSC in EOS-HSM-FPS supported by FPS DSC support structure.
- (4) Only load combinations 9 and 10 have results that differ from Table 3.9.1-7a.

Table 3.9.1-8
OTCP Stress Results – Load Combinations
 3 Pages

Load Comb No.	Service Level	DSC Orientation	Stress Category	Loads	Stress intensity (ksi)	Allowable Stress (ksi)	Stress Ratio
1	A	Vertical ⁽¹⁾	P _m	DW _v + max(PI ₍₂₀₎ ,BD,VD)	0.42	17.50	0.02
			P _m +P _b	DW _v + max(PI ₍₂₀₎ ,BD,VD)	3.95	26.25	0.15
			P _L	DW _v + max(PI ₍₂₀₎ ,BD,VD)	0.50	26.25	0.02
			P _m (or P _L)+P _b +Q	DW _v + max(PI ₍₂₀₎ ,BD,VD)	2.47	52.50	0.05
			P _m (or P _L)+P _b +Q+P _e	DW _v + max(PI ₍₂₀₎ ,BD,VD)+TH	10.57	52.50	0.20
2/3	A	Horizontal ⁽²⁾	P _m	DW _h + 1g axial + 1g transverse + 1g Vertical + PI ₍₂₀₎	0.49	17.50	0.03
			P _m +P _b	DW _h + 1g axial + 1g transverse + 1g Vertical + PI ₍₂₀₎	3.60	26.25	0.14
			P _L	DW _h + 1g axial + 1g transverse + 1g Vertical + PI ₍₂₀₎	1.39	26.25	0.05
			P _m (or P _L)+P _b +Q	DW _h + 1g axial + 1g transverse + 1g Vertical + PI ₍₂₀₎	4.53	52.50	0.09
			P _m (or P _L)+P _b +Q+P _e	DW _h + 1g axial + 1g transverse + 1g Vertical + PI ₍₂₀₎ + TH	11.15	52.50	0.21
4	A/B	Horizontal ⁽²⁾	P _m	DW _h + 135kips + PI ₍₂₀₎	0.58	17.50	0.03
			P _m +P _b	DW _h + 135kips + PI ₍₂₀₎	4.30	26.25	0.16
			P _L	DW _h + 135kips + PI ₍₂₀₎	0.76	26.25	0.03
			P _m (or P _L)+P _b +Q	DW _h + 135kips + PI ₍₂₀₎	3.07	52.50	0.06
			P _m (or P _L)+P _b +Q+P _e	DW _h + 135kips + TH	10.92	52.50	0.21
5	A/B	Horizontal ⁽²⁾	P _m	DW _h + 80 kips + PI ₍₂₀₎	0.56	17.50	0.03
			P _m +P _b	DW _h + 80 kips + PI ₍₂₀₎	4.18	26.25	0.16
			P _L	DW _h + 80 kips + PI ₍₂₀₎	0.80	26.25	0.03
			P _m (or P _L)+P _b +Q	DW _h + 80 kips + PI ₍₂₀₎	3.13	52.50	0.06
			P _m (or P _L)+P _b +Q+P _e	DW _h + 80 kips + TH	10.80	52.50	0.21

Table 3.9.1-8
OTCP Stress Results – Load Combinations
 3 Pages

Load Comb No.	Service Level	DSC Orientation	Stress Category	Loads	Stress intensity (ksi)	Allowable Stress (ksi)	Stress Ratio
6	D	Horizontal ⁽²⁾	P_m	DWh + 135 kips + $PI_{(20)}$	0.55	44.38	0.01
			$P_m + P_b$	DWh + 135 kips + $PI_{(20)}$	4.15	57.06	0.07
			P_L	DWh + 135 kips + $PI_{(20)}$	0.85	57.06	0.01
			P_m (or P_L) + P_b + Q	DWh + 135 kips + $PI_{(20)}$	NA		
7A	D	Horizontal ⁽²⁾	P_m	DWh + max.(SD_AWAY, SD_RAIL_EP, SD_TOP_RAIL_EP) + $PI_{(20)}$	9.82	44.38	0.22
			$P_m + P_b$	DWh + max.(SD_AWAY_EP, SD_RAIL_EP) + $PI_{(20)}$	25.08	57.06	0.44
			P_L	DWh + max.(SD_AWAY, SD_RAIL_EP, SD_TOP_RAIL_EP) + $PI_{(20)}$	16.07	57.06	0.28
			P_m (or P_L) + P_b + Q	DWh + max.(SD_AWAY_EP, SD_RAIL_EP) + $PI_{(20)}$	NA		
7B	D	Vertical	P_m	DWv + max.(ED_TOP, ED_BOT) + $PI_{(20)}$	2.90	44.38	0.07
			$P_m + P_b$	DWv + max.(ED_TOP, ED_BOT) + $PI_{(20)}$	16.06	57.06	0.28
			P_L	DWv + max.(ED_TOP, ED_BOT) + $PI_{(20)}$	3.21	57.06	0.06
			P_m (or P_L) + P_b + Q	DWv + max.(ED_TOP, ED_BOT) + $PI_{(20)}$	NA		
8	D	Horizontal ⁽²⁾	P_m	DWh + $PI_{(130)}$	2.39	44.38	0.05
			$P_m + P_b$	DWh + $PI_{(130)}$	25.74	57.06	0.45
			P_L	DWh + $PI_{(130)}$	2.38	57.06	0.04
			P_m or P_L) + P_b + Q	DWh + $PI_{(130)}$	NA		
9	A	Horizontal ⁽³⁾	P_m	DWh + $PI_{(20)}$	0.69	17.50	0.04
			$P_m + P_b$	DWh + $PI_{(20)}$	4.48	26.25	0.17
			P_L	DWh + $PI_{(20)}$	1.08	26.25	0.04
			P_m (or P_L) + P_b + Q	DWh + $PI_{(20)}$	4.04	52.50	0.08
			P_m (or P_L) + P_b + Q + P_e	DWh + $PI_{(20)}$ + TH	11.10	52.50	0.21

Table 3.9.1-8
OTCP Stress Results – Load Combinations
 3 Pages

Load Comb No.	Service Level	DSC Orientation	Stress Category	Loads	Stress intensity (ksi)	Allowable Stress (ksi)	Stress Ratio
10	D	Horizontal ⁽³⁾	P_m	DWh + max.(HS_TOP, HS_BOT)+PI ₍₂₀₎	1.61	44.38	0.04
			P_m+P_b	DWh + max.(HS_TOP, HS_BOT)+PI ₍₂₀₎	4.58	57.06	0.08
			P_L	DWh + max.(HS_TOP, HS_BOT)+PI ₍₂₀₎	5.01	57.06	0.09
			P_m (or P_L)+ P_b +Q	DWh + max.(HS_TOP, HS_BOT)+PI ₍₂₀₎	NA		
11	Test	Vertical	P_m	max. (PI(23)+155 kips ,PE _(14.7) +155 kips)	NA		
			P_m+P_b	max. (PI(23)+155 kips,PE _(14.7) +155 kips)	NA		
			P_L	max. (PI(23)+155 kips ,PE _(14.7) +155 kips)	NA		
			P_m or P_L)+ P_b +Q	max. (PI(23)+155 kips,PE _(14.7) +155 kips)	NA		

Notes:

- (1) DSC in transfer cask in vertical orientation. Only inner top cover is installed.
- (2) DSC in TC with TC in a horizontal orientation.
- (3) DSC in EOS-HSM supported on the steel rails.

Table 3.9.1-8a
OTCP Stress Results- Load Combination (Supported by FPS DSC Support Structure)
 3 Pages

Load Comb No.	Service Level	DSC Orientation	Stress Category	Loads	Stress intensity (ksi)	Allowable Stress (ksi)	Stress Ratio
1	A	Vertical ⁽¹⁾	P_m	$DW_v + \max(PI(20), BD, VD)$	0.42	17.50	0.02
			$P_m + P_b$	$DW_v + \max(PI(20), BD, VD)$	3.95	26.25	0.15
			P_L	$DW_v + \max(PI(20), BD, VD)$	0.50	26.25	0.02
			$P_m \text{ (or } P_L) + P_b + Q$	$DW_v + \max(PI(20), BD, VD)$	2.47	52.50	0.05
			$P_m \text{ or } P_L + P_b + Q + P_e$	$DW_v + \max(PI(20), BD, VD) + TH$	10.57	52.50	0.20
2/3	A	Horizontal ⁽²⁾	P_m	$DW_h + 1g \text{ axial} + 1g \text{ transverse} + 1g \text{ Vertical} + PI(20)$	0.49	17.50	0.03
			$P_m + P_b$	$DW_h + 1g \text{ axial} + 1g \text{ transverse} + 1g \text{ Vertical} + PI(20)$	3.60	26.25	0.14
			P_L	$DW_h + 1g \text{ axial} + 1g \text{ transverse} + 1g \text{ Vertical} + PI(20)$	1.39	26.25	0.05
			$P_m \text{ (or } P_L) + P_b + Q$	$DW_h + 1g \text{ axial} + 1g \text{ transverse} + 1g \text{ Vertical} + PI(20)$	4.53	52.50	0.09
			$P_m \text{ (or } P_L) + P_b + Q + P_e$	$DW_h + 1g \text{ axial} + 1g \text{ transverse} + 1g \text{ Vertical} + PI(20) + TH$	11.15	52.50	0.21
4	A/B	Horizontal ⁽²⁾	P_m	$DW_h + 135\text{kips} + PI(20)$	0.58	17.50	0.03
			$P_m + P_b$	$DW_h + 135\text{kips} + PI(20)$	4.30	26.25	0.16
			P_L	$DW_h + 135\text{kips} + PI(20)$	0.76	26.25	0.03
			$P_m \text{ (or } P_L) + P_b + Q$	$DW_h + 135\text{kips} + PI(20)$	3.07	52.50	0.06
			$P_m \text{ (or } P_L) + P_b + Q + P_e$	$DW_h + 135\text{kips} + TH$	10.92	52.50	0.21
5	A/B	Horizontal ⁽²⁾	P_m	$DW_h + 80 \text{ kips} + PI(20)$	0.56	17.50	0.03
			$P_m + P_b$	$DW_h + 80 \text{ kips} + PI(20)$	4.18	26.25	0.16
			P_L	$DW_h + 80 \text{ kips} + PI(20)$	0.80	26.25	0.03
			$P_m \text{ or } P_L + P_b + Q$	$DW_h + 80 \text{ kips} + PI(20)$	3.13	52.50	0.06
			$P_m \text{ (or } P_L) + P_b + Q + P_e$	$DW_h + 80 \text{ kips} + TH$	10.80	52.50	0.21

Table 3.9.1-8a
OTCP Stress Results- Load Combination (Supported by FPS DSC Support Structure)
 3 Pages

Load Comb No.	Service Level	DSC Orientation	Stress Category	Loads	Stress intensity (ksi)	Allowable Stress (ksi)	Stress Ratio
6	D	Horizontal ⁽²⁾	P _m	DWh + 135 kips + PI(20)	0.55	44.38	0.01
			P _m +P _b	DWh + 135 kips + PI(20)	4.15	57.06	0.07
			P _L	DWh + 135 kips + PI(20)	0.85	57.06	0.01
			P _m (or P _L)+P _b +Q	DWh + 135 kips + PI(20)	NA		
7A	D	Horizontal ⁽²⁾	P _m	DWh + max.(SD_AWAY, SD_RAIL_EP,SD_TOP_RAIL_EP)+ PI(20)	9.82	44.38	0.22
			P _m +P _b	DWh + max.(SD_AWAY_EP, SD_RAIL_EP)+ PI(20)	25.08	57.06	0.44
			P _L	DWh + max.(SD_AWAY, SD_RAIL_EP,SD_TOP_RAIL_EP)+ PI(20)	16.07	57.06	0.28
			P _m (or P _L)+P _b +Q	DWh + max.(SD_AWAY_EP, SD_RAIL_EP)+ PI(20)	NA		
7B	D	Vertical	P _m	DW _v + max.(ED_TOP, ED_BOT)+ PI(20)	2.90	44.38	0.07
			P _m +P _b	DW _v + max.(ED_TOP, ED_BOT)+ PI(20)	16.06	57.06	0.28
			P _L	DW _v + max.(ED_TOP, ED_BOT)+ PI(20)	3.21	57.06	0.06
			P _m (or P _L)+P _b +Q	DW _v + max.(ED_TOP, ED_BOT)+ PI(20)	NA		
8	D	Horizontal ⁽²⁾	P _m	DWh + PI(130)	2.39	44.38	0.05
			P _m +P _b	DWh + PI(130)	25.74	57.06	0.45
			P _L	DWh + PI(130)	2.38	57.06	0.04
			P _m (or P _L)+P _b +Q	DWh + PI(130)	NA		
9	A	Horizontal ⁽³⁾	P _m	DWh + PI(20)	1.11	17.50	0.06
			P _m +P _b	DWh + PI(20)	5.26	26.25	0.20
			P _L	DWh + PI(20)	2.30	26.25	0.09
			P _m (or P _L)+P _b +Q	DWh + PI(20)	7.37	52.50	0.14
			P _m (or P _L)+P _b +Q+P _c	DWh + PI(20) +TH	13.99	52.50	0.27

Table 3.9.1-8a
OTCP Stress Results- Load Combination (Supported by FPS DSC Support Structure)
 3 Pages

Load Comb No.	Service Level	DSC Orientation	Stress Category	Loads	Stress intensity (ksi)	Allowable Stress (ksi)	Stress Ratio
10	D	Horizontal ⁽³⁾	P_m	DWh + max.(HS_TOP, HS_BOT)+PI(20)	1.70	44.38	0.04
			P_m+P_b	DWh + max.(HS_TOP, HS_BOT)+PI(20)	4.48	57.06	0.06
			P_L	DWh + max.(HS_TOP, HS_BOT)+PI(20)	7.73	57.06	0.14
			P_m (or P_L)+ P_b +Q	DWh + max.(HS_TOP, HS_BOT)+PI(20)	NA		
11	Test	Vertical	P_m	max. (PI(23)+155 kips ,PE(14.7)+155 kips)	NA		
			P_m+P_b	max. (PI(23)+155 kips,PE(14.7)+155 kips)	NA		
			P_L	max. (PI(23)+155 kips ,PE(14.7)+155 kips)	NA		
			P_m (or P_L)+ P_b +Q	max. (PI(23)+155 kips,PE(14.7)+155 kips)	NA		

Notes:

- (1) DSC in transfer cask in vertical orientation. Only inner top cover is installed.
- (2) DSC in transfer cask, TC is in horizontal orientation.
- (3) DSC in EOS-HSM-FPS supported by FPS DSC support structure.
- (4) Maximum value with and without internal pressure.
- (5) Only load combinations 9 and 10 have results that differ from Table 3.9.1-8.

Table 3.9.1-9
ITCP Stress Results – Load Combinations
 3 Pages

Load Comb No.	Service Level	DSC Orientation	Stress Category	Loads	Stress intensity (ksi)	Allowable Stress (ksi)	Stress Ratio
1	A	Vertical ⁽¹⁾	P _m	DW _v + max(PI ₍₂₀₎ ,BD,VD)	0.80	17.50	0.05
			P _m +P _b	DW _v + max(PI ₍₂₀₎ ,BD,VD)	9.02	26.25	0.34
			P _L	DW _v + max(PI ₍₂₀₎ ,BD,VD)	0.67	26.25	0.03
			P _m (or P _L)+P _b +Q	DW _v + max(PI ₍₂₀₎ ,BD,VD)	5.20	52.50	0.10
			P _m (or P _L)+P _b +Q+P _e	DW _v + max(PI ₍₂₀₎ ,BD,VD)+TH	19.20	52.50	0.37
2/3	A	Horizontal ⁽²⁾	P _m	DW _h + 1g axial + 1g transverse + 1g Vertical + PI ₍₂₀₎	0.56	17.50	0.03
			P _m +P _b	DW _h + 1g axial + 1g transverse + 1g Vertical + PI ₍₂₀₎	3.66	26.25	0.14
			P _L	DW _h + 1g axial + 1g transverse + 1g Vertical + PI ₍₂₀₎	1.18	26.25	0.04
			P _m (or P _L)+P _b +Q	DW _h + 1g axial + 1g transverse + 1g Vertical + PI ₍₂₀₎	3.66	52.50	0.07
			P _m (or P _L)+P _b +Q+P _e	DW _h + 1g axial + 1g transverse + 1g Vertical + PI ₍₂₀₎ + TH	13.84	52.50	0.26
4	A/B	Horizontal ⁽²⁾	P _m	DW _h + 135kips + PI ₍₂₀₎	0.56	17.50	0.03
			P _m +P _b	DW _h + 135kips + PI ₍₂₀₎	4.31	26.25	0.16
			P _L	DW _h + 135kips + PI ₍₂₀₎	0.98	26.25	0.04
			P _m (or P _L)+P _b +Q	DW _h + 135kips + PI ₍₂₀₎	3.47	52.50	0.07
			P _m (or P _L)+P _b +Q+P _e	DW _h + 135kips + TH	14.49	52.50	0.28
5	A/B	Horizontal ⁽²⁾	P _m	DW _h + 80 kips + PI ₍₂₀₎	0.54	17.50	0.03
			P _m +P _b	DW _h + 80 kips + PI ₍₂₀₎	4.21	26.25	0.16
			P _L	DW _h + 80 kips + PI ₍₂₀₎	0.93	26.25	0.04
			P _m (or P _L)+P _b +Q	DW _h + 80 kips + PI ₍₂₀₎	3.33	52.50	0.06
			P _m (or P _L)+P _b +Q+P _e	DW _h + 80 kips + TH	14.39	52.50	0.27

Table 3.9.1-9
ITCP Stress Results – Load Combinations
 3 Pages

Load Comb No.	Service Level	DSC Orientation	Stress Category	Loads	Stress intensity (ksi)	Allowable Stress (ksi)	Stress Ratio
6	D	Horizontal ⁽²⁾	P_m	DWh + 135 kips + $PI_{(20)}$	0.54	44.38	0.01
			$P_m + P_b$	DWh + 135 kips + $PI_{(20)}$	4.18	57.06	0.07
			P_L	DWh + 135 kips + $PI_{(20)}$	0.89	57.06	0.02
			P_m (or P_L) + P_b + Q	DWh + 135 kips + $PI_{(20)}$	NA		
7A	D	Horizontal ⁽²⁾	P_m	DWh + max.(SD_AWAY, SD_RAIL_EP, SD_TOP_RAIL_EP) + $PI_{(20)}$	7.33	44.38	0.17
			$P_m + P_b$	DWh + max.(SD_AWAY_EP, SD_RAIL_EP) + $PI_{(20)}$	20.14	57.06	0.35
			P_L	DWh + max.(SD_AWAY, SD_RAIL_EP, SD_TOP_RAIL_EP) + $PI_{(20)}$	13.28	57.06	0.23
			P_m (or P_L) + P_b + Q	DWh + max.(SD_AWAY_EP, SD_RAIL_EP) + $PI_{(20)}$	NA		
7B	D	Vertical	P_m	DWv + max.(ED_TOP, ED_BOT) + $PI_{(20)}$	3.40	44.38	0.08
			$P_m + P_b$	DWv + max.(ED_TOP, ED_BOT) + $PI_{(20)}$	18.01	57.06	0.32
			P_L	DWv + max.(ED_TOP, ED_BOT) + $PI_{(20)}$	4.09	57.06	0.07
			P_m (or P_L) + P_b + Q	DWv + max.(ED_TOP, ED_BOT) + $PI_{(20)}$	NA		
8	D	Horizontal ⁽²⁾	P_m	DWh + $PI_{(130)}$	2.46	44.38	0.06
			$P_m + P_b$	DWh + $PI_{(130)}$	25.82	57.06	0.45
			P_L	DWh + $PI_{(130)}$	3.07	57.06	0.05
			P_m (or P_L) + P_b + Q	DWh + $PI_{(130)}$	NA		
9	A	Horizontal ⁽³⁾	P_m	DWh + $PI_{(20)}$	0.74	17.50	0.04
			$P_m + P_b$	DWh + $PI_{(20)}$	4.55	26.25	0.17
			P_L	DWh + $PI_{(20)}$	1.31	26.25	0.05
			P_m (or P_L) + P_b + Q	DWh + $PI_{(20)}$	4.51	52.50	0.09
			P_m (or P_L) + P_b + Q + P_e	DWh + $PI_{(20)}$ + TH	14.73	52.50	0.28

Table 3.9.1-9
ITCP Stress Results – Load Combinations
 3 Pages

Load Comb No.	Service Level	DSC Orientation	Stress Category	Loads	Stress intensity (ksi)	Allowable Stress (ksi)	Stress Ratio
10	D	Horizontal ⁽³⁾	P_m	DWh + max.(HS_TOP, HS_BOT)+PI ₍₂₀₎	2.05	44.38	0.05
			P_m+P_b	DWh + max.(HS_TOP, HS_BOT)+PI ₍₂₀₎	4.60	57.06	0.08
			P_L	DWh + max.(HS_TOP, HS_BOT)+PI ₍₂₀₎	3.73	57.06	0.07
			P_m (or P_L)+ P_b +Q	DWh + max.(HS_TOP, HS_BOT)+PI ₍₂₀₎	NA		
11	Test	Vertical	P_m	max. (PI(23)+155 kips ,PE _(14.7) +155 kips)	NA		
			P_m+P_b	max. (PI(23)+155 kips,PE _(14.7) +155 kips)	NA		
			P_L	max. (PI(23)+155 kips ,PE _(14.7) +155 kips)	NA		
			P_m (or P_L)+ P_b +Q	max. (PI(23)+155 kips,PE _(14.7) +155 kips)	NA		

Notes:

- (1) DSC in transfer cask in vertical orientation. Only inner top cover is installed.
- (2) DSC in TC with TC in a horizontal orientation.
- (3) DSC in EOS-HSM supported on the steel rails.

Table 3.9.1-9a
ITCP Stress Results- Load Combinations (Supported by FPS DSC Support Structure)
 3 Pages

Load Comb No.	Service Level	DSC Orientation	Stress Category	Loads	Stress intensity (ksi)	Allowable Stress (ksi)	Stress Ratio
1	A	Vertical ⁽¹⁾	P_m	DWv + max(PI(20),BD,VD)	0.80	17.50	0.05
			P_m+P_b	DWv + max(PI(20),BD,VD)	9.02	26.25	0.34
			P_L	DWv + max(PI(20),BD,VD)	0.67	26.25	0.03
			P_m (or P_L)+ P_b +Q	DWv + max(PI(20),BD,VD)	5.20	52.50	0.10
			P_m (or P_L)+ P_b +Q+ P_e	DWv + max(PI(20),BD,VD)+TH	19.20	52.50	0.37
2/3	A	Horizontal ⁽²⁾	P_m	DWh + 1g axial + 1g transverse + 1g Vertical + PI(20)	0.56	17.50	0.03
			P_m+P_b	DWh + 1g axial + 1g transverse + 1g Vertical + PI(20)	3.66	26.25	0.14
			P_L	DWh + 1g axial + 1g transverse + 1g Vertical + PI(20)	1.18	26.25	0.04
			P_m (or P_L)+ P_b +Q	DWh + 1g axial + 1g transverse + 1g Vertical + PI(20)	3.66	52.50	0.07
			P_m (or P_L)+ P_b +Q+ P_e	DWh + 1g axial + 1g transverse + 1g Vertical + PI(20) +TH	13.84	52.50	0.26
4	A/B	Horizontal ⁽²⁾	P_m	DWh + 135kips + PI(20)	0.56	17.50	0.03
			P_m+P_b	DWh + 135kips + PI(20)	4.31	26.25	0.16
			P_L	DWh + 135kips + PI(20)	0.98	26.25	0.04
			P_m (or P_L)+ P_b +Q	DWh + 135kips + PI(20)	3.47	52.50	0.07
			P_m (or P_L)+ P_b +Q+ P_e	DWh + 135kips + TH	14.49	52.50	0.28
5	A/B	Horizontal ⁽²⁾	P_m	DWh + 80 kips + PI(20)	0.54	17.50	0.03
			P_m+P_b	DWh + 80 kips + PI(20)	4.21	26.25	0.16
			P_L	DWh + 80 kips + PI(20)	0.93	26.25	0.04
			P_m (or P_L)+ P_b +Q	DWh + 80 kips + PI(20)	3.33	52.50	0.06
			P_m (or P_L)+ P_b +Q+ P_e	DWh + 80 kips + TH	14.39	52.50	0.27

Table 3.9.1-9a
ITCP Stress Results- Load Combinations (Supported by FPS DSC Support Structure)
 3 Pages

Load Comb No.	Service Level	DSC Orientation	Stress Category	Loads	Stress intensity (ksi)	Allowable Stress (ksi)	Stress Ratio
6	D	Horizontal ⁽²⁾	P _m	DWh + 135 kips + PI(20)	0.54	44.38	0.01
			P _m +P _b	DWh + 135 kips + PI(20)	4.18	57.06	0.07
			P _L	DWh + 135 kips + PI(20)	0.89	57.06	0.02
			P _m (or P _L)+P _b +Q	DWh + 135 kips + PI(20)	NA		
7A	D	Horizontal ⁽²⁾	P _m	DWh + max.(SD_AWAY, SD_RAIL_EP,SD_TOP_RAIL_EP)+ PI(20)	7.33	44.38	0.17
			P _m +P _b	DWh + max.(SD_AWAY_EP, SD_RAIL_EP)+ PI(20)	20.14	57.06	0.35
			P _L	DWh + max.(SD_AWAY, SD_RAIL_EP,SD_TOP_RAIL_EP)+ PI(20)	13.28	57.06	0.23
			P _m (or P _L)+P _b +Q	DWh + max.(SD_AWAY_EP, SD_RAIL_EP)+ PI(20)	NA		
7B	D	Vertical	P _m	DW _v + max.(ED_TOP, ED_BOT)+ PI(20)	3.40	44.38	0.08
			P _m +P _b	DW _v + max.(ED_TOP, ED_BOT)+ PI(20)	18.01	57.06	0.32
			P _L	DW _v + max.(ED_TOP, ED_BOT)+ PI(20)	4.09	57.06	0.07
			P _m (or P _L)+P _b +Q	DW _v + max.(ED_TOP, ED_BOT)+ PI(20)	NA		
8	D	Horizontal ⁽²⁾	P _m	DWh + PI(130)	2.46	44.38	0.06
			P _m +P _b	DWh + PI(130)	25.82	57.06	0.45
			P _L	DWh + PI(130)	3.07	57.06	0.05
			P _m (or P _L)+P _b +Q	DWh + PI(130)	NA		
9	A	Horizontal ⁽³⁾	P _m	DWh + PI(20)	0.57	17.50	0.03
			P _m +P _b	DWh + PI(20)	4.24	26.25	0.16
			P _L	DWh + PI(20)	1.13	26.25	0.04
			P _m (or P _L)+P _b +Q	DWh + PI(20)	4.04	52.50	0.08
			P _m (or P _L)+P _b +Q+P _c	DWh + PI(20) +TH	14.42	52.50	0.27

Table 3.9.1-9a
ITCP Stress Results- Load Combinations (Supported by FPS DSC Support Structure)
 3 Pages

Load Comb No.	Service Level	DSC Orientation	Stress Category	Loads	Stress intensity (ksi)	Allowable Stress (ksi)	Stress Ratio
10	D	Horizontal ⁽³⁾	P_m	DWh + max.(HS_TOP, HS_BOT)+PI(20)	1.90	44.38	0.04
			P_m+P_b	DWh + max.(HS_TOP, HS_BOT)+PI(20)	4.70	57.06	0.08
			P_L	DWh + max.(HS_TOP, HS_BOT)+PI(20)	3.96	57.06	0.07
			P_m (or P_L)+ P_b +Q	DWh + max.(HS_TOP, HS_BOT)+PI(20)	NA		
11	Test	Vertical	P_m	max. (PI(23)+155 kips ,PE(14.7)+155 kips)	NA		
			P_m+P_b	max. (PI(23)+155 kips,PE(14.7)+155 kips)	NA		
			P_L	max. (PI(23)+155 kips ,PE(14.7)+155 kips)	NA		
			P_m (or P_L)+ P_b +Q	max. (PI(23)+155 kips,PE(14.7)+155 kips)	NA		

Notes:

- (1) DSC in transfer cask in vertical orientation. Only inner top cover is installed.
- (2) DSC in transfer cask, TC is in horizontal orientation.
- (3) DSC in EOS-HSM-FPS supported by FPS DSC support structure.
- (4) Maximum value with and without internal pressure.
- (5) Only load combinations 9 and 10 have results that differ from Table 3.9.1-9.

Table 3.9.1-10
IBCP Stress Results – Load Combinations
 3 Pages

Load Comb No.	Service Level	DSC Orientation	Stress Category	Loads	Stress intensity (ksi)	Allowable Stress (ksi)	Stress Ratio
1	A	Vertical ⁽¹⁾	P _m	DW _v + max(PI ₍₂₀₎ , BD, VD)	0.43	17.50	0.02
			P _m +P _b	DW _v + max(PI ₍₂₀₎ , BD, VD)	1.00	26.25	0.04
			P _L	DW _v + max(PI ₍₂₀₎ , BD, VD)	0.44	26.25	0.02
			P _m (or P _L)+P _b +Q	DW _v + max(PI ₍₂₀₎ , BD, VD)	1.18	52.50	0.02
			P _m (or P _L)+P _b +Q+P _e	DW _v + max(PI ₍₂₀₎ , BD, VD)+TH	17.40	52.50	0.33
2/3	A	Horizontal ⁽²⁾	P _m	DWh + 1g axial + 1g transverse + 1g Vertical + PI ₍₂₀₎	0.40	17.50	0.02
			P _m +P _b	DWh + 1g axial + 1g transverse + 1g Vertical + PI ₍₂₀₎	0.67	26.25	0.03
			P _L	DWh + 1g axial + 1g transverse + 1g Vertical + PI ₍₂₀₎	0.80	26.25	0.03
			P _m (or P _L)+P _b +Q	DWh + 1g axial + 1g transverse + 1g Vertical + PI ₍₂₀₎	2.77	52.50	0.05
			P _m (or P _L)+P _b +Q+P _e	DWh + 1g axial + 1g transverse + 1g Vertical + PI ₍₂₀₎ + TH	18.99	52.50	0.36
4	A/B	Horizontal ⁽²⁾	P _m	DWh + 135kips + PI ₍₂₀₎	1.46	17.50	0.08
			P _m +P _b	DWh + 135kips + PI ₍₂₀₎	5.56	26.25	0.21
			P _L	DWh + 135kips + PI ₍₂₀₎	1.60	26.25	0.06
			P _m (or P _L)+P _b +Q	DWh + 135kips + PI ₍₂₀₎	6.71	52.50	0.13
			P _m (or P _L)+P _b +Q+P _e	DWh + 135kips + TH	22.93	52.50	0.44
5	A/B	Horizontal ⁽²⁾	P _m	DWh + 80 kips + PI ₍₂₀₎	0.47	17.50	0.03
			P _m +P _b	DWh + 80 kips + PI ₍₂₀₎	2.08	26.25	0.08
			P _L	DWh + 80 kips + PI ₍₂₀₎	0.79	26.25	0.03
			P _m (or P _L)+P _b +Q	DWh + 80 kips + PI ₍₂₀₎	3.05	52.50	0.06
			P _m (or P _L)+P _b +Q+P _e	DWh + 80 kips + TH	19.27	52.50	0.37

Table 3.9.1-10
IBCP Stress Results – Load Combinations
 3 Pages

Load Comb No.	Service Level	DSC Orientation	Stress Category	Loads	Stress intensity (ksi)	Allowable Stress (ksi)	Stress Ratio
6	D	Horizontal ⁽²⁾	P_m	DWh + 135 kips + $PI_{(20)}$	0.56	44.38	0.01
			$P_m + P_b$	DWh + 135 kips + $PI_{(20)}$	2.71	57.06	0.05
			P_L	DWh + 135 kips + $PI_{(20)}$	0.89	57.06	0.02
			P_m (or P_L) + $P_b + Q$	DWh + 135 kips + $PI_{(20)}$	NA		
7A	D	Horizontal ⁽²⁾	P_m	DWh + max.(SD_AWAY, SD_RAIL_EP, SD_TOP_RAIL_EP) + $PI_{(20)}$	18.03	44.38	0.41
			$P_m + P_b$	DWh + max.(SD_AWAY_EP, SD_RAIL_EP) + $PI_{(20)}$	23.81	57.06	0.42
			P_L	DWh + max.(SD_AWAY, SD_RAIL_EP, SD_TOP_RAIL_EP) + $PI_{(20)}$	23.67	57.06	0.41
			P_m (or P_L) + $P_b + Q$	DWh + max.(SD_AWAY_EP, SD_RAIL_EP) + $PI_{(20)}$	NA		
7B	D	Vertical	P_m	DWv + max.(ED_TOP, ED_BOT) + $PI_{(20)}$	6.56	44.38	0.15
			$P_m + P_b$	DWv + max.(ED_TOP, ED_BOT) + $PI_{(20)}$	21.21	57.06	0.37
			P_L	DWv + max.(ED_TOP, ED_BOT) + $PI_{(20)}$	5.05	57.06	0.09
			P_m (or P_L) + $P_b + Q$	DWv + max.(ED_TOP, ED_BOT) + $PI_{(20)}$	NA		
8	D	Horizontal ⁽²⁾	P_m	DWh + $PI_{(130)}$	1.10	44.38	0.02
			$P_m + P_b$	DWh + $PI_{(130)}$	5.44	57.06	0.10
			P_L	DWh + $PI_{(130)}$	1.80	57.06	0.03
			P_m (or P_L) + $P_b + Q$	DWh + $PI_{(130)}$	NA		
9	A	Horizontal ⁽³⁾	P_m	DWh + $PI_{(20)}$	0.58	17.50	0.03
			$P_m + P_b$	DWh + $PI_{(20)}$	1.30	26.25	0.05
			P_L	DWh + $PI_{(20)}$	1.12	26.25	0.04
			P_m (or P_L) + $P_b + Q$	DWh + $PI_{(20)}$	2.46	52.50	0.05
			P_m (or P_L) + $P_b + Q + P_e$	DWh + $PI_{(20)}$ + TH	18.68	52.50	0.36

Table 3.9.1-10
IBCP Stress Results – Load Combinations
 3 Pages

Load Comb No.	Service Level	DSC Orientation	Stress Category	Loads	Stress intensity (ksi)	Allowable Stress (ksi)	Stress Ratio
10	D	Horizontal ⁽³⁾	P_m	DWh + max.(HS_TOP, HS_BOT)+PI ₍₂₀₎	4.00	44.38	0.09
			P_m+P_b	DWh + max.(HS_TOP, HS_BOT)+PI ₍₂₀₎	12.66	57.06	0.22
			P_L	DWh + max.(HS_TOP, HS_BOT)+PI ₍₂₀₎	3.80	57.06	0.07
			P_m (or P_L)+ P_b +Q	DWh + max.(HS_TOP, HS_BOT)+PI ₍₂₀₎	NA		
11	Test	Vertical	P_m	max. (PI(23)+155 kips, PE _(14.7) +155 kips)	0.67	17.50	0.04
			P_m+P_b	max. (PI(23)+155 kips, PE _(14.7) +155 kips)	7.69	26.25	0.29
			P_L	max. (PI(23)+155 kips, PE _(14.7) +155 kips)	1.13	26.25	0.04
			P_m (or P_L)+ P_b +Q	max. (PI(23)+155 kips, PE _(14.7) +155 kips)	NA		

Notes:

- (1) DSC in transfer cask in vertical orientation. Only inner top cover is installed.
- (2) DSC in TC with TC in a horizontal orientation.
- (3) DSC in EOS-HSM supported on the steel rails.

Table 3.9.1-10a
IBCP Stress Results - Load Combinations (Supported by FPS DSC Support Structure)
 3 Pages

Load Comb No.	Service Level	DSC Orientation	Stress Category	Loads	Stress intensity (ksi)	Allowable Stress (ksi)	Stress Ratio
1	A	Vertical ⁽¹⁾	P_m	DW _v + max(PI(20),BD,VD)	0.43	17.50	0.02
			P_m+P_b	DW _v + max(PI(20),BD,VD)	1.00	26.25	0.04
			P_L	DW _v + max(PI(20),BD,VD)	0.44	26.25	0.02
			P_m (or P_L)+ P_b +Q	DW _v + max(PI(20),BD,VD)	1.18	52.50	0.02
			P_m (or P_L)+ P_b +Q+ P_e	DW _v + max(PI(20),BD,VD)+TH	17.40	52.50	0.33
2/3	A	Horizontal ⁽²⁾	P_m	DW _h + 1g axial + 1g transverse + 1g Vertical + PI(20)	0.40	17.50	0.02
			P_m+P_b	DW _h + 1g axial + 1g transverse + 1g Vertical + PI(20)	0.67	26.25	0.03
			P_L	DW _h + 1g axial + 1g transverse + 1g Vertical + PI(20)	0.80	26.25	0.03
			P_m (or P_L)+ P_b +Q	DW _h + 1g axial + 1g transverse + 1g Vertical + PI(20)	2.77	52.50	0.05
			P_m (or P_L)+ P_b +Q+ P_e	DW _h + 1g axial + 1g transverse + 1g Vertical + PI(20) +TH	18.99	52.50	0.36
4	A/B	Horizontal ⁽²⁾	P_m	DW _h + 135kips + PI(20)	1.46	17.50	0.08
			P_m+P_b	DW _h + 135kips + PI(20)	5.56	26.25	0.21
			P_L	DW _h + 135kips + PI(20)	1.60	26.25	0.06
			P_m (or P_L)+ P_b +Q	DW _h + 135kips + PI(20)	6.71	52.50	0.13
			P_m (or P_L)+ P_b +Q+ P_e	DW _h + 135kips + TH	22.93	52.50	0.44
5	A/B	Horizontal ⁽²⁾	P_m	DW _h + 80 kips + PI(20)	0.47	17.50	0.03
			P_m+P_b	DW _h + 80 kips + PI(20)	2.08	26.25	0.08
			P_L	DW _h + 80 kips + PI(20)	0.79	26.25	0.03
			P_m (or P_L)+ P_b +Q	DW _h + 80 kips + PI(20)	3.05	52.50	0.06
			P_m (or P_L)+ P_b +Q+ P_e	DW _h + 80 kips + TH	19.27	52.50	0.37

Table 3.9.1-10a
IBCP Stress Results - Load Combinations (Supported by FPS DSC Support Structure)
 3 Pages

Load Comb No.	Service Level	DSC Orientation	Stress Category	Loads	Stress intensity (ksi)	Allowable Stress (ksi)	Stress Ratio
6	D	Horizontal ⁽²⁾	P _m	DWh + 135 kips + PI(20)	0.56	44.38	0.01
			P _m +P _b	DWh + 135 kips + PI(20)	2.71	57.06	0.05
			P _L	DWh + 135 kips + PI(20)	0.89	57.06	0.02
			P _m (or P _L)+P _b +Q	DWh + 135 kips + PI(20)	NA		
7A	D	Horizontal ⁽²⁾	P _m	DWh + max.(SD_AWAY, SD_RAIL_EP,SD_TOP_RAIL_EP)+ PI(20)	18.03	44.38	0.41
			P _m +P _b	DWh + max.(SD_AWAY_EP, SD_RAIL_EP)+ PI(20)	23.81	57.06	0.42
			P _L	DWh + max.(SD_AWAY, SD_RAIL_EP,SD_TOP_RAIL_EP)+ PI(20)	23.67	57.06	0.41
			P _m (or P _L)+P _b +Q	DWh + max.(SD_AWAY_EP, SD_RAIL_EP)+ PI(20)	NA		
7B	D	Vertical	P _m	DW _v + max.(ED_TOP, ED_BOT)+ PI(20)	6.56	44.38	0.15
			P _m +P _b	DW _v + max.(ED_TOP, ED_BOT)+ PI(20)	21.21	57.06	0.37
			P _L	DW _v + max.(ED_TOP, ED_BOT)+ PI(20)	5.05	57.06	0.09
			P _m (or P _L)+P _b +Q	DW _v + max.(ED_TOP, ED_BOT)+ PI(20)	NA		
8	D	Horizontal ⁽²⁾	P _m	DWh + PI(130)	1.10	44.38	0.02
			P _m +P _b	DWh + PI(130)	5.44	57.06	0.10
			P _L	DWh + PI(130)	1.80	57.06	0.03
			P _m (or P _L)+P _b +Q	DWh + PI(130)	NA		
9	A	Horizontal ⁽³⁾	P _m	DWh + PI(20)	0.82	17.50	0.05
			P _m +P _b	DWh + PI(20)	1.55	26.25	0.06
			P _L	DWh + PI(20)	0.95	26.25	0.04
			P _m (or P _L)+P _b +Q	DWh + PI(20)	2.04	52.50	0.04
			P _m (or P _L)+P _b +Q+P _c	DWh + PI(20) +TH	18.26	52.50	0.35

Table 3.9.1-10a
IBCP Stress Results - Load Combinations (Supported by FPS DSC Support Structure)
 3 Pages

Load Comb No.	Service Level	DSC Orientation	Stress Category	Loads	Stress intensity (ksi)	Allowable Stress (ksi)	Stress Ratio
10	D	Horizontal ⁽³⁾	P_m	DWh + max.(HS_TOP, HS_BOT)+PI(20)	4.40	44.38	0.10
			P_m+P_b	DWh + max.(HS_TOP, HS_BOT)+PI(20)	13.56	57.06	0.24
			P_L	DWh + max.(HS_TOP, HS_BOT)+PI(20)	4.36	57.06	0.08
			P_m (or P_L)+ P_b +Q	DWh + max.(HS_TOP, HS_BOT)+PI(20)	NA		
11	Test	Vertical	P_m	max. (PI(23)+155 kips ,PE(14.7)+155 kips)	0.67	17.50	0.04
			P_m+P_b	max. (PI(23)+155 kips,PE(14.7)+155 kips)	7.69	26.25	
			P_L	max. (PI(23)+155 kips ,PE(14.7)+155 kips)	1.13	26.25	0.04
			P_m (or P_L)+ P_b +Q	max. (PI(23)+155 kips,PE(14.7)+155 kips)	NA		

Notes:

- (1) DSC in transfer cask in vertical orientation. Only inner top cover is installed.
- (2) DSC in transfer cask, TC is in horizontal orientation.
- (3) DSC in EOS-HSM-FPS supported by FPS DSC support structure.
- (4) Maximum value with and without internal pressure.
- (5) Conservatively, Level A allowables are taken for test conditions.
- (6) Only load combinations 9 and 10 have results that differ from Table 3.9.1-10.

Table 3.9.1-11
ITCP-DSC Shell Weld Stress Results – Load Combinations
 2 Pages

Load Comb No.	Service Level	DSC Orientation	Stress Category	Loads	Stress intensity (ksi)	Allowable Stress	Stress Ratio
1	A	Vertical ⁽¹⁾	P _L	DW _v + max(PI ₍₂₀₎ , BD, VD)	8.60	23.20	0.37
			P _L +P _b +Q+P _e	DW _v + max(PI ₍₂₀₎ , BD, VD) + TH	34.48	46.30	0.74
2	A	Horizontal ⁽²⁾	P _L	DWh + 1g axial + 1g transverse + 1g Vertical + PI ₍₂₀₎	5.95	23.20	0.26
			P _L +P _b +Q+P _e	DWh + 1g axial + 1g transverse + 1g Vertical + PI ₍₂₀₎ + TH	27.93	46.30	0.60
3	A	Horizontal ⁽²⁾	P _L	DWh + 1g axial + 1g transverse + 1g Vertical + PI ₍₂₀₎	5.95	23.20	0.26
			P _L +P _b +Q+P _e	DWh + 1g axial + 1g transverse + 1g Vertical + PI ₍₂₀₎ + TH	27.93	46.30	0.60
4	A/B	Horizontal ⁽²⁾	P _L	DWh + 135kips + PI ₍₂₀₎	6.02	23.20	0.26
			P _L +P _b +Q+P _e	DWh + 135kips + PI ₍₂₀₎ + TH	29.44	46.30	0.64
5	A/B	Horizontal ⁽²⁾	P _L	DWh + 80 kips + PI ₍₂₀₎	6.50	23.20	0.28
			P _L +P _b +Q+P _e	DWh + 80 kips + PI ₍₂₀₎ + TH	29.11	46.30	0.63
6	D	Horizontal ⁽²⁾	P _L	DWh + 135 kips + PI ₍₂₀₎	6.74	46.90	0.14
			P _L +P _b +Q+P _e	DWh + 135 kips + PI ₍₂₀₎ + TH	NA		
7A	D	Horizontal ⁽²⁾	P _L	DWh + max.(SD_AWAY, SD_RAIL_EP, SD_TOP_RAIL_EP) + PI ₍₂₀₎	35.77	46.90	0.76
			P _L +P _b +Q+P _e	DWh + max.(SD_AWAY_EP, SD_RAIL_EP) + PI ₍₂₀₎ + TH	NA		
7B	D	Vertical	P _L	DW _v + max.(ED_TOP, ED_BOT) + PI ₍₂₀₎	13.22	52.08	0.25
			P _L +P _b +Q+P _e	DW _v + max.(ED_TOP, ED_BOT) + PI ₍₂₀₎ + TH	NA		
8	D	Horizontal ⁽²⁾	P _L	DWh + PI ₍₁₃₀₎	16.41	46.90	0.35
			P _L +P _b +Q+P _e	DWh + PI ₍₁₃₀₎ + TH	NA		
9	A	Horizontal ⁽³⁾	P _L	DWh + PI ₍₂₀₎	8.27	23.20	0.36
			P _L +P _b +Q+P _e	DWh + PI ₍₂₀₎ + TH	31.18	46.30	0.67

Table 3.9.1-11
ITCP-DSC Shell Weld Stress Results – Load Combinations
 2 Pages

Load Comb No.	Service Level	DSC Orientation	Stress Category	Loads	Stress intensity (ksi)	Allowable Stress	Stress Ratio
10	D	Horizontal ⁽³⁾	P_L	DWh + max.(HS_TOP, HS_BOT)+PI ₍₂₀₎	18.93	46.90	0.40
			$P_L+P_b+Q+P_e$	DWh + max.(HS_TOP, HS_BOT)+PI ₍₂₀₎ + TH	NA		
11	Test	Vertical	P_L	max. (PI(23)+155 kips ,PE _(14.7) +155 kips)	NA		
			$P_L+P_b+Q+P_e$	max. (PI(23)+155 kips,PE _(14.7) +155 kips) + TH	NA		

Notes:

- (1) DSC in transfer cask in vertical orientation. Only inner top cover is installed.
- (2) DSC in TC with TC in a horizontal orientation.
- (3) DSC in EOS-HSM supported on the steel rails

Table 3.9.1-11a
ITCP-DSC Shell Weld Stress Results - Load Combinations (Supported by FPS DSC Support Structure)
 2 Pages

Load Comb No.	Service Level	DSC Orientation	Stress Category	Loads	Stress intensity (ksi)	Allowable Stress (ksi)	Stress Ratio
1	A	Vertical ⁽¹⁾	P _L	DW _v + max(PI(20),BD,VD)	8.60	23.20	0.37
			P _L +P _b +Q+P _e	DW _v + max(PI(20),BD,VD)+TH	34.48	46.30	0.74
2	A	Horizontal ⁽²⁾	P _L	DW _h + 1g axial + 1g transverse + 1g Vertical + PI(20)	5.95	23.20	0.26
			P _L +P _b +Q+P _e	DW _h + 1g axial + 1g transverse + 1g Vertical + PI(20) +TH	27.93	46.30	0.60
3	A	Horizontal ⁽²⁾	P _L	DW _h + 1g axial + 1g transverse + 1g Vertical + PI(20)	5.95	23.20	0.26
			P _L +P _b +Q+P _e	DW _h + 1g axial + 1g transverse + 1g Vertical + PI(20)+TH	27.93	46.30	0.60
4	A/B	Horizontal ⁽²⁾	P _L	DW _h + 135kips + PI(20)	6.02	23.20	0.26
			P _L +P _b +Q+P _e	DW _h + 135kips + PI(20) +TH	29.44	46.30	0.64
5	A/B	Horizontal ⁽²⁾	P _L	DW _h + 80 kips + PI(20)	6.50	23.20	0.28
			P _L +P _b +Q+P _e	DW _h + 80 kips + PI(20) +TH	29.11	46.30	0.63
6	D	Horizontal ⁽²⁾	P _L	DW _h + 135 kips + PI(20)	6.74	46.90	0.14
			P _L +P _b +Q+P _e	DW _h + 135 kips + PI(20) +TH	NA		
7A	D	Horizontal ⁽²⁾	P _L	DW _h + max.(SD_AWAY, SD_RAIL_EP,SD_TOP_RAIL_EP)+ PI(20)	35.77	46.90	0.76
			P _L +P _b +Q+P _e	DW _h + max.(SD_AWAY_EP, SD_RAIL_EP)+ PI(20) +TH	NA		
7B	D	Vertical	P _L	DW _v + max.(ED_TOP, ED_BOT)+ PI(20)	13.22	52.08	0.25
			P _L +P _b +Q+P _e	DW _v + max.(ED_TOP, ED_BOT)+ PI(20) +TH	NA		
8	D	Horizontal ⁽²⁾	P _L	DW _h + PI(130)	16.41	46.90	0.35
			P _L +P _b +Q+P _e	DW _h + PI(130) +TH	NA		
9	A	Horizontal ⁽³⁾	P _L	DW _h + PI(20)	7.64	23.20	0.33
			P _L +P _b +Q+P _e	DW _h + PI(20) +TH	31.40	46.30	0.68

Table 3.9.1-11a
ITCP-DSC Shell Weld Stress Results - Load Combinations (Supported by FPS DSC Support Structure)
 2 Pages

Load Comb No.	Service Level	DSC Orientation	Stress Category	Loads	Stress intensity (ksi)	Allowable Stress (ksi)	Stress Ratio
10	D	Horizontal ⁽³⁾	P _L	DWh + max.(HS_TOP, HS_BOT)+PI(20)	19.98	46.90	0.43
			P _L +P _b +Q+P _e	DWh + max.(HS_TOP, HS_BOT)+PI(20) +TH	NA		
11	Test	Vertical	P _L	max. (PI(23)+155 kips ,PE(14.7)+155 kips)	NA		
			P _L +P _b +Q+P _e	max. (PI(23)+155 kips,PE(14.7)+155 kips) +TH	NA		

Notes:

- (1) DSC in transfer cask in vertical orientation. Only inner top cover is installed.
- (2) DSC in transfer cask, TC is in horizontal orientation.
- (3) DSC in EOS-HSM-FPS supported by FPS DSC support structure.
- (4) Only load combinations 9 and 10 have results that differ from Table 3.9.1-11.

Table 3.9.1-12
OTCP-DSC Shell Weld Stress Results – Load Combinations
 2 Pages

Load Comb No.	Service Level	DSC Orientation	Stress Category	Loads	Stress intensity (ksi)	Allowable Stress	Stress Ratio
1	A	Vertical ⁽¹⁾	P _L	DW _v + max(PI ₍₂₀₎ ,BD,VD)	4.96	23.20	0.21
			P _L +P _b +Q+P _e	DW _v + max(PI ₍₂₀₎ ,BD,VD) + TH	21.15	46.30	0.46
2	A	Horizontal ⁽²⁾	P _L	DWh + 1g axial + 1g transverse + 1g Vertical + PI ₍₂₀₎	7.45	23.20	0.32
			P _L +P _b +Q+P _e	DWh + 1g axial + 1g transverse + 1g Vertical + PI ₍₂₀₎ + TH	26.42	46.30	0.57
3	A	Horizontal ⁽²⁾	P _L	DWh + 1g axial + 1g transverse + 1g Vertical + PI ₍₂₀₎	7.45	23.20	0.32
			P _L +P _b +Q+P _e	DWh + 1g axial + 1g transverse + 1g Vertical + PI ₍₂₀₎ + TH	26.42	46.30	0.57
4	A/B	Horizontal ⁽²⁾	P _L	DWh + 135kips + PI ₍₂₀₎	5.45	23.20	0.23
			P _L +P _b +Q+P _e	DWh + 135kips + PI ₍₂₀₎ + TH	20.82	46.30	0.45
5	A/B	Horizontal ⁽²⁾	P _L	DWh + 80 kips + PI ₍₂₀₎	5.78	23.20	0.25
			P _L +P _b +Q+P _e	DWh + 80 kips + PI ₍₂₀₎ + TH	22.80	46.30	0.49
6	D	Horizontal ⁽²⁾	P _L	DWh + 135 kips + PI ₍₂₀₎	5.87	46.90	0.13
			P _L +P _b +Q+P _e	DWh + 135 kips + PI ₍₂₀₎ + TH	NA		
7A	D	Horizontal ⁽²⁾	P _L	DWh + max.(SD_AWAY, SD_RAIL_EP,SD_TOP_RAIL_EP)+ PI ₍₂₀₎	31.73	46.90	0.68
			P _L +P _b +Q+P _e	DWh + max.(SD_AWAY_EP, SD_RAIL_EP)+ PI ₍₂₀₎ + TH	NA		
7B	D	Vertical	P _L	DW _v + max.(ED_TOP, ED_BOT)+ PI ₍₂₀₎	12.97	46.90	0.28
			P _L +P _b +Q+P _e	DW _v + max.(ED_TOP, ED_BOT)+ PI ₍₂₀₎ + TH	NA		
8	D	Horizontal ⁽²⁾	P _L	DWh + PI ₍₁₃₀₎	14.77	46.90	0.31
			P _L +P _b +Q+P _e	DWh + PI ₍₁₃₀₎ + TH	NA		
9	A	Horizontal ⁽³⁾	P _L	DWh + PI ₍₂₀₎	6.93	23.20	0.30
			P _L +P _b +Q+P _e	DWh + PI ₍₂₀₎ + TH	23.75	46.30	0.51

Table 3.9.1-12
OTCP-DSC Shell Weld Stress Results – Load Combinations
 2 Pages

Load Comb No.	Service Level	DSC Orientation	Stress Category	Loads	Stress intensity (ksi)	Allowable Stress	Stress Ratio
10	D	Horizontal ⁽³⁾	P_L	DWh + max.(HS_TOP, HS_BOT)+PI ₍₂₀₎	17.07	46.90	0.36
			$P_L+P_b+Q+P_e$	DWh + max.(HS_TOP, HS_BOT)+PI ₍₂₀₎ + TH	NA		
11	Test	Vertical	P_L	max. (PI(23)+155 kips ,PE _(14.7) +155 kips)	NA		
			$P_L+P_b+Q+P_e$	max. (PI(23)+155 kips,PE _(14.7) +155 kips) + TH	NA		

Notes:

- (1) Maximum value of load case with and without internal pressure.
- (2) DSC in TC with TC in a horizontal orientation.
- (3) DSC in HSM supported on the steel rails.

Table 3.9.1-12a
OTCP-DSC Shell Weld Stress Results - Load Combinations (Supported by FPS DSC Support Structure)
 2 Pages

Load Comb No.	Service Level	DSC Orientation	Stress Category	Loads	Stress intensity (ksi)	Allowable Stress (ksi)	Stress Ratio
1	A	Vertical ⁽¹⁾	P_L	DW _v + max(PI(20),BD,VD)	4.96	23.20	0.21
			$P_L+P_b+Q+P_e$	DW _v + max(PI(20),BD,VD)+TH	21.15	46.30	0.46
2	A	Horizontal ⁽²⁾	P_L	DW _h + 1g axial + 1g transverse + 1g Vertical + PI(20)	7.45	23.20	0.32
			$P_L+P_b+Q+P_e$	DW _h + 1g axial + 1g transverse + 1g Vertical + PI(20) +TH	26.42	46.30	0.57
3	A	Horizontal ⁽²⁾	P_L	DW _h + 1g axial + 1g transverse + 1g Vertical + PI(20)	7.45	23.20	0.32
			$P_L+P_b+Q+P_e$	DW _h + 1g axial + 1g transverse + 1g Vertical + PI(20) +TH	26.42	46.30	0.57
4	A/B	Horizontal ⁽²⁾	P_L	DW _h + 135kips + PI(20)	5.45	23.20	0.23
			$P_L+P_b+Q+P_e$	DW _h + 135kips + PI(20) +TH	20.82	46.30	0.45
5	A/B	Horizontal ⁽²⁾	P_L	DW _h + 80 kips + PI(20)	5.78	23.20	0.25
			$P_L+P_b+Q+P_e$	DW _h + 80 kips + PI(20) +TH	22.80	46.30	0.49
6	D	Horizontal ⁽²⁾	P_L	DW _h + 135 kips + PI(20)	5.87	46.90	0.13
			$P_L+P_b+Q+P_e$	DW _h + 135 kips + PI(20) +TH	NA		
7A	D	Horizontal ⁽²⁾	P_L	DW _h + max.(SD_AWAY, SD_RAIL_EP,SD_TOP_RAIL_EP)+ PI(20)	31.73	46.90	0.68
			$P_L+P_b+Q+P_e$	DW _h + max.(SD_AWAY_EP, SD_RAIL_EP)+ PI(20) +TH	NA		
7B	D	Vertical	P_L	DW _v + max.(ED_TOP, ED_BOT)+ PI(20)	12.97	46.90	0.28
			$P_L+P_b+Q+P_e$	DW _v + max.(ED_TOP, ED_BOT)+ PI(20) +TH	NA		
8	D	Horizontal ⁽²⁾	P_L	DW _h + PI(130)	14.77	46.90	0.31
			$P_L+P_b+Q+P_e$	DW _h + PI(130) +TH	NA		
9	A	Horizontal ⁽³⁾	P_L	DW _h + PI(20)	11.76	23.20	0.51
			$P_L+P_b+Q+P_e$	DW _h + PI(20) +TH	28.56	46.30	0.62

Table 3.9.1-12a
OTCP-DSC Shell Weld Stress Results - Load Combinations (Supported by FPS DSC Support Structure)
 2 Pages

Load Comb No.	Service Level	DSC Orientation	Stress Category	Loads	Stress intensity (ksi)	Allowable Stress (ksi)	Stress Ratio
10	D	Horizontal ⁽³⁾	P_L	DWh + max.(HS_TOP, HS_BOT)+PI(20)	22.43	46.90	0.48
			$P_L+P_b+Q+P_e$	DWh + max.(HS_TOP, HS_BOT)+PI(20) +TH	NA		
11	Test	Vertical	P_L	max. (PI(23)+155 kips ,PE(14.7)+155 kips)	NA		
			$P_L+P_b+Q+P_e$	max. (PI(23)+155 kips,PE(14.7)+155 kips) +TH	NA		

Notes:

- (1) DSC in transfer cask in vertical orientation. Only inner top cover is installed.
- (2) DSC in transfer cask, TC is in horizontal orientation.
- (3) DSC in HSM-FPS supported by FPS DSC support structure.
- (4) Only load combinations 9 and 10 have results that differ from Table 3.9.1-12.

Table 3.9.1-13
Weld Flaw Size for Controlling Load Combination

Service Level	Controlling Load Combination	Tensile Radial Stress SX (ksi)	Safety Factor SFm	Radial Stress including Safety Factor (Sx)x (SFm)	Allowable a/t	Subsurface Flaws		Surface Flaws	
						Weld Thickness 2t (inch)	Flaw Depth, 2a (inch)	Weld Thickness t (inch)	Flaw Depth, a (inch)
A	4	0.21	2.7	0.56	(0.99) 0.75	0.50	0.38	0.50	0.38
B	4	0.21	2.4	0.49	(0.99) 0.75	0.50	0.38	0.50	0.38
D	7A	3.65	1.3	4.75	(0.89) 0.75	0.50	0.38	0.50	0.38

Table 3.9.1-14
Lifting Lug Plate-DSC Shell Weld Stress Results – Load Combinations

Load Comb. No.	Service Level	DSC Orientation	Stress Category	Loads	Stress intensity (ksi)	Allowable Stress (ksi)	Stress Ratio
1	A	Vertical ⁽¹⁾	$P_m + P_b$	$DW_v + \max(PI_{(20)}, BD, VD)$	1.87	7.76	0.24
2	A	Horizontal ⁽²⁾	$P_m + P_b$	$DW_h + 1g \text{ axial} + 1g \text{ transverse} + 1g \text{ Vertical} + PI_{(20)}$	0.78	7.76	0.10
3	A	Horizontal ⁽²⁾	$P_m + P_b$	$DW_h + 1g \text{ axial} + 1g \text{ transverse} + 1g \text{ Vertical} + PI_{(20)}$	0.78	7.76	0.10
4	A/B	Horizontal ⁽²⁾	$P_m + P_b$	$DWh + 135 \text{ kips} + PI(20)$	0.61	7.76	0.08
5	A/B	Horizontal ⁽²⁾	$P_m + P_b$	$DWh + 80 \text{ kips} + PI(20)$	0.64	7.76	0.08
6	D	Horizontal ⁽²⁾	$P_m + P_b$	$DWh + 135 \text{ kips} + PI(20)$	0.63	15.52	0.04
7A	D	Horizontal ⁽²⁾	$P_m + P_b$	$DWh + \max.(SD_AWAY, SD_RAIL) + PI(20)$	3.45	15.52	0.22
7B	D	Vertical ⁽¹⁾	$P_m + P_b$	$DW_v + \max.(ED_TOP, ED_BOT) + PI_{(20)}$	0.98	15.52	0.06
8	D	Horizontal ⁽²⁾	$P_m + P_b$	$DW_h + PI_{(130)}$	3.96	15.52	0.26
9	A	Horizontal ⁽³⁾	$P_m + P_b$	$DW_h + PI_{(20)}$	0.66	7.76	0.08
10	D	Horizontal ⁽³⁾	$P_m + P_b$	$DWh + \max.(HS_TOP, HS_BOT) + PI(20)$	4.88	15.52	0.31
11	A	Vertical ⁽¹⁾	$P_m + P_b$	$\max. (PI_{(23)} + 155 \text{ kips}, PE_{(14.7)} + 155 \text{ kips})$	NA		

Notes:

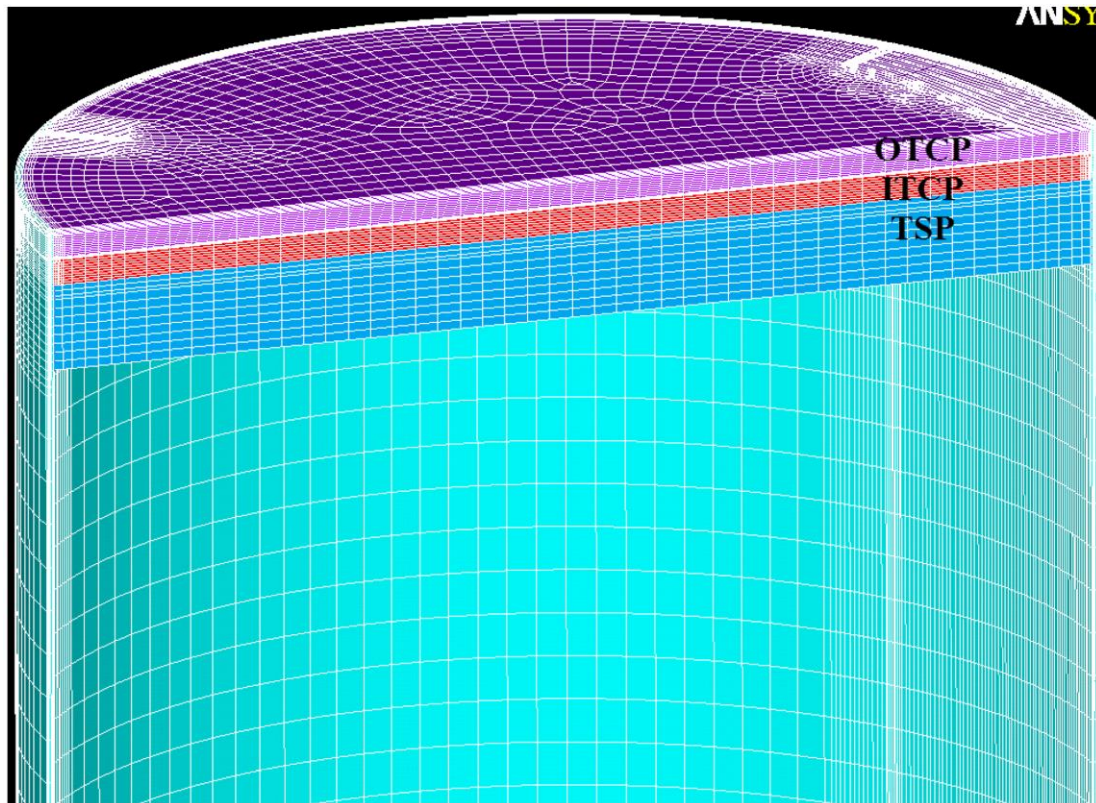
- (1) DSC in the transfer cask in vertical orientation and only the inner top cover plate is welded
- (2) DSC in the transfer cask, TC is in horizontal orientation and supported at 4 trunnion locations
- (3) DSC in the HSM supported on the steel rails

Table 3.9.1-15
Summary of Maximum Strain for Side Drop (Strain Criteria)⁽¹⁾

Load Case	Maximum Equivalent Plastic Strain (in/in)	Triaxiality Factor	Uniform Strain Limit (in/in)	Factor of Safety
Baseline 75g	0.065	-1.6 (1.0)	0.17	2.6
75g with 20% increase in yield strength	0.054	-1.6 (1.0)	0.17	3.1
75g with 40% increase in yield strength	0.045	-1.6 (1.0)	0.17	3.8

Notes:

- (1) The maximum equivalent plastic strains are conservatively compared with the uniform strain limits.



Length through the middle of the DSC not shown

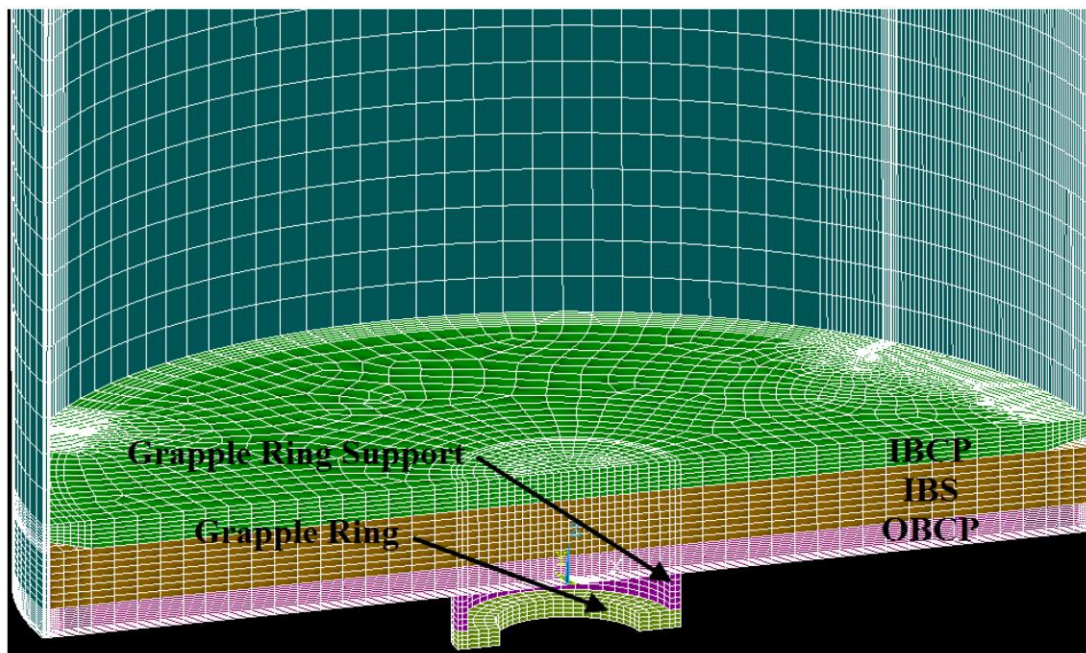


**Figure 3.9.1-1
DSC FEM**

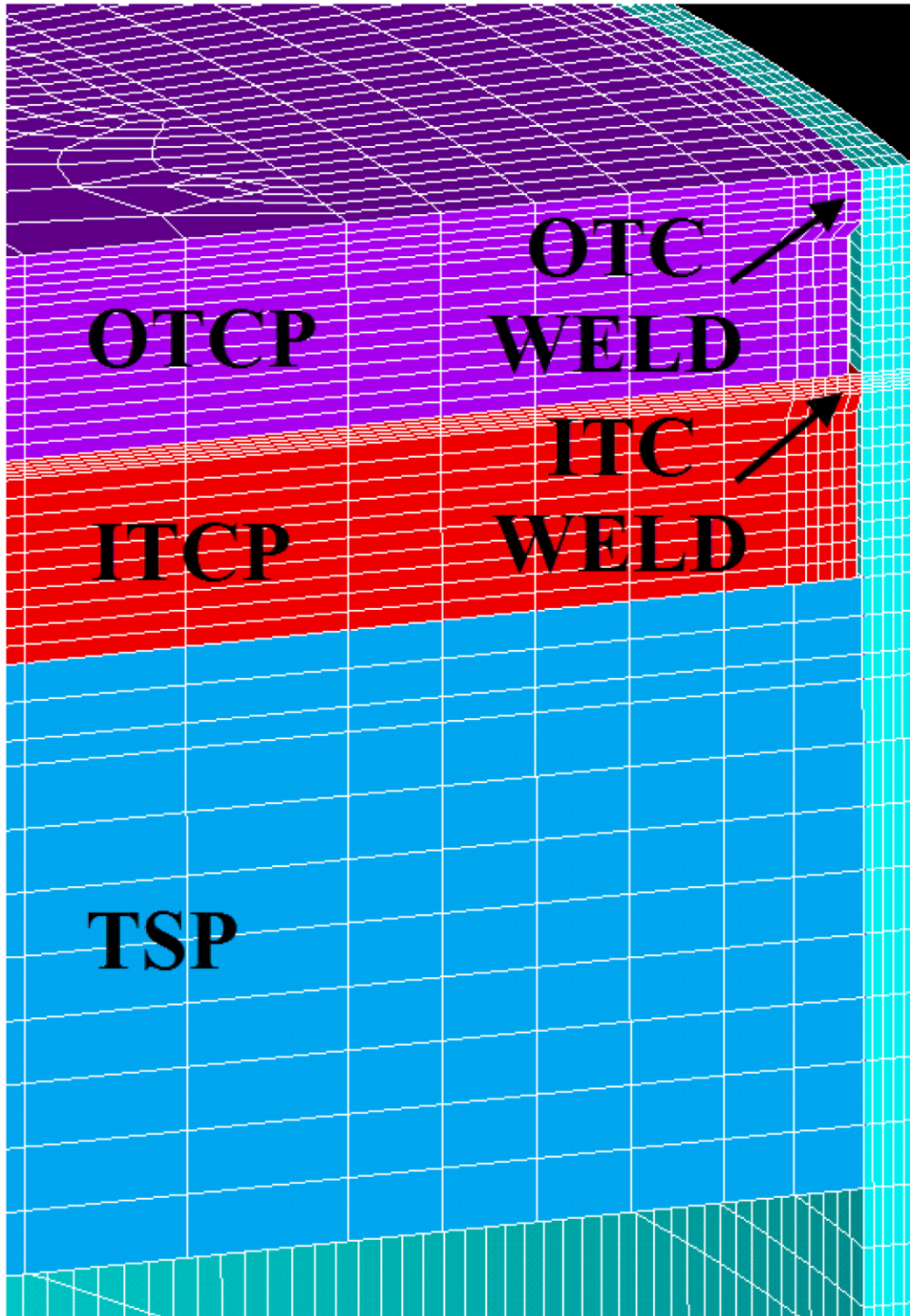


Figure 3.9.1-2
DSC FEM-Top End

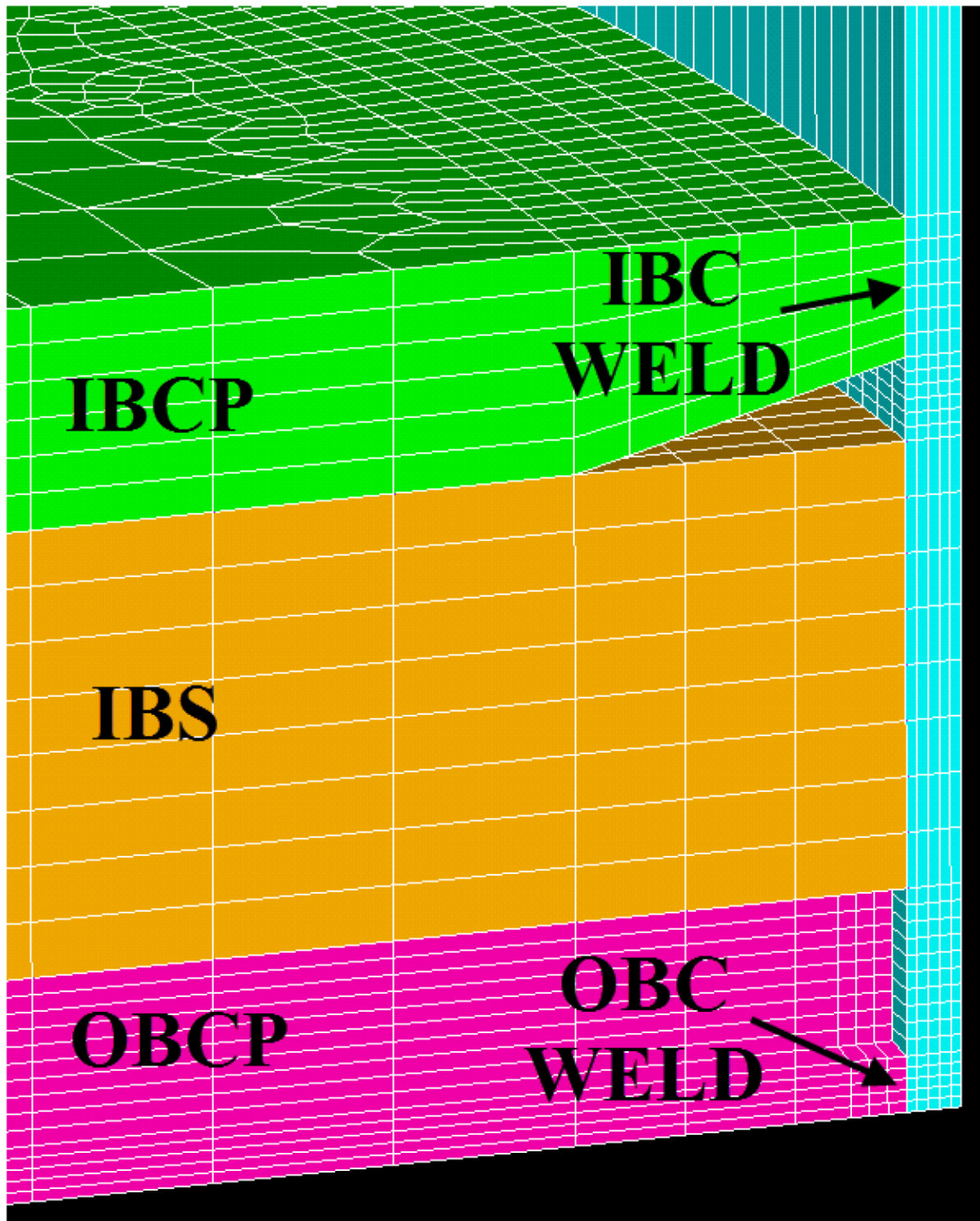


Figure 3.9.1-3
DSC FEM-Bottom End

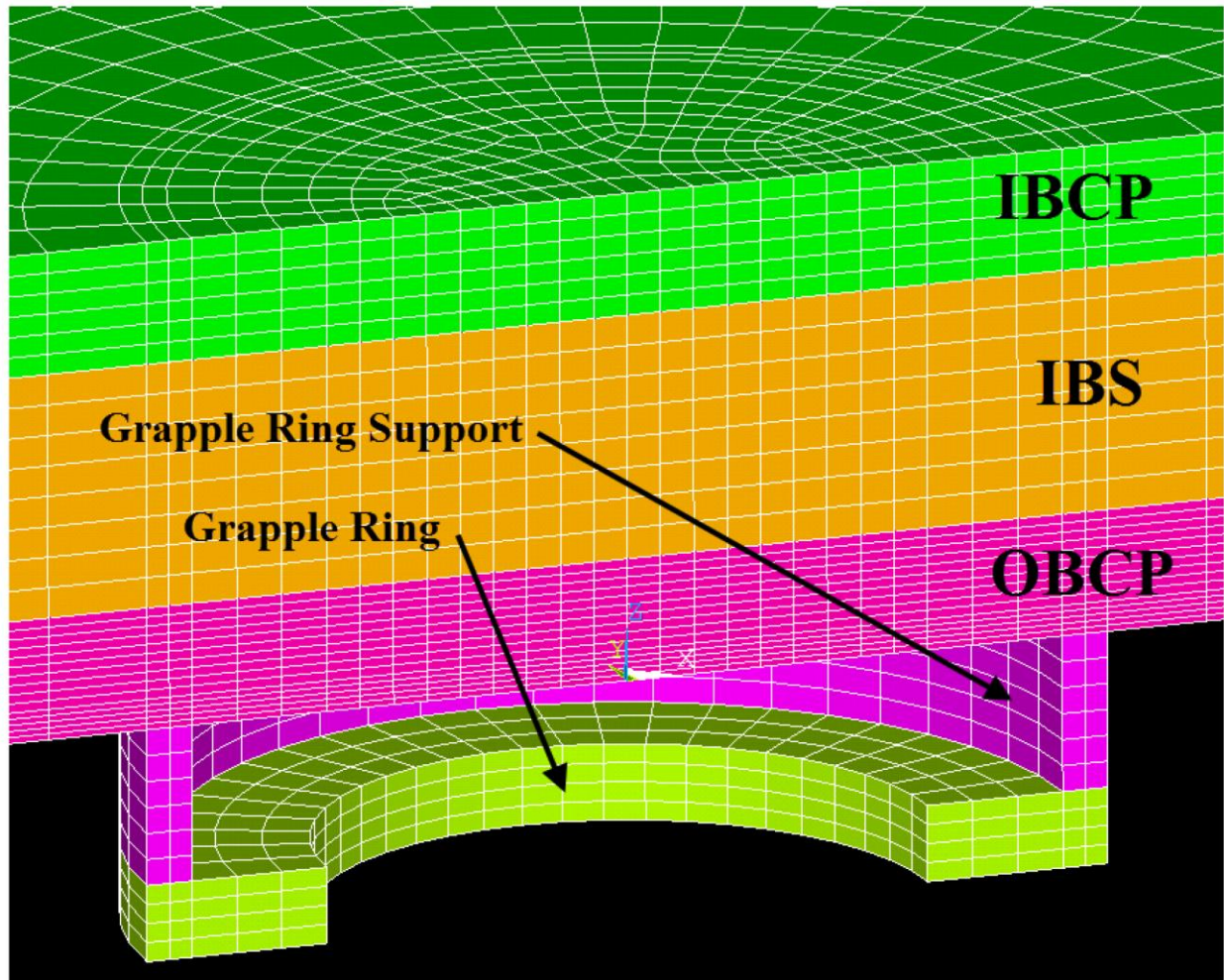


Figure 3.9.1-4
Mesh detail – Grapple Assembly

Figure 3.9.1-5
Not Used

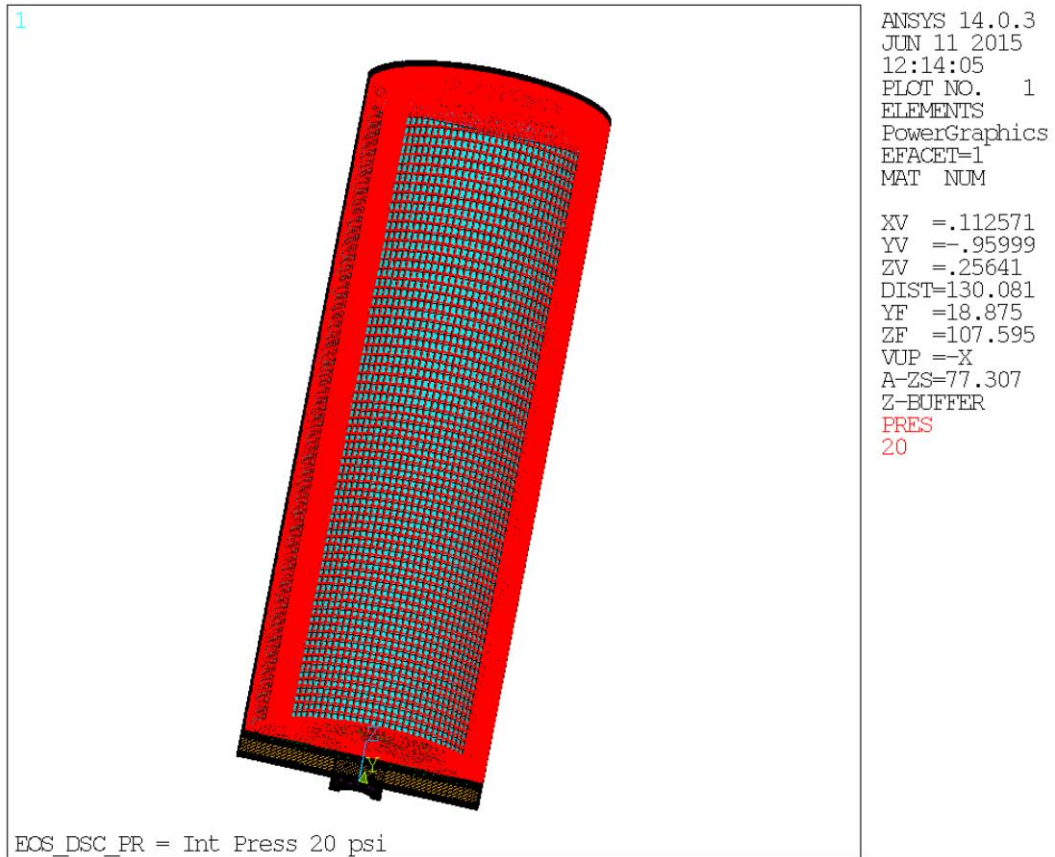


Figure 3.9.1-6
Internal Pressure – Load Application

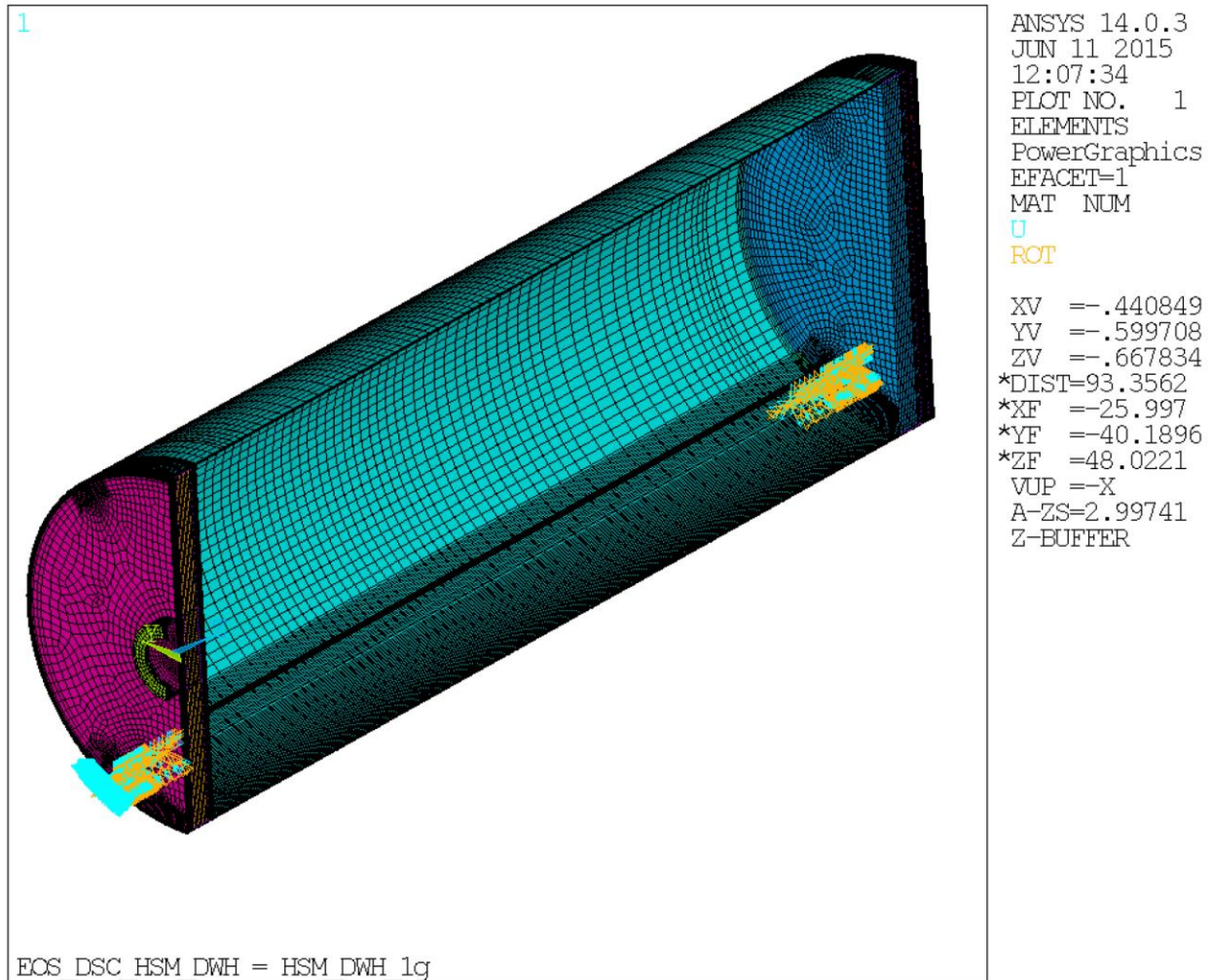


Figure 3.9.1-7
Dead Weight Simulation in EOS-HSM – Boundary Conditions

Note: Symmetry boundary conditions not shown for clarity.

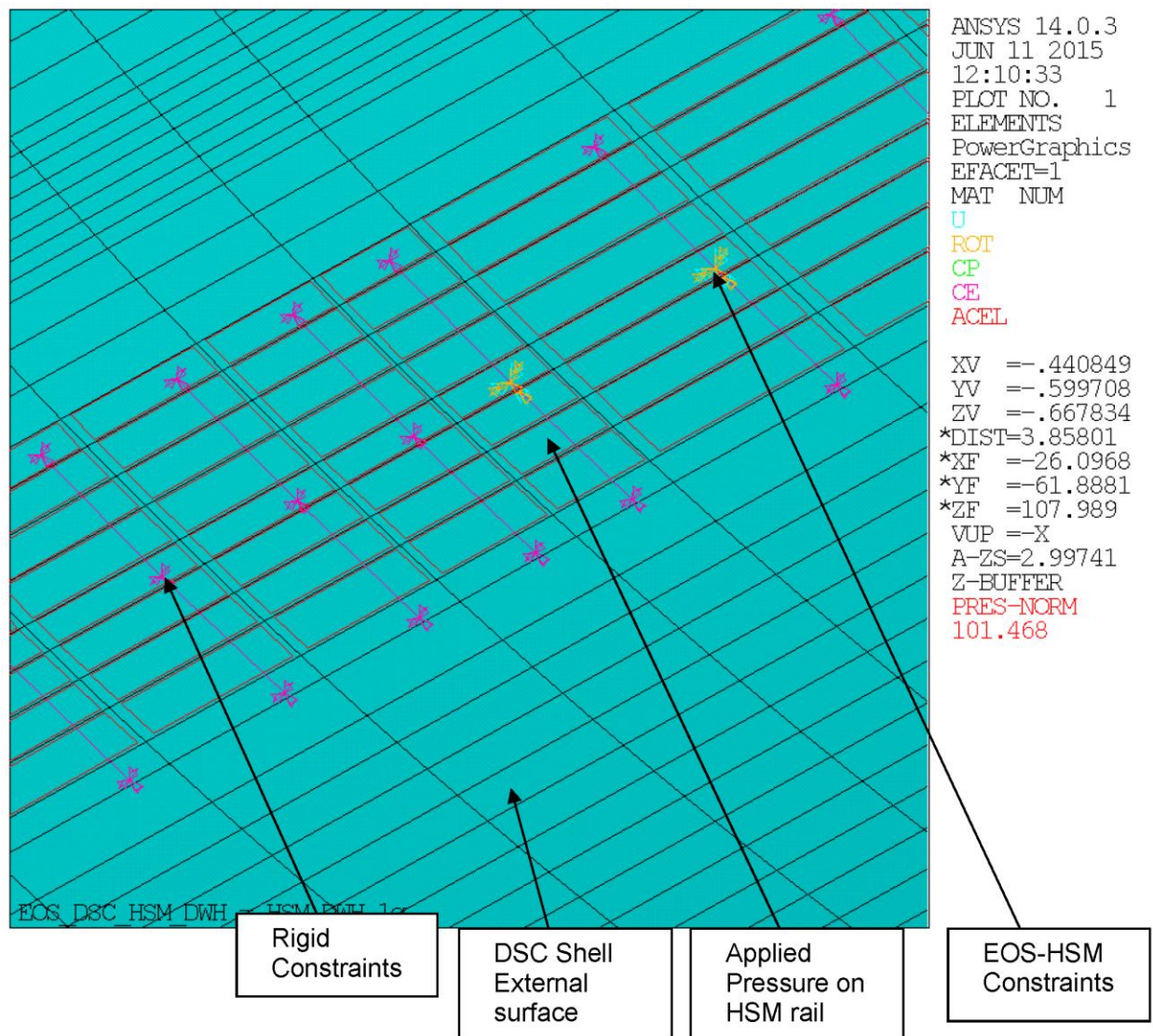


Figure 3.9.1-7a
Dead Weight Simulation in EOS-HSM Detail

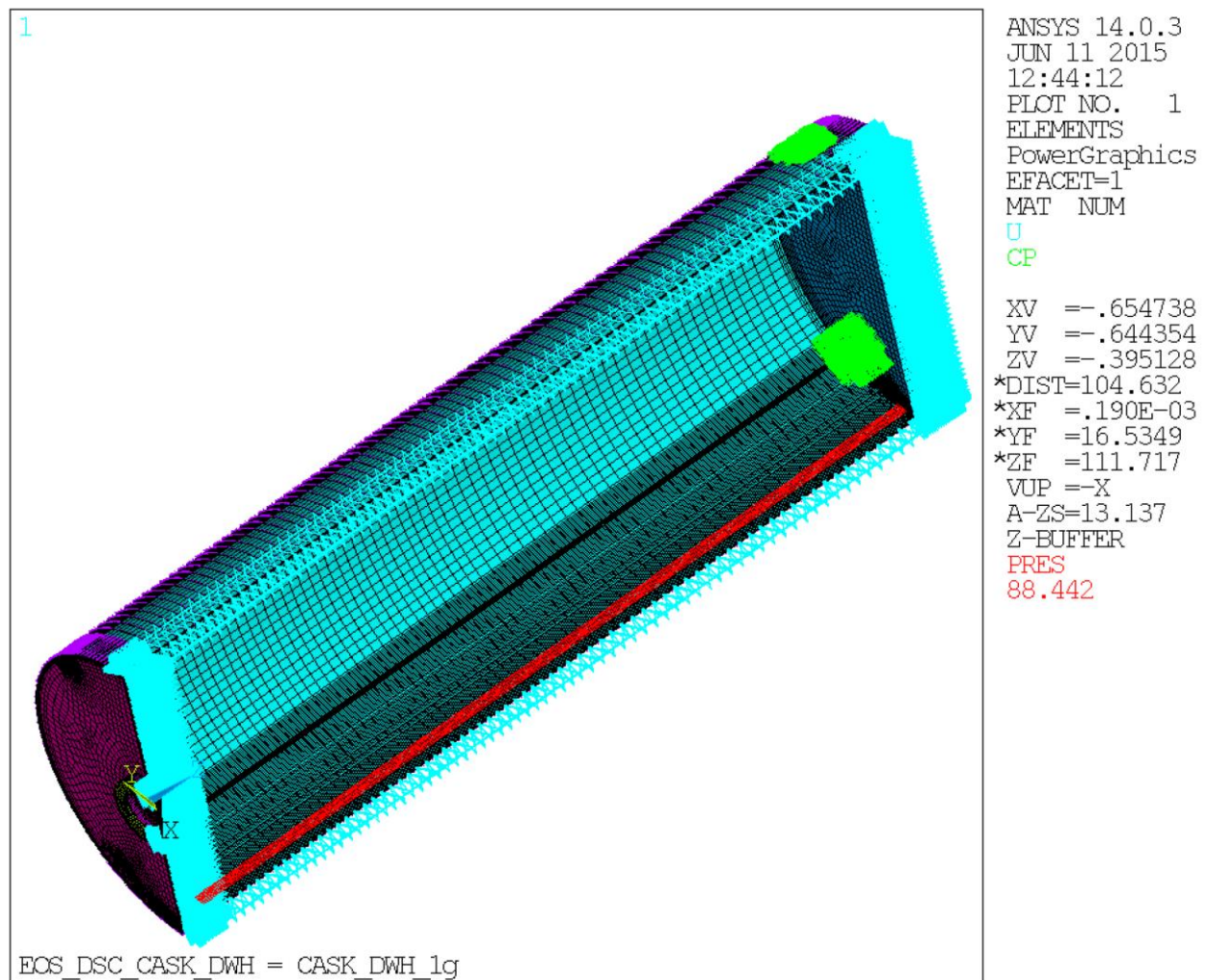


Figure 3.9.1-8
Dead Weight Simulation in EOS-TC

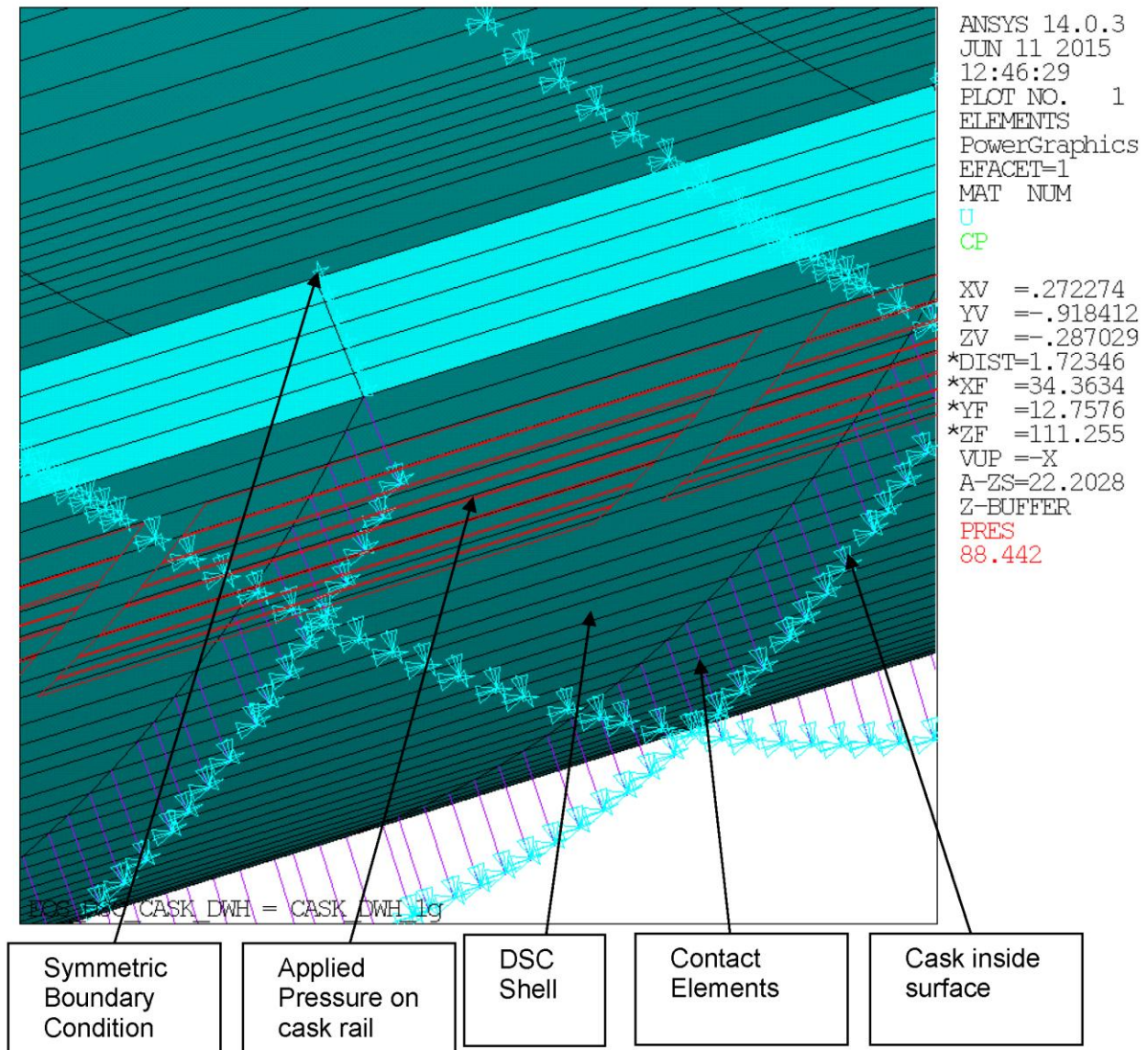


Figure 3.9.1-8a
Dead Weight Simulation in Cask Detail

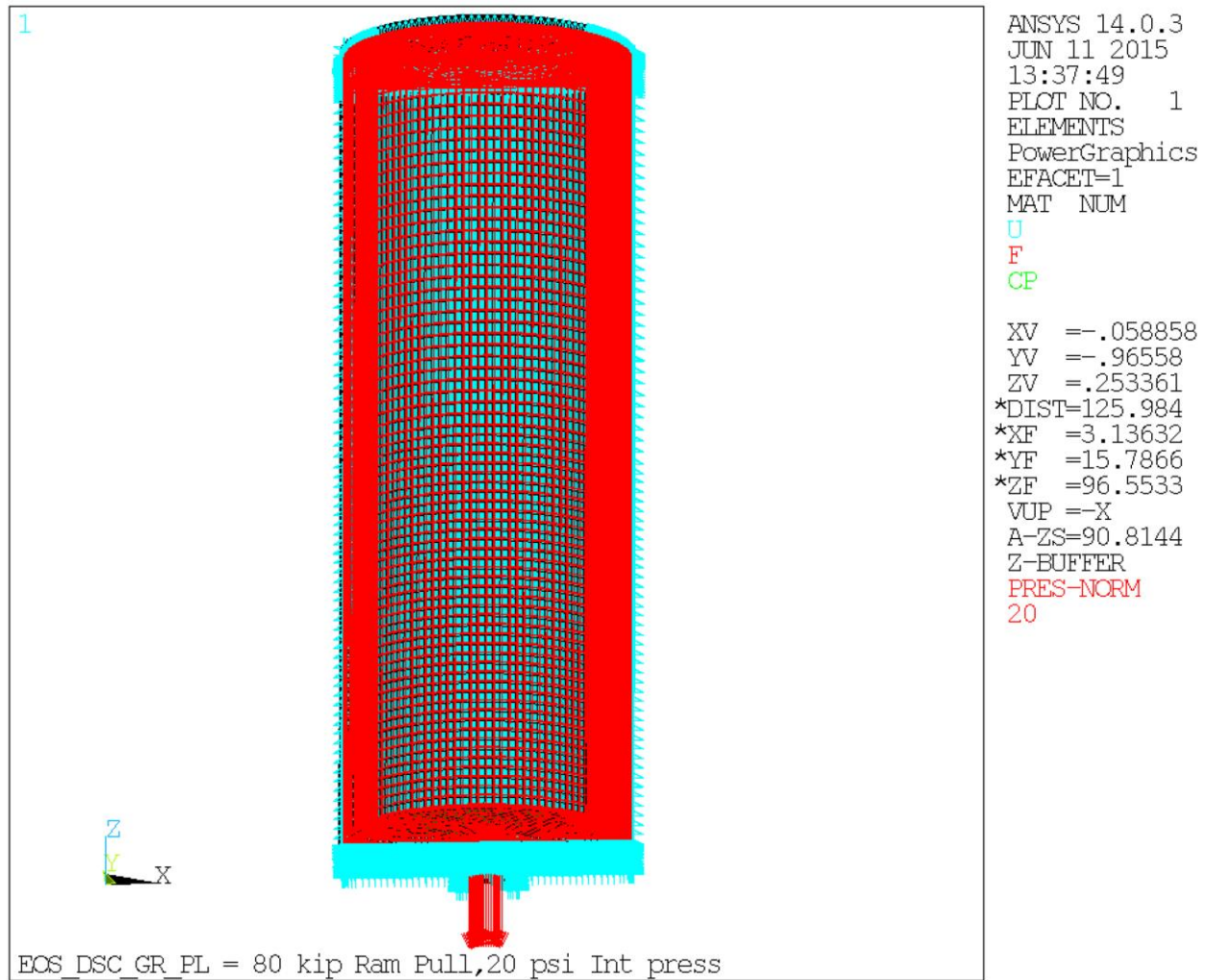


Figure 3.9.1-9
Pull Load with Internal Pressure

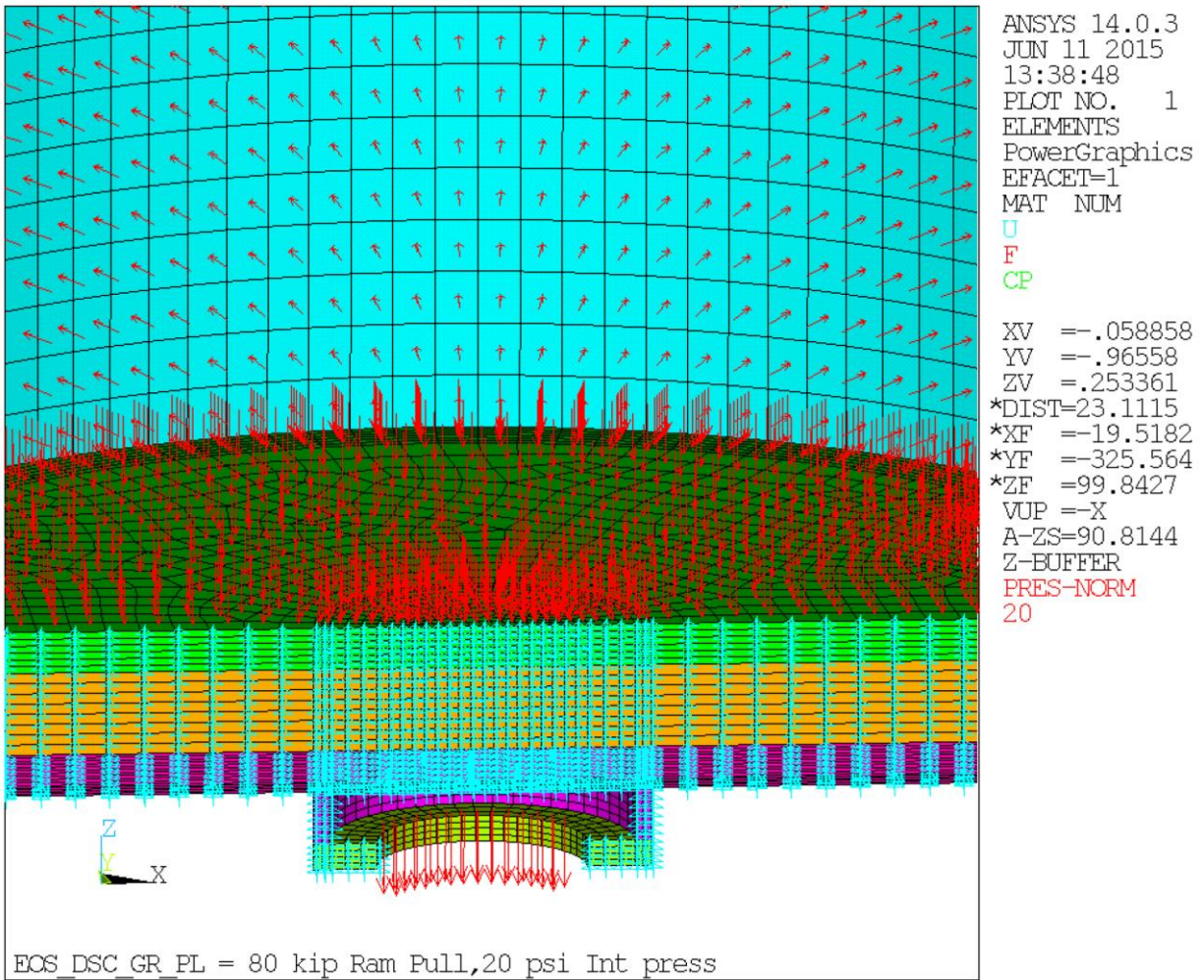


Figure 3.9.1-9a
Pull Load with Internal Pressure Detail

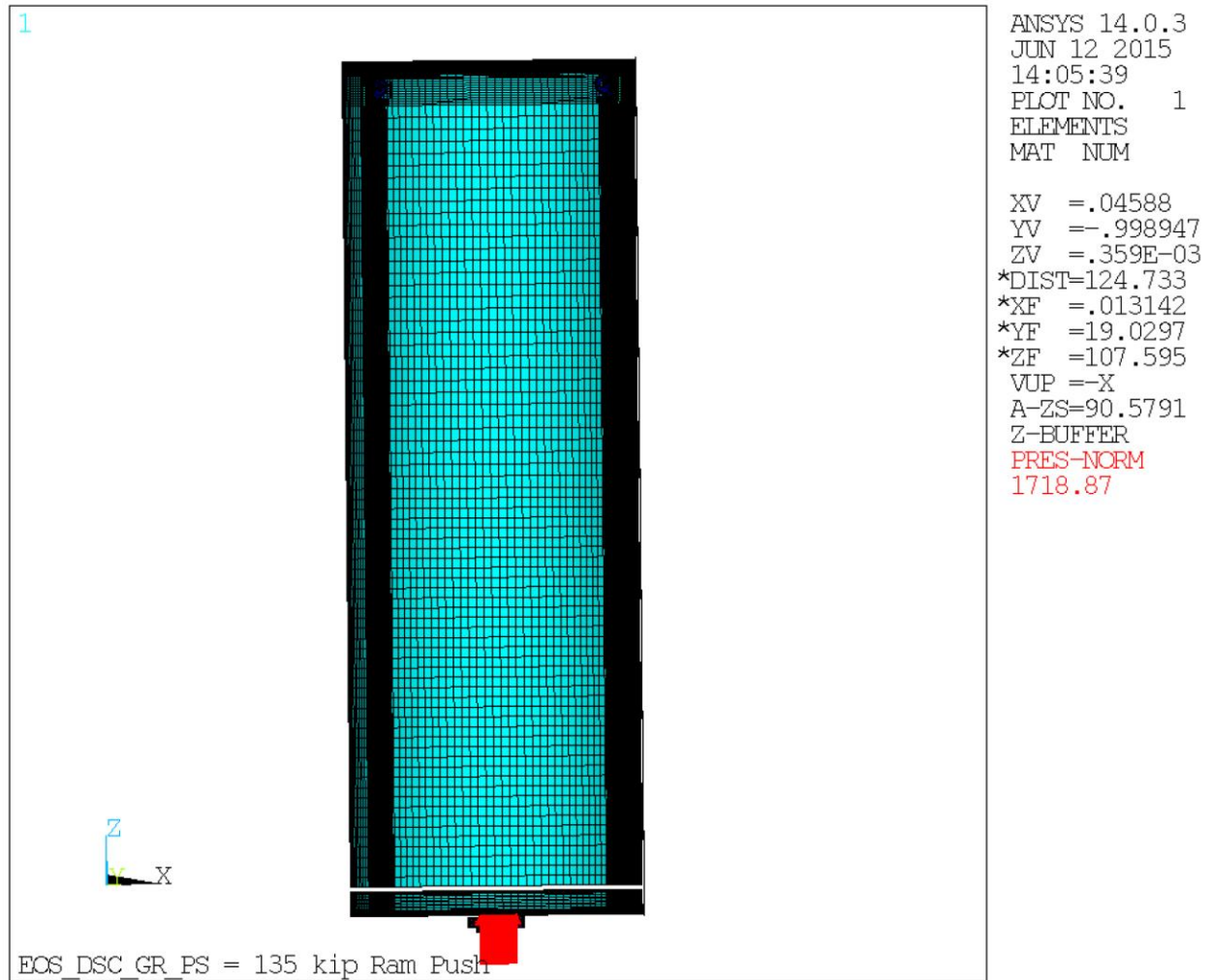


Figure 3.9.1-10
Push Load with Internal Pressure

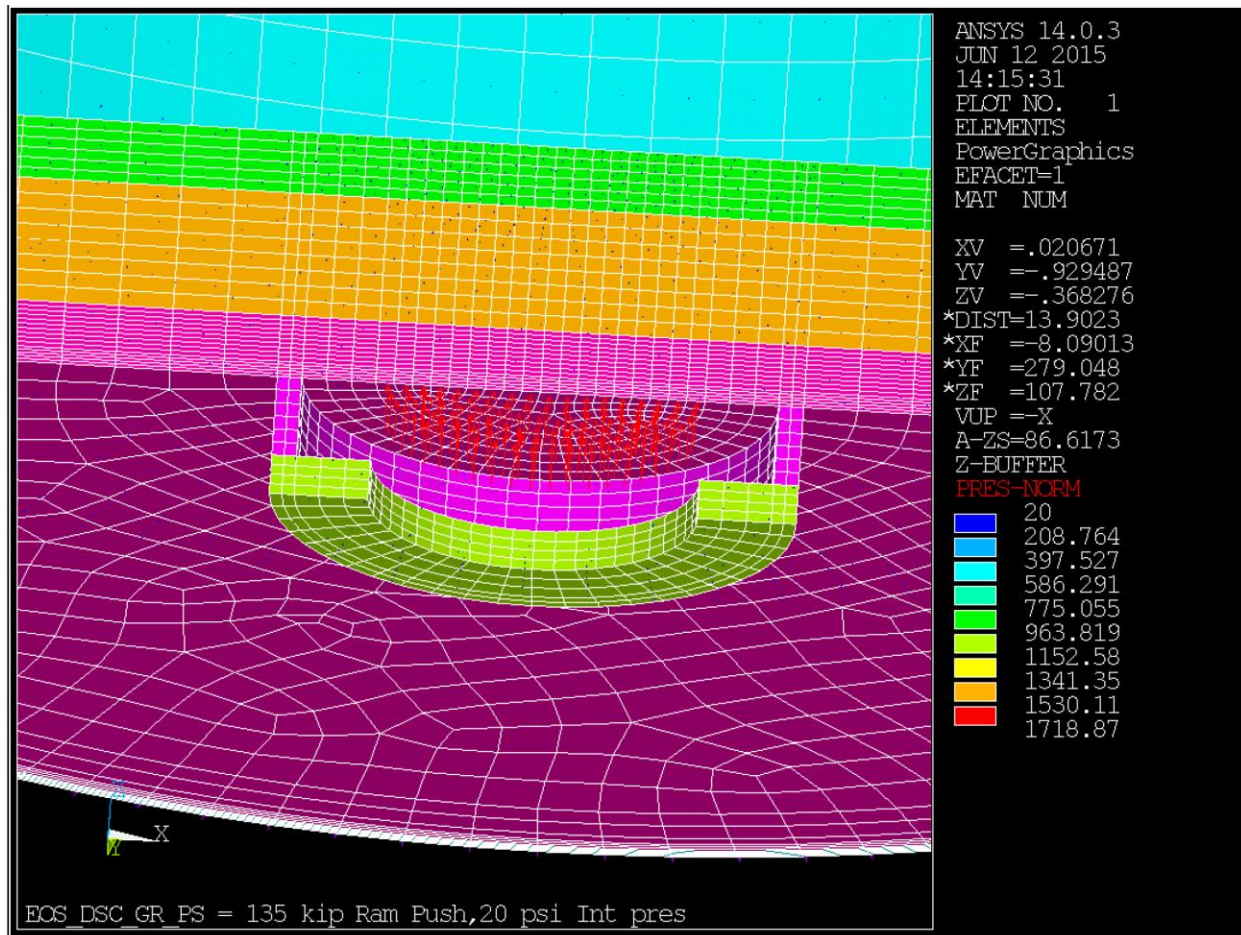


Figure 3.9.1-10a
Push Load with Internal Pressure Detail

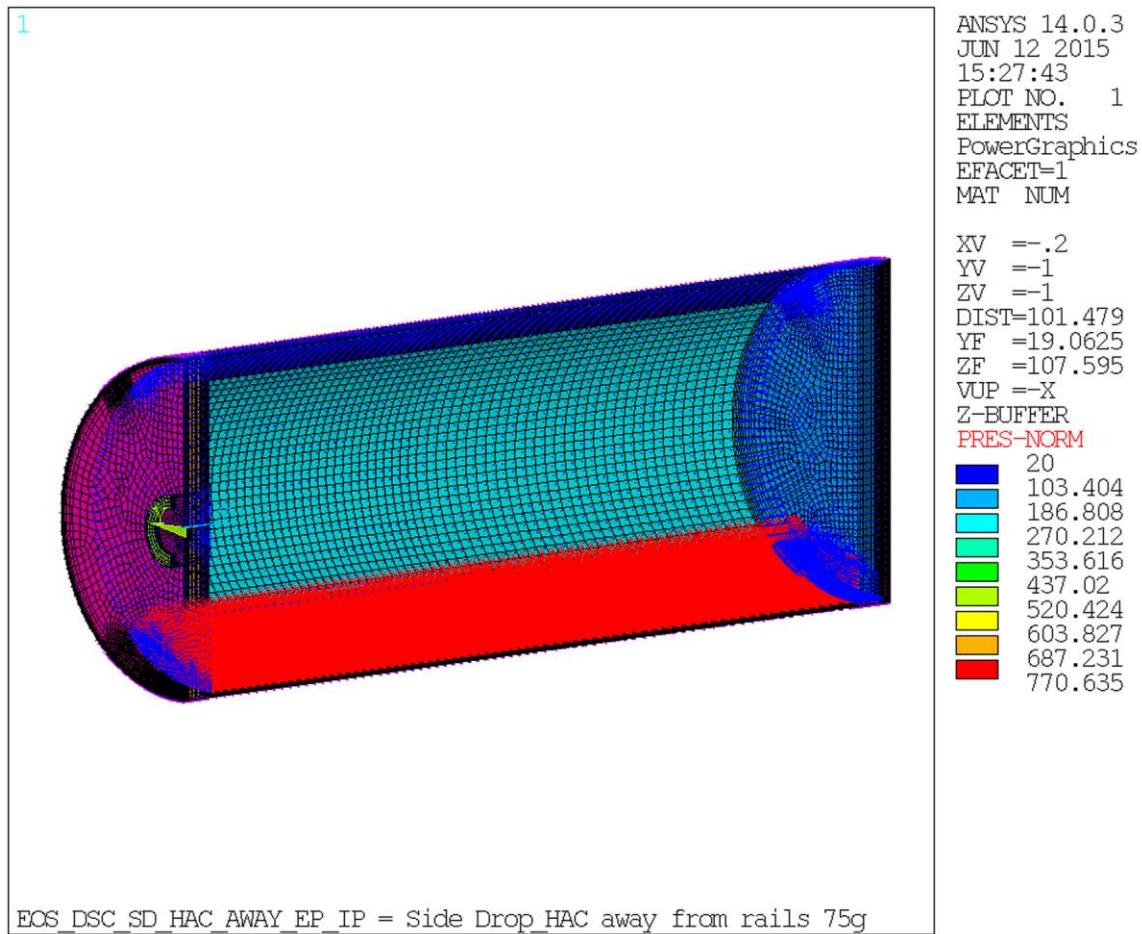


Figure 3.9.1-11
Side Drop away from Cask Rail

Note: Internal pressure of 20 psi is applied within the pressure boundary. The magnitude of internal pressure is very small compared to canister internals' uniform pressure load and therefore is not noticeable.

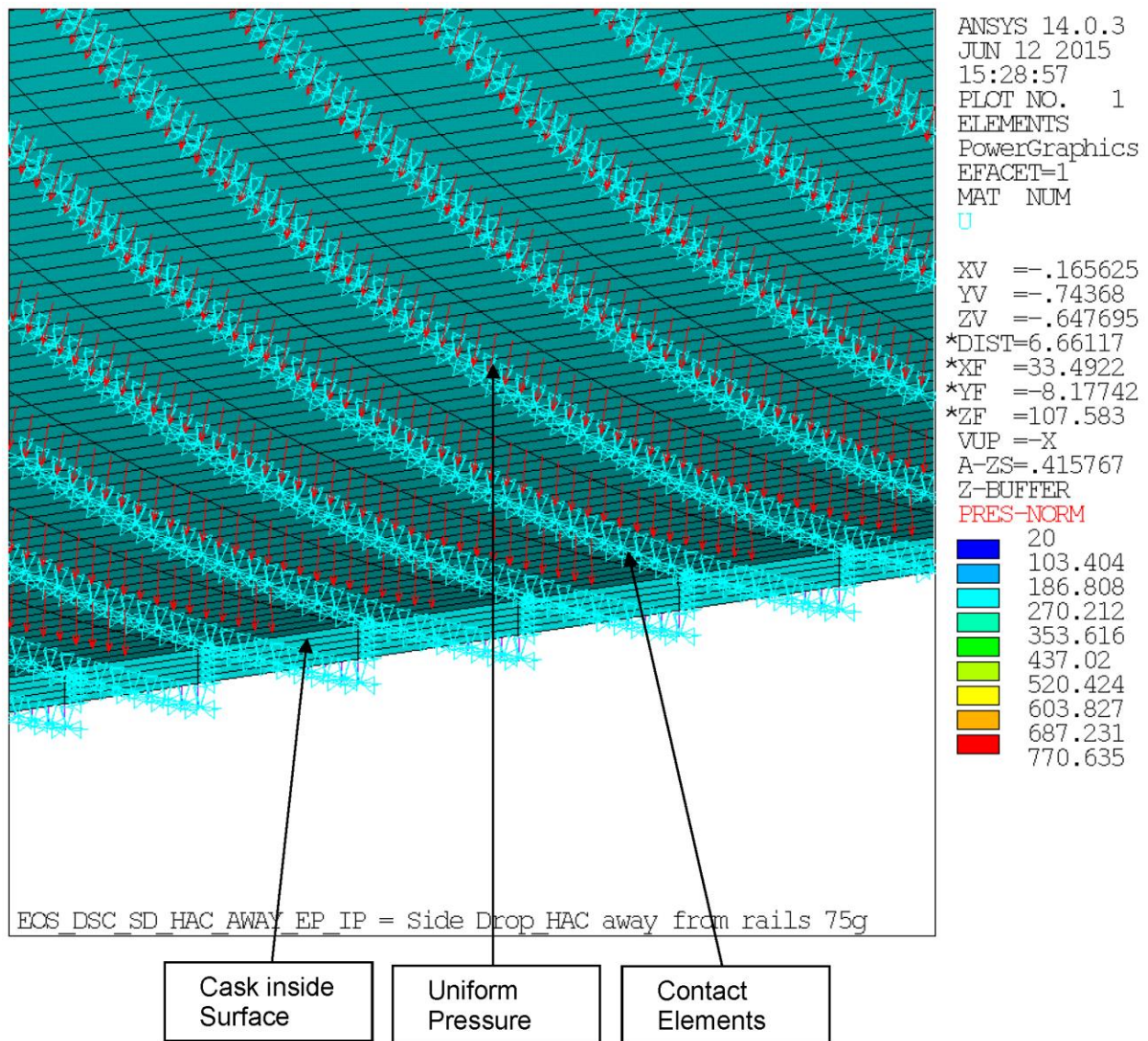


Figure 3.9.1-11a
Side Drop away from Cask Rail– Boundary Condition Details

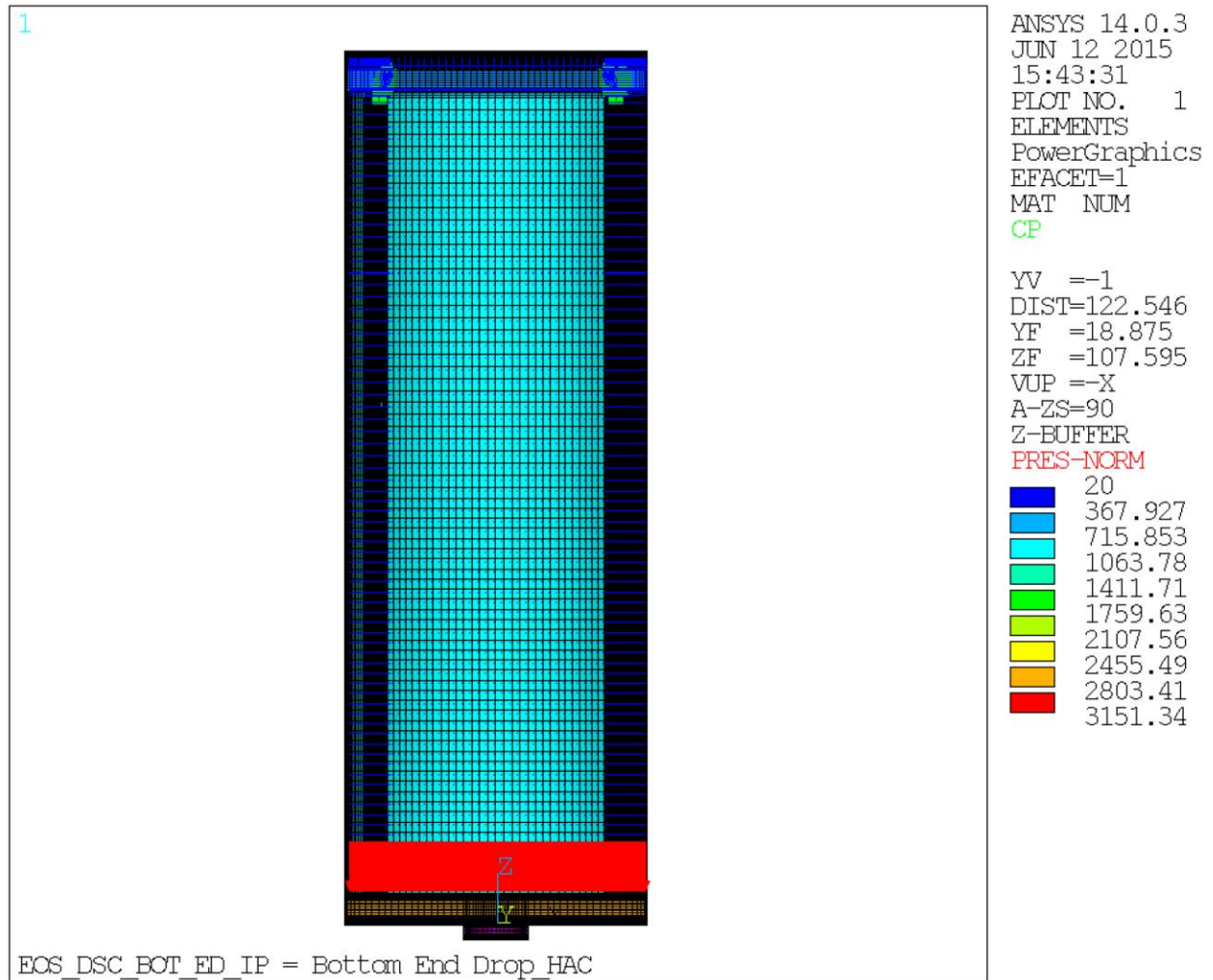


Figure 3.9.1-12
Bottom End Drop Simulation

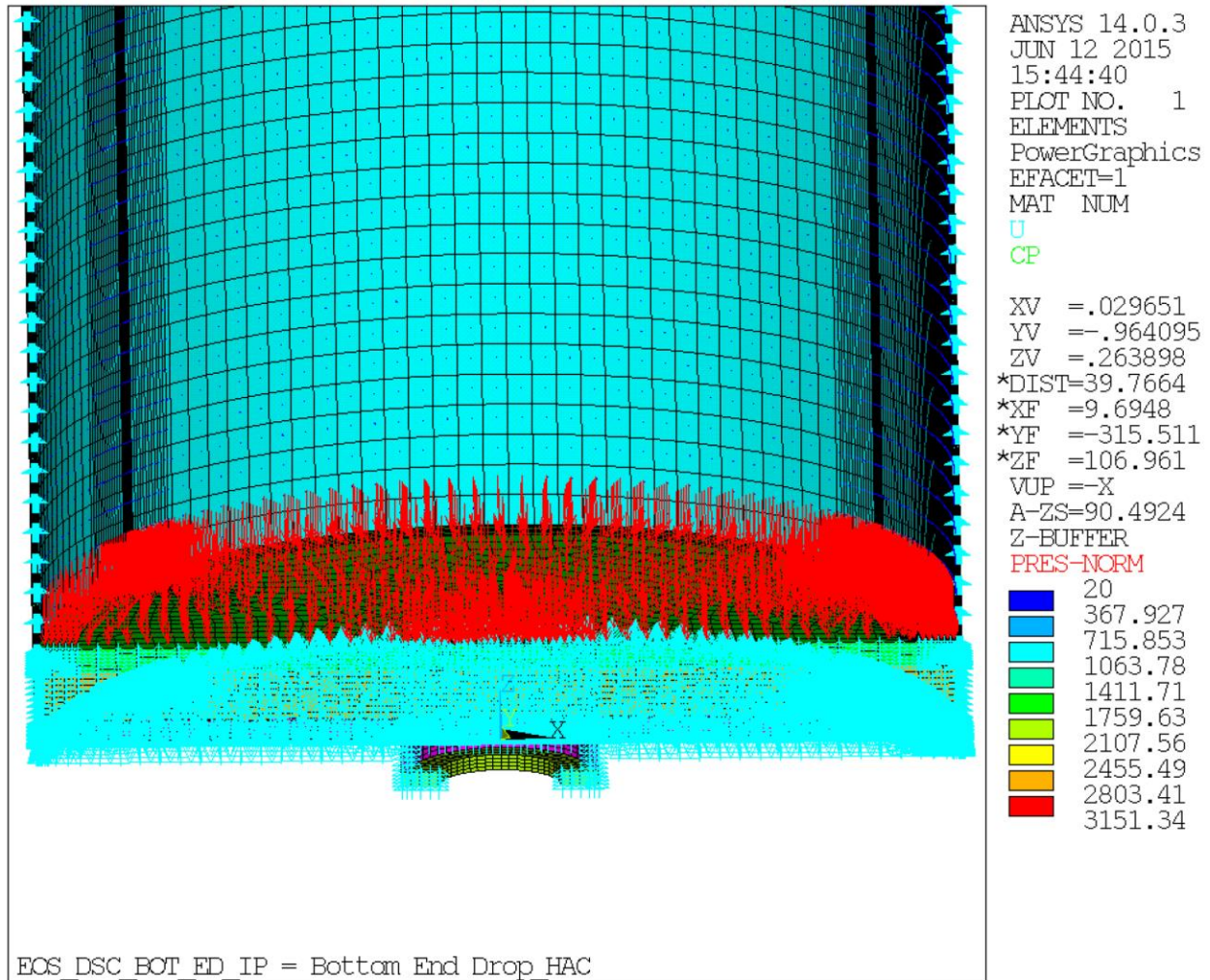


Figure 3.9.1-12a
Bottom End Drop Simulation Detail

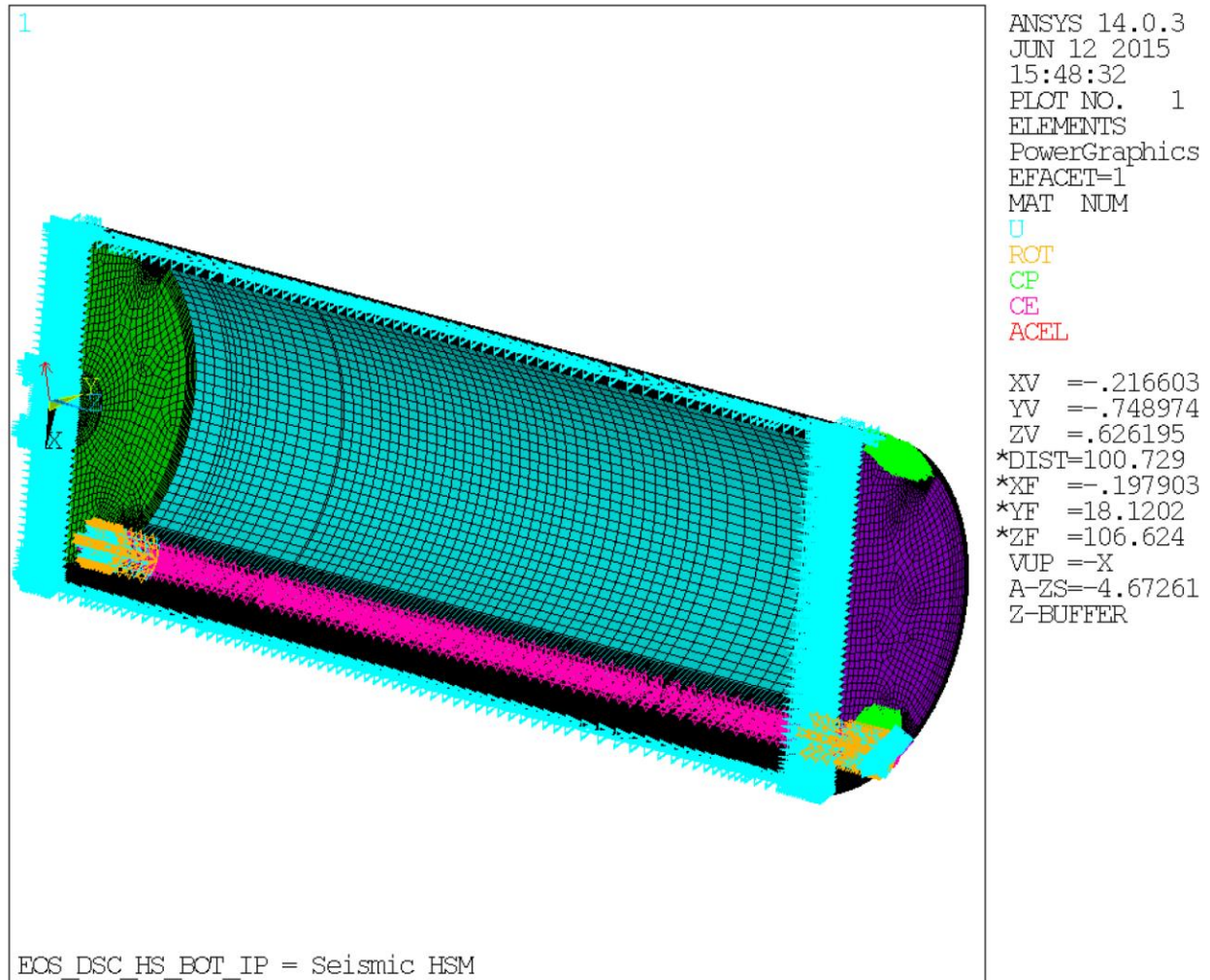


Figure 3.9.1-13
Seismic in EOS-HSM Simulation

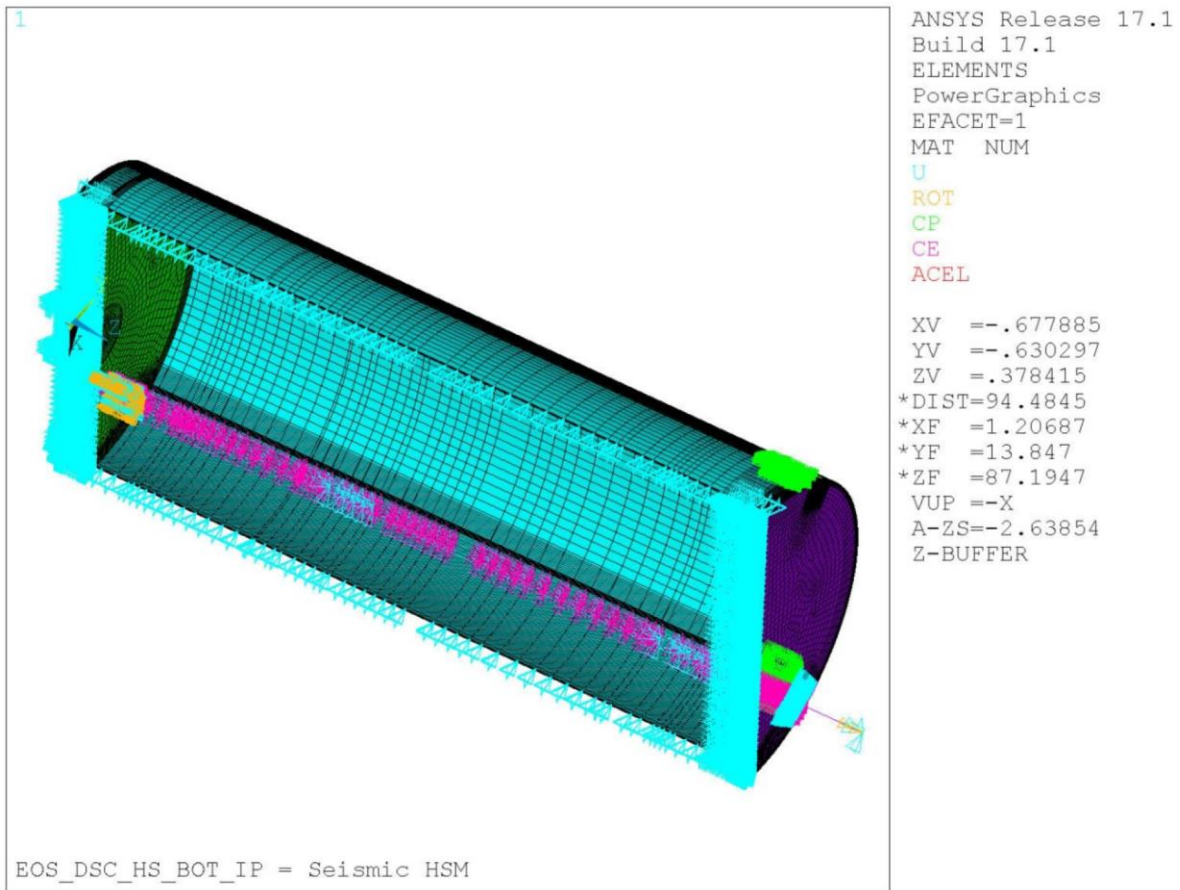


Figure 3.9.1-13a
High Seismic in EOS-HSM-FPS Simulation

Proprietary Information on Pages 3.9.1- 98 through 3.9.1- 100
Withheld Pursuant to 10 CFR 2.390

Figure 3.9.1-17
Not Used

Proprietary Information on Pages 3.9.1- 102 and 3.9.1- 103
Withheld Pursuant to 10 CFR 2.390

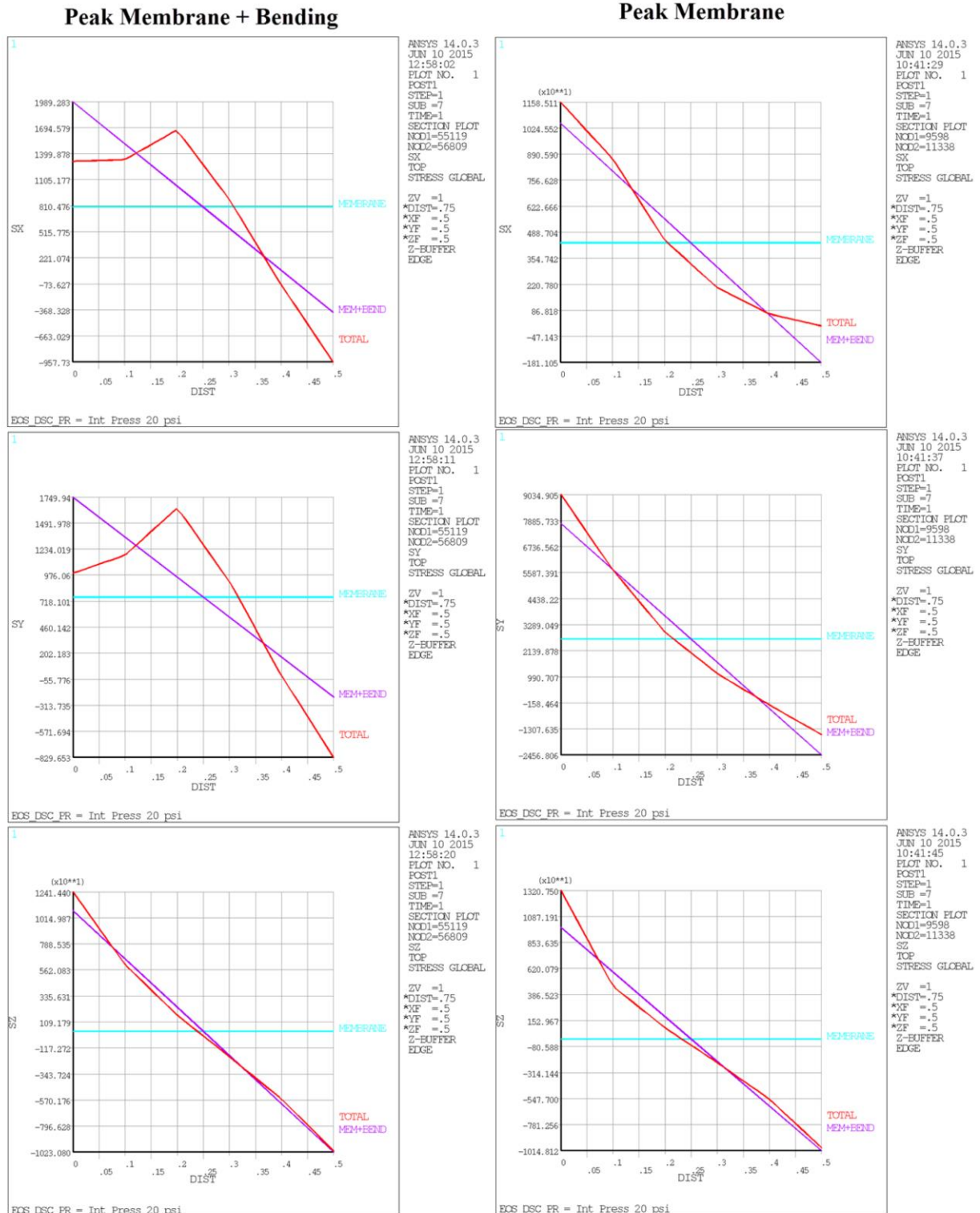


Figure 3.9.1-20
Maximum Linearized Component Stresses for Internal Pressure (Normal)
Load Case

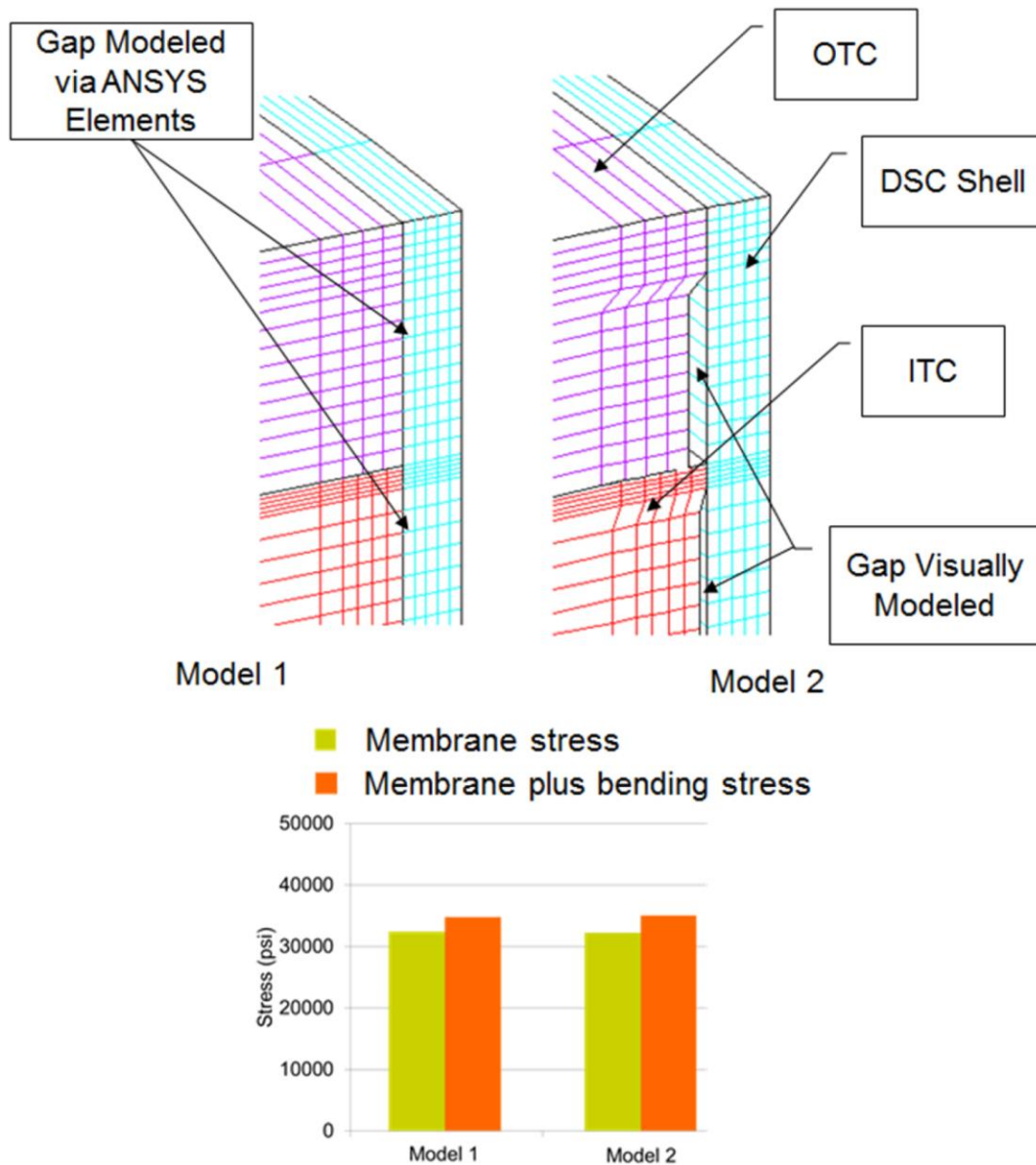


Figure 3.9.1-21
Mesh Sensitivity Study 01 – Models and ITCP Weld Stresses

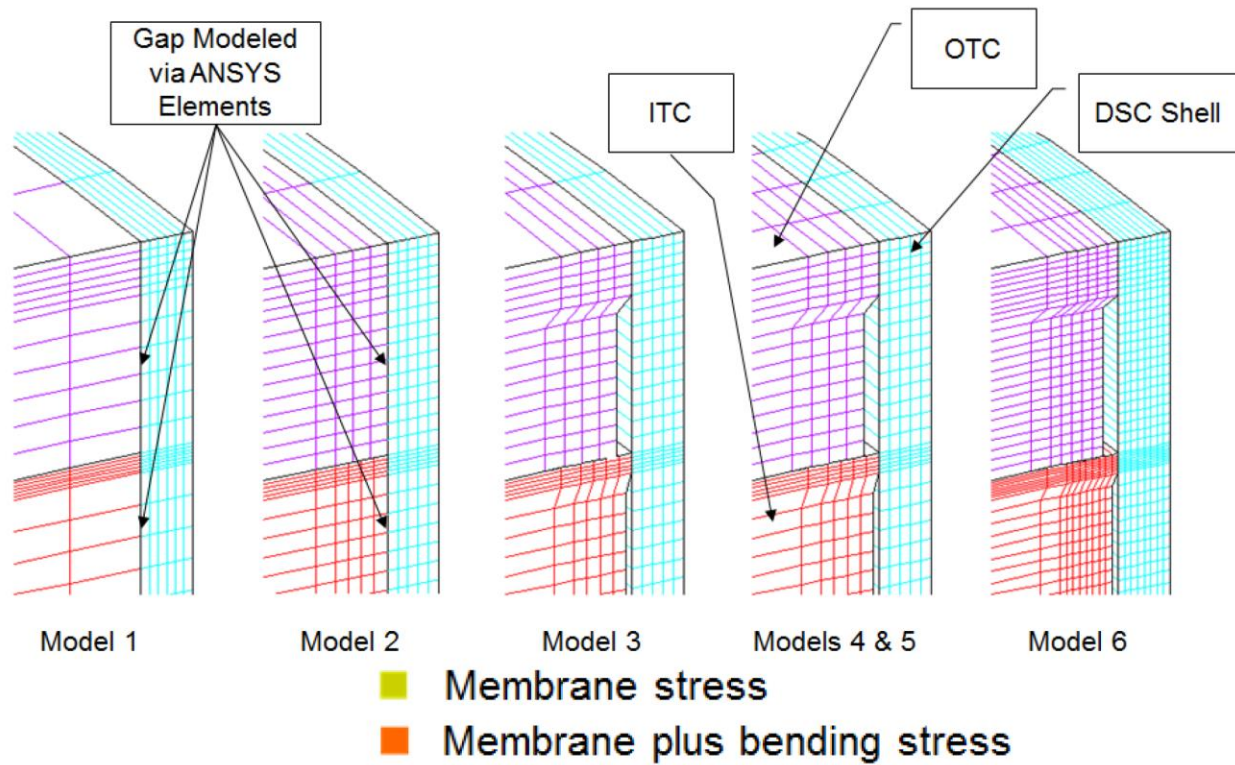


Figure 3.9.1-22
Mesh Sensitivity Study 02 – Models and ITCP Weld Stresses

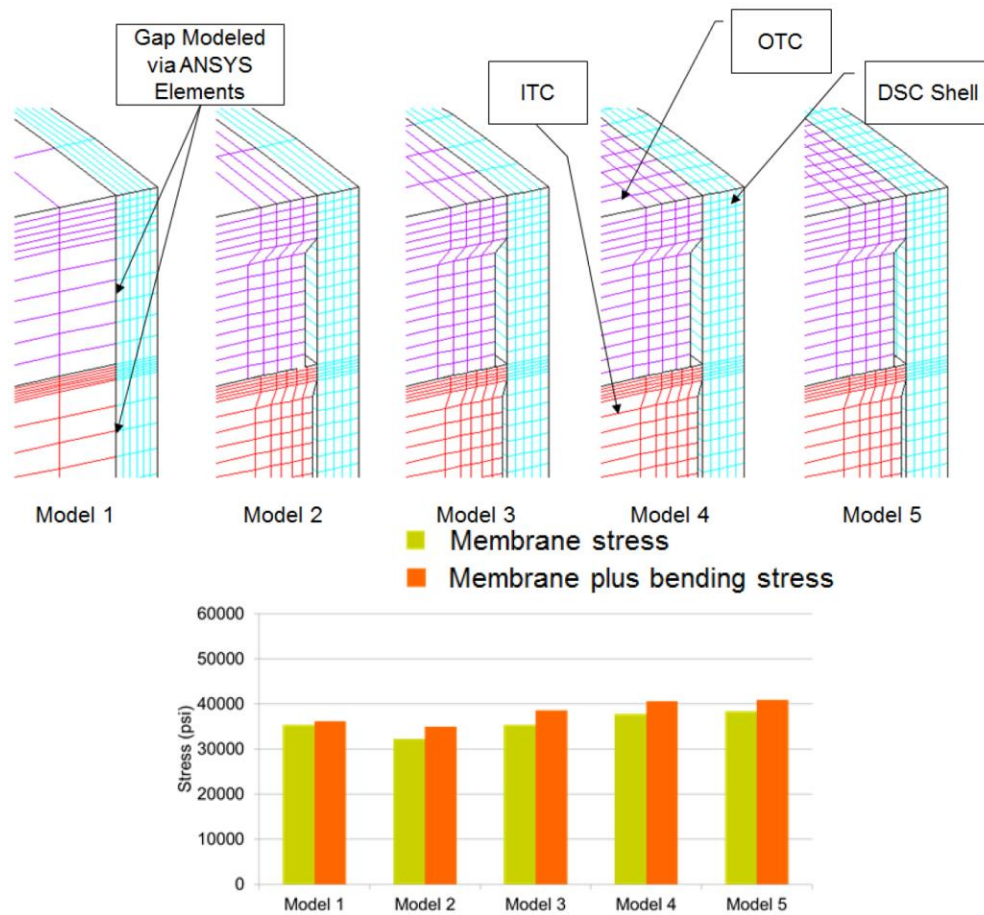


Figure 3.9.1-23
Mesh Sensitivity Study 03 – Models and ITCP Weld Stresses

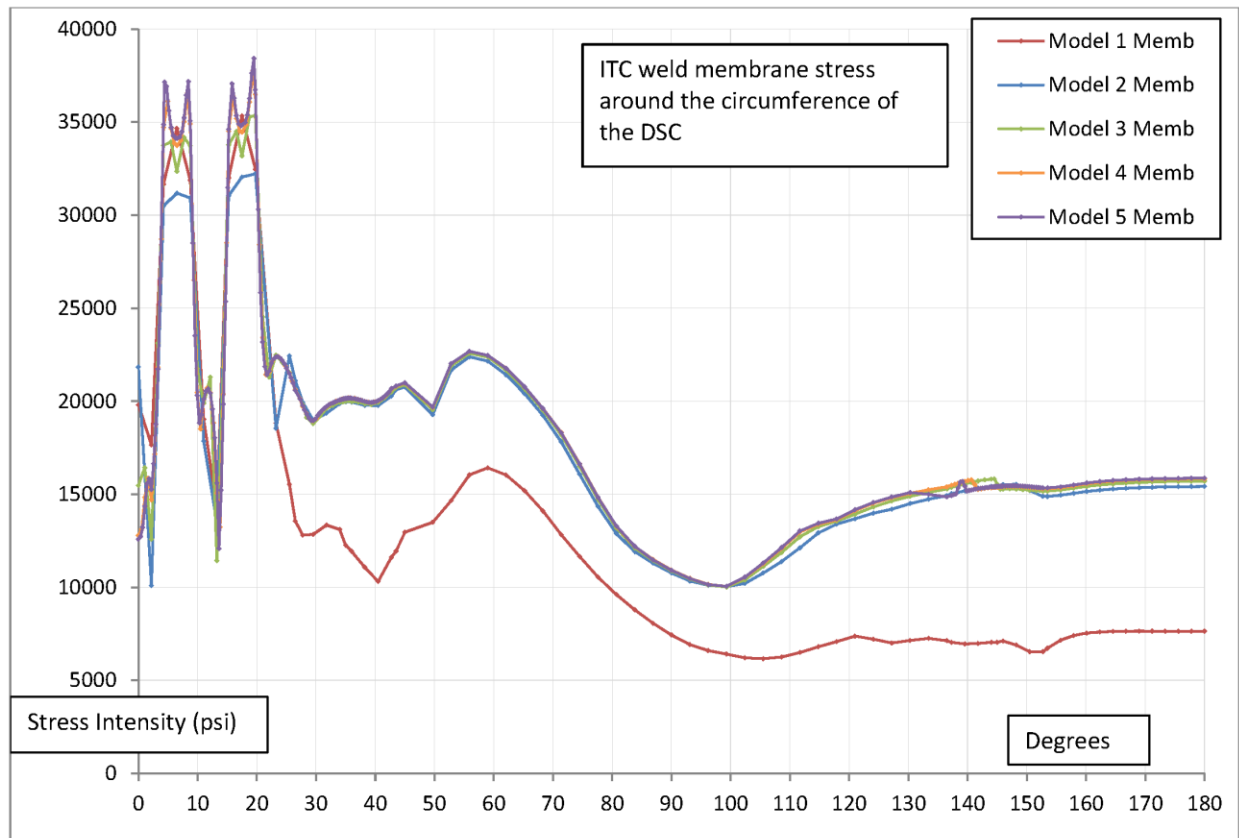


Figure 3.9.1-23a
Membrane Stresses around the Circumference within the ITCP Weld

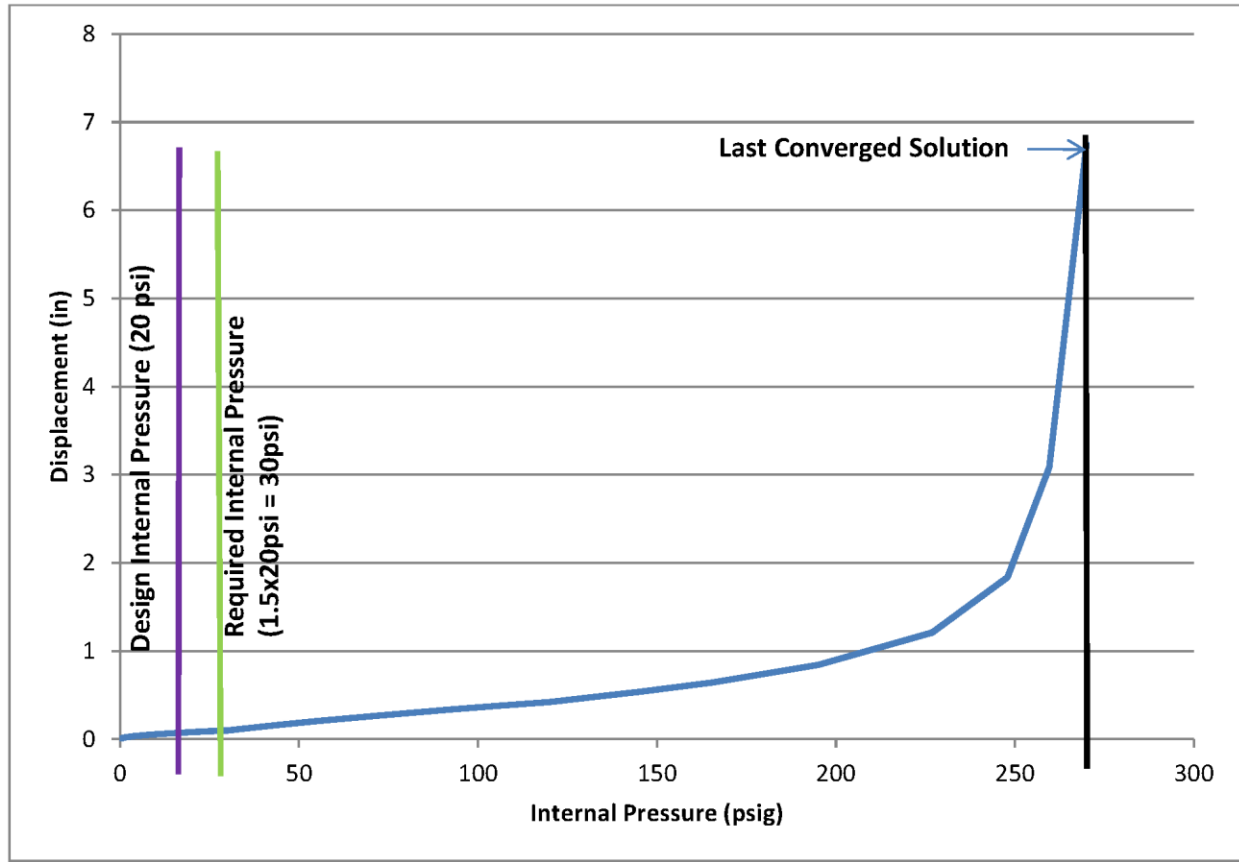


Figure 3.9.1-24
Limit Load – Load vs. Deflection – Internal Pressure

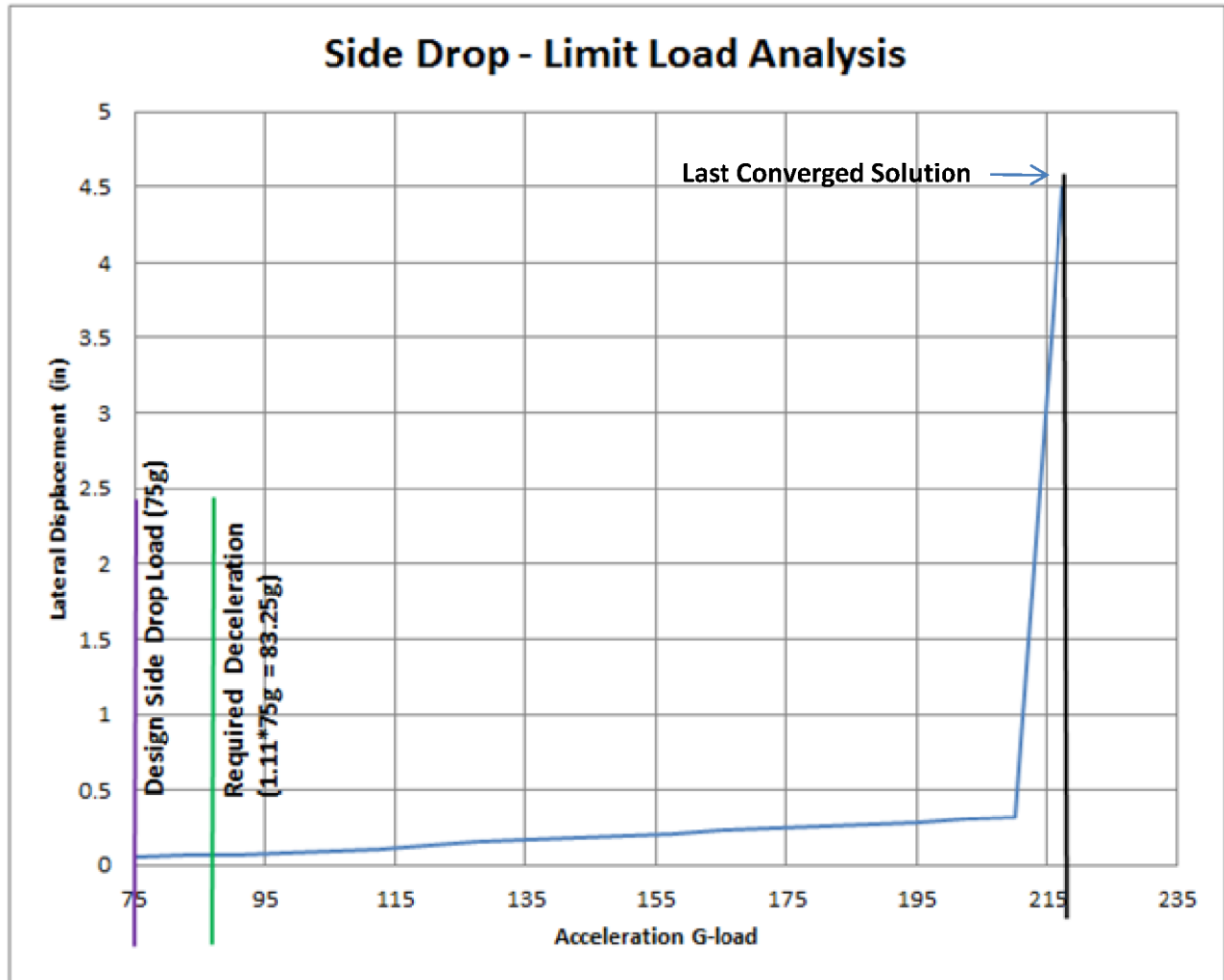
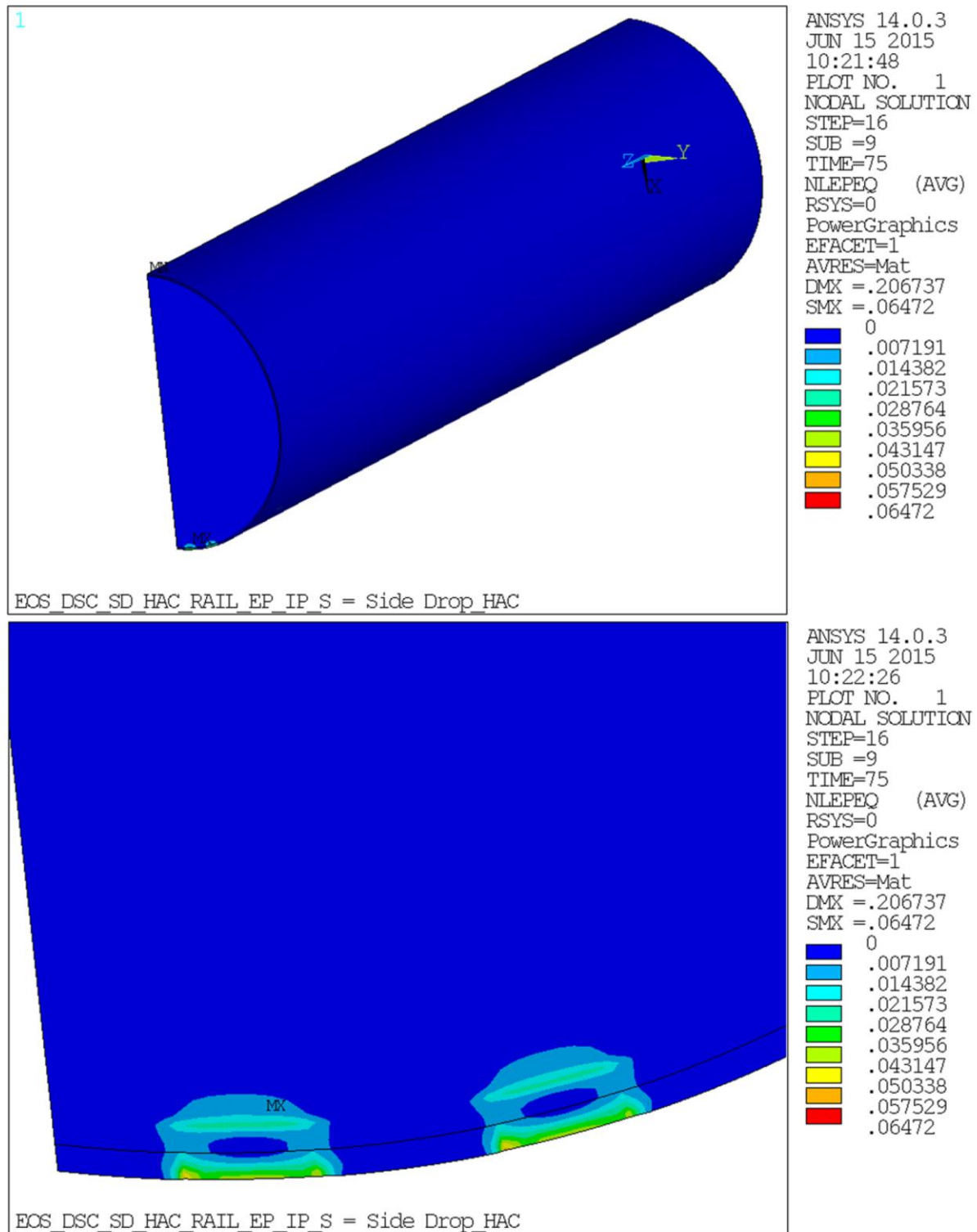


Figure 3.9.1-25
Limit Load – Load vs. Deflection – Side Drop Acceleration



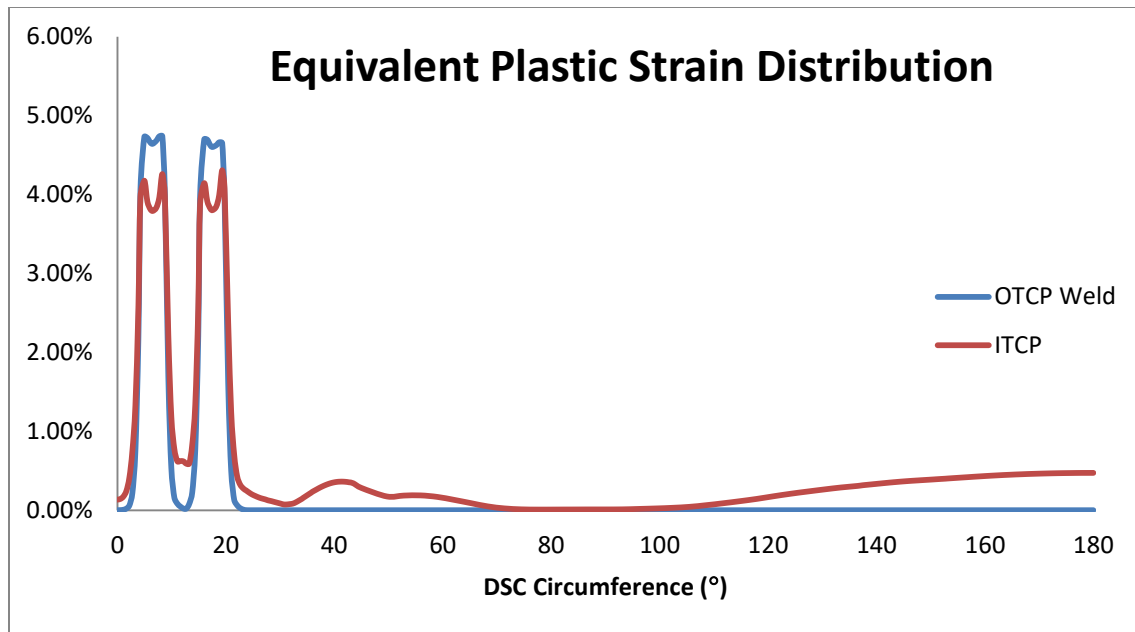


Figure 3.9.1-27
OTCP and ITCP Confinement Weld Equivalent Plastic Strain Distribution
for Strain Criteria Analysis

APPENDIX 3.9.2 EOS-37PTH AND EOS-89BTH BASKET STRUCTURAL ANALYSIS

Table of Contents

3.9.2 EOS-37PTH AND EOS-89BTH BASKET STRUCTURAL ANALYSIS	3.9.2-1
3.9.2.1 EOS-37PTH Basket Structural Evaluation for Normal/Off-Normal Loads.....	3.9.2-1
3.9.2.2 EOS-89BTH Basket Structural Evaluation for Normal/Off-Normal Loads.....	3.9.2-9
3.9.2.3 EOS-37PTH Basket Structural Evaluation for On-Site Accident Drop Loads.....	3.9.2-14
3.9.2.4 EOS-89BTH Basket Structural Evaluation for On-Site Accident Drop Loads.....	3.9.2-23
3.9.2.5 References	3.9.2-30

List of Tables

<i>Table 3.9.2-1</i>	<i>Threaded Fastener Stress Design Criteria (Normal / Off-Normal)</i>	<i>3.9.2-32</i>
<i>Table 3.9.2-2</i>	<i>Component Allowable Stresses (Normal / Off-Normal)</i>	<i>3.9.2-33</i>
<i>Table 3.9.2-3</i>	<i>EOS-37PTH Basket Stress Summary – Enveloped DW + Handling + Thermal</i>	<i>3.9.2-34</i>
<i>Table 3.9.2-4</i>	<i>EOS-89BTH Basket Stress Summary – Enveloped DW + Handling + Thermal</i>	<i>3.9.2-35</i>
<i>Table 3.9.2-5</i>	<i>Basket Grid Plate Accident Drop Strain Design Criteria</i>	<i>3.9.2-36</i>
<i>Table 3.9.2-6</i>	<i>EOS-37PTH Basket Grid Plate Strain Summary – Side Drops with and without Bolts and Tie Rods</i>	<i>3.9.2-37</i>
<i>Table 3.9.2-7</i>	<i>EOS-37PTH Basket Grid Plate Strain Summary – Enveloped Accident Conditions</i>	<i>3.9.2-38</i>
<i>Table 3.9.2-8</i>	<i>EOS-37PTH Basket Buckling Analysis Results Summary</i>	<i>3.9.2-39</i>
<i>Table 3.9.2-9</i>	<i>EOS-37PTH Basket Maximum Adjacent Fuel Compartment Relative Displacements</i>	<i>3.9.2-40</i>
<i>Table 3.9.2-10</i>	<i>EOS-89BTH Basket Grid Plate Strain Summary – Side Drops with and without Bolts and Tie Rods</i>	<i>3.9.2-41</i>
<i>Table 3.9.2-11</i>	<i>EOS-89BTH Basket Grid Plate Strain Summary – Enveloped Accident Conditions</i>	<i>3.9.2-42</i>
<i>Table 3.9.2-12</i>	<i>EOS-89BTH Basket Buckling Analysis Results Summary</i>	<i>3.9.2-43</i>
<i>Table 3.9.2-13</i>	<i>EOS-89BTH Basket Maximum Adjacent Fuel Compartment Relative Displacements</i>	<i>3.9.2-44</i>

List of Figures

Figure 3.9.2-1	EOS-37PTH Basket Assembly ANSYS Model (Components Only) – Isometric View	3.9.2-45
Figure 3.9.2-2	EOS-37PTH Basket Assembly ANSYS Model (Components Only) – Isometric View Upper-Left Quadrant	3.9.2-46
Figure 3.9.2-3	EOS-37PTH Basket Assembly Typical Grid Plate Intersection	3.9.2-47
Figure 3.9.2-4	EOS-37PTH Basket Assembly ANSYS Model (Components Only) – Front View	3.9.2-48
Figure 3.9.2-5	EOS-37PTH Basket Assembly ANSYS Model (Plate Thicknesses) Lower Right Quadrant	3.9.2-49
Figure 3.9.2-6	EOS-37PTH Basket Assembly ANSYS Model (with Contact Elements) – Lower Right Quadrant	3.9.2-50
Figure 3.9.2-7	EOS-37PTH Basket Assembly ANSYS Model–Transition Rail Bolt and Tie Rod Locations	3.9.2-51
Figure 3.9.2-8	EOS-37PTH Basket Assembly ANSYS Model – Fuel Load Applied as Pressure	3.9.2-52
Figure 3.9.2-9	Comparison of Applied Temperature Profile to Data from Thermal Analysis for EOS-37PTH Basket Plates – Hottest Cross-Section, LC # 6, Horizontal, Off-Normal Hot Transfer in EOS-TC125, Outdoor	3.9.2-53
Figure 3.9.2-10	EOS-37PTH Basket Assembly ANSYS Model – Applied Bounding Thermal Profile	3.9.2-54
Figure 3.9.2-11	EOS-37PTH Basket 198.43 Degree 1.581g, DW + Handling – Grid Plates, $P_m + P_b$ (stress intensity, psi)	3.9.2-55
Figure 3.9.2-12	EOS-89BTH Basket Assembly ANSYS Model (Components Only) – Isometric View	3.9.2-56
Figure 3.9.2-13	EOS-89BTH Basket Assembly ANSYS Model (Components Only) – Isometric View – Upper-Left Quadrant	3.9.2-57
Figure 3.9.2-14	EOS-89BTH Basket Assembly Typical Grid Plate Intersection	3.9.2-58
Figure 3.9.2-15	EOS-89BTH Basket Assembly ANSYS Model (Components Only) – Front View	3.9.2-59
Figure 3.9.2-16	EOS-89BTH Basket Assembly ANSYS Model (Plate Thicknesses) – Lower Right Quadrant	3.9.2-60
Figure 3.9.2-17	EOS-89BTH Basket Assembly ANSYS Model (with Contact Elements) – Lower Right Quadrant	3.9.2-61
Figure 3.9.2-18	EOS-89BTH Basket Assembly ANSYS Model – Transition Rail Bolt and Tie Rod Locations	3.9.2-62

<i>Figure 3.9.2-19</i>	<i>EOS-89BTH Basket Assembly ANSYS Model – Fuel Load Applied as Pressure.....</i>	<i>3.9.2-63</i>
<i>Figure 3.9.2-20</i>	<i>Comparison of EOS-89BTH and EOS-37PTH Temperatures (Curve Fits) LC # 8, Vertical, Normal Hot Transfer in EOS-TC125, Indoor.....</i>	<i>3.9.2-64</i>
<i>Figure 3.9.2-21</i>	<i>EOS-89BTH Basket Assembly ANSYS Model – Applied Bounding Thermal Profile.....</i>	<i>3.9.2-65</i>
<i>Figure 3.9.2-22</i>	<i>EOS-89BTH Basket 198.43 Degree 1.581g, DW + Handling – Grid Plates, $P_m + P_b$ (stress intensity, psi)</i>	<i>3.9.2-66</i>
<i>Figure 3.9.2-23</i>	<i>EOS-37PTH Basket 0 Degree 60g Side Drop (with bolts / tie rods) – Grid Plates, $\epsilon_m + \epsilon_b$ (Equivalent Plastic Strain, in/in)</i>	<i>3.9.2-67</i>
<i>Figure 3.9.2-24</i>	<i>EOS-89BTH Basket 270 Degree 60g Side Drop (with bolts / tie rods) – Grid Plates, ϵ_m (Equivalent Plastic Strain, in/in).....</i>	<i>3.9.2-68</i>
<i>Figure 3.9.2-25</i>	<i>EOS-89BTH Basket 180 Degree 60g Side Drop (without bolts / tie rods) – Grid Plates, $\epsilon_m + \epsilon_b$ (Equivalent Plastic Strain, in/in).....</i>	<i>3.9.2-69</i>
<i>Figure 3.9.2-26</i>	<i>EOS-37PTH / EOS-89BTH DSC Shell ANSYS Model - Isometric View.....</i>	<i>3.9.2-70</i>
<i>Figure 3.9.2-27</i>	<i>EOS -37PTH / EOS-89BTH DSC Shell ANSYS Model - End View</i>	<i>3.9.2-71</i>

3.9.2 EOS-37PTH AND EOS-89BTH BASKET STRUCTURAL ANALYSIS

This appendix evaluates the structural integrity of the EOS-37PTH and EOS-89BTH DSC basket for normal, off-normal, and side and end drop accident loads.

3.9.2.1 EOS-37PTH Basket Structural Evaluation for Normal/Off-Normal Loads

This section evaluates the structural integrity of the EOS-37PTH DSC basket for normal and off-normal loads. Onsite transfer conditions in the TC108, TC125, and TC135 transfer cask (TC) and storage conditions in the EOS-HSM are considered.

3.9.2.1.1 General Description

The EOS-37PTH DSC consists of a shell assembly that provides confinement and shielding, and an internal basket assembly that locates and supports the FAs. The basket is made up of interlocking, slotted plates to form an egg-crate type structure. The egg-crate structure forms a grid of 37 fuel compartments that house PWR spent fuel assemblies (SFAs). A typical stack-up of grid plates is composed of a structural steel plate, an aluminum plate for heat transfer and a neutron absorber plate (neutron poison) for criticality.

[

]

The basket structure is open at each end and therefore, when the EOS-TC is oriented vertically, longitudinal FA loads are applied directly to the cover plates/shield plugs of the DSC shell assembly and not to the basket assembly. When the EOS-TC is oriented horizontally, longitudinal FA loads from handling may be at least partially transferred to the basket assembly due to friction. The FAs are laterally supported in the basket's fuel compartments. The basket is laterally supported by the basket transition rails and the DSC inner shell.

The minimum open dimension of each fuel compartment cell is sized to allow storage of the applicable fuel, which provides clearance around the FAs. The length of the DSC shell/basket assemblies can be customized to accommodate different FA lengths. The basket length is less than the DSC cavity length to allow for thermal expansion and tolerances.

[

3.9.2.1.2 Dimensions and Materials

The key basket dimensions and materials are per Drawings EOS01-1010-SAR and EOS01-1011-SAR (Section 1.3.1).

The key DSC dimensions and materials are per Drawing EOS01-1001-SAR (Section 1.3.1).

The key EOS-TC dimensions are per Drawings in Section 1.3.4.

3.9.2.1.3 Material Properties

The mechanical properties of structural materials used for the basket assembly as a function of temperature are shown in Chapter 8.

3.9.2.1.4 Temperature Data

Temperature data from the thermal analyses in Chapter 4 at the axial location of hottest temperatures are considered for the thermal stress analysis and component evaluations. A bounding temperature gradient is used in the thermal stress analysis.

3.9.2.1.5 Fuel Data

Chapter 2 provides design characteristics for the types of pressurized water reactor (PWR) FAs to be considered. A bounding distributed weight of 11.0 lbs/in. in the active fuel region is considered in the deadweight and handling analyses.

3.9.2.1.6 Methodology

ANSYS 10.0A1 [3.9.2-2] is used for the evaluation of side loads and thermal loads. Hand calculations are performed to conservatively calculate the stresses due to the axial handling loads. Axial loads are combined with the corresponding side loads, as applicable. Load conditions for the vertical orientation of the DSC/TC are not controlling. Therefore, only the horizontal orientation is evaluated. However, the temperature gradient applied in the thermal analysis bounds the gradients applicable to both the horizontal and vertical orientations (see Section 3.9.2.1.6.1.4).

3.9.2.1.6.1 Finite Element Model

3.9.2.1.6.1.1 Analysis Model Description for Side Loads

In consideration of continuous support of the basket grid structure by the transition rails along the entire length, a 6-inch slice of the basket assembly is modeled, consisting of one-half the widths (basket axial direction) of the basket plates. One end of the 6-inch long model is at the symmetry plane of the horizontal plates and is at the free edges of the vertical plates. The opposite end of the 6-inch long model is at the symmetry plane of the vertical plates and is at the free edges of the horizontal plates. Symmetry boundary conditions ($U_Y = ROTX = ROTZ = 0$) are defined at the symmetry planes of the grid plates and at both cut faces of the transition rails and steel angle plates. Geometry plots of the ANSYS model are shown in Figure 3.9.2-1 through Figure 3.9.2-7.

The top and bottom regions of the basket assembly use grid plates with widths as small as 6 inches. The resulting ligaments at the 3-inch deep slots are only 3 inches wide, which is one-half of 6-inch wide ligaments for grid plates in the middle region. However, the tributary width for loading from fuel is also one-half of the tributary width for plates in the middle region, and the fuel distributed load is smaller at the ends since it is away from the active fuel region. Furthermore, the temperatures are lower at the top and bottom of the basket assembly. Therefore, the top and bottom regions of the basket assembly are bounded by the analyzed middle region.

The steel grid plates and the DSC shell are modeled using ANSYS Shell181 elements. No structural credit is taken for the poison plates or for the aluminum plates. The mass of the poison plates and aluminum plates is accounted for by increasing the density of the adjacent steel grid plates. Reinforcing steel angle plates in the R45 transition rails are also modeled using ANSYS Shell181 elements. The aluminum transition rails are modeled using ANSYS Solid185 elements.

Contact between the grid plates at the slots is modeled using ANSYS Conta178 elements (without friction). Initial gaps are defined for the contact elements based on the thickness stack-up of the steel, poison, and aluminum plates in each slot. Similarly, contact between the grid plates and the aluminum transition rails are modeled using ANSYS Conta178 elements (without friction). The initial gaps between the plates and the transition rails are considered closed. This implies that the unmodeled “sandwiched” aluminum, and poison plates are assumed to transfer loads normal to the plates. For stability and convergence purposes, soft springs (Combin14) are modeled coincident with the contact elements.

Bolts connecting the transition rails to the grid plates are modeled using ANSYS Beam4 elements. Nodes on the bolt elements are coupled to nodes on the grid plates, aluminum transition rails, and reinforcing steel angle plates in the rails, as applicable. At one end of each bolt, a contact element (Conta178) is defined in the axial direction of the bolt. The couples and contact element are defined so that only tension loads are transferred through the bolts (due to oversized bolt holes).

Similarly, tie rods for the R90 transition rail assemblies are modeled using ANSYS Beam4 elements. For loading other than thermal, the ends of tie rods are connected to the transition rails in the same manner as for the bolts, so that only tension loads are transferred. One Belleville spring washer is used at each end of the tie rods to allow for thermal growth of the R90 aluminum rail assemblies. Therefore, nonlinear Combin39 spring elements are used in lieu of the contact elements only for the thermal analyses (see Section 3.9.2.1.6.1.2). The thermal loading basically compresses the washer, so the tie rods behave like tension-only for other loads.

The DSC shell, when fully welded with cover plates, is much stiffer than the basket and therefore, for static analyses of the basket for small load levels such as deadweight and on-site handling loads, the DSC shell is considered to be rigid. Gaps between the basket and the DSC cylindrical shell are modeled using ANSYS Conta178 elements (without friction). Each gap element contains two nodes; one on each surface of the structures. Initial gaps are based on a basket outside diameter of 74.10 inches and a DSC inside diameter of 74.50 inches, and the side load orientation. Initial gaps are adjusted in consideration of the radial thermal growth of the basket relative to the growth of the DSC shell.

To consider bounding conditions, two sets of analyses are performed. The first set of analyses defines nominal gaps for a basket thermal growth, relative to the DSC shell, approximated to be 0.05 inches. The second set of analyses adjusts the gaps for a basket minimum thermal growth, relative to the DSC shell, of 0.0158 inch, calculated based on average temperatures of the basket and DSC shell at the hottest cross-section per Chapter 4.

Side loads due to transfer handling bound the loads applicable to storage in the EOS-HSM for which only deadweight is applicable. As discussed earlier, the DSC shell, when fully welded with cover plates, is much stiffer than the basket and therefore, for static analyses of the basket for small load levels such as deadweight and on-site handling loads, the DSC shell is considered to be rigid. Therefore the impact of the rail location is insignificant and one model envelopes the configuration when the DSC is inside the EOS-TC and EOS-HSM.

3.9.2.1.6.1.2 Analysis Model Description for Thermal Loads

The basket assembly thermal stress model is similar to the side-loaded model except that it excludes the DSC cylindrical shell (which does not restrain the thermal growth of the basket). One Belleville spring washer is used at each end of the tie rods to allow for thermal growth of the R90 aluminum rail assemblies. Therefore, nonlinear Combin39 spring elements are used in lieu of contact elements at one end of each tie rod for the thermal analyses. The force-deflection input is determined using data associated with the spring washer.

Boundary conditions for the transition rails and rail angle plates are removed from one end of the model to avoid fictitious thermal stresses that would occur if both ends were restrained. Two thermal cases are considered in consideration of the boundary conditions for the transition rails and rail angle plates: restraint at $y = 0$ inch (near end restraint), and restraint at $y = 6$ inches (far end restraint). Although the maximum stress results from these two cases are effectively the same, the results are combined with the deadweight and handling cases using ANSYS load combinations to preclude the conservatism of adding maximum stresses regardless of location. The consideration of two sets of boundary conditions for thermal ensures that the correct maximum stress in combination with deadweight and handling stress is obtained.

3.9.2.1.6.1.3 Material Properties in Analyses

The modeled components of the basket and DSC are based on lower bound material properties. The material properties used for stress analyses (except thermal stress analyses) are based on bounding average temperature values at the hottest section for off-normal transfer in a horizontal EOS-TC. Elastic analyses are used for all normal and off-normal conditions.

3.9.2.1.6.1.4 Loads

Load cases are based on the loads described in Chapter 2.

For side loading, the fuel weight load is modeled conservatively using a pressure load equivalent to the applicable acceleration, or G-load, times the FA weight divided by the basket fuel compartment area associated with the active fuel region length and the fuel compartment width between slots (8.79 inches). A fuel load of 11.0 lbs/in acting on the fuel compartment width between slots is applied to bound the load distribution in the active fuel region for all PWR fuel types identified in Chapter 2. Figure 3.9.2-8 shows the application of fuel weight pressure loads to the model.

For 0° and 180° side load orientations, the equivalent fuel assembly pressure acts only on the horizontal plates. For 90° and 270° side load orientations, the equivalent fuel assembly pressure acts only on the vertical plates. For other orientations, the equivalent FA pressure acts perpendicular to the horizontal and vertical plates, proportioned based on the Cosine and Sine of the orientation angle.

Based on the handling load combination required per Chapter 2, the following bounding normal side load conditions (DSC and basket in horizontal position) are evaluated:

- DW + 1g Vertical = 2.0g Vertical at $\theta = 180^\circ$
- DW + 0.5g Vert. + 0.5g Transverse = 1.58g at $\theta_{198} = 198.43^\circ$ *
- DW + 1.0g Transverse = 1.414g at $\theta_{225} = 225.0^\circ$ *

$$* \theta_{198} = 180^\circ + \tan^{-1}(0.5 / 1.5) = 198.43^\circ; \theta_{225} = 180^\circ + \tan^{-1}(1.0 / 1.0) = 225^\circ$$

Thermal stress analyses are based on a bounding temperature profile. The temperature profile used is represented by the following equation, labeled “EOS Basket Analysis” in Figure 3.9.2-9:

$$T(x) = -0.3952 x^2 + 3.4661 x + 790.29$$

Where,

$$T(x) = \text{Basket temperature as a function of radius, } x.$$

Figure 3.9.2-9 shows the raw temperature data (versus radius) for one load case from the thermal analyses, labeled “EOS-37PTH in EOS-TC125, Grid Plates, LC # 6” (worst-case temperature condition for steepness of radial temperature gradient). A comparison of the curves shows that the curve labeled as “EOS Basket Analysis,” which gives the temperatures versus radius used in the basket thermal stress analysis herein, provides the bounding steeper gradient.

3.9.2.1.6.2 Criteria

The basis for allowable stresses is obtained from Chapter 8 and ASME Section III, Division 1, Subsection NG [3.9.2-1]. The criteria are summarized in Chapter 3, Table 3-2. Allowable stresses for the threaded fasteners, used to connect the transition rails to the basket grid structure, are from Chapter 8 and Section NG-3230 of [3.9.2-1]. The criteria are summarized in Table 3.9.2-1. The component allowable stress values are summarized in Table 3.9.2-2. The allowable stresses are based on material properties at 700 °F for the grid plates and 550 °F for the transition rails, angle plates, bolts and tie rods. These temperatures bound the average temperatures at the hottest section for the grid plates and transition rails, respectively, summarized in Chapter 4 for off-normal transfer in a horizontal EOS-TC.

3.9.2.1.6.3 Creep Evaluation for Long Term Storage

The aluminum R90 rails are designed to resist the bearing loads due to the deadweight of the loaded basket for 80 years while stored in the EOS-HSM. For long-term creep effects, where loading on the aluminum transition rail redistributes over time, an average bearing stress is an appropriate value to consider.

Conservatively, it is assumed that the entire weight of the basket is resisted by the three pieces of a single aluminum R90 rail. The 1g deadweight load from the entire weight of a 6-inch long portion of the basket is approximately 3,416 lb. The area of the corresponding 6-inch long portion of the R90 rail that resists the load is approximately $= 156 \text{ in}^2$. However, credit for the outer portion of the width of the rail is excluded by conservatively considering only half of the rail width. The corresponding bearing stress is calculated as follows:

Basket 1g vertical bearing stress = Load / Area = 43.8 psi, or, 0.044 ksi.
(on aluminum R90 transition rail)

The individual compartment load at each SFA location on the supporting aluminum plate gives a much lower bearing stress. Using a conservative width of only 8 inches for a compartment gives:

SFA 1g vert. bearing stress = (Load / length) / Width = 1.375 psi, or, 0.0014 ksi.
(on aluminum plate)

The allowable bearing stresses are provided in Chapter 8, and based on Reference [3.9.2-3]; they represent the stress in Aluminum 1100 to produce a strain of 0.01 in 550,000 hours (approximately 63 years). However, the creep strain curve is so flat that the values at 80 years are approximately the same. The allowable bearing stress for Aluminum 1100 represents a conservative lower bound. The initial temperature values (time = 0) and the corresponding allowable bearing stresses in the basket aluminum components, to limit creep strain to 0.01, are as follows:

- 0.254 ksi in the hottest aluminum plate, with a starting temperature of 680 °F
- 0.758 ksi in the hottest R90 rail, with a starting temperature of 470 °F
- 0.876 ksi in a less than hottest R90 rail, based on a starting temperature of 440 °F

From Chapter 4 for normal conditions (applicable to long-term storage conditions) at the hottest cross-section of the basket, the average R90 transition rail temperature is not more than 469 °F, which is less than the above temperature of 470 °F for the hottest R90 rail. Similarly, from Chapter 4, for normal conditions, the hottest basket plate temperature is not more than 668 °F, which is less than the above temperature of 680 °F for the hottest aluminum plate. Based on this comparison of temperatures, and since the heat dissipation rate for the EOS-37PTH basket is better than that for the basket temperature data (temperature versus time) used in Reference [3.9.2-3], the allowable creep stresses given above are applicable to the aluminum components of the EOS-37PTH basket.

3.9.2.1.7 Results

3.9.2.1.7.1 Results for On-Site DW+Handling and Thermal Stress Analysis

Combined results for basket component stress results for normal condition deadweight + handling loads and thermal stress analysis are shown in Table 3.9.2-3. The tabulated results show that all stresses meet the corresponding Code limits.

ANSYS Force Summation Comparison

An ANSYS force summation for the basket components only, for the 2g deadweight plus handling load combination, is compared to the expected load as shown below:

Force Summation: $F_z = -6,831.256 \text{ lb}$
(in vertical direction (z), length of model is 6 inches)

Expected Load:

Basket weight / length w/o spent fuel: = 167.2 lb/in

Basket wt. w/o spent fuel (6" long) = 1,003 lb.

Spent fuel weight (6" long) = (11 lb/in) (6" length of basket) (37 SFAs)
= 2,442 lb.

Total weight of the basket, with spent fuel (6" long) = 3,445 lb (for 1g)

Expected Load at 2g (in vertical direction) = 6,890 lb.

The ANSYS load of 6,831 is within 1% of the hand-calculated weight load and therefore, is acceptable.

Similarly, the ANSYS 1g load is 3,416 lb, or half of the ANSYS 2g load, as expected.

3.9.2.1.7.2 Aluminum Components – Long Term Storage Deadweight Bearing Stress

The aluminum R90 rails are designed to resist the bearing loads due to the deadweight of the loaded basket for 80 years while stored in the EOS-HSM. A review of the R90 transition rail stresses in Figure 3.9.2-11 shows that for the 1g deadweight loading, the R90 rail carries most of the loading. The aluminum R45 rails take some of the bearing load but are not controlling. The stresses shown in Figure 3.9.2-11 are unaveraged stresses that include local and peak effects. However, for long-term creep effects, where loading on the aluminum transition rail redistributes over time, an average bearing stress is a more appropriate value to consider. The stresses calculated in Section 3.9.2.1.6.3 are compared to allowable stress values that are reduced to limit the effect due to creep.

Comparison of Aluminum Bearing Stress to Allowable Creep Stress from Section 3.9.2.1.6.3:

Component	Bearing Stress	Allowable Creep Stress	Stress/Allowable Ratio
Alum. Rail	0.044 ksi	0.758 ksi	0.0580
Alum. Plate	0.0014 ksi	0.254 ksi	0.0055

3.9.2.1.8 Conclusions

Finite element analyses and hand calculations for the EOS-37PTH basket assembly are performed for all normal and off-normal on-site conditions. Controlling stress intensities are reported in Table 3.9.2-3. A comparison of stress intensities to the corresponding allowable values indicate that all load conditions and combinations show acceptable stress levels, as applicable.

3.9.2.2 EOS-89BTH Basket Structural Evaluation for Normal/Off-Normal Loads

The basis for the fuel compartment allowable stress values is the ASME Code, Section III, Subsection NG (Reference [3.9.2-1]), as given in Chapter 8.

3.9.2.2.1 General Description

The EOS-89BTH DSCs consists of a shell assembly that provides confinement and shielding, and an internal basket assembly that locates and supports the FAs. The basket is made up of interlocking slotted plates to form an egg-crate type structure. The egg-crate structure forms a grid of 89 fuel compartments that house boiling water reactor (BWR) SFAs. A typical stack-up of grid plates is composed of a structural steel plate, an aluminum plate for heat transfer and a neutron absorber plate (neutron poison) for criticality.

The DSC shell and basket assemblies are detailed in drawings in Section 1.3.2.

The descriptions in Section 3.9.2.1.1 of the transition rails and basket are also applicable to the EOS-89BTH DSC.

3.9.2.2.2 Key Dimensions and Materials

The key basket dimensions and materials are per Drawings EOS01-1020-SAR and EOS01-1021-SAR Section 1.3.2.

The key DSC dimensions and materials are per Drawing EOS01-1001-SAR (Section 1.3.2):

The key EOS-TC dimensions are per the drawings in Section 1.3.4.

3.9.2.2.3 Material Properties

The mechanical properties of structural materials used for the basket assembly and canister as a function of temperature are shown in Chapter 8.

3.9.2.2.4 Temperature Data

Temperature data from the EOS-89BTH thermal analyses and from the EOS-37PTH thermal analyses in Chapter 4, at the axial location of hottest temperatures, are considered herein for the thermal stress analysis and component evaluations. The conservative temperature gradient used herein for the thermal stress analysis bounds the gradients for the EOS-89BTH basket. See Section 3.9.2.1.6.1.4 for further discussion.

3.9.2.2.5 Fuel Data

Chapter 2 provides design characteristics for the types of BWR FAs to be considered. A maximum FA weight of 705 lbs is used. A distributed weight of 705 lbs / 150 in. = 4.7 lbs/in is considered to be bounding in the active fuel region for the deadweight and handling analyses.

3.9.2.2.6 Methodology

Same as Section 3.9.2.1.6.

3.9.2.2.6.1 Finite Element Model

3.9.2.2.6.1.1 Analysis Model Description for Side Loads

Geometry plots of the ANSYS model are shown in Figure 3.9.2-12 through Figure 3.9.2-18. All other details of the analysis model description are the same as Section 3.9.2.1.6.1.1.

3.9.2.2.6.1.2 Analysis Model Description for Thermal Loads

Same as Section 3.9.2.1.6.1.2.

3.9.2.2.6.1.3 Material Properties in Analyses

Same as Section 3.9.2.1.6.1.3.

3.9.2.2.6.1.4 Loads

Load cases are based on the loads described in Chapter 2.

For side loading, the fuel weight load is modeled conservatively using a pressure load equivalent to the applicable acceleration, or g-load, times the FA weight divided by the basket fuel compartment area associated with the active fuel region length and the fuel compartment width between slots (5.85 inches). A fuel load of 4.7 lbs/in acting on the fuel compartment width between slots is applied to bound the load distribution in the active fuel region for all BWR fuel types identified in Chapter 2. Figure 3.9.2-19 shows the application of fuel weight pressure loads to the model.

For 0° and 180° side load orientations, the equivalent FA pressure acts only on the horizontal plates. For 90° and 270° side load orientations, the equivalent fuel assembly pressure acts only on the vertical plates. For other orientations, the equivalent FA pressure acts perpendicular to the horizontal and vertical plates, proportioned based on the Cosine and Sine of the orientation angle.

Based on the handling load combination, the following bounding normal side load conditions (DSC and basket in horizontal position) are evaluated:

- - DW + 1g Vertical = 2.0g Vertical at $\theta = 180^\circ$
- - DW + 0.5g Vert. + 0.5g Transverse = 1.58g at $\theta_{198} = 198.43^\circ$ *
- - DW + 1.0g Transverse = 1.414g at $\theta_{225} = 225.0^\circ$ *

* $\theta_{198} = 180^\circ + \tan^{-1}(0.5 / 1.5) = 198.43^\circ$; $\theta_{225} = 180^\circ + \tan^{-1}(1.0 / 1.0) = 225^\circ$

Thermal stress analyses are made based on a bounding temperature profile. The temperature profile used is represented by the following equation labeled “EOS Basket Analysis” in Figure 3.9.2-9:

$$T(x) = -0.3952 x^2 + 3.4661 x + 790.29$$

Where,

$T(x)$ = Basket temperature as a function of radius, x .

Due to the lower heat load in the EOS-89BTH DSC compared to the EOS-37PTH DSC, limited analyses are run in Chapter 4 to demonstrate that the maximum fuel cladding temperatures for the EOS-89BTH will be bounded by those for the EOS-37PTH. However, resulting maximum EOS-89BTH basket component temperatures are in some cases shown to be greater than for the EOS-37PTH basket component temperatures.

Figure 3.9.2-20 shows that although the EOS-89BTH grid plate temperatures are slightly greater than the EOS-37PTH grid plate temperatures, the gradients are similar. As shown in these figures and in comparison plots for other thermal cases, the analyzed temperature profile has a steeper temperature gradient than that for the raw data. Therefore, it can be concluded that the conservative temperature gradient used herein for the thermal stress analysis will bound the gradients for the EOS-89BTH basket. Figure 3.9.2-21 shows the bounding temperature profile applied to the ANSYS model.

3.9.2.2.6.2 Criteria

The basis for allowable stresses is obtained from Chapter 8 and ASME Section III, Division 1, Subsection NG (Reference [3.9.2-1]). The criteria are summarized in Chapter 3, Table 3-2.

Allowable stresses for the threaded fasteners, used to connect the transition rails to the basket grid structure, are from Chapter 8 and Section NG-3230 of [3.9.2-1]. The criteria are summarized in Table 3.9.2-1. The component allowable stress values are summarized in Table 3.9.2-2. The allowable stresses are based on material properties at 700 °F for the grid plates (except where noted otherwise) and 550 °F for the transition rails, angle plates, bolts and tie rods. These temperatures bound the average temperatures at the hottest section for the grid plates and transition rails, respectively, summarized in Chapter 4 for transfer in a horizontal EOS-TC (non-accident).

3.9.2.2.6.3 Creep Evaluation for Long Term Storage

The aluminum R90 rails are designed to resist the bearing loads due to the deadweight of the loaded basket for 80 years while stored in the EOS-HSM. For long-term creep effects, where loading on the aluminum transition rail redistributes over time, an average bearing stress is an appropriate value to consider.

Conservatively assuming that the entire weight of the basket is resisted by the three pieces of a single aluminum R90 rail, the 1g deadweight load from the entire weight of a 6-inch long portion of the basket is approximately 3,462 lb. The area of the corresponding 6-inch long portion of the R90 rail that resists the load is approximately $= 102 \text{ in}^2$. However, credit for the outer portion of the width of the rail is excluded by conservatively considering only half of the rail width. The corresponding bearing stress is calculated as follows:

Basket 1g vert. bearing stress = Load / Area = 67.9 psi, or, 0.068 ksi. (on aluminum R90 transition rail)

The individual compartment load at each SFA location on the supporting aluminum plate gives a much lower bearing stress. Using a conservative width of only 5 inches for a compartment gives:

$$\text{SFA 1g vert. bearing stress} = (\text{Load} / \text{length}) / \text{Width} = 0.940 \text{ psi, or,} \\ 0.00094 \text{ ksi. (on aluminum plate)}$$

The allowable bearing stresses are provided in Section 3.9.2.1.6.3. The initial temperature values (time = 0) and the corresponding allowable bearing stresses in the basket aluminum components, to limit creep strain to 0.01, are as follows:

- 0.254 ksi in the hottest aluminum plate, with a starting temperature of 680 °F
- 0.758 ksi in the hottest R90 rail, with a starting temperature of 470 °F
- 0.876 ksi in a less than hottest R90 rail, based on a starting temperature of 440 °F

From Chapter 4, for normal conditions (applicable to long-term storage conditions) at the hottest cross-section of the basket, the average R90 transition rail temperature is not more than 446 °F, which is less than the above temperature of 470 °F for the hottest R90 rail. Similarly, from Chapter 4, for normal conditions, the hottest basket plate temperature is not more than 676 °F, which is less than the above temperature of 680 °F for the hottest aluminum plate. Based on this comparison of temperatures, and since the heat dissipation rate for the EOS-89BTH basket is better than that for the basket temperature data (temperature versus time) used in Reference [3.9.2-3], the allowable creep stresses given above are applicable to the aluminum components of the EOS-89BTH basket.

3.9.2.2.7 Results

3.9.2.2.7.1 Results for On-Site DW+Handling and Thermal Stress Analysis

Combined results with controlling stress ratios for normal condition deadweight + handling loads and thermal analysis are shown in Table 3.9.2-4. The tabulated results show that all stresses meet the corresponding Code limits.

ANSYS Force Summation Comparison

An ANSYS force summation for the basket components only, for the 2g deadweight plus handling load combination, is compared to the expected load as shown below:

Force Summation: $F_z = -6,923.822 \text{ lb}$ (in vertical direction (z), length of model is 6")

Expected Load:

Basket weight / length w/o spent fuel $= (19,300 + 637 + 1,110 + 3,980) /$
 $166.0 + 1,720 / 175.0$
 $= 160.6 \text{ lb/in}$

Basket wt. w/o spent fuel (6" long) $= (160.6) (6") = 964 \text{ lb.}$

Spent fuel weight (6" long) $= (4.7 \text{ lb/in}) (6" \text{ length of basket}) (89 \text{ SFAs})$
 $= 2,510 \text{ lb.}$

Total weight of the basket, with spent fuel (6" long) = $964 + 2,510 = 3,474$ lb
(for 1g)

Expected Load at 2g (in vertical direction) = $2 (3,474) = 6,948$ lb.

The ANSYS load of 6,924 is within 0.4% of the hand-calculated weight load and therefore, is acceptable.

Similarly, the ANSYS 1g load is 3,462 lb, or half of the ANSYS 2g load, as expected.

3.9.2.2.7.2 Aluminum Components – Long Term Storage Deadweight Bearing Stress

The aluminum R90 rails are designed to resist the bearing loads due to the deadweight of the loaded basket for 80 years while stored in the EOS-HSM. A review of the R90 transition rail stresses in Figure 3.9.2-22 shows that for the 1g deadweight loading, the R90 rail carries most of the loading. The aluminum R45 rails take some of the bearing load but are not controlling. The stresses shown in Figure 3.9.2-22 are unaveraged stresses that include local and peak effects. However, for long-term creep effects, where loading on the aluminum transition rail redistributes over time, an average bearing stress is a more appropriate value to consider.

The stresses calculated in Section 3.9.2.2.6.3 are compared to allowable stress values that are reduced to limit the effect due to creep.

Comparison of Aluminum Bearing Stress to Allowable Creep Stress from Section 3.9.2.2.6.3:

Component	Bearing Stress	Allowable Creep Stress	Stress/Allowable Ratio
Alum. Rail	0.068 ksi	0.758 ksi	0.0897
Alum. Plate	0.00094 ksi	0.254 ksi	0.0037

3.9.2.2.7.3 Conclusions

Finite element analyses and hand calculations for the EOS-89BTH basket assembly are performed for all normal and off-normal on-site conditions. Controlling stress intensities are reported in Table 3.9.2-4. A comparison of stress intensities to the corresponding allowable values indicate that all load conditions show acceptable stress levels, as applicable.

3.9.2.3 EOS-37PTH Basket Structural Evaluation for On-Site Accident Drop Loads

This section evaluates the structural integrity of the EOS-37PTH DSC basket for on-site accident side and end drop loads. On-site transfer conditions in the EOS-TC108, EOS-TC125, or EOS-TC135 are considered for thermal properties used in the side drop load analyses.

3.9.2.3.1 General Description

Same as Section 3.9.2.1.1.

3.9.2.3.2 Key Dimensions and Materials

Same as Section 3.9.2.1.2.

3.9.2.3.3 Material Properties

Same as Section 3.9.2.1.3.

3.9.2.3.4 Temperature Data

Same as Section 3.9.2.1.4.

3.9.2.3.5 Fuel Data

Chapter 2 provides design characteristics for the types of pressurized water reactor (PWR) FAs to be considered. A bounding distributed weight of 11.0 lbs/in. in the active fuel region is considered for the on-site accident side drop analyses.

3.9.2.3.6 Methodology

ANSYS 10.0A1 and 17.1 [3.9.2-2] are used for the evaluation of on-site accident side drop loads. Hand calculations are performed to conservatively calculate the stresses due to the on-site axial end drop loads. Stresses due to the end drop loads are not controlling. Therefore, only the side drop load analysis results are presented.

3.9.2.3.6.1 Finite Element Model

3.9.2.3.6.1.1 Analysis Model Description for Side Loads

In consideration of continuous support of the basket grid structure by the transition rails along the entire length, a 6-inch slice of the basket assembly is modeled, consisting of one-half the widths of the basket plates. One end of the 6-inch long model is at the symmetry plane of the horizontal plates and is at the free edges of the vertical plates. The opposite end of the 6-inch long model is at the symmetry plane of the vertical plates and is at the free edges of the horizontal plates. Symmetry boundary conditions ($U_Y = ROTX = ROTZ = 0$) are defined at the symmetry planes of the grid plates and at both cut faces of the transition rails and steel angle plates. Geometry plots of the ANSYS model are shown in Figure 3.9.2-1 through Figure 3.9.2-8 (180 degree drop orientation shown).

The top and bottom regions of the basket assembly use grid plates with widths as small as 6 inches. The resulting ligaments at the 3-inch deep slots are only 3 inches wide, which is one-half of 6-inch wide ligaments for grid plates in the middle region. However, the tributary width for loading from fuel is also one-half of the tributary width for plates in the middle region, and the fuel distributed load is smaller at the ends since it is away from the active fuel region. Furthermore, the temperatures are lower at the top and bottom of the basket assembly. Therefore, the top and bottom regions of the basket assembly are bounded by the analyzed middle region.

The steel grid plates and the DSC shell are modeled using ANSYS Shell181 elements. No structural credit is taken for the poison plates or for the aluminum plates. The mass of the poison plates and aluminum plates is accounted for by increasing the density of the adjacent steel grid plates. Reinforcing steel angle plates in the R45 transition rails are also modeled using ANSYS Shell181 elements. The aluminum transition rails are modeled using ANSYS Solid185 elements.

Contact between the grid plates at the slots is modeled using ANSYS Conta178 elements (without friction). Initial gaps are defined for the contact elements based on the thickness stack-up of the steel, poison, and aluminum plates in each slot. Similarly, contact between the grid plates and the aluminum transition rails are modeled using ANSYS Conta178 elements (without friction). The initial gaps between the plates and the transition rails are considered closed. This implies that the unmodeled “sandwiched” aluminum and poison plates are assumed to transfer loads normal to the plates. For stability and convergence purposes, soft springs (Combin14) are modeled coincident with the contact elements.

Bolts connecting the transition rails to the grid plates are modeled using ANSYS Beam4 elements. Nodes on the bolt elements are coupled to nodes on the grid plates, aluminum transition rails, and reinforcing steel angle plates in the rails, as applicable. At one end of each bolt, a contact element (Conta178) is defined in the axial direction of the bolt. The couples and contact elements are defined such that only tension loads are transferred through the bolts (due to oversized bolt holes). Similarly, tie rods for the R90 transition rail assemblies are modeled using ANSYS Beam4 elements. The ends of tie rods are connected to the transition rails in the same manner as for the bolts, such that only tension loads are transferred. The Belleville spring washers used at the ends of the tie rods are considered to be compressed by thermal loading so the tie rods behave as tension-only for other loads. Additional side drop analyses are performed without the connection bolts and tie rods (assumed to fail) to demonstrate that they are not needed for an accident drop.

Gaps between the basket and the DSC cylindrical shell are modeled using ANSYS Conta178 elements (without friction). Initial gaps are based on a basket outside diameter of 74.10 inches and a DSC inside diameter of 74.50 inches, and the side load orientation. Initial gaps are adjusted in consideration of the radial thermal growth of the basket relative to the growth of the DSC shell. Each gap element contains two nodes; one on each surface of the structures. The flexibility of the DSC shell is considered. Therefore, additional gap elements (ANSYS Conta178) are modeled between the DSC and the EOS-TC cask, where the gap nodes specified at the inner side of the cask are restrained in the three translational directions. Initial gaps are based on a DSC outside diameter of 75.50 inches and an EOS-TC inner shell diameter of 76.25 inches, and the side load orientation. Initial gaps are adjusted in consideration of the radial thermal growth of the DSC shell relative to the growth of the cask. Cask rails are simulated by using the difference between cask and DSC radii, combined with the rail thickness, as applicable, and using zero gap contact elements at the rails in initial contact with the DSC and non-zero gap contact elements elsewhere between the DSC and the cask.

To consider the stiffening effect of the DSC end plates on the cylindrical shell, a simplified, half-length model of the DSC shell was used to get more realistic cylindrical shell side drop deformations for gap calculations. See Figure 3.9.2-26 and Figure 3.9.2-27. The model includes a thick cover plate representing the two cover plates, and contact elements to the nodes at the inner diameter of the cask and cask rails are modeled as described above for the basket model. Symmetry boundary conditions ($U_Y = ROT_X = ROT_Z = 0$) are defined at the end of the model opposite of the cover plate (mid-length of the DSC shell). Elastic-plastic material properties at 400 °F are defined for the shell, based on a bilinear material stress-strain curve with a 1% tangent modulus. The average shell temperature of a horizontally oriented DSC in an EOS-TC for off-normal conditions is less than 435 °F so an approximate value of 400 °F was used. A uniform pressure is applied to a range +/-45 degrees from the bottom to represent the basket and fuel load. Internal pressure and the associated stress stiffening effects are conservatively not modeled. The resulting shell displacements at the symmetry plane of the cylindrical shell, for the upper 140 degrees (+/-70 degrees) opposite from the point of drop, are applied for 180° and 270° side drop load analyses. For the 225° side drop load analyses, the shell displacements at the upper 60 degrees (+/-30 degrees) opposite from the point of drop are applied. This credits the stiffening effect of the DSC end plates while allowing the shell to locally displace around the cask rails based on interaction with loading from the basket components.

3.9.2.3.6.1.2 Material Properties in Analyses

The modeled components of the basket and DSC are based on lower bound material properties. The material properties used for stress/strain analyses are based on representative average temperature values.

For elastic-plastic strain and buckling analyses, bilinear material stress-strain curves are used with a 1% tangent modulus for all materials except the bolts and tie rods. This is consistent with previous licensed basket designs.

3.9.2.3.6.1.3 Loads

Load cases are based on the loads described in Chapter 2.

A 65 inch side drop is considered in various orientations to ensure the adequacy of the design under on-site accident side drop conditions. A side drop load of 60g is evaluated to bound the acceleration predicted in Appendix 3.9.3. A 75g end drop is also considered to conservatively envelop the effects of a 65-inch corner drop.

For side loading, the fuel weight load is modeled conservatively using a pressure load equivalent to the applicable acceleration, or G-load, times the fuel assembly weight divided by the basket fuel compartment area associated with the active fuel region length and the fuel compartment width between slots (8.79 inches). A fuel load of 11.0 lbs/in. acting on the fuel compartment width between slots is applied to bound the load distribution in the active fuel region for all PWR fuel types. Figure 3.9.2-8 shows the application of fuel weight pressure loads to the model (for a 180° side drop orientation).

For 0° and 180° side load orientations, the equivalent fuel assembly pressure acts only on the horizontal plates. For 90° and 270° side load orientations, the equivalent fuel assembly pressure acts only on the vertical plates. For other orientations, the equivalent fuel assembly pressure acts perpendicular to the horizontal and vertical plates, proportioned based on the Cosine and Sine of the orientation angle.

The following accident side drop load conditions (DSC and basket in horizontal position) are evaluated:

- 180° Side Drop on Rails *in TC108*
(due to symmetry, this also covers the 0° Side Drop *in TC108*)
- 270° Side Drop away from Rails *in TC108*
(due to symmetry, this also covers the 90° Side Drop *in TC108*)
- 225° Side Drop on Rails *in TC108*
(due to symmetry, this also covers other multiples of 45° Side Drop *in TC108*)
- 0° Side Drop on Rails *in TC125/135*
(due to symmetry, this also covers 90° and 270° Side Drops *in TC125/135*)
- 45° Side Drop on Rails *in TC125/135*
(due to symmetry, this also covers 315° Side Drop *in TC125/135*)
- 225° Side Drop on Rails *in TC125/135*
(due to symmetry, this also covers 135° Side Drop *in TC125/135*)

3.9.2.3.6.2 Criteria

The basis for allowable strains is obtained from Chapter 8. The strain criteria are discussed and summarized in Section 3.1.1.1.1.

The basket grid plate strain criteria are summarized in Table 3.9.2-5. The threaded fasteners, used to connect the transition rails to the basket grid structure, are not required to be evaluated because they are considered to fail (with analyses and calculations confirming that they are not needed for accident condition drops).

Section 3.9.2.4.6.3 demonstrates that uncontrolled crack propagation in the basket plates is not an issue for the selected high-strength low-alloy (HSLA) steel material.

3.9.2.3.7 Results

3.9.2.3.7.1 Results for Analysis of 60g Accident Side Loading

60g accident side drop loads are analyzed using the ANSYS model described in Section 3.9.2.3.6.1.1. Accident condition equivalent static elastic-plastic analyses are performed for computing the equivalent plastic strains.

The fuel weight load is modeled conservatively using a pressure load equivalent to the applicable acceleration, or G-load, times the maximum fuel assembly weight per length (11.0 lbs/in) divided by the fuel compartment width (8.79 inches).

At the 180° side load orientation, the equivalent 1g fuel assembly pressure, acting only on the horizontal plates, P_{180h} , is calculated as follows:

$$P_{180h} = 11.0 \text{ lbs/in} / (8.79") = 1.2514 \text{ psi}$$

At the 270° side load orientation, 1g acting only on the vertical plates:

$$P_{270v} = 11.0 \text{ lbs/in} / (8.79") = 1.2514 \text{ psi}$$

At 225° (45 degrees from bottom), 1g acting on the horizontal and vertical plates:

$$P_{225h} = P_{225v} = P_{180h} \sin(45^\circ) = 0.8849 \text{ psi}$$

The ANSYS unit (1g) accelerations, indicating direction of load, are:

180-degree	acel, 0, 0, 1
270-degree	acel, 1, 0, 0
225-degree	acel, 0.7071, 0, 0.7071

For side load analyses, the equivalent fuel assembly pressure loads and accelerations above are multiplied by the corresponding side load acceleration value (e.g., 60g).

Displacements, stresses, strains and forces for each converged load step are saved to ANSYS files.

Basket grid plate equivalent plastic strain results for accident condition 60g side drop loads are shown in Table 3.9.2-6. Results with controlling strain ratios are shown in Table 3.9.2-7. An ANSYS strain contour plot corresponding to the bounding equivalent plastic strain values is shown in Figure 3.9.2-23. The tabulated results show that all strains meet the corresponding allowable strain limits. As demonstrated in Section 3.9.2.4.6.3, uncontrolled crack propagation in the grid plates is not an issue for the selected HSLA steel material.

Analyses are run to 75g. The program stops at the load substep that fails to result in a converged solution, if convergence to 75g does not occur. The last converged load step is considered the buckling load. The buckling load values are compared with 60g, the required g-load for accident conditions, with results shown in Table 3.9.2-8. All analyses complete the 75g load step.

Stresses and strains in the aluminum basket transition rails are not explicitly evaluated. All analyzed drop conditions include the case where the connecting bolts and tie rods are assumed to fail, to demonstrate that the connection to the aluminum is not needed to maintain basket strains within the allowable strain limits. Therefore, the only significant stress in the basket aluminum rails is a bearing type stress where the transition rail is compressed between the basket grid plates and the inside surface of the EOS-DSC. Since bearing stresses are not required to be evaluated for accident conditions, no further evaluation of the basket transition rails is required.

ANSYS Force Summation Comparison

An ANSYS force summation for the basket components only, for the 60g side drop, is compared to the expected load as shown below:

From the ANSYS results for the 60g load step:

Force Summation: $F_z = -204,896.4 \text{ lb}$
(in vertical direction (z), length of model is 6 inches)

Expected Load:

Basket weight / length w/o spent fuel:

$$\begin{aligned} &= (18,900 + 1,080) / (181.5 - 0.9) + (983 + 4,790 + 4,370) / (181.5 - 1.25 - 0.9) \\ &= 167.2 \text{ lb/in.} \end{aligned}$$

Basket wt. w/o spent fuel (6 inches long) = (167.2) (6 inches) = 1,003 lb.

Spent fuel weight (6" long) = (11 lb/in) (6-inch length of basket) (37 SFAs)
= 2,442 lb.

Total weight of the basket, with spent fuel (6 inches long) = 1,003 + 2,442 =
3,445 lb (for 1g)

Expected Load at 60g (in vertical direction) = 60 (3,445) = 206,700 lb.

The ANSYS load of 204,896 is very similar to the hand-calculated weight load (within 1%) and therefore, is acceptable.

3.9.2.3.7.2 75g Accident End Drop Loading Calculations

Compressive stress associated with the 75g end drop condition is calculated using conservative loads and geometry. For the 75g end drop load condition, the steel grid plates are assumed to carry their own weight plus the weight of all of the aluminum components. The fuel assembly loads are applied directly to the cover plates/shield plugs of the DSC shell assembly and not to the basket assembly. The basket weight considered below bounds the weight summarized in Chapter 3, Table 3-6. The axial stress calculated below represents the general membrane stress in the steel grid plates. The local bearing and peak stresses at the intersections of the slots are not required to be evaluated for accident conditions. There is no significant out-of-plane bending in the grid plates for the 75g end drop condition.

75g axial load:

$$\sigma_{\text{Axial-75g}} = 75 (W_{\text{basket}}) / A_S \quad (\text{conservative to use full basket weight})$$

$$W_{\text{basket}} = 36.0 \text{ kips (conservative)}$$

Section Area, A_S = summation of plate lengths and thicknesses (from plate details), conservatively excluding slot widths and extensions beyond the last slot of each plate.

$$A_S = 4[0.281"(7)(8.80") + 0.281"(7)(8.80") + 0.281"(5)(8.80") + 0.313"(3)(8.80")]$$

$$= 221.0 \text{ in}^2$$

Therefore,

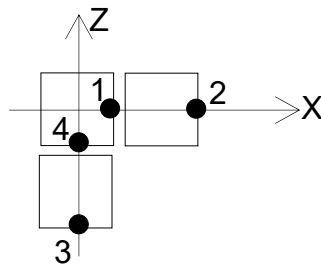
$$\sigma_{\text{Axial-75g}} = 75 (36.0) / 221.0$$

$$= 12.22 \text{ ksi}$$

This stress value is low (below yield), such that the 75g end drop load condition strains do not control and no further evaluation is required.

3.9.2.3.7.3 Adjacent Fuel Compartment Relative Displacements

Maximum relative perpendicular displacement from one fuel compartment plate to another is determined from the ANSYS results for the accident side drops. These differences are addressed in the criticality evaluations to ensure that the fuel assembly array pitch does not significantly change due to the accident side drop. The sketch below indicates the sign convention and typical locations where displacements are extracted.



The relative displacements are calculated as follows:

$$\Delta_{UX} = UX_2 - UX_1$$

$$\Delta_{UZ} = UZ_4 - UZ_3$$

Maximum relative displacements for those adjacent compartments that have moved closer together are tabulated in Table 3.9.2-9. Relative displacements that indicate fuel compartments have moved away from one another are ignored. The summary table includes results for analyses with bolts and tie rods modeled and for analyses without bolts and tie rods modeled.

3.9.2.3.7.4 Conclusions

Finite element analyses and hand calculations for the EOS-37PTH basket assembly are performed for all accident side and end drop on-site conditions. Controlling equivalent plastic strains are reported in Table 3.9.2-7. A comparison of strains to the corresponding allowable values indicates that all load conditions show acceptable results.

As demonstrated in Section 3.9.2.4.6.3, uncontrolled crack propagation in the grid plates is not an issue for the selected HSLA steel material.

3.9.2.4 EOS-89BTH Basket Structural Evaluation for On-Site Accident Drop Loads

This section evaluates the structural integrity of the EOS-89BTH DSC basket for on-site accident side and end drop loads. On-site transfer conditions in the EOS-TC108, EOS-TC125, or EOS-TC135 are considered for thermal properties used in the side drop load analyses.

3.9.2.4.1 General Description

Same as Section 3.9.2.2.1.

3.9.2.4.2 Key Dimensions and Materials

Same as Section 3.9.2.2.2.

3.9.2.4.3 Material Properties

Same as Section 3.9.2.2.3.

3.9.2.4.4 Temperature Data

Same as Section 3.9.2.2.4.

3.9.2.4.5 Fuel Data

Chapter 2 provides design characteristics for the types of BWR FAs to be considered. A maximum FA weight of 705 lbs is used. A distributed weight of 705 lbs / 150 in. = 4.7 lbs/in is considered to be bounding in the active fuel region for the on-site accident side drop analyses.

3.9.2.4.6 Methodology

ANSYS 10.0A1 and 17.1 [3.9.2-2] are used for the evaluation of on-site accident side drop loads. Hand calculations are performed to conservatively calculate the stresses due to the on-site axial end drop loads. Stresses due to the end drop loads are not controlling. Therefore, only the side drop load analysis results are presented.

3.9.2.4.6.1 Finite Element Model

3.9.2.4.6.1.1 Analysis Model Description for Side Loads

Geometry plots of the ANSYS model are shown in Figure 3.9.2-12 through Figure 3.9.2-18. All other details of the analysis model description are the same as Section 3.9.2.3.6.1.1.

3.9.2.4.6.1.2 Material Properties in Analyses

Same as Section 3.9.2.3.6.1.2.

3.9.2.4.6.1.3 Loads

Load cases are based on the loads described in Chapter 2.

A 65 inch side drop is considered in various orientations to ensure the adequacy of the design under on-site accident side drop conditions. A side drop load of 60g is evaluated to bound the acceleration predicted in Appendix 3.9.3. A 75g end drop is also considered to conservatively envelop the effects of a 65 inch corner drop.

For side loading, the fuel weight load is modeled conservatively using a pressure load equivalent to the applicable acceleration, or G-load, times the fuel assembly weight divided by the basket fuel compartment area associated with the active fuel region length and the fuel compartment width between slots (5.85 inches). A fuel load of 4.7 lbs/in acting on the fuel compartment width between slots is applied to bound the load distribution in the active fuel region for all BWR fuel types. Figure 3.9.2-19 shows the application of fuel weight pressure loads to the model (for a 180° side drop orientation).

For 0° and 180° side load orientations, the equivalent fuel assembly pressure acts only on the horizontal plates. For 90° and 270° side load orientations, the equivalent fuel assembly pressure acts only on the vertical plates. For other orientations, the equivalent fuel assembly pressure acts perpendicular to the horizontal and vertical plates, proportioned based on the Cosine and Sine of the orientation angle.

The following accident side drop load conditions (DSC and basket in horizontal position) are evaluated *for the rail configuration associated with the EOS-TC108*:

- 180° Side Drop on Rails
(due to symmetry, this also covers the 0° Side Drop)
- 270° Side Drop away from Rails
(due to symmetry, this also covers the 90° Side Drop)
- 225° Side Drop on Rails
(due to symmetry, this also covers other multiples of 45° Side Drop)

Side drop load conditions were also evaluated for the rail configuration associated with the EOS-TC125/135 and were found to not control.

3.9.2.4.6.2 Criteria

The basis for allowable strains is obtained from Chapter 8. The strain criteria are discussed and summarized in Section 3.1.1.1.1.

The basket grid plate strain criteria are summarized in Table 3.9.2-5. The threaded fasteners, used to connect the transition rails to the basket grid structure, are not required to be evaluated because they are considered to fail (with analyses and calculations confirming that they are not needed for accident condition drops).

Proprietary Information on This Page
Withheld Pursuant to 10 CFR 2.390

3.9.2.4.7 Results

3.9.2.4.7.1 Results for Analysis of 60g Accident Side Loading

60g accident side drop loads are analyzed using the ANSYS model described in Section 3.9.2.4.6.1.1. Accident condition equivalent static elastic-plastic analyses are performed for computing the equivalent plastic strains.

The fuel weight load is modeled conservatively using a pressure load equivalent to the applicable acceleration, or G-load, times the maximum fuel assembly weight per length (4.7 lbs/in) divided by the fuel compartment width (5.85 inches).

At the 180° side load orientation, the equivalent 1g fuel assembly pressure, acting only on the horizontal plates, P_{180h} , is calculated as follows:

$$P_{180h} = 4.7 \text{ lbs/in} / (5.85 \text{ inches}) = 0.8034 \text{ psi}$$

At the 270° side load orientation, 1g acting only on the vertical plates:

$$P_{270v} = 4.7 \text{ lbs/in} / (5.85 \text{ inches}) = 0.8034 \text{ psi}$$

At 225° (45 degrees from bottom), 1g acting on the horizontal and vertical plates:

$$P_{225h} = P_{225v} = P_{180h} \sin(45^\circ) = 0.5681 \text{ psi}$$

The ANSYS unit (1g) accelerations, indicating direction of load, are:

180-degree	acel, 0, 0, 1
270-degree	acel, 1, 0, 0
225-degree	acel, 0.7071, 0, 0.7071

For side load analyses, the equivalent fuel assembly pressure loads and accelerations above are multiplied by the corresponding side load acceleration value (e.g., 60g).

Displacements, stresses, strains and forces for each converged load step are saved to ANSYS files.

Basket grid plate equivalent plastic strain results for accident condition 60g side drop loads are shown in Table 3.9.2-10. Results with controlling strain ratios are shown in Table 3.9.2-11. ANSYS strain contour plots corresponding to the bounding equivalent plastic strain values are shown in Figure 3.9.2-24 and Figure 3.9.2-25. The tabulated results show that all strains meet the corresponding allowable strain limits. As demonstrated in Section 3.9.2.4.6.3, uncontrolled crack propagation in the grid plates is not an issue for the selected HSLA steel material.

Analyses are run to 75g. The program stops at the load substep that fails to result in a converged solution, if convergence to 75g does not occur. The last converged load step is considered the buckling load. The buckling load values are compared with 60g, the required g-load for accident conditions, with results shown in Table 3.9.2-8. All analyses complete the 75g load step.

Stresses and strains in the aluminum basket transition rails are not explicitly evaluated. All analyzed drop conditions include the case where the connecting bolts and tie rods are assumed to fail, to demonstrate that the connection to the aluminum is not needed to maintain basket strains within the allowable strain limits. Therefore, the only significant stress in the basket aluminum rails is a bearing type stress where the transition rail is compressed between the basket grid plates and the inside surface of the EOS-DSC. Since bearing stresses are not required to be evaluated for accident conditions, no further evaluation of the basket transition rails is required.

ANSYS Force Summation Comparison

An ANSYS force summation for the basket components only, for the 60g side drop, is compared to the expected load as shown below:

From the ANSYS results for the 60g load step:

Force Summation: $F_z = -207,687.2 \text{ lb}$
(in vertical direction (z), length of model is 6 inches)

Expected Load:

Basket weight / length w/o spent fuel:

$$= (19,300 + 637 + 1,110 + 3,980) / 166.0 + 1,720 / 175.0$$

$$= 160.6 \text{ lb/in}$$

$$\text{Basket wt. w/o spent fuel (6 inches long)} = (160.6) (6 \text{ inches}) = 964 \text{ lb.}$$

$$\text{Spent fuel weight (6 inches long)} = (4.7 \text{ lb/in}) (6\text{-inch length of basket}) (89 \text{ SFAs}) = 2,510 \text{ lb.}$$

Total weight of the basket, with spent fuel (6 inches long) = $964 + 2,510 = 3,474$ lb (for 1g)

Expected Load at 60g (in vertical direction) = $60 (3,474) = 208,440$ lb.

The ANSYS load of 207,687 is very similar to the hand-calculated weight load (within 0.4%) and therefore, is acceptable.

3.9.2.4.7.2 75g Accident End Drop Loading Calculations

Compressive stress associated with the 75g end drop condition is calculated using conservative loads and geometry. For the 75g end drop load condition, the steel grid plates are assumed to carry their own weight plus the weight of all of the aluminum components. The fuel assembly loads are applied directly to the cover plates/shield plugs of the DSC shell assembly and not to the basket assembly. The basket weight considered below bounds the weight summarized in Chapter 3, Table 3-7. The axial stress calculated below represents the general membrane stress in the steel grid plates of the holddown ring, for which the plate cross-sectional area is less than other sections of the basket. The local bearing and peak stresses at the intersections of the slots are not required to be evaluated for accident conditions. There is no significant out-of-plane bending in the grid plates for the 75g end drop condition.

75g axial load:

$$\sigma_{\text{Axial-75g}} = 75 (W_{\text{basket}}) / A_S \quad (\text{conservative to use full basket weight})$$

$$W_{\text{basket}} = 32.0 \text{ kips (conservative)}$$

Section Area, A_S = summation of plate lengths and thicknesses

The shortest length (top or bottom) of each holddown ring plate is considered, rounded down to the nearest tenth of an inch. The area is reduced by 10% to conservatively account for slots.

$$\begin{aligned} A_S &= 0.90(2)[0.250"(69.9") + 0.1875"(46.7") + 0.250"(69.9") + 0.250"(44.8") + \\ &\quad 0.250"(19.1") + 0.250"(19.1")] \\ &= 116.0 \text{ in}^2 \end{aligned}$$

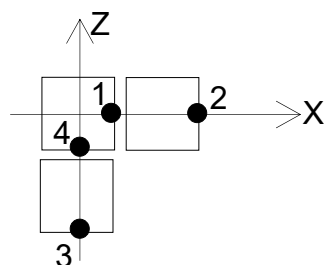
Therefore,

$$\begin{aligned} \sigma_{\text{Axial-75g}} &= 75 (32.0) / 116.0 \\ &= 20.69 \text{ ksi} \end{aligned}$$

This stress value is low (below yield), such that the 75g end drop load condition strains do not control and no further evaluation is required.

3.9.2.4.7.3 Adjacent Fuel Compartment Relative Displacements

Maximum relative perpendicular displacement from one fuel compartment plate to another is determined from the ANSYS results for the accident side drops. These differences are addressed in the criticality evaluations to ensure that the fuel assembly array pitch does not significantly change due to the accident side drop. The sketch below indicates the sign convention and typical locations where displacements are extracted.



The relative displacements are calculated as follows:

$$\Delta_{UX} = UX_2 - UX_1$$

$$\Delta_{UZ} = UZ_4 - UZ_3$$

Maximum relative displacements for those adjacent compartments that have moved closer together are tabulated in Table 3.9.2-13. Relative displacements that indicate fuel compartments have moved away from one another are ignored. The summary table includes results for analyses with bolts and tie rods modeled and for analyses without bolts and tie rods modeled.

3.9.2.4.7.4 Conclusions

Finite element analyses and hand calculations for the EOS-89BTH basket assembly are performed for all accident side and end drop on-site conditions. Controlling strains are reported in Table 3.9.2-11. A comparison of equivalent plastic strains to the corresponding allowable values indicates that all load conditions show acceptable results.

As demonstrated in Section 3.9.2.4.6.3, uncontrolled crack propagation in the grid plates is not an issue for the selected HSLA steel material.

3.9.2.5 References

- 3.9.2-1 American Society of Mechanical Engineers, "ASME Boiler and Pressure Vessel Code," Section III, Division 1, Subsection NG, 2010 Edition thru 2011 Addenda.
- 3.9.2-2 ANSYS Computer Code and User's Manual, Release 10.0 and 17.1.

- 3.9.2-3 AREVA TN Technical Report, "Evaluation of Creep of NUHOMS® Basket Aluminum Components under Long Term Storage Conditions," E-25768, Rev. 0 (Structural Integrity Associates, Inc. File No. TNI-20Q-302, Rev. 0).
- 3.9.2-4 NUREG/CR-1815, "Recommendations for Protecting Against Failure by Brittle Fracture in Ferritic Steel Shipping Containers Up to Four Inches Thick," U.S. Nuclear Regulatory Commission, June 1981.
- 3.9.2-5 [

Table 3.9.2-1
Threaded Fastener Stress Design Criteria (Normal / Off-Normal)

Stress Category	Allowable Stresses
	Normal / Off-Normal ⁽¹⁾
Primary + Secondary Membrane $P_m + Q_m^{(2)}$	$\min(0.9 S_y, 2/3 S_u)$
Primary + Secondary Shear $P_m + Q_m^{(3)(6)}$	$0.6 S_y$
Primary + Secondary Bearing $P_m + Q_m^{(4)}$	$2.7 S_y$
Primary Membrane $P_m^{(2)}$	S_m
Primary Shear $P_m^{(3)}$	$0.6 S_m$
Primary + Secondary Membrane + Bending $P_m + Q_m + P_b + Q_b^{(5)(6)}$	$\min(1.2 S_y, 8/9 S_u)$

- (1) Classification and stress limits are as defined in ASME Code, Section III, Subsection NG [3.9.2-1].
- (2) Averaged stress intensity on tensile stress area at threaded section.
- (3) Averaged stress across shear area of threaded section.
- (4) Averaged bearing stress under the fastener head.
- (5) Stress intensity, excluding effects of stress concentrations.
- (6) Not applicable to this evaluation; no significant thermal shear due to oversized/slotted holes, and no significant bending.

Table 3.9.2-2
Component Allowable Stresses (Normal / Off-Normal)

Component	Material	Temp. (°F)	Stress Category	Allowable Stress (ksi)
Steel Grid Plates	HSLA steel such as AISI 4130	700	P_m	24.96
			$P_m + P_b$	37.43
			$P_m + P_b + Q$	74.87
Rail Angle Plates	SA-516 Grade 70	550	P_m	20.00
			$P_m + P_b$	30.00
			$P_m + P_b + Q$	60.00
Transition Rails	Aluminum 6061	550	$P_m + P_b$	4.85
			$P_m + P_b + Q$	9.70
Bolts ⁽¹⁾	<i>A 564 Type 630 H1100</i>	550	Tension, P_m	44.15
			Tension, $P_m + Q_m$	84.56
			Shear, P_m	26.49
Tie Rods	<i>A 564 Type 630 H1100</i>	550	Tension, P_m	44.15
			Tension, $P_m + Q_m$	84.56

- (1) For basket side loading, only tension loads are transferred through the bolts and tie rods due to oversized/slotted bolts holes that allow for thermal expansion.

Table 3.9.2-3
EOS-37PTH Basket Stress Summary – Enveloped DW + Handling + Thermal

Load Combination	Component	Stress Category	Maximum Stress (ksi) ⁽¹⁾	Allowable Stress (ksi)	Stress Ratio
Enveloping Results for Normal Conditions in the EOS-TC	Grid Plates ⁽³⁾	P_m	$4.61+0.25=4.86$	24.96	0.195
		$P_m + P_b$	$23.95+0.25=24.20$	37.43	0.647
		$P_m + P_b + Q$	31.94	74.87	0.427
	Angle Plates	P_m	3.56	20.00	0.178
		$P_m + P_b$	4.63	30.00	0.154
		$P_m + P_b + Q$	12.75	60.00	0.213
	Transition Rails	$P_m + P_b$	2.72	4.85	0.560
		$P_m + P_b + Q$	8.57	9.70	0.883
	Bolts ⁽²⁾⁽⁴⁾	P_m	12.24	44.15	0.277
		$P_m + Q_m$	44.61	84.56	0.527
	Tie Rods ⁽²⁾	P_m	7.32	44.15	0.166
		$P_m + Q_m$	14.87	84.56	0.176

- (1) $P_m + P_b + Q$ values are determined using ANSYS load combinations.
- (2) Bolt and tie rod stresses listed are increased for the reduced area at the threads.
- (3) Grid plate stresses include hand calculated stresses for 0.5g axial, where controlled by the DW + (0.5g Vert., 0.5g Trans., 0.5g Ax.) Handling load combination.
- (4) Bolt maximum shear stress is $14.84 < 17.37$, with a stress ratio of 0.854 per conservative hand calculation for axial handling.

Table 3.9.2-4
EOS-89BTH Basket Stress Summary – Enveloped DW + Handling + Thermal

Load Combination	Component	Stress Category	Maximum Stress (ksi) ⁽¹⁾	Allowable Stress (ksi)	Stress Ratio
Enveloping Results for Normal Conditions in the EOS-TC	Grid Plates ⁽³⁾	P_m	4.30	24.96	0.172
		$P_m + P_b$	$17.11 + 0.42 = 17.53$	37.43	0.468
		$P_m + P_b + Q$	$23.23 + 0.42 = 23.65$	74.87	0.316
	Angle Plates	P_m	1.77	20.00	0.088
		$P_m + P_b$	2.58	30.00	0.086
		$P_m + P_b + Q$	12.52	60.00	0.209
	Transition Rails	$P_m + P_b$	4.47	4.85	0.921
		$P_m + P_b + Q$	11.77	9.70	1.214 ⁽⁴⁾
	Bolts ⁽²⁾⁽⁵⁾	P_m	6.15	28.95	0.212
		$P_m + Q_m$	24.47	78.21	0.313
	Tie Rods ⁽²⁾	P_m	2.99	28.95	0.103
		$P_m + Q_m$	8.59	78.21	0.110

- (1) $P_m + P_b + Q$ values are determined using ANSYS load combinations.
- (2) Bolt and tie rod stresses listed are increased for the reduced area at the threads.
- (3) Grid plate stresses include hand calculated stresses for 0.5g axial, where controlled by the DW + (0.5g Vert., 0.5g Trans., 0.5g Ax.) Handling load combination.
- (4) This level of stress occurs only at very small locations at locations of bolts, and they are considered to be peak stresses. In addition, most of this stress is due to thermal, occurs during initial heat-up, is not cyclic and therefore, is not a fatigue concern. Stresses away from these small areas are significantly lower and well within the allowable stress.
- (5) Bolt maximum shear stress is $14.92 < 17.37$, with a stress ratio of 0.859 per conservative hand calculation for axial handling.

Table 3.9.2-5
Basket Grid Plate Accident Drop Strain Design Criteria

Strain Category	Allowable Strains ⁽²⁾
	Accident ⁽¹⁾
Primary Membrane ϵ_m	1.0%
Primary Membrane + Bending $\epsilon_m + \epsilon_b$	3.0%
Primary + Peak $\epsilon_m + \epsilon_b + \epsilon_F$	10.0% ⁽³⁾
Compression or Buckling	Note 4

- (1) Basket strain limits are described in Chapter 3.
- (2) Equivalent plastic strain limits.
- (3) Membrane + bending equivalent plastic strains determined from the analyses conservatively include peak equivalent plastic strain, such that the limit on primary + peak does not need to be evaluated.
- (4) Determine the buckling load for each postulated drop orientation to demonstrate that the basket does not buckle within maximum drop load of 60g. Report the safety margin.

Table 3.9.2-6
EOS-37PTH Basket Grid Plate Strain Summary – Side Drops
with and without Bolts and Tie Rods

Side Drop Load Case ⁽³⁾	Fastener Status	Strain ⁽¹⁾ Category	Maximum Strain (in/in)	Allowable Strain (in/in)
60g, 180 deg. Side Drop	with Bolts/Tie Rods	ϵ_m	0.00000	0.01
		$\epsilon_m + \epsilon_b$	0.00797	0.03
	without ⁽²⁾ Bolts/Tie Rods	ϵ_m	0.00000	0.01
		$\epsilon_m + \epsilon_b$	0.00834	0.03
60g, 0 deg. Side Drop	with Bolts/Tie Rods	ϵ_m	0.00000	0.01
		$\epsilon_m + \epsilon_b$	0.00881	0.03
	without ⁽²⁾ Bolts/Tie Rods	ϵ_m	0.00000	0.01
		$\epsilon_m + \epsilon_b$	0.00809	0.03
60g, 45 deg. Side Drop	with Bolts/Tie Rods	ϵ_m	0.00000	0.01
		$\epsilon_m + \epsilon_b$	0.00485	0.03
	without ⁽²⁾ Bolts/Tie Rods	ϵ_m	0.00000	0.01
		$\epsilon_m + \epsilon_b$	0.00434	0.03

- (1) Equivalent plastic strain.
- (2) Bolts and tie rods are removed from the model for this analysis, assuming that they fail.
- (3) Controlling load cases (Drop on TC125/135 rails).

Table 3.9.2-7
EOS-37PTH Basket Grid Plate Strain Summary – Enveloped Accident
Conditions

Load Combination	Strain ⁽¹⁾ Category	Maximum Strain (in/in)	Allowable Strain (in/in)	Strain Ratio
Enveloping Results for Accident Conditions in the EOS-TC	ε_m	0.00000	0.01	0.000
	$\varepsilon_m + \varepsilon_b$	<i>0.00881</i>	0.03	<i>0.294</i>

(1) Equivalent plastic strain.

Table 3.9.2-8
EOS-37PTH Basket Buckling Analysis Results Summary

Load Condition ⁽²⁾	Last Converged Load (G)	Actual Max. Load (G)	Factor of Safety
60g 180 deg. drop, with bolts & tie rods	75.0 ⁽¹⁾	60.0	1.25
60g 0 deg. drop, with bolts & tie rods	75.0 ⁽¹⁾	60.0	1.25
60g 45 deg. drop, with bolts & tie rods	75.0 ⁽¹⁾	60.0	1.25
60g 180 deg. drop, without bolts & tie rods	75.0 ⁽¹⁾	60.0	1.25
60g 0 deg. drop, without bolts & tie rods	75.0 ⁽¹⁾	60.0	1.25
60g 45 deg. drop, without bolts & tie rods	75.0 ⁽¹⁾	60.0	1.25

(1) A maximum load of 75g was applied. Therefore, the buckling load and factor of safety may be greater.

(2) Controlling load conditions (Drop on TC125/135 rails).

Table 3.9.2-9
EOS-37PTH Basket Maximum Adjacent Fuel Compartment Relative Displacements

Load Condition	Drop Orientation ⁽²⁾	Maximum Absolute Relative Displacement (in) ⁽¹⁾			
		With Bolts & Tie Rods		Without Bolts & Tie Rods	
		Δ_{UX}	Δ_{UZ}	Δ_{UX}	Δ_{UZ}
60g Accident Side Drop	180°	0.039726	0.078975	0.062991	0.083127
	270°	0.075675	0.056695	0.077194	0.046207
	225°	0.072454	0.079197	0.072620	0.079586

- (1) For displacements that indicate fuel compartments have moved closer together. Obtained from results for the 60g load step.
- (2) Controlling drop orientations (Drop on TC125/135 rails)..

Table 3.9.2-10
EOS-89BTH Basket Grid Plate Strain Summary – Side Drops
with and without Bolts and Tie Rods

Side Drop Load Case	Fastener Status	Strain ⁽¹⁾ Category	Maximum Strain (in/in)	Allowable Strain (in/in)
60g, 180 deg. Side Drop	with Bolts/Tie Rods	ϵ_m	0.00000	0.01
		$\epsilon_m + \epsilon_b$	0.00595	0.03
	without ⁽²⁾ Bolts/Tie Rods	ϵ_m	0.00000	0.01
		$\epsilon_m + \epsilon_b$	0.00611	0.03
60g, 270 deg. Side Drop	with Bolts/Tie Rods	ϵ_m	0.00049	0.01
		$\epsilon_m + \epsilon_b$	0.00498	0.03
	without ⁽²⁾ Bolts/Tie Rods	ϵ_m	0.00000	0.01
		$\epsilon_m + \epsilon_b$	0.00491	0.03
60g, 225 deg. Side Drop	with Bolts/Tie Rods	ϵ_m	0.00000	0.01
		$\epsilon_m + \epsilon_b$	0.00264	0.03
	without ⁽²⁾ Bolts/Tie Rods	ϵ_m	0.00000	0.01
		$\epsilon_m + \epsilon_b$	0.00229	0.03

(1) Equivalent plastic strain.

(2) Bolts and tie rods are removed from the model for this analysis, assuming that they fail.

Table 3.9.2-11
EOS-89BTH Basket Grid Plate Strain Summary – Enveloped Accident
Conditions

Load Combination	Strain ⁽¹⁾ Category	Maximum Strain (in/in)	Allowable Strain (in/in)	Strain Ratio
Enveloping Results for Accident Conditions in the EOS-TC	ϵ_m	0.00049	0.01	0.049
	$\epsilon_m + \epsilon_b$	0.00611	0.03	0.204

(1) Equivalent plastic strain.

Table 3.9.2-12
EOS-89BTH Basket Buckling Analysis Results Summary

Load Condition	Last Converged Load (G)	Actual Max. Load (G)	Factor of Safety
60g 180 deg. drop, with bolts & tie rods	75.0 ⁽¹⁾	60.0	1.25
60g 270 deg. drop, with bolts & tie rods	75.0 ⁽¹⁾	60.0	1.25
60g 225 deg. drop, with bolts & tie rods	75.0 ⁽¹⁾	60.0	1.25
60g 180 deg. drop, without bolts & tie rods	66.975	60.0	1.12
60g 270 deg. drop, without bolts & tie rods	75.0 ⁽¹⁾	60.0	1.25
60g 225 deg. drop, without bolts & tie rods	75.0 ⁽¹⁾	60.0	1.25

(1) A maximum load of 75g was applied. Therefore, the buckling load and factor of safety may be greater.

Table 3.9.2-13
EOS-89BTH Basket Maximum Adjacent Fuel Compartment Relative Displacements

Load Condition	Drop Orientation	Maximum Absolute Relative Displacement (in) ⁽¹⁾			
		With Bolts & Tie Rods		Without Bolts & Tie Rods	
		Δ_{UX}	Δ_{UZ}	Δ_{UX}	Δ_{UZ}
60g Accident Side Drop	180°	0.021608	0.045477	0.022232	0.056033
	270°	0.032627	0.040907	0.040814	0.022854
	225°	0.031594	0.041521	0.027013	0.042423

- (1) For displacements that indicate fuel compartments have moved closer together. Obtained from results for the 60g load step.

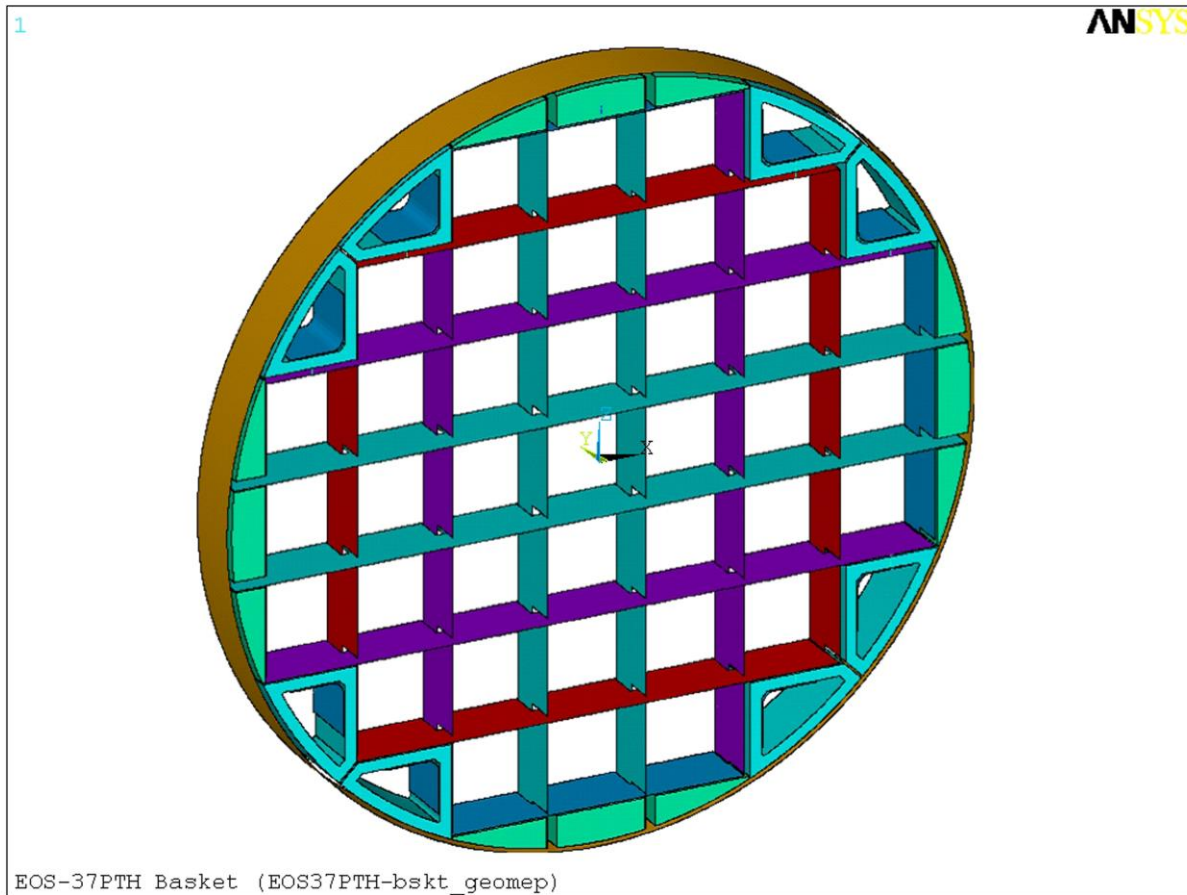


Figure 3.9.2-1
EOS-37PTH Basket Assembly ANSYS .Model (Components Only)
– Isometric View



Figure 3.9.2-2
EOS-37PTH Basket Assembly ANSYS Model (Components Only)
– Isometric View
Upper-Left Quadrant

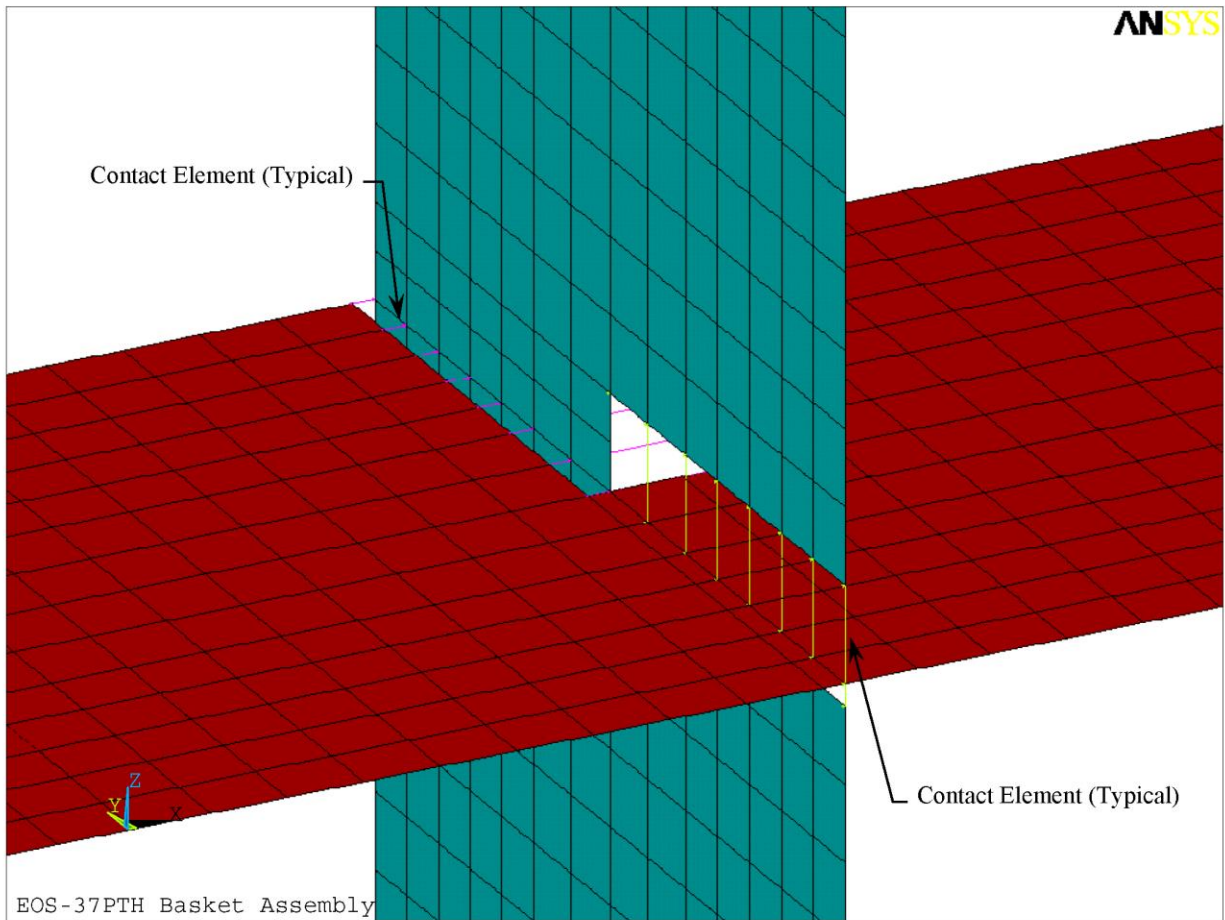


Figure 3.9.2-3
EOS-37PTH Basket Assembly Typical Grid Plate Intersection



Figure 3.9.2-4
EOS-37PTH Basket Assembly ANSYS Model (Components Only) – Front View



Figure 3.9.2-5
EOS-37PTH Basket Assembly ANSYS Model (Plate Thicknesses)
Lower Right Quadrant



Figure 3.9.2-6
EOS-37PTH Basket Assembly ANSYS Model (with Contact Elements) –
Lower Right Quadrant



Figure 3.9.2-7
EOS-37PTH Basket Assembly ANSYS Model
–Transition Rail Bolt and Tie Rod Locations

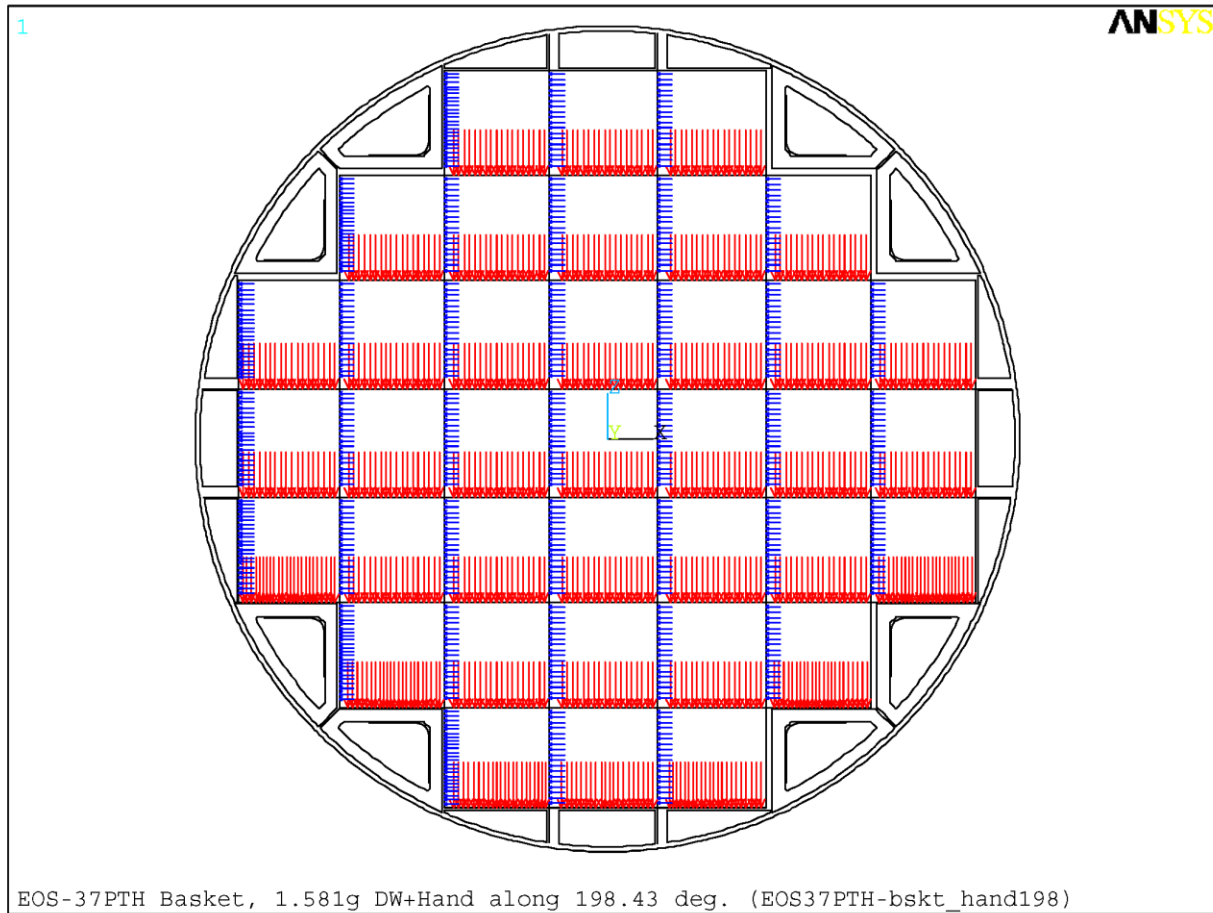


Figure 3.9.2-8
EOS-37PTH Basket Assembly ANSYS Model – Fuel Load Applied as Pressure

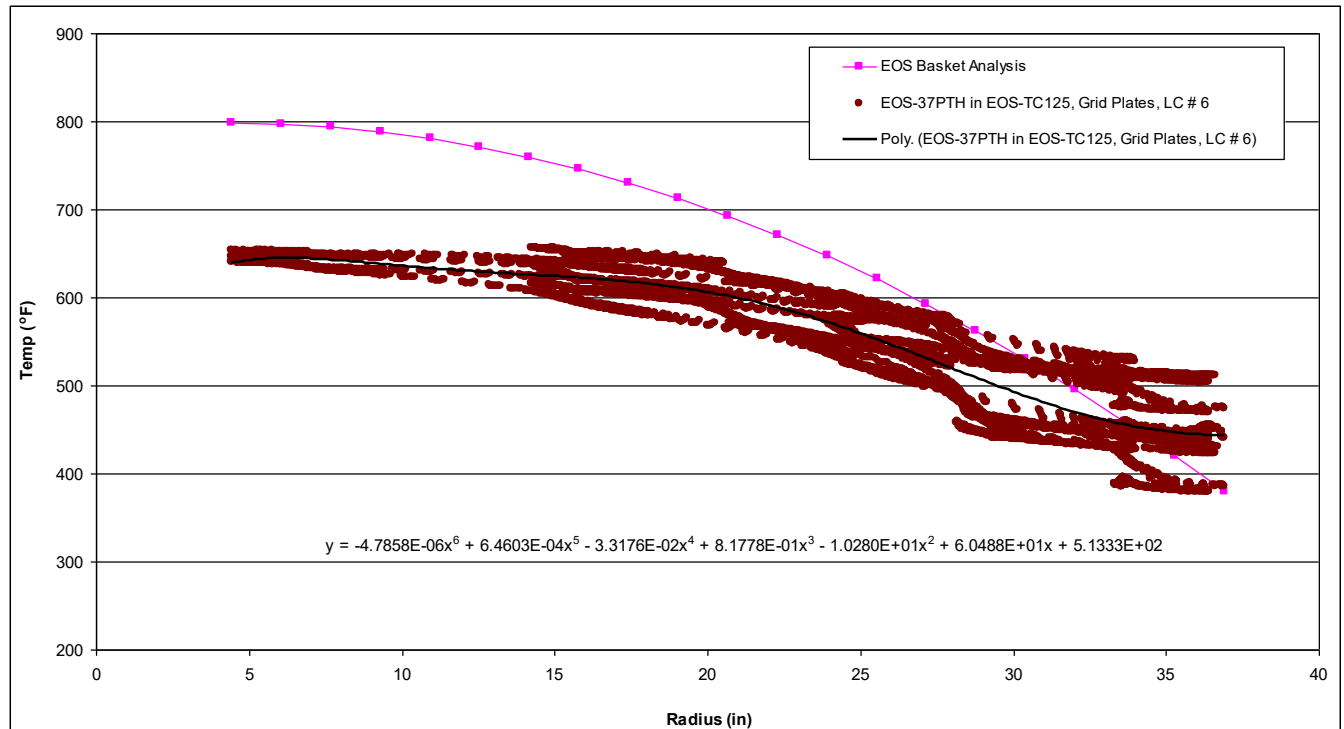


Figure 3.9.2-9
Comparison of Applied Temperature Profile to Data from Thermal Analysis
for EOS-37PTH Basket Plates – Hottest Cross-Section,
LC # 6, Horizontal, Off-Normal Hot Transfer in EOS-TC125, Outdoor

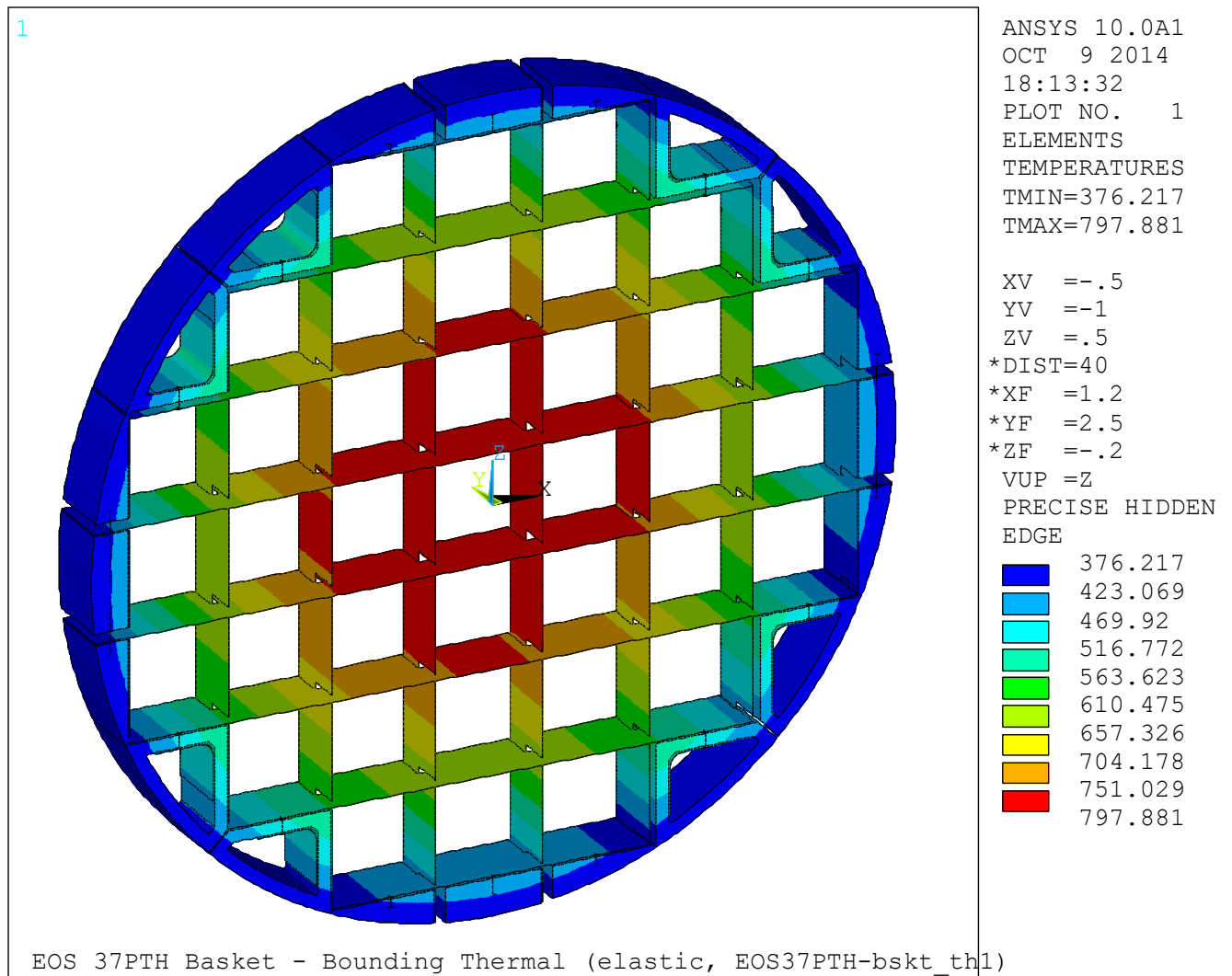


Figure 3.9.2-10
EOS-37PTH Basket Assembly ANSYS Model – Applied Bounding Thermal Profile

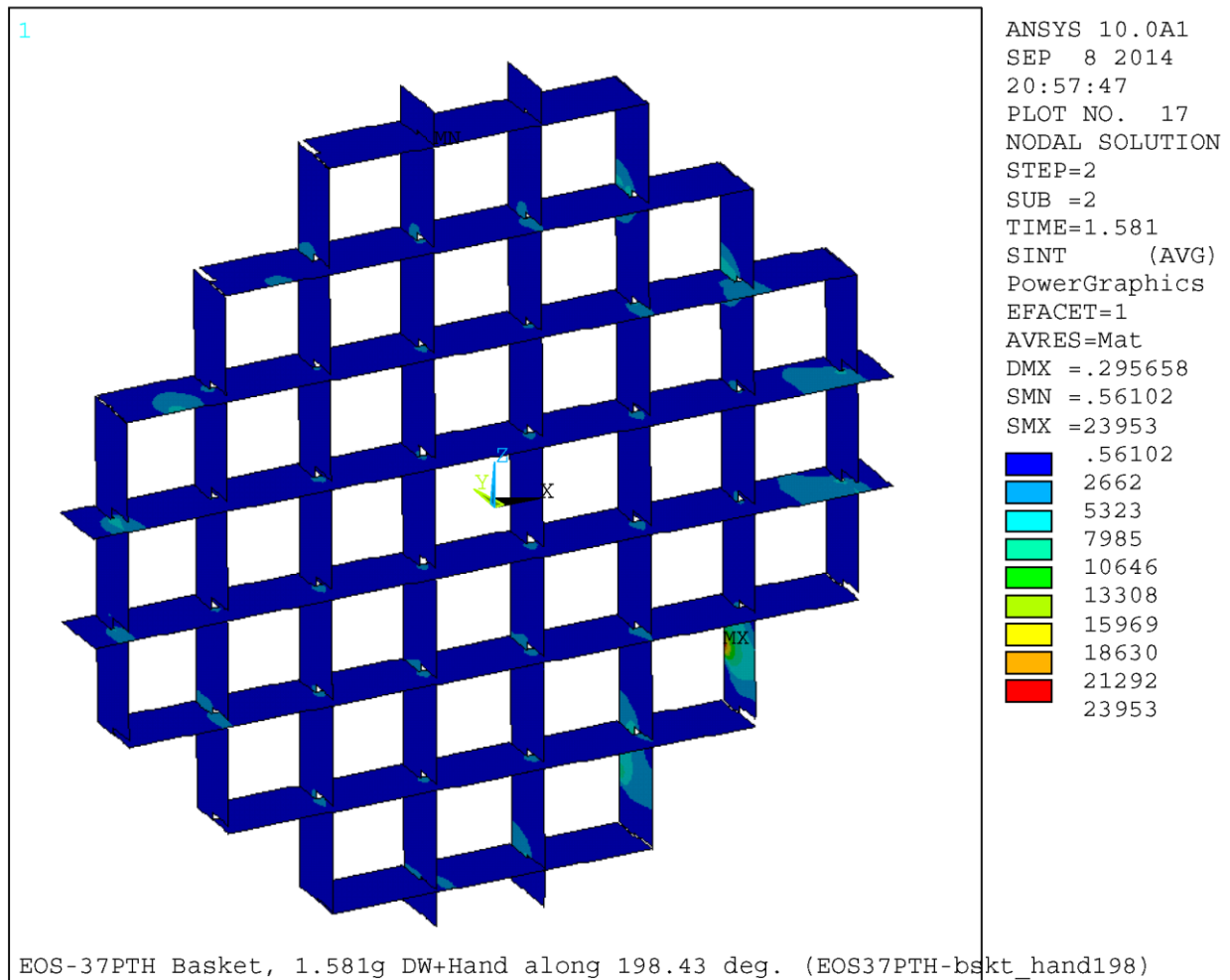


Figure 3.9.2-11
EOS-37PTH Basket 198.43 Degree 1.581g, DW + Handling
– Grid Plates, $P_m + P_b$ (stress intensity, psi)

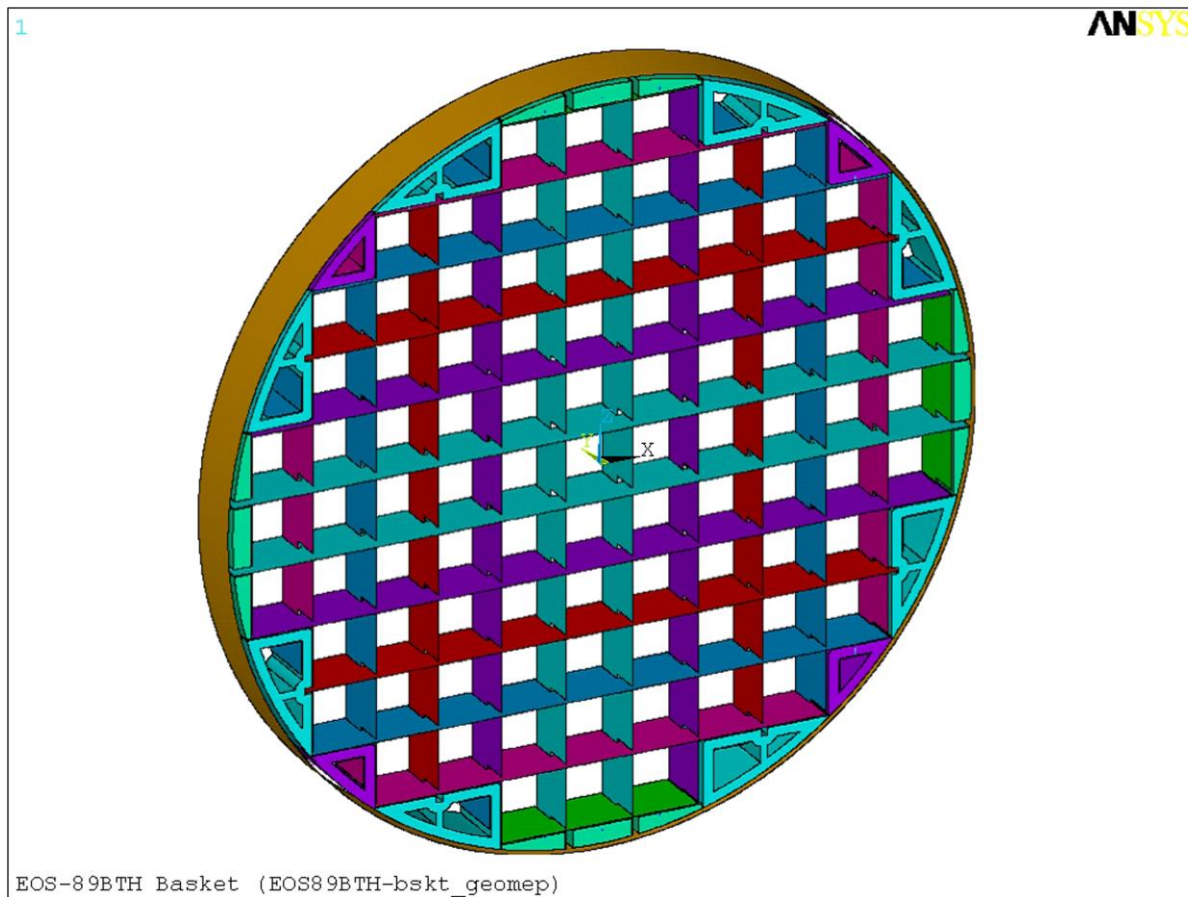


Figure 3.9.2-12
EOS-89BTH Basket Assembly ANSYS Model (Components Only) –
Isometric View




Figure 3.9.2-13
EOS-89BTH Basket Assembly ANSYS Model (Components Only) –
Isometric View –
Upper-Left Quadrant

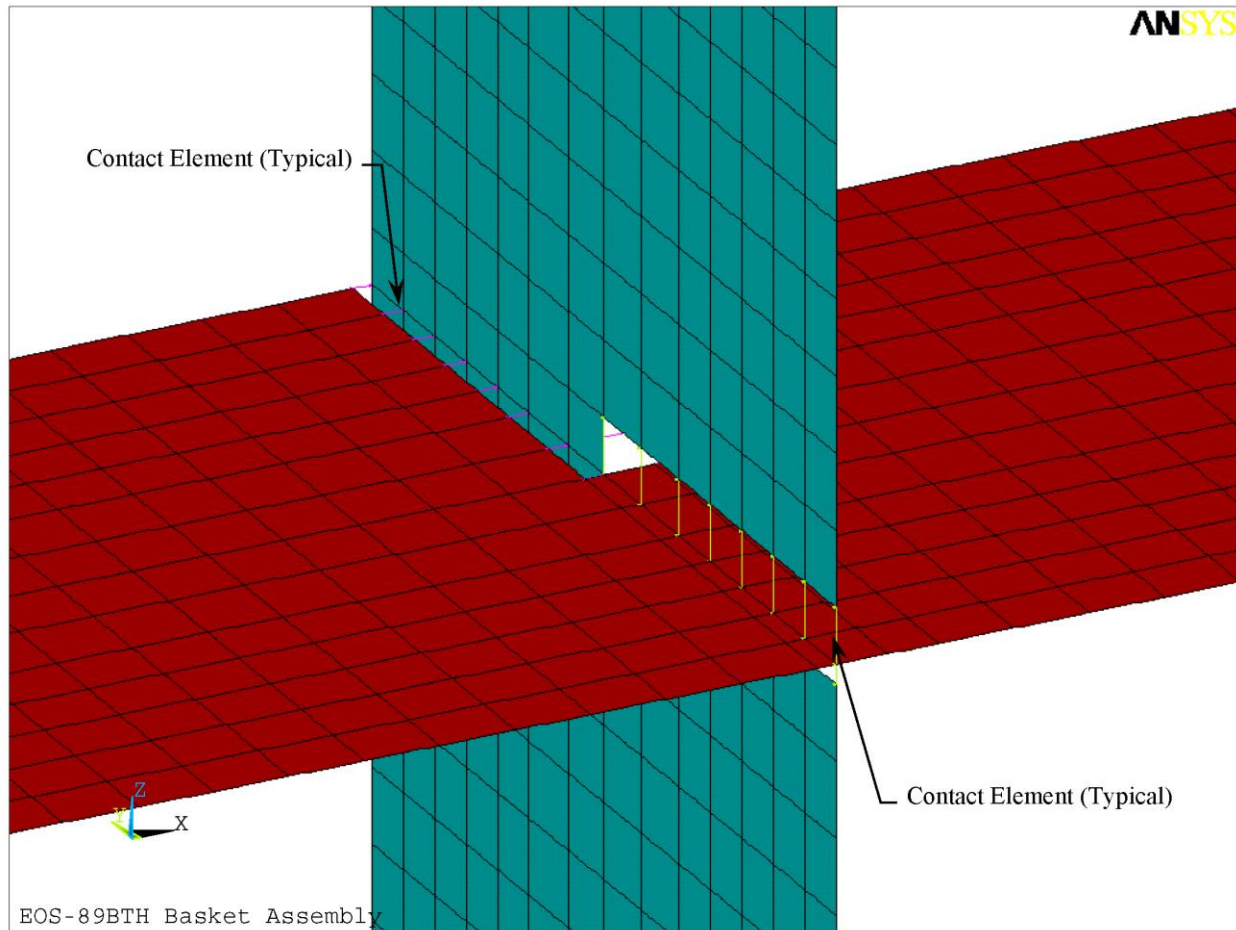


Figure 3.9.2-14
EOS-89BTH Basket Assembly Typical Grid Plate Intersection



Figure 3.9.2-15
EOS-89BTH Basket Assembly ANSYS Model (Components Only) – Front View



Figure 3.9.2-16
EOS-89BTH Basket Assembly ANSYS Model (Plate Thicknesses) –
Lower Right Quadrant



Figure 3.9.2-17
EOS-89BTH Basket Assembly ANSYS Model (with Contact Elements) –
Lower Right Quadrant

Figure 3.9.2-18
EOS-89BTH Basket Assembly ANSYS Model –
Transition Rail Bolt and Tie Rod Locations

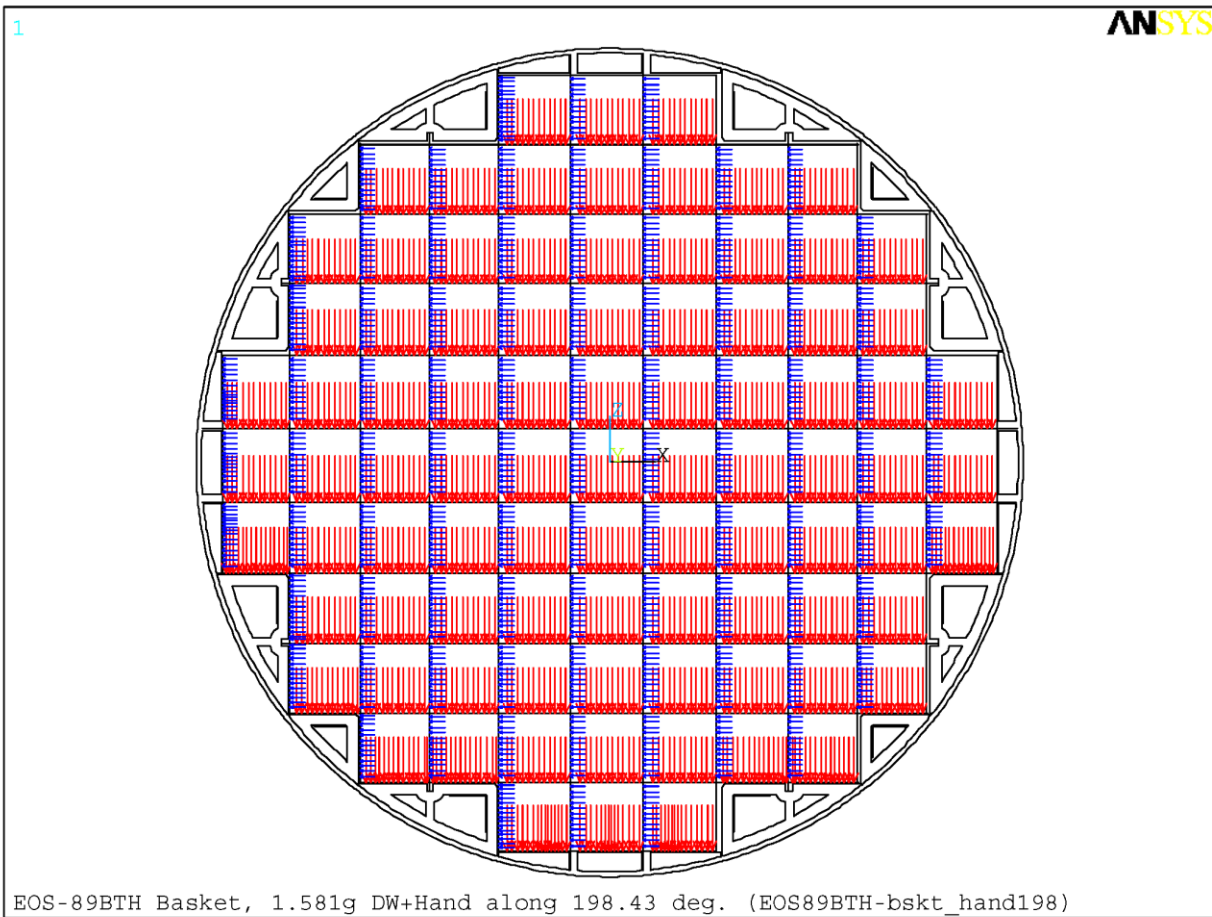


Figure 3.9.2-19
EOS-89BTH Basket Assembly ANSYS Model – Fuel Load Applied as Pressure

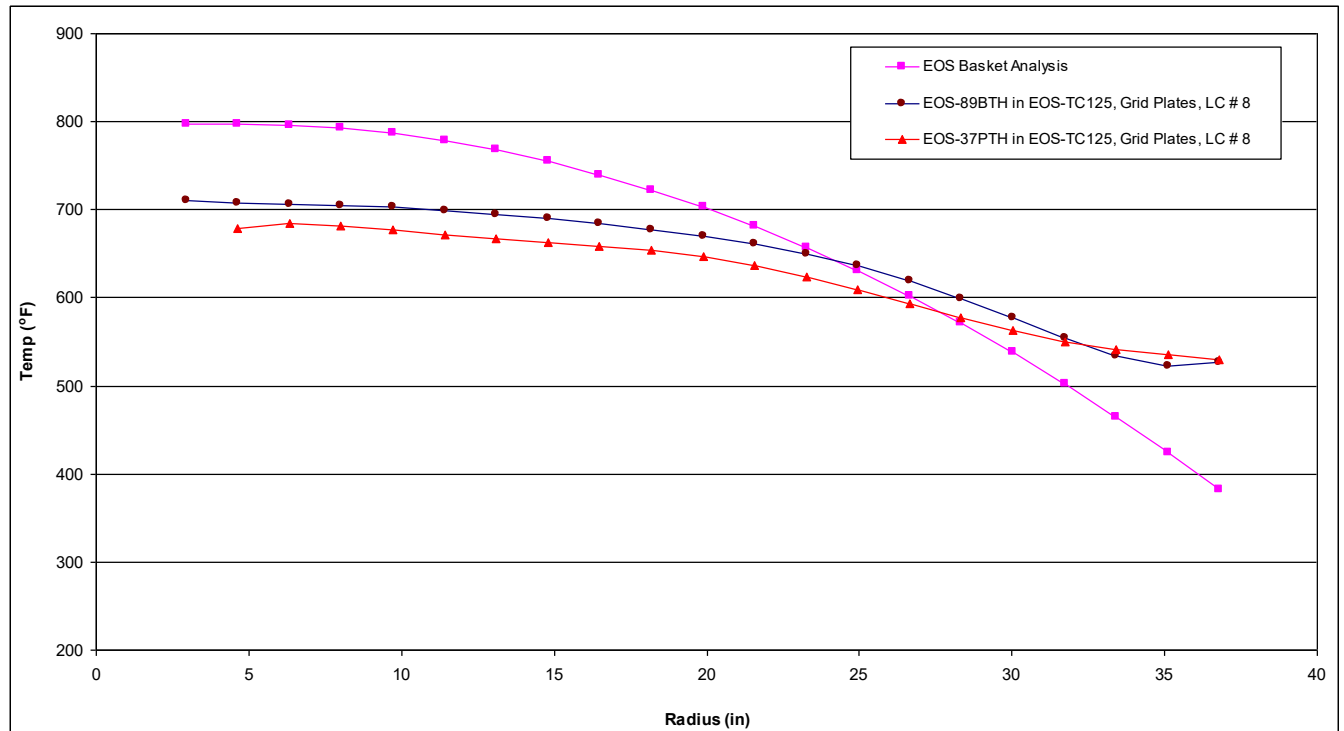


Figure 3.9.2-20
Comparison of EOS-89BTH and EOS-37PTH Temperatures (Curve Fits)
LC # 8, Vertical, Normal Hot Transfer in EOS-TC125, Indoor

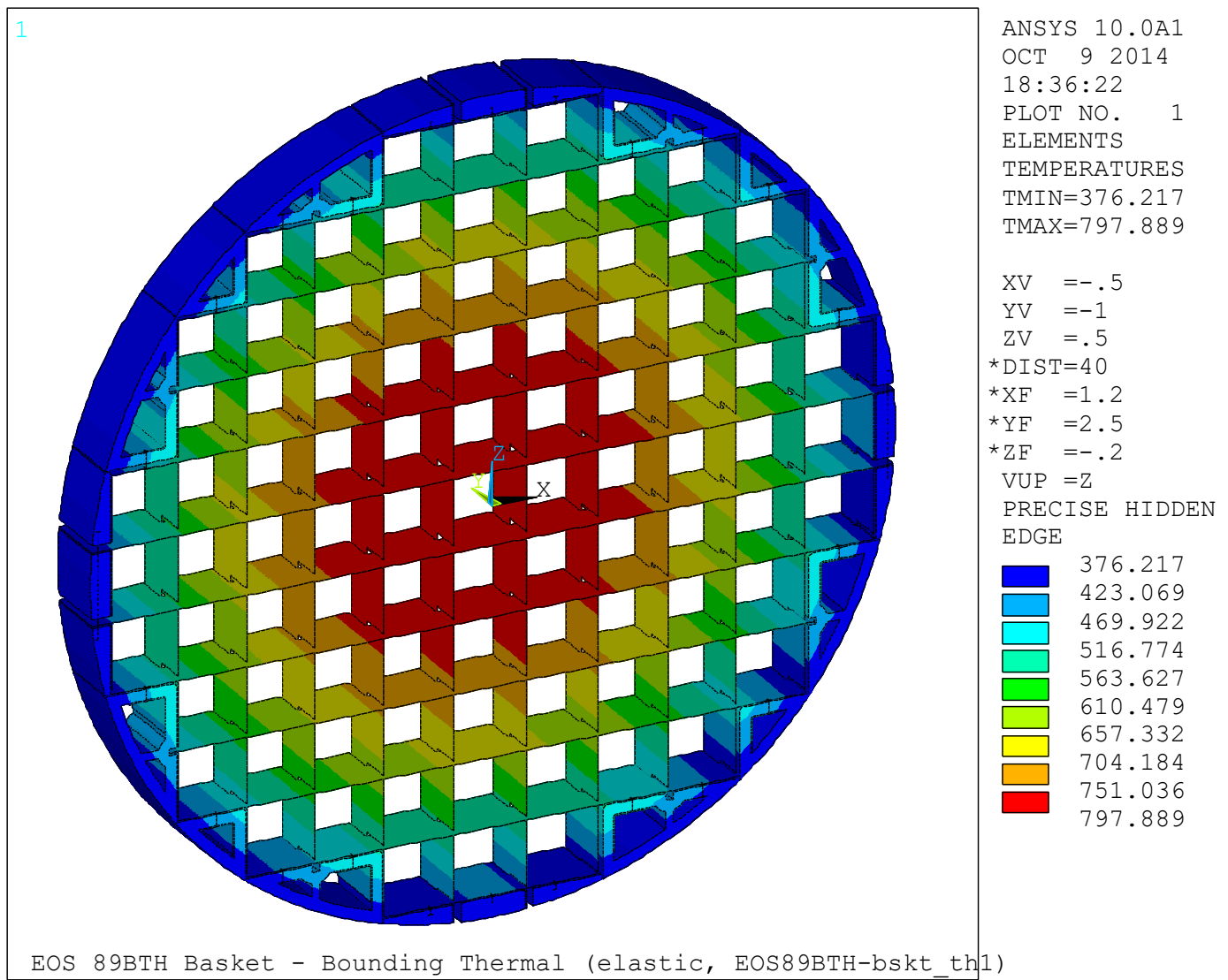


Figure 3.9.2-21
EOS-89BTH Basket Assembly ANSYS Model – Applied Bounding Thermal Profile

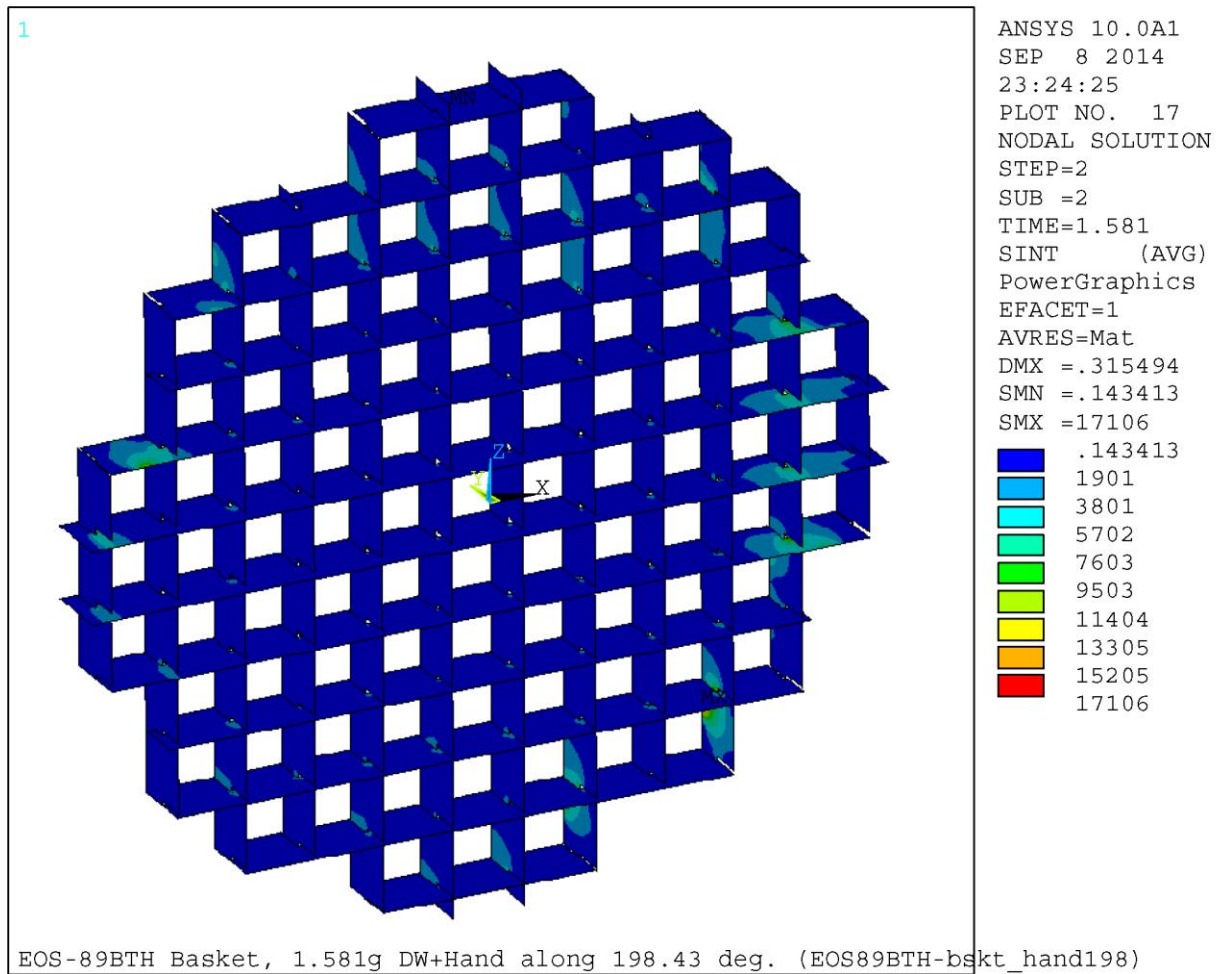


Figure 3.9.2-22
EOS-89BTH Basket 198.43 Degree 1.581g, DW + Handling
– Grid Plates, $P_m + P_b$ (stress intensity, psi)

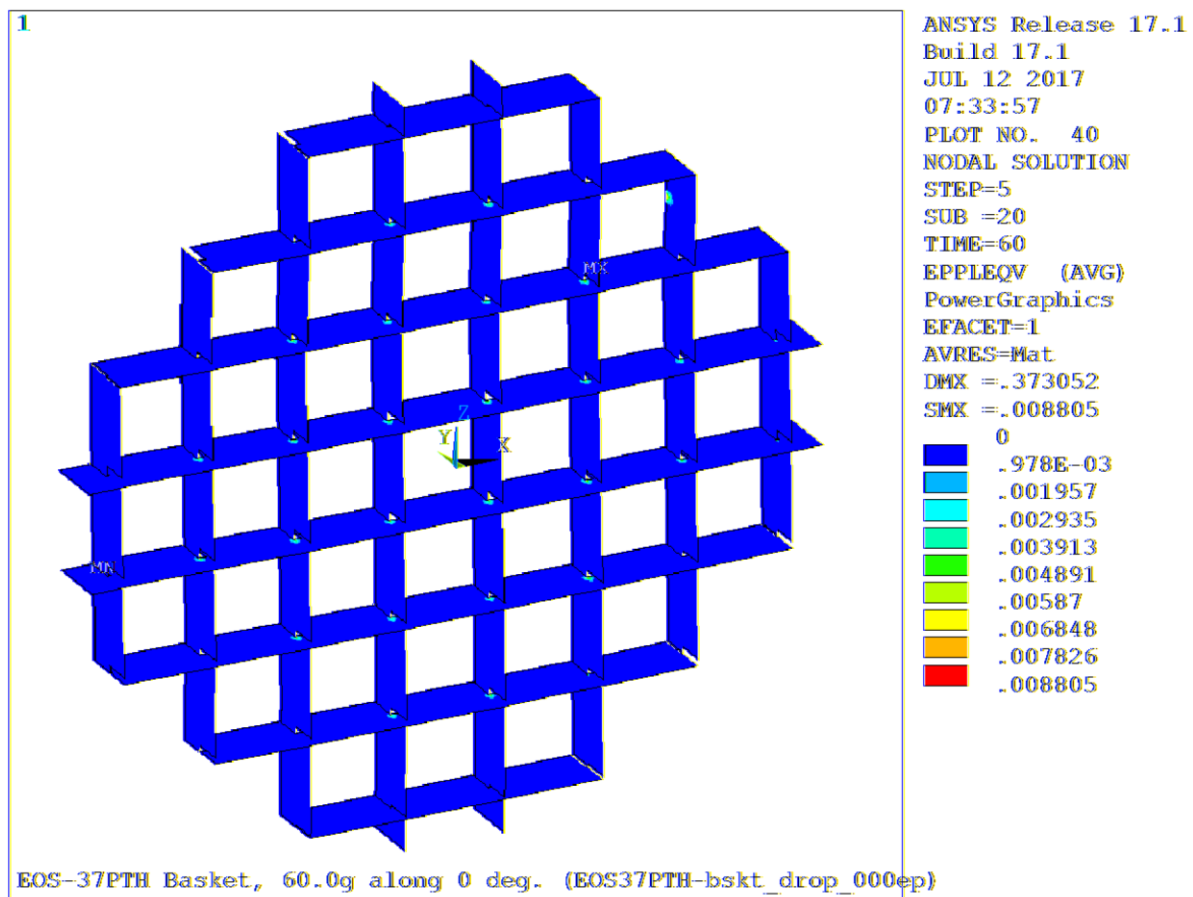


Figure 3.9.2-23
EOS-37PTH Basket 0 Degree 60g Side Drop (*with* bolts / tie rods)
– Grid Plates, $\epsilon_m + \epsilon_b$ (Equivalent Plastic Strain, in/in)

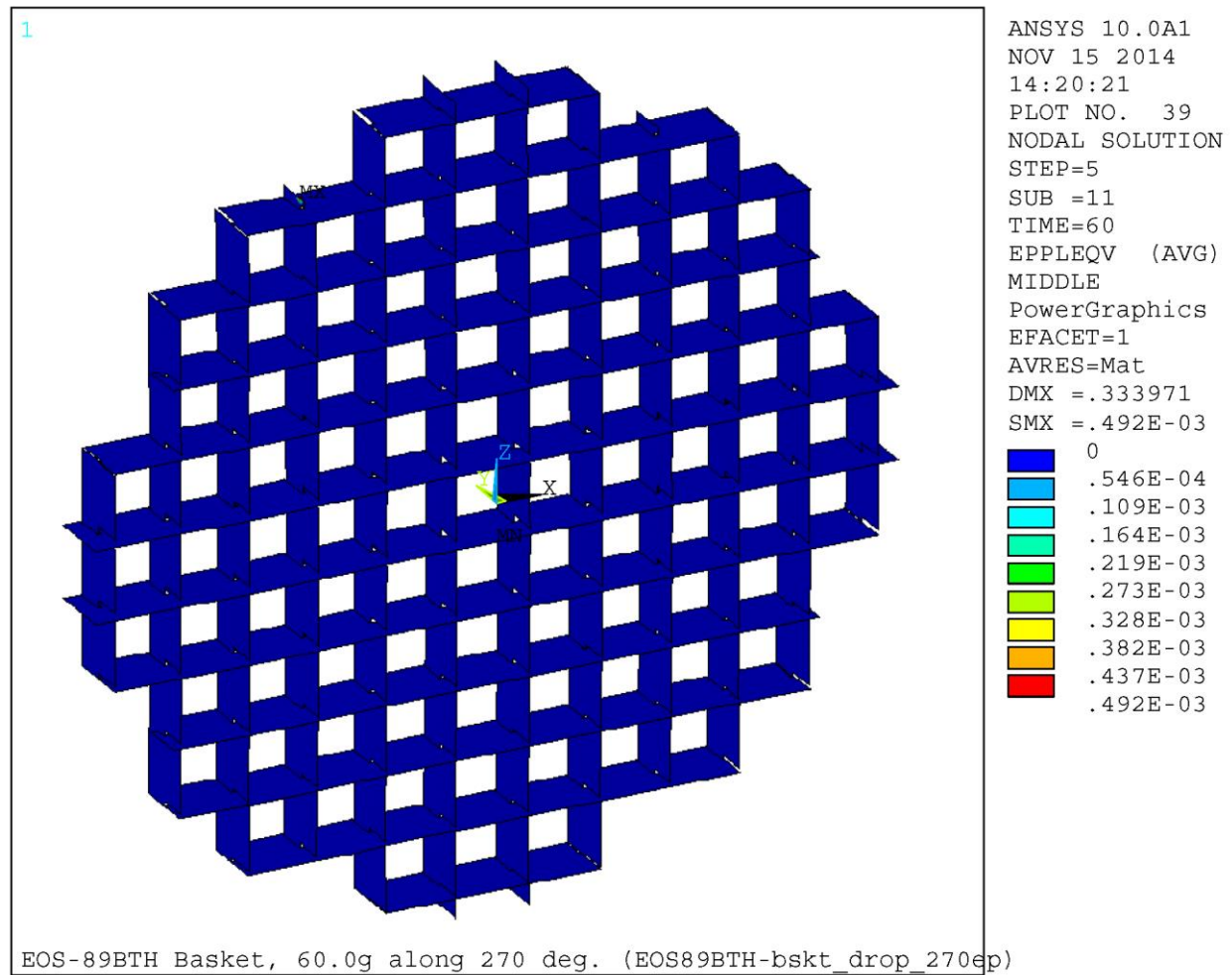


Figure 3.9.2-24
EOS-89BTH Basket 270 Degree 60g Side Drop (with bolts / tie rods)
– Grid Plates, ϵ_m (Equivalent Plastic Strain, in/in)

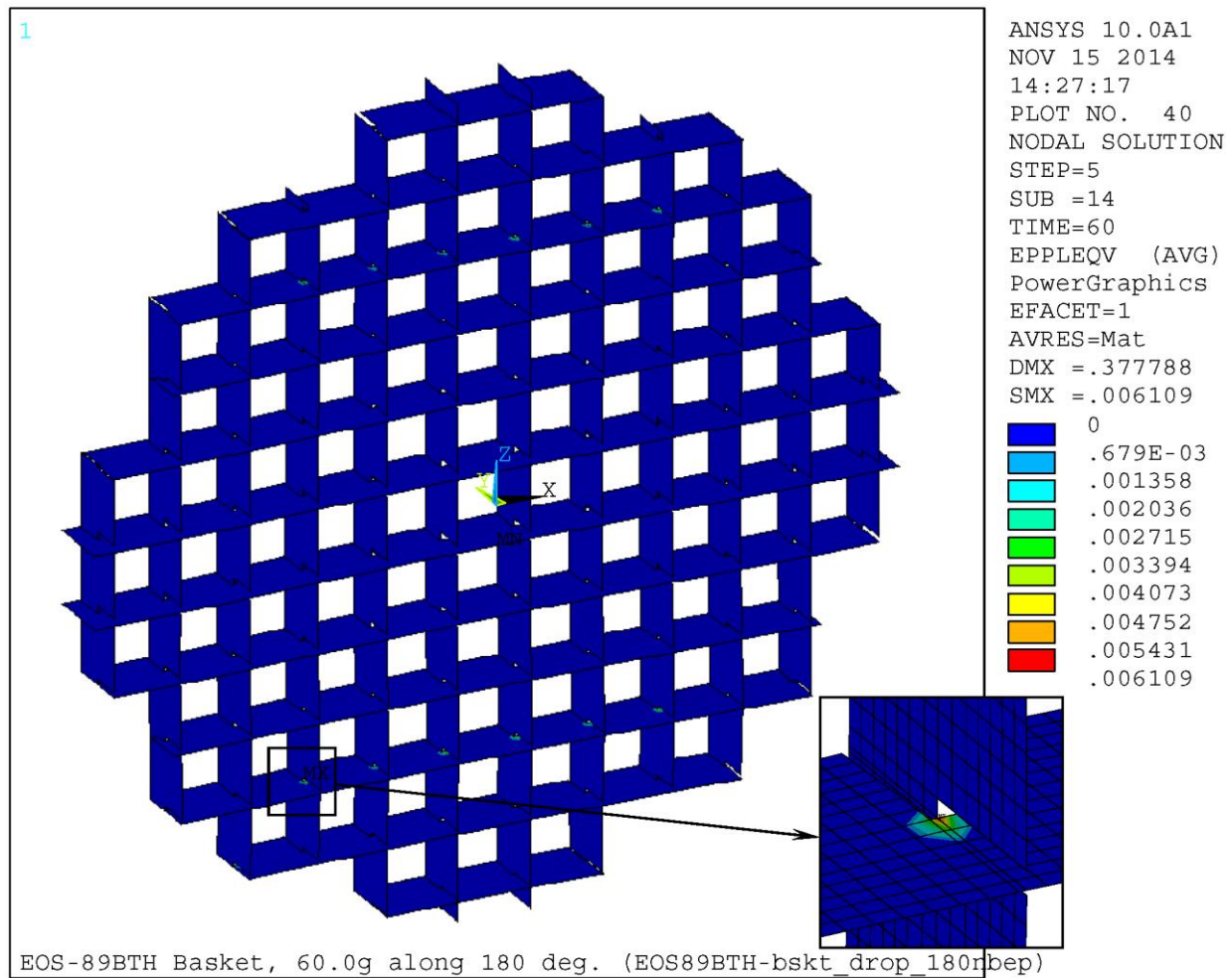


Figure 3.9.2-25
EOS-89BTH Basket 180 Degree 60g Side Drop (without bolts / tie rods)
– Grid Plates, $\epsilon_m + \epsilon_b$ (Equivalent Plastic Strain, in/in)

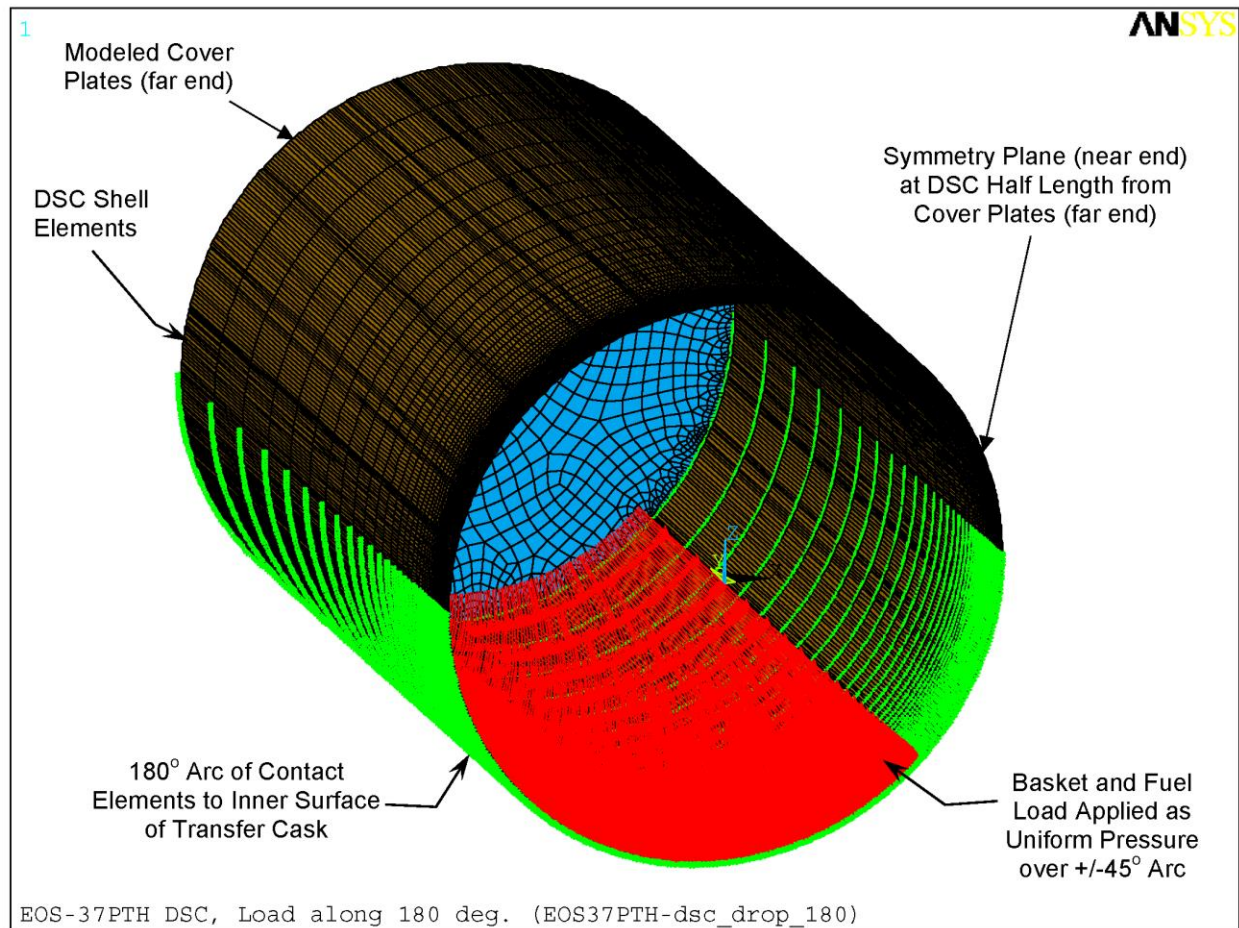


Figure 3.9.2-26
EOS-37PTH / EOS-89BTH DSC Shell ANSYS Model - Isometric View

(Half-length symmetric model, for determination of shell displacements at the symmetry plane, which are applied in side drop analyses. See also Figure 3.9.2-27.)

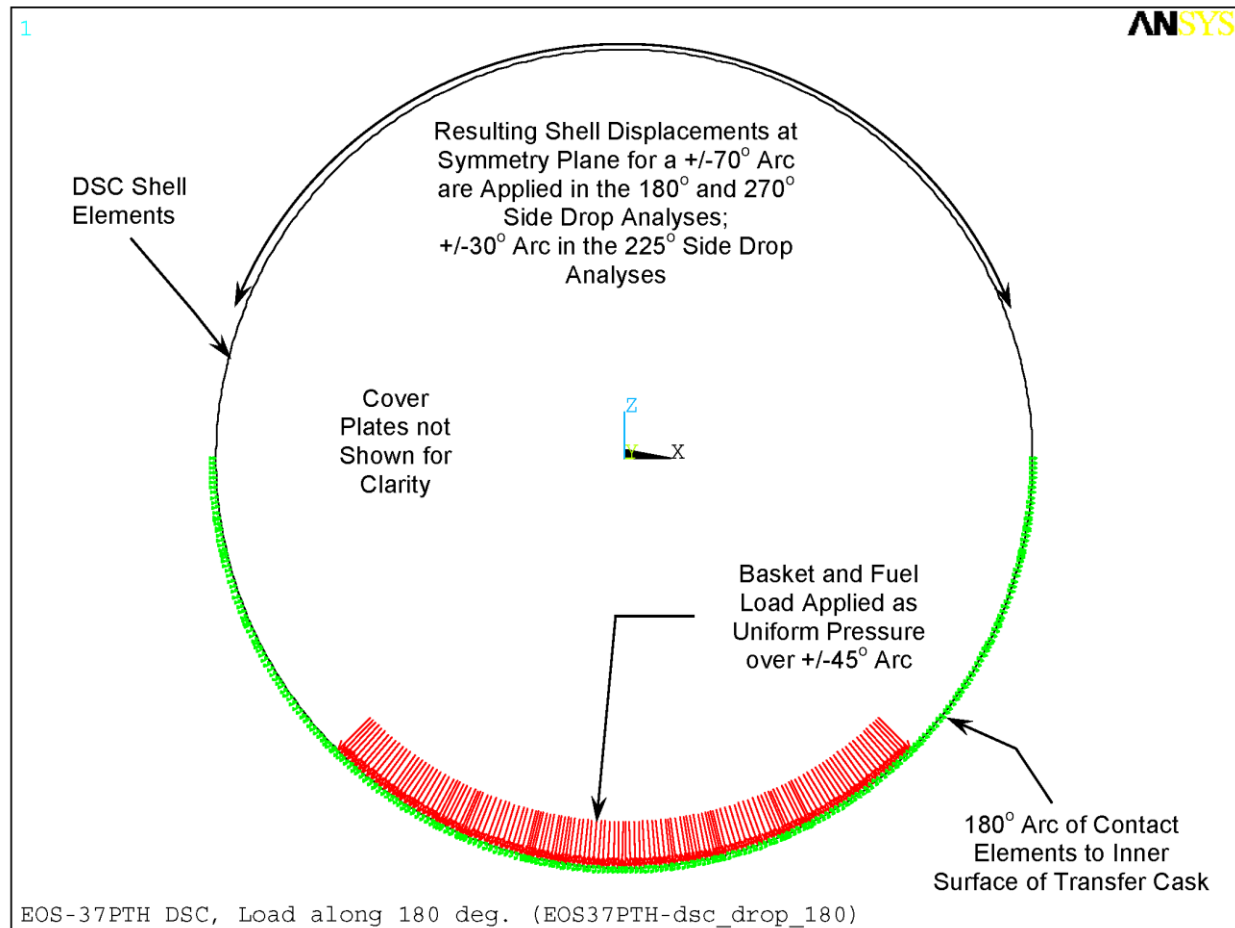


Figure 3.9.2-27
EOS -37PTH / EOS-89BTH DSC Shell ANSYS Model - End View

(Half-length symmetric model, for determination of shell displacements at the symmetry plane, which are applied in side drop analyses, cover plate elements not shown for clarity.)

APPENDIX 3.9.3

NUHOMS® EOS SYSTEM ACCIDENT DROP EVALUATION

Table of Contents

3.9.3 NUHOMS® EOS SYSTEM ACCIDENT DROP EVALUATION	3.9.3-1
3.9.3.1 Application Independent Parameters and Background.....	3.9.3-1
3.9.3.2 Benchmarking and Sensitivity	3.9.3-1
3.9.3.3 NUHOMS® EOS System with EOS-TC108 and EOS-37PTH Side and Corner Drop Evaluation using LS-DYNA.....	3.9.3-2
3.9.3.4 NUHOMS® EOS System with EOS-TC108 and EOS-89BTH Side and Corner Drop Evaluation using LS-DYNA.....	3.9.3-5
3.9.3.5 References	3.9.3-5

List of Figures

Figure 3.9.3-1	Overview of EOS-37PTH Model.....	3.9.3-7
Figure 3.9.3-2	Overview of EOS-37PTH Model.....	3.9.3-8
Figure 3.9.3-3	Overview of TC model	3.9.3-9
Figure 3.9.3-4	Overview of DSC model.....	3.9.3-10
Figure 3.9.3-5	Overview of EOS-37PTH Basket Model.....	3.9.3-11
Figure 3.9.3-6	EOS-37PTH Basket Plate Temperature Distribution (°F).....	3.9.3-12
Figure 3.9.3-7	Corner Drop Orientation	3.9.3-13
Figure 3.9.3-8	DELETED.....	3.9.3-14
Figure 3.9.3-9	EOS-TC108 with EOS-37PTH Side Drop TC Acceleration Time History (in/sec ²)	3.9.3-15
Figure 3.9.3-10	EOS-TC108 with EOS-37PTH Corner Drop TC Acceleration Time History (in/sec ²)	3.9.3-16
Figure 3.9.3-11	DELETED.....	3.9.3-17
Figure 3.9.3-12	DELETED.....	3.9.3-18
Figure 3.9.3-13	DELETED.....	3.9.3-19
Figure 3.9.3-14	DELETED.....	3.9.3-20
Figure 3.9.3-15	DELETED.....	3.9.3-21
Figure 3.9.3-16	DELETED.....	3.9.3-22
Figure 3.9.3-17	EOS-89BTH Overview of Basket Model	3.9.3-23
Figure 3.9.3-18	DELETED.....	3.9.3-24
Figure 3.9.3-19	EOS-TC108 with EOS-89BTH Side Drop TC Acceleration Time History Filtered at 150hz (in/sec ²)	3.9.3-25

Proprietary Information on Pages 3.9.3-1 through 3.9.3-13
Withheld Pursuant to 10 CFR 2.390

Figure 3.9.3-8
DELETED

Proprietary Information on Pages 3.9.3-15 and 3.9.3-16
Withheld Pursuant to 10 CFR 2.390

Figure 3.9.3-11
DELETED

Figure 3.9.3-12
DELETED

Figure 3.9.3-13
DELETED

Figure 3.9.3-14
DELETED

Figure 3.9.3-15
DELETED

Figure 3.9.3-16
DELETED

Proprietary Information on This Page
Withheld Pursuant to 10 CFR 2.390

Figure 3.9.3-18
DELETED

Proprietary Information on This Page
Withheld Pursuant to 10 CFR 2.390

APPENDIX 3.9.4 EOS-HSM STRUCTURAL ANALYSIS

Table of Contents

3.9.4 EOS-HSM STRUCTURAL ANALYSIS	3.9.4-1
3.9.4.1 General Description	3.9.4-1
3.9.4.2 Material Properties	3.9.4-3
3.9.4.3 Design Criteria	3.9.4-3
3.9.4.4 Load Cases	3.9.4-5
3.9.4.5 Load Combination	3.9.4-5
3.9.4.6 Finite Element Models	3.9.4-5
3.9.4.7 Normal Operation Structural Analysis	3.9.4-9
3.9.4.8 Off-Normal Operation Structural Analysis	3.9.4-10
3.9.4.9 Accident Condition Structural Analysis	3.9.4-11
3.9.4.10 Structural Evaluation	3.9.4-17
3.9.4.11 Conclusions	3.9.4-28
3.9.4.12 References	3.9.4-28

List of Tables

<i>Table 3.9.4-1</i>	<i>Design Pressures for Tornado Wind Flowing from Front Wall to Rear Wall and Vice Versa.....</i>	<i>3.9.4-30</i>
<i>Table 3.9.4-2</i>	<i>Design Pressures for Tornado Wind Flowing from Right Side to Left Side Wall and Vice Versa</i>	<i>3.9.4-31</i>
<i>Table 3.9.4-3</i>	<i>Spectral Acceleration Applicable to Different Components of EOS-HSM for Seismic Analysis.....</i>	<i>3.9.4-32</i>
<i>Table 3.9.4-3a</i>	<i>Spectral Acceleration Applicable to Different Components of EOS-HSMS-FPS for Seismic Analysis.....</i>	<i>3.9.4-32</i>
<i>Table 3.9.4-4</i>	<i>Load Cases for EOS-HSM Concrete Components Evaluation.....</i>	<i>3.9.4-33</i>
<i>Table 3.9.4-5</i>	<i>Load Combination for EOS-HSM Concrete Components Evaluation.....</i>	<i>3.9.4-34</i>
<i>Table 3.9.4-6</i>	<i>Strength Reduction Factors for Concrete.....</i>	<i>3.9.4-35</i>
<i>Table 3.9.4-7</i>	<i>Demand of EOS-HSM Concrete Components for Shear Forces and Moments.....</i>	<i>3.9.4-36</i>
<i>Table 3.9.4-8</i>	<i>Demand of EOS-HSM Concrete Components for Axial Forces and Moments.....</i>	<i>3.9.4-37</i>
<i>Table 3.9.4-9</i>	<i>Demand of EOS-HSMS Concrete Components for Shear Forces and Moments.....</i>	<i>3.9.4-38</i>
<i>Table 3.9.4-10</i>	<i>Demand of EOS-HSMS Concrete Components for Axial Forces and Moments.....</i>	<i>3.9.4-39</i>
<i>Table 3.9.4-11</i>	<i>Ultimate Shear/Moment Capacities of Concrete Components.....</i>	<i>3.9.4-40</i>
<i>Table 3.9.4-11a</i>	<i>Ultimate Shear/Moment Capacities of FPS Concrete Components</i>	<i>3.9.4-41</i>
<i>Table 3.9.4-12</i>	<i>Ultimate Axial/Moment Capacities of Concrete Components.....</i>	<i>3.9.4-42</i>
<i>Table 3.9.4-12a</i>	<i>Ultimate Axial/Moment Capacities of FPS Concrete Components</i>	<i>3.9.4-43</i>
<i>Table 3.9.4-13</i>	<i>Comparison of Highest Combined Shear Forces/Moments with the Capacities of EOS-HSM</i>	<i>3.9.4-44</i>
<i>Table 3.9.4-13a</i>	<i>Comparison of Highest Combined Shear Forces/Moments with the Capacities of EOS FPS HSM (Bounding).....</i>	<i>3.9.4-47</i>
<i>Table 3.9.4-14</i>	<i>Comparison of Highest Combined Axial Forces/Moments with the Capacities of EOS-HSM</i>	<i>3.9.4-50</i>
<i>Table 3.9.4-14a</i>	<i>Comparison of Highest Combined Axial Forces/Moments with the Capacities of EOS-HSM-FPS Option (Bounding).....</i>	<i>3.9.4-53</i>
<i>Table 3.9.4-14b</i>	<i>Comparison of Highest Combined Axial Forces/Moments of All EOS-HSM-FPS Configuration Options with the Applicable Capacities - Near Air Vent (Bounding)</i>	<i>3.9.4-56</i>
<i>Table 3.9.4-15</i>	<i>Load Cases for DSC Support Structure Evaluation</i>	<i>3.9.4-57</i>

<i>Table 3.9.4-16</i>	<i>Load Combination for DSC Support Structure Evaluation</i>	<i>3.9.4-57</i>
<i>Table 3.9.4-17</i>	<i>Summary of Demand to Capacity Ratio (D/C Ratio) for the Whole Cross Section</i>	<i>3.9.4-58</i>
<i>Table 3.9.4-17a</i>	<i>Summary of Demand to Capacity Ratio of the FPS DSC Support Structure.....</i>	<i>3.9.4-58</i>
<i>Table 3.9.4-18</i>	<i>Summary of Demand to Capacity Ratio (D/C Ratio) for the Flange Elements.....</i>	<i>3.9.4-59</i>
<i>Table 3.9.4-19</i>	<i>Summary of Demand to Capacity Ratio (D/C Ratio) for the Web Elements.....</i>	<i>3.9.4-59</i>
<i>Table 3.9.4-20</i>	<i>Summary of Demand to Capacity Ratio (D/C Ratio) for the Stiffener Elements</i>	<i>3.9.4-59</i>
<i>Table 3.9.4-21</i>	<i>Summary of Demand to Capacity Ratio (D/C Ratio) for the Accessories.....</i>	<i>3.9.4-60</i>
<i>Table 3.9.4-21a</i>	<i>Summary of Demand to Capacity Ratio (D/C Ratio) for FPS DSC Support Structure Accessories</i>	<i>3.9.4-60</i>
<i>Table 3.9.4-22</i>	<i>Summary of Demand to Capacity Ratio (D/C Ratio) for DSC Support Structure Welds</i>	<i>3.9.4-61</i>
<i>Table 3.9.4-22a</i>	<i>Summary of Demand to Capacity Ratio (D/C Ratio) for FPS DSC Support Structure Welds</i>	<i>3.9.4-61</i>
<i>Table 3.9.4-23</i>	<i>Modal Frequencies and Mass Participation of EOS-HSMS.....</i>	<i>3.9.4-62</i>
<i>Table 3.9.4-23a</i>	<i>Modal Frequencies and Mass Participation of EOS-HSMS-FPS</i>	<i>3.9.4-62</i>
<i>Table 3.9.4-24</i>	<i>Roof Heat Shield Modal Participating Mass Ratios for EOS-HSM and EOS-HSM-FPS Options.....</i>	<i>3.9.4-63</i>
<i>Table 3.9.4-25</i>	<i>Side Heat Shield Modal Participating Mass Ratios for EOS-HSM.....</i>	<i>3.9.4-64</i>
<i>Table 3.9.4-25a</i>	<i>Side Heat Shield Modal Participating Mass Ratios for EOS-HSM-FPS.....</i>	<i>3.9.4-66</i>
<i>Table 3.9.4-26</i>	<i>Ultimate Shear/Moment Capacities of Alternate Front Wall</i>	<i>3.9.4-67</i>
<i>Table 3.9.4-26a</i>	<i>Ultimate Shear/Moment Capacities of EOS-HSM-FPS Alternate Front Wall.....</i>	<i>3.9.4-68</i>
<i>Table 3.9.4-27</i>	<i>Ultimate Axial and Balanced Moment Capacities of Alternate Front Wall.....</i>	<i>3.9.4-69</i>
<i>Table 3.9.4-27a</i>	<i>Ultimate Axial/Moment Capacities of EOS-HSM-FPS Alternate Front Wall.....</i>	<i>3.9.4-70</i>
<i>Table 3.9.4-28</i>	<i>Comparison of Highest Combined Shear Forces/Moments with the Capacities of the Alternate Front Wall.....</i>	<i>3.9.4-71</i>
<i>Table 3.9.4-28a</i>	<i>Comparison of Highest Combined Shear Forces/Moments with Capacities of the EOS-HSM-FPS Alternate Front Wall (Bounding).....</i>	<i>3.9.4-73</i>

<i>Table 3.9.4-29</i>	<i>Comparison of Highest Combined Axial Forces/Moments with the Capacities of the Alternate Front Wall.....</i>	<i>3.9.4-76</i>
<i>Table 3.9.4-29a</i>	<i>Comparison of Highest Combined Axial Forces/Moments with Capacities of the EOS-HSM-FPS Alternate Front Wall (Bounding).....</i>	<i>3.9.4-78</i>

List of Figures

Figure 3.9.4-1	Analytical Model of EOS-HSM for Mechanical Load Analysis.....	3.9.4-81
Figure 3.9.4-1a	Analytical Model of EOS-HSM-FPS for Mechanical Load Analysis	3.9.4-82
Figure 3.9.4-2	Analytical Model of EOS-HSMS for Mechanical Load Analysis (Node to Node Contact at Segment Joint interface)	3.9.4-83
Figure 3.9.4-2a	Analytical Model of EOS-HSMS-FPS for Mechanical Load Analysis (Node to Node Contact at Segment Joint Interface).....	3.9.4-84
Figure 3.9.4-3	Temperature distribution of EOS-HSMS for Normal Thermal Hot Condition.....	3.9.4-85
Figure 3.9.4-3a	Temperature distribution of EOS-HSMS-FPS for Normal Thermal Hot Condition.....	3.9.4-86
Figure 3.9.4-4	Temperature distribution of EOS-HSMS for Blocked Vent Accident Thermal Condition.....	3.9.4-87
Figure 3.9.4-4a	Temperature distribution of EOS-HSMS-FPS for Blocked Vent Accident Thermal Condition.....	3.9.4-88
Figure 3.9.4-5	Symbolic Notation of Forces and Moments of EOS-HSM Concrete Components.....	3.9.4-89
Figure 3.9.4-6	Analytical Model of the W12x136 DSC Main Support Beam with Stiffeners and Open Web.....	3.9.4-90
Figure 3.9.4-7	Components of DSC Support Structure	3.9.4-91
Figure 3.9.4-7a	Components of FPS DSC Support Structure	3.9.4-92
Figure 3.9.4-8	Analytical Model of Coupled Roof Heat Shield and Connection Studs.....	3.9.4-93
Figure 3.9.4-9	Analytical Model of Coupled Side Heat Shield and Connection Studs.....	3.9.4-94
Figure 3.9.4-10	Horizontal Target and 5% Spectral Match (Horizontal 1, Hector Mine Earthquake)	3.9.4-95
Figure 3.9.4-11	Baseline Corrected Acceleration, Velocity and Displacement Time Histories (Horizontal 1, Hector Mine Earthquake).....	3.9.4-96
Figure 3.9.4-12	Horizontal Target and 5% Spectral Match (Horizontal 2, Hector Mine Earthquake)	3.9.4-97
Figure 3.9.4-13	Baseline Corrected Acceleration, Velocity and Displacement Time Histories (Horizontal 2, Hector Mine Earthquake).....	3.9.4-98
Figure 3.9.4-14	Vertical Target and 5% Spectral Match (Vertical Up, Hector Mine Earthquake).....	3.9.4-99
Figure 3.9.4-15	Baseline Corrected Acceleration, Velocity and Displacement Time Histories (Vertical Up, Hector Mine Earthquake)	3.9.4-100

<i>Figure 3.9.4-16</i>	<i>ISRS at Side Heat Shield Support Nodes due to Hector Mine Earthquake-Based Motion compatible with Enhanced RG 1.60 Spectra, 4% Damping, X-Direction</i>	<i>3.9.4-101</i>
<i>Figure 3.9.4-17</i>	<i>ISRS at Side Heat Shield Support Nodes due to Hector Mine Earthquake-Based Motion compatible with Enhanced RG 1.60 Spectra, 4% Damping, Y-Direction</i>	<i>3.9.4-102</i>
<i>Figure 3.9.4-18</i>	<i>ISRS at Side Heat Shield Support Nodes due to Hector Mine Earthquake-Based Motion compatible with Enhanced RG 1.60 Spectra, 4% Damping, Z-Direction</i>	<i>3.9.4-103</i>
<i>Figure 3.9.4-19</i>	<i>ISRS at Roof Heat Shield Support Nodes due to Hector Mine Earthquake-Based Motion compatible with Enhanced RG 1.60 Spectra, 4% Damping, X-Direction</i>	<i>3.9.4-104</i>
<i>Figure 3.9.4-20</i>	<i>ISRS at Roof Heat Shield Support Nodes due to Hector Mine Earthquake-Based Motion compatible with Enhanced RG 1.60 Spectra, 4% Damping, Y-Direction</i>	<i>3.9.4-105</i>
<i>Figure 3.9.4-21</i>	<i>ISRS at Roof Heat Shield Support Nodes due to Hector Mine Earthquake-Based Motion compatible with Enhanced RG 1.60 Spectra, 4% Damping, Z-Direction</i>	<i>3.9.4-106</i>

3.9.4 EOS-HSM STRUCTURAL ANALYSIS

The purpose of this appendix is to present the structural evaluation of the EOS-HSM due to all applied loads during storage, loading and unloading operation. The NUHOMS® EOS System consists of the dual-purpose (transportation and storage) EOS-37PTH and EOS-89BTH dry shielded canister (DSC), a horizontal storage module (EOS-HSM), an onsite transfer cask (EOS-TC), and associated ancillary equipment.

3.9.4.1 General Description

General description and operational features for the NUHOMS® EOS System is provided in Chapter 1. The EOS-HSM is a freestanding, reinforced concrete structure, designed to provide environmental protection and radiological shielding for the EOS-37PTH DSC or EOS-89BTH DSC. The drawings of the EOS-HSM, showing different components and overall dimensions, are provided in Chapter 1.

The EOS-HSM consists of a base unit and a roof unit. The roof unit rests mainly on the front and rear walls, and partly on the side walls of the base unit. The roof and the base are connected by bolts/embedments to form a single module via four steel brackets located at each of the interior upper corners of base unit.

Alternate designs of horizontal storage modules may be used in lieu of EOS-HSM as part of NUHOMS® EOS System. The EOS-HSMS is a multi-segment design of horizontal storage module which consists of two segments of the base unit and a roof unit. The two segments of the base unit of EOS-HSMS are connected by grouted, high-strength, threaded bars/embedments, and the base and roof are connected in a similar way to that of EOS-HSM.

An alternate Flat Plate Support (FPS) Rail design of horizontal storage module, the EOS-HSM-FPS, may also be used in lieu of EOS-HSM as a part of the NUHOMS® EOS System. EOS-HSM-FPS is modified from the EOS-HSM to support the FPS DSC Support Structure with concrete pedestals spaced along the length of the DSC Support Structure.

EOS-HSMS-FPS is a multi-segment design of the EOS-HSM-FPS which consists of two segments of the base unit and a roof unit. The alternate Base front wall thickness is 42" uniform thickness, as opposed to the original design which expanded from 42" to 54" at the bottom portion of the alternate front wall. The 42" thick lower portion of the rear wall is replaced with 24" thick (12" thick rear wall plus 12" thick rear pedestal) support pedestals.

The two segments of the base unit of EOS-HSMS-FPS are connected by grouted, high-strength, threaded bars/embedments, and the base and roof are connected in a similar way to that of EOS-HSM-FPS. EOS-HSM is used herein for all alternatives unless a unique situation is presented. EOS-HSM-FPS is used herein for both the EOS-HSM-FPS and EOS-HSMS-FPS unless a unique situation is presented. The EOS-HSM storage modules can be arranged either in a single-row array, or in back-to-back double-row arrays by placing a module next to, and in contact with, adjacent module(s) with thick end shield walls connected to the EOS-HSM at the end of the arrays. The thick rear shield walls are also connected to the back wall of the EOS-HSM, if the modules are placed in a single-row array.

The EOS-37PTH DSC or EOS-89BTH DSC is supported inside the EOS-HSM by DSC support structure. The DSC support structure is comprised of two main support beams, two extension plates and two nitronic sliding rails and it spans between the front wall and the rear wall of the base unit. The web of the main support beams has openings to allow the air flow around the DSC. The DSC support structure provides support for the DSC during storage and also acts as a sliding surface during the insertion and retrieval of DSC.

DSC support structure is used herein for both DSC support structure and FPS DSC support structure unless a unique situation is presented.

The EOS-37PTH DSC or EOS-89BTH DSC is supported inside the EOS-HSM-FPS by the FPS DSC support structure. The FPS DSC support structure is comprised of a stiffened flat-plate design that is supported at the front and rear walls of the EOS-HSM-FPS and additionally at two intermediate concrete support pedestals. The FPS DSC support structure provides support for the DSC during storage and also acts as a sliding surface during the insertion and retrieval of DSC. The FPS DSC support structure is only an option for the medium EOS-HSM and EOS-HSMS.

The width of EOS-HSM is 116 inches. The overall height of EOS-HSM is 240 inches including the outlet vent cover. Three different EOS-HSM lengths are available in order to accommodate DSCs of different lengths. The internal cavity of the EOS-HSM accommodates DSCs of variable length by varying the location of the axial retainer and by variation of gap between the DSC and the EOS-HSM back wall.

The air inlet vents located at the front lower corners of base unit extend through the bottom of side wall on both sides, which ultimately lead to the cavity of base unit. The air outlet vents are provided in the roof at both sides of the module.

The front wall of EOS-HSM base unit has round access door opening provided for transferring EOS-37PTH DSC or EOS-89BTH DSC into the module or retrieving it from the module. The door opening is closed by a shield door after the insertion of EOS-37PTH DSC or EOS-89BTH DSC. The EOS-HSM shield door is a combination of rectangular and cylindrical concrete block with steel backing plate on the inside face. The shield door provides environmental protection, including missile and shielding protection.

End shield walls are installed at each end of a module array to provide the required missile and shielding protection. Similarly, a rear shield wall is installed at the rear of each module of the single row module array for same purpose.

For thermal protection of the EOS-HSM concrete, a thin stainless steel heat shield is installed inside the EOS-HSM. The interior surface of the upper part of the side wall is protected with side heat shields, and the underside of the roof unit is protected with a roof heat shield. The roof heat shield has an upward slope at 10 degrees from center towards outlet vent. The heat shield guides the cooling air flow through the EOS-HSM.

During DSC insertion and retrieval operations, the EOS-TC is docked with the EOS-HSM docking surface and mechanically secured to the cask restraint embedments provided in the front wall of the base unit. These embedments are equally spaced on either side of the door opening and located near the lower embedment for door attachment.

3.9.4.2 Material Properties

The material properties used in the analysis and design of EOS-HSM and its components are discussed in detail in Chapter 8.

3.9.4.3 Design Criteria

The reinforced concrete EOS-HSM and the DSC support structure are important to safety components of NUHOMS® EOS System. Consequently, they are designed and analyzed to perform their intended functions under the extreme environmental and natural phenomena specified in 10 CFR 72.122 [3.9.4-1] and American National Standards Institute (ANSI) 57.9 [3.9.4-10]. These include tornado and wind, seismic, and flood design criteria. The design wind pressure is determined as per American Society of Civil Engineers (ASCE) 7-10 [3.9.4-15].

The concrete EOS-HSM and steel DSC support structures are designed to the requirements of American Concrete Institute (ACI) 349-06 [3.9.4-12] and the American Institute of Steel Construction (AISC) Manual of Steel Construction [3.9.4-14], respectively, using the load combinations prescribed by ANSI 57.9 [3.9.4-10]. When ACI-349-06 does not have enough information, ACI-318-08 [3.9.4-11] is used as supplement. The following table summarizes the Codes and Standards for design and fabrication of these components.

Component	Material	Applicable Code
EOS-HSM Concrete Components	Concrete	ACI 349-06 (Design) ACI 318-08 (Fabrication) ASCE 7-10 (Loads) ANSI/ANS 57.9-84 (Loads & Load Combination)
DSC Support Structure, Heat Shields and other Steel Components	Steel	AISC Manual of Steel Construction, 13 th Edition (Structural Steel) AWS D1.1, March 2010 (or later editions) (Structural Weld) ASCE 7-10 (Loads) ANSI/ANS 57.9-84 (Loads & Load Combination)

The ultimate strength method of ACI 349-06 [3.9.4-12] is used for the design of the EOS-HSM reinforced concrete structural components. The reinforcement is provided to meet the minimum flexural and shear reinforcement requirement of ACI 349-06 and to ensure that the provided design strength exceeds the required strength. Alternatively, for some cases, the minimum reinforcement area requirement can be waived for components with a flexural stress ratio of less than 0.66 as per Section 10.5.3 of ACI 349-06 [3.9.4-12].

The axial, shear and moment capacities for all the concrete components of the EOS-HSM calculated based on ACI 349-06 are provided in Table 3.9.4-11, Table 3.9.4-12, Table 3.9.4-26, and Table 3.9.4-27 for EOS-HSM and Table 3.9.4-26a and Table 3.9.4-27a for EOS-HSM-FPS. The capacities for blocked vent accident condition consider the strength reduction at elevated temperature.

The comparison of the Highest Combined Shear Force/Moment with the capacities for the EOS HSM is provided in Table 3.9.4-13 and the comparison of the Highest Combined Shear Force/Moment with the capacities for the Alternate Front wall is provided in Table 3.9.4-28.

The comparison of the highest combined shear force/moment with the capacities for the EOS HSM-FPS is provided in Table 3.9.4-13a and the comparison of the highest combined shear force/moment with the capacities for the Alternate Front wall is provided in Table 3.9.4-28a.

Similarly, the comparison of the highest combined axial force/moment with capacities for the EOS HSM is provided in Table 3.9.4-14 and comparison of the highest combined axial force/moments with capacities for the alternate front wall is provided in Table 3.9.4-29.

The comparison of the highest combined axial force/moment with the capacities for the EOS HSM-FPS is provided in Table 3.9.4-14a and the comparison of the highest combined shear force/moment with the capacities for the Alternate Front wall is provided in Table 3.9.4-29a.

The required steel strength, S , and required steel shear strength, S_v , for critical section of steel structure are calculated in accordance with the requirements of AISC Steel Construction Manual [3.9.4-14] using the Allowable Strength Design (ASD) method.

3.9.4.4 Load Cases

A summary of the design loads for EOS-HSM concrete component evaluation is provided in Table 3.9.4-4. This table also presents the applicable codes and standards for specific load. A summary of the design loads for DSC support structure is provided in Table 3.9.4-15.

3.9.4.5 Load Combination

The load combinations used in the structural analysis of EOS-HSM and DSC support structure comply with the requirement of 10 CFR 72.122 [3.9.4-1] and ANSI 57.9-84 [3.9.4-10]. Table 3.9.4-5 and Table 3.9.4-16 summarize the load combination requirement of EOS-HSM and DSC support structure, respectively.

3.9.4.6 Finite Element Models

EOS-HSM and EOS-HSMS have variable lengths to store DSCs of different lengths. EOS-HSM Long is analyzed and governs the structural design of EOS-HSM Short, Medium and Long. EOS-HSM-FPS and EOS-HSMS-FPS are only available and analyzed at a Medium length.

3.9.4.6.1 Finite Element Model to Evaluate EOS-HSM Concrete Components for Mechanical Loads

The structural analysis of an individual module provides a conservative estimate of the response of the EOS-HSM structural elements under the postulated static and dynamic loads for any EOS-HSM array configuration. The frame and shear wall action of the EOS-HSM concrete components are considered to be the primary structural system resisting the loads. The analytical model is evaluated for normal operating, off-normal, and postulated accident loads acting on the EOS-HSM.

A three-dimensional (3D) ANSYS finite element model (FEM) of the EOS-HSM, including all the concrete components, is developed. The eight-node brick element (ANSYS element type SOLID185) is used to model the concrete structure. Each node of the eight-node brick element has three translational degrees of freedom. The DSC is modeled using beam elements (ANSYS element type BEAM4). The DSC main support beam, W12x136 and the brace, C3x5 are also modelled using beam elements with appropriate section properties. The mass of the DSC is lumped at eleven discrete nodes of the beam using lumped mass elements (ANSYS element type MASS21). A plot of the ANSYS model of EOS-HSM and EOS-HSMS is shown in Figure 3.9.4-1 and Figure 3.9.4-2, respectively.

A three-dimensional (3D) ANSYS finite element model (FEM) of the EOS-HSM-FPS, including all the concrete components, is developed. The eight-node brick element (ANSYS element type SOLID185) is used to model the concrete structure. Each node of the eight-node brick element has three translational degrees of freedom. The DSC is modeled using beam elements (ANSYS element type BEAM4). The FPS DSC support structure consists of two composite plates (1"x12" and 1"x4").

For the FPS DSC support design, two DSC configurations are analyzed that represent the maximum and minimum lengths of DSCs designated for the EOS-HSM-FPS or EOS-HSMS-FPS designs. In these models the mass of the DSC is distributed along its length at discrete nodes using lumped mass elements (ANSYS element type MASS21). Plots of ANSYS models for the EOS-HSM-FPS and EOS-HSMS-FPS are shown in Figure 3.9.4-1a and Figure 3.9.4-2a, respectively.

The DSC support structure is incorporated into the EOS-HSM analytical model to transfer the load to concrete components. The connections of the support structure to the concrete structure are modeled using rigid beam elements. The various normal, off-normal and accident loads are applied to the analytical model and internal forces and moments are computed by performing a linear elastic finite element analysis.

The node coupling option of ANSYS is used to represent the appropriate connection between the base and roof of the EOS-HSM and EOS-HSM-FPS models. For EOS-HSMS and EOS-HSMS-FPS, the node to node contact element (ANSYS element type CONTA178) is used across the interface of the upper and lower segment to transfer the load from the roof and upper segment to the lower segment. The counter bore and rail extension baseplate groove at the door opening are not included in the FEM. Conservatively, the nodes at the bottom of EOS-HSM are constrained in all three translational degree of freedom, thus maximizing the EOS-HSM design forces and moments.

3.9.4.6.2 Finite Element Model of the EOS-HSM Concrete Structure for Thermal Stress Analysis

Thermal stress analyses of the EOS-HSM were performed using a 3D FEM, which includes only the concrete components. The connections of the door and the support structure rails to the EOS-HSM concrete structure are designed so that free thermal growth is permitted in these members when the EOS-HSM is subjected to thermal loads. Because of their free thermal growth, the door and the support structure do not induce thermal stresses in the concrete components of the EOS-HSM. Therefore, the analytical model of the EOS-HSM for thermal stress analysis of the concrete components does not include the DSC support structure and the door. The ANSYS models with temperature profile, which is used to perform thermal stress analysis of the concrete components, are shown in Figure 3.9.4-3, Figure 3.9.4-3a, Figure 3.9.4-4, and Figure 3.9.4-4a.

For the thermal load analysis, the bottom of the EOS-HSM ($y=0$ in ANSYS model) was restrained at one set of edge nodes (in axial and lateral directions) and friction forces were applied at the bottom of EOS-HSM base in the axial and lateral directions. One node in the front wall and two nodes in the back wall at $y=0$ are also restrained in vertical direction.

3.9.4.6.3 Finite Element Model for Structural Analysis of DSC Support Structure

A 3D FEM of the DSC main support beam with stiffener plates and rail extension baseplate is developed in the computer program ANSYS [3.9.4-19]. In the finite element model (FEM) for the DSC main support beam (W12x136), the W section of the main support beam is broken down into flange and web components represented individually by BEAM189 elements.

The beam elements (BEAM189) are arranged in a 2D plane aligned with the centerline of the beam, inclined 30 degrees from vertical along the length of the beam. Each element has three nodes with six degrees of freedom (three translational and three rotational) per node.

The web of the DSC main support beam has triangular openings, allowing for heat flow, resulting in vertical and diagonal web elements. The cross sections of these components are calculated and used to define the assigned cross sections for each component. A plot of the front portion of the model of the DSC main support beam model is shown in Figure 3.9.4-6.

The model is completely restrained at the bottom end of the rail extension baseplate. The ends of the DSC main support beam at the bottom are restrained for vertical displacement and rotation about longitudinal axis to simulate the simple support condition of the concrete pedestals at the front and rear walls. The support beam is also restrained laterally at the location of lateral braces.

The ETAB command of ANSYS is used to extract the beam element results due to individual load cases which then combined to determine the combined load results.

The FPS DSC support structure is a simple design comprised of flat plates. Therefore, hand calculation methodology was employed assuming it as a simply supported beam with concentrated load.

3.9.4.6.4 Finite Element Model for Structural Analysis of Heat Shield Panels and Connection Studs

The heat shields (coupled panel-stud system) are subjected to two loads: a combination of 1g dead load due to its own weight, and a seismic load that is dependent upon its natural frequency as well as the in-structure response spectra (ISRS) at the supports of the plate-stud system.

Modal time-history analysis of the EOS-HSM is performed using ANSYS computer code to determine the ISRS at the nodes at which the studs are supported. Applicable time-histories and modal properties for this evaluation are provided in Section 3.9.4.9.2.

ANSYS is also used to determine the natural vibration frequencies of the coupled panel-stud system. Shell elements (ANSYS element type SHELL63) are used to model the heat shield panel and beam elements (ANSYS element type BEAM4) are used for the studs. The FEM of the coupled panel-stud system is shown in Figure 3.9.4-8 and Figure 3.9.4-9.

The natural frequency of the plate-stud system is used to determine the appropriate g load from the ISRS. It is assumed that the heat shields are dynamically decoupled from the EOS-HSM because the concrete EOS-HSM is much more rigid than the heat shields and the weight of the heat shield is small as compared to the total weight of loaded EOS-HSM. Accordingly, the heat shields are not accounted for in the modal time-history analysis of the EOS-HSM, and the EOS-HSM is not considered in modal analysis of the heat shields.

3.9.4.7 Normal Operation Structural Analysis

The evaluation of the EOS-HSM is performed at normal operating condition. The following table shows the normal operating loads for which the EOS-HSM components are designed. The table also lists the individual EOS-HSM components that are affected by each loading.

Load Type	Components	
	EOS-HSM	DSC Support Structure
Dead Load	X	X
Live Load	X	X
Normal Handling	X	X
Normal Thermal	X	X
Wind Load	X	

The reinforced concrete and the steel DSC support structure of the EOS-HSM are analyzed for the normal, off-normal, and postulated accident conditions using FEMs described in Section 3.9.4.6. These models are used to evaluate concrete and support structure forces and moments due to dead load, live load, normal handling loads, normal thermal loads, and wind load. The methodology used to evaluate the effects of these normal loads is addressed in the following paragraphs.

3.9.4.7.1 EOS-HSM Dead Load (DL) Analysis

Dead loads are applied to the analytical model by application of 1g acceleration in the vertical direction where g is the gravitational acceleration (386.4 in/sec²). The 5% variation of dead load as indicated in ANSI/ANS 57.9 is not used because the heaviest design weight is used for analysis.

3.9.4.7.2 EOS-HSM Live load (LL) Analysis

Live load analysis is performed by applying 200 psf pressure on the roof. The DSC weight is also applied on the DSC support structure as a live load.

3.9.4.7.3 EOS-HSM Normal Operational Handling Load (R_o) Analysis

Normal operation assumes the canister is sliding over the DSC support structure due to a hydraulic ram force of up to 135,000 lbs (insertion) and 80,000 lbs (extraction) applied at the grapple ring. The normal operation handling load of 70,000 lbs is applied to each DSC main support structure in the axial direction resulting in a total applied load of 140,000 lbs on both beams which conservatively envelopes the total insertion/extraction force. The same magnitude of load of 70,000 lbs is also applied at each of the cask restraint embedment in opposite direction. In addition, the DSC weight is applied as a distributed load on both DSC support structure of the EOS-HSM.

3.9.4.7.4 EOS-HSM Normal Operating Thermal (T_o) Stress Analysis

The normal operating thermal (T_o) loads on EOS-HSM include the effect of design basis heat load up to 50 kW generated by DSC, plus the effect of normal ambient temperature range. To evaluate the effects of normal thermal loads on the EOS-HSM, heat transfer analyses for a range of normal ambient temperatures (-20 °F and 100 °F) are performed with DSC heat load of 50 kW. The normal thermal cold condition (-20 °F) is bounded by off-normal thermal cold condition (-40 °F). Therefore, off-normal thermal cold condition is used in place of normal thermal cold condition. The ambient condition that causes maximum temperature and maximum gradients in the concrete components is used in the analysis. The normal thermal hot condition is the governing case for this load case. The EOS-HSM thermal stress analysis was performed using thermal profiles and maximum temperatures that bounds those reported in Chapter 4.

3.9.4.7.5 EOS-HSM Design Basis Wind Load (W) Analysis

The DSC support structure and DSC inside the EOS-HSM are not affected by wind load. The concrete structure forces and moments due to design basis wind load (W) are bounded by the result of tornado generated wind load discussed in Section 3.9.4.9.1. Therefore, tornado generated wind load is conservatively used in the off-normal wind load combination C2, as seen in Table 3.9.4-5. Therefore, no separate analysis is performed for the design basis wind load case.

3.9.4.8 Off-Normal Operation Structural Analysis

This section describes the design basis off-normal events for the EOS-HSM components and presents analyses that demonstrate the adequacy of the design safety features of the EOS-HSM.

The following table shows the off-normal operating loads for which the EOS-HSM components are designed.

Load Type	Components	
	EOS-HSM	DSC Support Structure
Off-Normal Handling	X	X
Off-Normal Thermal	X	X

For an operating NUHOMS® EOS System, off-normal events could occur during fuel loading, TC handling, canister transfer, trailer towing, and other operational events. Two credible off-normal events as listed in the above table are defined that bound the range of off-normal conditions for EOS-HSM. The limiting off-normal events are defined as a jammed DSC during loading or unloading from the EOS-HSM and the extreme ambient temperatures of -40 °F (winter) and +117 °F (summer). These events bound the range of expected off-normal structural loads and off-normal temperatures range acting on the EOS-HSM. ANSYS FEMs described in Section 3.9.4.6 are used to evaluate concrete and support structure forces and moments due to these loads.

The FPS DSC support structure employs hand calculation methodology to calculate forces and moments by assuming it as a simply supported beam with concentrated load.

3.9.4.8.1 EOS-HSM Off-Normal Handling Loads (Ra) Analysis

This load case assumes that the EOS-TC is not accurately aligned with respect to the EOS-HSM resulting in binding of the DSC during a transfer operation causing the hydraulic pressure in the ram to increase. The ram force is limited to a maximum load of 135,000 lbs during insertion, as well as during retrieval. Therefore, for the DSC support structure, the off-normal jammed canister load (R_a) is defined as an axial load of 135 kips on one DSC support structure, plus a vertical load of one half the DSC weight (on both rails) at the most critical location.

3.9.4.8.2 EOS-HSM Off-Normal Thermal Loads Analysis

This load case is the same as the normal thermal load, but with an ambient temperature range from -40 °F to 117 °F. The temperature distributions for the extreme ambient conditions are used in the analysis for the concrete component evaluation.

3.9.4.9 Accident Condition Structural Analysis

The design basis accident events specified by ANSI/ANS 57.9-1984, and other credible accidents postulated to affect the normal safe operation of the EOS-HSM are addressed in this section.

Each accident condition is analyzed to demonstrate that the requirements of 10 CFR 72.122 are met and that adequate safety margins exist for the EOS-HSM design. The resulting accident condition stresses in the EOS-HSM components are evaluated and compared with the applicable code limits. The postulated accident conditions addressed in this section include:

- Tornado winds and tornado generated missiles (W_t , W_m)
- Design basis earthquake (E)

- Design basis flood (FL)
- Blocked Vent Accident Thermal (T_a)

ANSYS FEMs described in Section 3.9.4.6 are used to evaluate concrete and support structure forces and moments due to these loads.

The FPS DSC support structure employs hand calculation methodology to calculate forces and moments by assuming it as a simply supported beam with concentrated load.

3.9.4.9.1 Tornado Winds/Tornado Missile Load (W_t , W_m) Analysis

The most severe tornado generated wind and missile loads selected for analysis specified by NRC Regulatory Guide 1.76 [3.9.4-4] and NUREG-0800 [3.9.4-7]. The extreme design basis wind loads are less severe than tornado generated wind loads and, therefore, do not need to be addressed.

The tornado wind intensities used for the EOS-HSM analysis are obtained from NRC Regulatory Guide 1.76, Rev. 0 [3.9.4-4], which bound the design basis requirements. Region I intensities are utilized since they result in the most severe loading parameters. For this region, the maximum wind speed is 360 mph, the rotational speed is 290 mph, and the maximum translational speed is 70 mph. The radius of the maximum rotational speed is 150 ft, the pressure drop across the tornado is 3 psi and the rate of pressure drop is 2 psi per second [3.9.4-4].

The maximum wind speed used of 360 mph provides substantial conservatism relative to the maximum wind speed of 230 mph prescribed in current regulatory guidance in NRC Regulatory Guide 1.76 Revision 1 [3.9.4-22]. For the purposes of the structural evaluation as described in Chapter 3 and its associated appendices, as well as the accident evaluation as described in Chapter 12 the design basis tornado (DBT) refers to the bounding criteria from Regulatory Guide 1.76, Rev. 0 used in the analysis.

Tornado loads are generated for three separate loading phenomena:

- Pressure or suction forces created by drag as air impinges and flows past the EOS-HSM. These pressure or suction forces are due to tornado generated wind with maximum wind speed of 360 mph.
- Pressure or suction forces created by drag due to tornado generated pressure drop or differential pressure load of 3 psi.
- Impact, penetration and spalling forces created by tornado-generated missiles impinging on the EOS-HSM.

The determination of impact forces created by tornado missiles for the EOS-HSM is consistent with that presented in Section 2.3.1.2. The four types of missiles listed below envelope the missile spectrum of NUREG-0800, Revision 2, Section 3.5.1.4 [3.9.4-7]. These missiles also bound the design basis missile spectrum of NRC Regulatory Guide 1.76, Revision 1 [3.9.4-22] and NUREG 0800, Revision 3, Section 3.5.1.4 [3.9.4-8]. Evaluation of the effects of small diameter spherical missiles (artillery) is not required because there are no openings in the EOS-HSM leading directly to the DSC through which such missiles could pass.

1. Utility wooden pole, 13.5" diameter, 35' long, Weight = 1124 lbs, Impact velocity = 180 fps.
2. Armor piercing artillery shell 8" diameter, Weight = 276 lbs, Impact velocity = 185 fps.
3. Steel pipe, 12" diameter, Schedule 40, 15 ft long, Weight = 750 lbs, Impact velocity = 154 fps.
4. Automobile traveling through the air not more than 25 ft above the ground and having contact area of 20 sq. ft, Weight = 4000 lbs, Impact Horizontal Velocity = 195 fps.

Stability and stress analyses are performed to determine the response of the EOS-HSM to tornado wind pressure loads. The stability analyses are discussed in detail in Appendix 3.9.7. The stress analyses are performed using the ANSYS FEM of a single EOS-HSM to determine design forces and moments. These conservative analyses envelope the effects of wind pressures on the EOS-HSM array. Thus, the requirements of 10 CFR 72.122 are met.

The EOS-HSM is qualified for maximum design basis tornado (DBT) generated design wind loads of 218 psf and 154 psf on the windward and leeward EOS-HSM walls (See Table 3.9.4-1 and Table 3.9.4-2), and a pressure drop of 3 psi.

A single, stand-alone EOS-HSM is protected by shield walls, or an adjacent module on either side and at the rear. For an EOS-HSM array, the critical module is on the windward end of the array. This module has an end shield wall to protect the module from tornado missile impacts. The shield wall is also subjected to the 218 psf windward pressure load. The leeward side of the same end module in the array has no appreciable suction load due to the presence of the adjacent module. The 154 psf suction load is applicable to the end shield wall on the opposite end module in the array. A suction of 326 psf is also applied to the roof of each EOS-HSM in the array.

For the stress analyses, the DBT wind pressures are applied to the EOS-HSM as uniformly distributed loads. The rigidity of the EOS-HSM in the transverse direction, due to frame and shear wall action of the EOS-HSM, is the primary load transfer mechanism assumed in the analysis. The bending moments and shear forces at critical locations in the EOS-HSM concrete components are calculated by performing an analysis using the ANSYS analytical model of the EOS-HSM as described in Section 3.9.4.6. The resulting moments and forces are included in the EOS-HSM load combination results reported in Table 3.9.4-7 to Table 3.9.4-10 and in the EOS-HSM-FPS load combinations reported in Table 3.9.4-13a and Table 3.9.4-14a.

Conservatively, the design basis extreme wind pressure loads are assumed to be equal to those calculated for the DBT (based on 360 mph wind speed) in the formulation of EOS-HSM load combination results.

In addition, the adequacy of the EOS-HSM to resist tornado missile loads is checked using the modified National Defense Research Committee (NDRC) empirical formulae [3.9.4-13] for local damage evaluation, and response chart solution method [3.9.4-18] for global response. These evaluations are described in Section 3.9.4.10.6.

3.9.4.9.2 Earthquake (Seismic) Load (E) Analysis

The design basis seismic load used for analysis of the EOS-HSM components is as discussed in Section 2.3.4. Based on U.S. NRC (NRC) Regulatory Guide 1.61 [3.9.4-3], a damping value of four percent is used for seismic analysis of steel structural components and a damping value of seven percent is used for seismic analysis of concrete components of EOS-HSM. An evaluation of the frequency content of the loaded EOS-HSM is performed to determine the amplified accelerations associated with the design basis seismic response spectra for EOS-HSM.

The design basis accelerations for the EOS-HSM are amplified based on the results of the frequency analysis of the EOS-HSM. The results of the frequency analysis of the EOS-HSM structure (which includes a simplified model of the DSC) yield a lowest frequency of 18.7 Hz in the transverse direction and 32.7 Hz in the longitudinal direction. The lowest vertical frequency exceeds 45 Hz; therefore the spectral acceleration is not amplified in vertical direction. Thus, based on the Regulatory Guide 1.60 response spectra amplifications, and conservatively using ZPA accelerations of 0.50g and 0.33g in the horizontal and vertical directions, respectively, the corresponding seismic accelerations used for the design of the EOS-HSM are 0.936g and 0.628g in the transverse and longitudinal directions, respectively, and 0.333g in the vertical direction. The resulting amplified accelerations are given in Table 3.9.4-3.

An equivalent static analysis of the EOS-HSM is performed using the ANSYS model described in Section 3.9.4.6 by applying the amplified seismic accelerations load. These amplified accelerations are determined based on the frequency analysis of the EOS-HSM. The frequency analysis of EOS-HSM and multi-segment design EOS-HSMS was performed individually and found that EOS-HSMS yields bounding amplified acceleration. Therefore, the bounding amplified acceleration derived from modal analysis of EOS-HSMS is conservatively used for both EOS-HSM and EOS-HSMS.

Similarly, the frequency analysis of EOS-HSM-FPS and multi-segment design EOS-HSMS-FPS was performed individually and found that EOS-HSMS-FPS yields bounding amplified acceleration. Therefore, the bounding amplified acceleration derived from modal analysis of EOS-HSMS-FPS is conservatively used for both EOS-HSM-FPS and EOS-HSMS-FPS.

The responses for each orthogonal direction are combined using the square root of the sum of the squares (SRSS) method. The resulting moments and forces due to combined seismic load are included in the EOS-HSM load combination results.

For sites where the response spectra at the base of the HSM are larger than analyzed, more than one module may need to tie together to prevent significant sliding or to prevent the modules from banging into each other causing unacceptable damage. The reinforcement requirement may also need to be reviewed, and additional rebar may be added for such sites.

The stability evaluation of the EOS-HSM due to a 0.45g Horizontal/0.30g Vertical seismic load is discussed in Appendix 3.9.7.

For dynamic analysis, the stability evaluation shall be performed using the analysis methodology described in CoC 1029 [3.9.4-21].

Seismic analysis of the EOS-HSM heat shields consists of a modal time-history analysis of the EOS-HSM for obtaining the ISRS at heat shields support locations and an equivalent static analysis of the EOS-HSM heat shields using the seismic acceleration load corresponding to the ISRS obtained in the first step. The earthquake time histories compatible with the RG 1.60 spectra are used as seismic input motion. The acceleration, velocity, and displacement time histories and corresponding spectra of the motion in the two horizontal and vertical directions, all with 1.0g ZPA, are shown in Figure 3.9.4-10 through Figure 3.9.4-15. The ISRS of the side heat shield support nodes are shown in Figure 3.9.4-10, Figure 3.9.4-11, and Figure 3.9.4-12. Modal frequencies and mass participation factors of the EOS-HSMS are shown in Table 3.9.4-23 for *EOS-HSMS*, Table 3.9.4-23a for *EOS-HSMS-FPS for the minimum length DSC (governing configuration)*. From the modal time-history analysis, the ISRS with a damping value of four percent are obtained at the support locations of the heat shields are shown in Figure 3.9.4-16 through Figure 3.9.4-21. Modal participations factors for the *EOS-HSM* roof heat shield and side heat shield are shown in Table 3.9.4-24 and Table 3.9.4-25, respectively. *Similarly, EOS-HSM-FPS modal participations factors for the roof heat shield and side heat shield are shown in Table 3.9.4-24 and Table 3.9.4-25a, respectively.* The ISRS for the head heat shields is conservatively determined using ground motion based on the RG 1.60 spectra anchored at 0.50g and 0.33g in the horizontal and vertical directions, respectively.

3.9.4.9.3 Flood Load (FL) Analysis

Since the source of flooding is site specific, the exact source, or quantity of flood water, should be established by the licensee. However, for this generic evaluation of the EOS-HSM, bounding flooding conditions are specified that envelope those that are postulated for most plant sites. As described in Section 2.3.3, the design basis flooding load is specified as a 50-foot static head of water and a maximum flow velocity of 15 feet per second. Each licensee should confirm that this represents a bounding design basis for their specific ISFSI site.

Since the EOS-HSM is open to the atmosphere, static differential pressure due to flooding is not a design load.

The maximum drag pressure, D , acting on the EOS-HSM due to a 15 fps flood water velocity is calculated as follows:

$$D = \frac{C_D \rho_w V^2}{2g} \quad [3.9.4-20]$$

Where:

V = 15 fps, Flood water velocity

C_D = 2.0, Drag coefficient for flat plate

$$\begin{aligned}\rho_w &= 62.4 \text{ lb/ft}^3, \text{ Flood water density} \\ g &= 32.2 \text{ ft/sec}^2, \text{ Acceleration due to gravity} \\ D &= \text{Drag pressure (psf)}\end{aligned}$$

The resulting flood induced drag pressure is: $D = 436$ psf.

The following flood load cases are considered to account for different flow direction:

- Case 1: Flood water flow from front to rear of EOS-HSM
- Case 2: Flood water flow from rear to front of EOS-HSM
- Case 3: Flood water flow from right side to left side of EOS-HSM or vice versa

ANSYS FEM described in Section 3.9.4.6 is used for the structural evaluation. The results for flood load case are obtained by enveloping results from above load cases.

The stability evaluation of EOS-HSM due to flood load is discussed in Appendix 3.9.7.

3.9.4.9.4 Accident Blocked Vent Thermal (T_a) Stress Analysis

This accident conservatively postulates the complete blockage of the EOS-HSM ventilation air inlet and outlet openings.

Since the EOS-HSMs are located outdoors; there is a remote probability that the ventilation air inlet and outlet vent openings could become blocked by debris from events such as flooding, high wind and tornados. Design features, such as the perimeter security fence and the redundant protected location of the air inlet, and outlet vent openings and the screens reduce the probability of occurrence of such an accident. Nevertheless, for this conservative generic analysis, such an accident is postulated to occur and is analyzed.

The postulated accident thermal event occurs due to blockage of the air inlet and outlet vents under off-normal ambient temperatures range from -40 °F to 117 °F.

ANSYS FEM described in Section 3.9.4.6 is used for the structural analysis for accident blocked vent condition.

3.9.4.10 Structural Evaluation

The load categories associated with normal operating conditions, off-normal conditions and postulated accident conditions are described previously. The load combination results and design strengths of EOS-HSM components are presented in this section.

3.9.4.10.1 EOS-HSM Concrete Components

To determine the required strength (internal axial forces, shear forces, and bending moments) for each EOS-HSM concrete component, linear elastic finite element analyses are performed for the normal, off-normal, and accident loads using the analytical models described in Section 3.9.4.6 for mechanical and thermal loads.

The concrete design loads are multiplied by load factors and combined to simulate the most adverse load conditions. The load combinations listed in Table 3.9.4-5 are used to evaluate the concrete components. The bounding load combination results for each component are presented in Table 3.9.4-7 to Table 3.9.4-10 for EOS-HSM and Table 3.9.4-13a and Table 3.9.4-14a *for the EOS-HSM-FPS and EOS-HSMS-FPS configurations*. Table 3.9.4-11a, Table 3.9.4-12a, Table 3.9.4-13a, Table 3.9.4-14a, and Table 3.9.4-14b *provide concrete capacities and bounding results for the demand/capacity ratios for all analyzed HSM-DSC configurations*. The notations for the components of forces and moments and the concrete component planes in which capacities are computed are shown in Figure 3.9.4-5. The thermal stresses of EOS-HSM concrete components used in the load combination results are based on thermal results that bound those reported in Chapter 4. All load combination results are less than computed section capacities.

The required strength, U , for critical sections of concrete is calculated in accordance with the requirements of ANSI 57.9 [3.9.4-10] and ACI 349-06 [3.9.4-12], including the strength reduction factors defined in ACI 349-06, Section 9.3. The design strength of EOS-HSM concrete components exceeds the factored design loads. Thus, the EOS-HSM concrete components are adequate to perform their intended function. EOS-HSM construction details such as construction joints and reinforcement bar splices is detailed on the construction drawings.

3.9.4.10.2 DSC Support Structure

The DSC main support beams, stiffener plates, extension baseplates, DSC stop plates and braces members of the DSC support structure and 12"x1" plates, tubesteel spacers, stop plates, and extension baseplates of the FPS DSC support structure are evaluated using the allowable strength design method of the AISC Manual of Steel Construction [3.9.4-14]. The maximum temperature used in the stress analysis of the support steel bounds the maximum temperature reported in Chapter 4.

The load combination results for each of these components are provided in Table 3.9.4-17 to Table 3.9.4-22 for the DSC support structure and Table 3.9.4-17a, Table 3.9.4-21a, and Table 3.9.4-22a for the FPS DSC support structure. The maximum value of demand to capacity ratio of DSC support structure is less than 1.0. Thus, DSC support structure is adequately strong to resist the reasonably foreseeable loads applied to it.

3.9.4.10.3 EOS-HSM Shield Door

The shield door is free to grow in the radial direction when subjected to thermal loads. Therefore, there are no stresses in the door due to thermal growth. The dead weight, tornado wind, differential pressure and flood loads cause insignificant stresses in the door compared to stresses due to missile impact load. Therefore, the door is evaluated only for the missile impact load.

The minimum thickness of concrete component to prevent perforation, and scabbing are 18.5 inches and 27.7 inches, respectively. Thus, the 30.5-inch thick door is adequate to protect from local damage due to missile impact. The computed maximum ductility ratio for the door is less than 1, which satisfies the ductility requirement if compared against the allowable ductility ratio of 10 as per ACI 349-06 [3.9.4-12]. Therefore, the concrete door meets the ductility requirement and is adequate to protect from global effect of missile impact.

For the door anchorage, the controlling load is tornado generated differential pressure drop load. The maximum tensile force per bolt (four door attachment bolts), is 7.6 kips. The design strength of door attachment embedment (nonductile) as per Section D.3.6.3 of ACI 349-06 [3.9.4-12] is 17.99 kips, which is greater than 7.6 kips, thus satisfying the ACI 349-06 code requirement.

3.9.4.10.4 EOS-HSM Heat Shield

The roof heat shield assembly consists of four panels. Each panel section is a v-shaped in transverse direction with v-notch at the center of the EOS-HSM width. The roof heat shield panels are connected to the roof by fifteen, $\frac{3}{4}$ -10UNC bolts. The natural lateral frequency of a typical panel/connection stud system is determined from ANSYS computer code. The maximum interaction ratio for combined axial and bending stress in the connection bolts is 0.503 and 0.550 for EOS-HSM and EOS-HSM-FPS options, respectively, which is less than 1.0. The maximum bending moment in roof heat shield panel is 22.29 in-lb/in. and 23.30 in-lb/in, respectively for the EOS-HSM and EOS-HSM-FPS options, respectively, which is also less than the panel moment capacity of 59.59 in-lb/in.

The side wall heat shield assembly also consists of four panels. The side wall heat shield panels are attached to the EOS-HSM short and long base unit side wall by seventeen 1/2-13UNC bolts on both sides and EOS-HSM medium base unit side wall by fifteen 1/2-13UNC bolts on both sides. The maximum interaction ratio for combined axial and bending stress in connection bolts is 0.563 and 0.271 for EOS-HSM and EOS-HSM-FPS options, respectively, which is less than 1.0. The maximum bending moment in side heat shield panel is 46.98 in-lb/in and 20.38 in-lb/in, respectively for the EOS-HSM and EOS-HSM-FPS options, respectively., which is also less than the panel moment capacity of 59.59 in-lb/in.

The maximum temperature used in the stress analysis of the heat shields bounds the maximum temperatures reported in Chapter 4. The size of the slot hole provided in the panel at the connection bolt location is sufficiently large to allow for free thermal expansion. Therefore, neither of roof heat shield panel and side wall heat shield panel is subjected to thermal stress.

3.9.4.10.5 EOS-HSM DSC Axial Restraint

The DSC axial restraint consists of a capped steel tube embedment located within the bottom center of the round access opening of the EOS-HSM front wall, and a 2-inch by 4-inch solid bar steel retainer that drops into the embedment cavity after DSC transfer is complete. The drop-in retainer extends approximately 5 inches above the top of embedment to provide axial restraint of the DSC. The maximum seismically induced shear load in the retainer is 140.5 kips and 134.67 kips for EOS-HSM and EOS-HSM-FPS options, respectively. The allowable shear strength of the axial retainer is 196.0 kips. The maximum seismically induced moment in the retainer is 281.0 in-kips and 269.33 in-kips for EOS-HSM and EOS-HSM-FPS options, respectively, taking a moment arm of 2 inches, conservatively. The allowable flexural strength of axial retainer is 344.9 in-kips. Hence, the DSC axial retainer design is adequate to perform its intended function.

3.9.4.10.6 Evaluation of Concrete Components for Missile Loading

Missile impact effects are assessed in terms of local damage and overall structural response. Local damage that occurs in the immediate vicinity of the impact area is assessed in terms of penetration, perforation, spalling and scabbing. Evaluation of local effects is essential to ensure that protected items (the DSC and fuel) would not be damaged by a missile perforating a protective barrier, or by secondary missiles such as scabbing particles. Evaluation of overall structural response is essential to ensure that protected items are not damaged or functionally impaired by deformation or collapse of the impacted structure.

The tornado-generated missiles are conservatively assumed to strike normal to the surface with the long axis of the missile parallel to the line of flight to maximize the local effects. Plastic deformation to absorb the energy input by the tornado-generated missile load is desirable and acceptable, provided that the overall integrity of the structure is not impaired. Due to complex physical process associated with missile impact effects, the EOS-HSM structure is primarily evaluated conservatively by application of empirical formulae.

3.9.4.10.6.1 Local Damage Evaluation

Local missile impact effects consist of (a) missile penetration into the target, (b) missile perforation through the target, and (c) spalling and scabbing of the target. This also includes punching shear in the region of the target. Per F.7.2.3 of ACI 349-06 [3.9.4-12], if the concrete thickness is at least 20% greater than that required to prevent perforation, the punching shear requirement of the code need not be checked.

The following enveloping missiles are considered for local damage:

- Utility wooden pole
- Armor piercing artillery shell
- 12-inch diameter schedule 40 steel pipe

Large deformable missiles such as automobiles are incapable of producing significant local damage. Concrete thickness satisfying the global structural response requirements including punching shear is considered to preclude unacceptable local damage. Therefore, the local effects from an automobile are evaluated using punching shear criteria of ACI 349-06 [3.9.4-12].

The following empirical formulae are used to determine the local damage effects on reinforced concrete target:

B. Modified NDRC formulas for penetration depth [3.9.4-13]:

$$x = \sqrt{4KNWd \left(\frac{v_o}{1000 d} \right)^{1.8}}, \text{ for } x/d \leq 2.0$$

$$x = \left[KNW \left(\frac{v_o}{1000 d} \right)^{1.8} \right] + d, \text{ for } x/d > 2.0$$

Where,

x = Missile penetration depth, inches

$$K = \text{concrete penetrability factor} = \frac{180}{\sqrt{f'_c}}$$

N = projectile shape factor
 = 0.72 flat nosed
 = 0.84 blunt nosed
 = 1.0 bullet nosed (spherical end)
 = 1.14 very sharp nose

W = weight of missile, lb

v_o = striking velocity of missile, fps

d = effective projectile diameter, inches.

for a solid cylinder, d = diameter of projectile and

for a non-solid cylinder, $d = (4A_c/\pi)^{1/2}$

A_c = projectile impact area, in²

C. Modified NDRC formula for perforation thickness [3.9.4-13]:

$$\frac{e}{d} = 3.19 \left(\frac{x}{d} \right) - 0.718 \left(\frac{x}{d} \right)^2, \text{ for } x/d \leq 1.35$$

$$\frac{e}{d} = 1.32 + 1.24 \left(\frac{x}{d} \right), \text{ for } 1.35 \leq x/d \leq 13.5$$

Where,

e = perforation thickness, in.

In order to provide an adequate margin of safety the design thickness $t_d = 1.2e$
 [3.9.4-12]

D. Modified NDRC formula for scabbing thickness [3.9.4-13]:

$$\frac{s}{d} = 7.91 \left(\frac{x}{d} \right) - 5.06 \left(\frac{x}{d} \right)^2, \text{ for } x/d \leq 0.65$$

$$\frac{s}{d} = 2.12 + 1.36 \left(\frac{x}{d} \right), \text{ for } 0.65 \leq x/d \leq 11.75$$

Where,

s = scabbing thickness, in.

In order to provide an adequate margin of safety the design thickness $t_d = 1.2s$
 [3.9.4-12]

The concrete targets of the EOS-HSM that may be subjected to local damage due to missile impact are:

- 44-inch thick roof

- 42-inch thick (minimum) front wall
- 36-inch thick end shield wall
- 36-inch thick rear shield wall
- 30.5-inch thick shielding door

The minimum thickness of concrete target components listed above is 30.5 inches. So, the required perforation thickness and require scabbing thickness is compared against 30.5 inches to ensure the adequacy of design.

3.9.4.10.6.1.1 Local Impact Effects of Utility Wooden Pole Missile

Per section 6.4.1.2.5 of [3.9.4-13], utility wooden pole missiles do not have sufficient strength to penetrate a concrete target and that the scabbing thickness required for wood missiles is substantially less than that required for a steel missile with the same mass and velocity. Practically, wooden pole missiles do not appear to be capable of causing local damage to the 12-inch or thicker walls (also see Section 2.1.1 of [3.9.4-18]). Since none of the concrete targets are less than 12 inches thick, the postulated wood missiles do not cause any local damage to the EOS-HSM concrete component.

3.9.4.10.6.1.2 Local Impact Effects of Armor Piercing Artillery Shell Missile

The penetration depth for this missile is calculated using the NDRC Formula as given in Section 3.9.4.10.6.1 (a) and the parameters used in the formula are as listed below:

$d = 8.0$ in.	effective diameter of missile
$W = 276$ lb	weight of missile
$v_o = 185$ fps	striking velocity of missile
$f'_c = 5000$ psi	concrete compressive strength
$K = 180/\sqrt{5000} = 2.55$	concrete penetrability factor
$N = 0.84$	projectile shape factor (blunt nosed)
Penetration depth, $x = 4.6$ in.	for $x/d (= 0.58) \leq 2.0$
Perforation thickness, $e = 12.9$ in.	for $x/d (= 0.58) \leq 1.35$
Required perforation thickness = $1.2 * 12.9 = 15.5$ in. < 30.5 in.	
Scabbing thickness, $s = 23.1$ in.	for $x/d (= 0.58) \leq 0.65$
Required scabbing thickness = $1.2 * 23.1 = 27.7$ in. < 30.5 in.	

Therefore, penetration, perforation and scabbing of the concrete components of EOS-HSM do not occur due to this missile impact.

3.9.4.10.6.1.3 Local Impact Effects of 12-Inch Diameter Schedule 40 Steel Pipe Missile

The penetration depth for this missile is calculated using the NDRC Formula as given in Section 3.9.4.10.6.1 (A) and the parameters used in the formula are as listed below:

$\phi = 12.75$ in. outer diameter of 12" dia. schedule 40 steel pipe.

$A_c = 15.74$ in² missile impact area (cross sectional area of steel)

$d = (4 \cdot 15.74 / \pi)^{1/2} = 4.5$ in. effective diameter of missile

$W = 750$ lb weight of missile

$v_o = 154$ fps striking velocity of missile

$f'_c = 5000$ psi concrete compressive strength

$K = 180 / \sqrt{5000} = 2.55$ concrete penetrability factor

$N = 0.72$ projectile shape factor (flat nosed)

Penetration depth, $x = 7.6$ in. for $x/d (= 1.69) \leq 2.0$

Perforation thickness, $e = 15.4$ in. for $1.35 \leq x/d (= 1.69) \leq 13.5$

Required perforation thickness = $1.2 \cdot 15.4 = 18.5$ in. < 30.5 in. OK

Scabbing thickness, $s = 19.9$ in. for $0.65 \leq x/d (= 1.69) \leq 11.75$

Required scabbing thickness = $1.2 \cdot 19.9 = 23.9$ in. < 30.5 in. OK

Therefore, penetration, perforation and scabbing of the concrete components of EOS-HSM do not occur due to this missile impact.

3.9.4.10.6.2 Global Structural Response

When a missile strikes a structure, large forces develop at the missile-structure interface, which decelerate the missile and accelerate the structure. The response of the structure depends on the dynamic properties of the structure and the time dependent nature of the applied loading (interface force-time function). The force-time function is, in turn, dependent on the type of impact (elastic or plastic) and the nature and extent of local damage.

In an elastic impact, the missile and the structure deform elastically, remain in contact for a short period of time (duration of impact), and subsequently disengage due to the action of elastic interface restoring forces.

In a plastic impact, the missile or the structure (or both) may sustain permanent deformation or damage (local damage). Elastic restoring forces are small, and the missile and the structure tend to remain in contact after impact. Plastic impact is much more common than elastic impact, which is rarely encountered. Test data have indicated that the impact from all postulated tornado-generated missiles can be characterized as a plastic impact.

If the interface forcing function can be defined or conservatively idealized, the structure can be modeled mathematically, and conventional analytical or numerical techniques can be used to predict structural response. If the interface forcing function cannot be defined, the same mathematical model of the structure can be used to determine structural response by application of conservation of momentum and energy balance techniques with due consideration for type of impact (elastic or plastic).

In either case, in lieu of a more rigorous analysis, a conservative estimate of structural response can be obtained by first determining the response of the impacted structural element, and then applying its reaction forces to the supporting structure. The predicted structural response enables assessment of structural design adequacy in terms of strain energy capacity, deformation limits, stability and structural integrity.

The overall structural response of each component as a whole (global response) is determined by single degree of freedom analysis using response charts solution method of [3.9.4-18].

The following enveloping missiles are considered for global structural response:

- Utility wooden pole
- Armor piercing artillery shell
- 12-inch diameter schedule 40 steel pipe
- Automobile missile

The peak interface force and impact duration for each missile are calculated as follows:

A. Utility Wooden Pole Missile

For wooden missile, the interface forcing function is a rectangular pulse having a force magnitude of F and duration t_i , per Section 2.3.1 of [3.9.4-18]

$$F = PA$$

$$t_i = M_m v_c / F$$

Where,

F = interface force (lb)

P = interface pressure (psi) = 2500 psi for wood missiles [3.9.4-18]

A = cross sectional area of the missile (in^2) = $\pi * 13.52/4 = 143.1 \text{ in}^2$

t_i = impact duration (sec)

W_m = weight of missile (lb) = 1124 lb

$$M_m = \text{missile mass (lb-sec}^2/\text{ft)} = W_m/g = 1124 \text{ lb} / 32.2 \text{ ft/sec}^2 = 34.9 \text{ lb-sec}^2/\text{ft}$$

$$v_c = \text{change in velocity during impact (conservatively } = v_s) \text{ (fps)} = 180 \text{ fps}$$

Therefore,

$$F = 358 \text{ kip and } t_i = 0.018 \text{ sec}$$

B. Armor Piercing Artillery Shell

For solid steel missile, the concrete is a soft target per section 6.4.2 of [3.9.4-13] with a penetration depth of 4.6 in. The interface forcing function is a rectangular pulse per Section 6.4.2.1.1 of [3.9.4-13].

$$F = W_m V_0^2 / 2gX$$

$$t_i = 2X/V_0$$

Where,

F = interface force (lb)

t_i = impact duration (sec)

W_m = missile weight (lb) = 276 lb

V_0 = initial velocity of the missile (fps) = 185 fps

X = penetration depth = 4.6 in.

Therefore,

$$F = 383 \text{ kip and } t_i = 0.00414 \text{ sec}$$

C. 12-Inch Diameter Schedule 40 Steel Pipe

For steel pipe missile, the interface forcing function is a triangular pulse per Section 2.3.2 of [3.9.4-18].

$$t_i = 400M_m / PA$$

$$F = (2M_m v_s) / t_i$$

Where,

F = peak interface force (lb)

P = collapse stress of pipe (psi) = 60000 psi

A = cross sectional metal area of the missile (in^2) = 15.74 in^2

t_i = impact duration (sec)

W_m = weight of missile (lb) = 750 lb

M_m = missile mass (lb-sec²/ft) = $W_m/g = 750 \text{ lb} / 32.2 \text{ ft/sec}^2 = 23.29 \text{ lb-sec}^2/\text{ft}$

v_s = striking velocity of missile = 154 fps

Therefore,

$F = 718 \text{ kip}$ and $t_i = 0.01 \text{ sec}$

D. Automobile Missile

For automobile missile, the interface forcing function per 2.3.3 of [3.9.4-18] is as follows:

$F_t = 0.625 v_c W \sin(20t) \quad 0 < t \leq 0.0785 \text{ sec}$

$F_t = 0 \quad t > 0.0785 \text{ sec}$

Where,

F_t = force as a function of time (lb)

W = weight of automobile (lb) = 4000 lb

v_c = change in velocity during impact (conservatively = v_s) (fps) = 195 fps

Therefore,

$F = 488 \text{ kip}$ and $t_i = 0.0785 \text{ sec}$

The end wall, rear wall, base front wall, roof and door of EOS-HSM are evaluated for global response, since these components may interface with missile loading. The end/rear walls and door are idealized as a simply supported plate while the base front wall and roof are idealized as simply supported beam for structural response. The yield resistance and fundamental period of vibration of concrete components is then determined based on the assumed idealized boundary condition using the equations given in Section 4.4 of [3.9.4-18]. The calculated value of yield resistance, R_y , and fundamental period of vibration, T_n , for different concrete components are tabulated below.

Component	R_y (kip)	T_n (sec)
End Wall	446.1	0.0180
Rear Wall	919.9	0.0065
Base Front Wall	1116.1	0.0045
Roof	402.0	0.0301
Door	1211.0	0.00208

In the response chart solution method, the structural response is determined by entering the chart with calculated values of C_T and C_R to determine the ductility ratio, μ , which is compared against the allowable ductility ratio as given in Appendix F of ACI 349-06 [3.9.4-12]. The dimensionless ratios, C_T and C_R , are defined as follows:

$$C_R = \frac{R_y}{F} \qquad C_T = \frac{t_i}{T_n}$$

The maximum value of ductility ratio of all five components is found to be less than 10. The allowable ductility ratio per ACI 349-06 [3.9.4-12] is 10. Hence, the global response of EOS-HSM is within deformation limit meeting the ductility requirement.

Each component is also evaluated for punching shear capacity with interfacing utility wooden pole missile and automobile missile. All the components have punching shear capacity greater than the peak missile interface force.

3.9.4.11 Conclusions

The load categories associated with normal operating conditions, off-normal conditions and postulated accident conditions are described and analyzed in previous sections. The load combination results for EOS-HSM components important-to-safety are also presented. Comparison of the results with the corresponding design capacity shows that the design strength of the EOS-HSM is greater than the strength required for the most critical load combination.

3.9.4.12 References

- 3.9.4-1 Code of Federal Regulation Title 10, Part 72 (10CFR Part 72), "Licensing Requirements for the Independent Storage of Spent Nuclear Fuel, High-Level Radioactive Waste, and Reactor-Related Greater than Class C Waste."
- 3.9.4-2 U.S. Nuclear Regulatory Commission, Regulatory Guide 1.60, "Design Response Spectra for Seismic Design of Nuclear Power Plants," Revision 1, 1973.
- 3.9.4-3 U.S. Nuclear Regulatory Commission, Regulatory Guide 1.61, "Damping Values for Seismic Design of Nuclear Power Plants," Revision 1, March 2007.
- 3.9.4-4 U.S. Nuclear Regulatory Commission, Regulatory Guide 1.76, "Design Basis Tornado for Nuclear Power Plants," Revision 0, April 1974.
- 3.9.4-5 U.S. Nuclear Regulatory Commission, Regulatory Guide 1.92, "Combining Modal Responses and Spatial Components in Seismic Response Analysis," Revision 3, October 2012.
- 3.9.4-6 U.S. Nuclear Regulatory Commission, Regulatory Guide 1.122, "Development of Floor Design Response Spectra for Seismic Design of Floor-Supported Equipment or Components," Revision 1, 1978.

- 3.9.4-7 NUREG-0800, Standard Review Plan, Section 3.5.1.4, “Missiles Generated by Natural Phenomena,” Revision 2, July 1981.
- 3.9.4-8 NUREG-0800, Standard Review Plan, Section 3.3.1, “Wind Loading,” Section 3.3.2 “Tornado Loads,” and Section 3.5.1.4 “Missiles Generated by Tornado and Extreme Winds,” Revision 3, March 2007.
- 3.9.4-9 NUREG-1536, “Standard Review Plan for Spent Fuel Dry Storage Systems at a General License Facility,” Revision 1, U.S. Nuclear Regulatory Commission, July 2010.
- 3.9.4-10 ANSI/ANS 57.9-1984, “Design Criteria for an Independent Spent Fuel Storage Installation (Dry Storage Type),” American National Standards Institute, American Nuclear Society.
- 3.9.4-11 ACI-318-08, “Building Code Requirement for Structural Concrete,” American Concrete Institute.
- 3.9.4-12 ACI 349-06, “Code Requirements for Nuclear Safety Related Concrete Structures,” American Concrete Institute.
- 3.9.4-13 American Society of Civil Engineers, “Structural Analysis and Design of Nuclear Plant Facilities,” ASCE Publication No. 58.
- 3.9.4-14 American Institute of Steel Construction, AISC Manual of Steel Construction, 13th Edition.
- 3.9.4-15 American Society of Civil Engineers, “Minimum Design Loads for Buildings and Other Structures,” ASCE 7-10 (formerly ANSI A58.1).
- 3.9.4-16 AREVA Inc., “Updated Final Safety Analysis Report for the Standardized NUHOMS® Horizontal Modular Storage System for Irradiated Nuclear Fuel,” Revision 17, USNRC Docket Number 72-1004, *March 2018*.
- 3.9.4-17 Bechtel Power Corporation, “Design of Structures for Missile Impact,” Topical Report BCTOP-9A, Revision 2, San Francisco, California.
- 3.9.4-18 Bechtel Corporation, “Design Guide Number C-2.45 for Design of Structures for Tornado Missile Impact,” Rev. 0, April 1982.
- 3.9.4-19 “ANSYS Computer Code and User’s Manual”, Release 14.0.3 *and Release 17.1*.
- 3.9.4-20 Binder, Raymond C., “Fluid Mechanics,” 3rd Edition, Prentice-Hall, Inc, 1973.
- 3.9.4-21 AREVA Inc., “Updated Final Safety Analysis Report For The Standardized Advanced NUHOMS® Horizontal Modular Storage System For Irradiated Nuclear Fuel,” Revision 7, US NRC Docket Number 72-1029, *April 2016*.
- 3.9.4-22 U.S. Nuclear Regulatory Commission, Regulatory Guide 1.76, “Design Basis Tornado for Nuclear Power Plants,” Revision 1, March 2007.

Table 3.9.4-1
Design Pressures for Tornado Wind Flowing from Front Wall to Rear Wall
and Vice Versa

Component	Velocity Pressure, q_v (psf)	External Pressure Coefficient, C_p	Internal Pressure Coefficient, (GC_{pi})	Max. Design Pressure, $q_v * (G * C_p - GC_{pi})$ (psf)
Windward(Front/Rear Wall)	254	0.80	± 0.18	218
Leeward(Rear/Front Wall)		-0.30 ⁽¹⁾		-110
Side(Right Side Wall)		-0.70		-197
Side(Left Side Wall)		-0.70		-197
Roof		-1.30		-326

Notes:

1. The C_p value is taken for $L/B = 116"/268" \approx 0.40$ when analyzing EOS-HSM and ≈ 0.47 when analyzing EOS-HSM-FPS.
2. The gust effect factor, $G=0.85$ considering the EOS-HSM as rigid.

Table 3.9.4-2
Design Pressures for Tornado Wind Flowing from Right Side to Left Side
Wall and Vice Versa

Component	Velocity Pressure, q_v (psf)	External Pressure Coefficient, C_p	Internal Pressure Coefficient, (GC_{pi})	Max. Design Pressure, $q_v*(G*C_p - GC_{pi})$ (psf)
Side(Front Wall)	254	-0.70	± 0.18	-197
Side(Rear Wall)		-0.70		-197
Windward(Right/Left Side Wall)		0.80		218
Leeward(Left/Right Side Wall)		-0.50 ⁽¹⁾		-154
Roof		-1.30		-326

Notes:

1. The C_p value is taken for $L/B = 116"/268" \approx 0.40$ when analyzing EOS-HSM and ≈ 0.47 when analyzing EOS-HSM-FPS.
2. The gust effect factor, $G=0.85$ considering the EOS-HSM as rigid.

Table 3.9.4-3
Spectral Acceleration Applicable to Different Components of EOS-HSM for
Seismic Analysis

Direction	Frequency (Hz)	Spectral Acceleration Corresponding to ZPA = 0.5g horizontal & 0.333 g vertical ⁽¹⁾		
		at 3% Damping (for DSC)	at 4% Damping (for DSC support structure)	at 7% Damping (for concrete components)
X (Transverse)	18.7	1.229g	1.156g	0.936g
Y (Vertical)	60.3	0.333g	0.333g	0.333g
Z (Longitudinal)	32.7	0.694g	0.677g	0.628g

(1) Seismic loading conservatively exceeds the design basis ZPA values of 0.45g horizontal and 0.30g vertical.

Table 3.9.4-3a
Spectral Acceleration Applicable to Different Components of EOS-HSMS-
FPS for Seismic Analysis

Direction	Frequency (Hz)	Spectral Acceleration Corresponding to Design ZPA		
		at 3% Damping (for DSC)	at 4% Damping (for DSC support structure)	at 7% Damping (for concrete)
X (Transverse)	19.2	1.194g	1.125g	0.917g
Y (Vertical)	60.6	0.333g	0.333g	0.333g
Z	31.4	0.724g	0.704g	0.647g

Table 3.9.4-4
Load Cases for EOS-HSM Concrete Components Evaluation

Design Load Type	Load Notation	Design Parameters	Applicable Codes / References
Normal			
Dead	DL	Includes self-weight with 160 pcf density for concrete and 0.28 pci for steel support structure.	ANSI/ANS 57.9-1984 [3.9.4-10]
Live	LL	Design live load of 200 psf on roof which includes snow and ice load and DSC weight of 135 kip applied on DSC support rails.	ANSI/ANS 57.9-1984 [3.9.4-10] & ASCE 7-10 [3.9.4-15]
Normal Handling	R _o	The concrete module is evaluated for 140 kip DSC insertion load as a normal handling load. The DSC weight is also applied at both rail support locations (4 points).	
Normal Thermal	T _o	DSC with spent fuel rejecting up to 50.0 kW of decay heat. Extreme ambient air temp. -20 °F and 100 °F. Reference temperature = 70 °F.	
Off-Normal/Accidental			
Off-Normal Handling	R _a	For the steel support structure the magnitude of this load is 135 kip both for DSC insertion and retrieval, applied to one rail. The DSC weight is also applied at one rail support location (two points).	
Accidental Thermal	T _a	Enveloped of Off-Normal and Accidental Thermal (vent blocked) condition. Accidental thermal condition is same as off-normal condition with ambient temperature range of -40 °F to 117 °F. Reference temperature = 70 °F	
Earthquake	E	Zero period acceleration of 0.5g in horizontal and 0.333g in vertical direction with enhancement in frequency above 9 Hz and 7% damping. ⁽¹⁾	NRC Reg. Guide 1.60 [3.9.4-2] & Reg. Guide 1.61 [3.9.4-3]
Flood	FL	Maximum flood height of 50 ft and max. velocity of water 15 ft/sec	10 CFR Part 72 [3.9.4-1]
Wind/Tornado Wind	W/W _t	Maximum wind speed of 360 mph, and a pressure drop of 3 psi	ASCE 7-10 [3.9.4-15] & NRC Reg Guide 1.76 [3.9.4-4]
Tornado Generated Missile	W _m	4 types of tornado-generated missiles	NUREG-0800 Section 3.5.1.4 [3.9.4-7]

(1) Seismic loading conservatively exceeds the design basis ZPA values of 0.45g horizontal and 0.30g vertical.

Table 3.9.4-5
Load Combination for EOS-HSM Concrete Components Evaluation

Combination Number	Load Combination	Event
C1	$1.4 \text{ DL} + 1.7 (\text{LL} + \text{R}_o)$	Normal
C2	$1.05 \text{ DL} + 1.275 (\text{LL} + \text{T}_o + \text{W})$	Off-Normal – Wind
C3	$1.05 \text{ DL} + 1.275 (\text{LL} + \text{T}_o + \text{R}_a)$	Off-Normal – Handling
C4	$\text{DL} + \text{LL} + \text{T}_o + \text{E}$	Accident – Earthquake
C5	$\text{DL} + \text{LL} + \text{T}_o + \text{W}_t$	Accident – Tornado
C6	$\text{DL} + \text{LL} + \text{T}_o + \text{FL}$	Accident – Flood
C7	$\text{DL} + \text{LL} + \text{T}_a$	Accident – Thermal

Note: See Table 3.9.4-4 for notation.

Table 3.9.4-6
Strength Reduction Factors for Concrete

Type of Stress	Strength Reduction Factor, ϕ
Tension - Controlled	0.90
Compression - Controlled	0.65
Shear	0.75
Torsion	0.75
Bearing	0.65

Note: The strength reduction factors are taken from ACI 349-06, Section 9.3 [3.9.4-12].

Table 3.9.4-7
Demand of EOS-HSM Concrete Components for Shear Forces and Moments

Component	Load Combination	M₁ (in-kip/ft)	M₂ (in-kip/ft)	V_{o1} (kip/ft)	V_{o2} (kip/ft)	V_i (kip/ft)
1. Rear Wall Bottom (32")	C1 through C6	338.7	708.7	6.3	9.8	51.6
	C7	232.8	270.8	1.9	2.7	25.3
2. Rear Wall Top (12")	C1 through C6	36.9	106.6	5.1	6.4	13.7
	C7	24.5	69.3	4.2	2.9	7.6
3. Front Wall Bottom (54")	C1 through C6	1024.0	1877.2	14.2	13.0	57.6
	C7	1049.1	1735.2	3.1	3.1	25.2
4. Front Wall Top (42")	C1 through C6	949.7	1768.7	28.5	25.6	90.4
	C7	1353.1	2485.3	26.1	24.4	48.3
5. Side Wall Bottom (24")	C1 through C6	269.3	182.9	15.4	14.8	23.5
	C7	143.4	396.3	14.3	18.6	11.1
6. Side Wall Bottom (14")	C1 through C6	91.4	38.0	11.4	6.1	14.4
	C7	64.0	117.2	12.1	12.7	11.1
7. Side Wall Top (12")	C1 through C6	285.3	195.0	12.3	11.9	38.5
	C7	341.2	151.8	10.6	10.6	46.5
8. Roof (44")	C1 through C6	622.2	1831.5	46.1	49.5	21.5
	C7	283.6	1004.2	11.6	24.3	22.5

Table 3.9.4-8
Demand of EOS-HSM Concrete Components for Axial Forces and Moments

Component	Load Combination	T₁ (kip/ft)	T₂ (kip/ft)	C₁ (kip/ft)	C₂ (kip/ft)	M_{1P} (in-kip/ft)	M_{2P} (in-kip/ft)
1. Rear Wall Bottom (32")	C1 through C6	33.8	32.1	46.4	104.4	299.6	428.3
	C7	13.4	5.5	40.5	44.6	66.4	124.1
2. Rear Wall Top (12")	C1 through C6	9.5	23.6	7.5	29.6	36.9	43.4
	C7	7.1	40.0	15.1	15.8	20.1	45.8
3. Front Wall Bottom (54")	C1 through C6	72.2	65.6	51.3	122.3	1019.5	773.8
	C7	19.8	0.0	32.0	59.8	485.3	0.0
4. Front Wall Top (42")	C1 through C6	97.7	77.5	86.6	256.2	737.5	1137.7
	C7	22.1	32.8	38.7	98.9	1352.7	1796.9
5. Side Wall Bottom (24")	C1 through C6	28.0	37.6	48.2	70.2	267.5	158.6
	C7	22.5	58.7	28.0	38.8	97.1	324.9
6. Side Wall Bottom (14")	C1 through C6	19.4	16.5	47.6	15.9	75.9	37.9
	C7	31.5	62.9	21.9	6.1	64.0	117.2
7. Side Wall Top (12")	C1 through C6	27.5	49.7	157.1	103.7	44.4	49.0
	C7	56.9	11.7	138.0	108.7	64.5	132.3
8. Roof (44")	C1 through C6	24.4	67.5	35.4	107.1	621.8	1817.3
	C7	11.5	59.9	4.8	90.8	239.4	751.2

Table 3.9.4-9
Demand of EOS-HSMS Concrete Components for Shear Forces and Moments

Component	Load Combination	M₁ (in-kip/ft)	M₂ (in-kip/ft)	V_{o1} (kip/ft)	V_{o2} (kip/ft)	V_i (kip/ft)
1. Rear Wall Bottom (32")	C1 through C6	335.6	694.6	6.9	11.3	55.5
	C7	215.2	297.1	2.2	2.5	24.5
2. Rear Wall Top (12")	C1 through C6	69.4	110.3	4.9	7.7	52.9
	C7	25.1	66.2	3.2	3.0	8.5
3. Front Wall Bottom (54")	C1 through C6	970.2	1882.1	13.4	13.0	60.8
	C7	1028.4	1436.7	3.6	3.1	26.2
4. Front Wall Top (42")	C1 through C6	1077.5	1501.8	28.7	28.3	130.5
	C7	1500.8	2424.0	24.8	21.4	46.8
5. Side Wall Bottom (24")	C1 through C6	193.1	161.2	13.3	12.6	20.9
	C7	140.6	409.0	14.6	17.4	13.1
6. Side Wall Bottom (14")	C1 through C6	67.4	38.9	10.9	6.6	15.4
	C7	58.5	115.7	12.0	12.0	9.8
7. Side Wall Top (12")	C1 through C6	265.9	224.6	12.1	12.1	59.3
	C7	307.9	138.6	10.6	10.6	37.7
8. Roof (44")	C1 through C6	623.2	1839.1	39.3	49.8	22.3
	C7	291.1	979.2	10.2	21.8	20.8

Table 3.9.4-10
Demand of EOS-HSMS Concrete Components for Axial Forces and Moments

Component	Load Combination	T₁ (kip/ft)	T₂ (kip/ft)	C₁ (kip/ft)	C₂ (kip/ft)	M_{1P} (in-kip/ft)	M_{2P} (in-kip/ft)
1. Rear Wall Bottom (32")	C1 through C6	25.0	42.4	49.3	108.5	248.3	344.0
	C7	14.6	10.9	39.7	47.3	58.8	295.8
2. Rear Wall Top (12")	C1 through C6	51.4	43.7	306.1	132.2	44.1	29.1
	C7	7.5	34.8	21.9	22.4	21.2	42.4
3. Front Wall Bottom (54")	C1 through C6	54.1	88.6	75.0	117.7	800.5	412.6
	C7	20.5	0.0	35.3	62.5	486.1	0.0
4. Front Wall Top (42")	C1 through C6	111.6	103.8	426.5	336.5	352.2	907.9
	C7	45.6	80.0	65.8	163.9	1500.8	992.9
5. Side Wall Bottom (24")	C1 through C6	34.7	28.2	49.3	60.0	181.8	159.6
	C7	21.0	55.2	26.4	33.8	98.8	342.5
6. Side Wall Bottom (14")	C1 through C6	20.6	15.0	45.9	16.8	64.3	38.9
	C7	29.8	57.3	21.0	10.2	57.2	115.7
7. Side Wall Top (12")	C1 through C6	50.8	62.0	257.1	233.8	40.9	63.2
	C7	51.8	58.5	121.8	240.2	63.3	62.7
8. Roof (44")	C1 through C6	24.9	76.4	38.8	114.5	623.0	1824.9
	C7	10.4	46.9	4.9	94.0	246.1	746.4

Table 3.9.4-11
Ultimate Shear/Moment Capacities of Concrete Components

Component	Thermal Condition	V_{ui}	V_{uo1}	V_{uo2}	M_{u1}	M_{u2}
		kips/ft	kips/ft	kips/ft	kip-in/ft	kip-in/ft
1. Rear Wall Bottom (32")	Normal	90.4	38.3	38.3	886.8	886.8
	Accident	85.6	36.3	36.3	837.1	837.1
2. Rear Wall Top (12")	Normal	65.0	12.8	12.8	290.4	290.4
	Accident	61.4	12.2	12.2	273.8	273.8
3. Front Wall Bottom (54")	Normal	196.0	64.3	64.3	3,791.7	3,791.7
	Accident	185.4	61.0	61.0	3,578.1	3,578.1
4. Front Wall Top (42")	Normal	180.7	49.0	49.0	2,875.6	2,875.6
	Accident	170.9	46.5	46.5	2,712.9	2,712.9
5. Side Wall Bottom (24")	Normal	102.1	27.8	27.8	919.3	919.3
	Accident	96.6	26.4	26.4	867.3	867.3
6. Side Wall Bottom (14")	Normal	89.4	15.1	15.1	489.8	489.8
	Accident	84.5	14.3	14.3	461.7	461.7
7. Side Wall Top (12")	Normal	86.8	12.6	12.6	404.0	404.0
	Accident	82.1	11.9	11.9	380.6	380.6
8. Roof (44")	Normal	151.4	51.5	51.5	2,283.1	2,283.1
	Accident	143.3	48.9	48.9	2,154.6	2,154.6

Notes:

V_{ui} = Minimum of ultimate in plane shear capacities in planes 1 and 2.

V_{uo1} = Minimum ultimate out of plane shear capacity in plane 1.

V_{uo2} = Minimum ultimate out of plane shear capacity in plane 2.

M_{u1} = Minimum ultimate moment capacity in plane 1.

M_{u2} = Minimum ultimate moment capacity in plane 2.

Planes 1 and 2 are defined in Figure 3.9.4-5.

Ultimate shear/moment capacities of alternate front wall rebar layout reported in Table 3.9.4-26.

Table 3.9.4-11a
Ultimate Shear/Moment Capacities of FPS Concrete Components

Component	Thermal Condition	V_{ui}	V_{uo1}	V_{uo2}	M_{u1}	M_{u2}
		kip/ft	kip/ft	kip/ft	kip-in/ft	kip-in/ft
1. Rear Wall Side (24")	Normal	80.2	28.1	28.1	648.2	648.2
	Accident	75.9	26.6	26.6	611.8	611.8
2. Rear Wall Mid & Top (12")	Normal	65.0	12.8	12.8	290.4	290.4
	Accident	61.4	12.2	12.2	273.8	273.8
3. Interior Pedestal (12")	Normal	65.0	12.8	12.8	290.4	290.4
	Accident	61.4	12.2	12.2	273.8	273.8
4. Front Wall (42")	Normal	180.7	49.0	49.0	2,875.6	2,875.6
	Accident	170.9	46.5	46.5	2,712.9	2,712.9
5. Side Wall Bottom (24")	Normal	102.1	27.8	27.8	919.3	919.3
	Accident	96.6	26.4	26.4	867.3	867.3
6. Side Wall Bottom (14")	Normal	89.4	15.1	15.1	489.8	489.8
	Accident	84.5	14.3	14.3	461.7	461.7
7. Side Wall Top (12")	Normal	86.8	12.6	12.6	404.0	404.0
	Accident	82.1	11.9	11.9	380.6	380.6
8. Roof (44")	Normal	151.4	51.5	51.5	2,283.1	2,283.1
	Accident	143.3	48.9	48.9	2,154.6	2,154.6

Notes:

V_{ui} = Minimum of ultimate in plane shear capacities in planes 1 and 2.

V_{uo1} = Minimum ultimate out of plane shear capacity in plane 1.

V_{uo2} = Minimum ultimate out of plane shear capacity in plane 2.

M_{u1} = Minimum ultimate moment capacity in plane 1.

M_{u2} = Minimum ultimate moment capacity in plane 2.

Planes 1 and 2 are defined in Figure 3.9.4-5.

Table 3.9.4-12
Ultimate Axial/Moment Capacities of Concrete Components

Component	Thermal Condition	P_{tu}	P_{cu}	P_{ub1}	P_{ub2}	M_{ub1}	M_{ub2}
		kips/ft	kips/ft	kips/ft	kips/ft	kip-in/ft	kip-in/ft
1. Rear Wall Bottom (32")	Normal	59.6	880.4	490.2	490.2	4,802.8	4,802.8
	Accident	56.3	793.9	465.0	465.0	4,367.5	4,367.5
2. Rear Wall Top (12")	Normal	59.6	350.0	163.0	163.0	747.1	747.1
	Accident	56.3	316.5	154.6	154.6	687.3	687.3
3. Front Wall Bottom (54")	Normal	152.7	1,513.4	822.0	822.0	14,501.4	14,501.4
	Accident	144.2	1,365.9	779.7	779.7	13,222.4	13,222.4
4. Front Wall Top (42")	Normal	152.7	1,195.1	625.7	625.7	9,097.3	9,097.3
	Accident	144.2	1,079.5	593.5	593.5	8,318.6	8,318.6
5. Side Wall Bottom (24")	Normal	85.9	682.2	355.5	355.5	2,951.3	2,951.3
	Accident	81.1	616.2	337.2	337.2	2,699.1	2,699.1
6. Side Wall Bottom (14")	Normal	85.9	417.0	191.9	191.9	1,081.2	1,081.2
	Accident	81.1	377.5	182.1	182.1	995.7	995.7
7. Side Wall Top (12")	Normal	85.9	364.0	159.1	159.1	806.6	806.6
	Accident	81.1	329.8	151.0	151.0	744.4	744.4
8. Roof (44")	Normal	114.5	1,227.8	659.5	659.5	9,425.2	9,425.2
	Accident	108.1	1,108.0	625.5	625.5	8,597.8	8,597.8

Notes:

P_{tu} = Minimum of ultimate tensile capacities in planes 1 and 2.

P_{cu} = Minimum of ultimate compressive capacities in plane 1 and 2.

P_{ub1} = Minimum of ultimate balanced section compressive capacity in plane 1.

P_{ub2} = Minimum of ultimate balanced section compressive capacity in plane 2.

M_{ub1} = Minimum of ultimate balanced section moment capacity in plane 1.

M_{ub2} = Minimum of ultimate balanced section moment capacity in plane 2.

Planes 1 and 2 are defined in Figure 3.9.4-5.

Ultimate axial and balanced moment capacities of alternate front wall rebar layout reported in Table 3.9.4-26.

Table 3.9.4-12a
Ultimate Axial/Moment Capacities of FPS Concrete Components

Component	Thermal Condition	P_{tu}	P_{cu}	P_{ub1}	P_{ub2}	M_{ub1}	M_{ub2}
		kips/ft	kips/ft	kips/ft	kips/ft	kip-in/ft	kip-in/ft
1. Rear Wall Side (24")	Normal	59.6	668.2	359.3	359.3	2,782.8	2,782.8
	Accident	56.3	602.9	340.8	340.8	2,538.0	2,538.0
2. Rear Wall Mid & Top (12")	Normal	59.6	350.0	163.0	163.0	747.1	747.1
	Accident	56.3	316.5	154.6	154.6	687.3	687.3
3. Interior Pedestal (12")	Normal	59.6	350.0	163.0	163.0	747.1	747.1
	Accident	56.3	316.5	154.6	154.6	687.3	687.3
4. Front Wall (42")	Normal	152.7	1,195.1	625.7	625.7	9,097.3	9,097.3
	Accident	144.2	1,079.5	593.5	593.5	8,318.6	8,318.6
5. Side Wall Bottom (24")	Normal	85.9	682.2	355.5	355.5	2,951.3	2,951.3
	Accident	81.1	616.2	337.2	337.2	2,699.1	2,699.1
6. Side Wall Bottom (14")	Normal	85.9	417.0	191.9	191.9	1,081.2	1,081.2
	Accident	81.1	377.5	182.1	182.1	995.7	995.7
7. Side Wall Top (12")	Normal	85.9	364.0	159.1	159.1	806.6	806.6
	Accident	81.1	329.8	151.0	151.0	744.4	744.4
8. Roof (44")	Normal	114.5	1,227.8	659.5	659.5	9,425.2	9,425.2
	Accident	108.1	1,108.0	625.5	625.5	8,597.8	8,597.8

Notes:

P_{tu} = Minimum of ultimate tensile capacities in planes 1 and 2

P_{cu} = Minimum of ultimate compressive capacities in plane 1 and 2

P_{ub1} = Minimum of ultimate balanced section compressive capacity in plane 1

P_{ub2} = Minimum of ultimate balanced section compressive capacity in plane 2

M_{ub1} = Minimum of ultimate balanced section moment capacity in plane 1

M_{ub2} = Minimum of ultimate balanced section moment capacity in plane 2

Planes 1 and 2 are defined in Figure 3.9.4-5

Table 3.9.4-13
Comparison of Highest Combined Shear Forces/Moments with the Capacities of EOS-HSM
 3 Pages

Component	Load Combination	Quantity	V ₁	V _{o1}	V _{o2}	M ₁	M ₂
			kips/ft	kips/ft	kips/ft	kip-in/ft	kip-in/ft
1. Rear Wall Bottom (32")	C1 through C6	Computed	51.62	6.26	9.79	338.75	708.70
		Capacity	90.43	38.26	38.26	886.79	886.79
		Ratio	0.57	0.16	0.26	0.38	0.80
	C7	Computed	25.29	1.86	2.71	232.79	270.83
		Capacity	85.58	36.30	36.30	837.08	837.08
		Ratio	0.30	0.05	0.07	0.28	0.32
2. Rear Wall Top (12")	C1 through C6	Computed	13.70	5.12	6.40	36.93	106.65
		Capacity	64.97	12.81	12.81	290.38	290.38
		Ratio	0.21	0.40	0.50	0.13	0.37
	C7	Computed	7.64	4.22	2.95	24.52	69.33
		Capacity	61.43	12.15	12.15	273.80	273.80
		Ratio	0.12	0.35	0.24	0.09	0.25
3. Front Wall Bottom (54")	C1 through C6	Computed	57.56	14.24	13.02	1023.97	1877.23
		Capacity	195.97	64.28	64.28	3791.72	3791.72
		Ratio	0.29	0.22	0.20	0.27	0.50
	C7	Computed	25.23	3.12	3.11	1049.12	1735.23
		Capacity	185.37	60.98	60.98	3578.11	3578.11
		Ratio	0.14	0.05	0.05	0.29	0.48

Table 3.9.4-13
Comparison of Highest Combined Shear Forces/Moments with the Capacities of EOS-HSM
 3 Pages

Component	Load Combination	Quantity	V ₁	V _{o1}	V _{o2}	M ₁	M ₂
			kips/ft	kips/ft	kips/ft	kip-in/ft	kip-in/ft
4. Front Wall Top (42")	C1 through C6	Computed	90.42	28.50	25.62	949.69	1768.70
		Capacity	180.69	49.00	49.00	2875.63	2875.63
		Ratio	0.50	0.58	0.52	0.33	0.62
	C7	Computed	48.32	26.12	24.35	1353.14	2485.27
		Capacity	170.88	46.49	46.49	2712.91	2712.91
		Ratio	0.28	0.56	0.52	0.50	0.92
5. Side Wall Bottom (24")	C1 through C6	Computed	23.50	15.39	14.78	269.28	182.86
		Capacity	102.12	27.84	27.84	919.26	919.26
		Ratio	0.23	0.55	0.53	0.29	0.20
	C7	Computed	11.06	14.31	18.56	143.44	396.28
		Capacity	96.57	26.41	26.41	867.25	867.25
		Ratio	0.11	0.54	0.70	0.17	0.46
6. Side Wall Bottom (14")	C1 through C6	Computed	14.39	11.42	6.10	91.36	38.03
		Capacity	89.39	15.11	15.11	489.85	489.85
		Ratio	0.16	0.76	0.40	0.19	0.08
	C7	Computed	11.13	12.14	12.65	63.98	117.21
		Capacity	84.50	14.34	14.34	461.69	461.69
		Ratio	0.13	0.85	0.88	0.14	0.25

Table 3.9.4-13
Comparison of Highest Combined Shear Forces/Moments with the Capacities of EOS-HSM
 3 Pages

Component	Load Combination	Quantity	V ₁	V _{o1}	V _{o2}	M ₁	M ₂
			kips/ft	kips/ft	kips/ft	kip-in/ft	kip-in/ft
7. Side Wall Top (12")	C1 through C6	Computed	38.48	12.32	11.88	285.32	195.00
		Capacity	86.84	12.57	12.57	403.96	403.96
		Ratio	0.44	0.98	0.95	0.71	0.48
	C7	Computed	46.54	10.56	10.64	341.15	151.85
		Capacity	82.08	11.92	11.92	380.58	380.58
		Ratio	0.57	0.89	0.89	0.90	0.40
8. Roof (44")	C1 through C6	Computed	21.46	46.12	49.54	622.18	1831.53
		Capacity	151.43	51.55	51.55	2283.14	2283.14
		Ratio	0.14	0.89	0.96	0.27	0.80
	C7	Computed	22.51	11.56	24.29	283.58	1004.18
		Capacity	143.25	48.90	48.90	2154.63	2154.63
		Ratio	0.16	0.24	0.50	0.13	0.47

Notes:

Load Combinations C1 through C6 include normal thermal condition and C7 includes accidental thermal condition.

Comparison of highest combined shear forces/moments with capacities for alternate front wall rebar layout reported in Table 3.9.4-28.

Table 3.9.4-13a
Comparison of Highest Combined Shear Forces/Moments with the Capacities of EOS FPS HSM
(Bounding)
3 Pages

Component	Load Comb. ⁽¹⁾	Quantity	V _I	V _{o1}	V _{o2}	M ₁	M ₂
			kips/ft	kips/ft	kips/ft	kip-in/ft	kip-in/ft
1. Rear Wall Side (24")	C1 through C6	Demand	36.4	15.8	24.0	192.7	353.7
		Capacity	80.2	28.1	28.1	648.2	648.2
		Ratio	0.45	0.56	0.85	0.30	0.55
	C7	Demand	8.3	4.6	8.4	160.1	217.4
		Capacity	75.9	26.6	26.6	611.8	611.8
		Ratio	0.11	0.17	0.31	0.26	0.36
2. Rear Wall Center and Top (12")	C1 through C6	Demand	53.0	11.3	10.7	68.9	140.9
		Capacity	65.0	12.8	12.8	290.4	290.4
		Ratio	0.81	0.88	0.84	0.24	0.49
	C7	Demand	12.2	9.2	5.2	69.9	105.4
		Capacity	61.4	12.2	12.2	273.8	273.8
		Ratio	0.20	0.76	0.43	0.26	0.38
3. Interior Pedestal (12")	C1 through C6	Demand	49.6	12.4	11.5	41.3	41.3
		Capacity	65.0	12.8	12.8	290.4	290.4
		Ratio	0.76	0.97	0.90	0.14	0.14
	C7	Demand	23.9	2.5	10.2	30.1	31.4
		Capacity	61.4	12.2	12.2	273.8	273.8
		Ratio	0.39	0.20	0.84	0.11	0.11

Table 3.9.4-13a
Comparison of Highest Combined Shear Forces/Moments with the Capacities of EOS FPS HSM
(Bounding)
3 Pages

Component	Load Comb. ⁽¹⁾	Quantity	V _I	V _{o1}	V _{o2}	M ₁	M ₂
			kips/ft	kips/ft	kips/ft	kip-in/ft	kip-in/ft
4. Front Wall Top (42")	C1 through C6	Demand	128.4	29.3	44.1	1446.2	2379.2
		Capacity	180.7	49.0	49.0	2875.6	2875.6
		Ratio	0.71	0.60	0.90	0.50	0.83
	C7	Demand	58.3	23.6	41.7	1499.3	2436.3
		Capacity	170.9	46.5	46.5	2712.9	2712.9
		Ratio	0.34	0.51	0.90	0.55	0.90
5. Side Wall Bottom (24")	C1 through C6	Demand	29.7	17.2	16.2	215.3	235.5
		Capacity	102.1	27.8	27.8	919.3	919.3
		Ratio	0.29	0.62	0.58	0.23	0.26
	C7	Demand	17.4	16.9	15.8	145.2	408.5
		Capacity	96.6	26.4	26.4	867.3	867.3
		Ratio	0.18	0.64	0.60	0.17	0.47
6. Side Wall Bottom (14")	C1 through C6	Demand	22.0	13.6	9.0	75.8	68.3
		Capacity	89.4	15.1	15.1	489.8	489.8
		Ratio	0.25	0.90	0.59	0.15	0.14
	C7	Demand	14.3	12.1	12.3	65.8	134.1
		Capacity	84.5	14.3	14.3	461.7	461.7
		Ratio	0.17	0.84	0.85	0.14	0.29

Table 3.9.4-13a
Comparison of Highest Combined Shear Forces/Moments with the Capacities of EOS FPS HSM
(Bounding)
3 Pages

Component	Load Comb. ⁽¹⁾	Quantity	V _I	V _{o1}	V _{o2}	M ₁	M ₂
			kips/ft	kips/ft	kips/ft	kip-in/ft	kip-in/ft
7. Side Wall Top (12")	C1 through C6	Demand	76.6	11.8	11.3	334.2	192.0
		Capacity	86.8	12.6	12.6	404.0	404.0
		Ratio	0.88	0.94	0.90	0.83	0.48
	C7	Demand	44.1	10.2	10.4	335.4	145.4
		Capacity	82.1	11.9	11.9	380.6	380.6
		Ratio	0.54	0.85	0.87	0.88	0.38
8. Roof (44")	C1 through C6	Demand	26.5	45.7	48.4	596.6	1859.3
		Capacity	151.4	51.5	51.5	2283.1	2283.1
		Ratio	0.18	0.89	0.94	0.26	0.81
	C7	Demand	21.8	16.1	8.6	309.2	990.6
		Capacity	143.3	48.9	48.9	2154.6	2154.6
		Ratio	0.15	0.33	0.18	0.14	0.46

Notes:

(1) Comb C1 through C6 include normal thermal, Comb C7 include accident thermal

Table 3.9.4-14
Comparison of Highest Combined Axial Forces/Moments with the Capacities of EOS-HSM
 3 Pages

Component	Load Combination	Quantity	P (Comp)	P ₁ (Tens)	P ₂ (Tens.)	M _{1p} ⁽¹⁾	M _{2p} ⁽¹⁾
			kips/ft	kips/ft	kips/ft	kip-in/ft	kip-in/ft
1. Rear Wall Bottom (32")	C1 through C6	Computed	104.39	33.78	32.11	299.64	428.28
		Capacity	880.39	59.64	59.64	427.42	738.10
		Ratio	0.12	0.57	0.54	0.70	0.58
	C7	Computed	44.56	13.37	5.46	66.43	124.05
		Capacity	793.88	56.33	56.33	826.20	806.31
		Ratio	0.06	0.24	0.10	0.08	0.15
2. Rear Wall Top (12")	C1 through C6	Computed	29.63	9.50	23.56	36.93	43.42
		Capacity	349.99	59.64	59.64	279.91	238.59
		Ratio	0.08	0.16	0.40	0.13	0.18
	C7	Computed	15.84	7.09	40.00	20.08	45.85
		Capacity	316.52	56.33	56.33	249.52	79.84
		Ratio	0.05	0.13	0.71	0.08	0.57
3. Front Wall Bottom (54")	C1 through C6	Computed	122.27	72.22	65.59	1019.49	773.80
		Capacity	1513.35	152.68	152.68	1998.10	3368.23
		Ratio	0.08	0.47	0.43	0.51	0.23
	C7	Computed	59.82	19.82	0.00	485.33	0.00
		Capacity	1365.94	144.20	144.20	3244.10	3578.11
		Ratio	0.04	0.14	0.00	0.15	0.00

Table 3.9.4-14
Comparison of Highest Combined Axial Forces/Moments with the Capacities of EOS-HSM
 3 Pages

Component	Load Combination	Quantity	P (Comp)	P ₁ (Tens)	P ₂ (Tens.)	M _{1p} ⁽¹⁾	M _{2p} ⁽¹⁾
			kips/ft	kips/ft	kips/ft	kip-in/ft	kip-in/ft
4. Front Wall Top (42")	C1 through C6	Computed	256.17	97.70	77.54	737.46	1137.66
		Capacity	1195.11	152.68	152.68	2524.84	1880.68
		Ratio	0.21	0.64	0.51	0.29	0.60
	C7	Computed	98.93	22.08	32.83	1352.68	1796.91
		Capacity	1079.52	144.20	144.20	2297.59	2299.51
		Ratio	0.09	0.15	0.23	0.59	0.78
5. Side Wall Bottom (24")	C1 through C6	Computed	70.20	27.97	37.58	267.46	158.64
		Capacity	682.20	85.88	85.88	664.87	738.53
		Ratio	0.10	0.33	0.44	0.40	0.21
	C7	Computed	38.81	22.46	58.73	97.14	324.92
		Capacity	616.18	81.11	81.11	627.12	331.04
		Ratio	0.06	0.28	0.72	0.15	0.98
6. Side Wall Bottom (14")	C1 through C6	Computed	47.63	19.43	16.50	75.91	37.93
		Capacity	417.00	85.88	85.88	450.17	484.24
		Ratio	0.11	0.23	0.19	0.17	0.08
	C7	Computed	21.85	31.53	62.90	63.98	117.21
		Capacity	377.50	81.11	81.11	337.69	236.42
		Ratio	0.06	0.39	0.78	0.19	0.50

Table 3.9.4-14
Comparison of Highest Combined Axial Forces/Moments with the Capacities of EOS-HSM
 3 Pages

Component	Load Combination	Quantity	P (Comp)	P ₁ (Tens)	P ₂ (Tens.)	M _{1p} ⁽¹⁾	M _{2p} ⁽¹⁾
			kips/ft	kips/ft	kips/ft	kip-in/ft	kip-in/ft
7. Side Wall Top (12")	C1 through C6	Computed	157.07	27.52	49.71	44.42	49.00
		Capacity	363.96	85.88	85.88	386.56	170.14
		Ratio	0.43	0.32	0.58	0.11	0.29
	C7	Computed	138.02	56.91	11.68	64.54	132.35
		Capacity	329.77	81.11	81.11	114.93	358.64
		Ratio	0.42	0.70	0.14	0.56	0.37
8. Roof (44")	C1 through C6	Computed	107.11	24.43	67.55	621.82	1817.34
		Capacity	1227.83	114.51	114.51	2237.29	2106.43
		Ratio	0.09	0.21	0.59	0.28	0.86
	C7	Computed	90.83	11.47	59.85	239.44	751.16
		Capacity	1107.99	108.15	108.15	2085.65	1488.26
		Ratio	0.08	0.11	0.55	0.11	0.50

Notes:

1. M_{1p} and M_{2p} are moments at the same location and for the same load combination as P₁ and P₂. M_{1p} and M_{2p} occur at the same location simultaneously with P₁ and P₂, i.e., $M_1 = [(P_{tu} - P_1)/P_{tu}] * M_{u1}$.
2. Load Combinations C1 to C6 include normal thermal, C7 include accident thermal.
3. Comparison of highest combined axial forces/moments with capacities for alternate front wall rebar layout reported in Table 3.9.4-29.

Table 3.9.4-14a
Comparison of Highest Combined Axial Forces/Moments with the Capacities of EOS-HSM-FPS Option
(Bounding)
3 Pages

Component	Load Comb. ⁽¹⁾	Quantity	P (Comp)	P ₁ (Tens)	P ₂ (Tens.)	M _{1p} ⁽²⁾	M _{2p} ⁽²⁾
			kips/ft	kips/ft	kips/ft	kip-in/ft	kip-in/ft
1. Rear Wall Side (24")	C1 through C6	Demand	70.3	25.3	49.3	190.8	202.7
		Capacity	668.2	59.6	59.6	430.1	569.0
		Ratio	0.11	0.42	0.83	0.49	0.89
	C7	Demand	44.1	28.0	17.6	160.1	180.6
		Capacity	602.9	56.3	56.3	324.9	608.7
		Ratio	0.07	0.50	0.31	0.52	0.36
2. Rear Wall Center and Top (12")	C1 through C6	Demand	284.2	53.3	41.9	47.5	48.0
		Capacity	350.0	59.6	59.6	241.3	276.6
		Ratio	0.81	0.89	0.70	0.82	0.30
	C7	Demand	34.7	48.6	36.5	11.3	75.7
		Capacity	316.5	56.3	56.3	47.0	112.0
		Ratio	0.11	0.86	0.65	0.29	0.78
3. Interior Pedestal (12")	C1 through C6	Demand	168.7	49.6	35.1	41.3	40.4
		Capacity	350.0	59.6	59.6	57.1	255.4
		Ratio	0.48	0.83	0.59	0.48	0.18
	C7	Demand	84.1	13.2	14.5	30.1	4.3
		Capacity	316.5	56.3	56.3	243.4	271.8
		Ratio	0.27	0.23	0.26	0.12	0.02

Table 3.9.4-14a
Comparison of Highest Combined Axial Forces/Moments with the Capacities of EOS-HSM-FPS Option
(Bounding)
3 Pages

Component	Load Comb. ⁽¹⁾	Quantity	P (Comp)	P ₁ (Tens)	P ₂ (Tens.)	M _{1p} ⁽²⁾	M _{2p} ⁽²⁾
			kips/ft	kips/ft	kips/ft	kip-in/ft	kip-in/ft
4. Front Wall Top (42")	C1 through C6	Demand	386.6	135.5	127.5	619.9	1205.3
		Capacity	1195.1	152.7	152.7	1117.0	1381.3
		Ratio	0.32	0.89	0.84	0.89	0.89
	C7	Demand	142.3	41.9	31.4	1486.8	1733.0
		Capacity	1079.5	144.2	144.2	2360.9	2367.6
		Ratio	0.13	0.29	0.22	0.68	0.76
5. Side Wall Bottom (24") ⁽³⁾	C1 through C6	Demand	55.4	56.0	68.9	204.0	171.0
		Capacity	682.2	85.9	85.9	677.9	283.5
		Ratio	0.08	0.65	0.80	0.32	0.88
	C7	Demand	37.6	22.1	74.8	69.8	381.7
		Capacity	616.2	81.1	81.1	667.6	138.0
		Ratio	0.06	0.27	0.92	0.11	5.38 ⁽³⁾
6. Side Wall Bottom (14")	C1 through C6	Demand	62.0	32.0	55.8	41.3	66.6
		Capacity	417.0	85.9	85.9	424.1	319.6
		Ratio	0.15	0.37	0.65	0.10	0.28
	C7	Demand	21.3	31.0	65.8	65.8	134.1
		Capacity	377.5	81.1	81.1	368.3	192.2
		Ratio	0.06	0.38	0.81	0.19	0.89

Table 3.9.4-14a
Comparison of Highest Combined Axial Forces/Moments with the Capacities of EOS-HSM-FPS Option
(Bounding)
3 Pages

Component	Load Comb. ⁽¹⁾	Quantity	P (Comp)	P ₁ (Tens)	P ₂ (Tens.)	M _{1p} ⁽²⁾	M _{2p} ⁽²⁾
			kips/ft	kips/ft	kips/ft	kip-in/ft	kip-in/ft
7. Side Wall Top (12")	C1 through C6	Demand	222.5	72.8	86.3	53.7	53.9
		Capacity	364.0	85.9	85.9	402.0	148.2
		Ratio	0.61	0.85	1.01 ⁽⁴⁾	0.30	0.73
	C7	Demand	176.4	44.8	60.4	90.0	113.7
		Capacity	329.8	81.1	81.1	185.0	379.1
		Ratio	0.53	0.55	0.74	0.52	0.59
8. Roof (44")	C1 through C6	Demand	154.2	42.0	74.8	475.0	1732.7
		Capacity	1227.8	114.5	114.5	1459.0	1974.0
		Ratio	0.13	0.37	0.65	0.33	0.88
	C7	Demand	93.5	31.9	54.9	233.4	938.5
		Capacity	1108.0	108.1	108.1	2148.0	2075.4
		Ratio	0.08	0.29	0.51	0.11	0.46

Notes:

1. Comb C1 through C6 include normal thermal, Comb C7 include accident thermal
2. M1p and M2p are moments at the same location and for the same load combination as P1 and P2. M1p and M2p occur at the same location simultaneously with P1 and P2, i.e., $M1 = [(P_{tu} - P1)/P_{tu}] * Mu1$
3. See Table 3.9.4-14b for the results of detailed analysis of side wall local demand to capacity ratio for overstressed region above/adjacent to air vent.
4. The maximum load ratio of the side wall is 1.01, based on the lower tension capacity. Detailed analysis of the side wall local demand to capacity ratio, with actual rebar spacing for the overstressed region, gives maximum load ratio 0.85.

Table 3.9.4-14b
Comparison of Highest Combined Axial Forces/Moments of All EOS-HSM-FPS Configuration Options with the
Applicable Capacities - Near Air Vent (Bounding)

Component	Load Comb. ⁽¹⁾	Quantity	P ₁ (Tens.)	P ₂ (Tens.)	P ₁ (Comp)	P ₂ (Comp)	M _{1p} ⁽²⁾	M _{2p} ⁽²⁾
			kips/ft	kips/ft	kips/ft	kips/ft	kip-in/ft	kip-in/ft
5B. Side Wall Above/Adjacent Air Vent (24")	C1 through C6	Demand	56.0	68.9	55.4	38.9	204.0	233.9
		Capacity	85.9	232.0	682.2	760.0	677.9	1842.4
		Ratio	0.65	0.30	0.08	0.05	0.32	0.13
	C7	Demand	22.1	74.8	37.6	22.3	69.8	408.5
		Capacity	81.1	219.1	616.2	689.9	667.6	1458.1
		Ratio	0.27	0.34	0.06	0.03	0.11	0.28

Notes:

- Comb C1 through C6 include normal thermal, Comb C7 include accident thermal
- M_{1p} and M_{2p} are moments at the same location and for the same load combination as P₁ and P₂. M_{1p} and M_{2p} occur at the same location simultaneously with P₁ and P₂, i.e., $M_1 = [(P_{tu} - P_1)/P_{tu}] * M_{u1}$

Table 3.9.4-15
Load Cases for DSC Support Structure Evaluation

Load Type Nomenclature	Load Type Description
D	Dead load – self weight of rails
L	Live load – weight of the DSC
Ro	Normal handling load
To	Normal thermal load
Ra	Off-normal handling load
Ta	Envelope of off-normal and accident thermal loads
E	Earthquake load

Table 3.9.4-16
Load Combination for DSC Support Structure Evaluation

Load Combination ID	Load Combination	Event
N1	$1.0 S > D + L + Ro$	Normal
N2	$1.0 S > D + L + Ro$	Normal – Insertion/Extraction
N3	$1.3 S > D + L + Ra + To$	Off-normal – Handling
A5S	$1.6 S > D + L + E + To$	Accident – Earthquake
A5V	$1.4 Sv > D + L + E + To$	Accident – Earthquake
A8S	$1.7 S > D + L + Ta$	Accident – Thermal
A8V	$1.4 Sv > D + L + Ta$	Accident – Thermal

Table 3.9.4-17
Summary of Demand to Capacity Ratio (D/C Ratio) for the Whole Cross
Section

Load Combination	Demand/Capacity Ratio	Maximum D/C Ratio and Controlling Action
N3 Strong	0.118	0.729 in Weak Axis Bending in load case A5 Seismic
N1 Weak	0.193	
A5S Weak	0.729	
A8S Weak	0.002	

Table 3.9.4-17a
Summary of Demand to Capacity Ratio of the FPS DSC Support Structure

		Normal			Off-normal		
		73" Span	46" Span	40" Span	73" Span	46" Span	40" Span
Capacities	Tension, P_{nt} [kips]	359	359	359	466	466	466
	Compression, P_{nc} [kips]	449	463	466	584	602	605
	Flexure (Weak-Axis), M_n [kips-in]	596	428	428	775	556	556
	Shear, V_n [kips]	147	147	147	191	191	191
Demand	Tension, P_{nt} [kips]	N/A			135	135	135
	Compression, P_{nc} [kips]				135	135	135
	Flexure (Weak-Axis), M_n [kips-in]				653	416	358
	Flexure (Strong-Axis), M_n [kips-in]				177	876	17
	Shear, V_n [kips]				36	36	36
Demand to Capacity Ratio	Tension, P_{nt}	N/A			0.29	0.29	0.29
	Compression, P_{nc}				0.23	0.22	0.22
	Flexure (Weak-Axis), M_n [kips-in]				0.84	0.75	0.64
	Shear, V_n				0.19	0.19	0.19
	Combined Compression and Flexure				0.98	0.89	0.80

Table 3.9.4-18
Summary of Demand to Capacity Ratio (D/C Ratio) for the Flange Elements

Load Combination	Flange Demand/Capacity Type Ratio			Maximum D/C Ratio and Controlling Action
	Axial Compression	Strong Bending	Weak Bending	
N1	0.314	0.02	0.228	0.388 Axial Compression in load case N3
N3	0.388	0.226	0.225	
A5S	0.265	0.022	0.229	
A8S	0.114	0.012	0.136	
N2	0.3	0.023	0.271	

Table 3.9.4-19
Summary of Demand to Capacity Ratio (D/C Ratio) for the Web Elements

Load Combination	Web Demand/Capacity Type Ratio			Maximum D/C Ratio and Controlling Action
	Axial Compression	Strong Bending	Weak Bending	
N1	0.747	0.08	0.012	0.761 in Axial Compression in load case A5 Seismic
N3	0.7	0.007	0.007	
A5S	0.761	0.076	0.014	
A8S	0.407	0.038	0.008	
N2	0.693	0.091	0.012	

Table 3.9.4-20
Summary of Demand to Capacity Ratio (D/C Ratio) for the Stiffener Elements

Load Combination	Stiffener Demand/Capacity Type Ratio			Maximum D/C Ratio and Controlling Action
	Axial Compression	Strong Bending	Weak Bending	
N1	0.162	0.023	0.707	0.805 in Weak Axis Bending in load case A5 Seismic
N3	0.059	0.372	0.372	
A5S	0.153	0.026	0.805	
A8S	0.096	0.014	0.434	
N2	0.156	0.02	0.529	

Table 3.9.4-21
Summary of Demand to Capacity Ratio (D/C Ratio) for the Accessories

Item	Demand/Capacity Ratio
Stop plate	0.784
DSC seismic impact	0.027
Extension baseplate	0.864
Lateral braces	0.636

Table 3.9.4-21a
Summary of Demand to Capacity Ratio (D/C Ratio) for FPS DSC Support Structure Accessories

Item	Demand/Capacity Ratio
12"x1" Plate	0.82
Tubesteel Spacer	0.80
Stop Plate	0.96
Rail Extension Baseplate	0.57

Table 3.9.4-22
Summary of Demand to Capacity Ratio (D/C Ratio) for DSC Support
Structure Welds

Weld between	Demand/Capacity Ratio
Stop plate and rail	0.363
Extension baseplate and rail	0.141
Stiffener and lateral brace	0.291
Stiffener plate and rail	0.668

Table 3.9.4-22a
Summary of Demand to Capacity Ratio (D/C Ratio) for FPS DSC Support
Structure Welds

Weld between	Demand/Capacity Ratio
4"x1" Plate and 12"x1" Plate	0.27
Stiffener and 12" x 1" Plate	0.94
Stop Plate and Support ⁽¹⁾	0.96
Tubesteel Spacer and 12" x 1" Plate	0.81
Extension Baseplate and 12" x 1" Plate	0.33
Nitronic Plate to 4"x1" Plate	0.74

Notes:

1. Full penetration weld and qualification of base metal qualifies the welds - see Table 3.9.4-21a.

Table 3.9.4-23
Modal Frequencies and Mass Participation of EOS-HSMS

Mode	Frequency (Hz)	Mass Participation					
		X-Direction		Y-Direction		Z-Direction	
		Mass (lb-s ² /in)	%	Mass (lb-s ² /in)	%	Mass (lb-s ² /in)	%
1	18.7	696	56%	-	-	-	-
2	31.7	-	-	-	-	-	-
3	32.7	-	-	-	-	711	57%
4	33.6	-	-	-	-	-	-
5	37.6	20	2%	-	-	-	-
6	49.8	291	23%	-	-	-	-
7	60.3	-	-	489	39%	-	-
8	67.3	-	-	-	-	323	26%
9	69.2	-	-	-	-	-	-
10	70.4	-	-	-	-	-	-

Table 3.9.4-23a
Modal Frequencies and Mass Participation of EOS-HSMS-FPS

Mode	Frequency (Hz)	Mass Participation					
		X-Direction		Y-Direction		Z-Direction	
		Mass (lb-s ² /in)	%	Mass (lb-s ² /in)	%	Mass (lb-s ² /in)	%
1	19.2	636.8	55.0%	-	-	-	-
2	31.4	-	-	1.4	0.1%	788.7	68.1%
3	34.1	-	-	-	-	-	-
4	35.7	10.8	0.9%	-	-	-	-
5	36.8	258.3	22.3%	-	-	-	-
6	39.4	9.1	0.8%	-	-	-	-
7	43.4	-	-	1.3	0.1	119.2	10.3%
8	60.6	-	-	451.0	38.9	-	-
9	72	-	-	-	-	-	-
10	71.1	-	-	302.6	26.1%	-	-

Table 3.9.4-24
Roof Heat Shield Modal Participating Mass Ratios for EOS-HSM and EOS-HSM-FPS Options

Frequency (Hz)	Participating Mass Ratio		
	X-Direction	Y-Direction	Z-Direction
5.86	0.026	0.000	0.000
7.40	0.000	0.000	0.573
11.29	0.000	0.000	0.000
12.71	0.003	0.000	0.000
13.77	0.000	0.000	0.000
15.53	0.000	0.000	0.159
20.51	0.003	0.000	0.000
23.54	0.000	0.000	0.000
24.51	0.000	0.974	0.000
25.01	0.943	0.000	0.000
25.89	0.000	0.000	0.000
27.22	0.000	0.004	0.000
32.84	0.000	0.000	0.000
35.49	0.002	0.000	0.000
36.77	0.000	0.000	0.000
40.90	0.000	0.000	0.020
41.06	0.000	0.000	0.000
43.97	0.001	0.000	0.000
44.67	0.000	0.000	0.000
48.45	0.000	0.000	0.000
48.66	0.000	0.000	0.040
51.44	0.000	0.000	0.000
54.01	0.000	0.000	0.006
60.36	0.000	0.000	0.000
66.09	0.000	0.000	0.000
66.19	0.000	0.000	0.000
68.80	0.000	0.000	0.007
74.25	0.000	0.000	0.000
78.30	0.000	0.000	0.000
80.56	0.000	0.000	0.000
80.69	0.000	0.000	0.000
81.37	0.000	0.000	0.046
82.17	0.000	0.000	0.000
86.31	0.000	0.000	0.000
89.52	0.000	0.000	0.006
95.39	0.000	0.000	0.000
97.21	0.000	0.000	0.000

Table 3.9.4-25
Side Heat Shield Modal Participating Mass
Ratios for EOS-HSM
(2 Sheets)

Frequency (Hz)	Participating Mass Ratio		
	X-Direction	Y-Direction	Z-Direction
3.97	0.684	0.000	0.000
4.51	0.154	0.000	0.000
6.57	0.006	0.000	0.000
7.42	0.004	0.000	0.000
7.69	0.000	0.000	0.000
9.21	0.000	0.000	0.000
10.43	0.010	0.000	0.000
15.53	0.000	0.000	0.000
16.55	0.000	0.001	0.000
16.74	0.042	0.000	0.000
17.39	0.000	0.000	0.000
17.78	0.018	0.000	0.001
19.63	0.000	0.001	0.000
22.45	0.000	0.000	0.000
24.59	0.001	0.000	0.000
26.88	0.000	0.000	0.000
29.15	0.000	0.000	0.000
29.75	0.001	0.000	0.001
30.11	0.004	0.000	0.000
32.69	0.016	0.000	0.002
33.60	0.000	0.002	0.000
36.04	0.000	0.000	0.000
38.72	0.014	0.000	0.001
39.05	0.000	0.000	0.000
42.87	0.000	0.000	0.000
43.01	0.000	0.000	0.000
44.44	0.000	0.000	0.000
46.77	0.001	0.000	0.000
48.98	0.001	0.000	0.001
49.35	0.000	0.009	0.000
50.17	0.003	0.000	0.000
53.29	0.005	0.000	0.001
55.11	0.000	0.018	0.000
56.77	0.000	0.000	0.004
59.53	0.000	0.000	0.034

Table 3.9.4-25
Side Heat Shield Modal Participating Mass
Ratios for EOS-HSM
(2 Sheets)

Frequency (Hz)	Participating Mass Ratio		
	X-Direction	Y-Direction	Z-Direction
61.20	0.000	0.096	0.000
64.18	0.000	0.000	0.179
64.44	0.000	0.001	0.000
65.87	0.000	0.000	0.000
66.19	0.001	0.000	0.425
67.23	0.000	0.509	0.000
68.47	0.002	0.000	0.255
70.35	0.000	0.326	0.000
71.92	0.000	0.000	0.009
74.26	0.000	0.001	0.000
75.55	0.000	0.000	0.059
76.08	0.000	0.002	0.000
79.42	0.000	0.000	0.000
81.57	0.002	0.000	0.015
83.62	0.000	0.018	0.000
83.79	0.000	0.000	0.001
86.33	0.001	0.000	0.001
88.01	0.000	0.001	0.000
91.46	0.000	0.002	0.000
92.25	0.000	0.000	0.000
92.56	0.000	0.000	0.000
93.78	0.000	0.001	0.000
96.86	0.003	0.000	0.001
97.14	0.000	0.000	0.000

Table 3.9.4-25a
Side Heat Shield Modal Participating Mass Ratios for EOS-HSM-FPS

Frequency (Hz)	Modal Effective Mass Fraction		
	X-Direction	Y-Direction	Z-Direction
5.59	0.803	0.000	0.000
6.52	0.000	0.000	0.000
8.39	0.001	0.000	0.000
9.67	0.000	0.000	0.000
13.78	0.000	0.000	0.000
14.50	0.000	0.001	0.000
17.16	0.016	0.000	0.000
19.49	0.000	0.000	0.000
19.65	0.000	0.001	0.000
22.72	0.000	0.000	0.000
24.35	0.088	0.000	0.000
27.48	0.000	0.000	0.000
27.52	0.000	0.000	0.002
33.60	0.000	0.000	0.000
35.10	0.020	0.000	0.000
35.79	0.000	0.000	0.000
36.87	0.000	0.000	0.001
39.73	0.000	0.000	0.000
42.82	0.009	0.000	0.000
45.82	0.010	0.000	0.000
47.08	0.000	0.000	0.011
50.33	0.000	0.001	0.000

Frequency (Hz)	Modal Effective Mass Fraction		
	X-Direction	Y-Direction	Z-Direction
51.76	0.000	0.000	0.000
55.71	0.000	0.000	0.000
55.76	0.000	0.000	0.000
56.89	0.000	0.008	0.000
63.43	0.000	0.000	0.000
64.14	0.000	0.000	0.000
64.80	0.000	0.040	0.000
68.13	0.000	0.000	0.000
71.50	0.000	0.000	0.006
72.71	0.000	0.000	0.000
74.05	0.006	0.000	0.000
78.80	0.000	0.000	0.901
79.32	0.000	0.737	0.000
80.78	0.002	0.000	0.000
85.84	0.000	0.165	0.000
87.58	0.000	0.026	0.000
87.97	0.000	0.000	0.023
89.65	0.013	0.000	0.000
91.71	0.000	0.000	0.046
92.02	0.000	0.000	0.000
98.44	0.000	0.000	0.000
99.87	0.000	0.000	0.001

Table 3.9.4-26
Ultimate Shear/Moment Capacities of Alternate Front Wall

Component	Thermal Condition	V_{ui}	V_{uo1}	V_{uo2}	M_{u1}	M_{u2}
		kip/ft	kip/ft	kip/ft	kip-in/ft	kip-in/ft
3. Front Wall Bottom (54")	Normal	148.31	42.45	65.55	3,041.40	2,599.68
	Accident	140.26	40.28	62.19	2,869.52	2,453.93
4. Front Wall Top (42")	Normal	157.09	35.58	46.69	2,566.64	2,238.71
	Accident	148.61	33.75	44.29	2,420.78	2,112.66
4. Front Wall Middle (42")	Normal	181.44	43.59	47.58	2,565.76	2,806.10
	Accident	171.58	41.36	45.14	2,420.22	2,647.21
4. Front Wall Bottom (42")	Normal	135.48	49.32	47.74	2,766.98	1,819.51
	Accident	128.18	46.79	45.29	2,610.56	1,717.30

Notes:

V_{ui} = Minimum of ultimate in plane shear capacities in planes 1 and 2

V_{uo1} = Minimum ultimate out of plane shear capacity in plane 1

V_{uo2} = Minimum ultimate out of plane shear capacity in plane 2

M_{u1} = Minimum ultimate moment capacity in plane 1

M_{u2} = Minimum ultimate moment capacity in plane 2

Planes 1 and 2 are defined in Figure 3.9.4-5

Table 3.9.4-26a
Ultimate Shear/Moment Capacities of EOS-HSM-FPS Alternate Front Wall

Component	Thermal Condition	V_{ui}	V_{uo1}	V_{uo2}	M_{u1}	M_{u2}
		Kips/ft	Kips/ft	Kips/ft	In-kips/ft	In-kips/ft
Front Wall Top (42")	Normal	130.25	35.50	45.18	2,566.64	1,612.46
	Accident	123.24	33.68	42.87	2,420.78	1,521.80
Front Wall Mid Upper Side (42")	Normal	154.84	43.59	44.83	2,565.76	2,153.87
	Accident	146.45	41.36	42.53	2,420.22	2,032.24
Front Wall Mid Upper Center (42")	Normal	106.69	43.59	44.79	2,565.76	1,218.03
	Accident	100.96	41.36	42.49	2,420.22	1,149.74
Front Wall Mid Lower Side (42")	Normal	140.33	43.59	44.82	2,565.76	1,909.71
	Accident	132.74	41.36	42.52	2,420.22	1,802.07
Front Wall Mid Lower Center (42")	Normal	91.13	43.59	44.71	2,565.76	894.29
	Accident	86.28	41.36	42.42	2,420.22	844.27
Front Wall Mid Center (42")	Normal	176.35	43.59	44.87	2,565.76	2,642.55
	Accident	166.75	41.36	42.56	2,420.22	2,492.74
Front Wall Bottom (42")	Normal	130.25	49.00	50.28	2,892.11	1,796.75
	Accident	123.24	46.49	47.70	2,728.44	1,695.85

Notes:

V_{ui} = Minimum of ultimate in plane shear capacities in planes 1 and 2

V_{uo1} = Minimum ultimate out of plane shear capacity in plane 1

V_{uo2} = Minimum ultimate out of plane shear capacity in plane 2

M_{u1} = Minimum ultimate moment capacity in plane 1

M_{u2} = Minimum ultimate moment capacity in plane 2

Planes 1 and 2 are defined in Figure 3.9.4-5

Table 3.9.4-27
Ultimate Axial and Balanced Moment Capacities of Alternate Front Wall

Component	Thermal Condition	P_{tu}	P_{cu}	P_{ub1}	P_{ub2}	M_{ub1}	M_{ub2}
		kips/ft	kips/ft	kips/ft	kips/ft	kip-in/ft	kip-in/ft
3. Front Wall Bottom (54")	Normal	102.06	1,014.54	542.30	839.81	9,952.43	13,776.69
	Accident	96.39	916.25	514.44	796.54	9,088.71	12,515.78
4. Front Wall Top (42")	Normal	124.36	968.35	453.12	596.68	7,119.07	8,523.67
	Accident	117.47	875.40	429.90	566.00	6,546.80	7,803.89
4. Front Wall Middle (42")	Normal	153.58	1,195.59	556.08	607.30	8,443.62	8,947.22
	Accident	145.04	1,079.97	527.54	576.11	7,763.11	8,193.92
4. Front Wall Bottom (42")	Normal	98.42	1,166.23	629.94	610.99	9,046.99	8,334.65
	Accident	92.96	1,052.14	597.57	579.54	8,266.99	7,612.34

Notes:

- P_{tu} = Minimum of ultimate tensile capacities in planes 1 and 2
 Separate plane 1 and plane 2 values are calculated in "Concapsh_B.xlsx" and used in "EOS-HSM[s]_Demand_Rev.0_0221R2.xlsx"
- P_{cu} = Minimum of ultimate compressive capacities in plane 1 and 2
- P_{ub1} = Minimum of ultimate balanced section compressive capacity in plane 1
- P_{ub2} = Minimum of ultimate balanced section compressive capacity in plane 2
- M_{ub1} = Minimum of ultimate balanced section moment capacity in plane 1
- M_{ub2} = Minimum of ultimate balanced section moment capacity in plane 2
- Planes 1 and 2 are defined in Figure 3.9.4-5

Table 3.9.4-27a
Ultimate Axial/Moment Capacities of EOS-HSM-FPS Alternate Front Wall

Component	Thermal Condition	P _{tu}		P _{cu}		P _{ub1}	P _{ub2}	M _{ub1}	M _{ub2}
		plane 1 Kips/ft	plane 2 Kips/ft	plane 1 Kips/ft	plane 2 Kips/ft	Kips/ft	Kips/ft	In- kips/ft	In- kips/ft
Front Wall Top (42")	Normal	151.21	92.15	968.55	1162.89	452.07	578.28	7,110.37	8,036.23
	Accident	142.84	87.03	875.59	1048.97	428.90	548.51	6,539.49	7,359.85
Front Wall Mid Upper Side (42")	Normal	153.58	124.72	1089.51	1127.19	556.08	572.77	7,535.83	7,833.62
	Accident	145.04	117.79	984.50	1017.67	527.54	543.33	6,901.82	7,170.99
Front Wall Mid Upper Center (42")	Normal	153.58	69.98	1089.51	1045.01	556.08	573.84	7,535.83	6,725.66
	Accident	145.04	66.10	984.50	942.31	527.54	544.27	6,901.82	6,121.83
Front Wall Mid Lower Side (42")	Normal	153.58	110.36	1089.51	1066.50	556.08	573.02	7,535.83	7,181.25
	Accident	145.04	104.23	984.50	962.69	527.54	543.55	6,901.82	6,552.64
Front Wall Mid Lower Center (42")	Normal	153.58	51.32	1089.51	1035.08	556.08	573.39	7,535.83	6,512.28
	Accident	145.04	48.47	984.50	932.89	527.54	543.82	6,901.82	5,920.78
Front Wall Mid Center (42")	Normal	153.58	153.58	1089.51	1089.51	556.08	572.45	7,535.83	7,672.60
	Accident	145.04	145.04	984.50	984.50	527.54	543.06	6,901.82	7,017.02
Front Wall Bottom (42")	Normal	153.58	92.15	1195.59	1162.89	625.63	643.74	9,108.20	8,454.89
	Accident	145.04	87.03	1079.97	1048.97	593.49	610.58	8,328.86	7,694.69

Notes:

P_{tu} = Minimum of ultimate tensile capacities in planes 1 and 2P_{cu} = Minimum of ultimate compressive capacities in plane 1 and 2P_{ub1} = Minimum of ultimate balanced section compressive capacity in plane 1P_{ub2} = Minimum of ultimate balanced section compressive capacity in plane 2M_{ub1} = Minimum of ultimate balanced section moment capacity in plane 1M_{ub2} = Minimum of ultimate balanced section moment capacity in plane 2

Planes 1 and 2 are defined in Figure 3.9.4-5

Table 3.9.4-28
Comparison of Highest Combined Shear Forces/Moments with the Capacities of the Alternate Front Wall
2 Pages

Component	Load Comb.	Quantity	V _I	V _{o1}	V _{o2}	M ₁	M ₂
			Kips/ft	kips/ft	kips/ft	kip-in/ft	kip-in/ft
3. Front Wall Bottom (54")	C1 through C6	Computed	57.6	14.2	13.0	1024.0	1877.2
		Capacity	148.3	42.5	65.6	3041.4	2599.7
		Ratio	0.39	0.34	0.20	0.34	0.72
	C7	Computed	25.2	3.1	3.1	1049.1	1735.2
		Capacity	140.3	40.3	62.2	2869.5	2453.9
		Ratio	0.18	0.08	0.05	0.37	0.71
4. Front Wall Top (42")	C1 through C6	Computed	28.8	28.5	14.0	949.7	1453.5
		Capacity	157.1	35.6	46.7	2566.6	2238.7
		Ratio	0.18	0.80	0.30	0.37	0.65
	C7	Computed	9.8	26.1	13.0	1353.1	1584.6
		Capacity	148.6	33.8	44.3	2420.8	2112.7
		Ratio	0.07	0.77	0.29	0.56	0.75
4. Front Wall Middle (42")	C1 through C6	Computed	90.4	6.4	25.6	938.6	1768.7
		Capacity	181.4	43.6	47.6	2565.8	2806.1
		Ratio	0.50	0.15	0.54	0.37	0.63
	C7	Computed	48.3	6.3	24.4	1326.9	2485.3
		Capacity	171.6	41.4	45.1	2420.2	2647.2
		Ratio	0.28	0.15	0.54	0.55	0.94

Table 3.9.4-28
Comparison of Highest Combined Shear Forces/Moments with the Capacities of the Alternate Front Wall
2 Pages

Component	Load Comb.	Quantity	V _I	V _{o1}	V _{o2}	M ₁	M ₂
			Kips/ft	kips/ft	kips/ft	kip-in/ft	kip-in/ft
4. Front Wall Bottom (42")	C1 through C6	Computed	48.0	8.8	13.1	463.1	399.4
		Capacity	135.5	49.3	47.7	2767.0	1819.5
		Ratio	0.35	0.18	0.27	0.17	0.22
	C7	Computed	12.1	3.9	6.0	1058.0	509.5
		Capacity	128.2	46.8	45.3	2610.6	1717.3
		Ratio	0.09	0.08	0.13	0.41	0.30

Notes:

1. Load Combinations C1 through C6 include normal thermal condition, C7 includes accidental thermal condition.

Table 3.9.4-28a
Comparison of Highest Combined Shear Forces/Moments with Capacities of the EOS-HSM-FPS Alternate
Front Wall (*Bounding*)

3 Pages

Component	Load Comb. ⁽¹⁾	Quantity	V _I	V _{o1}	V _{o2}	M ₁	M ₂
			Kips/ft	kips/ft	kips/ft	kip-in/ft	kip-in/ft
4A. Front Wall Top (42")	C1 through C6	Demand	46.0	16.9	31.2	1102.1	1471.7
		Capacity	130.2	35.5	45.2	2566.6	1612.5
		Ratio	0.35	0.47	0.69	0.43	0.91
	C7	Demand	11.2	12.4	29.6	1442.3	1215.0
		Capacity	123.2	33.7	42.9	2420.8	1521.8
		Ratio	0.09	0.37	0.69	0.60	0.80
4B. Front Wall Mid Upper Side (42")	C1 through C6	Demand	118.8	0.0	39.8	1077.7	1336.6
		Capacity	154.8	43.6	44.8	2565.8	2153.9
		Ratio	0.77	0.00	0.89	0.42	0.62
	C7	Demand	45.3	0.0	36.8	1103.5	1827.7
		Capacity	146.5	41.4	42.5	2420.2	2032.2
		Ratio	0.31	0.00	0.87	0.46	0.90
4C. Front Wall Mid Upper Center (42")	C1 through C6	Demand	70.9	29.3	27.7	1104.6	547.8
		Capacity	106.7	43.6	44.8	2565.8	1218.0
		Ratio	0.66	0.67	0.62	0.43	0.45
	C7	Demand	17.7	23.6	29.3	1420.5	545.4
		Capacity	101.0	41.4	42.5	2420.2	1149.7
		Ratio	0.18	0.57	0.69	0.59	0.47

Table 3.9.4-28a
Comparison of Highest Combined Shear Forces/Moments with Capacities of the EOS-HSM-FPS Alternate
Front Wall (*Bounding*)

3 Pages

Component	Load Comb. ⁽¹⁾	Quantity	V _I	V _{o1}	V _{o2}	M _I	M ₂
			Kips/ft	kips/ft	kips/ft	kip-in/ft	kip-in/ft
4D. Front Wall Mid Lower Side (42")	C1 through C6	Demand	101.8	0.0	38.1	965.6	1283.7
		Capacity	140.3	43.6	44.8	2565.8	1909.7
		Ratio	0.73	0.00	0.85	0.38	0.67
	C7	Demand	29.8	0.0	29.4	766.6	1212.7
		Capacity	132.7	41.4	42.5	2420.2	1802.1
		Ratio	0.22	0.00	0.69	0.32	0.67
4E. Front Wall Mid Lower Center (42")	C1 through C6	Demand	73.6	18.6	17.8	1446.2	901.2
		Capacity	91.1	43.6	44.7	2565.8	894.3
		Ratio	0.81	0.43	0.40	0.56	1.01 ⁽²⁾
	C7	Demand	58.3	9.3	7.8	1190.5	736.2
		Capacity	86.3	41.4	42.4	2420.2	844.3
		Ratio	0.68	0.23	0.18	0.49	0.87
4F. Front Wall Mid Center (42")	C1 through C6	Demand	116.0	0.0	40.2	600.3	1832.5
		Capacity	176.3	43.6	44.9	2565.8	2642.5
		Ratio	0.66	0.00	0.90	0.23	0.69
	C7	Demand	47.5	0.0	30.2	653.7	2350.1
		Capacity	166.8	41.4	42.6	2420.2	2492.7
		Ratio	0.28	0.00	0.71	0.27	0.94

Table 3.9.4-28a
Comparison of Highest Combined Shear Forces/Moments with Capacities of the EOS-HSM-FPS Alternate
Front Wall (*Bounding*)

3 Pages

Component	Load Comb. ⁽¹⁾	Quantity	V _I	V _{o1}	V _{o2}	M ₁	M ₂
			Kips/ft	kips/ft	kips/ft	kip-in/ft	kip-in/ft
4G. Front Wall Bottom (42")	C1 through C6	Demand	52.7	11.7	43.6	391.5	687.8
		Capacity	130.2	49.0	50.3	2892.1	1796.8
		Ratio	0.40	0.24	0.87	0.14	0.38
	C7	Demand	16.3	3.1	20.5	445.3	489.5
		Capacity	123.2	46.5	47.7	2728.4	1695.9
		Ratio	0.13	0.07	0.43	0.16	0.29

Notes:

1. Load Combinations C1 through C6 include normal thermal, Comb C7 includes accident thermal
2. The maximum load ratio from front wall mid lower center is 1.01 based on lower moment capacity. The maximum load ratio (M₂) excluding the critical section is 0.87. The load ratio M₂ for the critical section using weighted average for a section across both mid lower center and mid lower side is 0.67.

Table 3.9.4-29
Comparison of Highest Combined Axial Forces/Moments with the Capacities of the Alternate Front Wall
2 Pages

Component	Load Comb.	Quantity	P (Comp)	P ₁ (Tens)	P ₂ (Tens.)	M _{1p} ⁽¹⁾	M _{2p} ⁽¹⁾
			kips/ft	kips/ft	kips/ft	kip-in/ft	kip-in/ft
3. Front Wall Bottom (54")	C1 through C6	Computed	122.3	72.2	65.6	1019.5	773.8
		Capacity	1014.5	123.3	102.1	1260.1	2165.3
		Ratio	0.12	0.59	0.64	0.81	0.36
	C7	Computed	59.8	19.8	0.0	485.3	0.0
		Capacity	916.3	116.5	96.4	2537.9	2453.9
		Ratio	0.07	0.17	0.00	0.19	0.00
4. Front Wall Top (42")	C1 through C6	Computed	58.5	97.7	33.5	737.5	788.5
		Capacity	968.4	150.8	124.4	2249.7	1982.4
		Ratio	0.06	0.65	0.27	0.33	0.40
	C7	Computed	18.7	22.1	31.7	1352.7	1439.2
		Capacity	875.4	142.5	117.5	2045.7	1543.4
		Ratio	0.02	0.15	0.27	0.66	0.93
4. Front Wall Middle (42")	C1 through C6	Computed	256.2	94.0	77.5	721.7	1137.7
		Capacity	1195.6	153.6	153.6	2337.3	1840.9
		Ratio	0.21	0.61	0.50	0.31	0.62
	C7	Computed	98.9	13.8	32.8	1326.9	1796.9
		Capacity	1080.0	145.0	145.0	2209.2	2246.2
		Ratio	0.09	0.09	0.23	0.60	0.80

Table 3.9.4-29
Comparison of Highest Combined Axial Forces/Moments with the Capacities of the Alternate Front Wall
2 Pages

Component	Load Comb.	Quantity	P (Comp)	P ₁ (Tens)	P ₂ (Tens.)	M _{1p} ⁽¹⁾	M _{2p} ⁽¹⁾
			kips/ft	kips/ft	kips/ft	kip-in/ft	kip-in/ft
4. Front Wall Bottom (42")	C1 through C6	Computed	66.4	77.3	33.8	450.5	177.3
		Capacity	1166.2	145.8	98.4	1612.9	1422.3
		Ratio	0.06	0.53	0.34	0.28	0.12
	C7	Computed	31.9	18.8	1.0	453.5	405.9
		Capacity	1052.1	137.7	93.0	2566.1	1700.6
		Ratio	0.03	0.14	0.01	0.18	0.24

Notes:

- 1 M_{1p} and M_{2p} are moments at the same location and for the same load combination as P₁ and P₂. M_{1p} and M_{2p} occur at the same location simultaneously with P₁ and P₂.
- 2 C1 through C6 include normal thermal, C7 includes accident thermal

Table 3.9.4-29a
Comparison of Highest Combined Axial Forces/Moments with Capacities of the EOS-HSM-FPS Alternate Front Wall (*Bounding*)

3 Pages

Component	Load Comb. ⁽¹⁾	Quantity	P ₁ (Tens.)	P ₂ (Tens.)	P ₁ (Comp)	P ₂ (Comp)	M _{1p} ⁽²⁾	M _{2p} ⁽²⁾
			kips/ft	kips/ft	kips/ft	kips/ft	kip-in/ft	kip-in/ft
4A. Front Wall Top (42")	C1 through C6	Demand	120.0	58.2	38.6	53.3	790.6	662.5
		Capacity	151.2	92.1	968.5	1162.9	2077.5	1007.5
		Ratio	0.79	0.63	0.04	0.05	0.64	0.70
	C7	Demand	20.9	20.5	15.3	20.2	1442.3	814.6
		Capacity	142.8	87.0	875.6	1049.0	2103.7	1521.2
		Ratio	0.15	0.24	0.02	0.02	0.70	0.70
4B. Front Wall Mid Upper Side (42")	C1 through C6	Demand	45.2	51.2	73.5	122.3	419.6	737.8
		Capacity	115.5	87.2	1089.5	1127.2	1860.7	1323.2
		Ratio	0.75	0.70	0.07	0.11	0.55	0.89
	C7	Demand	10.6	0.0	39.1	54.6	881.1	0.0
		Capacity	145.0	117.8	984.5	1017.7	2378.6	2032.2
		Ratio	0.07	0.00	0.04	0.05	0.37	0.00
4C. Front Wall Mid Upper Center (42")	C1 through C6	Demand	114.2	45.4	56.4	29.0	764.9	253.3
		Capacity	153.6	70.0	1089.5	1045.0	2185.2	1000.5
		Ratio	0.74	0.65	0.05	0.03	0.46	0.56
	C7	Demand	22.7	0.8	24.1	14.2	1414.7	142.6
		Capacity	145.0	66.1	984.5	942.3	2209.5	1148.3
		Ratio	0.16	0.01	0.02	0.02	0.69	0.12

Table 3.9.4-29a
Comparison of Highest Combined Axial Forces/Moments with Capacities of the EOS-HSM-FPS Alternate
Front Wall (*Bounding*)

3 Pages

Component	Load Comb. ⁽¹⁾	Quantity	P ₁ (Tens.)	P ₂ (Tens.)	P ₁ (Comp)	P ₂ (Comp)	M _{1p} ⁽²⁾	M _{2p} ⁽²⁾
			kips/ft	kips/ft	kips/ft	kips/ft	kip-in/ft	kip-in/ft
4D. Front Wall Mid Lower Side (42")	C1 through C6	Demand	98.0	76.7	185.5	175.6	619.9	455.8
		Capacity	153.6	110.4	1089.5	1066.5	1722.1	1908.9
		Ratio	0.64	0.70	0.17	0.16	0.67	0.62
	C7	Demand	20.4	19.6	47.7	86.8	275.2	895.0
		Capacity	145.0	104.2	984.5	962.7	2407.9	1591.1
		Ratio	0.14	0.19	0.05	0.09	0.12	0.59
4E. Front Wall Mid Lower Center (42")	C1 through C6	Demand	100.0	30.2	207.0	76.9	1372.2	321.8
		Capacity	153.6	51.3	1089.5	1035.1	2262.5	682.6
		Ratio	0.65	0.59	0.19	0.07	0.61	0.79
	C7	Demand	2.0	0.0	77.1	39.3	325.7	0.0
		Capacity	145.0	48.5	984.5	932.9	2420.2	844.3
		Ratio	0.01	0.00	0.08	0.04	0.14	0.00
4F. Front Wall Mid Center (42")	C1 through C6	Demand	118.7	104.5	386.6	296.9	271.7	1143.2
		Capacity	153.6	153.6	1089.5	1089.5	2223.3	1386.5
		Ratio	0.77	0.68	0.35	0.27	0.46	0.83
	C7	Demand	41.9	28.5	56.3	139.3	446.2	1635.4
		Capacity	145.0	145.0	984.5	984.5	2413.5	2365.6
		Ratio	0.29	0.20	0.06	0.14	0.23	0.69

Table 3.9.4-29a
Comparison of Highest Combined Axial Forces/Moments with Capacities of the EOS-HSM-FPS Alternate Front Wall (*Bounding*)

3 Pages

Component	Load Comb. ⁽¹⁾	Quantity	P ₁ (Tens.)	P ₂ (Tens.)	P ₁ (Comp)	P ₂ (Comp)	M _{1p} ⁽²⁾	M _{2p} ⁽²⁾
			kips/ft	kips/ft	kips/ft	kips/ft	kip-in/ft	kip-in/ft
4G. Front Wall Bottom (42")	C1 through C6	Demand	44.4	64.6	88.3	87.5	391.5	278.9
		Capacity	153.6	92.1	1195.6	1162.9	2719.9	952.4
		Ratio	0.29	0.70	0.07	0.08	0.14	0.38
	C7	Demand	31.6	10.3	17.2	21.6	326.5	449.9
		Capacity	145.0	87.0	1080.0	1049.0	2145.7	1654.9
		Ratio	0.22	0.12	0.02	0.02	0.15	0.27

Notes:

- 1 Load Combinations C1 through C6 include normal thermal, Combination C7 includes accident thermal
- 2 M_{1p} and M_{2p} are moments at the same location and for the same load combination as P₁ and P₂. M_{1p} and M_{2p} occur at the same location simultaneously with P₁ and P₂, i.e. $M_1 = [(P_{tu} - P_1)/P_{tu}] * M_{u1}$

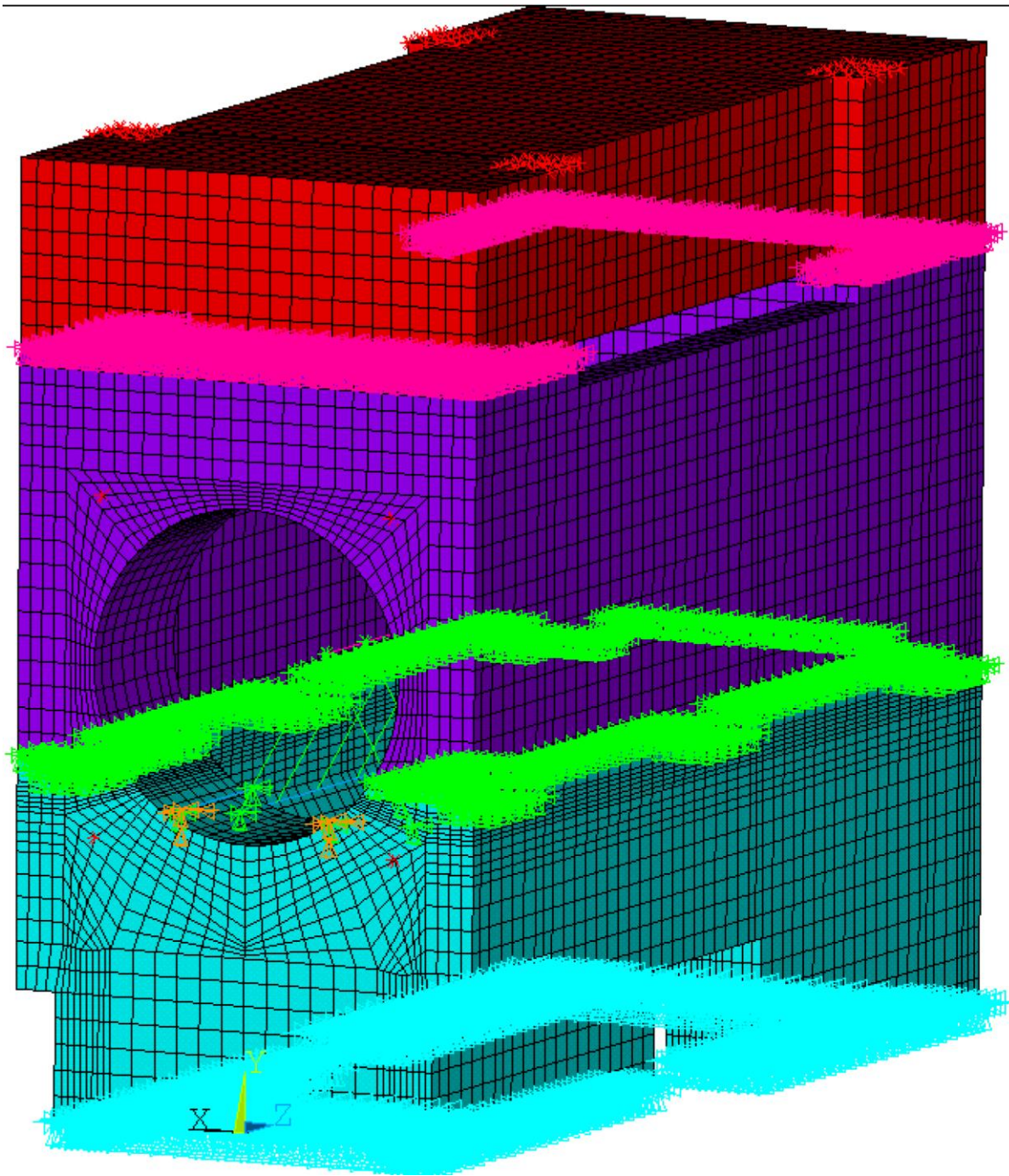


Figure 3.9.4-1
Analytical Model of EOS-HSM for Mechanical Load Analysis

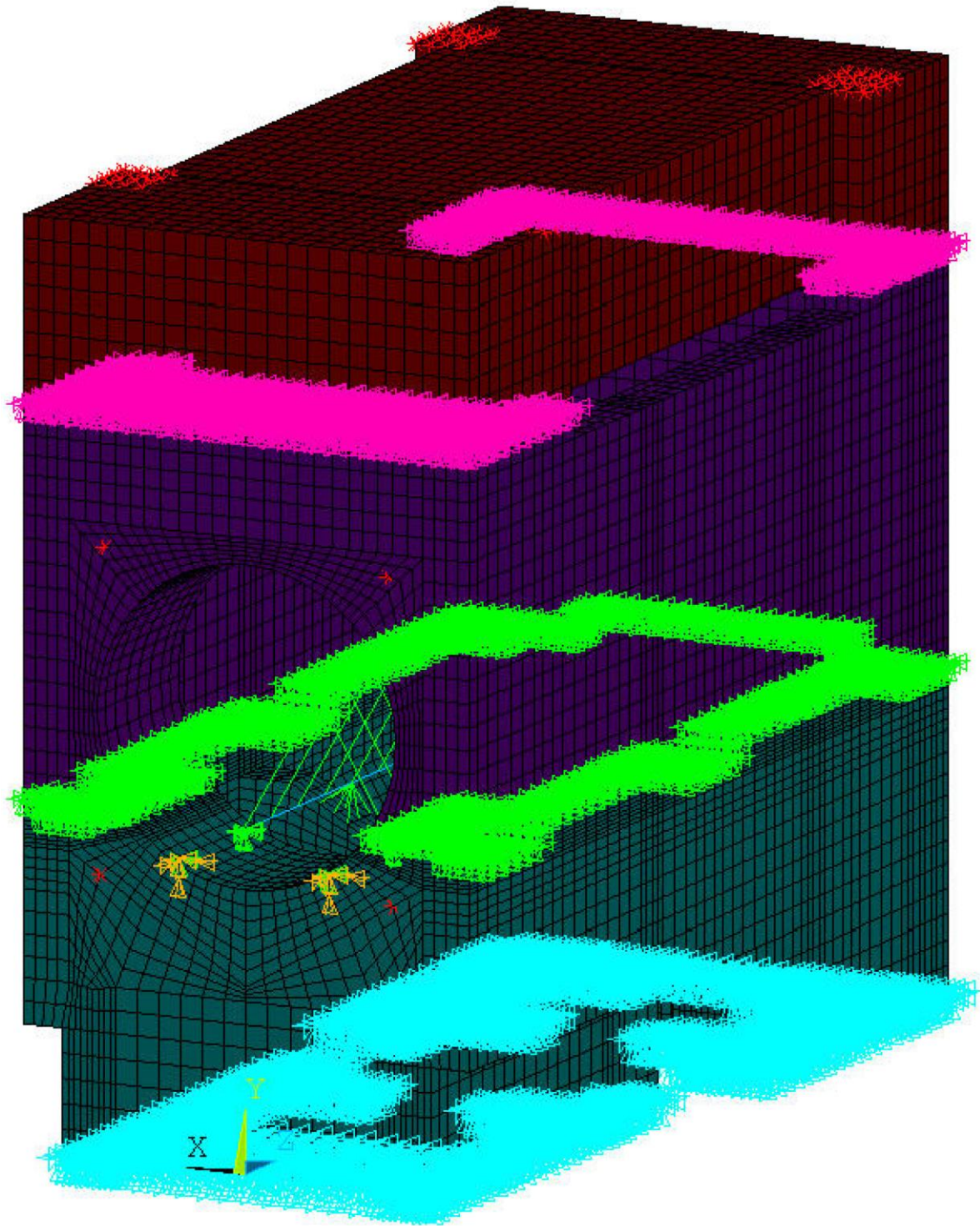


Figure 3.9.4-1a
Analytical Model of EOS-HSM-FPS for Mechanical Load Analysis

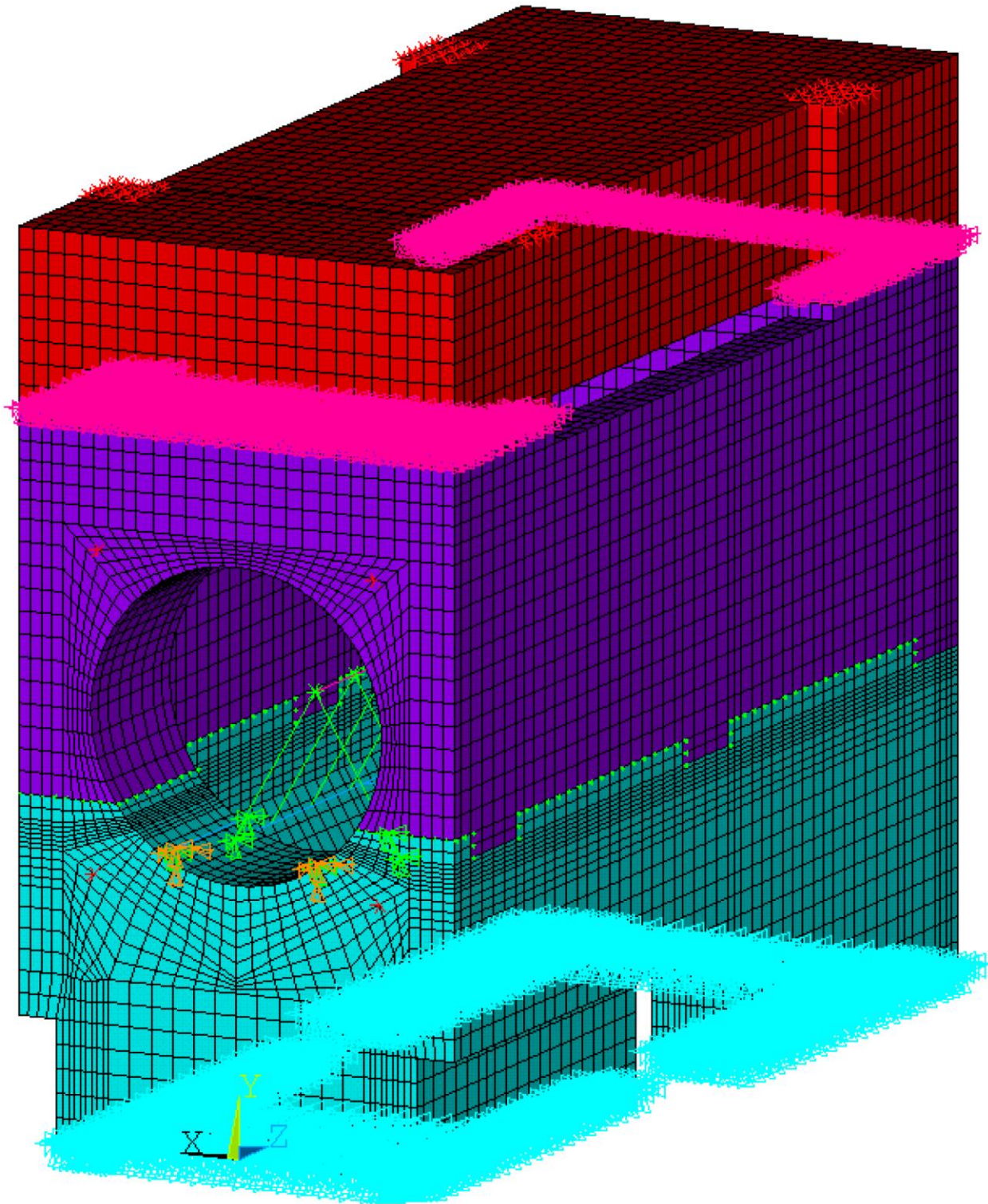


Figure 3.9.4-2
Analytical Model of EOS-HSMS for Mechanical Load Analysis
(Node to Node Contact at Segment Joint interface)

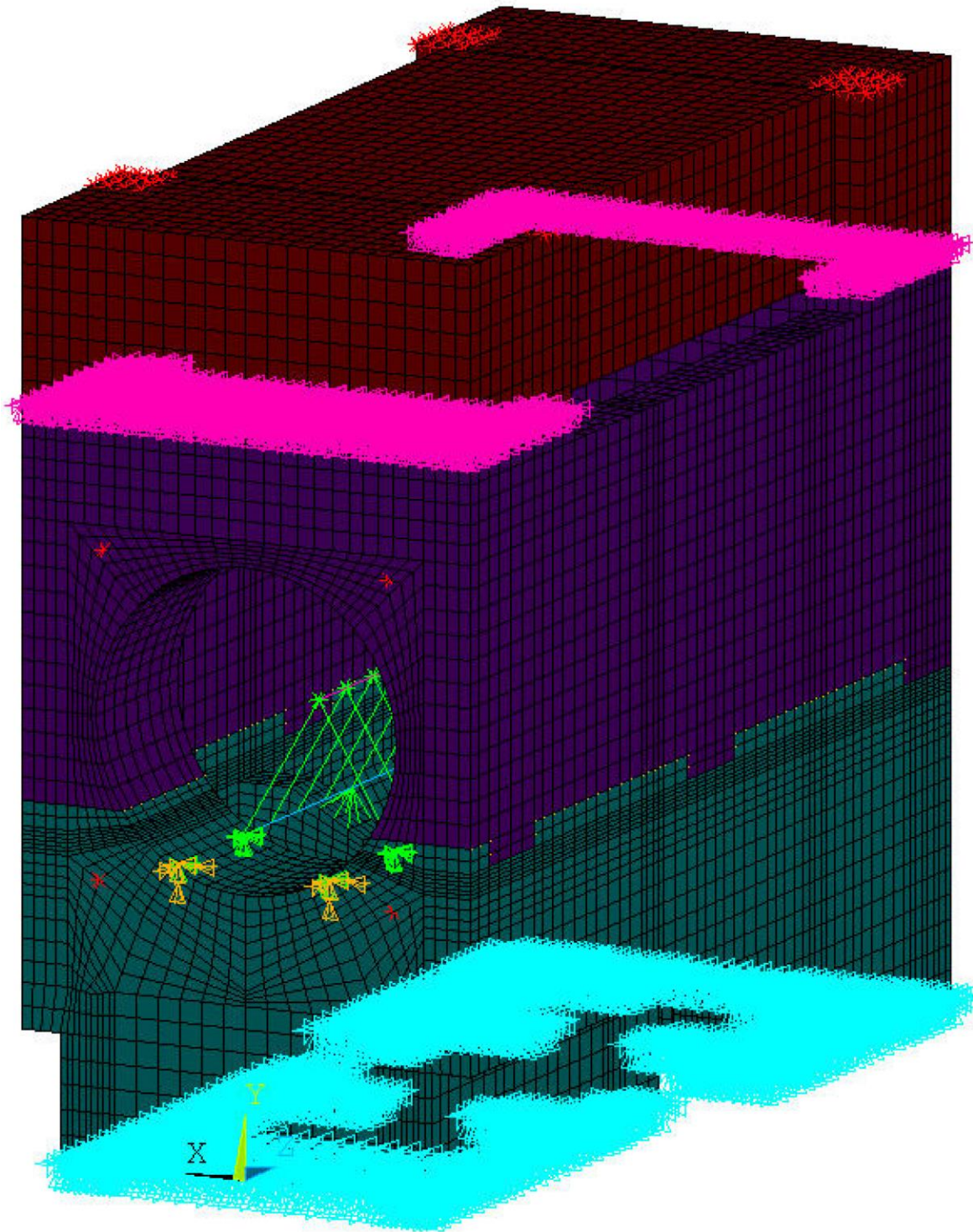


Figure 3.9.4-2a
Analytical Model of EOS-HSMS-FPS for Mechanical Load Analysis
(Node to Node Contact at Segment Joint Interface)

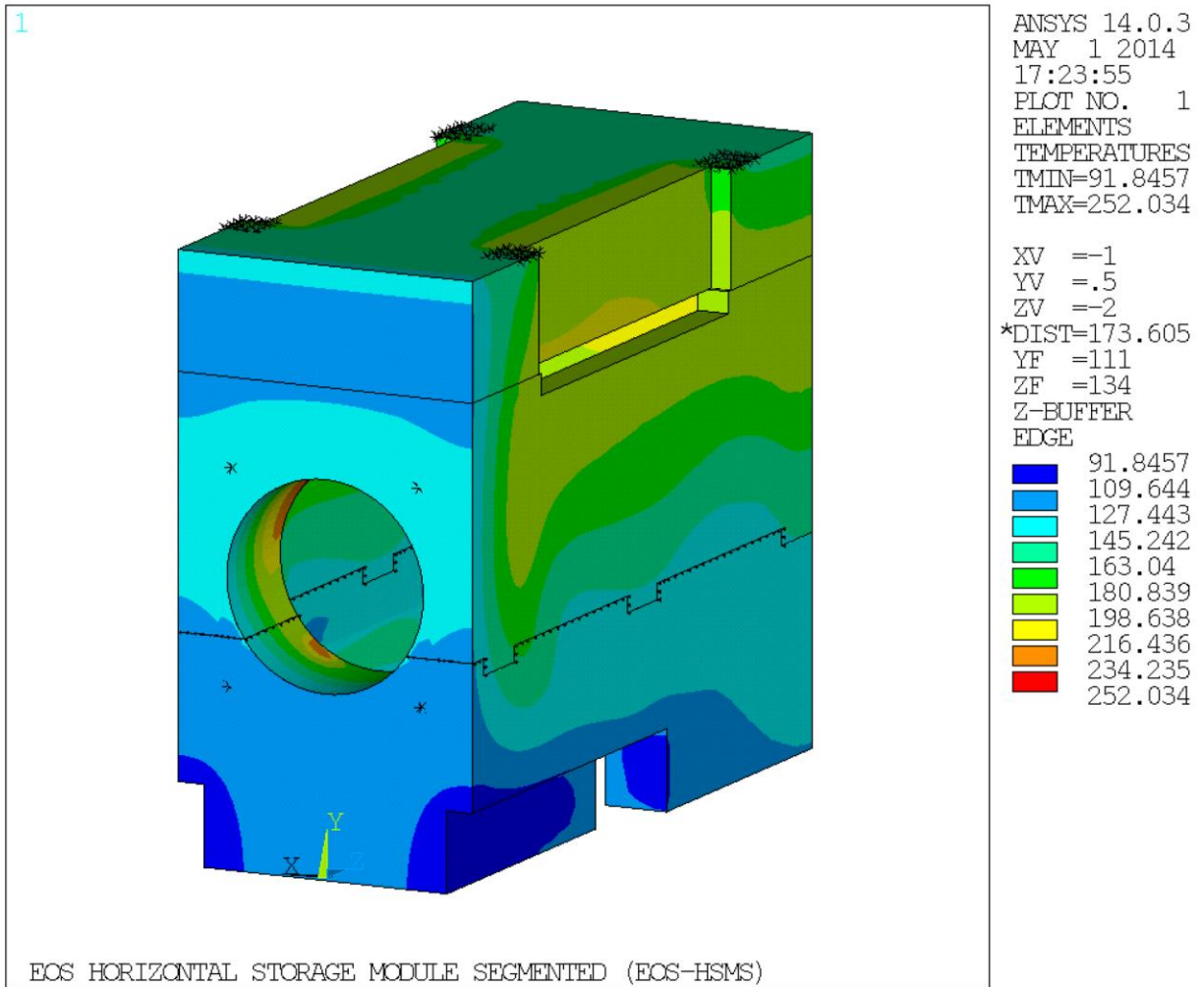


Figure 3.9.4-3
Temperature distribution of EOS-HSMS for Normal Thermal Hot Condition

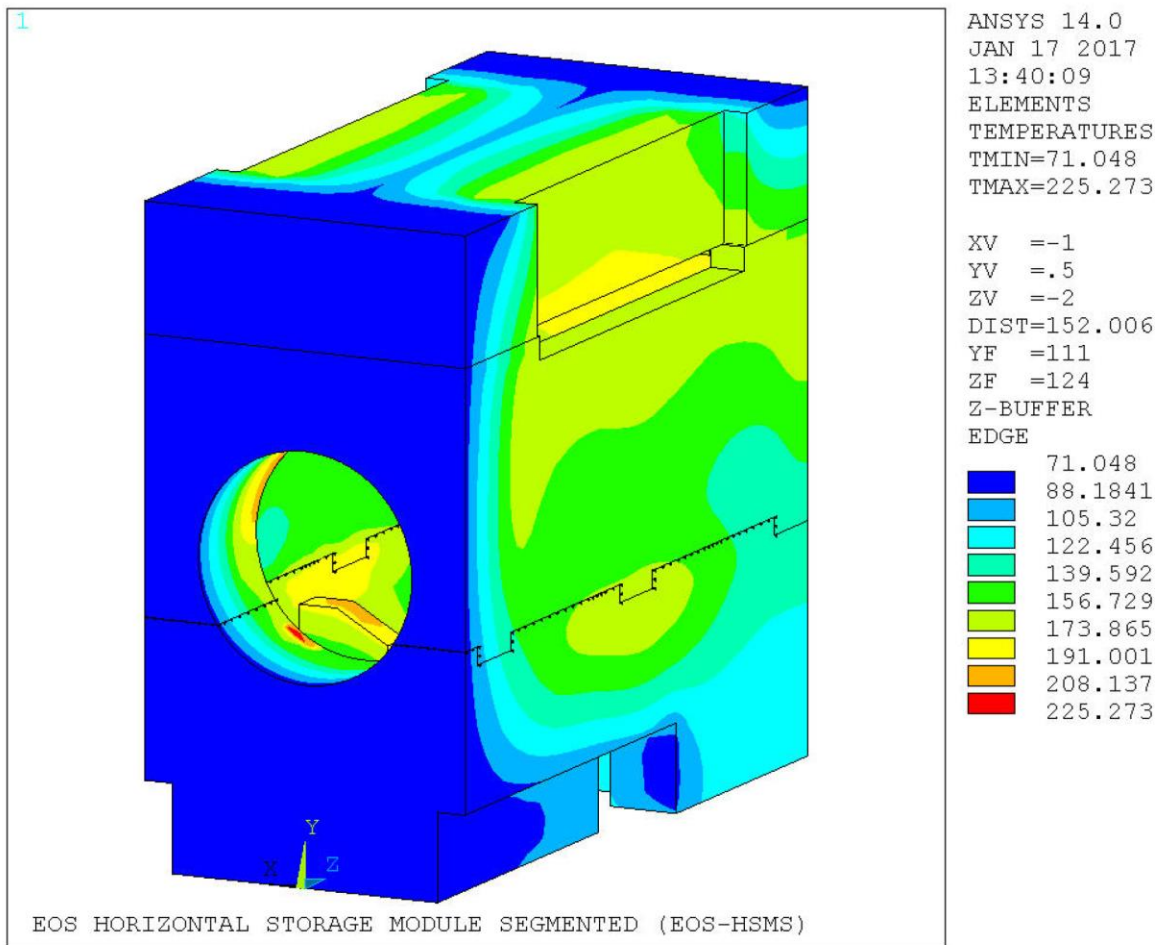


Figure 3.9.4-3a
Temperature distribution of EOS-HSMS-FPS for Normal Thermal Hot Condition

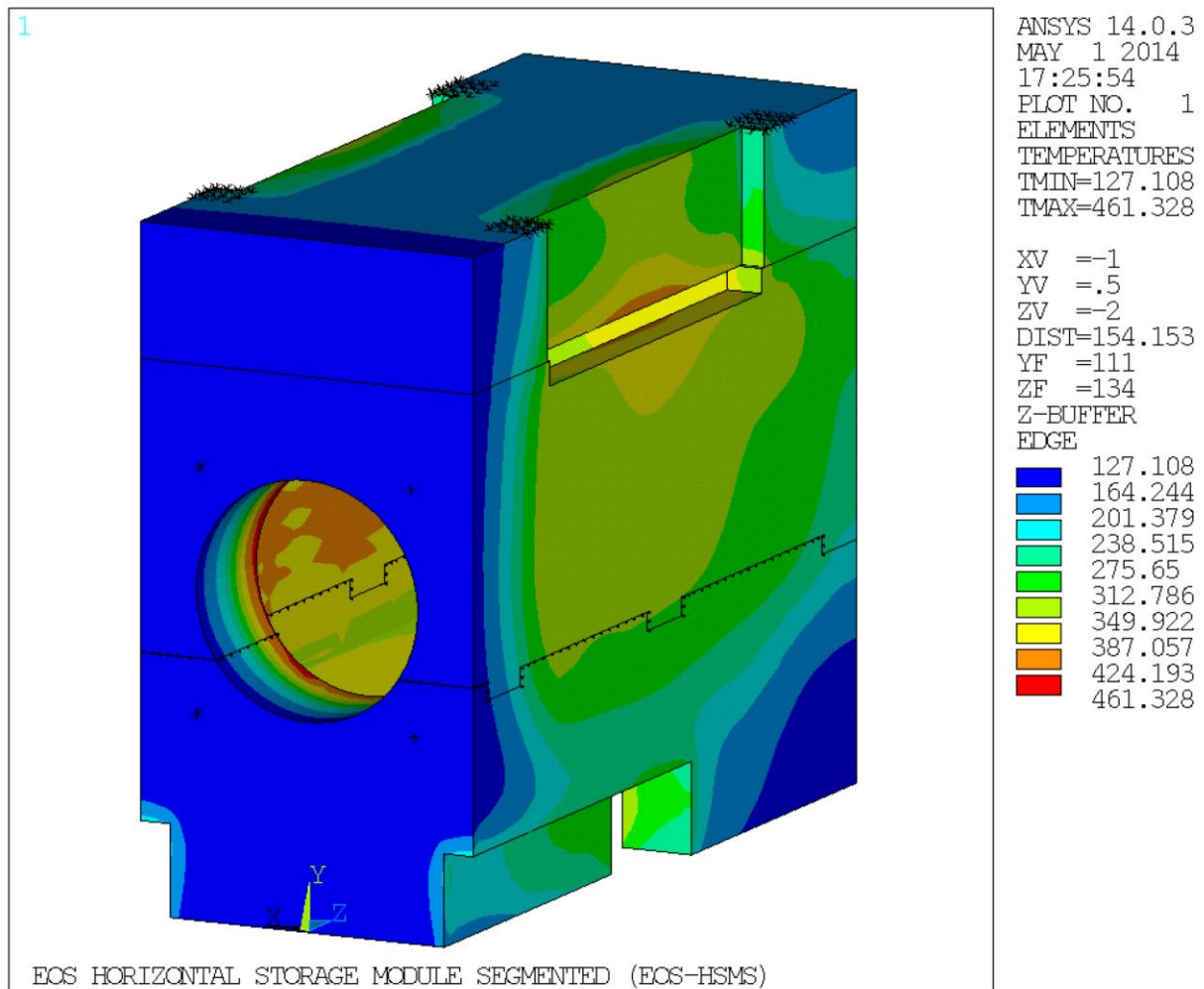
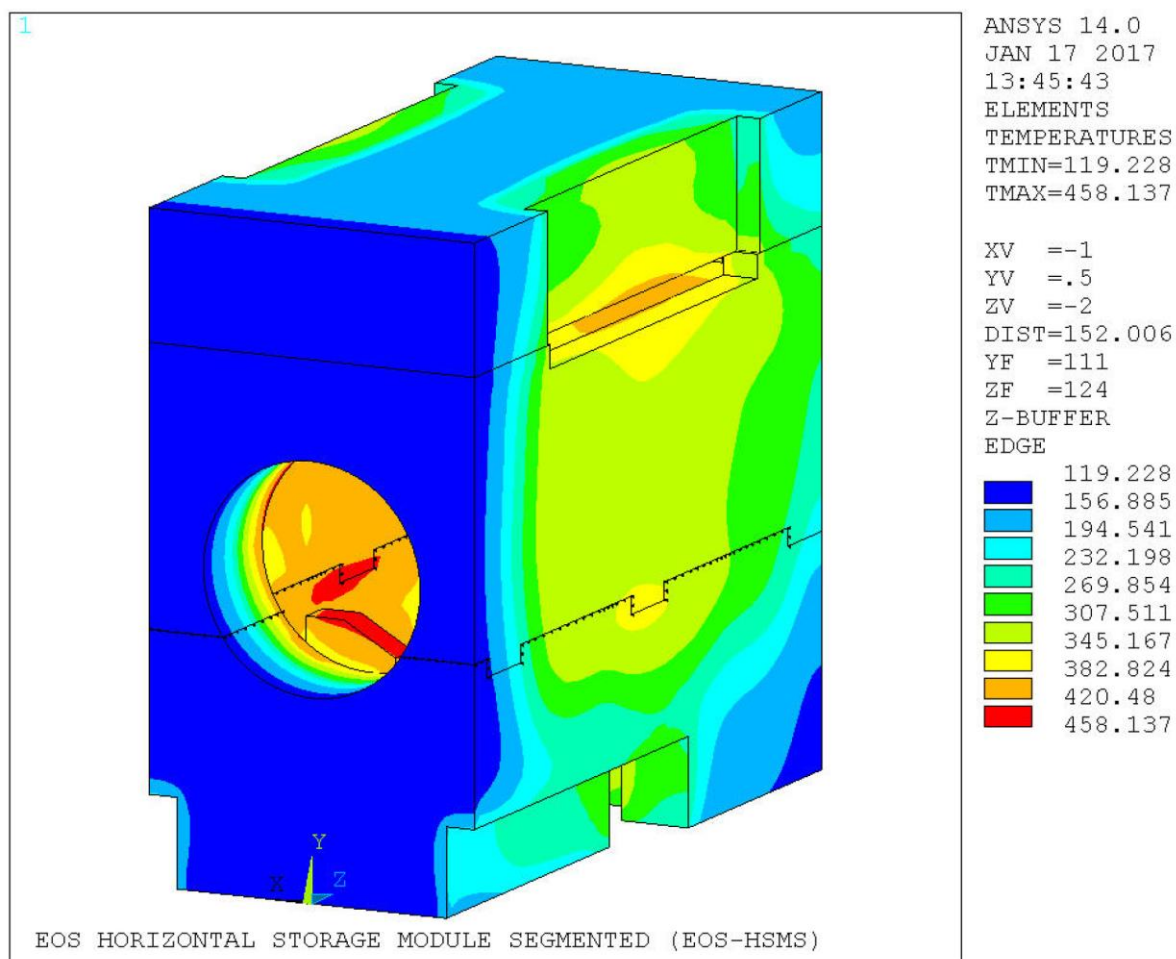


Figure 3.9.4-4
Temperature distribution of EOS-HSMS for Blocked Vent Accident Thermal Condition



Note: Bounding temperature distribution of EOS-HSMS-FPS used for design basis accident blocked vent thermal stress analysis, which is conservative compared to the temperature profile provided in Figure 4.9.5-8(e)

Figure 3.9.4-4a
Temperature distribution of EOS-HSMS-FPS for Blocked Vent Accident Thermal Condition

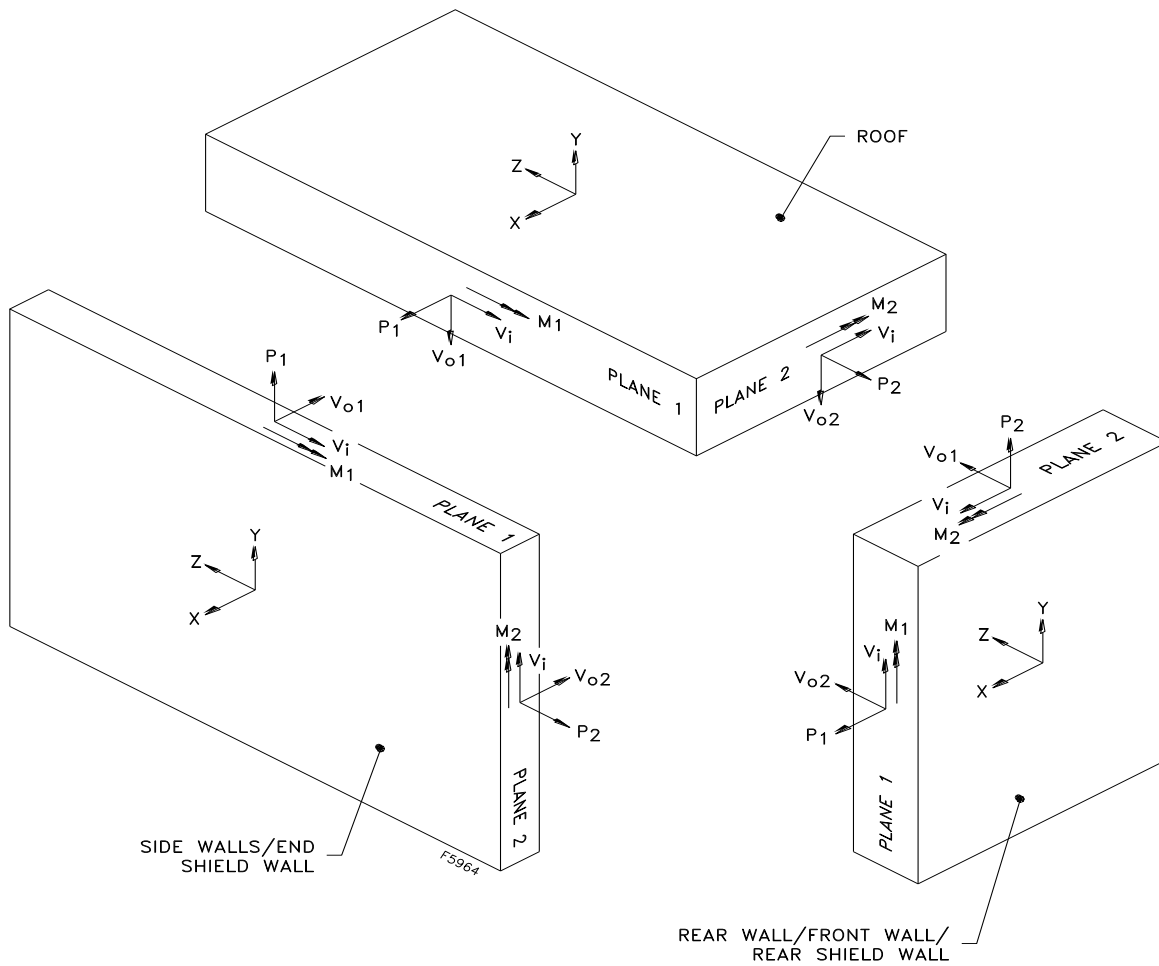


Figure 3.9.4-5
Symbolic Notation of Forces and Moments of EOS-HSM Concrete Components

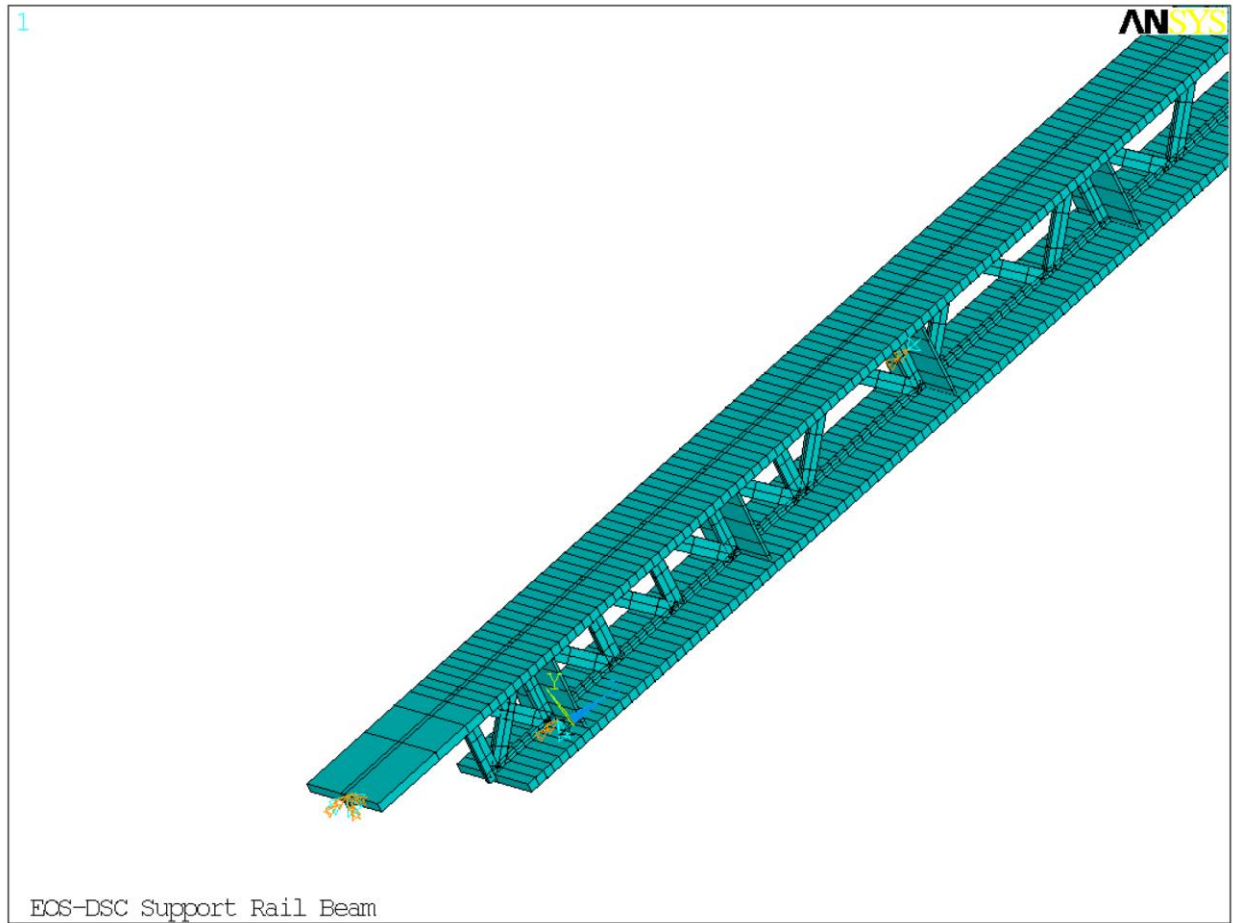


Figure 3.9.4-6
Analytical Model of the W12x136 DSC Main Support Beam with Stiffeners
and Open Web

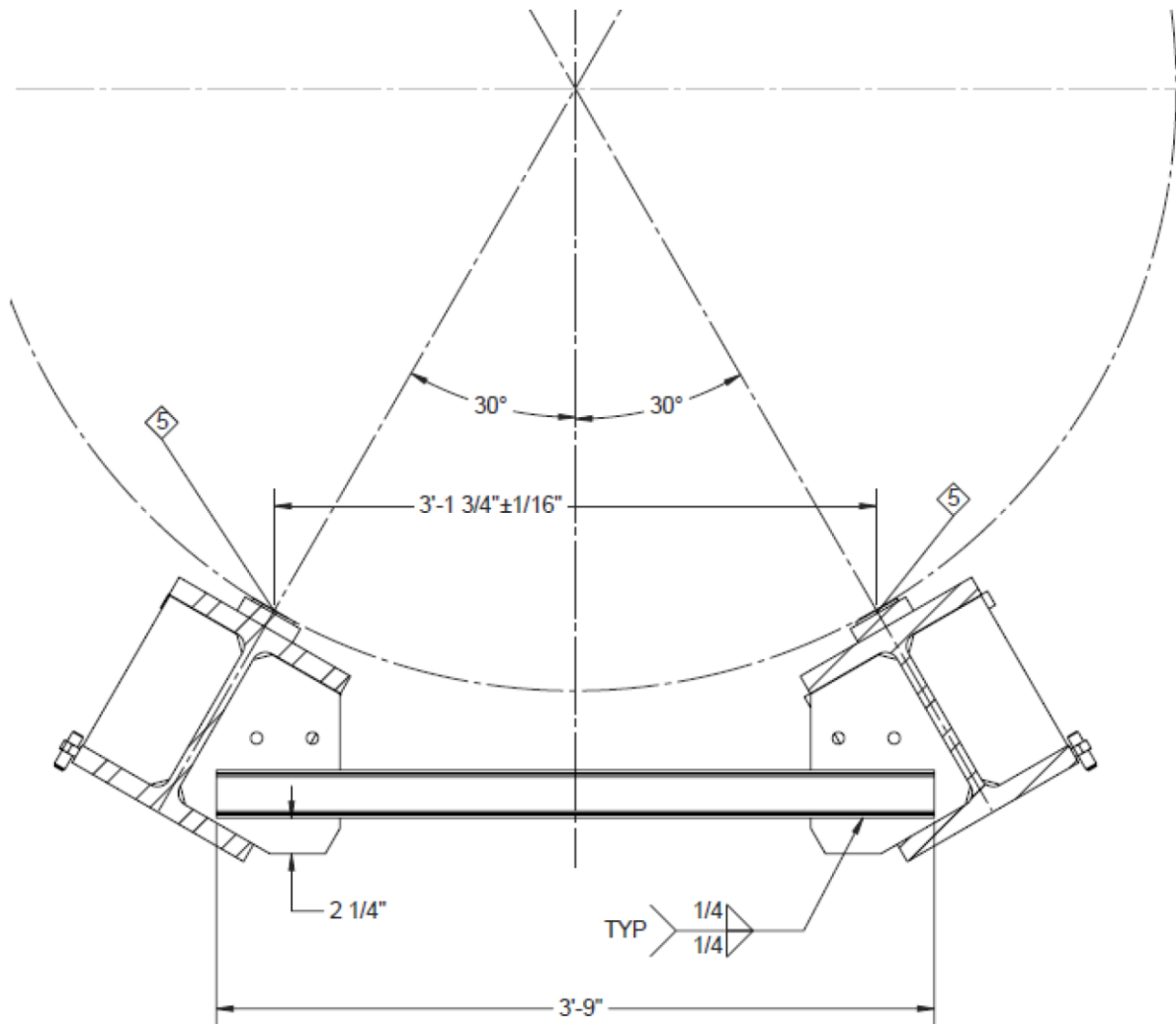


Figure 3.9.4-7
Components of DSC Support Structure

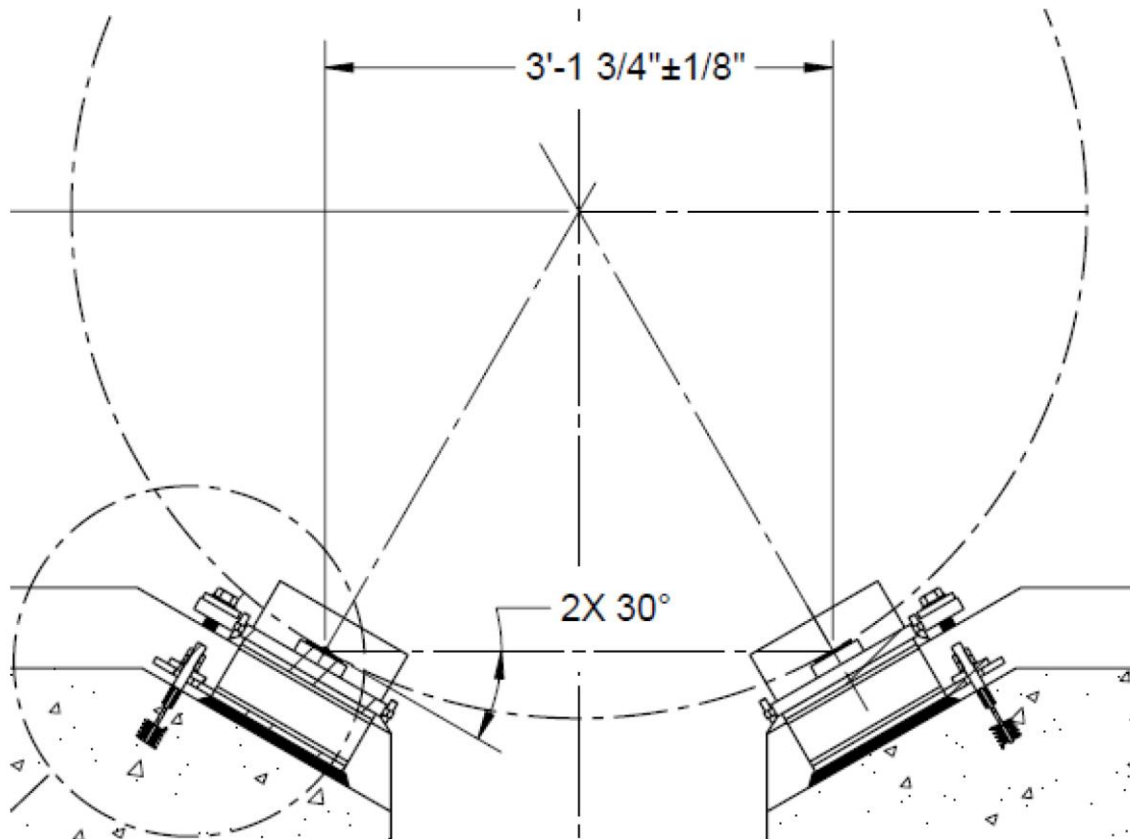


Figure 3.9.4-7a
Components of FPS DSC Support Structure

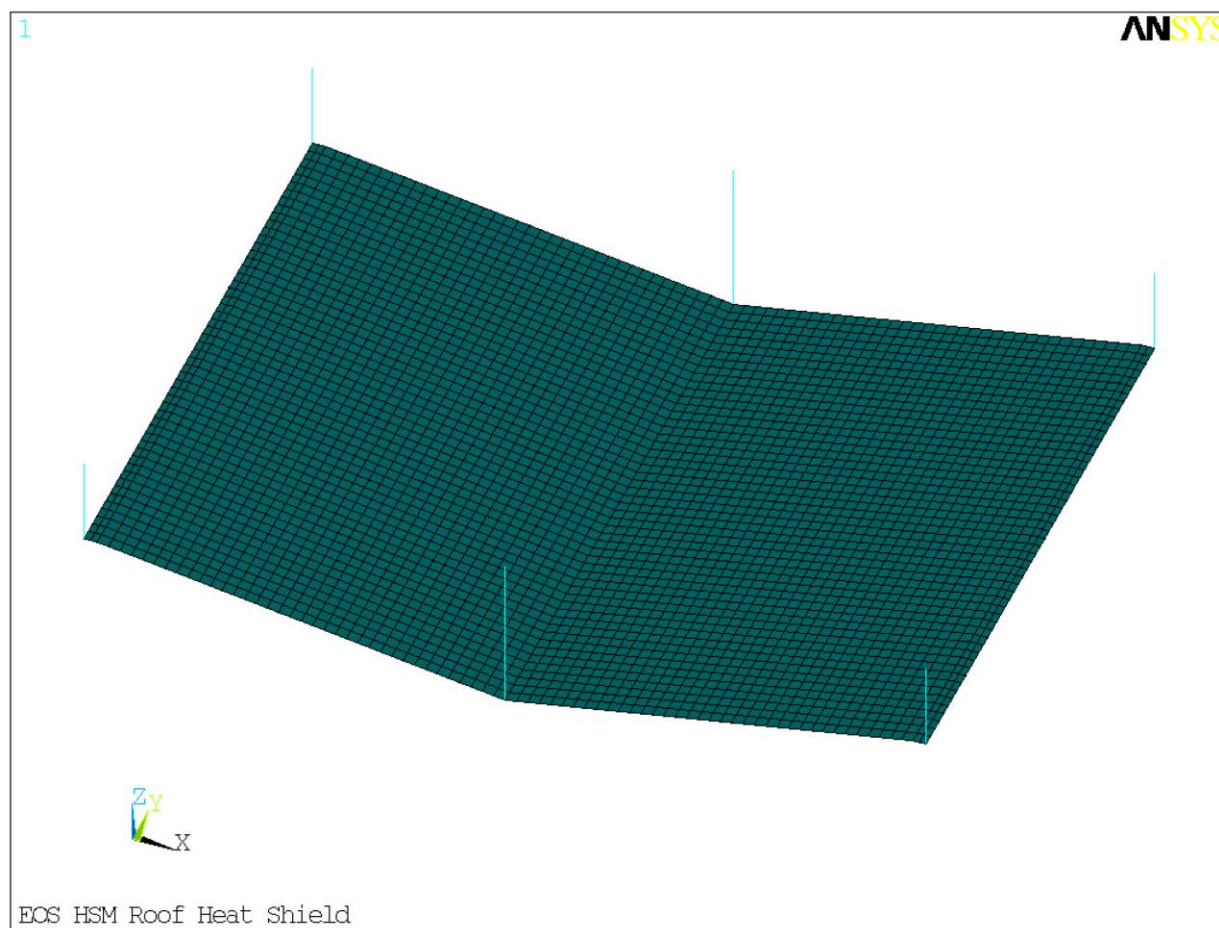


Figure 3.9.4-8
Analytical Model of Coupled Roof Heat Shield and Connection Studs

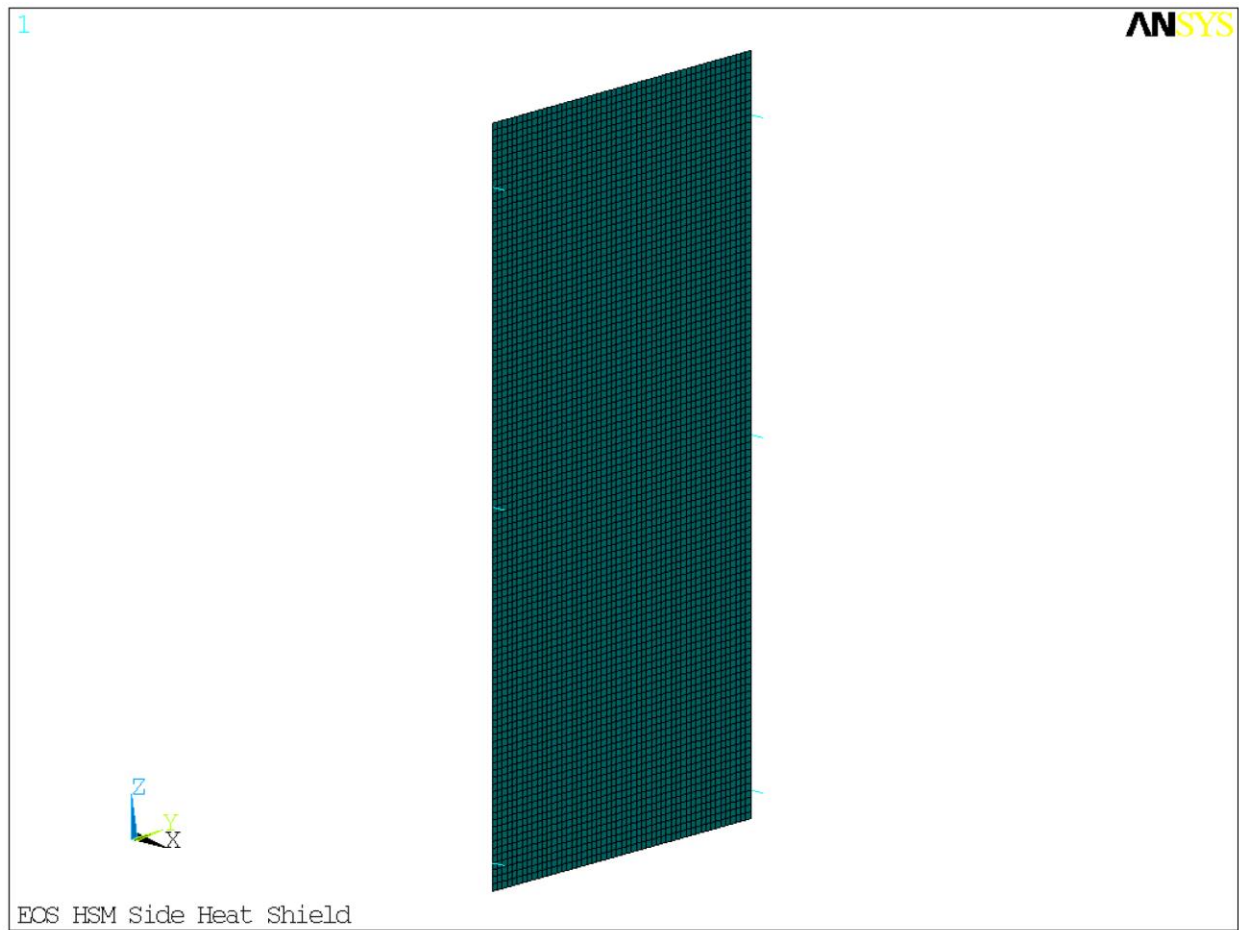


Figure 3.9.4-9
Analytical Model of Coupled Side Heat Shield and Connection Studs

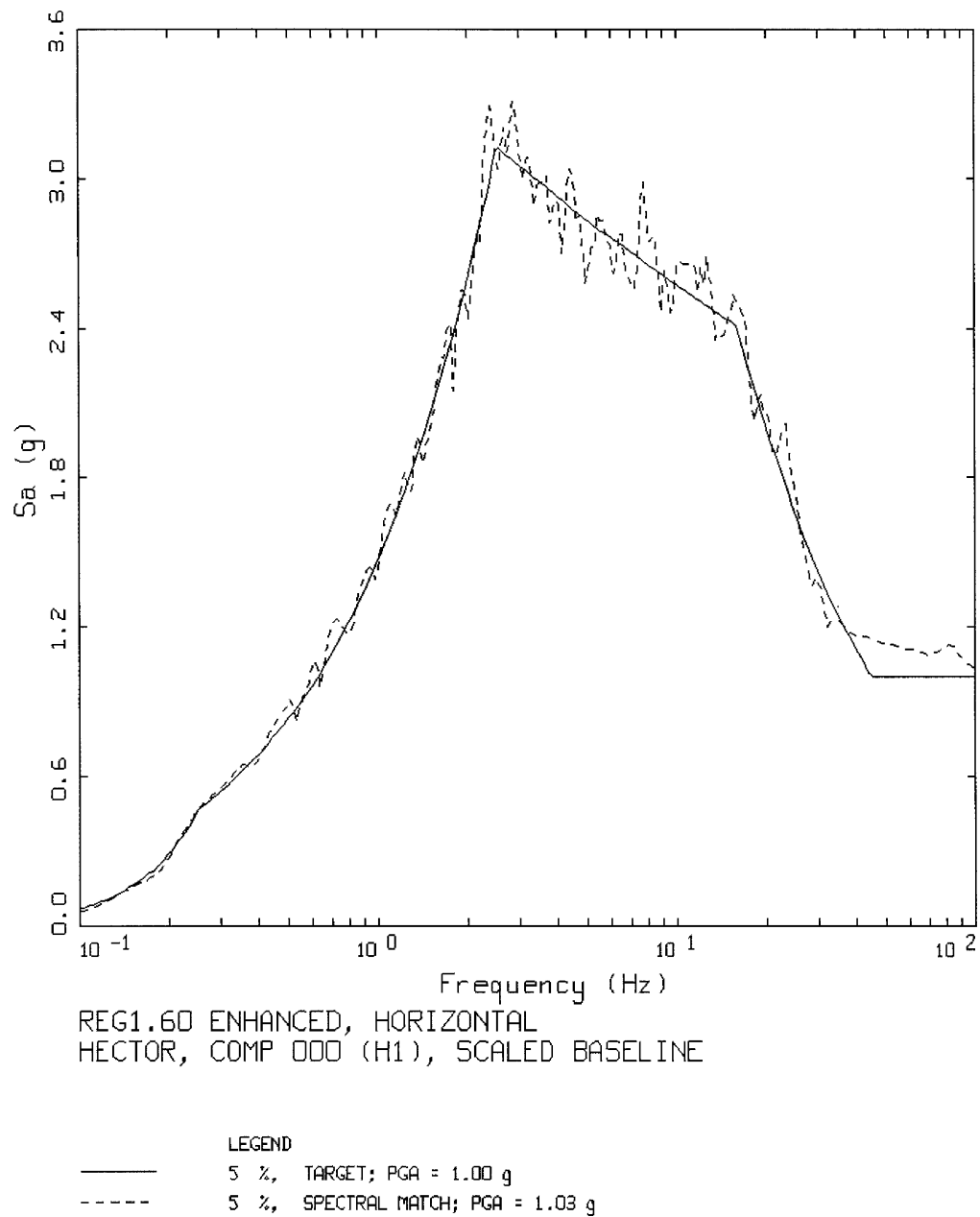
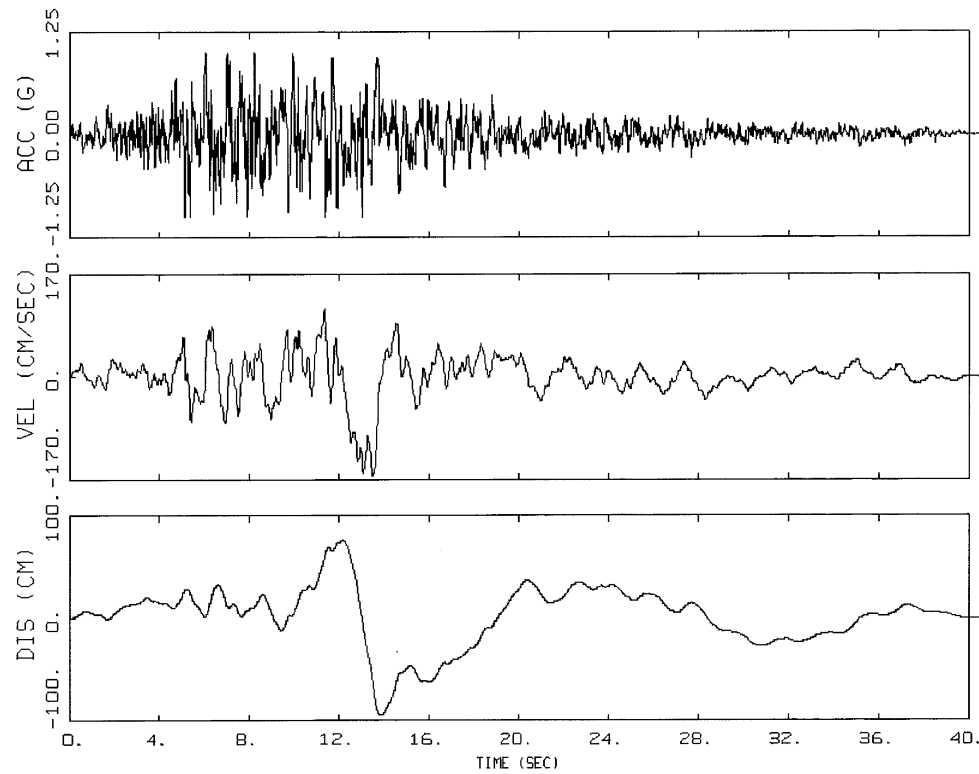
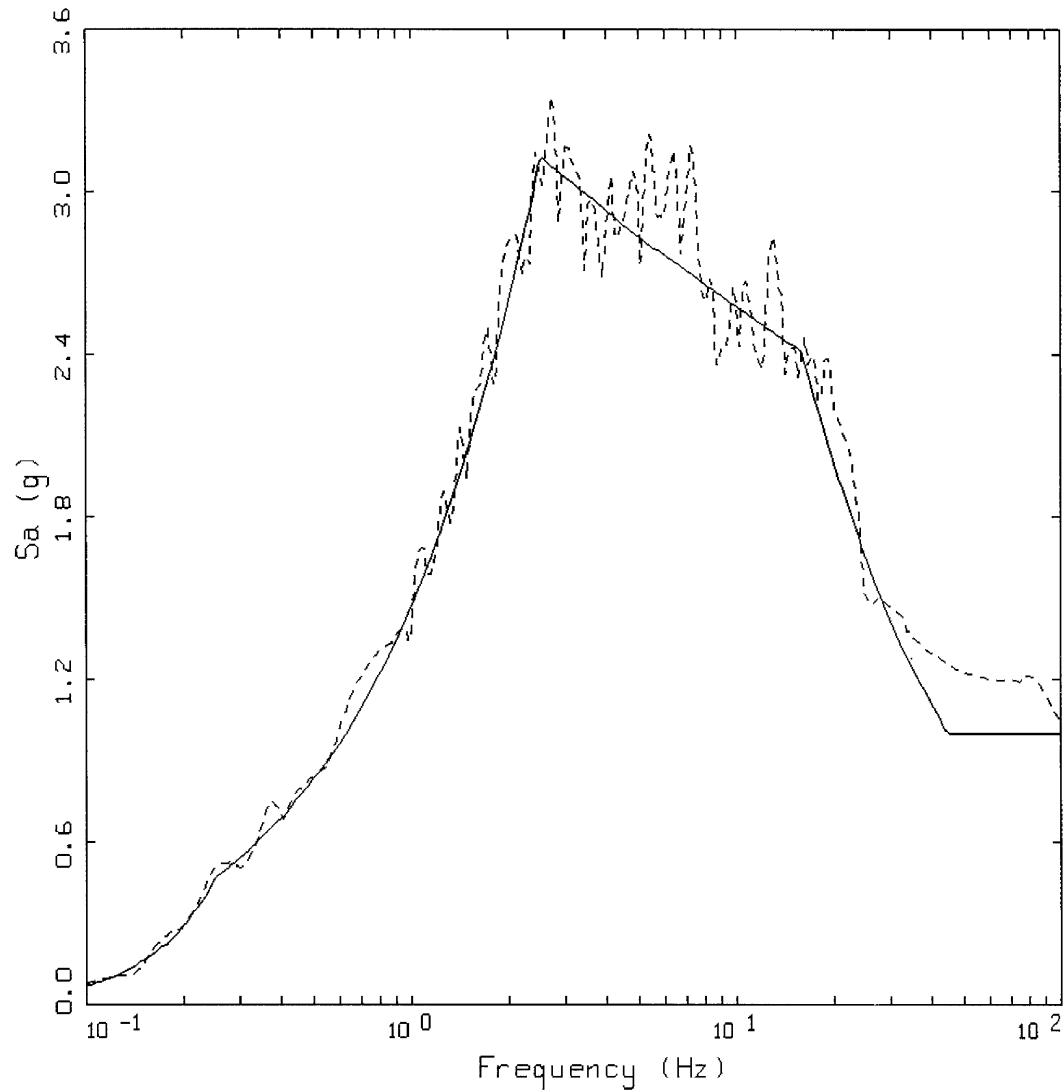


Figure 3.9.4-10
Horizontal Target and 5% Spectral Match (Horizontal 1, Hector Mine Earthquake)



REG1.6D ENHANCED, HORIZONTAL
HECTOR, COMP 000 (H1), SCALED BASELINE

Figure 3.9.4-11
Baseline Corrected Acceleration, Velocity and Displacement Time Histories
(Horizontal 1, Hector Mine Earthquake)



LEGEND
—— 5 %, TARGET; PGA = 1.00 g
----- 5 %, SPECTRAL MATCH; PGA = 1.05 g

Figure 3.9.4-12
Horizontal Target and 5% Spectral Match (Horizontal 2, Hector Mine Earthquake)

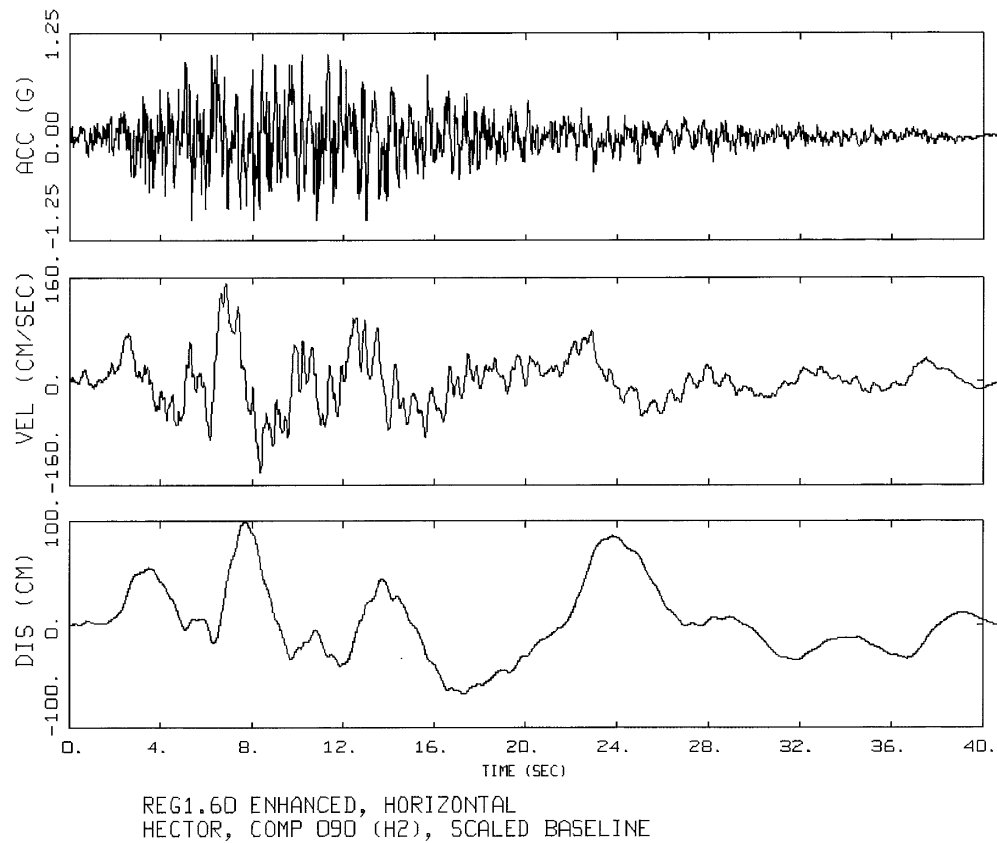
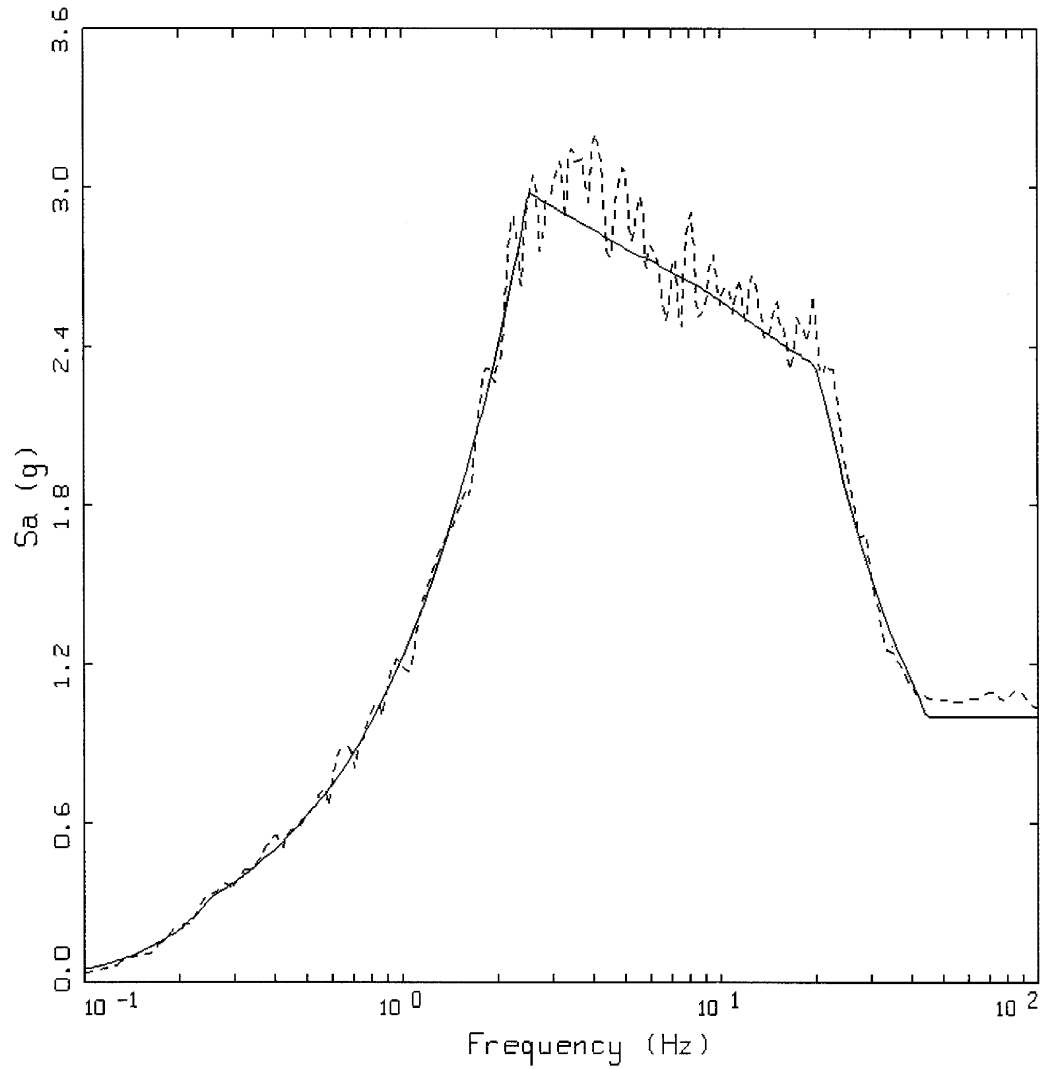


Figure 3.9.4-13
Baseline Corrected Acceleration, Velocity and Displacement Time Histories
(Horizontal 2, Hector Mine Earthquake)



LEGEND
—— 5 %, TARGET; PGA = 1.00 g
----- 5 %, SPECTRAL MATCH; PGA = 1.03 g

Figure 3.9.4-14
Vertical Target and 5% Spectral Match (Vertical Up, Hector Mine Earthquake)

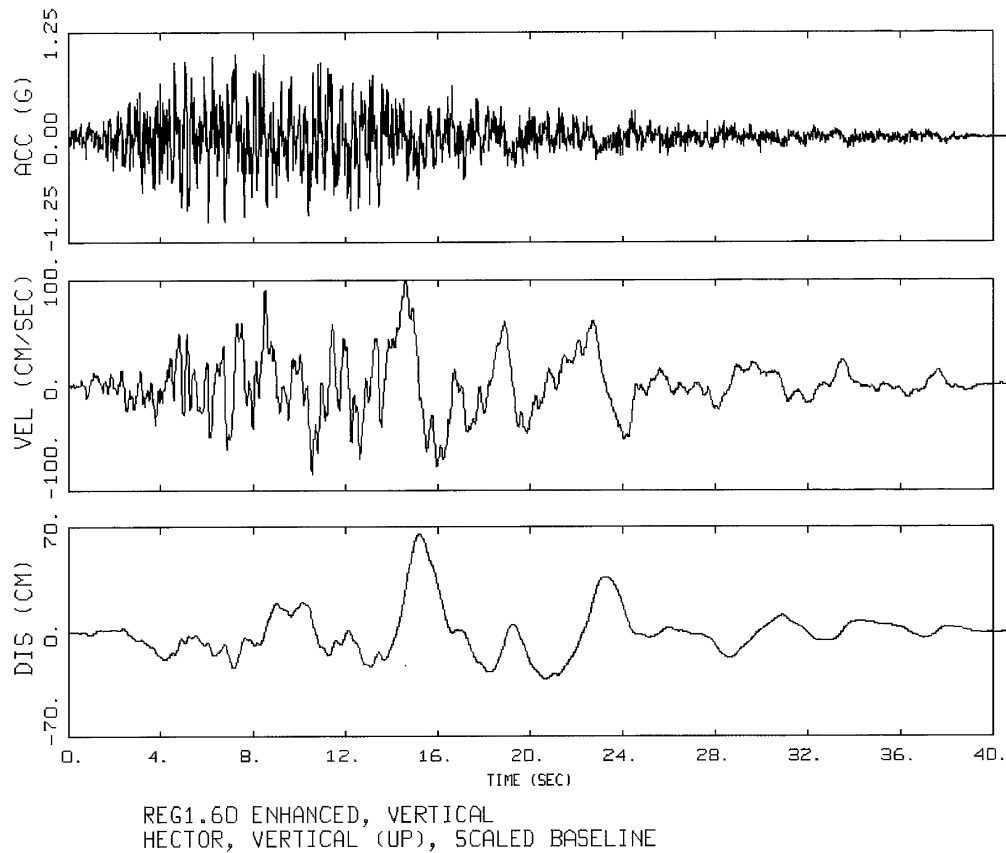


Figure 3.9.4-15
Baseline Corrected Acceleration, Velocity and Displacement Time Histories
(Vertical Up, Hector Mine Earthquake)

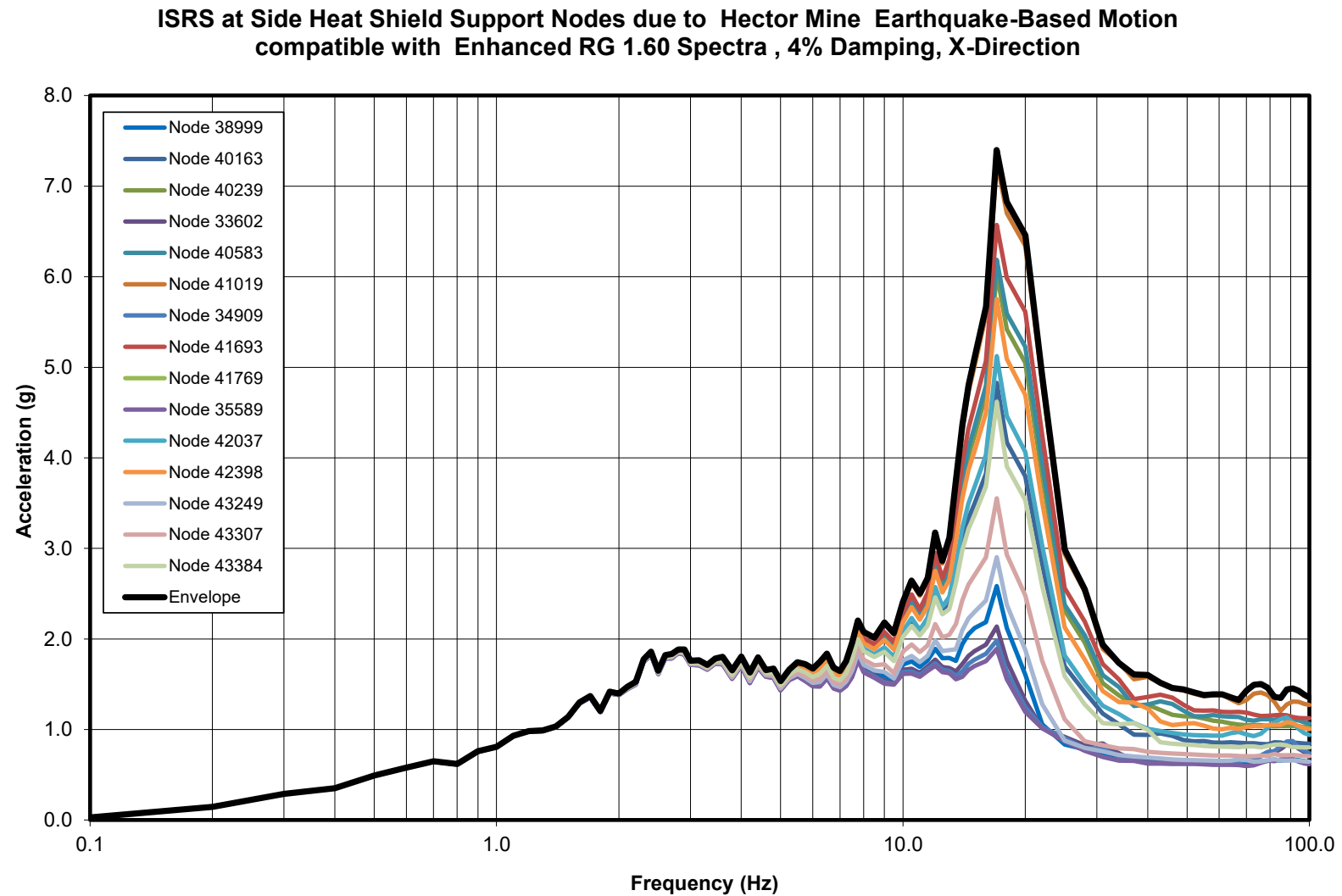


Figure 3.9.4-16
ISRS at Side Heat Shield Support Nodes due to Hector Mine Earthquake-Based Motion compatible with Enhanced RG 1.60 Spectra, 4% Damping, X-Direction

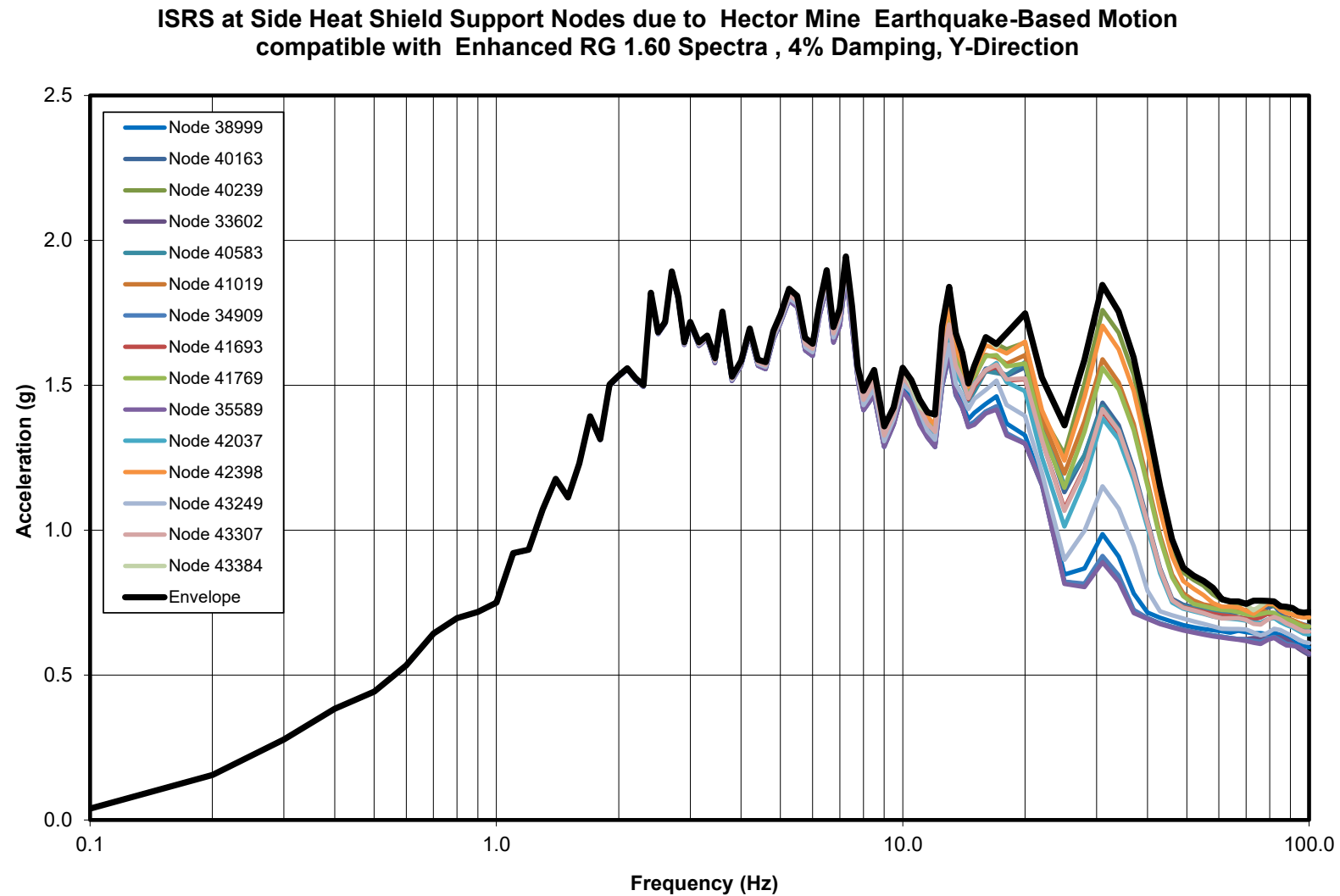


Figure 3.9.4-17
ISRS at Side Heat Shield Support Nodes due to Hector Mine Earthquake-Based Motion compatible with Enhanced RG 1.60 Spectra, 4% Damping, Y-Direction

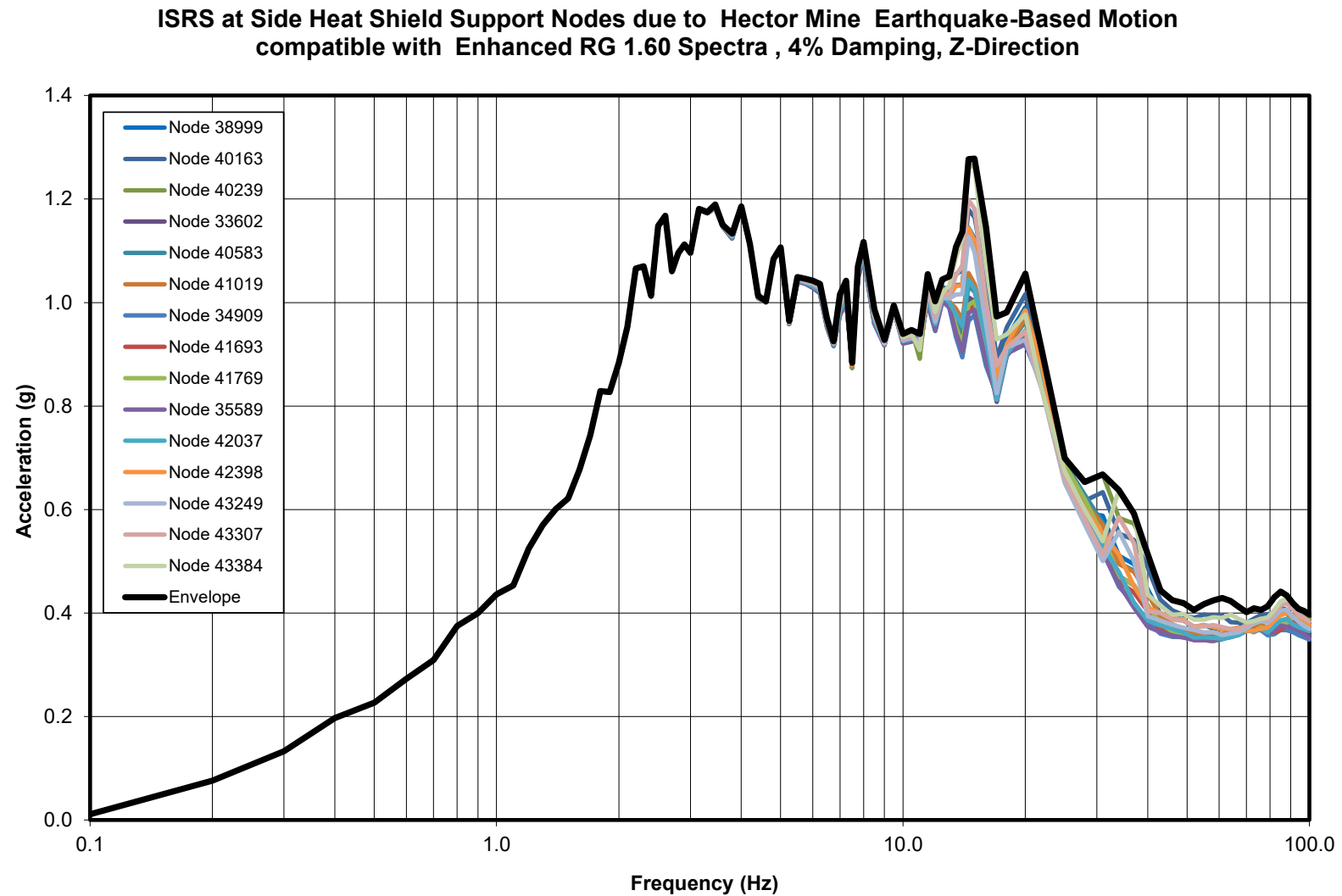


Figure 3.9.4-18
ISRS at Side Heat Shield Support Nodes due to Hector Mine Earthquake-Based Motion compatible with Enhanced RG 1.60 Spectra, 4% Damping, Z-Direction

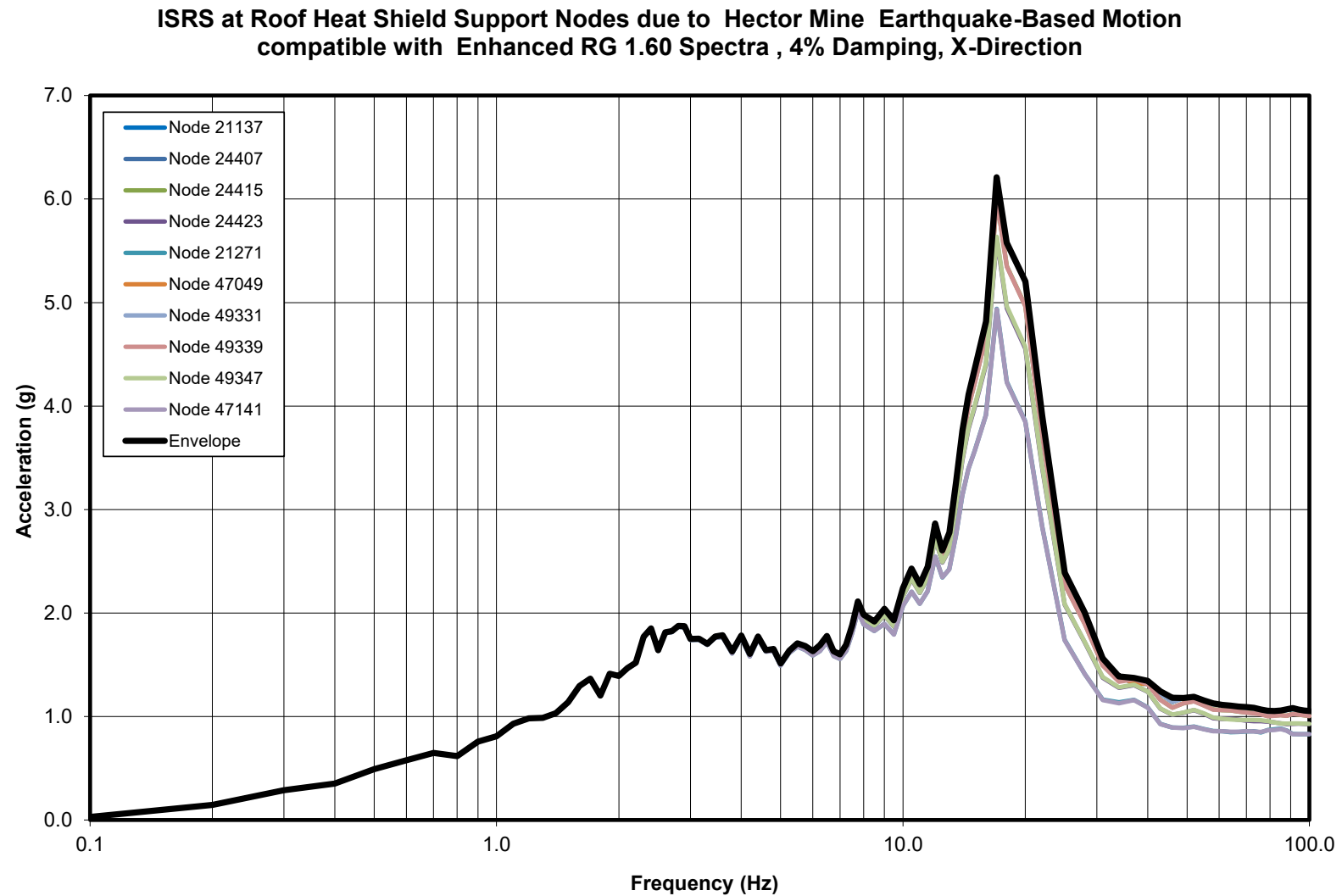


Figure 3.9.4-19
ISRS at Roof Heat Shield Support Nodes due to Hector Mine Earthquake-Based Motion compatible with Enhanced RG 1.60 Spectra, 4% Damping, X-Direction

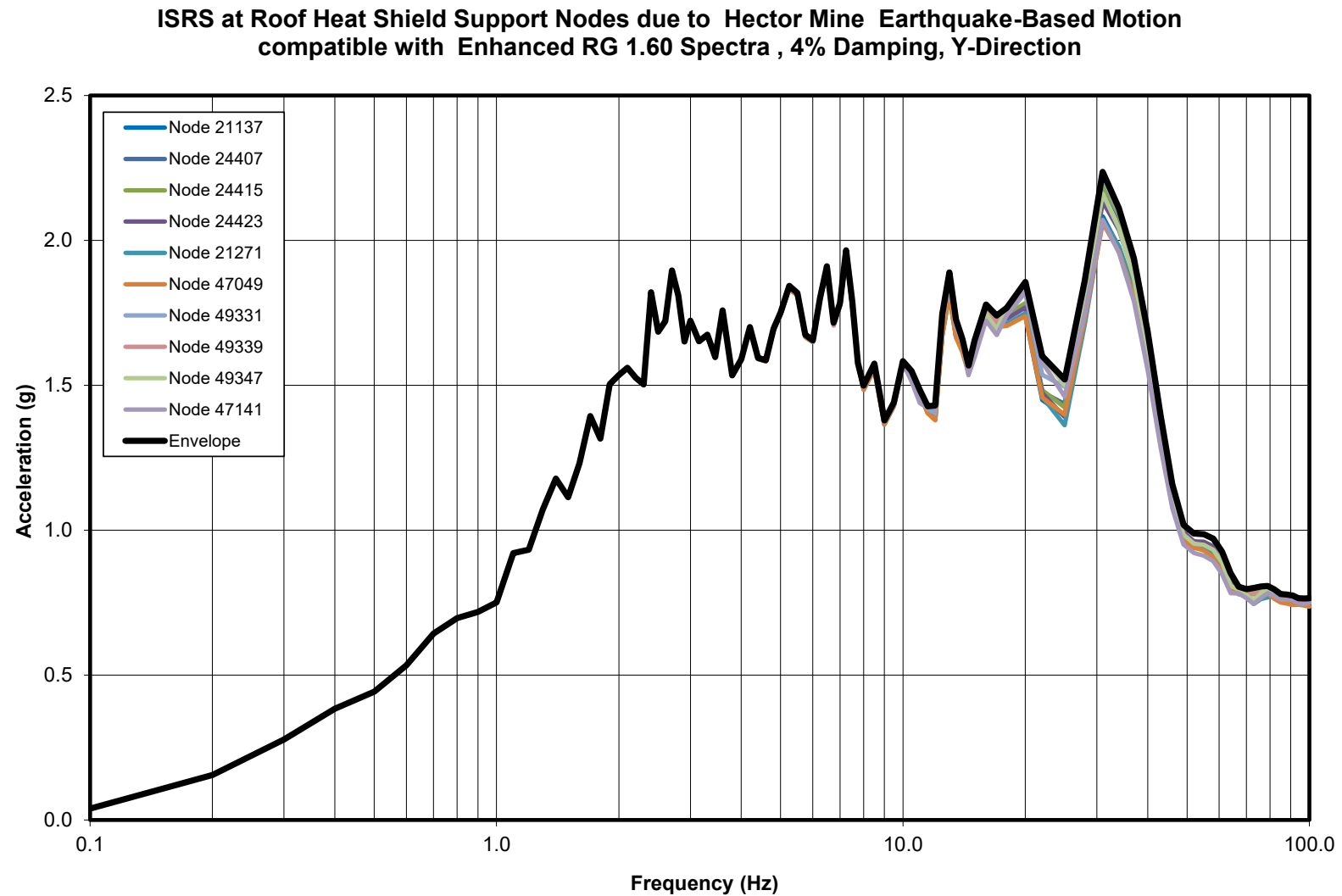


Figure 3.9.4-20
ISRS at Roof Heat Shield Support Nodes due to Hector Mine Earthquake-Based Motion compatible with Enhanced RG 1.60 Spectra, 4% Damping, Y-Direction

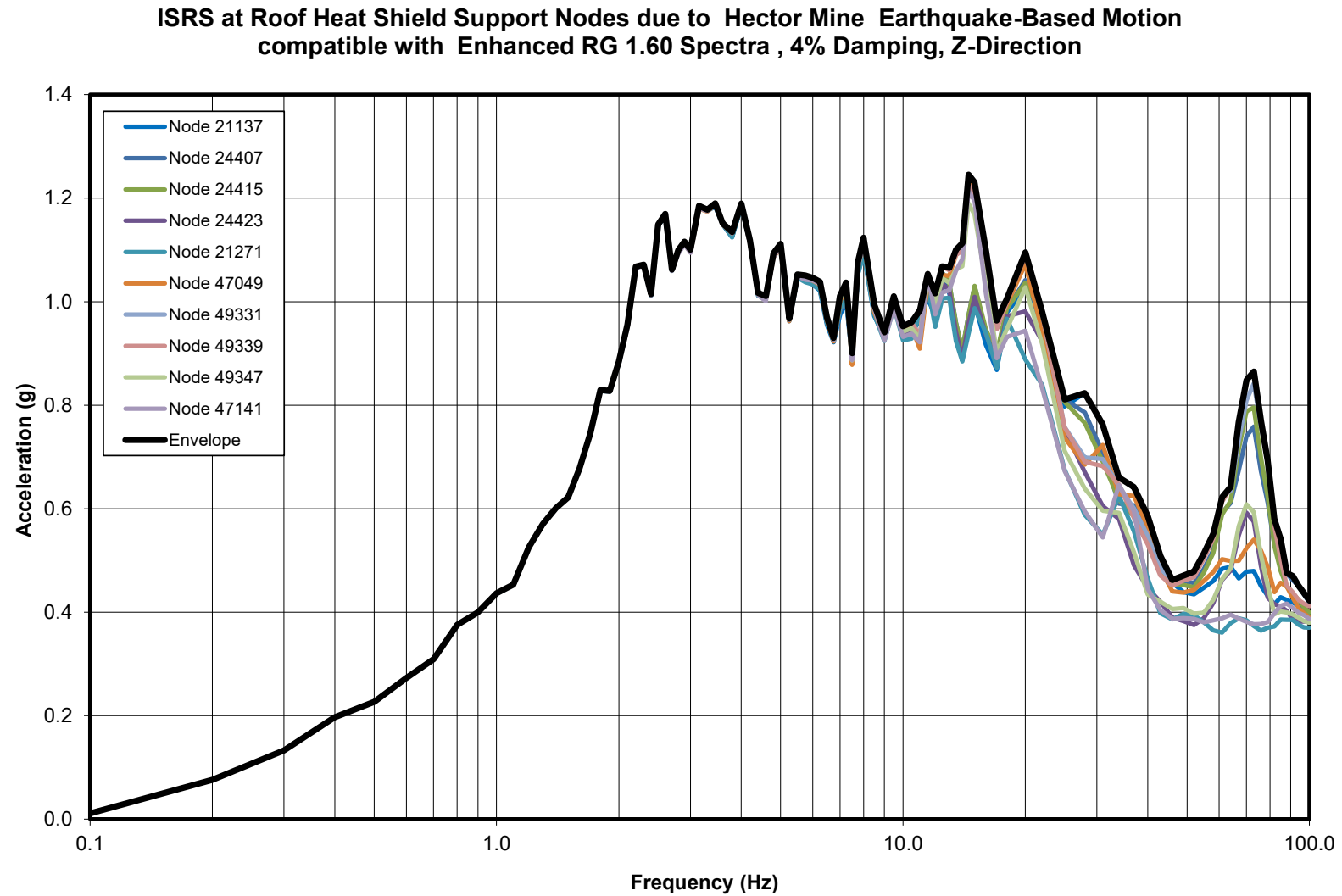


Figure 3.9.4-21
ISRS at Roof Heat Shield Support Nodes due to Hector Mine Earthquake-Based Motion compatible with Enhanced RG 1.60 Spectra, 4% Damping, Z-Direction

APPENDIX 3.9.5
NUHOMS® EOS-TC BODY STRUCTURAL ANALYSIS

Table of Contents

3.9.5 NUHOMS® EOS-TC BODY STRUCTURAL ANALYSIS	3.9.5-1
3.9.5.1 General Information	3.9.5-1
3.9.5.2 EOS Transfer Cask Accident (Side and End) Drop Evaluation for 65g Static Load.....	3.9.5-1
3.9.5.3 Lead Gamma Shielding Slump Evaluation	3.9.5-2
3.9.5.4 EOS Transfer Cask Trunnions and Local Shell Stress Evaluation	3.9.5-3
3.9.5.5 EOS Transfer Cask Neutron Shield Shell Structural Evaluation	3.9.5-9
3.9.5.6 EOS Transfer Cask, Trunnion, and Neutron Shield Shell Fatigue Requirements.....	3.9.5-14
3.9.5.7 References	3.9.5-15

List of Tables

Table 3.9.5-1	EOS-TCMAX Stress Result Summary Table – 65g Side Drop	3.9.5-16
Table 3.9.5-2	EOS-TCMAX Stress Result Summary Table – 65g Top End Drop.....	3.9.5-17
Table 3.9.5-3	EOS-TCMAX Stress Result Summary Table – 65g Bottom End Drop	3.9.5-18
Table 3.9.5-4	Stress Result Summary Table for the Trunnions	3.9.5-19
Table 3.9.5-5	Acceptance Criteria for the Stress Evaluation	3.9.5-21
Table 3.9.5-6	Stress Result Summary for the Neutron Shield Panel model	3.9.5-22
Table 3.9.5-7	Weld Stress Result Summary for the Neutron Shield Panel model.....	3.9.5-23

List of Figures

Figure 3.9.5-1	3D Half Symmetric Finite Element Model for Drop Loads	3.9.5-24
Figure 3.9.5-2	Pressure Load and Boundary Condition Plots – 65g Side Drop	3.9.5-25
Figure 3.9.5-3	Pressure Load and Boundary Condition Plots – 65g End Drop.....	3.9.5-26
Figure 3.9.5-4	Stress Intensity (psi) plot for EOS-TCMAX – 65g Side Drop	3.9.5-27
Figure 3.9.5-5	Deformation plot (in.) for EOS-TCMAX (scaled up) – 65g Side Drop	3.9.5-27
Figure 3.9.5-6	Stress Intensity (psi) plot for EOS-TCMAX – 65g Top End Drop	3.9.5-28
Figure 3.9.5-7	Stress Intensity (psi) plot for EOS-TCMAX – 65g Top End Drop	3.9.5-28
Figure 3.9.5-8	Upper Trunnion Sectional View	3.9.5-29
Figure 3.9.5-9	Cut Section Finite Element Model of EOS-TCMAX (Top and Bottom)	3.9.5-30
Figure 3.9.5-10	Pressure Load and Boundary Condition Plots	3.9.5-31
Figure 3.9.5-11	Stress Intensity (psi) Plot for Load Case 3g.....	3.9.5-32
Figure 3.9.5-12	Stress Intensity (psi) Plot for Load Case Horizontal Transfer on Skid	3.9.5-33
Figure 3.9.5-13	EOS-TC108 Meshed Model	3.9.5-34
Figure 3.9.5-14	EOS-TC125 Meshed Model	3.9.5-35
Figure 3.9.5-15	EOS-TC108 Neutron Shield Panel Stress Intensity ($P_m + P_b$) Plot Load Case E1	3.9.5-36
Figure 3.9.5-16	EOS-TC108 I-Beam Stress Intensity ($P_m + P_b$) Plot Load Case E1	3.9.5-37
Figure 3.9.5-17	EOS-TC135 Neutron Shield Shell Stress Intensity Plot under Pressure Load (40 psig)	3.9.5-38
Figure 3.9.5-18	EOS-TC135 I-Beam Stress Intensity Plot under Pressure Load (40 psig).....	3.9.5-39
Figure 3.9.5-19	EOS-TC125 Temperature Distribution Plot	3.9.5-40
Figure 3.9.5-20	EOS-TC108 Temperature Distribution Plot	3.9.5-41
Figure 3.9.5-21	Bottom and Top, respectively, End Drops - Load 65g - Lead Slump Displacements.....	3.9.5-42

3.9.5 NUHOMS® EOS-TC BODY STRUCTURAL ANALYSIS

3.9.5.1 General Information

This appendix covers the structural evaluation of the transfer cask (TC) when carrying a loaded DSC. The TC structure is designed to American Society of Mechanical Engineers (ASME) NF-3200 [3.9.5-3] stress limits to the greatest degree practical. The trunnions and trunnion welds to the TC top ring are designed to American National Standards Institute (ANSI) N14.6 [3.9.5-2] stress limits for non-redundant lifting. Structural evaluation of the TC for the missile impact load cases is covered in Appendix 3.9.7, and not presented in this Appendix.

A geometric- and load-bounding representation, enveloping the three EOS-TCs (EOS-TC108, EOS-TC125 and EOS-TC135), is referred to as EOS-TCMAX in this evaluation. The geometric dimensions for this bounding model are selected to yield the most bounding stresses and deformations.

3.9.5.2 EOS Transfer Cask Accident (Side and End) Drop Evaluation for 65g Static Load

The purpose of this section is to summarize the structural evaluation of the EOS-TC for the postulated accident side and end drop conditions. The Service Level D drop evaluations are done by means of 3-D elastic-plastic model. Structural integrity of the design is evaluated by means of plastic analysis criteria of Reference [3.9.5-3].

3.9.5.2.1 Material Properties

Mechanical properties of cask components are evaluated at a temperature of 400 °F, except for the trunnions, which are evaluated at 367 °F. These temperatures exceed the maximum temperature of cask body for all cask designs. A bilinear stress-strain curve with a 5% tangent modulus is used for steel components. The lead material is modeled by bilinear kinematic hardening method. All the EOS-TC material properties are listed in Chapter 8.

3.9.5.2.2 Design Criteria

The EOS-TC is analyzed using ASME code, Section III, Appendix F requirements service level D allowable stresses for plastic analysis.

3.9.5.2.3 Methodology

ANSYS [3.9.5-4] is used for the evaluation of side and end drop loads. A static load of 65g is applied and a plastic evaluation is performed for the postulated accident drop loads and compared against the Level D stress allowables.

A 65g drop load is considered bounding for the cask design in the accident conditions. Combination of side and end drop are considered bounding for the corner drop, since the corner accidents decelerations are significantly below 65g magnitude.

3.9.5.2.3.1 Finite Element Model

A 3D half symmetric model is used to perform accident drop evaluations. ANSYS SOLID185 elements were used to model the EOS-TC components. ANSYS Surface to Surface contact CONTA173 were used to model the contacting surface. Top cover bolts were modeled using COMBIN39 spring elements. Welds are modeled by means of nodal couples in all three directions. The finite element model is shown in Figure 3.9.5-1.

3.9.5.2.3.2 Loads and Boundary Conditions

For the side drop evaluation the DSC weight is specified using a cosine distributed pressure load for an angle span of 90°. Symmetry boundary conditions are applied on the cut plane. On the impact side the EOS-TC structural shell is fixed for a small 15° arc in radial direction and over total length. The applied pressure load and the boundary conditions are shown in Figure 3.9.5-2.

For the end drop evaluation the DSC weight is uniformly distributed on the lid/inner bottom end plate. Symmetry boundary conditions are applied on the cut plane. The cask is supported at the impacting surface for the top and bottom end drop. The applied pressure load and the boundary conditions are shown in Figure 3.9.5-3.

3.9.5.2.3.3 Results

The maximum stress intensity and the deformation plots for the 65g side drop are shown in Figure 3.9.5-4 and Figure 3.9.5-5. As shown in Table 3.9.5-1, all stresses are within allowable limits for the side drop condition.

The maximum stress intensity for the 65g top and bottom end drop are shown in Figure 3.9.5-6 and Figure 3.9.5-7. As shown in Table 3.9.5-2 and Table 3.9.5-3, all stresses are within allowable limits for the both top and bottom end drop condition.

3.9.5.3 Lead Gamma Shielding Slump Evaluation

The extent of lead slump in the TC during a vertical/end drop scenario is presented exclusive of side drop results, as a side drop would induce only negligible amounts of slump in the lead shielding.

The lead material conforms to the ASTM B29 specification for standard commercial lead, except that the density is increased from the reference 0.41 lb/in³ to 0.615 lb/in³ in order to conservatively bound the largest weight of shielding available.

The lead is assumed to fill the available cavity in the TC, such that any deformation of the inner shell will be carried into the lead shielding. The material is modeled with a multi-linear, kinematic hardening stress response to applied strains as detailed in Chapter 8.

The lead slump is modeled as subjected to a conservative 65g vertical load. This load induces a maximum slump of 2.2 inches in the vertical direction. The mesh for this vertical load is shown in Figure 3.9.5-3, while the displacements of the lead under top and bottom 65g accelerations are shown in Figure 3.9.5-21.

See Chapter 12 for the shielding evaluation of this slump.

3.9.5.4 EOS Transfer Cask Trunnions and Local Shell Stress Evaluation

The purpose of this section is to summarize the structural evaluation of the EOS-TC upper trunnions, the welds between the top/bottom rings and the upper/lower trunnions, respectively, and the shell stresses during lifting and handling operations for transfer conditions.

The EOS-TC is lifted by the two upper trunnions. Two lower pocket trunnions in the bottom ring of the cask form the rotational axis for the cask on the support skid during up-ending and down-ending of the cask. These lower pocket trunnions also provide support for the bottom end of the cask during transfer operations.

A geometric- and load-bounding representation, enveloping the three EOS-TCs (EOS-TC108, EOS-TC125 and EOS-TC135), is referred to as EOS-TCMAX in this evaluation. The geometric dimensions for this bounding model are selected to yield the most bounding stresses and deformations.

The evaluation is performed in the following steps:

- The upper trunnions, bottom ring and the welds between the trunnions and the shell are evaluated using hand calculations.
- The cask shell stresses are evaluated using ANSYS code [3.9.5-4].

3.9.5.4.1 Methodology and Acceptance Criteria

The conservatively bounding weights of the EOS-TC and DSC components employed for the analysis are as follows:

- Unloaded EOS-TC135 136,000 lb
- Loaded EOS-37PTH DSC 134,000 lb

- Total 270,000 lb

The upper trunnions and trunnion welds to the cask top ring are designed in accordance with the allowable stresses defined by ANSI N14.6 [3.9.5-2] for a non-redundant lifting device.

For the vertical configuration, the dead weight load includes the self-weight of the loaded EOS-TC with the bounding EOS-37PTH DSC payload full of water. This load considers the EOS-TC hanging vertically by the two upper trunnions. The weight of the DSC is applied as a uniform pressure on the bottom end plate of the EOS-TCMAX. A dynamic load factor (DLF) of 1.15 is used to include the effects of dynamic interactions.

During transfer of the EOS-TC on the trailer, the EOS-37PTH DSC will rest on the EOS-TC inner shell. The EOS-37PTH DSC weight is therefore applied as a pressure to the inner shell using a cosine shaped load amplitude variation. The EOS-TC will be in contact with the saddle, latch and the lower trunnion pockets; the lower trunnion pocket was modeled in ANSYS as vertically constrained nodes. Similarly, the semicircular half section of the upper trunnion is constrained in radial direction. See Figure 3.9.5-10 for a diagram showing the boundary conditions for various loading conditions.

During down-ending operations on the transfer trailer, the EOS-TC will rotate about the lower trunnion pockets, at which time, the contact between the lifting yoke and the upper trunnion will separate and the total load will be supported by the lower trunnion pockets.

For thermal stress analysis, temperature profiles and maximum component temperatures are based on the thermal analyses described in Chapter 4. Only two load cases are evaluated for thermal stress analysis, depending on the bounding cases, based on the maximum reported temperatures for normal and off-normal conditions. Displacement constraints are applied simply to prevent rigid body motion.

For all analyses except thermal analysis material properties are taken at a conservative temperature of 400 °F. For all analyses, except thermal analysis, material properties are taken at a conservative temperature of 400 °F for the entire cask, except for the trunnions, which are taken at a conservative 367 °F. The allowable stresses for the EOS-TC components are obtained from Chapter 3, Table 3-3 and is reproduced for the pertaining load cases in Table 3.9.5-4.

3.9.5.4.2 Trunnion and Weld Evaluation

The EOS-TC has two upper trunnions to lift the cask during the lifting and handling operations. The upper trunnions are welded to the cask through partial penetration groove welds with fillet covers.

The upper trunnions are single shoulder trunnions as shown in Figure 3.9.5-8. The upper trunnions are evaluated for its critical section, Section A-A shown in Figure 3.9.5-8, for the maximum total weight of the TC.

The maximum total weight is calculated as:

$$F_v = W_L \times \text{DLF} / N_{tr} = 155,250 \text{ lb}$$

Where,

F_v = Maximum lift weight

W_L = Total weight of the TC and DSC = 270,000 lb

DLF = Dynamic load factor = 1.15

N_{tr} = Number of trunnions = 2

The shear stress in Section A-A for 1g is:

$$\text{Shear Stress (ksi)} = F_v / S_{AA} = 3.29 \text{ ksi}$$

Where S_{AA} is the section area and the bending stress is:

$$\frac{M_{AA}}{I_{AA}} \times \frac{D_1}{2} = 6.59 \text{ ksi}$$

Where,

M_{AA} = Bending moment at Section A-A

I_{AA} = Moment of Inertia at Section A-A, and

D_1 = Trunnion diameter.

At a service load level of 1g the maximum stress intensity within the upper trunnion itself is 9.31ksi, leading to 6g and 10g stress intensities of 55.9 ksi and 93.1 ksi, respectively.

The upper trunnion is welded to the top ring via a 1.25 inch partial penetration groove weld with a 3/8 inch fillet cover. These welds are also evaluated per the ANSI 14.6 criteria. The direct shear load on the trunnion is considered to be resisted by contact/bearing due to the very tight tolerances to which the parts are machined.

Per Paragraph 4.2.1.1 of ANSI N14.6 [3.9.5-2], the combined shear stress and the maximum tensile stress are compared to the material yield and ultimate strengths considering safety factors of 6 and 10, respectively. Both the base metal and weld metal stresses are evaluated. Only the ultimate stress of the weld metal is considered. For the base metal, both yield and ultimate stress checks are performed.

The normal stress, f_n , and shear stress, f_v , components on each critical plane of the weld are calculated and then the combined maximum equivalent stress is calculated and compared to the bounding allowable stress for the trunnion base metal, weld metal, and top ring base metal. The maximum equivalent stress is calculated as:

$$f_{eqv} = \sqrt{(f_n)^2 + 3(f_v)^2}$$

The bending moment considered in the weld is calculated as the shear load, F_v times the moment arm of 2.62, which is the distance from the load application to the top ring:

$$M = F_v \times 2.62 = 155,250 \text{ lbs} \times 2.62 \text{ in} = 406,755 \text{ in} - \text{lbs}$$

Therefore, the bending load on the weld is

$$f_b = \frac{M}{I_{weld}} = \frac{406,755}{78.54} = 5,179 \text{ lb/in}$$

Where,

$$I_{weld} = \frac{\pi}{4}(D_2)^2 = 78.54 \text{ in}^2$$

The trunnion base metal shear stress, f_{vTBM} , is caused by the bending load of 5,179 lb/in calculated above. The base metal length is the depth of the J-groove, 1.25 inch, plus the 3/8 inch cover, for a total length of 1.625 inches.

$$f_{vTBM} = \frac{5,179 \text{ lb/in}}{1.625 \text{ in}} = 3,187 \text{ psi}$$

The maximum equivalent stress is, therefore:

$$f_{eqv,TBM} = \sqrt{3}f_{vTBM} = 5,520 \text{ psi}$$

The minimum throat distance through the weld metal is $\sqrt{1.25^2 + 0.375^2} = 1.305$ inches. The weld throat is inclined at an angle of $\tan^{-1} \frac{0.375}{1.25} = 16.7$ degrees. The stress on the minimum throat is a combination of tension and shear.

$$f_{v,weld} = \frac{5,179 \text{ lb/in}}{1.305 \text{ in}} \cos(16.7) = 3,801 \text{ psi}$$

$$f_{n,weld} = \frac{5,179 \text{ lb/in}}{1.305 \text{ in}} \sin(16.7) = 1,140 \text{ psi}$$

The weld metal maximum equivalent stress is:

$$f_{eqv,weld} = \sqrt{(f_{n,weld})^2 + 3(f_{v,weld})^2} = \sqrt{(1,140)^2 + 3(3,801)^2} = 6,682 \text{ psi}$$

The cask top ring base metal stress components are conservatively calculated considering a 45-degree weld bevel. The actual length of base metal for the J-groove geometry is larger. The length of the beveled edge is, therefore, taken as $1.414 \times 1.25 = 1.77$ inches. The top ring base metal shear stress is:

$$f_{vTRBM} = \frac{5,179 \frac{lb}{in}}{1.77 \text{ in}} \cos(45) = 2,069 \text{ psi}$$

The top ring base metal normal stress is:

$$f_{nTRBM} = \frac{5,179 \frac{lb}{in}}{1.77 \text{ in}} \times \sin(45) = 2,069 \text{ psi}$$

The base metal maximum equivalent stress is, therefore:

$$f_{eqv,TRBM} = \sqrt{(f_{nTRBM})^2 + 3(f_{vTRBM})^2} = \sqrt{2,069^2 + 3 \times 2,069^2} = 4,138 \text{ psi}$$

The allowable stresses for each of these stress components are as follows:

Trunnion base metal allowable stress:

$$F_{TBM} = \min\left(\frac{S_y}{6}, \frac{S_u}{10}\right) = \min\left(\frac{82.8}{6}, \frac{113.7}{10}\right) = \min(13.8, 11.4) = 11.4 \text{ ksi}$$

Top ring base metal allowable stress:

$$F_{TRBM} = \min\left(\frac{S_y}{6}, \frac{S_u}{10}\right) = \min\left(\frac{32.0}{6}, \frac{70.0}{10}\right) = \min(5.33, 7.0) = 5.33 \text{ ksi}$$

Weld metal allowable stress:

$$F_w = \min\left(\frac{S_y}{6}, \frac{S_u}{10}\right) = \min\left(NA, \frac{68.6}{10}\right) = 6.86 \text{ ksi}$$

The ultimate stress of the weld metal, ER308L, at 250 °F is 68.6 ksi to match the weaker of the two joined base metals. Using material properties at 250 °F is conservative as the maximum temperature at the weld zone between the top ring and trunnion is 225 °F.

The calculated stresses and comparisons to allowable values for the 1g critical lift (including a dynamic load factor of 1.15) are summarized in Table 3.9.5-4.

The lower trunnion pockets provided in the bottom ring support the EOS-TC during the various handling and transfer operations. The bearing stress in the bottom ring is analyzed for a bounding load of (1g vertical + 1g horizontal + 1g transverse + 1g dead weight). The maximum bearing stress between the bottom trunnions and the bottom ring is 10.8 ksi.

3.9.5.4.3 Shell Evaluation

A single 3D FEM is prepared for the bounding dimensions of the EOS-TCs, which accounts for the minimum thickness, longest length and bounding DSC weight. The following components were modeled with SOLID185 elements:

- Top ring
- Bottom ring
- Inner shell
- Outer shell
- Lead shielding
- Upper trunnions
- Bottom end plate
- Ram access penetration ring
- Top lid

The parts that are not modeled include the EOS-TC rails, bottom neutron shields, inner and outer neutron shield panel, bottom neutron shield plate, and the bottom cover plate, since these components will not significantly affect the evaluation.

Because all of the components of the EOS-TC are not modeled in the FEM, the densities of various components are modified in order to achieve the overall weight of the EOS-TC135. The total weight of the EOS-TCMAX model is 136,000 lb, which is conservatively higher than the overall weight of the EOS-TC135.

The weld between the top trunnions and top ring is modeled by coupling the nodes in all degrees of freedom. The nodes between inner/outer shell with top/bottom rings are merged together as these locations are not in the high stress locations. Contact between components is created using CONTA173 and TARGE170 surface-to-surface contact elements.

The finite element model for the EOS-TCMAX is shown in Figure 3.9.5-9.

3.9.5.4.4 Results

The stress values in the upper trunnions, shell welds and top and bottom ring are below the allowable values. Table 3.9.5-4 summarizes the calculated stress, allowable stress, and safety margin for each item and load case.

There are two upper trunnion and two lower trunnion pockets on the transfer cask. The upper trunnions are used for lifting and are welded to the cask top ring. The maximum stress in the trunnion and the trunnion to cask top ring weld are evaluated in accordance with the allowables defined by ANSI N14.6.

The maximum stress intensity for the upper trunnion is 93.1 ksi with a margin of 0.22 (10g load). The maximum weld stress is 6.68 ksi with a margin of 0.03 (1g critical lift with 1.15 DLF). The maximum bearing stress for the lower trunnion pocket is 10.8 ksi with a margin of 1.97. The maximum shell stress in the top ring (3g test load) is 32.6 ksi with a margin of 0.31. The maximum stress intensity in the bottom ring (load case HBOT) is 56.3 ksi with a margin of 0.14. The stress contour plots for the 3g test load case and the horizontal transfer load case are shown in Figure 3.9.5-11 and Figure 3.9.5-12, respectively. Since all margins are above zero, the system is shown to be capable of withstanding the prescribed loads.

3.9.5.5 EOS Transfer Cask Neutron Shield Shell Structural Evaluation

The purpose of this section is to summarize the evaluation of the stresses in the neutron shield shell structure of the NUHOMS® EOS-TCs (EOS-TC108, EOS-TC125 and EOS-TC135) due to prescribed loads during fuel loading and transfer operations.

Neutron shield shell is evaluated for all the applied loads during fuel loading and transfer operations as summarized Chapter 2, Table 2-8, except the accident drop loads as the complete loss of neutron shield is assumed in calculating the maximum combined gamma and neutron dose rates. Due to the differences in designs, separate finite element models are setup for the EOS-TC108, EOS-TC125, and EOS-TC135. The evaluation is performed using ANSYS [3.9.5-4].

Material properties, where not explicitly stated, are conservatively taken at 300 °F from the tables in Chapter 8 and the resulting stresses in the neutron shield shell components are compared with the stress criteria listed in Chapter 3, Table 3-5.

3.9.5.5.1 EOS-TC108 Neutron Shield Shell

A 120° segment of the neutron shield shell assembly for EOS-TC108 is modeled. The FEMs are developed using the nominal dimensions per the drawings in Chapter 1, Section 1.3.

Components (neutron shield panel, upper/lower flanges and the I-beams) are modeled using ANSYS SHELL181 3-D shell elements. The elements have 6 degrees of freedom (3 translational and 3 rotational) at each of the four nodes. The interfaces between the mating surfaces are modeled using ANSYS CONTA173 and TARGE170 surface to surface contact elements that allow the transfer of loads. EOS-TC is not modeled explicitly in this model, it is assumed fixed and the interaction between the neutron shield shell inner panel and EOS-TC is simulated using ANSYS CONTA178 node to node contact elements. The interaction between the I-beam faces and the seam plates is simulated using RBE3 constrained equations and ANSYS CONTA175, and TARGE170 node-to-surface contact elements, wherein the RBE3 constrained equation is created between the nodes of the I-beam face to transfer all the forces to the center node onto a single node at the center of the I-beam face. This node is then used to create a node to surface contact between the seam plate surface.

The fillet welds for EOS-TC108 neutron shield assembly are simulated using couplings at the interface of neutron shield inner panel to I-beams and at interface of the neutron shield outer panel to I-beam welds. Welds at other locations are full penetration welds, thus nodes at these weld locations are merged in order to achieve the appropriate behavior.

The FEM for the EOS-TC108 neutron shield assembly is shown in Figure 3.9.5-13.

Horizontal Transfer / Seismic Loads

The horizontal transfer and seismic loads are enveloped by analyzing the neutron shield shell for an internal pressure load of 20 psig and (1g DW + 1g vertical + 1g lateral + 1g axial) accelerations.

Along with this load, the annulus of the neutron shield shell is also subjected to hydrostatic pressure load, which varies linearly with height with maximum at the bottom. Conservatively, a uniform internal pressure equal to the maximum hydrostatic pressure ($p = \rho g d_1 = 0.0361 \times 2.24 \times 90.25 = 7.30 \text{ psig}$) is added. Therefore, the equivalent uniform pressure of 27.5 psig is applied to the model.

This equivalent pressure is applied on the inner walls of the annulus created between the inner neutron shield panel and the outer neutron shield panel. It is also applied on the faces of the I-beams that are exposed to the water.

The neutron shield shell assembly will rest on the EOS-TC. Thus, in order to simulate the effect, ANSYS CONTA178 node-to- node contacts are created between the inner face of the inner panel and the EOS-TC. The EOS-TC surface is not modeled explicitly and the degrees of freedom of free nodes representing the outer surface of the EOS-TC are constrained in all translational directions (UX, UY and UZ).

Nodes at the cut face of 120° segment are constrained in the hoop (UY) direction.

Test Pressure

The EOS-TC108 neutron shield is analyzed in the vertical position and at the room temperature (70 °F) for the test pressure load case.

In addition to hydrostatic pressure due to the water in the neutron shield, an internal pressure of 25 psig (~125% of 20 psig pressure) is also applied for this analysis. The hydrostatic pressure will vary with the height, maximum pressure being at the bottom of the neutron shield shell. This pressure is applied as the triangular varying load. Therefore, the maximum equivalent pressure applied to the model is 31.14 psig.

This equivalent pressure is applied on the inner walls of the annulus between the inner neutron shield panel and the outer neutron shield panel. It is also applied on the faces of the I-beams that are exposed to water.

For pressure test, the neutron shield shell is in the vertical orientation and the nodes at the location of the leg supports are constrained in all directions.

The stresses due to this equivalent pressure in test pressure load are compared with the level B allowable at room temperature.

Vertical Lift

The vertical lift load includes a DLF of 1.15 for pressure load, so the equivalent pressure applied during vertical transfer is 27.06 psig.

This equivalent pressure is applied on the inner walls of the annulus between the inner neutron shield panel and the outer neutron shield panel. It is also applied on the faces of the I-beams that are exposed to the neutron shield.

Thermal Loads

For thermal stress analysis, two temperature distributions from the thermal evaluations documented in Chapter 4 are used. The first load case corresponds to the EOS-TC108 loaded with EOS-37PTH DSC, heat load of 41.8 kW, off-normal hot conditions, outdoor and horizontal position of the TC. The second load case corresponds to the EOS-TC108 loaded with the EOS-89BTH DSC, heat load of 34.44 kW, normal hot conditions, indoor and vertical position of the TC. The temperature distributions are shown in Figure 3.9.5-20.

3.9.5.5.2 EOS-TC125 and EOS-TC135 Neutron Shield Shells

The EOS-TC125 / EOS-TC135 neutron shield shell assembly is analyzed for postulated load conditions using a 3D 180° half-symmetric FEMs. The FEMs are developed using the nominal dimensions per the drawings in Chapter 1, Section 1.3.

All components (EOS-TC shells, neutron shield panel, neutron shield panel support ring plates, and the I-beams) are modeled using ANSYS SOLID185 3-D solid elements. The elements have 3 translational degrees of freedom at each of the eight nodes (no rotational degrees of freedom). The interfaces between the mating surfaces are modeled using ANSYS CONTA173 and TARGE170 surface-to-surface contact elements that allow the transfer of loads.

The welds at the interface of outer shell to I-beams and at the interface of neutron shield plate support ring plates to EOS-TC outer shell are modeled using couplings.

The nodes at slot welds between the I-beam and neutron shield panel are merged in order to achieve appropriate behavior. The weld between neutron shield panel and neutron shield panel support ring are full penetration welds. Thus, nodes at these weld locations are merged in order to achieve the appropriate behavior.

The FEM for the EOS-TC125 neutron shield assembly is shown in Figure 3.9.5-14. It is also representative of the EOS-TC135 neutron shield assembly FEM.

The resulting stresses in the neutron shield shell components are compared with the stress criteria listed in Chapter 3, Table 3-5.

Horizontal Transfer / Seismic Loads

The horizontal transfer and seismic loads are enveloped by analyzing the neutron shield shell for an internal pressure load of 25 psig and (2g vertical + 2g lateral + 2g axial) accelerations.

Along with this load the annulus of the neutron shield shell is also subjected to hydrostatic pressure load which varies linearly with height with maximum at the bottom. Conservatively, a uniform internal pressure equal to the maximum hydrostatic pressure is added. Therefore the equivalent pressure of 40 psig is applied to the model.

This equivalent pressure is applied in the annulus of the neutron shield shell. It is also applied on the faces of the I-Beams which are exposed to the water.

During the horizontal transfer, the EOS-TC is supported by the trunnions and saddle. Therefore, in order to simulate the effect, degree of freedom of nodes at the trunnion locations on the outer surface of the EOS-TC are constrained in axial (upper trunnions) direction and in radial (lower trunnion pockets) direction.

Symmetric boundary conditions are applied at the cut face of the model.

Test Pressure and Vertical Lift

The neutron shield is analyzed in the vertical position and at the room temperature (70 °F) for the test pressure load case.

In addition to hydrostatic pressure due to the water in the neutron shield, an internal pressure of 32 psig (~125% of 25 psig pressure) is also applied for this analysis. The hydrostatic pressure will vary with the height, maximum pressure being at the bottom of the neutron shield shell. The maximum equivalent pressure at the bottom of the cask is calculated to be 38.78 psig. The test pressure load case is enveloped by the horizontal transfer / seismic load case and therefore is not evaluated separately.

Similarly, the maximum pressure during the vertical lift is calculated to be 32.79 psig, which is also enveloped by the horizontal transfer / seismic load case and not evaluated separately.

Thermal Loads

For thermal stress analysis, two temperature distributions from the thermal evaluations documented in Chapter 4 are used. The first load case corresponds to the EOS-TC125 loaded with EOS-37PTH DSC, heat load of 50 kW, off-normal hot conditions, outdoor and horizontal position of the TC. The second load case corresponds to the EOS-TC125 loaded with the EOS-37PTH DSC, heat load of 36.35 kW, normal hot conditions, indoor and vertical position of the TC. The temperature distributions are shown in Figure 3.9.5-19.

3.9.5.5.3 Results

The stress results for the neutron shield shells are summarized in Table 3.9.5-6 and Table 3.9.5-7. The stress contour plots of the EOS-TC108 neutron shield shell for the horizontal transfer/seismic load case are shown in Figure 3.9.5-15 and Figure 3.9.5-16. Also the stress contour plots of the EOS-TC135 neutron shield shell for the horizontal transfer / seismic load case are shown in Figure 3.9.5-17 and Figure 3.9.5-18.

3.9.5.6 EOS Transfer Cask, Trunnion, and Neutron Shield Shell Fatigue Requirements

The transfer cask (TC) and trunnion are designed in accordance with the applicable guidelines of the ASME Code, Section III, Division 1, and Subsection NF for Class 1 vessels, except for the neutron shield tank, which is designed to ASME Code, Section III, Division 1, and Subsection ND. Neither one of these subsections require a fatigue evaluation for low cycle loads. Therefore, the fatigue evaluation is not required for the EOS-TC per ASME code criteria.

3.9.5.7 References

- 3.9.5-1 Blodgett, O.W., “Design of Welded Structure,” published by James F. Lincoln Arc Welding Foundation, June 1966.
- 3.9.5-2 ANSI N14.6, “Special Lifting Devices for Shipping Containers Weighing 10,000 Pounds or more,” 1993.
- 3.9.5-3 American Society of Mechanical Engineers, “ASME Boiler and Pressure Vessel Code, 2010 Edition with 2011 Addenda.
- 3.9.5-4 ANSYS Computer Code and User’s Manual, Version 14.0.

Table 3.9.5-1
EOS-TCMAX Stress Result Summary Table – 65g Side Drop

STRESS CLASSIFICATION- SERVICE LEVEL D – SUMMARY TABLE				
EOS-TC Components	Stress Category	Maximum Stress (ksi)	Allowable Stress (ksi)	Max. Stress Ratio
Outer Shell	P _M	44.14	49.0	0.90
	P _L +P _B	54.72	63.0	0.87
Inner Shell	P _M	45.43	49.0	0.93
	P _L +P _B	50.41	63.0	0.80
Top Cover Plate	P _M	41.58	49.0	0.85
	P _L +P _B	55.78	63.0	0.89
Top Ring	P _M	43.45	49.0	0.89
	P _L +P _B	59.93	63.0	0.95
Bottom Ring	P _M	42.24	49.0	0.86
	P _L +P _B	53.70	63.0	0.85
Bottom End Plate	P _M	47.04	49.0	0.96
	P _L +P _B	50.49	63.0	0.80
RAM Access	P _M	39.41	49.0	0.80
	P _L +P _B	49.40	63.0	0.78
Bottom Neutron	P _M	46.21	49.0	0.94
	P _L +P _B	46.67	63.0	0.74

Table 3.9.5-2
EOS-TCMAX Stress Result Summary Table – 65g Top End Drop

#	Component	Max Stress (ksi) /Stress Ratio			Allowable (ksi)		
		PM	PL	PM+PB	PM	PL	PM+PB
1	Outer Shell	24.4 49.7%	36.3 57.6%	36.3 57.6%	49.0	63.0	63.0
2	Inner Shell	25.7 52.4%	37.9 60.1%	37.9 60.1%	49.0	63.0	63.0
3	Top Cover Plate	12.4 25.2%	18.8 29.8%	18.8 29.8%	49.0	63.0	63.0
4	Top Ring	13.0 26.6%	17.8 28.3%	17.8 28.3%	49.0	63.0	63.0
5	Bottom Ring	3.4 7.0%	6.2 9.9%	6.2 9.9%	49.0	63.0	63.0
6	Bottom End Plate	6.1 12.4%	11.8 18.8%	11.8 18.8%	49.0	63.0	63.0
7	RAM Access Penetration Ring	4.8 9.8%	6.4 10.2%	6.4 10.2%	49.0	63.0	63.0
8	Bottom Neutron Shield Pane	3.8 7.8%	7.0 11.1%	7.0 11.1%	49.0	63.0	63.0

Table 3.9.5-3
EOS-TCMAX Stress Result Summary Table – 65g Bottom End Drop

#	Component	Max Stress (ksi) / Stress Ratio			Allowable (ksi)		
		PM	PL	PM+PB	PM	PL	PM+PB
1	Outer Shell	25.1 51.3%	39.3 62.4%	39.3 62.4%	49.0	63.0	63.0
2	Inner Shell	18.1 37.0%	26.7 42.3%	26.7 42.3%	49.0	63.0	63.0
3	Top Cover Plate	4.1 8.5%	10.8 17.2%	10.8 17.2%	49.0	63.0	63.0
4	Top Ring	1.5 3.1%	2.6 4.1%	2.6 4.1%	49.0	63.0	63.0
5	Bottom Ring	22.5 45.8%	32.5 51.6%	32.5 51.6%	49.0	63.0	63.0
6	Bottom End Plate	16.4 33.5%	32.8 52.1%	32.8 52.1%	49.0	63.0	63.0
7	RAM Access Penetration Ring	25.4 51.8%	29.8 47.3%	29.8 47.3%	49.0	63.0	63.0
8	Bottom Neutron Shield Panel	10.2 20.8%	29.9 47.5%	29.9 47.5%	49.0	63.0	63.0

Table 3.9.5-4
Stress Result Summary Table for the Trunnions
(2 Pages)

Description	Calculated Stress (ksi)	Allowable Stress (ksi)	Margin
Manual Calculation for Upper Trunnions			
Stress intensity at A-A at 6g	55.86	82.80	0.48
Stress intensity at A-A at 10g	93.10	113.70	0.22
Manual Calculation for Weld Stresses and Lower Trunnion Pocket			
Trunnion Base Metal Max Equiv. Stress	5.52	11.40 ⁽¹⁾	1.07
Weld Metal Max Equiv. Stress	6.68	6.86 ⁽²⁾	0.03
Top Ring Base Metal Max Equiv. Stress	4.14	5.33 ⁽¹⁾	0.29
Load Case :3g (Test Load - Service level B)			
Top Ring Shell Stress (P_m)	16.58	28.46	0.72
Top Ring Shell Stress ($P_m + P_b$)	32.55	42.69	0.31
Bottom Ring Shell Stress (P_m)	10.44	28.46	1.73
Bottom Ring Shell Stress ($P_m + P_b$)	13.37	42.69	2.19
Load Case :DW Upper Trunnion (Service Level A) Vertical TC			
Top Ring Shell Stress (P_m)	6.75	21.40	2.17
Top Ring Shell Stress ($P_m + P_b$)	12.40	32.40	1.61
Top Ring Shell Stress ($P_m + P_b$) + Q	40.13	64.20	0.60
Bottom Ring Shell Stress (P_m)	3.76	21.40	4.69
Bottom Ring Shell Stress ($P_m + P_b$)	4.82	32.40	5.73
Bottom Ring Shell Stress ($P_m + P_b$) + Q	32.54	64.20	0.97
Load Case : DW Lower Trunnion (Service Level A) Vertical TC			
Top Ring Shell Stress (P_m)	1.36	21.40	14.72
Top Ring Shell Stress ($P_m + P_b$)	1.43	32.40	21.59
Top Ring Shell Stress ($P_m + P_b$) + Q	29.16	64.20	1.20
Bottom Ring Shell Stress (P_m)	11.52	21.40	0.86
Bottom Ring Shell Stress ($P_m + P_b$)	23.22	32.40	0.40
Bottom Ring Shell Stress ($P_m + P_b$) + Q	50.94	64.20	0.26
Load Case : Horizontal Transfer on Skid (1g axial) (Service Level B) Horizontal TC			
Top Ring Shell Stress (P_m)	7.39	28.46	2.85
Top Ring Shell Stress ($P_m + P_b$)	13.68	42.69	2.12
Top Ring Shell Stress ($P_m + P_b$) + Q	41.40	64.20	0.55
Bottom Ring Shell Stress (P_m)	17.47	28.46	0.63
Bottom Ring Shell Stress ($P_m + P_b$)	28.56	42.69	0.50

Table 3.9.5-4
Stress Result Summary Table for the Trunnions
 (2 Pages)

Description	Calculated Stress (ksi)	Allowable Stress (ksi)	Margin
Bottom Ring Shell Stress ($P_m + P_b$) + Q	56.28	64.20	0.14
Load Case : Horizontal Transfer on Skid (-1g axial) (Service Level B) Horizontal TC			
Top Ring Shell Stress (P_m)	5.25	28.46	4.42
Top Ring Shell Stress ($P_m + P_b$)	8.66	42.69	3.93
Top Ring Shell Stress ($P_m + P_b$) + Q	36.39	64.20	0.76
Bottom Ring Shell Stress (P_m)	16.12	28.46	0.77
Bottom Ring Shell Stress ($P_m + P_b$)	20.43	42.69	1.09
Bottom Ring Shell Stress ($P_m + P_b$) + Q	48.15	64.20	0.33

Notes:

(1) Lower of $S_y/6$ or $S_u/10$

(2) Equal to $S_u/10$

Table 3.9.5-5
Acceptance Criteria for the Stress Evaluation

Item	Stress Type	Service Levels A	Service Level B
Top Ring and Bottom Ring	Primary Membrane (P _m)	S _m	Same as Level A, increased by a factor of 1.33
	Primary Membrane + Bending (P _m + P _b)	1.5 S _m	
	Primary Membrane + Bending + Thermal Stress (Q)	3.0 S _m	
Upper Trunnions	Stress Intensity at 6g loads	S _y	
	Stress Intensity at 10g loads	S _u	
	Primary Membrane (P _m)	S _m	Same as Level A, increased by a factor of 1.33
	Primary Membrane + Bending (P _m + P _b)	1.5 S _m	
	Primary Membrane + Bending + Thermal Stress (Q)	3.0 S _m	
Welds	Maximum Equivalent Stress for Critical Lift (1g)	S _u /10 (Weld Metal and Base Metal)	
		S _y /6 (Base Metal)	
	Combined Weld Stress	min(0.3xS _u , 0.4xS _y)	Same as Level A, increased by a factor of 1.33
Bottom Ring	Bearing Stress	S _y	

Table 3.9.5-6
Stress Result Summary for the Neutron Shield Panel model

TC	Load Case ⁽¹⁾	Component	P _m (ksi)	Allowable (ksi)	Ratio	P _m +P _b (ksi)	Allowable (ksi)	Ratio	P _m +P _b +Q (ksi)	Allowable (ksi)	Ratio
125	E2	Neutron Shield Panel	10.92	20.00	0.55	25.57	30.00	0.85	37.69	48.00	0.79
125	E2	I-Beam	4.69	16.60	0.28	6.55	24.90	0.26	16.20	39.84	0.41
135	E2	Neutron Shield Panel	10.92	20.00	0.55	26.18	30.00	0.87	38.30	48.00	0.80
135	E2	I-Beam	5.06	16.60	0.30	6.96	24.90	0.28	16.60	39.84	0.42
108	A1	Neutron Shield Panel	5.18	5.50	0.94	6.77	8.25	0.82	11.40	13.20	0.86
108	A1	I-Beam	1.45	5.50	0.26	7.64	8.25	0.93	12.21	13.20	0.92
108	E1	Neutron Shield Panel	5.23	5.50	0.95	7.07	8.25	0.86	11.70	13.20	0.89
108	E1	I-Beam	1.56	5.50	0.28	8.18	8.25	0.99	12.75	13.20	0.97
108	B1	Neutron Shield Panel	5.86	6.60	0.89	7.80	9.90	0.79	12.43	14.40	0.86
108	B1	I-Beam	1.68	6.60	0.25	8.77	9.90	0.89	13.34	14.40	0.93

Note

- (1) The load cases are numbered per Chapter 2, Table 2-8, except E1 and E2 are the enveloping horizontal transfer/seismic load cases as described in the main body of the appendix

Table 3.9.5-7
Weld Stress Result Summary for the Neutron Shield Panel model

TC	Load Case ⁽¹⁾	Weld #	Stress (ksi)	Allowable	Ratio	S (ksi)
125	E2	Transfer Cask Outer Shell to I-Beam Fillet Weld	9.0	13.4	66.9%	20.0
125	E2	Neutron Shield Panel and I-Beam Slot Weld	4.9	13.4	36.7%	20.0
125	E2	Neutron Shield Panel Support and TC Outer Shell	7.9	13.4	58.8%	20.0
135	E2	Transfer Cask Outer Shell to I-Beam Fillet Weld	9.6	13.4	71.5%	20.0
135	E2	Neutron Shield Panel and I-Beam Slot Weld	4.9	13.4	36.7%	20.0
135	E2	Neutron Shield Panel Support and TC Outer Shell	9.3	13.4	68.9%	20.0
108	A1	Neutron Shield Panel Inner and I-Beam	0.8	3.0	26.6%	5.5
108	A1	Neutron Shield Panel Outer and I-Beam	1.3	3.0	44.2%	5.5
108	E1	Neutron Shield Panel Inner and I-Beam	0.9	3.0	29.9%	5.5
108	E1	Neutron Shield Panel Outer and I-Beam	1.4	3.0	47.3%	5.5
108	B1	Neutron Shield Panel Inner and I-Beam	0.9	3.7	25.5%	6.0
108	B1	Neutron Shield Panel Outer and I-Beam	1.5	3.7	41.9%	6.0

Note

- (1) The load cases are numbered per Chapter 2, Table 2-8, except E1 and E2 are the enveloping horizontal transfer/seismic load cases as described in the main body of the appendix

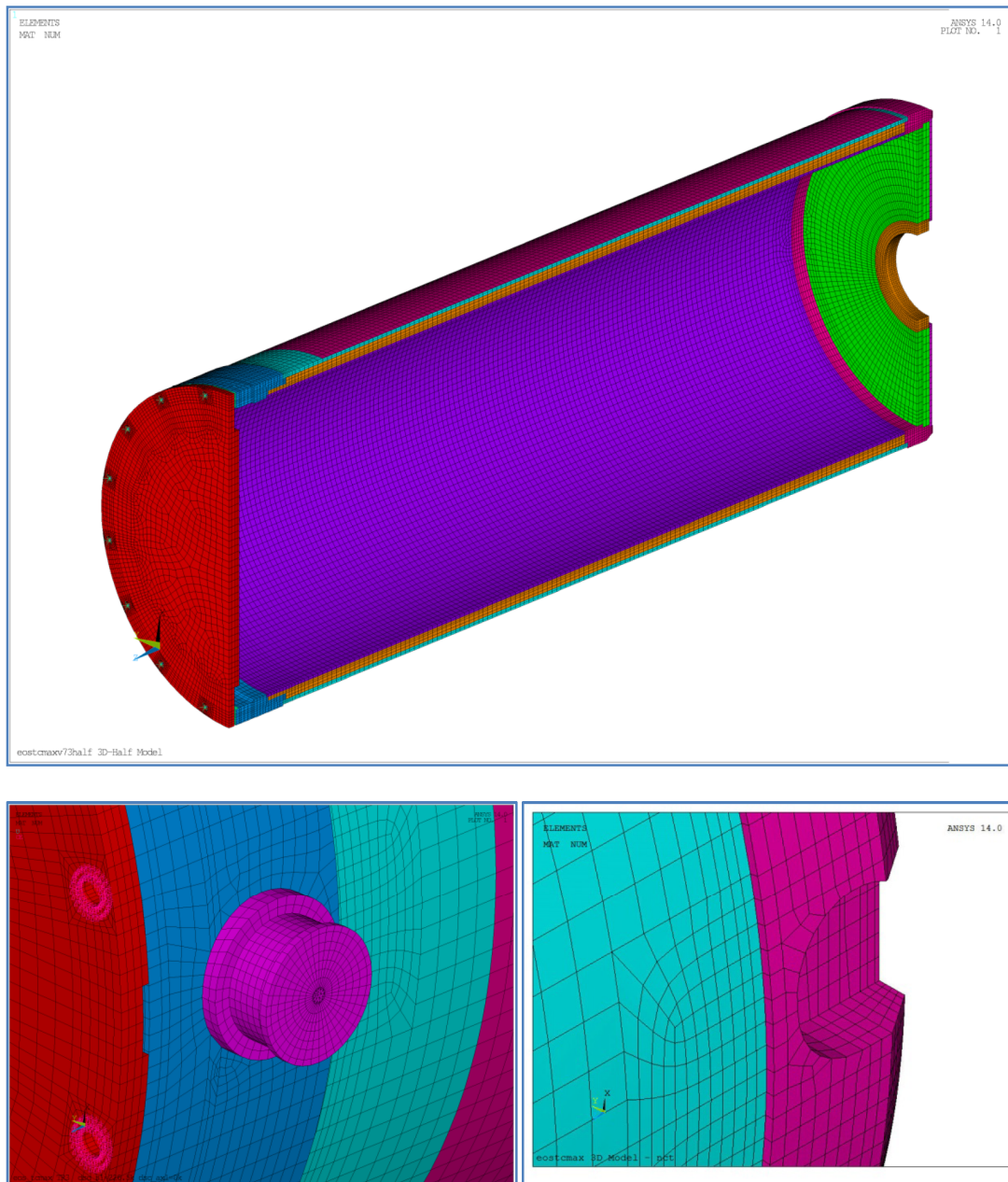


Figure 3.9.5-1
3D Half Symmetric Finite Element Model for Drop Loads

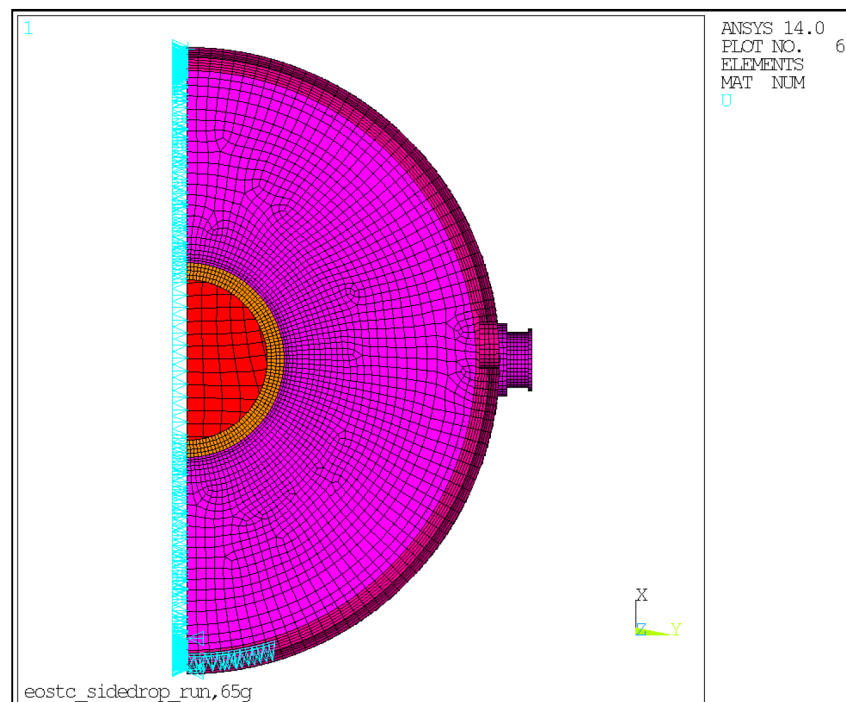
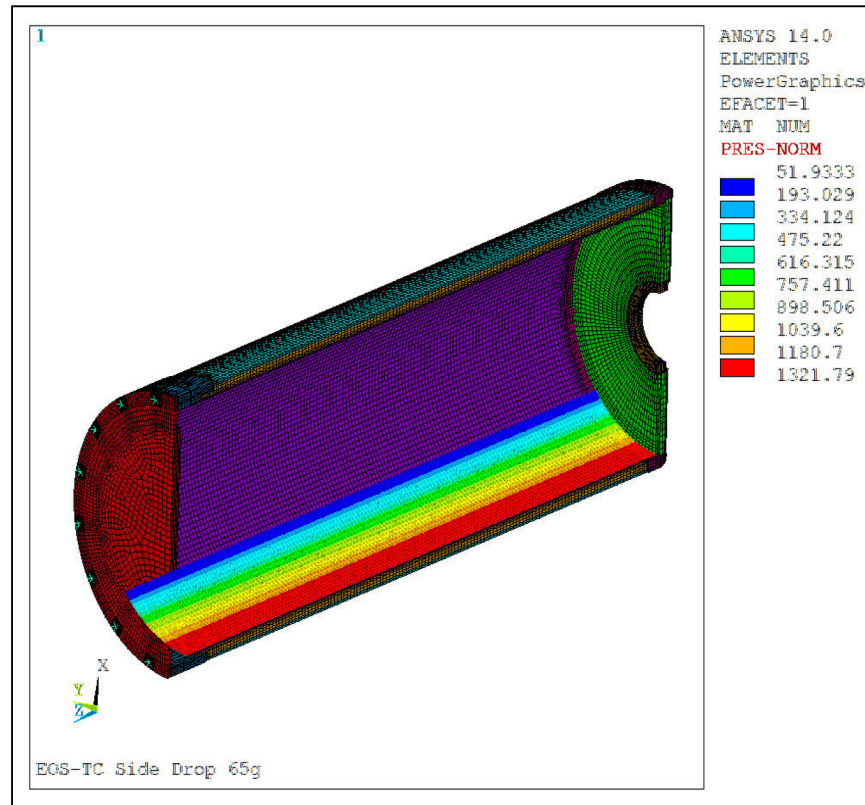


Figure 3.9.5-2
Pressure Load and Boundary Condition Plots – 65g Side Drop

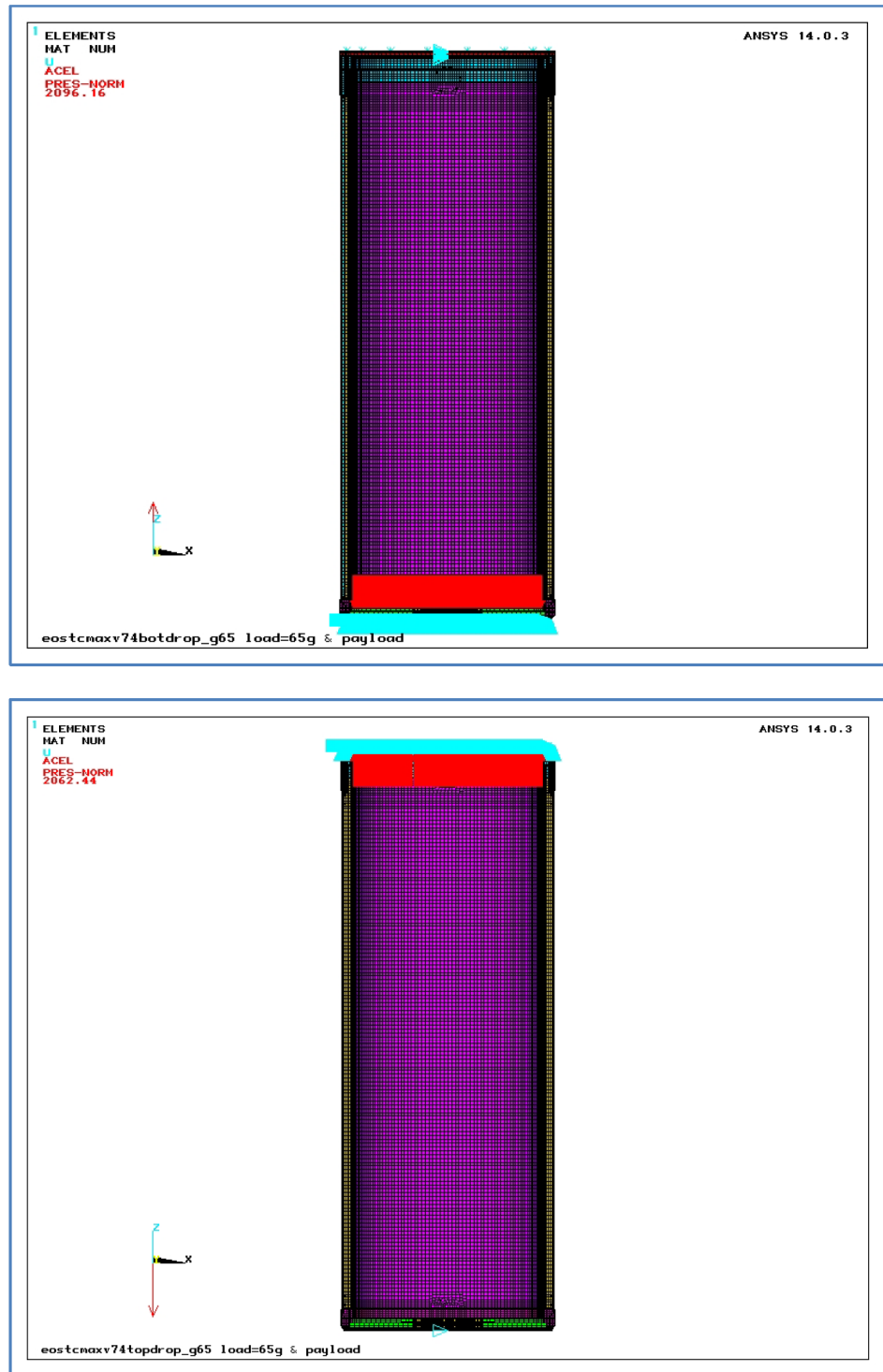


Figure 3.9.5-3
Pressure Load and Boundary Condition Plots – 65g End Drop

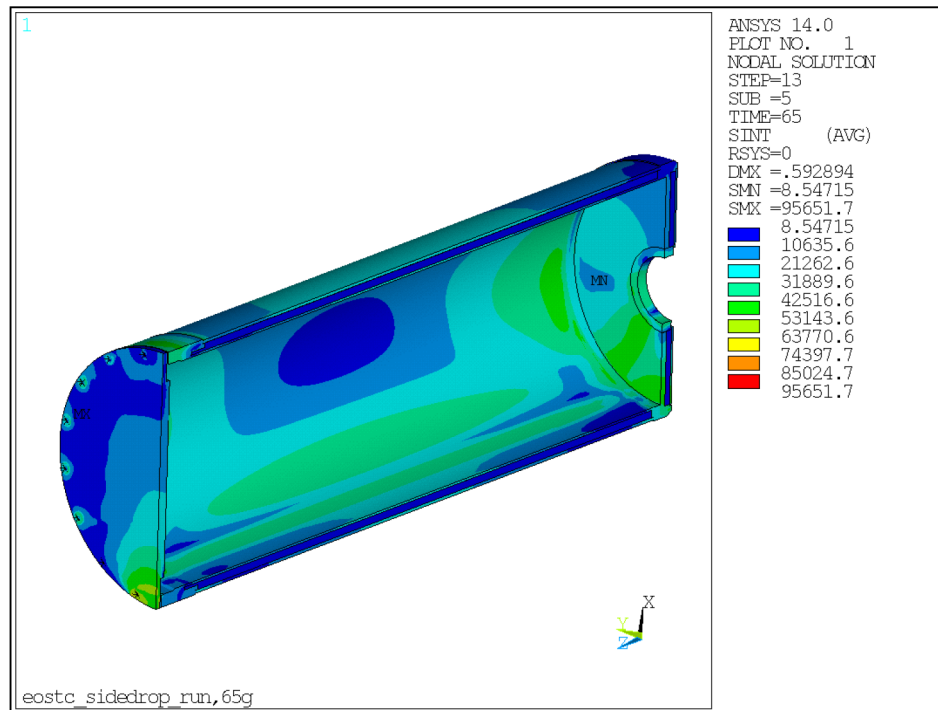


Figure 3.9.5-4
Stress Intensity (psi) plot for EOS-TCMAX – 65g Side Drop

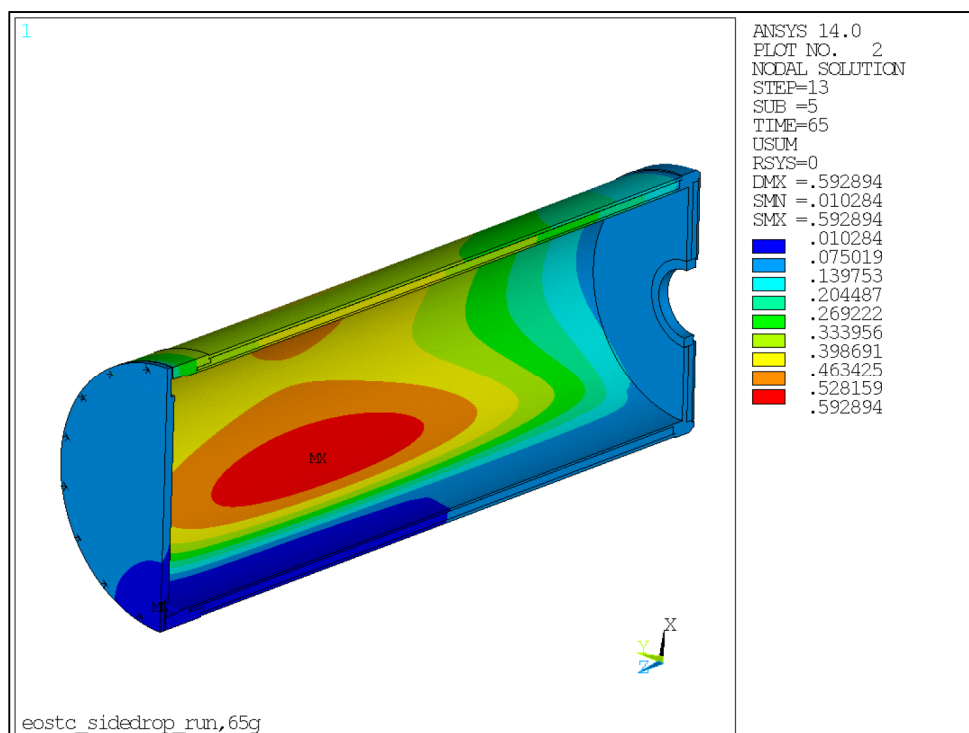


Figure 3.9.5-5
Deformation plot (in.) for EOS-TCMAX (scaled up) – 65g Side Drop

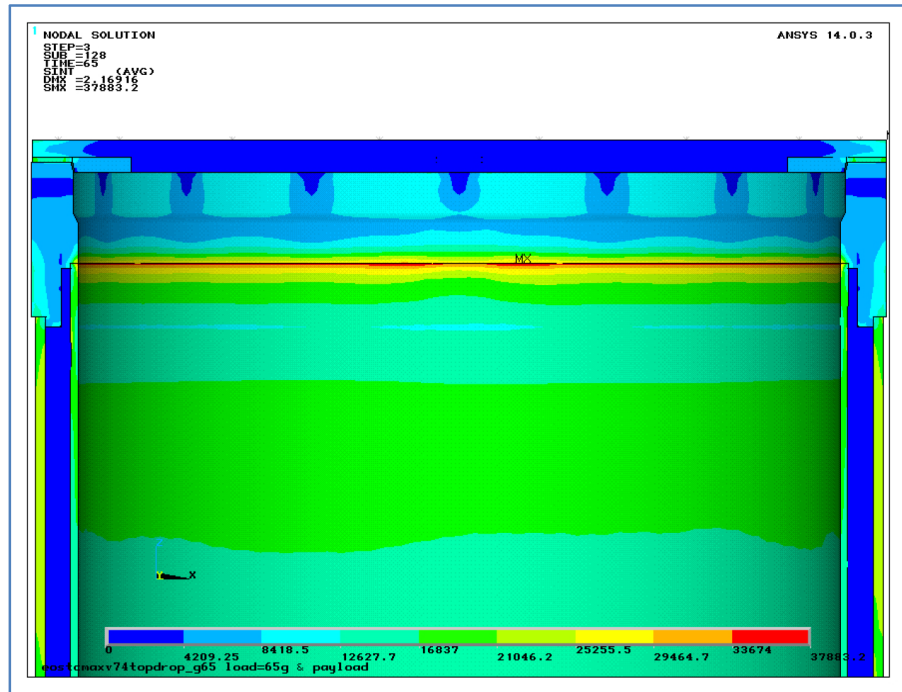


Figure 3.9.5-6
Stress Intensity (psi) plot for EOS-TCMAX – 65g Top End Drop

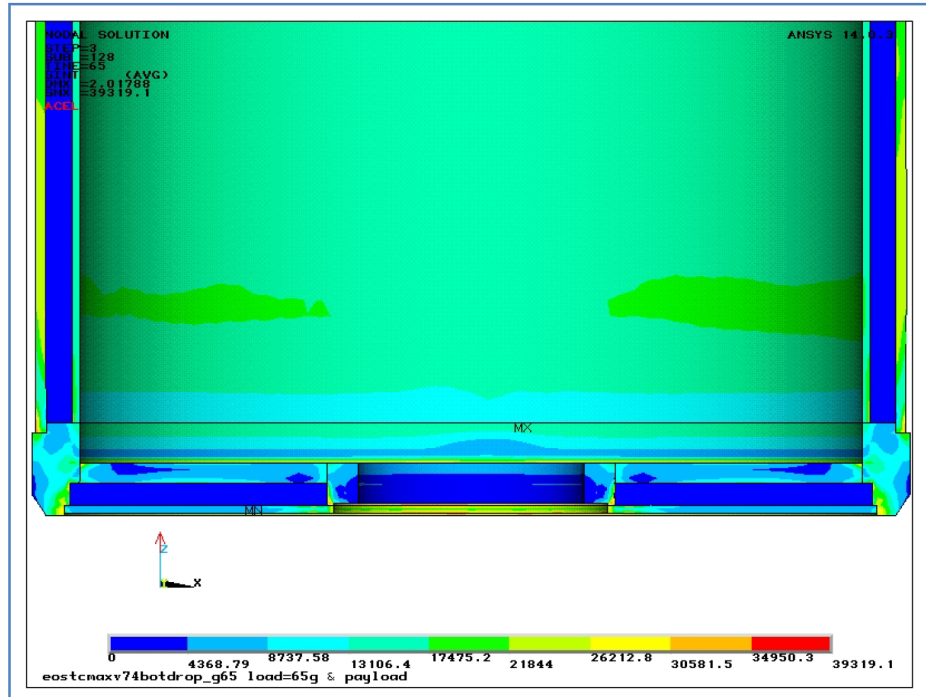


Figure 3.9.5-7
Stress Intensity (psi) plot for EOS-TCMAX – 65g Top End Drop

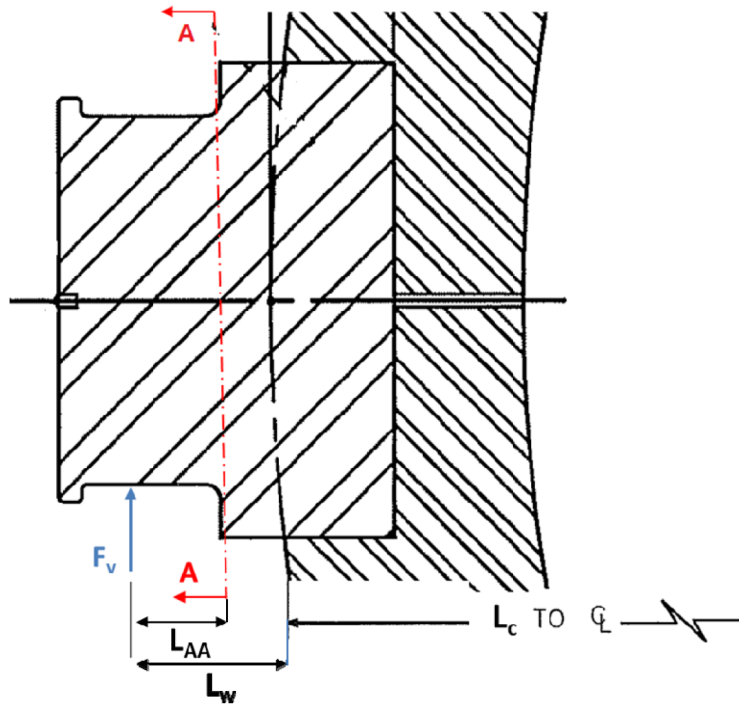


Figure 3.9.5-8
Upper Trunnion Sectional View

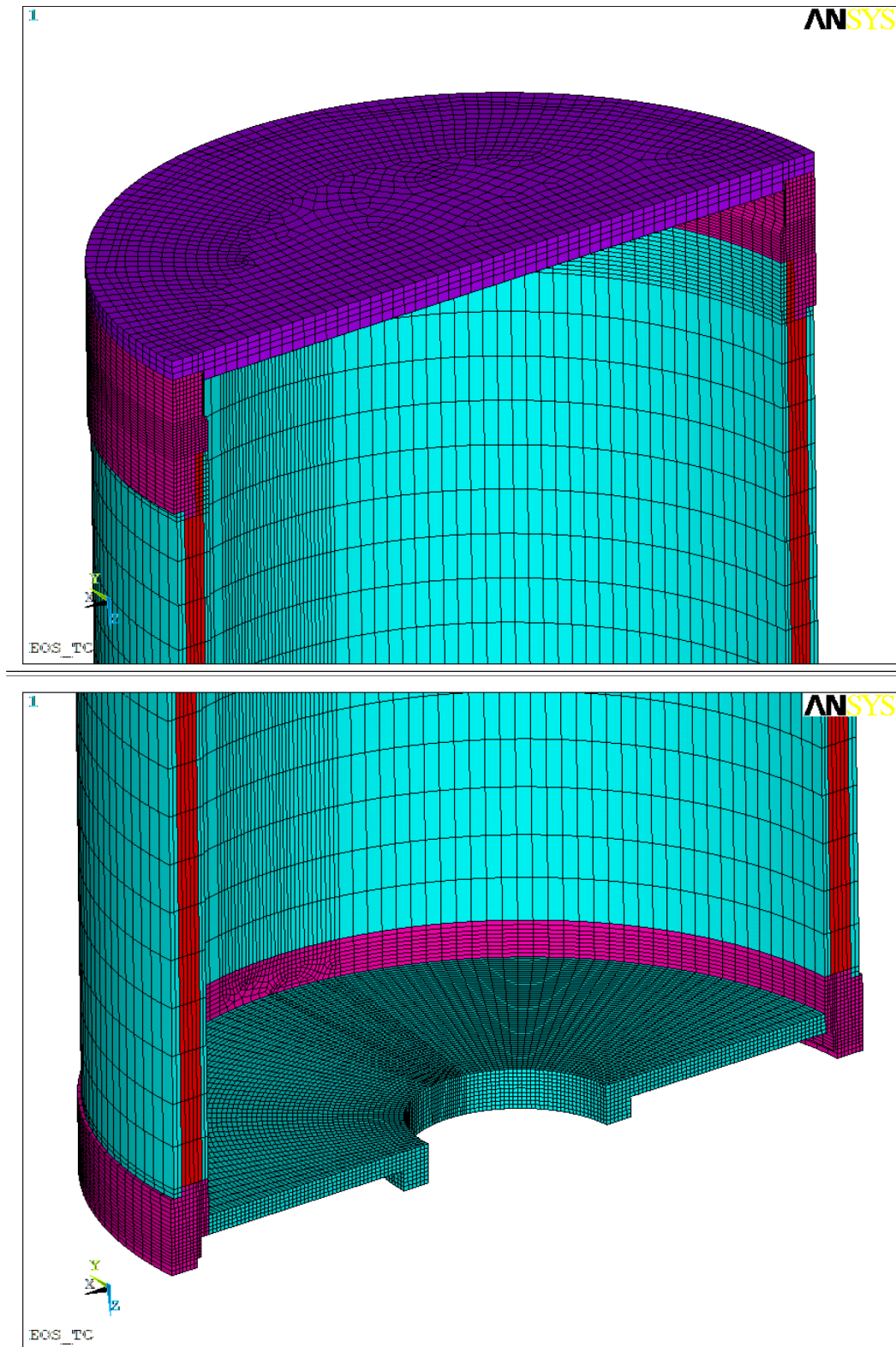


Figure 3.9.5-9
Cut Section Finite Element Model of EOS-TCMAX (Top and Bottom)

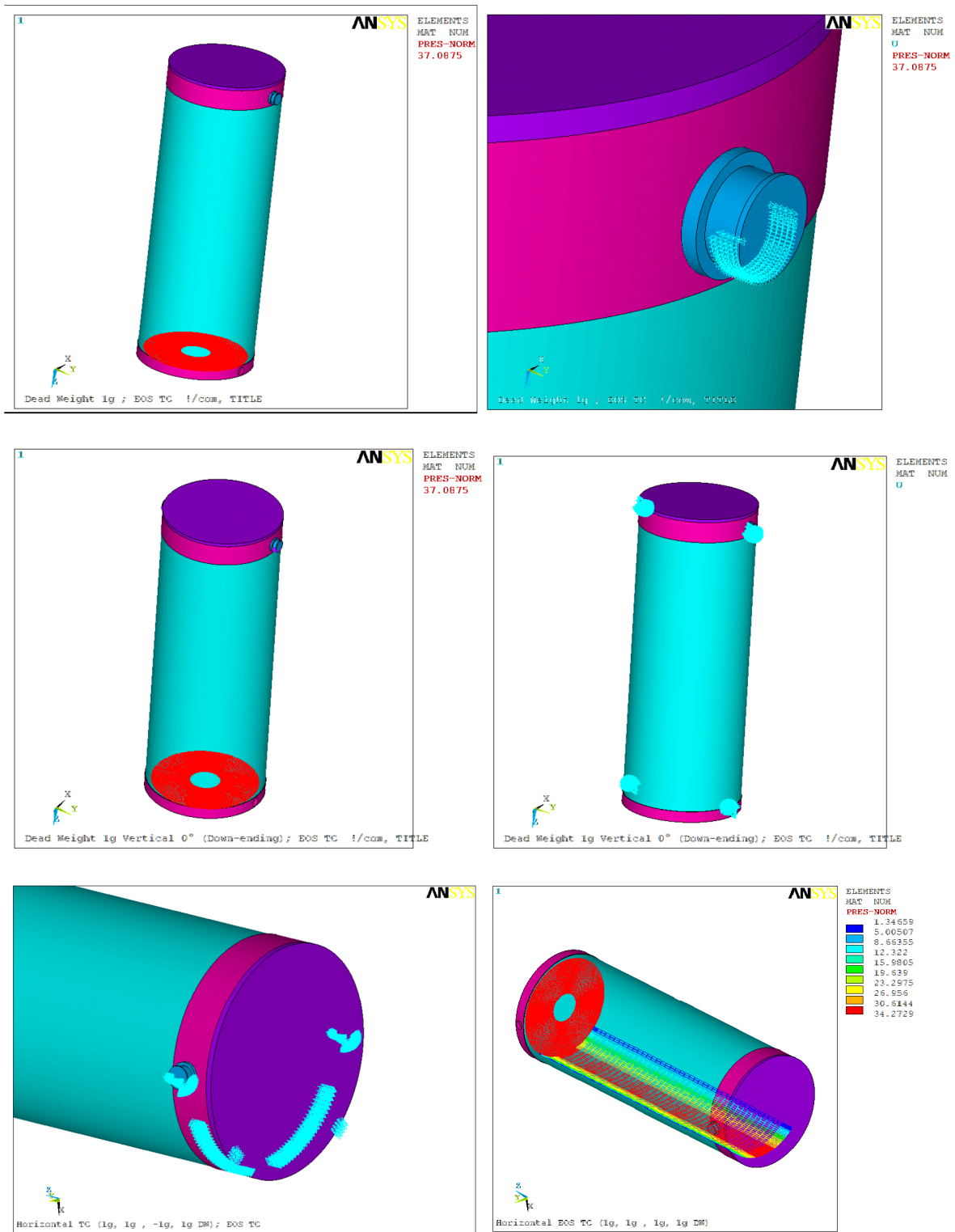


Figure 3.9.5-10
Pressure Load and Boundary Condition Plots

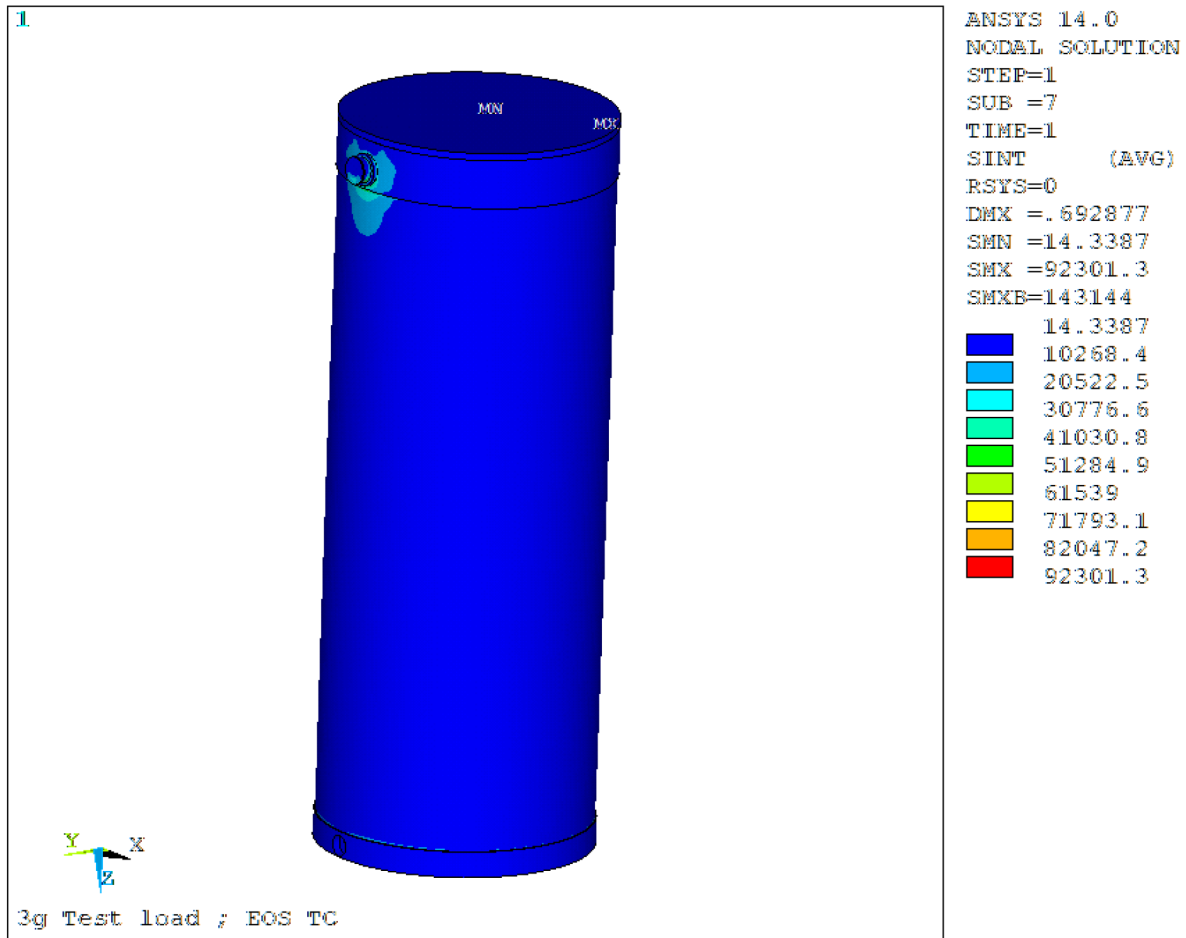


Figure 3.9.5-11
Stress Intensity (psi) Plot for Load Case 3g

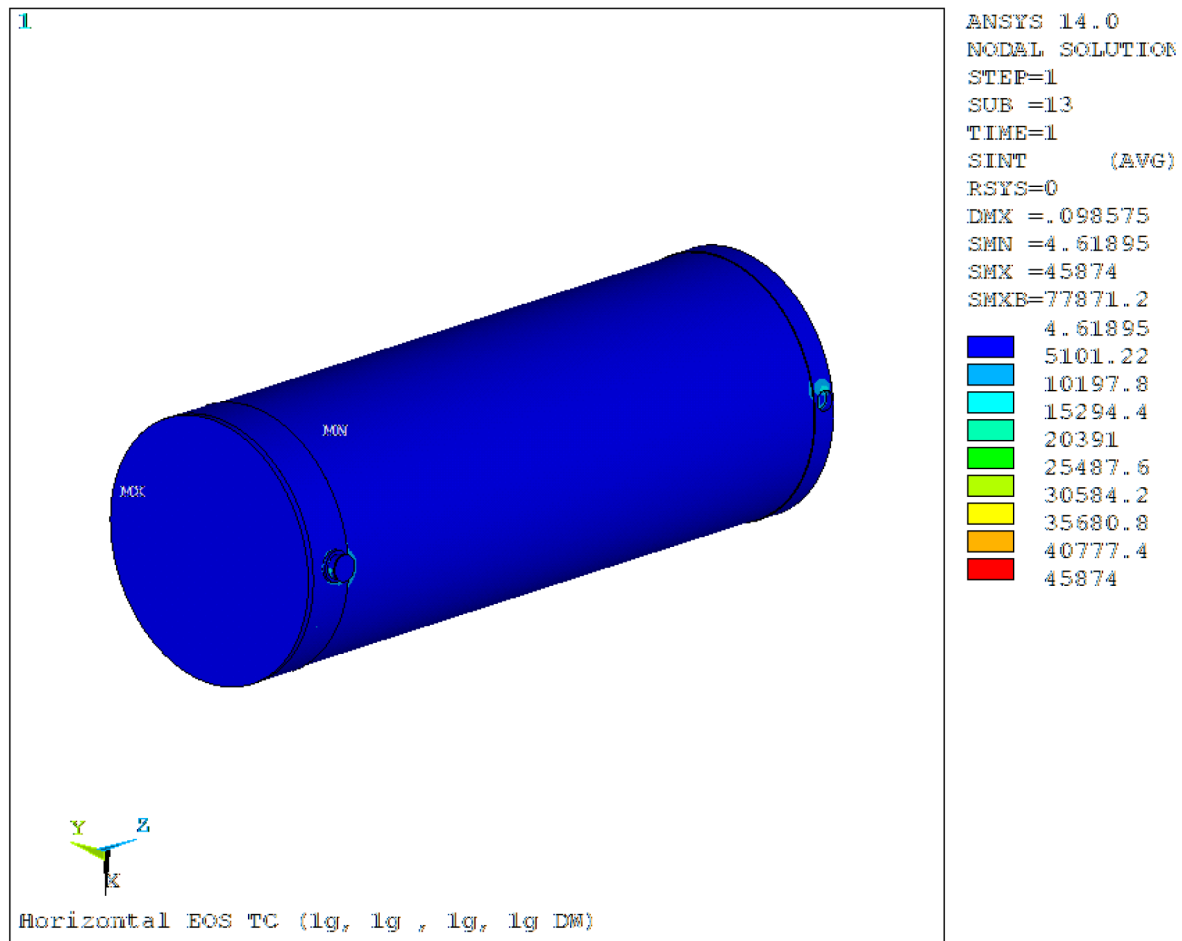


Figure 3.9.5-12
Stress Intensity (psi) Plot for Load Case Horizontal Transfer on Skid

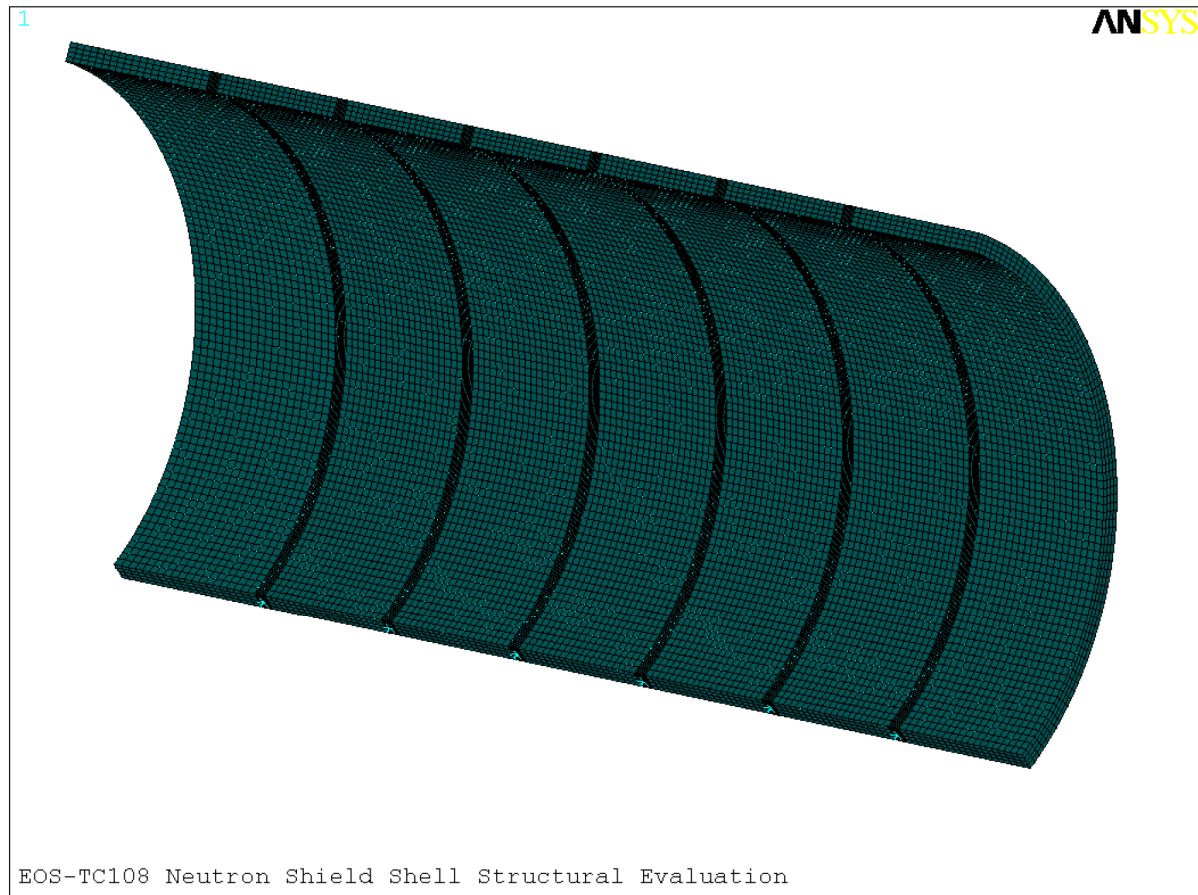


Figure 3.9.5-13
EOS-TC108 Meshed Model

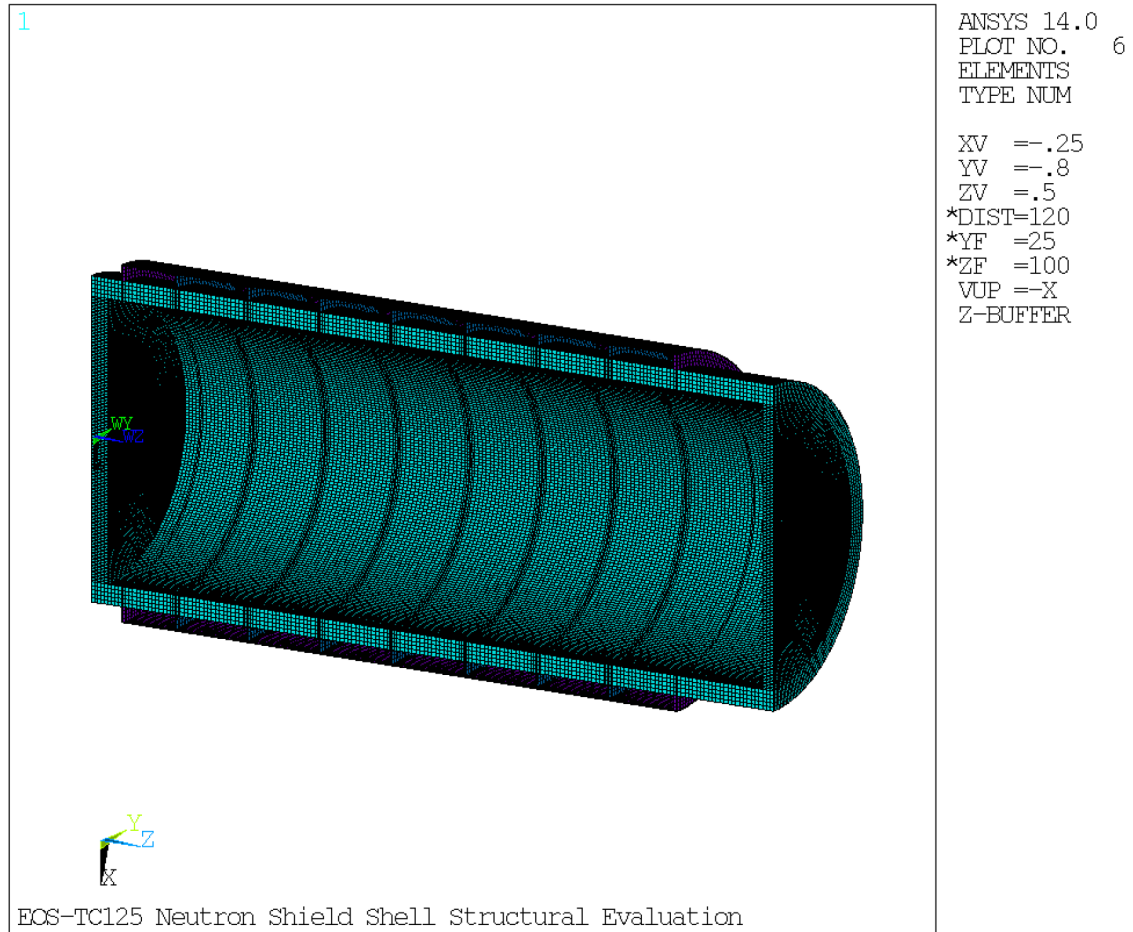


Figure 3.9.5-14
EOS-TC125 Meshed Model

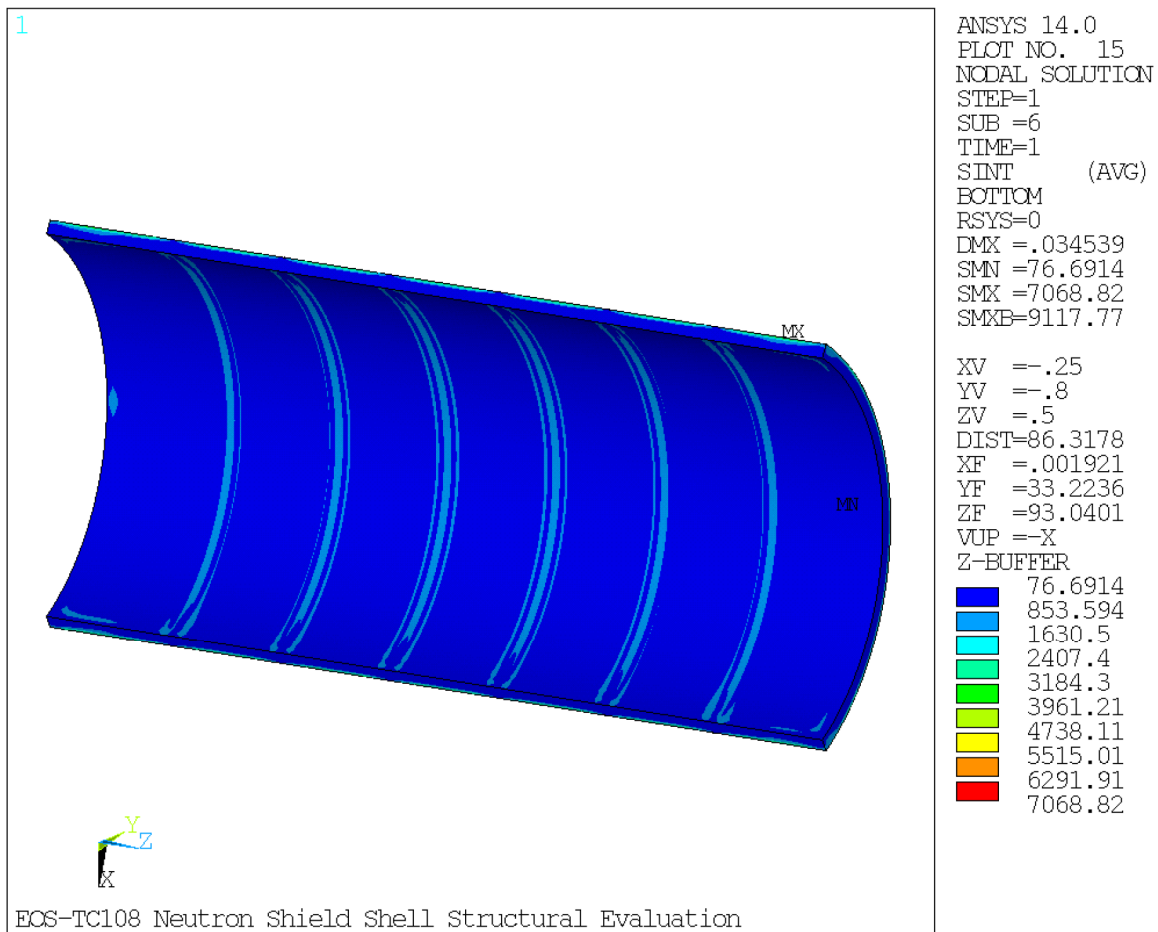


Figure 3.9.5-15
EOS-TC108 Neutron Shield Panel Stress Intensity (P_m+P_b) Plot Load Case E1

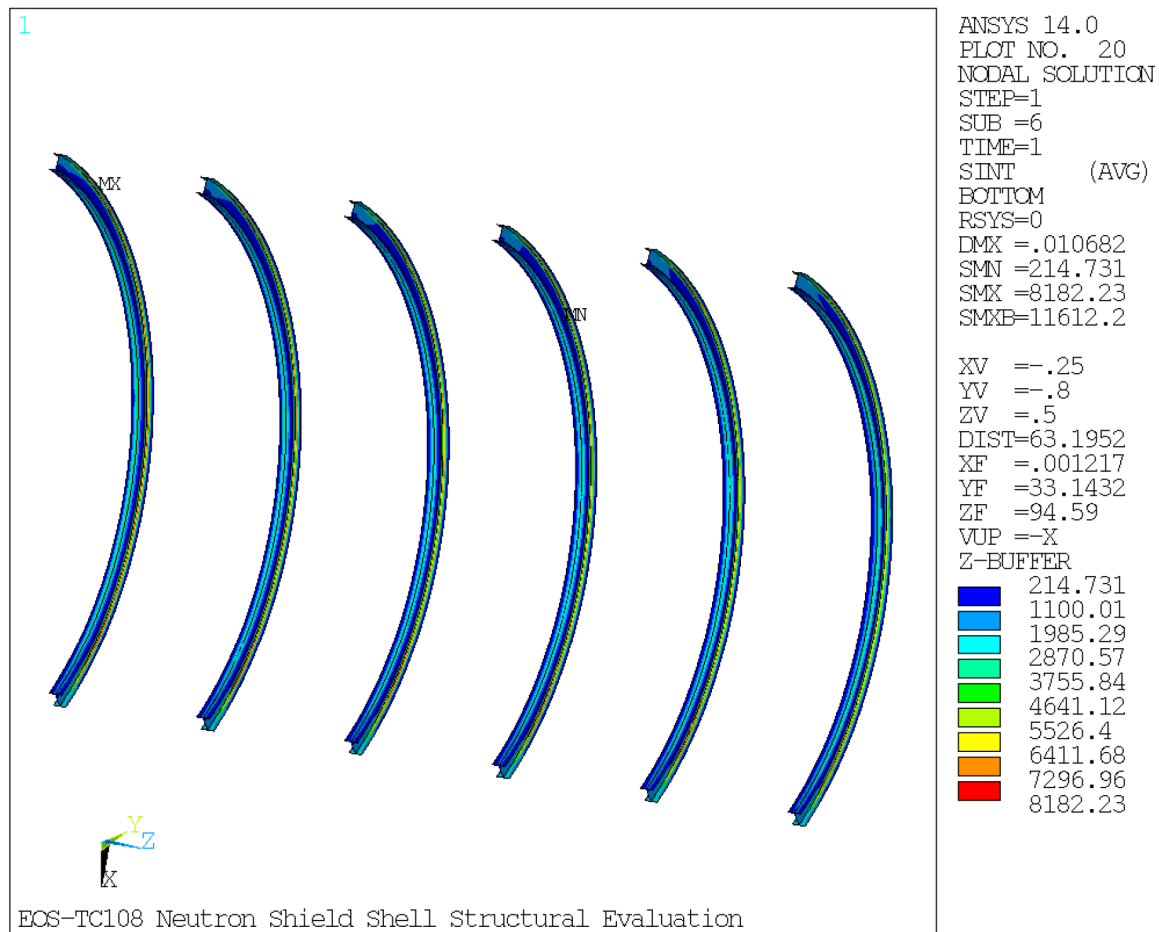


Figure 3.9.5-16
EOS-TC108 I-Beam Stress Intensity (P_m+P_b) Plot Load Case E1

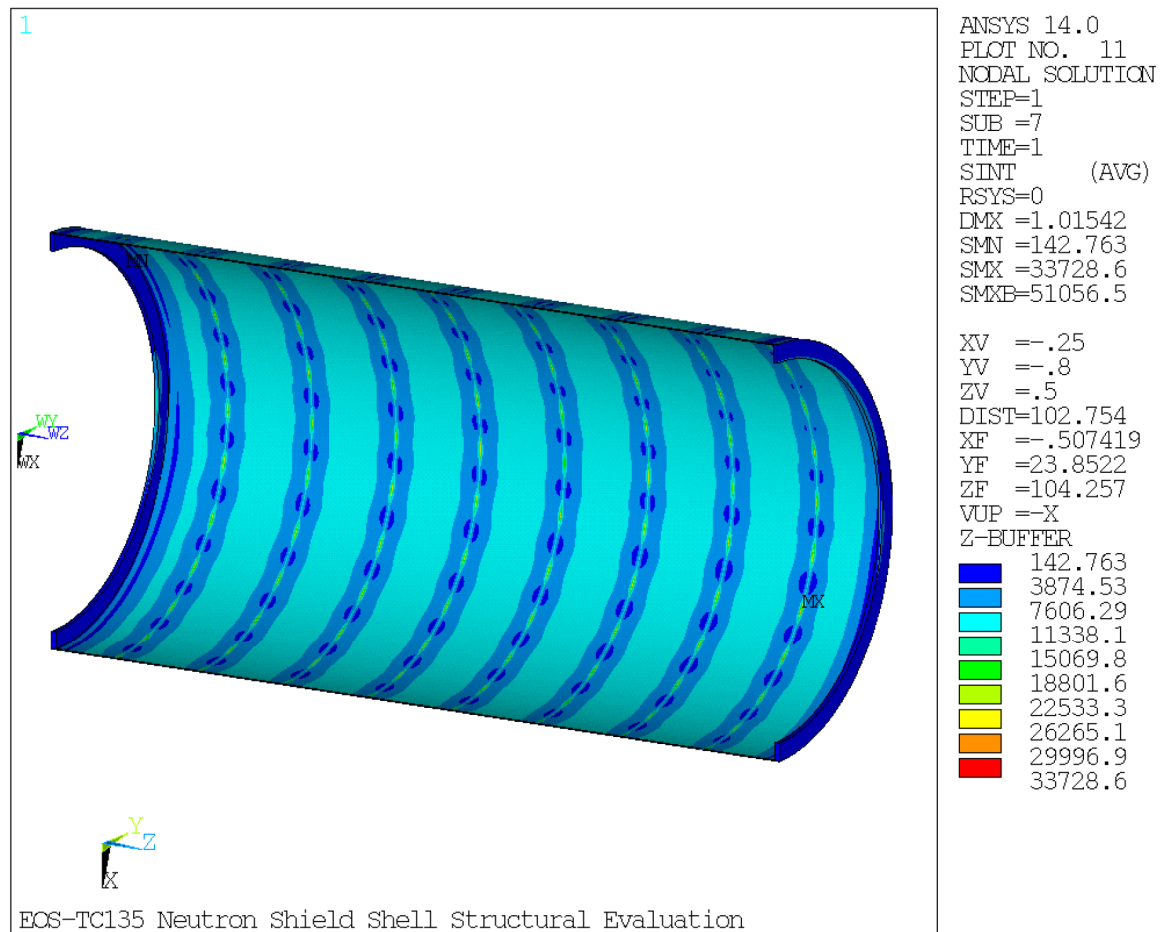


Figure 3.9.5-17
EOS-TC135 Neutron Shield Shell Stress Intensity Plot under Pressure Load
(40 psig)

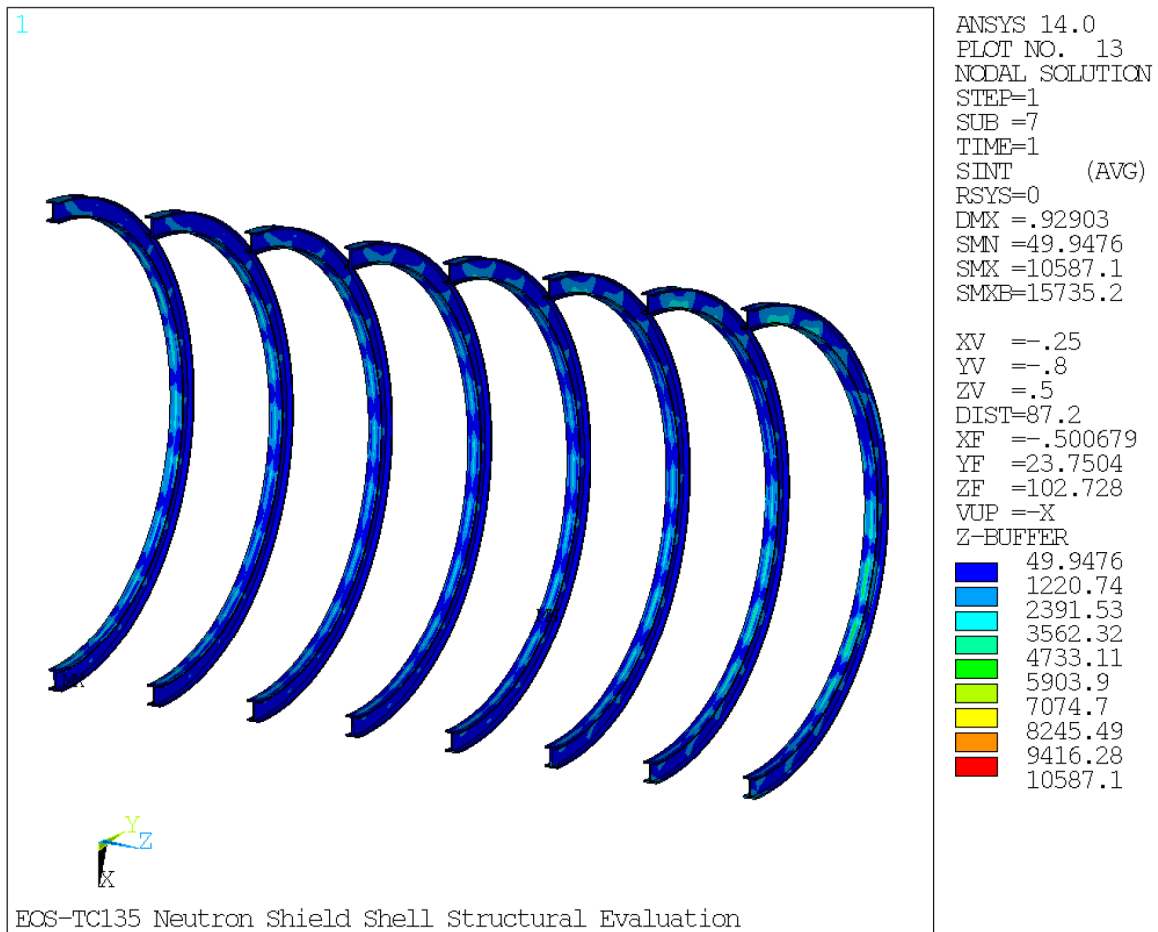


Figure 3.9.5-18
EOS-TC135 I-Beam Stress Intensity Plot under Pressure Load (40 psig)

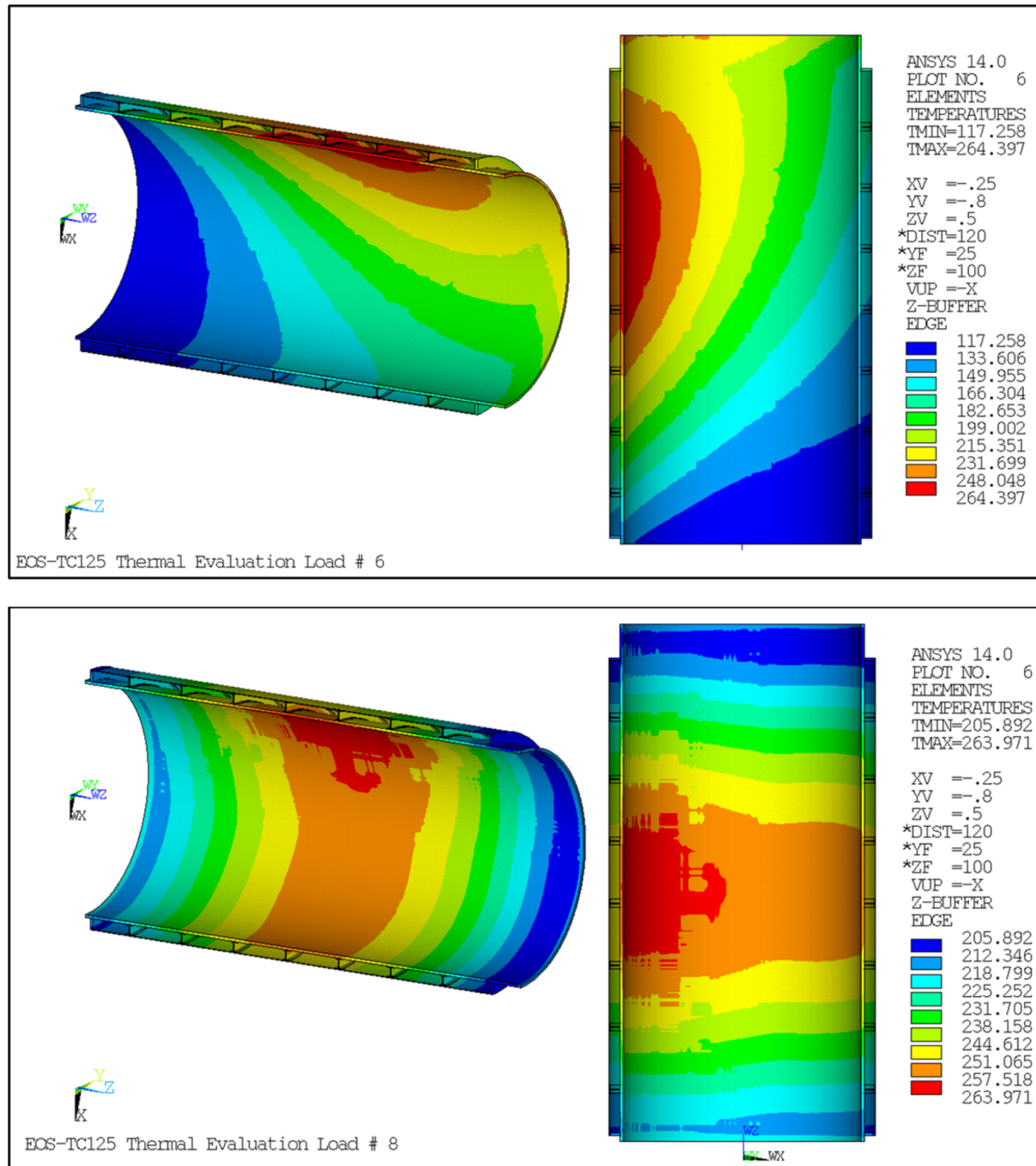


Figure 3.9.5-19
EOS-TC125 Temperature Distribution Plot

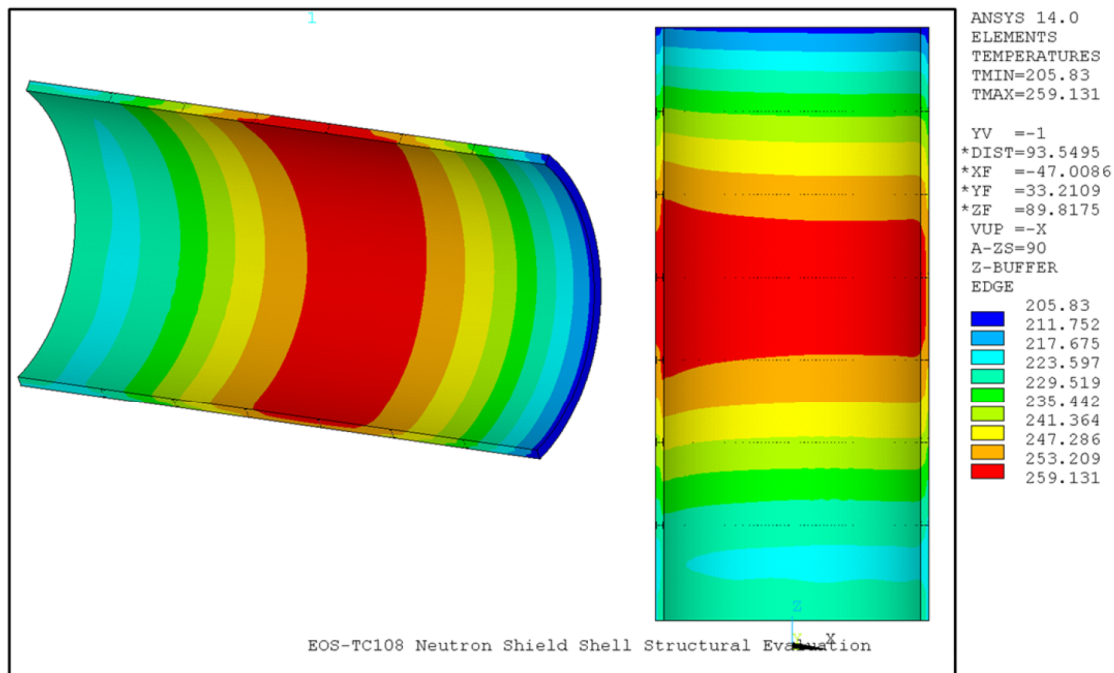
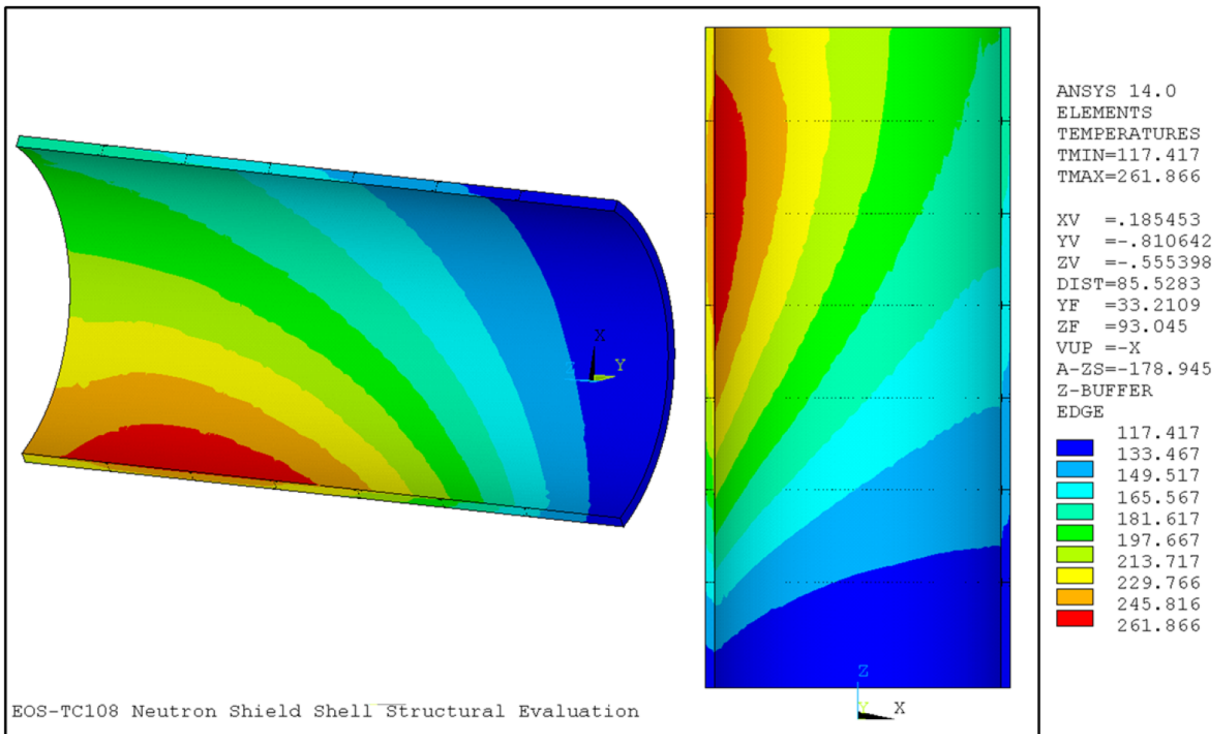


Figure 3.9.5-20
EOS-TC108 Temperature Distribution Plot

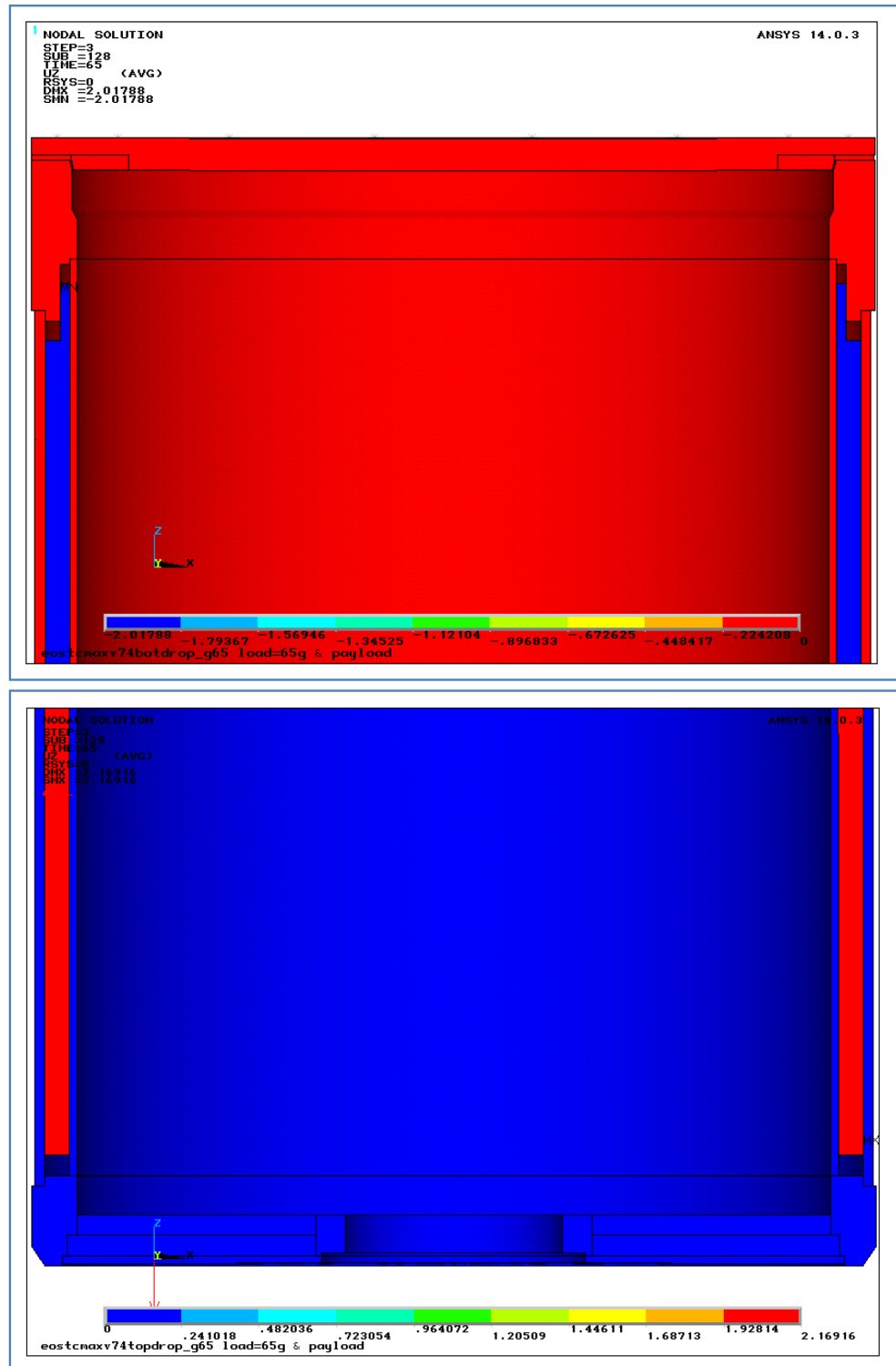


Figure 3.9.5-21
Bottom and Top, respectively, End Drops - Load 65g - Lead Slump
Displacements

Proprietary Information on Pages 3.9.6-i through 3.9.6-iv and 3.9.6-1 through 3.9.6-55
Withheld Pursuant to 10 CFR 2.390

APPENDIX 3.9.7 NUHOMS® EOS SYSTEM STABILITY ANALYSIS

Table of Contents

3.9.7 NUHOMS® EOS SYSTEM STABILITY ANALYSIS	3.9.7-1
3.9.7.1 EOS-HSM Stability Evaluation	3.9.7-1
3.9.7.2 EOS Transfer Cask Missile Stability and Stress Evaluation	3.9.7-14
3.9.7.3 References	3.9.7-31

List of Tables

Table 3.9.7-1	Sizes and Weight for Various EOS-HSM Models.....	3.9.7-33
Table 3.9.7-2	Missile Load Data for EOS-HSM Stability Analysis	3.9.7-33
Table 3.9.7-3	Design Pressures for Tornado Wind Loading.....	3.9.7-34
Table 3.9.7-4	Summary of EOS-HSM Sliding and Stability Results	3.9.7-35
Table 3.9.7-5	Design-Basis Tornado Missile Spectrum and Maximum Horizontal Speed for EOS-TC Stability Analysis.....	3.9.7-36
Table 3.9.7-6	Cask and DSC Weights in Different Configuration and Their Geometric Properties	3.9.7-37
Table 3.9.7-7	EOS-TC Analysis Results.....	3.9.7-38
Table 3.9.7-8	Combined Tornado Effect.....	3.9.7-39

List of Figures

Figure 3.9.7-1	EOS-HSM Dimensions for Stability Analysis.....	3.9.7-40
Figure 3.9.7-2	Angle of Rotation from Time-Dependent Analysis Due to Tornado Wind and Massive Missile Loading for EOS- HSM Short.....	3.9.7-41
Figure 3.9.7-3	Angle of Rotation from Time-Dependent Analysis Due to Tornado Wind and Massive Missile Loading for EOS- HSM Medium.....	3.9.7-42
Figure 3.9.7-3a	Angle of Rotation from Time Dependent Analysis due to Wind and Massive Missile Loading for EOS-HSM-FPS.....	3.9.7-42
Figure 3.9.7-4	Angle of Rotation from Time-Dependent Analysis Due to Tornado Wind and Massive Missile Loading for EOS- HSM Long.....	3.9.7-43
Figure 3.9.7-5	Sliding Displacement from Time-Dependent Analysis Due to Tornado Wind and Massive Missile Loading for EOS- HSM Short.....	3.9.7-43
Figure 3.9.7-6	Sliding Displacement from Time-Dependent Analysis Due to Tornado Wind and Massive Missile Loading for EOS- HSM Medium.....	3.9.7-44
Figure 3.9.7-6a	Sliding Displacement from Time Dependent Analysis due to Wind and Massive Missile Loading for EOS-HSM-FPS	3.9.7-44
Figure 3.9.7-7	Sliding Displacement from Time-Dependent Analysis Due to Tornado Wind and Massive Missile Loading for EOS- HSM Long	3.9.7-45
Figure 3.9.7-8	Stability of the DSC on the DSC Support Structure	3.9.7-46
Figure 3.9.7-9	Arrangement of EOS-TC, Skid and Transfer Trailer at Rest.....	3.9.7-47
Figure 3.9.7-10	Stability Geometry of TC on Transfer Trailer	3.9.7-48
Figure 3.9.7-11	Angle of Rotation (Time-Dependent)-Wind and Missile Loading for EOS-TC	3.9.7-49

3.9.7 NUHOMS® EOS SYSTEM STABILITY ANALYSIS

3.9.7.1 EOS-HSM Stability Evaluation

The sliding and overturning stability analyses due to design basis wind, flood, seismic, and massive missile impact loads are performed using hand calculations. The NUHOMS® EOS System consists of a reinforced concrete horizontal storage module (EOS-HSM) loaded with a dry shielded canister (DSC) (EOS-37PTH or EOS-89BTH).

3.9.7.1.1 General Description

The system consists of the dual-purpose (transport/storage) EOS-37PTH and EOS-89BTH DSCs, the EOS-HSM, and the onsite transfer cask (EOS-TC) with associated ancillary equipment. Each EOS-HSM is designed to store a DSC containing up to either 37 pressurized water reactor (PWR) or 89 boiling water reactor (BWR) spent fuel assemblies (SFAs).

The EOS-HSM storage modules can be arranged in both single-row or back-to-back-row arrays, with thick shield walls connected to the EOS-HSM at the ends of the arrays (end shield walls) and at the back end of the module (rear shield walls), if single-row arrays are used.

In the standard configuration, the EOS-HSM consists of two main segments: a base and a roof. The roof is installed on top of the base and is connected to it by bolts/embedments via four stiffened steel brackets located at each of the interior upper corners of the module's cavity. Alternate designs of horizontal storage modules may be used in lieu of EOS-HSM as part of the NUHOMS® EOS System.

The EOS-HSMS is a multi-segment design of a horizontal storage module, which consists of two segments of the base unit and a roof unit. The two segments of the base unit of EOS-HSMS are connected by grouted, high-strength, threaded bars/embedments, and the base and roof are connected in a similar way to that of EOS-HSM. An alternate Flat Plate Support Rail design of horizontal storage module, the EOS-HSM-FPS, may also be used in lieu of EOS-HSM as a part of the NUHOMS® EOS System. EOS-HSM-FPS is modified from the EOS-HSM to support the FPS DSC Support Structure with concrete pedestals spaced along the length of the DSC Support Structure. EOS-HSMS-FPS is a multi-segment design of the EOS-HSM-FPS, which consists of two segments of the base unit and a roof unit. The two segments of the base unit of EOS-HSMS-FPS are connected by grouted, high-strength, threaded bars/embedments, and the base and roof are connected in a similar way to that of EOS-HSM-FPS. EOS-HSM is used herein for all alternatives unless a unique situation is presented. EOS-HSM-FPS is used herein for both the EOS-HSM-FPS and EOS-HSMS-FPS unless a unique situation is presented.

3.9.7.1.2 Material Properties

The EOS-HSM assembly is constructed of reinforced concrete and steel. This analysis considers rigid body motions. Therefore, the mechanical properties of the materials are not used as design inputs in this evaluation.

3.9.7.1.3 Mass Properties

The mass properties of the EOS-HSM are listed in Table 3.9.7-1. Bounding values of concrete density (140 pcf, 150 pcf, and 160 pcf) are considered.

3.9.7.1.4 Friction Coefficients

The static analyses are performed using a concrete-to-concrete friction coefficient of 0.6.

3.9.7.1.5 Methodology

The stability of the EOS-HSM unit is evaluated for four load cases that may cause overturning and sliding of a single freestanding module. These four load cases are:

- Tornado-generated wind loads
- Massive missile impact loads
- Flood loads
- Seismic loads

3.9.7.1.6 Assumptions

1. The analyses assume that the dynamic coefficient of friction is equal to the static coefficient. This assumption maximizes the rocking uplift displacements of the EOS-HSM (particularly for the high friction coefficient analysis cases).
2. The differential pressure load caused by the tornado pressure drop does not affect the overall stability of the EOS-HSM and is ignored. The structure is vented, and so any differential pressure is very brief, while the internal and external pressures equilibrate. Since the structure is symmetric, the temporary internal pressure in the EOS-HSM caused by the negative tornado pressure does not cause any unbalanced loads on the EOS-HSM that would cause sliding and/or overturning.
3. This stability evaluation is applicable to both the standard EOS-HSM design, as well as the segmented EOS-HSMS design. The weight and inertia properties of the EOS-HSM and the EOS-HSMS are the same.

3.9.7.1.7 Loads and Boundary Conditions

3.9.7.1.7.1 Earthquake Input

The seismic stability evaluation is performed for a horizontal acceleration of 0.45g and vertical acceleration of 0.30g.

In addition, a 1.1 load factor is added to the seismic load.

3.9.7.1.7.2 Wind and Tornado Input

The EOS-HSM is evaluated for overturning and sliding due to the design basis tornado (DBT) specified in Chapter 2. The DBT is based on the NRC Reg. Guide 1.76 Region I Intensities. The maximum wind speed is 360 mph. The tornado loads are generated for three separate loading phenomena, as follows, which is combined in accordance with Section 3.3.2 of NUREG-0800 [3.9.7-1] (i.e. tornado wind load is concurrent with (additive to) tornado missile loads).

1. Pressure or suction forces created by drag as air impinges and flows past the EOS-HSM with a maximum tornado wind speed of 360 mph.
2. Suction forces due to a tornado generated pressure drop or differential pressure load of 3 psi.
3. Impact forces created by tornado-generated missiles impinging on the EOS-HSM.

Per NUREG-0800, the total tornado load on a structure is combined as follows:

$$\begin{aligned} W_t &= W_p \\ W_t &= W_w + 0.5W_p + W_m \end{aligned}$$

Where,

$$\begin{aligned} W_t &= \text{Total tornado load} \\ W_w &= \text{Load from tornado wind effect} \\ W_p &= \text{Load from tornado atmospheric pressure change effect} \\ W_m &= \text{Load from tornado missile impact effect} \end{aligned}$$

Note that W_p is not applicable to the stability analysis as discussed in Section 3.9.7.1.6. Thus, the load combination for tornado loading for this analysis is simplified to:

$$W_t = W_w + W_m$$

In addition, a 1.1 load factor is added to Dead weight + Tornado load.

The envelope of a range of missiles from Chapter 2 is used for the missile impact load.

As seen from Table 3.9.7-2 the automobile impact on to the EOS-HSM has the maximum momentum and is considered as bounding evaluation.

3.9.7.1.7.3 Flood Input

The EOS-HSM is evaluated for a flood height of 50 feet with a water velocity of 15 fps.

In addition, a 1.1 load factor is added to Dead weight + Flood load per Table 2-7 of Chapter 2.

3.9.7.1.8 Stability Analysis

The load categories associated with the EOS-HSM stability analysis are described in the previous section. The analysis steps and results for each load category are presented in this section.

3.9.7.1.8.1 Design Basis Tornado

The EOS-HSM is evaluated for forces created by drag as air impinges and flows past the EOS-HSM with a maximum tornado wind speed of 360 mph.

For sliding and overturning analysis, it is assumed that the module is subjected to the load due to 218 psf windward pressure loading acting on the end shield wall. The leeward side of the same module is subjected to a wind suction load of 154 psf. A suction of 326 psf is applied to the roof, including the top part of the shield walls. The loads are shown in Table 3.9.7-3.

In addition, missiles loads are combined with the tornado wind load per NUREG-800 [3.9.7-1].

3.9.7.1.8.1.1 Static Overturning Analysis due to Tornado Wind

The loaded EOS-HSM, the rear wall, one corner block, and one end shield wall rotates about B, shown in Figure 3.9.7-1. The other end shield wall and corner block rotates about point A, shown in Figure 3.9.7-1. Conservatively, the overturning of the loaded module with one end shield wall about point B is considered for the stabilizing moment.

In the overturning analysis of the EOS-HSM, the effects of tornado wind forces are first determined. An overturning moment is then calculated and is compared with a stabilizing moment. The minimum safety factor against overturning computed for all the three design lengths of EOS-HSM due to tornado wind is 1.59.

3.9.7.1.8.1.2 Dynamic Overturning Analysis of Tornado Wind Concurrent with Massive Missile Impact Loading

A dynamic analysis based on the conservation of energy is conducted for the combined effects of wind and concurrent massive missile impact loading. The effects of the concurrent massive missile impact loads are used in determining the initial angular momentum from the conservation of angular momentum equation using the wind loads from the previous section. Then the angle of rotation is determined from the conservation of energy of the concurrent loading.

The wind loads are calculated conservatively for EOS-HSM Long:

$$F_{hw} = (F_{windward} + F_{leeward})(L_{base})(h_{HSM+roof})$$

$$F_{vw} = (F_{roof})(L_{base})(w_{HSM+shield})$$

The concurrent wind loading is accounted for by reducing the inertia that resists motion in the denominator of the equation.

$$\omega_B = \frac{m_m \cdot d_m \cdot v_i}{m_m \cdot d_m^2 + I_{tot} - \left(\frac{F_{hw}}{g}\right)\left(\frac{h}{2}\right)^2 - \left(\frac{F_{vw}}{g}\right)\left(\frac{w}{2}\right)^2}$$

Where,

F_{hw} = Horizontal tornado wind load

F_{vw} = Vertical tornado wind load

ω_B = Angle of rotation

m_m = Mass of the missile

d_m = Distance from missile impact to floor

v_i = Initial missile velocity

I_{tot} = Total moment of inertia of HSM + Front end shield wall

h = Height of HSM + roof

w = Width of HSM + end shield wall

The conservation of energy is used for overturning.

Rotational Kinetic Energy = Change in Potential Energy – Work Done by Horizontal Wind force

$$\frac{I_{tot}\omega_B^2}{2} = (W - F_{vw}) \cdot r \cdot [\sin(\beta + \theta) - \sin\beta] - F_{hw} \cdot r \cdot [\cos(\beta + \theta) - \cos\beta]$$

Where,

θ = Angle of tipping

β = Angle from the horizontal to center of gravity (CG) of EOS-HSM (68.3°)

- r = Diagonal distance from CG to point B
 I_{tot} = Total moment of Inertia of HSM + Left end shield wall
 W = Weight of the loaded HSM + Left end shield wall

The loaded EOS-HSM is stable against overturning as tip-over does not occur until the CG rotates past the edge (point B, Figure 3.9.7-1) of the HSM to an angle of more than $90^\circ - 68.3^\circ = 21.7^\circ$

A loaded EOS-HSM rotates a maximum of 0.7 degrees, which is less than the 21.7 degrees required to overturn the module.

3.9.7.1.8.1.3 Time-Dependent Overturning Analysis of Tornado Wind Concurrent with Massive Missile Impact Loading

In addition to the dynamic overturning analysis, a time dependent analysis is used to ensure the absence of any overturning.

An approximate relationship for the deceleration of an automobile impacting a rigid wall is given by:

$$\begin{aligned}
 -\ddot{x} &= 12.5g \cdot x & \text{Eq. D - 1 of [3.9.7-4]} \\
 -\ddot{x} &= \text{Deceleration (ft/sec}^2\text{)} \\
 x &= \text{Distance automobile crushes into target (ft)}
 \end{aligned}$$

A force time history is obtained:

$$F = 0.625V_s W_m \sin 20t \quad \text{Eq. D - 6 of [3.9.7-4]}$$

The overturning moment is:

$$M_{ot} = F \cdot d_m + \frac{F_{hw}h}{2}$$

Where,

- d_m = Distance from missile impact to floor
 h = Vertical height to the top of EOS-HSM and is a function of rotation

The stabilizing moment is:

$$M_{st} = (W_{HSM} - F_{vw}) \cdot r \cos(\beta + \theta) + W_{end\ shield} \cdot r_{end} \cos(\gamma + \theta)$$

Where,

- W_{HSM} = Weight of the loaded EOS-HSM
 r = Diagonal distance from CG to point B
 θ = Angle of rotation
 r_{end} = Diagonal distance from CG of end shield wall to point B
 γ = Angle from horizontal to CG of end shield wall

The moment causing acceleration is:

$$M_{acc} = M_{ot} - M_{st}$$

The angular velocity is:

$$\omega_i = \left[\frac{M_{acc,i} + M_{acc,i-1}}{2} \cdot (t_i - t_{i-1}) \right] / I_{tot} + \omega_{i-1}$$

Where,

- i = Index for current time step
- i-1 = Index for previous time step
- I_{tot} = Total moment of Inertia of HSM + Left end shield wall

The angle of rotation is:

$$\theta_i = \left[\frac{\omega_i + \omega_{i-1}}{2} \cdot (t_i - t_{i-1}) \right] + \theta_{i-1}$$

The angles of rotation resulting from these analyses are shown in Figure 3.9.7-2 through Figure 3.9.7-4. The governing angle of rotation is 3.12 degrees, which is less than the 21.7 degrees required to overturn the module.

3.9.7.1.8.1.4 Sliding Analysis for Tornado Wind Concurrent with Massive Missile Impact loading

The combined wind + missile impact case is considered for EOS-HSM sliding analysis based on the conservation of energy.

First, the conservation of momentum is used for the sliding analysis.

$$V = \frac{m \cdot v_i}{M/1.07 + m - F_{hw}/386.4}$$

Where,

- V = Initial linear velocity of module after impact
- v_i = Initial velocity of missile
- m = Mass of the missile
- M₁ = Mass of empty EOS-HSM Short
- M₂ = Mass of end shield wall
- M₃ = Mass of governing loaded EOS-89BTH DSC
- M = Total mass = M₁ + M₂ + M₃
- 1.07 is the factor used to account for the uncertainty of the concrete density.

Then using the conservation of energy:

Friction Energy

= Initial Kinetic Energy of System + Work done by Wind

$$\mu \cdot (gM/1.07 - F_{vw})d = \frac{(M/1.07 + m) \cdot V^2}{2} + F_{hw}d$$

Where,

- μ = 0.6 coefficient of friction for concrete-to-concrete surfaces
- F_{vw} = Uplift force generated by DBT wind pressure on the roof
- d = Sliding distance of EOS-HSM
- F_{hw} = Sliding force generated by DBT wind pressure

The sliding distance of the EOS-HSM module is calculated to be 1.62 inches.

3.9.7.1.8.1.5 Time-Dependent Sliding Analysis for Tornado Wind Concurrent with Massive Impact Loading

In addition to the dynamic sliding analysis, a time dependent analysis is used to provide a bounding sliding displacement.

The total force causing sliding is:

$$F_{slide} = F + F_{hw}$$

The resisting force from friction is:

$$F_{resis} = \mu(W - F_{vw})$$

Therefore the force causing acceleration is:

$$F_{acc} = F_{slide} - F_{resis}$$

The velocity is:

$$v_i = \left[\frac{F_{acc,i} + F_{acc,i-1}}{2} \cdot (t_i - t_{i-1}) \right] / m_{tot} + v_{i-1}$$

Where,

- i = Index for current time step
- $i-1$ = Index for previous time step
- m_{tot} = Total mass of loaded EOS-HSM and both end shield walls including adjustment for density uncertainty

The sliding displacement is:

$$x_i = \left[\frac{v_i + v_{i-1}}{2} \cdot (t_i - t_{i-1}) \right] + x_{i-1}$$

The sliding displacements resulting from these analyses are shown in Figure 3.9.7-5 through Figure 3.9.7-7. The governing sliding displacement is 1.30 inches which is bounded by sliding distance of 1.62 inches resulting from dynamic sliding analysis as calculated in Section 3.9.7.1.8.1.4.

3.9.7.1.8.2 Flood Loads

The EOS-HSM is designed for a flood height of 50 feet and water velocity of 15 fps. The module is evaluated for the effects of a water current of 15 fps impinging on the side of a submerged EOS-HSM. Under 50 feet of water, the inside of the module is rapidly filled with water. Therefore, the EOS-HSM components are not evaluated for the 50 feet static head of water.

Calculation of the drag pressure due to design flood is shown in Appendix 3.9.4.

3.9.7.1.8.2.1 Overturning Analysis

The factor of safety against overturning of a single EOS-HSM with shield walls, for the postulated flooding conditions, is calculated by summing moments about the bottom outside corner of a single, freestanding EOS-HSM. The factors of safety against overturning for a single, freestanding EOS-HSM due to the postulated design basis flood water velocity are 1.14, 1.12, 1.11, and 1.13 for the EOS-HSM Short, EOS-HSM Medium, EOS-HSM-FPS Medium, and EOS-HSM Long, respectively.

3.9.7.1.8.2.2 Sliding Analysis

The factor of safety against sliding of a freestanding single EOS-HSM due to the maximum postulated flood water velocity of 15 fps is calculated using methods similar to those described above. The effective weight of the EOS-HSM including the DSC and end shield wall acting vertically downward, less the effects of buoyancy acting vertically upward is calculated. The factors of safety against sliding for a single, freestanding EOS-HSM due to the postulated design basis flood water velocity are 1.12, 1.09, 1.08, and 1.11 for the EOS-HSM Short, EOS-HSM Medium, EOS-HSM-FPS Medium, and EOS-HSM Long, respectively.

3.9.7.1.8.3 Seismic Load

The EOS-HSM is evaluated for maximum values for seismic accelerations of 0.45g in the horizontal direction and 0.30g in the vertical direction. Both the loaded EOS-HSM and the empty EOS-HSM are considered for these loads. The EOS-HSM and one end shield wall rotate about B, shown in Figure 3.9.7-1. The other end shield wall, corner blocks and rear shield walls are conservatively ignored.

The combination of 100% of horizontal acceleration and 40% of vertical acceleration is used.

3.9.7.1.8.3.1 Static Overturning Analysis of the EOS-HSM due to Seismic Load

The stabilizing and overturning moments are calculated and compared, and the case considering the bounding 140 pcf concrete density and the minimum DSC weight to minimize the stabilizing moment is shown below. The stability overturning analysis shown is for the governing EOS-HSM Long model. A factor of 1.07 (150 pcf/140 pcf) reduces the considered mass to the 140 pcf lower bound case. The 160 pcf upper bound is also considered, but not shown here.

$$\text{Stabilizing Moment} = M_{st} = (W_{HSM} + W_{DSC}) \times d_{HSM-B} + W_{end_shield_wall} \times d_{end_shield_wall-B}$$

$$M_{st} = \left(\frac{330kip}{1.07} + 134kip \right) \times (48in) + \left(\frac{187.1kip}{1.07} \right) \times (124in)$$

$$M_{st} = 42,900 \text{ kip-in}$$

Where a factor of 1.07 (150pcf/140pcf) is used to account for the uncertainty of the concrete density.

Overturning Moment =

$$M_{ot} = 0.4a_v \times (W_{HSM}x_{HSM} + W_{DSC}x_{DSC} + W_{wall}x_{wall}) + a_h(W_{HSM}y_{HSM} + W_{DSC}y_{DSC} + (W_{wall}h_{wall})/2)$$

$$M_{ot} = 0.4 \times 0.30g \times \left[\frac{330kip}{1.07} \times 48in + 134kip \times 48in + \frac{187.1kip}{1.07} \times 124in \right] + 0.45g \times \left[\frac{330kip}{1.07} \times 126.5 + 134kip \times 106in + \frac{187.1kip}{1.07} \times 111in \right]$$

$$M_{ot} = 37,800 \text{ kip-in}$$

Where,

W_{HSM}, W_{DSC} = Weight of empty HSM and DSC = 330 kip, 134 kip respectively

d_{HSM-B} = respective distance between the CG of the HSM and the point of rotation B (Figure 3.9.7-1) = 116 in./2 - 10 in. = 48 in.

$d_{end_shield_wall-B}$ = respective distance between the CG of the end shield wall and the point of rotation B (Figure 3.9.7-1) = 36 in./2 + 116 in. - 10 in. = 124 in.

a_v, a_h = vertical and horizontal seismic accelerations

x_{HSM} = horizontal distance between the CG of the HSM and the point of rotation B = 48 in. (Figure 3.9.7-1)

x_{DSC}	=	horizontal distance between the CG of the DSC and the point of rotation B = 48 in. (Figure 3.9.7-1)
x_{wall}	=	horizontal distance from the CG of the end shield wall to the point of rotation B = 124 in. (Figure 3.9.7-1)
y_{HSM}	=	vertical distance from the CG of the HSM and the point of rotation B = 126.5 in. (Figure 3.9.7-1)
y_{DSC}	=	vertical distance from the CG of the HSM and the point of rotation B = 106 in. (Figure 3.9.7-1)
h_{wall}	=	vertical distance from the CG of the end shield wall to the point of rotation B = 111 in. (Figure 3.9.7-1)

The maximum acceptable acceleration values before tipping occurs are calculated below:

$$M_{st} = 42,900kip \cdot in \geq 1.1M_{ot} = 1.1 \left\{ 0.4a_v \times \left[\frac{330kip}{1.07} \times 48in + 134kip \times 48in + \frac{187.1kip}{1.07} \times 124in \right] + a_h \left[\frac{330kip}{1.07} \times 126.5 + 134kip \times 106in + \frac{187.1kip}{1.07} \times 111in \right] \right\}$$

And assuming $a_v = \frac{2}{3}a_h$

$$a = 0.46g, a_v = 0.31g$$

The safety factor of $M_{st}/1.1M_{ot} = 1.03$ and is greater than 1 and is the governing safety factor for all load cases. Therefore, it is concluded that the EOS-HSM is stable for seismic loads of up to 0.45g horizontal and 0.30g vertical.

3.9.7.1.8.3.2 Static Sliding Analysis of the EOS-HSM due to Seismic Load

The resisting friction force and horizontal seismic force are calculated and compared and the case considering the bounding 140 pcf concrete density and the minimum DSC weight to minimize the resisting friction force is shown below. The static sliding analysis is shown for the governing EOS-HSM Long model. Cases where the EOS-HSM is loaded versus empty and has one end shield wall versus no shield walls are also considered.

$$\text{Friction force resisting sliding} = F_{st} = \mu(W_{HSM} + W_{DSC})(1 - 0.40 a_v)$$

$$F_{st} = 0.6 \times \left(\frac{330kip}{1.07} + 134kip \right) \times (1 - 0.40 \times 0.30)$$

$$F_{st} = 233 \text{ kip}$$

$$\text{Applied horizontal seismic force} = F_{hs} = a_h (W_{HSM} + W_{DSC})$$

$$F_{hs} = 0.45 \times \left(\frac{330kip}{1.07} + 134kip \right)$$

$$F_{hs} = 199\text{kip}$$

Where,

μ = friction coefficient = 0.6

a_v, a_h = vertical and horizontal seismic accelerations = 0.30g, 0.45g respectively

x, y = are the horizontal and vertical distance between the CG and point of rotation B

The maximum acceptable acceleration values before sliding occurs are calculated below:

$$\begin{aligned} F_{st} &= 0.6 \times \left(\frac{330\text{kip}}{1.07} + 134\text{kip} \right) \times (1 - 1.1 \times 0.40 a_v) \geq 1.1 F_{hs} \\ &= 1.1 a_h \left(\frac{330\text{kip}}{1.07} + 134\text{kip} \right) \end{aligned}$$

And assuming $a_v = \frac{2}{3} a_h$

$$a = 0.47g, a_v = 0.32g$$

The safety factor of $F_{st}/1.1F_{hs}=1.07$ and is greater than 1 and is the governing safety factor for all load cases. Therefore, it is concluded that the EOS-HSM is stable for seismic loads of up to 0.45g horizontal and 0.30g vertical.

3.9.7.1.8.3.3 Seismic Stability of the DSC on DSC Support Structure inside the EOS-HSM

This evaluation is performed for the DSC resting on the support rails inside the EOS-HSM, which includes the stability of the DSC against lifting off from one of the rails during a seismic event and potential sliding off of the DSC from the support structure. The horizontal equivalent static acceleration of 0.45g is applied laterally to the center of gravity of the DSC. The point of rigid body rotation of the DSC is assumed to be the center of the support rail. The applied moment acting on the DSC is calculated by summing the overturning moments.

The stabilizing moment, acting to oppose the applied moment, is calculated and compared with the overturning moment to obtain the maximum acceleration to preclude sliding and overturning of the DSC.

Weight of the DSC = W (kip)

$$\text{DSC outer radius} = R = 75.5''/2 = 37.8''$$

$$\text{Angle } \theta = 30^\circ$$

$$Z = 37.75 \sin(30^\circ) = 18.88''$$

$$Y = 37.75 \cos(30^\circ) = 32.69''$$

$$\text{Vertical Seismic Acceleration} = 0.30g$$

$$\text{Horizontal Seismic Acceleration} = 0.45g$$

$$\text{Vertical seismic force (kips)} = W \times 0.30 \times 0.4 = 0.12W = F_v$$

$$\text{Horizontal seismic force (kips)} = W \times 0.45 = 0.45W = F_h$$

The overturning moment =

$$1.1F_h \times Y = 1.1 \times 0.45W \times 32.69 = 16.18W \text{ kip-in}$$

The stabilizing moment =

$$(W - 1.1F_v) \times Z = (W - 1.1 \times 0.12W) \times 18.88 = 16.39W \text{ kip-in}$$

Therefore, the margin of safety (*SF*) against DSC lift off from the DSC support rails inside the HSM obtained from this analysis is:

$$SF = \frac{M_{st}}{M_{ot}} = \frac{16.39W}{16.18W} = 1.01$$

The safety factor of $M_{st}/M_{ot}=1.01$ is greater than 1. Therefore, the DSC is stable against lifting off the DSC support rails in the EOS-HSM. The evaluation to determine the maximum seismic acceleration before any uplift of the DSC occurs is shown.

$$M_{st} = (W - 1.1 \times 0.4a_v W) \times 18.88 \geq M_{ot} = 1.1 \times a_h W \times 32.69$$

$$\text{And assuming } a_v = \frac{2}{3} a_h$$

$$a_h = 0.46g, a_v = 0.30g$$

Therefore, the maximum horizontal and vertical acceleration are determined to be 0.45g and 0.30g, respectively.

3.9.7.1.8.4 Interaction of EOS-HSM with Adjacent Modules

For the overturning and sliding analyses due to tornado wind plus missile and flood loading, a single module with one end shield wall is considered. For the seismic sliding and overturning analyses in Section 3.9.7.1.8.3, the cases both with and without an end shield wall are considered, where the same weight and moment of inertia is consistently used for sliding force/overturning moment and for friction force/stabilizing moment in each case.

In the actual scenarios, there is either an end shield wall on one side and another module on the other side, or one module on each side. In the case of sliding, the tornado wind plus missile impact loads the end shield wall plus the HSM module and incur a displacement. The maximum displacement is already obtained in Sections 3.9.7.1.8.1.4 and 3.9.7.1.8.1.5 assuming no resisting force from the adjacent module. With the presence of the adjacent module, the displacement can be transferred into a load onto the adjacent module and result in the maximum displacement if it is perfectly elastic (coefficient of restitution = 1). Then this displacement can be transferred into a load for the next adjacent module with a maximum displacement. However, concrete has a much lower coefficient of restitution (COR) of about 0.1. Energy absorption due to contact (due to the low COR=0.1) results in less critical sliding and overturning results. Impact due to sliding would be distributed over the large side/rear wall surface areas. Impact due to tipping would be localized at the free edges/corners of the modules. Any local damage in these corners or edges would not affect the structural, thermal, or shielding performance of the EOS-HSM. Therefore, the displacement of the adjacent module cannot reach the maximum displacement since there is some energy loss. Thus, the maximum displacement obtained in Sections 3.9.7.1.8.1.4 and 3.9.7.1.8.1.5 is conservative and bounding. This conservatism also applies to overturning and the cases due to flood loads.

3.9.7.1.9 Results

For the maximum seismic acceleration of 0.45g horizontal and 0.30g vertical, no sliding will occur. Also, there will be no overturning at this set of seismic accelerations.

For flood, wind, and missile impact, it is also determined that the uplift values are small and so the DSC remains stable on the support rails. For seismic loading, it is also determined that there is no uplift of the DSC.

In the case of an uneven surface of the concrete pad, shims under the end and rear shield walls can be placed to restore the HSM to its horizontal configurations.

Table 3.9.7-4 shows a summary of the bounding results from the analyses in Section 3.9.7.1.8. Thus, a maximum horizontal acceleration of 0.45g and a vertical acceleration of 0.30g can be exerted on the EOS-HSM before any uplift or sliding occurs. Also there is no DSC lift-off due to this seismic loading.

3.9.7.2 EOS Transfer Cask Missile Stability and Stress Evaluation

3.9.7.2.1 General Description

The stability, stresses, and penetration resistance of the EOS-TCs (TC108, TC125 and TC135) due to design basis tornado and missile impact are evaluated in this section.

3.9.7.2.2 Material Properties

The material properties of the cask outer shell, and top cover plate at 400 °F are taken from Chapter 8.

3.9.7.2.3 Assumptions

1. The gust factor value of 0.85 is taken from Section 6.5.8.1 of ASCE 7-05 [3.9.7-5].
2. The bolted bottom cover plate assembly is protected by transfer equipment attached to skid assembly during the transfer operations, and therefore DBT and missile load is not consider for bottom cover plate.
3. The impact between massive missile and EOS-TC is assumed to be perfectly plastic impact and the missile mass is attached to EOS-TC after impact.
4. The stresses in trunnion/saddle due to DBT and missile impact are bounded by seismic loads. The evaluations of trunnions are performed separately in Appendix 3.9.5.

3.9.7.2.4 Design Input/Data

The most severe tornado-generated wind and missile loads specified by Regulatory Guide 1.76 [3.9.7-6] are selected as the design basis.

3.9.7.2.4.1 DBT Velocity Pressure

The DBT Region I intensities are utilized since they result in the most severe loading parameters. For this region, the maximum wind speed is 230 mph, the rotational speed is 184 mph, and the maximum translational speed is 46 mph. The radius of the maximum rotational speed is 150 feet, the pressure drop across the tornado is 1.2 psi and the rate of pressure drop is 0.5 psi per second.

The maximum velocity pressure, q_z , evaluated at height z based on the maximum tornado velocity (v) is calculated using the relationship given in [3.9.7-5].

$$q_z = 0.00256 K_z K_{zt} K_d I(v)^2$$

The maximum tornado wind speed, V , is the resultant of the maximum rotational speed (184 mph) and the translational speed (46 mph) of the tornado.

The design wind force, F , on the EOS-TC due to this velocity pressure, q_z , is
 $F = q_z G C_f A_f$ lb Section 6.5.15 of Ref. [3.9.7-5]

Where,

G = gust-effect factor = 0.85 (Assumption 1)

C_f = Force coefficient = conservatively taken as 0.82 (by linear interpolation of h/D value of 1.69) from Figure 6-21 of [3.9.7-5],

A_f = Projected area normal to the wind and geometry considered is shown in Figure 3.9.7-9 and is calculated for Case E of Table 3.9.7-6. This has a maximum projected area that is conservative.

Projected area of the cask = (Length of the cask, L_c) x (Diameter of the cask, D_c)

Projected area of the skid = (Length of the Skid, L_s) x (Height of the skid, H_s)

Projected area of the trailer = (Length of the trailer, L_t) x (Height of the Trailer, H_t)

Total projected area (Cask + Skid + Trailer),

Design wind force $F = 22.36$ kips

3.9.7.2.4.2 DBT Generated Missile Parameters

The tornado-generated missile impact evaluation is performed for a spectrum of missiles and are summarized in Table 3.9.7-5.

3.9.7.2.5 Methodology

The following analyses are performed for the cask and components using hand calculations:

- Stability analysis
- Stress analysis
- Penetration analysis

A load factor of 1.1 is applied to the tornado and seismic loads for stability analyses.

3.9.7.2.5.1 Combined Tornado Effects

Individual DBT, missile load, and combination of these loads are calculated assuming these act simultaneously and are shown in Table 3.9.7-8. Since the EOS-TC is vented, the differential atmospheric pressure is neglected.

3.9.7.2.6 Structural Evaluation

3.9.7.2.6.1 Design Basis Wind Pressure Loads

3.9.7.2.6.1.1 Stability Analysis due to DBT Wind Pressure Load

Total weight of the assembly (EOS-TC, skid and the trailer), W_C = Weight of (cask + skid + trailer)

The restoring moment is least for the assembly with minimum weight. Assuming the trailer and skid remain the same, the minimum weight of all the possible EOS-TC and DSC combinations per Table 3.9.7-6, is bounding for the stability analysis.

Considering the minimum weight of EOS-TC108 loaded with EOS-89BTH DSC (Case B, Table 3.9.7-6) is minimum (199.289 kips), a conservative weight of 170 kips is used for the evaluation.

Thus, the restoring moment, $M_{st} = (\text{Total weight}) \times (\text{Half width of the trailer})$

Conservatively assuming that the combined geometry of the cask/skid/trailer has a solid vertical projected area and ignoring the reduction in total wind pressure due to the open areas and shape factor, the maximum overturning moment, M_{ot} , for the cask/skid/trailer due to DBT wind pressure is:

$$M_{ot} = 2F \times H$$

Where,

H = Center of the cask/skid/trailer height

F = Design wind pressure

Accounting for the load factor of 1.1 on the overturning moment:

$$\text{Factor of safety against overturning} = 1.1 \times \frac{M_{st}}{M_{ot}} = 3.92$$

3.9.7.2.6.1.2 Stress Analysis

3.9.7.2.6.1.2.1 *Stresses in the Cask Shell due to DBT Wind Pressure Load*

Assuming the cask is simply supported and subjected to a uniform load, p, over the entire length, thus using Case 8c, Table 13.3 of Ref. [3.9.7-7], Page 650:

$$\text{Circumferential membrane stress} = \sigma_2 = 0.492 B p R^{\frac{3}{4}} L^{\frac{-1}{2}} t^{\frac{-5}{4}}$$

$$\text{Circumferential bending stress} = \sigma_2' = 1.217 B^{-1} p R^{\frac{1}{4}} L^{\frac{1}{2}} t^{\frac{-7}{4}}$$

$$\text{Axial membrane stress } \sigma_l = 0.1188 B^3 p R^{1/4} L^{1/2} t^{-7/4}$$

Total force = F = 22.36 kips (Section 3.9.7.2.4.1)

Force per inch, p, is maximum for the minimum length of the cask, thus the bounding minimum length, L (EOS-TC108, Case A Table 3.9.7-6) is taken conservatively

$$p = F / L$$

$$B = [12(1-\nu^2)]^{1/8}, \text{ where } \nu \text{ is the Poisson's ratio (= 0.3 for stainless steel)}$$

Circumferential membrane stress is maximum for the minimum cask length as it is inversely related to the cask length, whereas circumferential bending stress and axial membrane stress is maximum for the maximum cask length since they are directly related to the cask length.

Also, circumferential membrane stress, circumferential bending stress and axial membrane stress are maximum for the maximum cask radius since they are directly related to cask radius:

Bounding minimum cask length = (EOS-TC108, Case A, Table 3.9.7-6)

Bounding maximum cask length = (EOS-TC135, Case E, Table 3.9.7-6)

Bounding maximum cask radius = (EOS-TC135, Case E, Table 3.9.7-6)

Circumferential membrane stress $\sigma_2 = 0.086$ ksi

Circumferential bending stress, $\sigma_2 = 3.85$ ksi

Axial membrane stress, $\sigma_1 = 1.25$ ksi

Primary membrane stress intensity = $\sigma_1 = 0.135$ ksf = 0.0009 ksi

Membrane plus bending, S.I. = 5.19 ksi

3.9.7.2.6.1.2.2 *Stresses in Top Cover Plate due to DBT Wind Pressure Load*

Assuming the plate is simply supported at edges and subjected to a uniform load, q , (load per unit area) over the entire area, thus using Case 10a, Table 11.2 of Roark's Formula for Stress and Strain [3.9.7-7], Page 488 and 509:

$$M_c = qa^2 L_{17}, \text{ where } L_{17} = \frac{1}{4} \left\{ 1 - \frac{1-\nu}{4} \right\} \text{ for } r_o = 0.$$

$$\text{Thus, } M_c = \frac{qa^2(3+\nu)}{16}$$

$$q = 0.135 \text{ ksf} \quad M_c = 0.37 \text{ kip-in/in}$$

$$\sigma = \frac{6M_c}{t_1^2} = 0.21 \text{ ksi}$$

Primary membrane stress intensity = $\sigma_m = 0.135$ ksf = 0.0009 ksi

Membrane plus bending, S.I. = 0.21 ksi

3.9.7.2.6.2 Massive Missile Impact

3.9.7.2.6.2.1 Stability Analysis due to Massive Missile Impact Load

Stability analysis is done to analyze the most critical impact (Missile B, Table 3.9.7-5) when the missile hits the cask on the side. However, it is conservatively assumed that the missile hits the top most part of the cask as shown in Figure 3.9.7-10.

Using Table 3.9.7-6 and from conservation of momentum,

$$(H_i)_o = (H_a)_o$$

Where,

$(H_i)_o$ is the angular momentum about point O before impact $= R_1 v_i M_m$

$(H_a)_o$ is the angular momentum about point O after impact

$$= R_1^2 \omega_i M_m + (I_c)_o \omega_i$$

R_1 is the distance from point O to the impact point

v_i is the impact velocity of the missile

M_m is the mass of the missile

M_c is the mass of the cask assembly

ω_i is the angular velocity of the missile about point O just after the impact

$(I_c)_o$ is the mass moment of inertia of the cask about an axis through point O

Therefore, by conserving the momentum before and after the impact:

$$R_1 v_i M_m = R_1^2 \omega_i M_m + (I_c)_o \omega_i$$

$$\omega_i = \frac{R_1 v_i M_m}{R_1^2 M_m + (I_c)_o}$$

From the conservation of energy, $KE_i + PE_i = KE_f + PE_f$

Where,

$$KE_i \text{ is the initial kinetic energy of the cask and missile} = \frac{(I_c)_o \omega_i^2}{2} + \frac{R_1^2 \omega_i^2 M_m}{2}$$

$$KE_f \text{ is the final kinetic energy of the cask and missile} = \frac{(I_c)_o \omega_f^2}{2} + \frac{R_1^2 \omega_f^2 M_m}{2}$$

PE_i is the initial potential energy of the cask and missile = 0

PE_f is the final potential energy of cask and missile = (weight of the cask) x (change in height of the C.G.)

Therefore:

$$\frac{(I_c)_o \omega_i^2}{2} + \frac{R_1^2 \omega_i^2 M_m}{2} = \frac{(I_c)_o \omega_f^2}{2} + \frac{R_1^2 \omega_f^2 M_m}{2} + w_c h$$

$$\omega_f^2 = \frac{[(I_c)_o + R_1^2 M_m] \omega_i^2 - 2w_c h}{[(I_c)_o + R_1^2 M_m]}$$

From Figure 3.9.7-10 $h = R_2[\sin(\phi + \theta) - \sin(\phi)]$

$$\text{Hence, } \omega_f^2 = \frac{[(I_c)_o + R_1^2 M_m] \omega_i^2 - 2w_c R_2[\sin(\phi + \theta) - \sin(\phi)]}{[(I_c)_o + R_1^2 M_m]}$$

The cask stops rotating when the angular velocity, $\omega_f = 0$ and

$$\omega_i = \frac{R_1 v_i M_m}{R_1^2 M_m + (I_c)_o}$$

$$\text{Thus, } \sin \phi \cos \theta + \sin \theta \cos \phi = \frac{(R_1 v_i M_m)^2}{2w_c R_2 [(I_c)_o + R_1^2 M_m]} + \sin \phi$$

$$(I_c)_o = (I_c)_{CG} + M_c R_2^2 \quad (\text{From parallel axis theorem})$$

Where,

$(I_c)_{CG}$ is the mass moment of inertia of the cask about center of gravity of EOS-TC.

Conservatively, the bounding (maximum) loaded cask weight from Case B (EOS-TC108 with EOS-89BTH DSC) of Table 3.9.7-6 (i.e., 199.29 kips) is taken, which is further decreased to 170 kips such that it is more conservative, because this results in maximum impact force and hence, the maximum primary membrane stress, circumferential membrane and bending stress intensity.

Hence, the total weight of the TC (EOS-TC, Skid and the Trailer), $W_c = 170 + 10 + 35 = 215$ kips

So the total mass of the TC assembly (EOS-TC, Skid and Trailer), $M_c = (215 \times 1000)/32.2 = 6,677.02$ lbm

$$(I_c)_{CG} = \frac{M_c R_c^2}{2} = 43,991.21 \text{ ft}^2 \text{ lbm}$$

$$M_c R_2^2 = 698,769.51 \text{ ft}^2 \text{ lbm}$$

$$(I_c)_o = 7.43 \times 10^5 \text{ ft}^2 \text{ lbm}$$

By substituting the parameters of cask and stability geometry in above equation,
 $\sin(\theta + \phi) = 0.015 + 0.8433 = 0.8583$,

Angle of Cask CG about pivot “O” relative to horizontal, $\phi = \tan^{-1}(L1/R)$ where R is the half width of trailer (5.5 ft assumed) and L1 is calculated to be 43 in. + 17 in. + (87/2) = 103.5 in. = 8.63 ft (See Figure 3.9.7-10). Therefore, $\phi = 57.49^\circ$ and Solving above equation, $\theta = \sin^{-1}(0.8583) - 57.49 = 59.13 - 57.49 = 1.64^\circ$

The maximum angle for the tip over the cask occurs when the CG is directly above the point of rotation.

$$\text{i.e. } \theta_{tip} = 90^\circ - \phi = 32.52^\circ \quad \theta_{tip} = \tan^{-1} R/R_2 = \tan^{-1} 5.5/10.6 = 27.42^\circ$$

Accounting for the load factor of 1.1 on the tornado missile load by increasing the angle of rotation:

Since $\theta_{tip} \gg 1.1 \times \theta$, the tip over of the cask does not occur.

3.9.7.2.6.2.2 Stress Analysis

3.9.7.2.6.2.2.1 *Stresses in Cask Shell due to Massive Missile Impact Load*

The missile impact is analyzed by taking Automobile 16.4 feet x 6.6 feet x 4.3 feet (Case B of Table 3.9.7-5) for evaluation of stresses in cask shell and top cover plates. The stresses in the cask shell due to the massive missile impact will be highest for an impact at the cask mid length. The impact force due to the massive missile is calculated by determining the work done in elevating the cask center of gravity the vertical distance corresponding to the angle of rotation (1.64°) resulting from impact.

The angle of rotation of the cask due to the massive missile impact is 1.64° , therefore, the impact force (P) including a dynamic load factor of 2.0 is given by:

$$P = 2.0 \times W_c \times \cos(90^\circ - \theta)$$

Total weight of cask, W_c (EOS-TC, Skid and the Trailer) = 253.30 + 10 + 35 = 298.30 kips (Table 3.9.7-6 for enveloping EOS-TC weight)

W_c is considered to be approximately 300 kips, resulting in 17.17 kips

Assuming the cask is simply supported and subjected to a concentrated load, p , over short length $2b$ (Conservatively taken as 4.3 feet), thus using Case 8b, Table 13.3 of Roark's Formula for Stress and Strain [3.9.7-7], Page 650:

$$\text{Circumferential membrane stress, } \sigma_2 = 0.130 B p R^{\frac{3}{4}} b^{\frac{-3}{2}} t^{\frac{-5}{4}}$$

Circumferential bending stress, $\sigma_2' = 1.56B^{-1}pR^{\frac{1}{4}}b^{\frac{-1}{2}}t^{\frac{-7}{4}}$

Axial membrane stress, $\sigma_1 = 0.153B^3pR^{\frac{1}{4}}b^{\frac{-1}{2}}t^{\frac{-7}{4}}$

Force per inch, p, is maximum for the minimum length of Automobile 16.4 feet x 6.6 feet x 4.3 feet (Case B of Table 3.9.7-5):

$P = F / \text{minimum dimension of Automobile}$

$B = [12(1-\nu^2)]^{1/8}$, where ν is the Poisson's ratio (= 0.3 for stainless steel)

Also, circumferential membrane stress, circumferential bending stress and axial membrane stress are maximum for the maximum cask radius since they are directly related to cask radius:

Bounding maximum cask radius = EOS-TC135, Case E of Table 3.9.7-6

Circumferential membrane stress $\sigma_2 = 0.39$ ksi

Circumferential bending stress $\sigma_2' = 10.03$ ksi

Axial membrane stress, $\sigma_1 = 3.27$ ksi

Primary Membrane Stress Intensity = $3.27 + 0.39 = 3.66$ ksi

Membrane plus Bending, $S.I. = \sigma_2 + \sigma_2' = 13.69$ ksi

3.9.7.2.6.2.2.2 Stresses in Top Cover Plate due to Massive Missile Impact Load

The impact on the top cover plate is assumed to be perfectly inelastic impact (Assumption 10) and the automobile (massive missile) is assumed to attach to the EOS-TC after impact.

Let

v_s = Striking velocity of the automobile normal to EOS-TC

$w_{missile}$ = Weight of missile

The impact force acting on the EOS-TC due to the massive missile automobile will be

$W_m = 0.625xv_s \times w_{missile} \times \sin(20t)$ lbs (Bechtel topical Report, Ref. [3.9.7-4])

Where,

t = time from the instant initial impact (sec)

$w_m = 337500$ lbs = 337.5 kips

Assuming the plate is simply supported at edges and subjected to a uniform load 'q' (load per unit area) over the entire area, thus using case 10a, Table 11.2 of Ref. [3.9.7-7], Page 509:

$$M_c = qa^2 L_{17}, \text{ where } L_{17} = \frac{1}{4} \left\{ 1 - \frac{1-\nu}{4} \right\} \text{ for } r_o = 0.$$

$$\text{Thus, } M_c = \frac{qa^2(3+\nu)}{16}$$

$$M_c = \frac{p}{\pi a^2} \frac{a^2(3+\nu)}{16} = \frac{p(3+\nu)}{\pi 16}$$

$$\sigma = \frac{6M_c}{t^2} = \frac{6}{t^2} \frac{p(3+\nu)}{\pi 16} = 12.59 \text{ ksi}$$

Primary Membrane Stress= Total force acting on the EOS-TC due to massive missile automobile/ Area of top cover plate = 0.06 ksi

Therefore, Primary membrane + bending stress in the top cover plate will be 0.06 + 12.59 = 12.65 ksi

3.9.7.2.6.3 Missile Penetration Resistance Analysis

3.9.7.2.6.3.1 Penetration Analysis

In order to evaluate the system for resistance towards the missile penetration, the minimum thickness required to resist the bounding missile (Case A, Table 3.9.7-5) is calculated using two different relations:

- Nelm's formula [3.9.7-8] is used to determine the minimum required thickness for puncture resistance.
- The Ballistic Research Laboratory formula is used to calculate the missile penetration distance and the minimum required thickness for puncture resistance.

It is assumed that the missile is rigid and the mass and velocity of the missile for the evaluation is taken from Table 3.9.7-5.

Nelms' Formula (page 54 of Reference [3.9.7-8])

$$E_F/S = 2.4d^{1.6}t^{1.4}$$

Where,

E_F is the incipient puncture energy of the prismatic cask jacket (inch-lbs)
 S is the ultimate tensile strength of the jacket material (cask outer shell) (ksi)

t is the thickness of the jacket material (inch)
 d is the diameter of the punch/missile (6.625 inch)

Assuming all the kinetic energy of the missile is getting converted to the incipient puncture energy of the prismatic cask jacket.

$$E_F = \frac{1}{2} M_m v_m^2$$

Where,

M_m and v_m are the mass and velocity of the missile, respectively.

$$E_F/S = 2.4d^{1.6}t^{1.4}$$

$$t^{1.4} = 0.281 \Rightarrow t = 0.404 \text{ inch}$$

Ballistic Research Laboratory Relation (page 2-3 of [3.9.7-4])

$$T = \frac{\left(\frac{MV_s^2}{2} \right)^{2/3}}{672D}$$

Where,

T is the steel plate thickness to just perforate (inch)
 D is the diameter of the punch/missile (= 6.625 inch)
 M_s is the mass of the striking missile (= 8.91 lbs.sec²/ft)
 V is the velocity of the striking missile normal to target surface (=135 fps)
 $T = 0.421$ inch

The thickness t_p , of a steel barrier required to prevent perforation should exceed the thickness for threshold of perforations. It is recommended by [3.9.7-4] to increase the thickness, T , by 25 percent to prevent perforation.

Thus, minimum thickness of the barrier should be, $t_p = 1.25T$ inch = 0.526 inch

Out of the thickness calculated by the two methods, the threshold thickness evaluated by Ballistic Research Laboratory relation is bounding. Thus the minimum thickness required to prevent perforation in the EOS-TC is 0.526 inch.

Thickness of the cask outer shell (1 inch) >> 0.526 inch

Thickness of the top cover plate (3.25 inch) >> 0.526 inch

Since the cask shell, and top covers are much thicker than the depth of penetration; demonstrating that during a DBT, the cask is not be penetrated by the missiles specified in Table 3.9.7-5, thus protecting the DSC.

3.9.7.2.6.3.2 Localized Peak Stress Analysis due to Missile Impact Load

In order to evaluate the localized peak stresses occurring due to the missile impact on to the cask, impact force is calculated as follows:

$$F\Delta t = G_f - G_i$$

Where,

Δt is the time of contact = 0.05 sec (more conservative than impact time 0.075 sec [3.9.7-4])

G_f is the linear momentum at time $t = t_f = mv_f$

G_i is the linear momentum at time $t = t_i = mv_i$

v is the velocity

m is the mass

Subscripts i and f represent initial and final states, respectively.

$$F = \frac{m(v_i - v_f)}{(t_f - t_i)} = \frac{m(v_i - v_f)}{(\Delta t)}$$

Assuming that the system stops after the impact, i.e. $v_f = 0$

$$F = \frac{m(v_i)}{(\Delta t)} = 24.1 \text{ Kips}$$

The impact force is dynamic as calculated using the rate of change of momentum; hence a dynamic load factor is not required.

3.9.7.2.6.3.2.1 *Localized Peak Stresses in the Cask Shell due to Missile Impact Load*

Assuming the cask is a cylindrical shell with closed ends and end support, subjected to a uniform radial load, p , over a small area A , thus using Case 8a, Table 13.3 of Roark's Formula for Stress and Strain [3.9.7-7], Page 649:

$$\frac{R}{t} = 43.5$$

$r = 3.3125$ -in. radius of Schedule 40 Pipe (Case A, Table 3.9.7-5)

The localized peak stress region is taken at '2t' away from impact, hence $r = 5.3125$ inches is used to simulate the peak stress region.

$$\frac{A}{R^2} = \frac{\pi(5.3125)^2}{43.5^2} = 0.0469$$

By interpolation,

$$\sigma_2 \left(\frac{t^2}{F} \right) = 0.74$$

$$\sigma_2' = 0.74 \left(\frac{F}{t^2} \right) = 0.74 \left(\frac{24.1}{1^2} \right) = 17.83 \text{ ksi}$$

By interpolation,

$$\sigma_2 \left(\frac{Rt}{F} \right) = 6.37$$

$$\sigma_2 = 6.37 \left(\frac{F}{Rt} \right) = 6.37 \left(\frac{24.1}{43.5 \times 1} \right) = 3.53 \text{ ksi}$$

Force applied by the missile on to the cask = 24.1 kips

$$\text{Area of missile striking face} = \frac{\pi}{4} \times 6.625^2 = 34.47 \text{ in}^2$$

$$\text{Therefore, radial membrane stress } \sigma_3 = \frac{24.1}{34.47} = 0.70 \text{ ksi}$$

As the weight of the missile (287 lb) is much less than the weight of the overall cask, thus stresses in the axial direction (σ_1) will be negligible.

Therefore, conservatively Primary Membrane stress

$$\sigma_m = \max(\sigma_1 + \sigma_2, \sigma_2 + \sigma_3, \sigma_3 + \sigma_1) = 3.53 + 0.70 = 4.23 \text{ ksi}$$

$$\text{Primary Membrane plus Bending stress, } \sigma_m + \sigma_b = 4.23 + 17.83 = 22.06 \text{ ksi}$$

3.9.7.2.6.3.2.2 Localized Peak Stresses in Top Cover Plate due to Missile Impact Load

Assuming the top cover plate is a circular plate simply supported at the edges and subjected to a uniform load over a small area A of radius r_o , thus using case 16, Table 11.2 of Roark's Formula for Stress and Strain, Page 514 [3.9.7-7]:

$$M_{\max} = \frac{W}{4\pi} \left[(1+\nu) \ln \left(\frac{a}{r_o} \right) + 1 \right] \text{ at } r = 0$$

Where, a is the plate outer radius = 43.5 inch

$r_o = 5.3125$ inches

W is the load = 24.1 kips

t is the thickness of the top cover plate = 3.25 inches

$M_{max} = 7.16$ Kip-in/in

$$\sigma = \frac{6M_{max}}{t^2} = 4.07 \text{ ksi}$$

Force applied by the missile onto the cask = 24.1 kips

Area of missile striking face = 34.47 in²

Therefore, radial membrane stress = 24.1/34.47 = 0.70 ksi

Primary membrane plus bending stress = 4.07+ 0.70 = 4.77 ksi

3.9.7.2.6.4 Stability Analysis for EOS-TC due to Seismic Load

During any seismic event in a loaded EOS-TC in the horizontal position on the skid and the trailer, it will be subjected to overturning moment. The peak ground acceleration in the horizontal (a_h) and the vertical direction (a_v) due to seismic event is 0.45 g and 0.30 g, respectively.

An overturning moment due to seismic load is calculated assuming the seismic load is acting on the cask center from the ground. The vertical seismic load is combined with the horizontal load using the 100-40-40 combination method (i.e., 40% of the vertical component acting simultaneously with 100% of the horizontal component). The stability analysis due to seismic overturning moment is performed below:

The overturning moment produced in the cask due to seismic effect is:

$$M_{ot} = a_h \times W \times L_1 + 0.4a_v \times W \times R$$

This overturning moment is resisted by the restoring moment:

$$M_{st} = W \times R$$

The variables are defined as follows:

a_h = horizontal seismic acceleration = 0.45g

W = weight of cask (results are independent of cask weight)

L_1 = vertical location of cask center of gravity = $\frac{(17+43+\frac{87}{2})}{12} = 8.63$ feet
(Figure 3.9.7-9 and Figure 3.9.7-10)

R = horizontal distance from point of rotation to cask center of gravity =
 $\frac{11ft}{2} = 5.5$ feet (Figure 3.9.7-9 and Figure 3.9.7-10)

The factor of safety against overturning, including a load factor of 1.1 on the overturning moment is:

$$\begin{aligned}\frac{M_{st}}{1.1M_{ot}} &= \frac{W \times R}{1.1(a_h \times W \times L_1 + 0.4a_v \times W \times R)} \\ &= \frac{5.5}{1.1(0.45 \times 8.63 + 0.4 \times 0.30 \times 5.5)} = 1.10\end{aligned}$$

The maximum acceptable acceleration value before tipping occurs is calculated below:

$$\begin{aligned}a_v &= \frac{2}{3}a_h \\ M_{st} &> 1.1M_{ot} \rightarrow W \times R > 1.1 \left(a_h \times W \times L_1 + 0.4 \frac{2}{3} a_h \times W \times R \right) \\ \frac{R}{1.1} &> a_h \left(L_1 + 0.4 \frac{2}{3} \times R \right) \\ a_h &< \frac{R}{1.1 \left(L_1 + 0.4 \frac{2}{3} \times R \right)} = \frac{5.5}{1.1(8.63 + 0.267 \times 5.5)} = 0.49g \\ a_h &= 0.49, \quad a_v = 0.33g\end{aligned}$$

The safety factor against overturning is 1.10 based on the design basis accelerations and including a load factor of 1.1 on the overturning moment. The EOS-TC can have up to 0.49g horizontal seismic acceleration and 0.33g vertical seismic acceleration before the cask can start to overturn. Therefore, the EOS-TC will maintain its stability during the seismic event.

3.9.7.2.6.5 Analysis of Cask for DBT Wind Load and DBT Missile Load Combination

Per NUREG-0800, the total tornado load on a structure is combined as follows:

$$\begin{aligned}W_t &= W_p \\ W_t &= W_w + 0.5W_p + W_m\end{aligned}$$

Where,

$$\begin{aligned}W_t &= \text{Total tornado load} \\ W_w &= \text{Load from tornado wind effect} \\ W_p &= \text{Load from tornado atmospheric pressure change effect} \\ W_m &= \text{Load from tornado missile impact effect}\end{aligned}$$

Note that W_p is not applicable to the stability analysis as discussed in Section 3.9.7.1.6. Therefore, the load combination for tornado loading for this analysis is simplified to:

$$W_t = W_w + W_m$$

The envelope of a range of missiles listed in Table 3.9.7-5 is used for the missile impact load evaluation. The automobile missile, with a size of 16.4 ft x 6.6 ft x 4.3 ft (Case B of Table 1), impact on to the EOS-TC has the maximum momentum and is considered as the bounding case.

3.9.7.2.6.5.1 Overtuning Analysis due to Concurrent Tornado Loads

A dynamic analysis for the combined effects of wind and concurrent massive missile impact loading is conducted. The effects of the concurrent missile impact loads are used in determining the initial angular momentum from the conservation of angular momentum equations using the wind loads from the previous section. Then the angle of rotation is determined from the conservation of the concurrent loading.

Angular velocity of the missile about point O just after the impact is:

$$\omega_i = \frac{R_1 v_i M_m}{R_1^2 M_m + (I_c)_o}$$

The concurrent wind load is accounted for by reducing the inertia that resists motion in the denominator of the equation of angular velocity of the missile about point O just after the impact

$$\omega_i = \frac{R_1 v_i M_m}{R_1^2 M_m + (I_c)_o - W_w \times L_1^2}$$

Where R_1, v_i, M_m and $(I_c)_o$ are defined in Section 3.9.7.2.6.2.1

Using the relation presented in Section 3.9.7.2.6.2.1 and reducing the inertia that resists motion in the denominator of the equation,

$$\sin(\theta + \phi) = \frac{(R_1 v_i M_m)^2}{2w_c R_2 [(I_c)_o + R_1^2 M_m - W_w \times L_1^2]} + \sin \phi$$

$$\sin(\theta + \phi) = 0.0174 + 0.8433$$

$$(\theta + \phi) = \sin^{-1}(0.8607) = 59.40^\circ$$

$$\theta = 59.40^\circ - 57.49^\circ = 1.91^\circ$$

The maximum angle for the tip over of the cask occurs when the CG is directly above the point of rotation. The maximum angle for tip over calculated in Section 3.9.7.2.6.2.1 is $\theta_{tip} = 32.51^\circ$. Since $1.1\theta \times < 1/3 \theta_{tip}$, tip over of the EOS-TC cask will not occur.

3.9.7.2.6.5.2 Time-Dependent Overturning due to Concurrent Tornado Loads

In addition to the dynamic overturning analysis, a time dependent analysis is used to ensure the absence of any overturning.

An approximate relationship for the deceleration of an automobile impacting a rigid wall is given by:

$$-\ddot{x} = 12.5g * x \quad [3.9.7-4]$$

Where, $-\ddot{x} = 12.5g \cdot x$ Eq. D-1 of [3.9.7-4]

$$\begin{aligned} -\ddot{x} &= \text{Deceleration (ft/sec}^2\text{)} \\ x &= \text{Distance automobile crushes into target (ft)} \end{aligned}$$

A force time history is obtained:

$$W_m = 0.625 \times v_s \times w_{missile} \times \sin(20t)$$

The overturning moment is:

$$M_{ot} = W_m \times L + q_z \times L_\theta^2 \times L_T$$

Where,

$$\begin{aligned} L_\theta &= \text{Height to the top of the cask system, which is dependent on rotation } \theta. \\ L &= \text{Initial height of the cask system} \\ L_T &= \text{Length of the trailer} \\ q_z &= \text{DBT velocity pressure} \end{aligned}$$

And the stabilizing moment is:

$$M_{st} = W_c * R_2 * \cos(\phi + \theta)$$

The moment causing acceleration is:

$$M_{acc} = M_{ot} - M_{st}$$

The angular velocity is:

$$\omega_i = \frac{\left[\frac{M_{acc,i} + M_{acc,i-1}}{2} * (t_i - t_{i-1}) \right]}{(I_c)_o} + \omega_{i-1}$$

Where,

i = index for the current time step
 $i - 1$ = index for the previous time step

The angle of rotation is:

$$\theta_i = \left[\frac{\omega_i + \omega_{i-1}}{2} * (t_i - t_{i-1}) \right] + \theta_{i-1}$$

Accounting for the required load factor of 1.1 on the design basis tornado, the angle of rotation resulting from the analysis is shown in Figure 3.9.7-11. The governing angle of rotation is $7.55 \times 1.1 = 8.31$ degrees, which is less than the $(1/3) \times$ tip angle $(\Theta_{tip}) = (1/3) \times 32.51^\circ = 10.84^\circ$. The factor of safety against tipping is $10.84/8.31 = 1.30$. Therefore, the EOS-TC will not tip over due to wind concurrent with massive missile impact load combination.

3.9.7.2.7 Results

The factor of safety against tip overturn is greater than 1 for the individual DBT wind pressure load and seismic load. Also, the angle of rotation (θ) due to massive missile impact load, concurrent tornado loads is less than critical tipping angle $(1/3 \times \theta_{tip})$. Therefore, EOS-TC remains stable on the trailer during transfer operations. The primary membrane intensity and combined membrane plus bending stresses due to DBT and missile impact are calculated to be below the allowable stresses. The maximum missile penetration depth is found to be 0.526 inch, which is less than the thickness of the EOS-TC outer shell and top cover plate of 1 inch and 3.25 inches, respectively.

The resultant stresses for the bounding individual DBT, missiles impact and combined tornado load are summarized in Table 3.9.7-7 and Table 3.9.7-8, respectively.

3.9.7.3 References

- 3.9.7-1 NUREG-0800, Standard Review Plan, "Missiles Generated by Natural Phenomena", Revision 2, U.S. Nuclear Regulatory Commission, July 1981.
- 3.9.7-2 American Society of Civil Engineers, ASCE 7-10, "Minimum Design Loads for Buildings and Other Structures."

- 3.9.7-3 Raymond C. Binder, “Fluid Mechanics,” Prentice-Hall, Inc, 1943.
- 3.9.7-4 Bechtel Report BC-TOP-9A Rev. 2, “Topical Report – Design of Structures for Missile Impact,” September 1974.
- 3.9.7-5 American Society of Civil Engineers Standard, ASCE 7-05, “Minimum Design Loads for Buildings and Other Structures,” (Formerly ANSI A58.1).
- 3.9.7-6 U.S. Nuclear Regulatory Commission, Regulatory Guide 1.76, “Design Basis Tornado for Nuclear Power Plants,” Revision 1, March 2007.
- 3.9.7-7 R.G Budynas and W.C Young, “Roark’s Formula for Stress and Strain,” Eighth Edition, McGraw-Hill Book Company.
- 3.9.7-8 H. A. Nelms, “Structural Analysis of Shipping Casks, Effects of Jacket Physical properties and Curvature on Puncture Analysis,” Vol.3, ORNL TM-312, Oak Ridge National Laboratory, Oak Ridge Tennessee, June 1968.

Table 3.9.7-1
Sizes and Weight for Various EOS-HSM Models

EOS-HSM Module	Total Length of EOS-HSM (in.)	Nominal Weight of Empty HSM (lbs.)
EOS-HSM Short	228	292,000
EOS-HSM Medium	248	314,000
EOS-HSM-FPS Medium	248	307,000
EOS-HSM Long	268	330,000

Table 3.9.7-2
Missile Load Data for EOS-HSM Stability Analysis

Missile	Mass (lbs.)	Dimensions	Velocity (fps)	Momentum (lbs-fps)
Utility Wooden Pole	1,124	13.5-inch Diameter 35 feet Long	180	202,320
Armor Piercing Artillery Shell	276	8-inch Diameter	185	51,060
Steel Pipe	750	12-inch Sch. 40 15 feet Long	154	115,500
Automobile	4,000	20 ft ² Contact Area	195	780,000

Table 3.9.7-3
Design Pressures for Tornado Wind Loading

Wall Orientation (1)	Velocity Pressure (psf)	Ext. Pressure Coefficient (2)	Int. Pressure Coefficient (3)	Max/Min Design Pressure (psf) (4)
Front	253.8	0.680	± 0.18	218
Left	253.8	-0.595		-197
Rear ⁽⁵⁾	253.8	-0.425		-154
Right	253.8	-0.595		-197
Top	253.8	-1.105		-326

Notes:

1. Wind direction assumed to be from front. Wind loads from other directions may be found by rotating above table values to desired wind direction.
2. These values are calculated using the external pressure coefficients from Figure 27.4-1 of [3.9.7-2] times the gust effect factor (0.85) from Section 26.9 of [3.9.7-2].
3. Internal pressure coefficient from Table 26.11-1 of [3.9.7-2].
4. These values are computed based on Equation 27.4-1 of [3.9.7-2].
5. The bounding C_p of -0.5 from an L/B ratio of 0-1 is used for wind in all directions from Figure 27.4-1 of [3.9.7-2].

Table 3.9.7-4
Summary of EOS-HSM Sliding and Stability Results

Loading	Tornado Wind + Missile		Flood		Seismic for Loaded EOS-HSM with End Shield Wall	
Result	Maximum Sliding Distance (in)	Maximum Rocking Uplift ⁽³⁾ (°)	Safety Factor against Sliding	Safety Factor against Tipping	Maximum Acceleration before Sliding ⁽¹⁾ (horiz / vert) (g)	Maximum Acceleration before Tipping ⁽²⁾ (horiz / vert) (g)
EOS-HSM Short	1.62	3.4	1.12	1.14	0.45 / 0.30	>0.45 / 0.30
EOS-HSM Medium	1.62	2.8	1.09	1.12	0.45 / 0.30	>0.45 / 0.30
EOS-HSM-FPS Medium	1.62	2.7	1.08	1.11	0.45 / 0.30	>0.45 / 0.30
EOS-HSM Long	1.62	2.4	1.11	1.13	0.45 / 0.30	>0.45 / 0.30

Notes:

1. Maximum acceleration to preclude sliding is 0.47g / 0.32g, but seismic load is limited to 0.45g / 0.30g based on static stability analysis of DSC on the support structure.
2. Maximum acceleration to preclude tipping is 0.46g / 0.31g, but seismic load is limited to 0.45g / 0.30g based on stability analysis of DSC on the support structure.
3. A 1.1 required factor is applied for the wind load to the angles from Figure 3.9.7-2 to Figure 3.9.7-4.

Table 3.9.7-5
Design-Basis Tornado Missile Spectrum and Maximum Horizontal Speed for EOS-TC Stability Analysis

Case #	Missile ⁽¹⁾	Weight (lbs)	Horizontal Impact Velocity ⁽²⁾ (fps)
A	Schedule 40 Pipe (φ 6.625 inch x 15 ft long) ⁽⁵⁾	287	135
B	Automobile (16.4 ft x 6.6 ft x 4.3 ft) ⁽³⁾⁽⁴⁾	4000	135
C	Solid Steel Sphere (φ 1 inch)	0.147	26

Notes:

1. Missiles are assumed to strike at 90 degrees to the surface with the longitudinal axis of the missile parallel to the striking angle.
2. Vertical striking velocity is 67% of the horizontal.
3. Automobile missile (Case B) bounds all other cases for stability and stresses and therefore only Case B is evaluated for stability and associated stresses.
4. The automobile missile (Case B) considered to impact at all altitudes less than 30 ft above all grade levels within 0.5 mile of the plant structure.
5. Schedule 40 pipe (Case A) bounds all other items for penetration resistance and for local stresses and therefore Case A is evaluated for the penetration resistance.

Table 3.9.7-6
Cask and DSC Weights in Different Configuration and Their Geometric Properties

CASE	Configuration	Cask without NSP Assembly ⁽¹⁾ (lbs)	DSC Weight ⁽²⁾ (lbs)	Minimum Weight (lbs)	Maximum Weight (lbs)	Cask Diameter ⁽¹⁾ (inches)	Length ⁽¹⁾ (inches)
A	TC108/37PTH	86,289	119,000	205,289	220,289	85.5	206.76
			134,000				
B	TC108/89BTH	86,289	113,000	199,289	206,289	85.5	206.76
			120,000				
C	TC125/37PTH	108,802	119,000	227,802	242,802	87	208.21
			134,000				
D	TC125/89BTH	108,802	113,000	221,802	228,802	87	208.21
			120,000				
E	TC135/37PTH	119,230	119,000	238,230	253,230	87	228.71
			134,000				

Note:

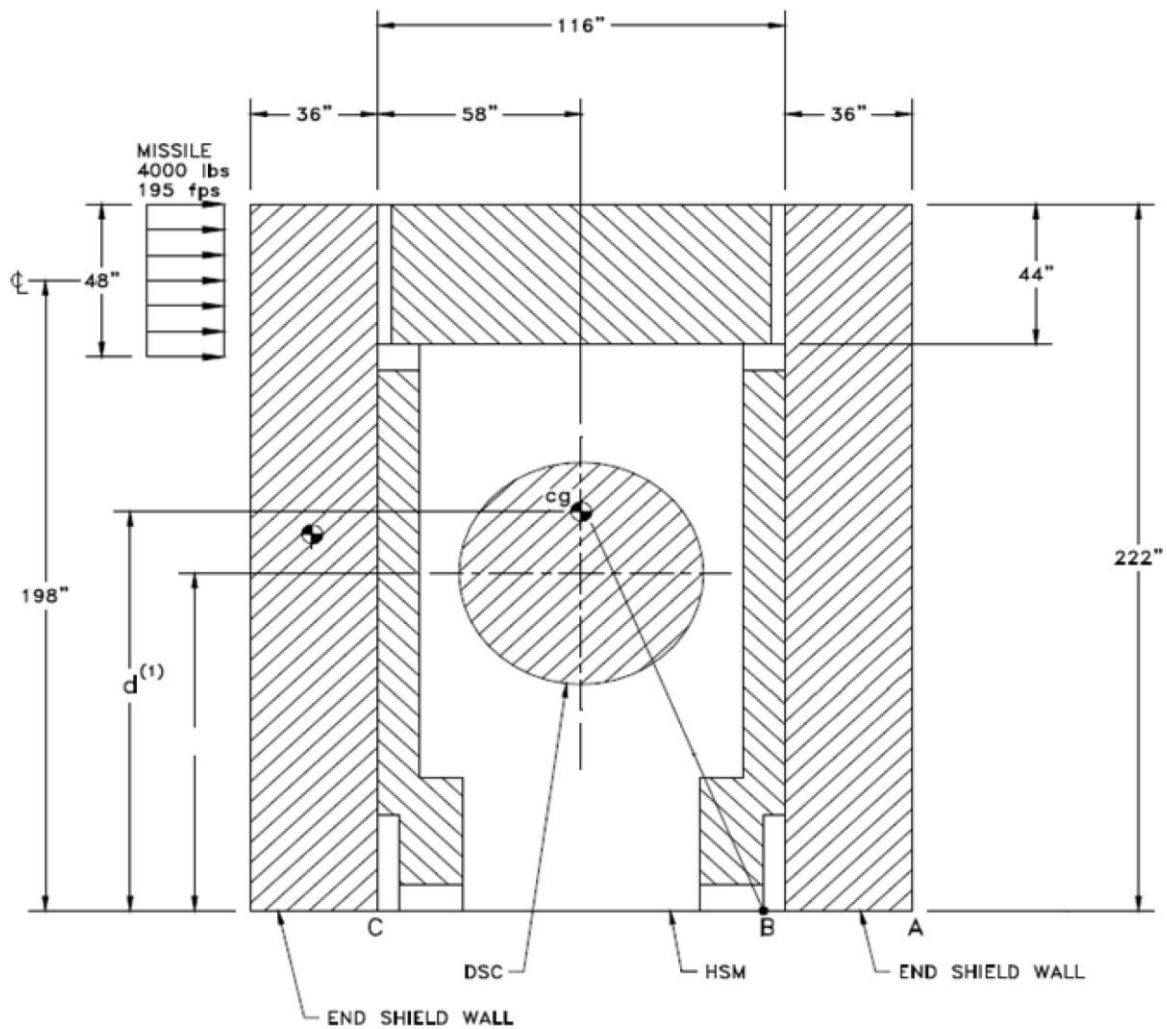
1. Weight of TC without NSP assembly and their geometric parameter in different configuration is taken from Section 3.2.
2. Weight of 37PTH and 89BTH DSC weights are taken from Section 3.2.

Table 3.9.7-7
EOS-TC Analysis Results

Load Description	Stress Category	Calculated Stress (ksi)		Allowable Stress (ksi)	Impact Force (kips)
		Cask Shell	Top Cover Plate		
Wind Pressure Loads	Primary Membrane	1.34	0	39	22.36
	Membrane + Bending	5.19	0.21	58.5	
Massive Missile	Primary Membrane	3.66		39	17.17
	Membrane + Bending	13.69		58.5	
	Primary Membrane		0.06	39	337.5
	Membrane + Bending		12.65	58.5	
Penetration Resistance	Primary Membrane	4.23	0.70	39	24.1
	Membrane + Bending	22.06	4.77	58.5	

Table 3.9.7-8
Combined Tornado Effect

Load Description	Stress Category	Combined Stress (ksi)		Allowable stress (ksi)
		Cask Shell	Top Cover Plate	
Wind pressure load + Massive Missile	Primary Membrane	5.0	0.06	39
	Membrane + Bending	18.88	12.86	58.5



⁽¹⁾ d = distance to CG of EOS-HSM

Figure 3.9.7-1
EOS-HSM Dimensions for Stability Analysis

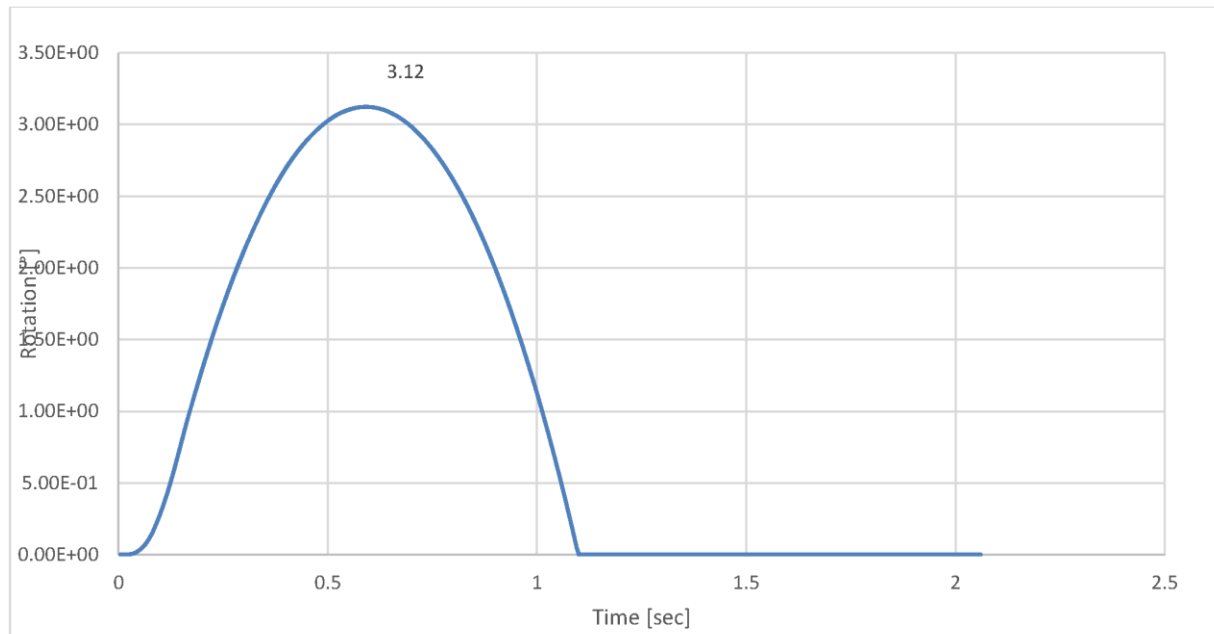


Figure 3.9.7-2
Angle of Rotation from Time-Dependent Analysis Due to Tornado Wind and
Massive Missile Loading for EOS- HSM Short

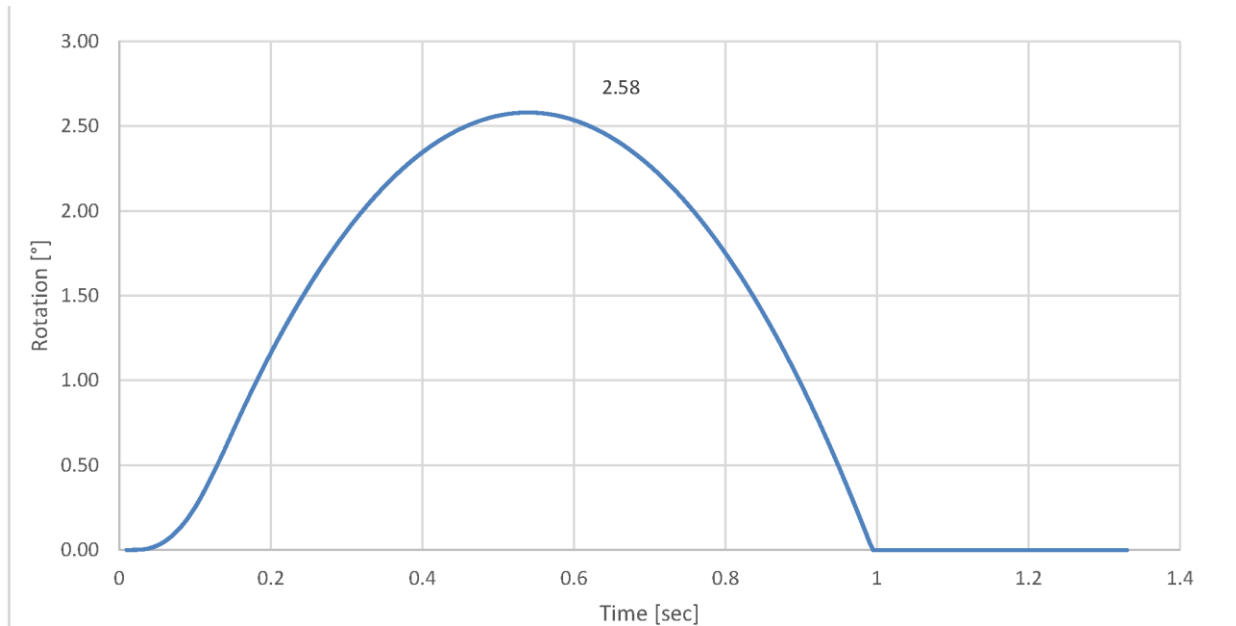


Figure 3.9.7-3
Angle of Rotation from Time-Dependent Analysis Due to Tornado Wind and Massive Missile Loading for EOS- HSM Medium

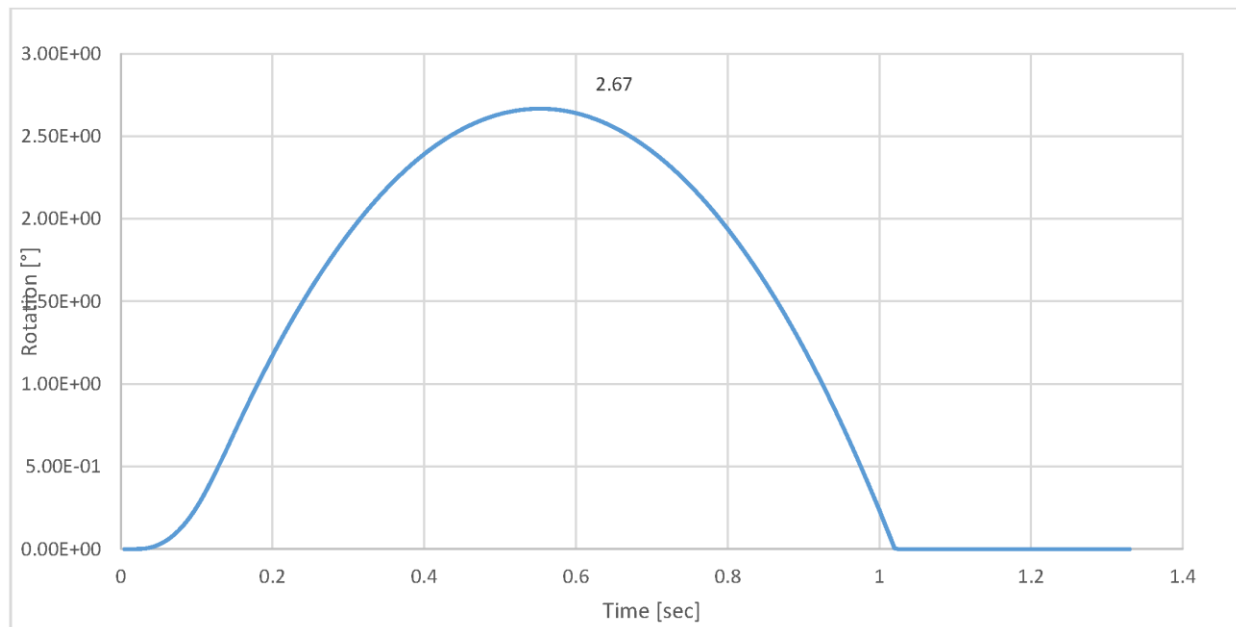


Figure 3.9.7-3a
Angle of Rotation from Time Dependent Analysis due to Wind and Massive Missile Loading for EOS-HSM-FPS

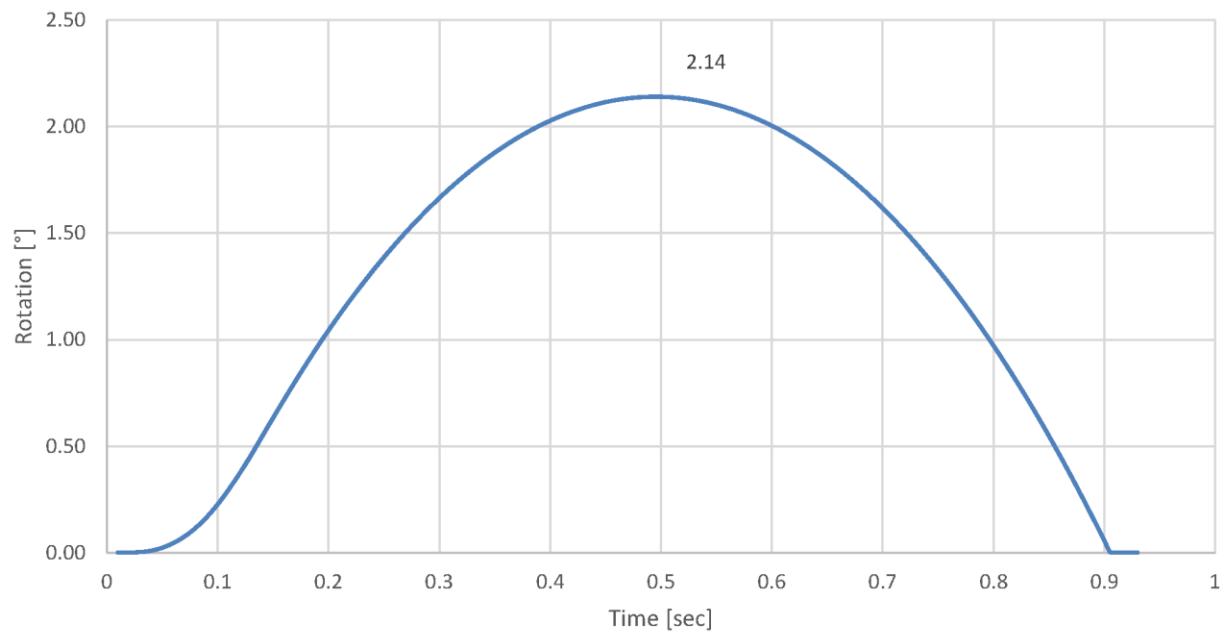


Figure 3.9.7-4
Angle of Rotation from Time-Dependent Analysis Due to Tornado Wind and
Massive Missile Loading for EOS- HSM Long

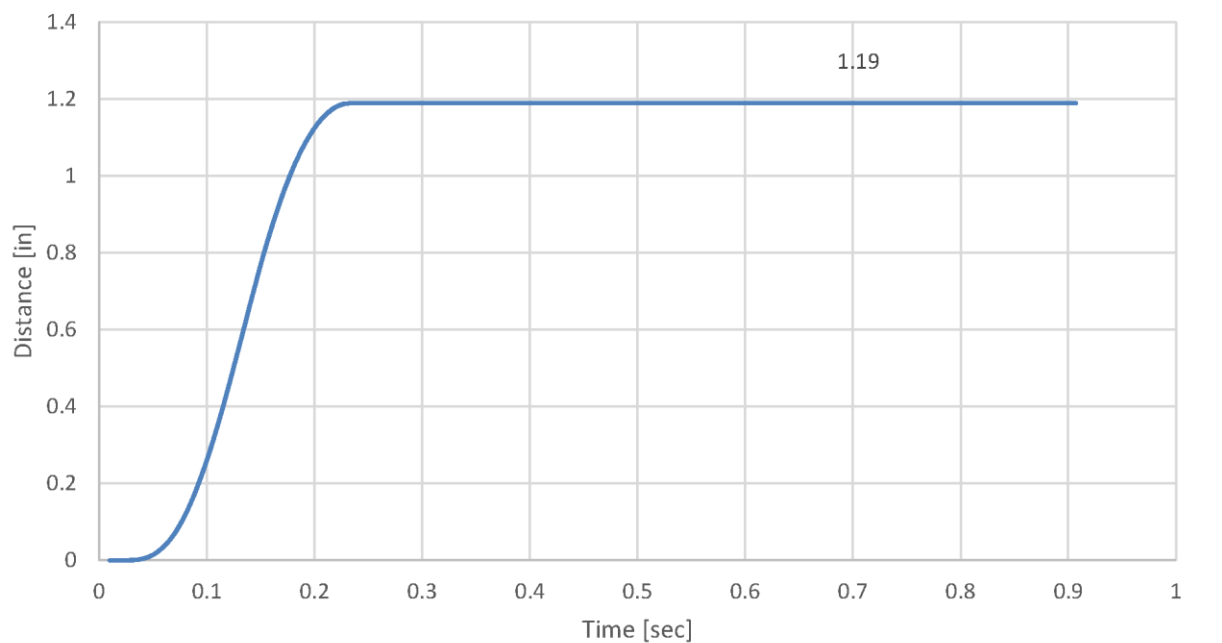


Figure 3.9.7-5
Sliding Displacement from Time-Dependent Analysis Due to Tornado Wind
and Massive Missile Loading for EOS- HSM Short

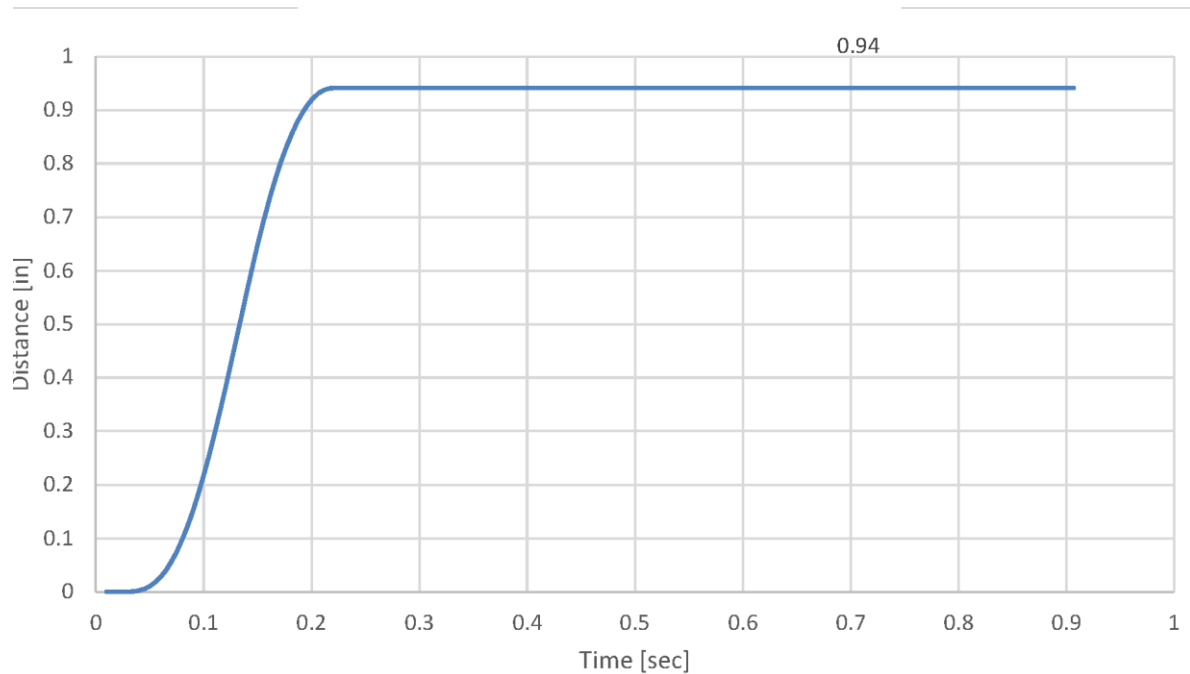


Figure 3.9.7-6
Sliding Displacement from Time-Dependent Analysis Due to Tornado Wind
and Massive Missile Loading for EOS- HSM Medium

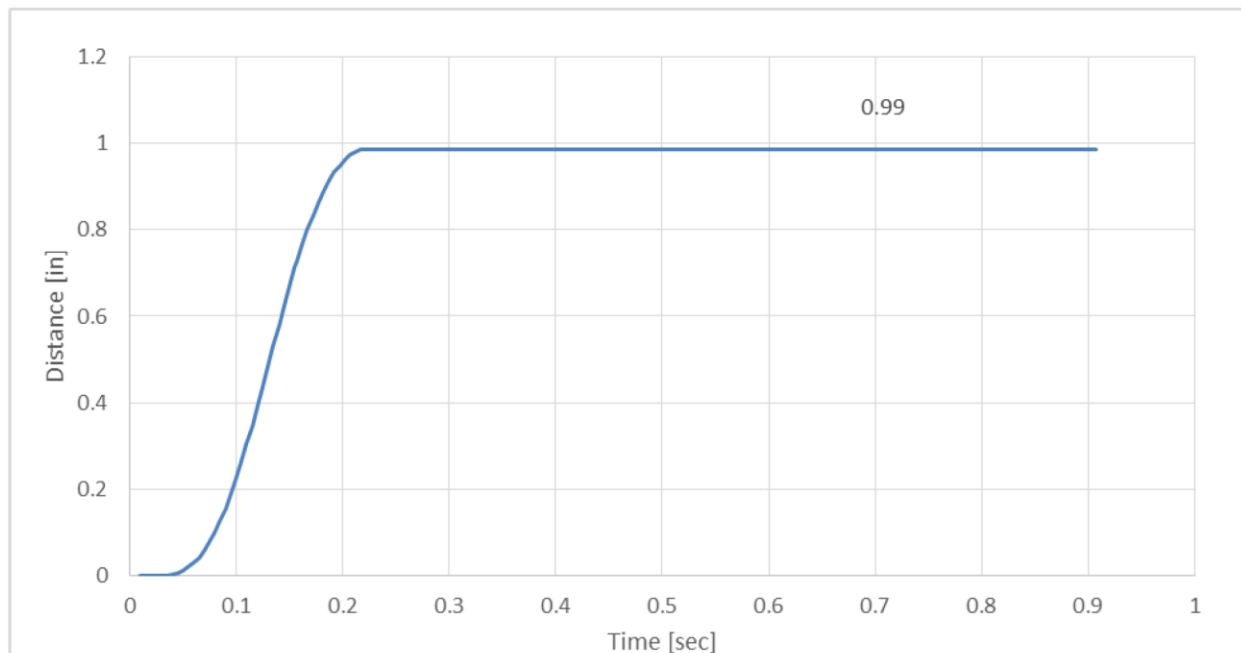


Figure 3.9.7-6a
Sliding Displacement from Time Dependent Analysis due to Wind and
Massive Missile Loading for EOS-HSM-FPS

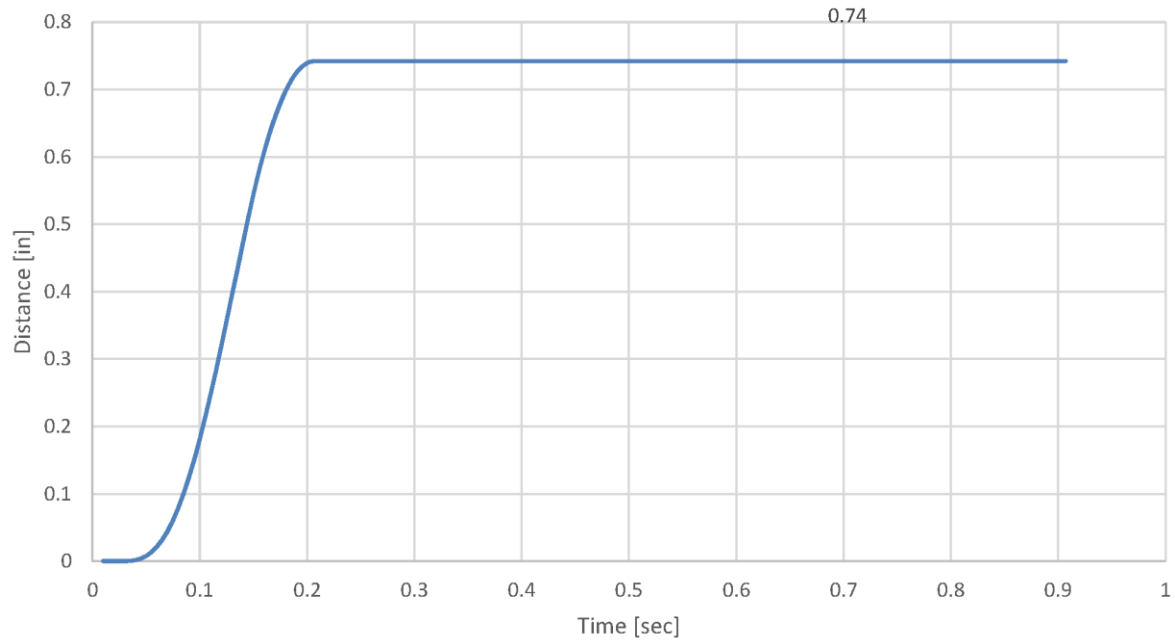


Figure 3.9.7-7
Sliding Displacement from Time-Dependent Analysis Due to Tornado Wind
and Massive Missile Loading for EOS- HSM Long

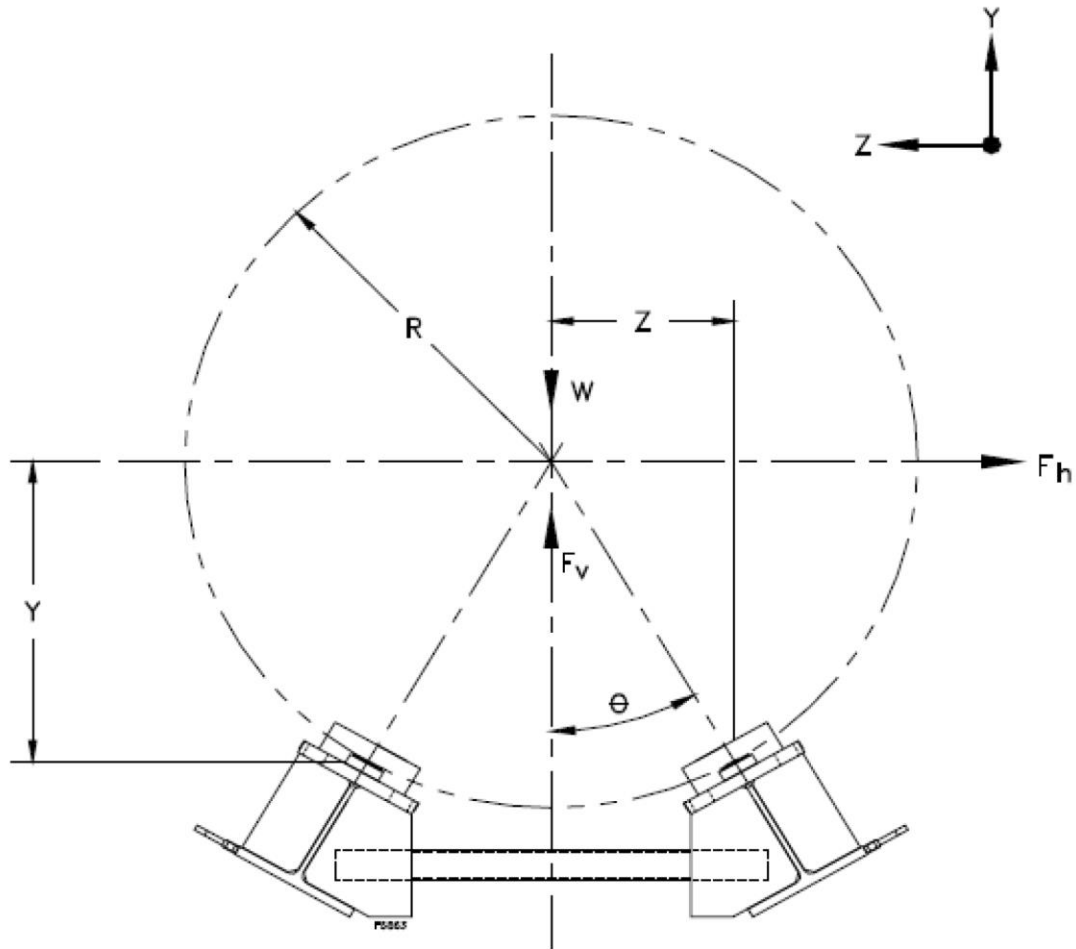


Figure 3.9.7-8
Stability of the DSC on the DSC Support Structure

Note: The EOS-HSM-FPS DSC support structure is not shown in this figure

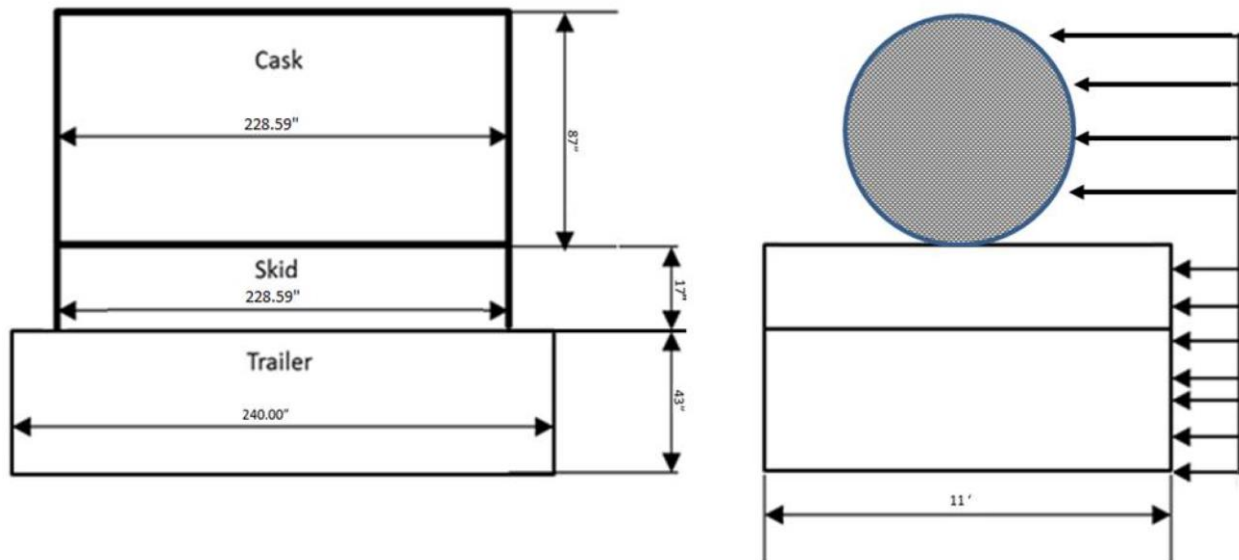


Figure 3.9.7-9
Arrangement of EOS-TC, Skid and Transfer Trailer at Rest

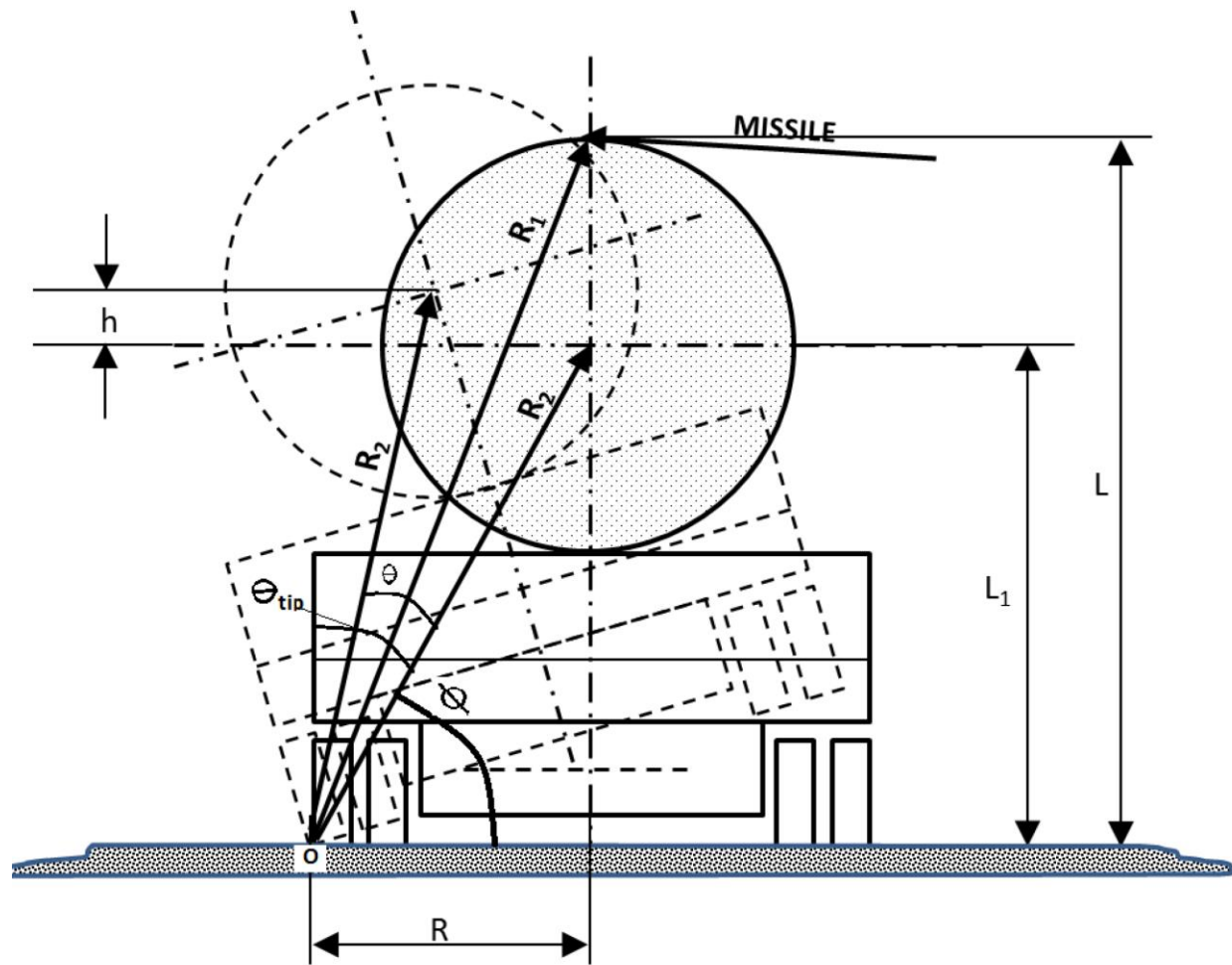


Figure 3.9.7-10
Stability Geometry of TC on Transfer Trailer

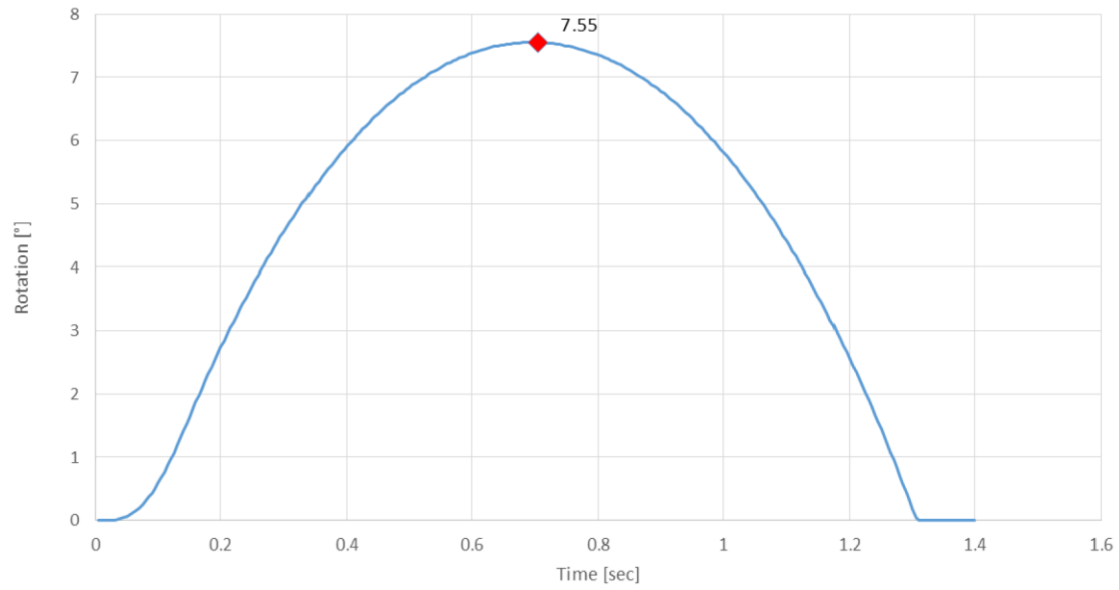


Figure 3.9.7-11
Angle of Rotation (Time-Dependent)-Wind and Missile Loading for EOS-TC